

INMATEH -

**AGRICULTURAL
ENGINEERING**

SEPTEMBER - DECEMBER

No liability is assumed by the editorial staff for the content of scientific papers and opinions published in this volume. They represent the author's point of view

Editorial

The National Institute of Research-Development for Machines and Installations designed to Agriculture and Food Industry - INMA Bucharest has the oldest and most prestigious research activity in the field of agricultural machinery and mechanizing technologies in Romania.

Short History

- ✓ *In 1927, the first research Center for Agricultural Machinery in Agricultural Research Institute of Romania - ICAR (Establishing Law was published in O.D. no. 97/05.05.1927) was established;*
- ✓ *In 1930, was founded The Testing Department of Agricultural Machinery and Tools by transforming Agricultural Research Centre of ICAR- that founded the science of methodologies and experimental techniques in the field (Decision no. 2000/1930 of ICAR, Manager - GHEORGHE IONESCU ȘIȘEȘTI);*
- ✓ *In 1952, was established the Research Institute for Mechanization and Electrification of Agriculture - ICMA Băneasa, by transforming the Department of Agricultural Machines and Tools Testing;*
- ✓ *In 1979, the Research Institute of Scientific and Technological Engineering for Agricultural Machinery and Tools - ICSITMUA was founded - subordinated to Ministry of Machine Building Industry - MICM, by unifying ICMA subordinated to MAA with ICPMA subordinated to MICM;*
- ✓ *In 1996 the National Institute of Research-Development for Machines and Installations designed to Agriculture and Food Industry - INMA was founded - according to G.D. no.1308/25.11.1996, by reorganizing ICSITMUA, G.D no. 1308/1996 coordinated by the Ministry of Education and Research G.D. no. 823/2004;*
- ✓ *In 2008 INMA has been accredited to carry out research and developing activities financed from public funds under G.D. no. 551/2007, Decision of the National Authority for Scientific Research - ANCSno. 9634/2008.*

As a result of widening the spectrum of communication, dissemination and implementation of scientific research results, in 2000 was founded the institute magazine, issued under the name of SCIENTIFIC PAPERS (INMATEH), ISSN 1583 – 1019.

*Starting with volume 30, no. 1/2010, the magazine changed its name to INMATEH - *Agricultural Engineering*, appearing both in print format (ISSN 2068 - 4215), and online (ISSN online: 2068 - 2239). The magazine is bilingual, abstract being published in native language and English, with a rhythm of three issues / year: January-April, May-August, September-December and is recognized by CNCSIS – with B⁺ category. Published articles are from the field of AGRICULTURAL ENGINEERING: technologies and technical equipment for agriculture and food industry, renewable energy, machinery testing, environment, transport in agriculture etc. and are evaluated by specialists inside the country and abroad, in mentioned domains.*

*Technical level and performance processes, technology and machinery for agriculture and food industry increasing, according to national requirements and European and international regulations, as well as exploitation of renewable resources in terms of efficiency, life, health and environment protection represent referential elements for the magazine „INMATEH - *Agricultural Engineering*”.*

We are thankful to all readers, publishers and assessors.

Editor in chief,

Ph. D. Eng. Vladut Nicolae-Valentin

Managing Editorial Board - INMA Bucharest**Editor in Chief****VLADUȚ Nicolae-Valentin**

Ph.D.Eng, SR I

E-mail: inmatehjournal@gmail.com**Executive Editor****POPA Lucreția**

Ph.D.Eng, SR I

Assistant Editor**MATACHE Mihai-Gabriel**

Ph.D.Eng, SR I

Logistic support, database**MURARU Virgil, Ph.D.Eng, SR I****ȚICU Tania, techn.****Scientific Secretary****Cârdei Petre, math.****Official translators****RADU Daniela-Cristina, Prof. English, French****Editorial Board**

- Acad. Prof. Ph.D. TABĂRA Valeriu - Romania, President of ASAS - Academy of Agricultural and Forestry Sciences "Gheorghe Ionescu Șişești";
- Ph.D. BOGOESCU Marian - Romania, Vicepresident of ASAS - Academy of Agricultural and Forestry Sciences "Gheorghe Ionescu Șişești";
- Hon.Prof.Ph.D.Eng. PIRNA Ion - Romania, President of the Department of Agricultural Mechanization of ASAS - Academy of Agricultural and Forestry Sciences "Gheorghe Ionescu Șişești";
- Ph.D. Eng. NICOLESCU C. Mihai - Romania, Scientific General Secretary of the ASAS-Academy of Agricultural and Forestry Sciences "Gheorghe Ionescu Șişești";
- Assoc.Prof. Ph.D. Eng. BELC Nastasia - Romania, IBA Bucharest;
- Ph.D. Eng. BUȚU Alina - Romania, INSB Bucharest;
- Prof. Ph.D. Eng. PARASCHIV Gigel - Romania, P.U. Bucharest;
- Prof. Ph.D.Eng. BIRIȘ Sorin - Romania, P.U. Bucharest;
- Prof. Ph.D. Eng. VLASE Sorin - Romania, "Transilvania" University Brașov;
- Prof. Ph.D.Eng. BURNETE Nicolae - Romania, Technical University Cluj Napoca;
- Prof. Ph.D. Eng. FILIP Nicolae - Romania, Technical University Cluj Napoca;
- Prof. Ph.D. Eng. VOICU Gheorghe - Romania, P.U. Bucharest;
- Prof. Ph.D. Eng. GERGEN Iosif -Romania,USAMVB Timișoara;
- Prof. Ph.D. Eng. ȚENU Ioan - Romania, USAMV Iași;
- Assoc.Prof.Ph.D.Eng. BUNGESCU Sorin - Romania, USAMVB Timișoara;
- Prof. Ph.D.Eng. FENYVESI László - Hungary, Hungarian Institute of Agricultural Engineering Godolo;
- Assist.Prof.Ph.D.Eng. BILANDZIJA Nikola - Croatia, University of Zagreb;
- Ph.D. BIOCCA Marcello - Italy Agricultural Research Council, Agricultural Engineering Research Unit;
- Prof.Ph.D.Eng. MIHAILOV Nikolay - Bulgaria, University of Rousse;
- Assoc.Prof.Ph.D.Eng. ATANASOV At. - Bulgaria, University of Rousse;
- Assoc.Prof. Ph.D. ERTEKIN Can - Turkey, Akdeniz University Antalya;
- Prof. Ph.D.Sc. Eng. VARTUKAPTEINIS Kaspars - Latvia, Latvia University of Agriculture, Institute of Agricultural Machinery;
- ir. HUYGHEBAERT Bruno - Belgium, Walloon Agricultural Research Center CRA-W;
- Prof.Ph.D. Eng. FABBRO Dal Inacio Maria - Brazil, Campinas State University;
- Prof. Ph.D. Eng. DE WRACHIEN Daniele - Italy, State University of Milan;
- Prof. Ph.D.Guanxin YAO - P.R.China, Along Agriculture R&DTechnology and Management Consulting Co., Ltd;
- Prof. Ph.D. Eng. GONZÁLEZ Omar - Republic of Cuba, Central University "Marta Abreu" de las Villas;
- Assist. Prof.Dr. KABAŞ Önder –Turkey, Akdeniz University.
- Asist.Prof.Dr. SELVİ Kemal Çağatay - Turkey, Ondokuz Mayıs University.

In the present, *INMATEH - Agricultural Engineering* journal is indexed in the next international databases:
 ELSEVIER /SciVerse SCOPUS, CLARIVATE ANALYTICS' WEB OF SCIENCE- Emerging Sources Citation Index (ESCI),
 ULRICHS Web: Global Serials Directory, CABI, SCPIO, Index COPERNICUS International,
 EBSCO Publishing, Elektronische Zeitschriftenbibliothek

INMATEH - Agricultural Engineering**vol. 56, no.3 / 2018**

NATIONAL INSTITUTE OF RESEARCH-DEVELOPMENT FOR MACHINES AND
 INSTALLATIONS DESIGNED TO AGRICULTURE AND FOOD INDUSTRY -
 INMA Bucharest

6 Ion Ionescu de la Brad Blvd., sector 1, Bucharest

Three issues per year,
 e-ISSN: 2068 – 2239
 p ISSN: 2068 – 4215

Edited by: INMA Bucharest

Copyright: INMA Bucharest / Romania

CONTENT

		Page(s)
1.	<p>EXPERIMENTAL RESEARCH ON THE MOVEMENT STABILITY OF A PLOUGHING AGGREGATE, COMPOSED ACCORDING TO THE “PUSH-PULL” SCHEME / PĒC «PUSH-PULL» SHĒMAS KOMPLEKTĒTA ARŠANAS AGREGĀTA KUSTĪBAS STABILITĀTES EKSPERIMENTĀLS PĒTĪJUMS</p> <p>Ph.D. Ivanovs S.¹⁾, Prof.PhD. Bulgakov V.²⁾, Prof.PhD. Adamchuk V.³⁾, Prof.PhD. Kyurchev V.⁴⁾, Prof.PhD. Kuvachov V.⁴⁾</p> <p>¹⁾Latvia University of Agriculture / Latvia; ²⁾National University of Life and Environmental Sciences of Ukraine / Ukraine; ³⁾National Scientific Centre “Institute for Agricultural Engineering and Electrification” / Ukraine; ⁴⁾Tavria State Agrotechnological University / Ukraine</p>	9
2.	<p>RESEARCH ON THE VIBRATION OF MINI TILLER / 微耕机的振动研究</p> <p>Ph.D. Eng. Liang X.C. [*], Prof. Ph.D. Chen J., Ms.Stud. Eng. Wang Z. Southwest University, College of Engineering and Technology, Chongqing Key Laboratory of Agricultural Equipment for Hilly and Mountainous Regions / P. R. China</p>	17
3.	<p>ANALYSIS OF THE WORKS PERFORMED BY PNEUMATIC AND MECHANICAL SEEDING DEVICE WITHOUT USING VACUUM / АНАЛІЗ РОБОТИ ПНЕВМОМЕХАНІЧНОГО ВИСІВНОГО АПАРАТА БЕЗ ВИКОРИСТАННЯ ВАКУУМУ</p> <p>Lect. Ph.D. Eng. Vasytkovska K.V., Lect. Ph.D. Eng. Vasytkovskyi O.M., Prof. Ph.D. Eng. Sviren M.O., Lect. Ph.D. Agric. Kulik G.A. Central Ukrainian National Technical University / Ukraine</p>	25
4.	<p>PRODUCTION TESTS OF A SEED DRILL CPH 2000 FOR DIRECT SOWING / ESSAIS AU CHAMP D’UN SEMOIR CPH 2000 POUR LE SEMIS DIRECT</p> <p>Warouma Arifa¹⁾, Haidenko Oleh²⁾</p> <p>¹⁾Dan Dicko Dan Koulodo University of Maradi, Niger Republic ²⁾Institute of Steppe Agriculture of the National Academy of Agrarian Sciences of Ukraine</p>	31
5.	<p>RESEARCH ON THE RATIONAL REGIMES OF WHEAT SEEDS DRYING / ДОСЛІДЖЕННЯ РАЦІОНАЛЬНИХ РЕЖИМІВ СУШІННЯ НАСІННЯ ПШЕНИЦІ</p> <p>Assoc. Prof.Ph.D.Eng. Paziuk V.M.¹⁾, Assoc. Prof. Ph.D. Eng. Liubin M.V. ²⁾, Assoc. Prof. Ph.D. Eng. Yaropud V.M. ²⁾, Assoc. Prof. Ph.D. Eng. Tokarchuk O.A. ²⁾, Assoc. Prof. Ph.D. Eng. Tokarchuk D.M. ²⁾</p> <p>¹⁾Institute of technical thermal physics NAS of Ukraine ²⁾Vinnitsa National Agrarian University / Ukraine</p>	39
6.	<p>AN ANALYSIS OF EIGHT TILLAGE METHODS IN A SILTY-CLAY SOIL: PROPOSAL FOR FLEXIBLE TILLAGE CYCLES / ANALISI DI OTTO METODI DI LAVORAZIONE DI TERRENI LIMO-ARGILLOSI: PROPOSTA DI CICLI FLESSIBILI DI LAVORAZIONE</p> <p>Fanigliulo R., Biocca M., Pochi D. Consiglio per la ricerca in agricoltura e l'analisi dell'economia agraria (CREA), Centro di ricerca Ingegneria e Trasformazioni agroalimentari (Research Centre for Engineering and Agro-Food Processing), Monterotondo (Rome), Italy</p>	49
7.	<p>TECHNIQUE FOR CALCULATING THE RESULTANT FORCE AND MOMENT OF SOIL RESISTANCE TO CUTTING BY BLADE OF ROTARY TILLAGE TOOL / МЕТОДИКА РАСЧЕТА РЕЗУЛЬТИРУЮЩЕЙ СИЛЫ И МОМЕНТА СОПРОТИВЛЕНИЯ ПОЧВЫ РЕЗАНИЮ ЛЕЗВИЕМ ЛОПАСТНОГО РОТАЦИОННОГО РАБОЧЕГО ОРГАНА</p> <p>Prof. PhD. Eng. Sc. Akimov A.P.[*], Asst. Prof. PhD. Eng. Sc. Konstantinov Y.V., Asst. Prof. PhD. Stepanov A.V. Chuvash State Agricultural Academy / Russia</p>	59
8.	<p>NUMERIC MODEL OF THE GRAIN MIXTURE FLOW IN A CYLINDRICAL SIEVE WHICH REVOLVES AROUND THE INCLINED AXIS / ДОСЛІДЖЕННЯ РУХУ ЗЕРНОВОЇ СУМІШІ В ЦИЛІНДРИЧНОМУ РЕШЕТІ, ЩО ОБЕРТАЄТЬСЯ НАВКОЛО НАХИЛЕНОЇ ОСІ</p> <p>Lect. Ph.D.Eng. Naumenko M., Lect. Ph.D.Eng. Sokol S., Lect. Ph.D. Eng. Filipenko D., Lect. Ph.D. Eng.Guridova V., Prof. Ph.D. Agri.Sci. Kharytonov M. Dnipro State Agrarian and Economics University, Faculty of Agrarian Engineering / Ukraine</p>	67
9.	<p>RESEARCHES ON THE MONITORING OF AIR PRESSURE IN THE TIRES AT ROAD TRANSPORT MEANS / CERCETARI PRIVIND MONITORIZAREA PRESIUNII AERULUI DIN PNEURI LA MIJLOACELE DE TRANSPORT RUTIERE</p> <p>Ph.D. Eng. Ciupercă R., Ph.D. Stud. Eng. Persu C., Ph.D. Eng. Nedelcu A., Ph.D. Eng. Popa L., Ph.D. Stud. Eng. Zaica A., Ph.D. Stud. Eng. Ștefan V. National Institute of Research-Development for Machines and Installations designed to Agriculture and Food Industry – INMA, Bucharest / Romania</p>	75

		Page(s)
10.	<p>RESEARCHES REGARDING THE OPTIMIZATION OF IMPURITIES REMOVAL TECHNOLOGY FROM THE CEREAL AND INDUSTRIAL PLANT SEEDS FOR ESTABLISHING ECOLOGICAL CROPS / CERCETĂRI PRIVIND OPTIMIZAREA TEHNOLOGIEI DE ELIMINARE A IMPURITĂȚILOR DIN MASA DE SEMINȚE DE CEREALE ȘI PLANTE TEHNICE DESTINATE ÎNFIINȚĂRII CULTURILOR ECOLOGICE</p> <p>Ph.D. Eng. Păun A.¹⁾, Eng. Stroescu Gh.¹⁾, Ph.D. Eng. Vișan A.L.¹⁾, Ph.D. Eng. Olan M.¹⁾, Ph.D. Stud. Eng. Zaica Alexandru¹⁾, Lect.Ph.D.Eng. Moiceanu G.²⁾</p> <p>¹⁾ National Institute of Research-Development for Machines and Installations designed to Agriculture and Food Industry – INMA, Bucharest / Romania; ²⁾ Politehnica University of Bucharest / Romania</p>	83
11.	<p>RESEARCH OF YELLOW-FEATHER CHICKEN BREEDING MODEL BASED ON SMALL CHICKEN CHAMBER / 基于小型鸡舍的黄羽鸡精细化养殖模式研究</p> <p>MAE. Stud. Heyang Yao¹⁾, Ms. Qiyue Sun¹⁾, Assoc. Prof. Ph.D. Xiuguo Zou^{*1)}, MEE. Stud. Siyu Wang²⁾, Senior Exper. Shixiu Zhang¹⁾, MAE. Stud. Shikai Zhang¹⁾, Ms. Shuyue Zhang¹⁾</p> <p>¹⁾ College of Engineering, Nanjing Agricultural University / China; ²⁾ School of environmental science and Engineering, Nanjing University of Information Science and Technology / China</p>	91
12.	<p>RESEARCH ON TEMPERATURE PREPARATION OF DIESEL BIOFUEL IN AN ENERGY VEHICLE FUEL TANK / ДОСЛІДЖЕННЯ ТЕМПЕРАТУРНОЇ ПІДГОТОВКИ ДИЗЕЛЬНОГО БІОПАЛИВА В ПАЛИВНОМУ БАКУ ЕНЕРГОЗАСОБУ</p> <p>Prof.D.Sc. Golub G.A.¹⁾, Ph.D. Eng. Chuba V.V.¹⁾, Ph.D. Eng. Kepko O.I.^{*2)}</p> <p>¹⁾National University of Life and Environmental Sciences of Ukraine, Kyiv / Ukraine; ²⁾Uman National University of Horticulture, Uman / Ukraine</p>	10 1
13.	<p>NUMERICAL ANALYSES OF AIR VELOCITY AND TEMPERATURE DISTRIBUTION IN POULTRY HOUSE USING COMPUTATIONAL FLUID DYNAMICS</p> <p>آنالیز عددی توزیع سرعت و دما در مرغداری با استفاده از دینامیک سیالات محاسباتی</p> <p>Ph.D. Stud. Eng. Pourvosoghi N¹⁾, Assoc.Prof. Ph.D. Eng. Nikbakht A.M.^{*1)}, Assoc.Prof. Ph.D. Eng. Sharifian F.¹⁾, Assist.Prof. Ph.D. Eng. Najafi R.²⁾</p> <p>¹⁾Department of Mechanical Engineering of Biosystems, Urmia University / Iran ²⁾Department of Animal Science, Urmia University / Iran</p>	10 9
14.	<p>RESEARCH ON SUNFLOWER SEEDS SEPARATION BY AIRFLOW / ДОСЛІДЖЕННЯ ПРОЦЕСУ СЕПАРАЦІЇ НАСІННЯ СОЛЯШНИКУ ПІД ДІЄЮ ПОВІТРЯНОГО ПОТОКУ</p> <p>Ph.D. Aliev E.B.¹⁾, Ph.D. Yaropud V.M.²⁾, Ph.D. Dudin V.Yr.³⁾, Ph.D. Pryshliak V.M.²⁾, Ph.D. Pryshliak N.V.²⁾, Ph.D. Ivlev V. V.³⁾</p> <p>¹⁾Institute of Oilseed Crops NAAS, Zaporizhzhia / Ukraine, ²⁾Vinnitsa National Agrarian University / Ukraine ³⁾ Dnipro State Agrarian and Economic University / Ukraine</p>	11 9
15.	<p>DESIGN OF SHAPED-HOLE VOLUME-VARIABLE PRECISION SEEDER / 变容量型孔轮式排种器设计</p> <p>Lect. Ph.D. Jiaxin Zheng¹⁾, M.S. Yanyu Gao¹⁾, Lect. Ph.D. Hongfang Yuan²⁾, Lect. Ph.D. Rong Chen^{*1)}</p> <p>¹⁾ School of Mechanical and Electrical Engineering, Yunnan Agricultural University, Kunming /China; ²⁾ Key Laboratory of Bionics Engineering, Ministry of Education, Jilin University, Changchun / China</p>	12 9
16.	<p>RESEARCH AND DEVELOPMENT OF AIR-SUCTION CORN PRECISION SEED METERING DEVICE / 气吸式精量玉米播种器的研究与开发</p> <p>Prof. Ph.D. Eng. Lv Xiaorong^{*1)}, Prof. Ph.D. Eng. Zhang Lihua¹⁾, Ph.D. Eng. Lv Xiaolian²⁾, M.A. Stud. Eng. Tian Zhiwei¹⁾</p> <p>¹⁾ Sichuan Agricultural University, College of Machinery & Electronics / China; ²⁾ Chuzhou University, College of Machinery & Automotive Engineering / China</p>	13 7
17.	<p>DESIGN AND EXPERIMENTAL STUDY OF THE FINGER-TYPE LIFTER TEST BENCH FOR <i>Cerasus humilis</i> BRANCHES / 拨指式钙果扶禾试验台的设计与试验</p> <p>As. M.S. Stud. Eng. Yongqiang He, Prof. Ph.D. Eng. Junlin He[*]), Ph.D. Stud. Eng. Xiaobin Du, M.S. Stud. Eng. Dawei Fang</p> <p>College of Engineering, Shanxi Agriculture University, Taigu / China</p>	14 7
18.	<p>DESIGN AND TEST ON CONTROL SYSTEM OF AUTOMATIC SEEDLING FEEDING MECHANISM FOR TRANSPLANTING MACHINE / 移栽机自动送苗机构控制系统设计和试验</p> <p>As. Ph.D. Stud. Eng. Yong Zhang^{1,2)}, A/Prof. Ph.D. Eng. KaiXing Zhang^{*1)}, M.S. Stud. Eng. Chao Song¹⁾, Prof. Ph.D. Eng. XianXi Liu.¹⁾, Prof. Ph.D. Eng. ZhengHe Song³⁾</p> <p>¹⁾ College of Mechanical and Electrical Engineering, Shandong Agricultural University, Taian / China; ²⁾ School of Information And Electronic Engineering, Shandong Technology and Business University, Yantai / China; ³⁾ College of Engineering, China Agricultural University, Beijing / China</p>	155
19.	<p>THE EFFECT OF POTATOES' COMPRESSIVE MECHANICAL PROPERTIES UNDER DIFFERENT MOISTURE CONTENTS: AN EXPERIMENTAL STUDY / 不同含水率下马铃薯压缩力学特性影响的试验研究</p> <p>Ph.D. Yu Fan^{1,2)}, A. Prof. Ph.D. Ping Zhao^{*1)}, Prof. Ph.D. Lichun Qiu¹⁾, M.S. Jizhe Zhao¹⁾</p> <p>¹⁾ Agricultural University of Shenyang, Shenyang 110886, China ²⁾ Heilongjiang Agricultural Economy Vocational College, Mudanjiang / China</p>	165

		Page(s)
20.	<p>THE INFLUENCE OF BULK MATERIAL FLOW ON TECHNICAL AND ECONOMICAL PERFORMANCE OF A SCREW CONVEYOR / ВПЛИВ ПОТОКУ СИПКОГО МАТЕРІАЛУ НА ТЕХНІКО-ЕКОНОМІЧНІ ПОКАЗНИКИ РОБОТИ ГВИНТОВОГО КОНВЕЄРА</p> <p>Prof. Ph.D. Eng. Hevko R.B.¹⁾, Prof. Ph.D. Eng. Baranovsky V.M.²⁾, Prof. Ph.D. Eng. Lyashuk O.L.,²⁾ Prof. Ph.D. Eng. Pohrishchuk B.V.¹⁾ Assoc. Prof. Ph.D. Eng. Gumeniuk Y.P.¹⁾ Assoc. Ph.D. Eng. Klendii O.M.,³⁾ Assoc. Ph.D. Eng. Dobizha N.V.¹⁾</p> <p>¹⁾Ternopil National Economical University / Ukraine; ²⁾Ternopil Ivan Puluj National Technical University ³⁾Separated Subdivision of National University of Life and Environmental Sciences of Ukraine, Berezhany Agrotechnical Institute / Ukraine</p>	175
21.	<p>THE NUMERICAL SIMULATION OF HYDRODYNAMICS AND MASS TRANSFER PROCESSES FOR VENTILATING SYSTEM EFFECTIVE LOCATION / ЧИСЕЛЬНЕ ДОСЛІДЖЕННЯ ГІДРОДИНАМІКИ І ТЕПЛОПЕРЕНОСУ У ПТАШНИКУ ДЛЯ ЕФЕКТИВНОГО РОЗМІЩЕННЯ ВЕНТИЛЯЦІЙНОГО ОБЛАДНАННЯ</p> <p>Prof. Ph.D. Eng. Gorobets V.G.¹⁾, Senior lecturer Ph.D. Eng. Trokhaniak V.I.¹⁾, Assoc. Prof. Ph.D. Eng. Rogovskii I.L.¹⁾, Senior lecturer Ph.D. Eng. Titova L.L.¹⁾, Senior lecturer Ph.D. Eng. Lendiel T.I.¹⁾, Assoc. Prof. Ph.D. Eng. Dudnyk A.O.¹⁾, PhD student Masiuk M.Yu.¹⁾</p> <p>¹⁾ National University of Life and Environmental Sciences of Ukraine / Ukraine</p>	185
22.	<p>STUDY ON NDVI OPTIMIZATION OF CORN VARIABLE FERTILIZER APPLICATOR / 变量施肥机 NDVI 的优化研究</p> <p>Ph.D. Hongli Liu¹⁾, Prof. Xi Wang²⁾, M.S. Jin Bing-kun²⁾</p> <p>¹⁾ College of Engineering, Heilongjiang Bayi Agricultural University, Daqing/China; ²⁾ Western University, 1151 Richmond Street, London, Ontario / Canada</p>	193
23.	<p>EFFECT OF PRE-SOAKING AND GRAIN SHAPE ON COOKING ENERGY OF PARBOILED AND RAW RICE / තම්බන ලද සහ කැකුළු සහල් ඇටවල භෞමික හා පිසීමට කලින් පෙතවීම සහල් පිසීමේ ශක්ති පරිභෝජනය මත බලපෑම</p> <p>K. G. Gunasekara ¹⁾, D. A. N. Dharmasena ²⁾ and F. H. C. A. Silva ²⁾</p> <p>¹⁾ Postgraduate Institute of Agriculture, University of Peradeniya, Peradeniya, Sri Lanka ²⁾ Department of Agricultural Engineering, Faculty of Agriculture, University of Peradeniya, Sri Lanka</p>	203
24.	<p>DETECTION AND CLASSIFICATION OF BRUISES IN "RED DELICIOUS" APPLE FRUITS BY APPLYING PIEZOELECTRIC TRANSDUCERS / تشخیص و طبقه‌بندی کوفتگی سیب "رد دلشیز" با استفاده از ترانس‌دیوسرهای پیزوالکتریک</p> <p>Ph.D. Stud. Mehrdad Foj Laley¹⁾, Assoc. Prof. Parviz Ahmadi Moghadam¹⁾, As Prof. Ali Hasanpour¹⁾, As prof. Vahid Rostampour¹⁾</p> <p>¹⁾ Department of Mechanical Engineering of Biosystems, Urmia University, Urmia / Iran</p>	211

EXPERIMENTAL RESEARCH ON THE MOVEMENT STABILITY OF A PLOUGHING AGGREGATE, COMPOSED ACCORDING TO THE “PUSH-PULL” SCHEME

PĒC «PUSH-PULL» SHĒMAS KOMPLEKTĒTA ARŠANAS AGREGĀTA KUSTĪBAS STABILITĀTES EKSPERIMENTĀLS PĒTĪJUMS

PhD. Ivanovs S.¹⁾, Prof.PhD. Bulgakov V.²⁾, Prof.PhD. Adamchuk V.³⁾,
Prof.PhD. Kyurchev V.⁴⁾, Prof.PhD. Kuvachov V.⁴⁾

¹⁾Latvia University of Agriculture / Latvia;

²⁾National University of Life and Environmental Sciences of Ukraine / Ukraine;

³⁾National Scientific Centre “Institute for Agricultural Engineering and Electrification” / Ukraine;

⁴⁾Tavria State Agrotechnological University / Ukraine

Tel: +37129403708; E-mail: semjons@apollo.lv

Keywords: *ploughing aggregate, «push-pull», movement stability, experimental researches.*

ABSTRACT

The conducted researches on a ploughing aggregate, composed according to the "push-pull" scheme as part of the HTZ-16131 tractor with a frontal two-bottom plough and a rear-mounted four-bottom plough, show that there is a positive correlation between the input impact – the turning angle of the driven wheels of the tractor, and the output parameter – its relative bearing. The maximum value of the mutual correlation function between these parameters is quite high, reaching mark 0.88. The researched ploughing aggregate, operating according to the "push-pull" scheme, has satisfactory path indicators. The path variations of the furrow laid by this aggregate are of a low-frequency nature. Arrangement of the supporting wheel of the frontal plough outside the furrow and its movement across an undeveloped agrophone does not lead to the deterioration in the steering ability of the explored ploughing aggregate.

ABSTRAKTS

Pēc «push-pull» shēmas komplektētu aršanas agregātu: traktora HTZ-16131 ar pakaļējās uzkares četru korpusu un ar frontālo divu korpusu arklu pētījumi liecina, ka starp ieejas parametru – traktora vadriteņu pagrieziena leņķi un izejas parametru – agregāta kursa leņķi pastāv pozitīva korelācijas sakarība. Savstarpējās korelācijas funkcijas maksimālā vērtība starp šiem parametriem ir pietiekami augsta un sasniedz atzīmi 0.88. Pētāmajam, pēc «push-pull» shēmas komplektētajam aršanas agregātam ir apmierinoši trajektorijas parametri. Ar šo agregātu veidotās vagas trajektorijas svārstībām ir zema frekvence. Frontālā arkla atbalsta riteņa novietojums vagā vai uz neapstrādāta agroфона nesamazina pētāmā aršanas agregāta vadāmību.

INTRODUCTION

Despite the high energy intensity, arable farming still occupies an important place in the soil tillage system (Barwicki et al., 2014; Meca and Cârdei, 2012). Under the conditions of many soil and climatic zones it is impossible to replace completely ploughing with other ways of soil treatment, such as boardless and shallow ploughing. Therefore, constant search is going on for improved machines and operating tools for ploughing, there is continued improvement of the aggregation schemes, and so on (Rucins and Vilde, 2005; Nadykto et al., 2017).

For instance, already now there is a widespread scheme in the world of a ploughing aggregate, composed of a tractor, a frontal and a rear-mounted plough, conventionally called "push-pull" (Bulgakov et al., 2008; Nadykto et al., 2016). But practical experience of their use has shown that, in case the frontal ploughing tool is not properly attached, there may arise not loading but, conversely, unloading of the frontal driven wheels of the tractor with inevitable loss of stability and steering ability of the entire ploughing aggregate (Bulgakov et al., 2017; Nadykto et al., 2017). Hence it follows that the presence of a frontal plough may significantly worsen the stability of the movement of the ploughing aggregate, composed according to the "push-pull" scheme.

According to the scientific hypothesis, developed by us, it was assumed that increase in the adhesive force of the aggregating tractor due to the use of a frontal plough can ensure increased operating width of

the ploughing aggregate, composed according to the "push-pull" scheme, at least by the width of one plough body in contrast to the aggregates with only one rear-mounted implement. Increase in the adhesive force of the aggregating tractor should, in its turn, lead to increase in the stability of the operating movement, reduced skidding of its propulsors and the specific fuel consumption by the ploughing aggregate, composed according to the "push-pull" scheme (Macmillan, 2002).

When choosing a scheme for aggregating a frontal implement, there is a variant prevailing among the scientists about a pivotal attachment of the implement to the tractor (Dontsov, 2008). They explain the choice of such a constructive solution by the fact that the ploughing implement, when encountering a mechanical obstacle, may deviate aside and avoid being damaged. Besides, it is claimed that, in order to ensure stable movement of the frontally mounted implement, the instantaneous turning centre of the frontally mounted tractor linkage must be in front of the suspension axis.

Certain attention should be paid to the postulate that, in order to increase the stability of the movement of the frontal pivotally attached implement, its operating elements must be arranged in the form of a wedge (Dontsov, 1989).

Some scientists argue that the stability of the movement of the tools operating in the pushing mode can be ensured by introducing flexible elements into the structure of the frontally mounted mechanism of the aggregating tractor (Ploschadnov et al., 2005).

Therefore, to ensure efficient application of the ploughing machine-and-tractor aggregates in agriculture, which are composed according to the "push-pull" scheme, it is expedient to study more deeply the stability issues of their movement.

The aim of this study is to increase the stability of the movement in a horizontal plane of a ploughing aggregate, assembled according to the "push-pull" scheme on the basis of data obtained during the field experimental data.

MATERIALS AND METHODS

The experimental studies were carried out on the basis of modern methods of conducting field experimental studies using strain gauge equipment and a measuring complex based on the analogue-to-digital converter. Processing of the obtained data on a PC was carried out by statistical methods applying a correlation-spectral analysis.

As a research object was chosen a ploughing machine-and-tractor aggregate on the basis of the tractor HTZ-16131 (Fig. 1). The technological part of the machine-and-tractor aggregate included a test sample of a two-bottom frontal plough (Fig. 2) and a rear-mounted tensometric plough (Fig. 3) with a 35 cm operating width of each body.



Fig. 1 - Tractor HTZ-16131 in the aggregate with a frontal (two-bottom) plough and a rear-mounted (four-bottom) strain-gauge plough (the "push-pull" scheme)

In the theoretical studies conducted by us it was established that, in order to avoid insufficient loading and, on the contrary, unloading of the front wheels of the aggregating tractor with a rated tractive effort of 30...32 kN, the frontal plough should have two bodies, and the rear plough should have 4 bodies (the "2 + 4" scheme) (Nadykto et al., 2017). Thus an experimental ploughing machine-and-tractor aggregate was composed, working according.



Fig. 2 - A frontal double-bottom plough



Fig. 3 - A rear-mounted tensometric plough

In the theoretical studies conducted by us it was established that, in order to avoid insufficient loading and, on the contrary, unloading of the front wheels of the aggregating tractor with a rated tractive effort of 30...32 kN, the frontal plough should have two bodies, and the rear plough should have 4 bodies (the "2 + 4" scheme) (Nadykto *et al.*, 2017). Thus an experimental ploughing machine-and-tractor aggregate was composed, working according to the "2 + 4" scheme and equipped with a frontal two-bottom plough and a rear-mounted four-bottom plough.

The first pass of the aggregate across the selected section of the field during the field experimental studies was carried out using a stable reference point, which ensured rectilinearity. Then the aggregate, composed according to the "push-pull" scheme, moved across a control section, 250 m long, in the forward and reverse directions.

The movement of the aggregating tractor HTZ-16131 within the above-described ploughing aggregate took place by means of the right-side wheels in the furrow, and with the left-side ones running across the undeveloped agrophone. It was assumed that the nature of the vertical oscillations of the left and the right sideboards of the aggregating tractor is practically the same.

Taking into account the design features of the researched ploughing aggregate, a set of measuring and recording equipment was developed using an analogue-to-digital converter that ensured unbiased assessment of the parameters to be studied.

To record the relative bearing of the tractor working within the ploughing machine-and-tractor aggregate, composed according to the "push-pull" scheme, a gyroscopic semi-compass GPK-52 was used, which was located in the zone of the longitudinal coordinate of the centre of mass of tractor HTZ-16131 (Fig. 4). The alternating current of voltage 36 V and a frequency of 400 Hz, necessary for the GPK-52 operation, were produced by a special PT-70 converter (Fig. 5).

The deviation of the path of the furrow from the straight line was measured by a metric ruler. The base straight line was staked out with a length of 250 m. The measurements were carried out in steps of 1 m. The frontal and the rear-mounted ploughs of the ploughing aggregate to be researched were adjusted to a depth of 25 cm. The aggregate moved on the control section with a forward velocity, which was determined by means of a track-measuring wheel and was fixed on the PC within the velocity range of 1.4...2.2 m·s⁻¹ allowed from agrotechnical standpoint.

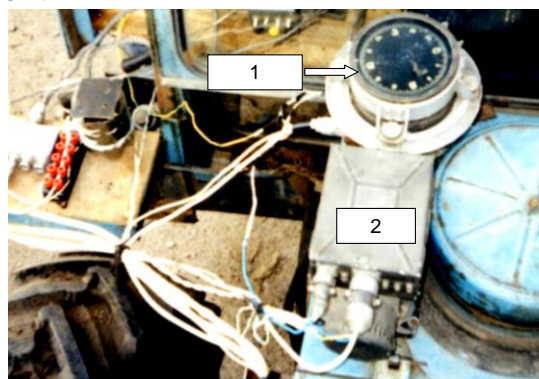


Fig. 4 - Installation of the gyroscopic semi-compass GPK-52 (1) and the current transducer PT-70 (2) on tractor HTZ-16131

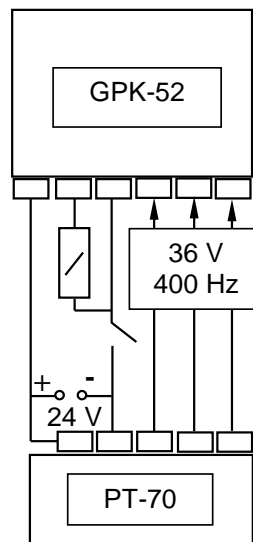


Fig. 5 - The connection diagram of the gyroscopic semi-compass GPK-52 with the PT-70 current transducer

Experimental researches of this ploughing aggregate were carried out on an agrophone (disked sunflower stubble), the average moisture content of which in the 0...30 cm layer was 13.8%. The soil density was within the range of 1.26...1.29 g·cm⁻³. Weediness of the field did not exceed 95 g·m⁻².

RESULTS

It has been established during the conducted research that the variation in the relative bearing (φ) of the tractor was insignificant, the dispersion of the process was 0.96 deg². Analysis of the normalised spectral density of this process showed that the frequency range of its course is 0...3 s⁻¹ (Fig. 6).

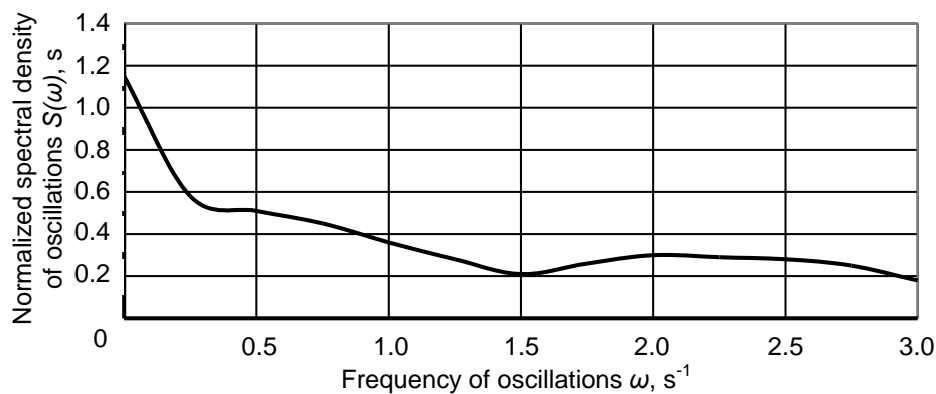


Fig. 6 - Normalised spectral density of variations of the relative bearing of the aggregating tractor HTZ-16131

Having determined the mean square deviation and the normalised spectral density of variations of relative bearing φ , we found the required experimental amplitude-frequency characteristic of the experimental ploughing aggregate (Fig. 7).

The nature of the experimental amplitude-frequency characteristic of the experimental ploughing aggregate shows (Fig. 7) that tractor HTZ 16131, together with the frontal plough, responds most noticeably to disturbances the frequency of which occurs within the range of 1...2 s⁻¹. In general, the process of changing the experimental amplitude of the frequency-frequency characteristic of the ploughing aggregate is close to the theoretical one (Bulgakov et al., 2016). The actual discrepancy between these comparable characteristics is not more than 8%.

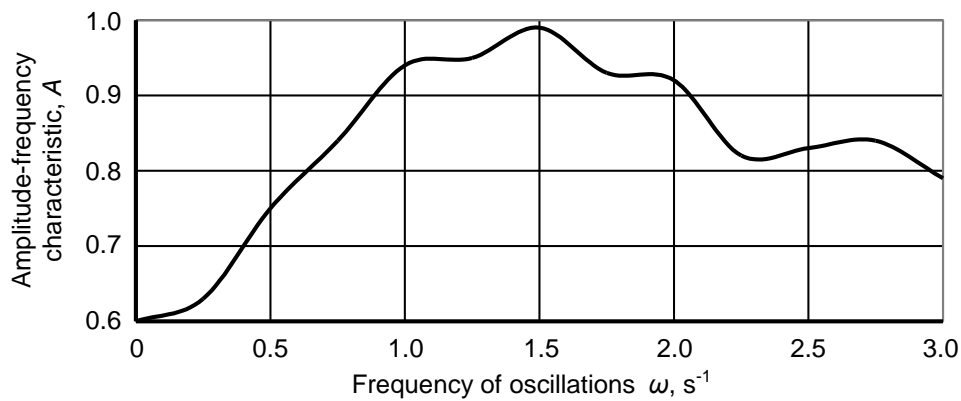


Fig. 7 - An experimental amplitude-frequency characteristic of the researched ploughing machine-and-tractor aggregate

By the conducted research it was established that the ploughing aggregate, composed according to the "push-pull" scheme of tractor HTZ-16131 with a frontal two-bottom and a rear-mounted four-bottom plough, has satisfactory path indicators. The basis for such a conclusion is the nature of variations of the furrow path, laid by this aggregate. In reality, they are of a sufficiently low frequency (Fig. 8).

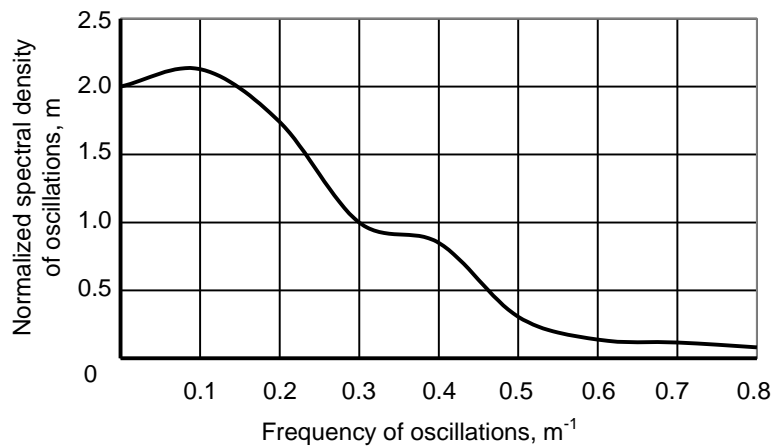


Fig. 8 - Normalised spectral density of the furrow path variations laid by the aggregate operating according to the "push-pull" scheme

The main dispersion spectrum, the value of which is 69.16 cm^2 , is concentrated in the frequency range $0 \dots 0.50 \text{ m}^{-1}$. At a velocity of the aggregate movement $2 \text{ m} \cdot \text{s}^{-1}$, it is $0 \dots 1.0 \text{ s}^{-1}$ or only $0 \dots 0.16 \text{ Hz}$. The length of the correlation link of the furrow path variations of the ploughing aggregate is at least 11 m.

Such a result is satisfactory since the cut-off frequency of the spectral density of the furrow path variations is 0.50 m^{-1} , which is only twice as large as the frequency that represents the acceptable non-rectilinearity of the row crops (Nadykto et al., 2009).

Since the tractor HTZ-16131 with aggregated ploughs moves with its right-side wheels along the furrow, the statistical characteristics of the turning angle of its driven wheels (parameter α) do not differ significantly from the similar dispersion characteristics, or from the normalised correlation function and spectral density, representing variations of the furrow path.

However, as relates to the relative bearing of the aggregating tractor (parameter φ), the statistical characteristics are basically different. Due to the lateral drift angles of the tires of the running wheels of the aggregating tractor, the energy (it is the same dispersion) and the internal structure of the variations of its relative bearing are a little different. In a numerical expression, the dispersion of the variations of parameter φ was 2.96 deg. , and parameter $\alpha - 2.10 \text{ deg.}$

The statistical processing on the PC was performed by 250 ordinates of the parameters α and φ . For such arrays of initial data, the tabular value F of Fisher's ratio test at the statistical significance level of 0.05 turned out to be equal to 1.39 (Dospechov, 2012; Gerber and Green, 2012).

Because the actual value F of Fisher's ratio test (equal to 1.41) is greater than the tabular (equal, 1.39), the null hypothesis about the equality of the estimated variances is not rejected. With a probability of 95%, it can be claimed that the variation dispersion of the relative bearing of the tractor is by no means greater than a similar indicator for the relative bearing of its driven wheels.

Perhaps because of this the variations spectrum of parameter φ is wider in comparison with angle α . Thus, if the cut-off frequency for the spectral density of the variations of the driven wheel turning angle is 0.3 s^{-1} , then for the relative bearing it is approximately 0.42 s^{-1} (Fig. 9).

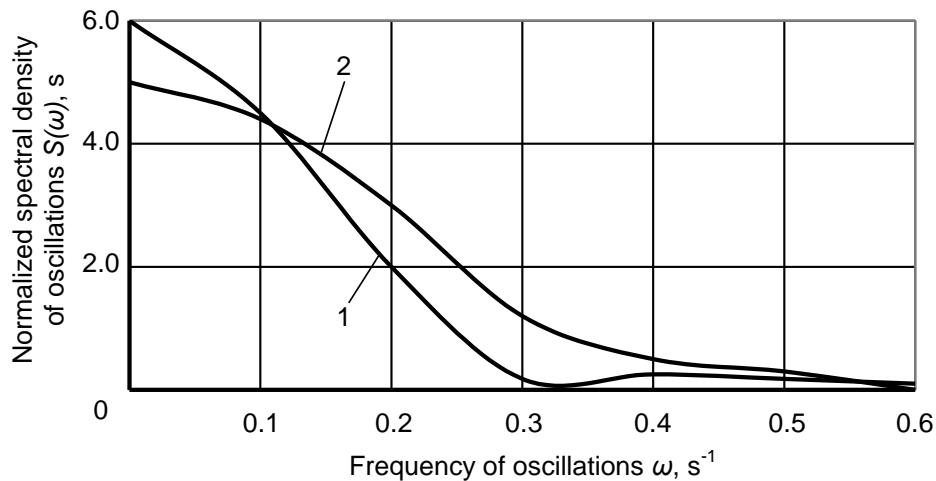


Fig. 9 - Normalised spectral densities of variations of the driven wheels turning angle of the tractor HTZ-16131 (1) and its relative bearing (2)

Despite the difference in the nature of variations of parameters α and φ , there is a close correlation between them. It is unambiguously represented by the normalised correlation function. Analysis of its behaviour shows (Fig. 10) that there is a positive correlation between the input impact – the turning angle of the driven wheels of the tractor, and the output parameter – its relative bearing. The maximum value of the mutual correlation function is quite high, reaching mark 0.88.

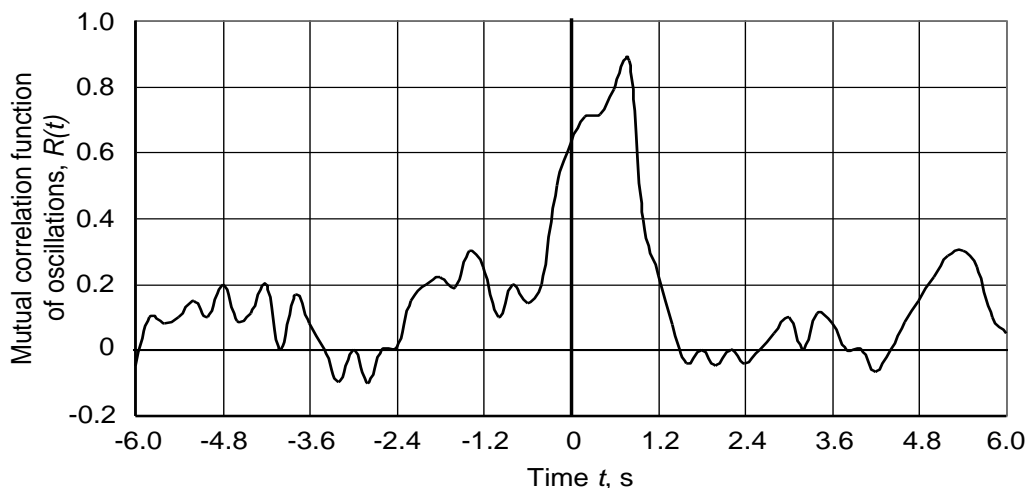


Fig. 10 - Mutual correlation function of variations in the relative bearing of the tractor HTZ-16131 by the turning angle of its driven wheels

The shift of the maximum value of the mutual correlation function to the right indicates that the relative bearing of the aggregating tractor is the turning function of its driven wheels, and not vice versa. If this maximum were in the second quadrant, value α would be considered as a reaction of the operator-driver to such a disturbance as an unwanted turn of the tractor body to one or the other side.

The shift of the maximum value of the mutual correlation function to the right of the vertical axis by 0.8 s indicates that it takes place precisely at the time when the change in the relative bearing of the tractor for the control action – the turning angle of its driven wheels – is delayed.

On the basis of what was laid out above, you can conclude the main thing. In the proposed variant of the ploughing machine-and-tractor aggregate, composed according to the "push-pull" scheme, the supporting wheel of the frontal plough is running outside the furrow. On the field it is moving across an undeveloped agrophone. This is in contrast to the world-wide variants of ploughing aggregates operating according to the "push-pull" scheme, which provide for the movement of the supporting wheel of the frontal implement in the furrow thus as if providing satisfactory control and stability of the movement of such an aggregate. But, on the basis on the analysis of the above-mentioned mutual correlation function (Fig. 10), it can be claimed that this decision does not lead to deterioration in the control of the movement of the researched ploughing aggregate assembled according the "push-pull" scheme.

The conducted research allows substantiating practical recommendations on the choice of a scheme and parameters of the ploughing aggregate, composed according to the "push-pull" scheme on the basis of the tractor HTZ-16131, from the position of satisfactory stability of its movement. So, the scheme of placing the tractor in the structure of ploughing aggregate is direct. When working in an aggregate with frontal and rear-mounted ploughs, the tractor HTZ-16131 should move with the right-side wheels running in the furrow. The air pressure in the tires should be as follows: the frontal wheels (with the tractor running straight) - 0.125 MPa, the rear wheels – 0.170 MPa. Any mobility of the frontal plough in a horizontal plane relative to the tractor is undesirable. During the operation the supporting wheel of the frontal plough moves outside the furrow. Although its removal from the connecting triangle of the frontal plough reduces the vertical load on the frontal wheels of the tractor, the change of this indicator is significant. Proceeding from this, when choosing the location of the wheel mentioned, it is necessary to carry out constructive limitations.

CONCLUSIONS

1. The ploughing aggregate, composed according to the "push-pull" scheme as part of the HTZ-16131 tractor with a frontal two-bottom and a rear-mounted four-bottom plough, has satisfactory path indicators. The variations of the furrow path laid by this aggregate are of a low-frequency nature. The basic dispersion spectrum, the value of which is 69.16 cm², is concentrated within the frequency range 0...0.50 m⁻¹. At the velocity of the ploughing aggregate 2.0 m·s⁻¹, it is 0...1.0 s⁻¹ or only 0...0.16 Hz.

2. There is a positive correlation between the input impact – the turning angle of the driven wheels of the tractor HTZ-16131, and the output parameter – its relative bearing. The maximum value of the mutual correlation function between these parameters is quite high, reaching mark 0.88. The shift of the maximum value of the mutual correlation function to the right by 0.8 s indicates that the relative bearing of the tractor is the turning function of its driven wheels, but the reaction of the tractor to the control impact lags precisely by the same time.

3. Arrangement of the supporting wheel of the frontal plough outside the furrow and its movement across an undeveloped agrophone does not lead to deterioration in the steering ability and stability of the movement of the researched ploughing aggregate, composed according to the "push-pull" scheme.

REFERENCES

- [1] Barwicki J., Gach St., Ivanovs S., (2012), Proper utilization of soil structure for crops today and conservation for future generations. *Proceedings of 11th International Scientific Conference "Engineering for Rural Development"*, Volume 11, pp.10-15, Jelgava/Latvia;
- [2] Bulgakov V., Kravchuk V., Nadykto V., (2008), Aggregation of ploughs (Агрегатирование плугов). *Р.Н. Agrarian Science*, 152 p., Kyiv/Ukraine;
- [3] Bulgakov V., Adamchuk V., Nadykto V., Kistechok O., Olt J., (2017), Theoretical research into the stability of motion of the ploughing tractor-implement unit operating on the 'push-pull' principle // *Agronomy Research*, 15(4), 1517-1529, Tartu/Estonia;
- [4] Dontsov I., (1989), Influence of the linkage parameters on stability of rectilinear uncontrolled motion of a frontal implement (Влияние параметров навески на устойчивость прямолинейного неуправляемого движения фронтального орудия) / *Collection of scientific works VISKHOM (Сборник научных трудов ВИСХОМ)*, 119 p., Moscow/Russia;
- [5] Dontsov I., (2008), Stability of the MTA movement with frontal and rear-mounted implements (Устойчивость движения МТА с орудиями фронтальной и задней навески), *Tractors and agricultural machinery (Тракторы и сельскохозяйственные машины)*, No.9, pp.27-29, Moscow/Russia;

- [6] Dospechov B., (2012), Methodology of a field experiment (Методика полевого опыта (с основами статистической обработки результатов исследований). *Agropromizdat*, 352 p. Moscow / Russia
- [7] Gerber A., Green D., (2012), *Field Experiments: Design, Analysis and Interpretation*, 480 p., Yale/USA;
- [8] Meca V. A., Cârdei P., (2012), Studies and researches for the unification of resistance expression of machines designed to soil tillage with applications in optimization of their working regime, *INMATEH - Agricultural Engineering*, vol. 36, No. 1/2012, Bucharest / Romania;
- [9] Nadykto V., Nazarova O., Chernaya T., (2009), The frequency-dispersion indicator of non-rectilinearity of the row crops rows (Частотно-дисперсионный показатель непрямолинейности рядков пропашных культур) / *Tractors and agricultural machinery (Тракторы и сельскохозяйственные машины)*, No.8. p. 12-14, Moscow/Russia;
- [10] Nadykto V., Kyurchev V., Beloev H., Kistechok A., (2017), Study of push-pull plough combination / *Journal of Agriculture and Environment*, Volume 1, No 1, pp. 4-9;
- [11] Nadykto V., Ivanovs S., Kistechok OI., (2016), Research on the draft-and-power and agrotechnical indicators of the work of a ploughing aggregate, created according to the scheme "push-pull" / *Journal of Research and Applications in Agricultural Engineering* Nr. 62(1), pp. 136.-139, Poznan/Poland;
- [12] Macmillan, R.H. (2012). *The Mechanics of Tractor Implement Performance. Theory and Worked Examples*. University of Melbourne, 165 p. Melbourne/Australia;
- [13] Ploschadnov A., Kursov I., Marshalov E., (2005), Increasing the stability of the movement of machine-and-tractor aggregates (Повышение устойчивости движения машинно-тракторных агрегатов). *Collection of scientific works of Tula State University (Известия Тульского государственного университета)*, pp.171-176, Tula/Russia;
- [14] Rucins A., Vilde A., (2005), Modelling forces acting on the plough body. *Simulation in Wider Europe - 19th European Conference on Modelling and Simulation, ECMS 2005*, pp. 425-430, Riga/Latvia.

RESEARCH ON THE VIBRATION OF MINI TILLER

微耕机的振动研究

Ph.D. Eng. Liang X.C. ^{*)}, Prof. Ph.D. Chen J., Ms. Stud. Eng. Wang Z.

Southwest University, College of Engineering and Technology, Chongqing Key Laboratory
of Agricultural Equipment for Hilly and Mountainous Regions / P. R. China

Tel: 86-023-68251265; E-mail: dylb1978@swu.edu.cn

Keywords: mini tiller, vibration, hilly and mountainous regions, experiment, analysis

ABSTRACT

The mini tiller is a type of agricultural equipment used for hilly and mountainous regions. The intense vibration it produces causes harm to the manipulator's body. Hence, it is imperative to analyse reported studies on the mini tiller, especially addressing the limitations of this machine. The mini tiller, brand 1z-105, was selected to be used as a prototype in several experiments using three different conditions. The data was analyzed in the time and frequency domains and the effects on the human body were explored. Finally, suggestion was made regarding the handling comfort of the mini tiller if it is articulated.

摘要

微耕机是丘陵山区重要的农业装备，然而其强烈的振动对操作者身体带来巨大的伤害。基于此，首先简要分析了微耕机的研究现状，尤其是使用中存在的问题。再以 1z-105 微耕机为研究对象，完成了其在三种工况下的振动实验。通过对微耕机的振动信号进行了时域和频域分析，探讨了微耕机作业时对人体的影响。最后基于结果分析，给出了未来微耕机提高操作舒适性的建议，为微耕机的性能改进提供理论依据。

INTRODUCTION

China is a country with complex land formation. The statistics indicate that over 60% of the area is comprised of hilly and mountainous regions, and more than 40% of agricultural acreage is located in this terrain. It is difficult to implement modernization and mechanization for agriculture in hilly regions, resulting in the limitation of using large agricultural equipment. The mini tiller is driven by a gasoline or diesel internal combustion engine of 2~7.5 kW, weighs 50~150 kg, and has a tilling depth of 10~16 cm. Due to the advantages, such as being multifunctional, small in size and light weight, it is popular.

Although such characteristics are advantageous in hilly or mountainous terrain, the mini tiller has significant disadvantages, including severe vibration which cannot be endured. Studies suggest that the intense vibration can cause moving disorders, damage to various body organs including the ear, spine and gastrointestinal disorders, and neurological disease (Ahmadian H., et al., 2012; Li, et al., 2016). Another disadvantage is operator fatigue caused by the operator walking behind the machine during tilling for 15~20 km (Mehta C. R., et al., 1997). In Italy, 13% of injuries from all accidents are related to the use of power tillers (Fabbri A., et al., 2017). With increasing urbanization, the older generation will be the operators of such equipment, and severe injuries, even death, are reported frequently. The handling comfort of mini tillers needs to be improved.

The biggest shortcoming of the mini tiller is the production of strong vibrations by the engine, rotary blade and uneven soil tilling. In addition, it is hard to find elastic components in the mini tiller resulting in the vibration amplitude to be difficult to buffer. During the tilling process, tires are replaced by the rotary blade, and almost all modules are assembled on a rigid rack. The harsh operating environment and the design faults, which are a result of lowering the cost, make the performance unacceptable for operators. Vibration is a complicated movement for the human body to react to, and some factors including vibration magnitude, frequency, duration time, input position, etc., are especially significant to the effects. It appears that some environmental elements, including light, heat and noise, are also relative to the effects of vibration (British Standards 6481, 1987, ISO 2631/1, 1985). There are multiple studies reported in the literature on the effects of vibration. The disease White Hand syndrome can be caused by vibration, and the mechanism of

the illness has been reported (Ragni L., et al., 1999). In order to determine optimal properties of the mini tiller, the vibrational mechanism of the tiller is analyzed and some measures for reducing vibration have been introduced (Yang J., et al., 2005). The Finite Element Method (FEM) is an effective low cost method used to achieve an optimized structure of agriculture machinery (Xu F., et al., 2008). The steering system must also be flexible in agricultural equipment (Nafchi A. M., et al., 2011). The majority of the vibration is from the engine and the vibration effect of different fuels must be considered (Heidary B., et al., 2013). Studies on the transmission of vibrations from the blade to the body are not easy to analyse. Therefore, it is crucial to establish a vibration model and reduce the vibration experienced by the operator (Fabbri A., et al., 2017). Parts of the vibration is generated during the tilling process and the geometry of blade and the scoop angle characteristics of a handheld tiller's rotary blade has been explored (Zhang Y. H., et al., 2016). Vibrational testing and a response analysis of the power tiller are essential (Xu H. B., et al., 2016).

The structure of mini tillers requires the structural optimization of the handlebars using vibration modal analysis (Niu P., et al., 2017). In reference [15], pre-stress means are used to analyse the vibration of the mini tiller, and the consistency between theoretical outcome and test data has been achieved (Wang Z., et al., 2018).

Improving the handling comfort of the mini tiller is filled with challenges, due to several factors contributing to the performance, such as rotation speed of the engine, the geometry of rotary blade, the soil type, the depth and width of tilling (Vaghela, et al., 2013, Fajardo A. L., et al., 2014, Matin M.A., et al., 2015). High value-added agriculture needs more advanced equipment with low pollution and satisfactory performance, especially in facility agriculture such as in the greenhouse. Therefore, tests for this study were finished in the two soils of the greenhouse.

MATERIALS AND METHODS

Compared to field experiments, the theoretical analysis of the mini tiller is easy and cost effective to conduct. However, not all the characteristics can be described precisely. For example, the soil model is hard to build, and some details of soil structure must be omitted to simplify the model.

The experimental location was situated at 29.81° N latitude and 106.42 ° E longitude, and field tests were completed on April 5, 2017. The mini tiller had worked for two years and its technique condition was good. The air temperature in the greenhouse was 21.5°C and the soil texture was a sandy loam. The parameters of mini tiller are listed in Table 1.

Table 1

Specification of the mini tiller

Mini tiller item	Parameter
Engine type	Four stroke direct injection
Related power	4.41 kW
Related rotation speed	3600 min/r
Cylinder number	1
Tilling depth	10-12 cm
Tilling width	75 cm
Transmission	2 forward and 1 reverse
Cooling system	Air cooling
Blade	Machete

The experimental scenario of mini tiller is recorded in Figure 1. The three-dimensional acceleration sensor was 356A16, which was produced by the PCB Company in the US. The frequency scope was 0.3~6 kHz, and measured range was -50~50 g. In addition, the sensitivity of the instrument in x-, y- and z- coordinate directions was 98.2, 101.0 and 98.5 mv/g, respectively. The acquisition card was NI 9234, which was made in NI Company in the US, the input voltage was -5~5 V and the rate of digital signal was 51.2 kHz. The vibration was transmitted from the rotary blade and engine to the body through the handlebar of the mini tiller, so the acceleration sensor was attached to the end of bar using the 502 glue. The coordinate directions of sensor and the whole measuring system are shown in Figure 1.

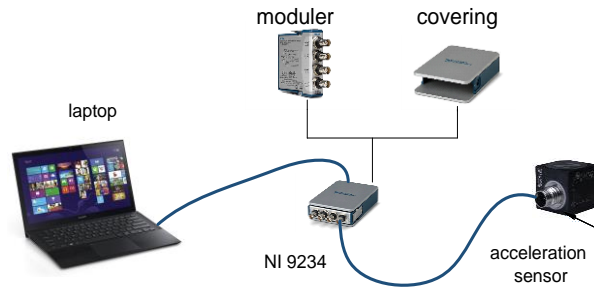


Fig. 1 - Sensor in the mini tiller and connection relation for different components

An experiment was undertaken in a greenhouse, as described below. Firstly, the acceleration sensor was situated outside of the handlebar, and uses a data cable to link the sensor, the acquisition card and USB port of the laptop. Secondly, vibration signals from the mini tiller with no load were collected using LabVIEW program when the tiller was operated. Thirdly, vibration signals were gathered while the tiller was running with a full load. During the process, the throttle was fixed in the open position and the gear ratio was unchanged. The experiments were repeated on two different grounds. Soil 1, had a moisture content of 13.5%, and average firmness of 0.41-0.63. The corresponding parameters in soil 2 were 9.4% and 0.58-0.75, respectively. The principle of vibration signal disposing is described in Figure 2.

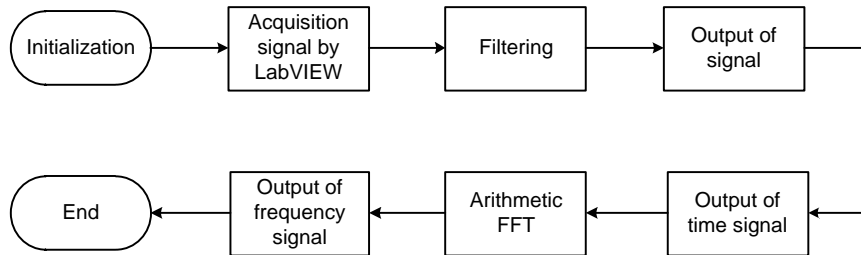


Fig. 2 - The principle of vibration signal disposing

RESULTS

Results under different conditions are recorded and shown in Figure 3. The mini tiller working without a load and the acceleration signal is shown in Figure 3a.

The mini tiller working under full load on soil that was less firm in texture is shown in Figure 3b.

In Figure 3c the experiment is repeated on a firmer textured soil.

The outcomes are expressed in a narrower frequency band in Figure 3d.

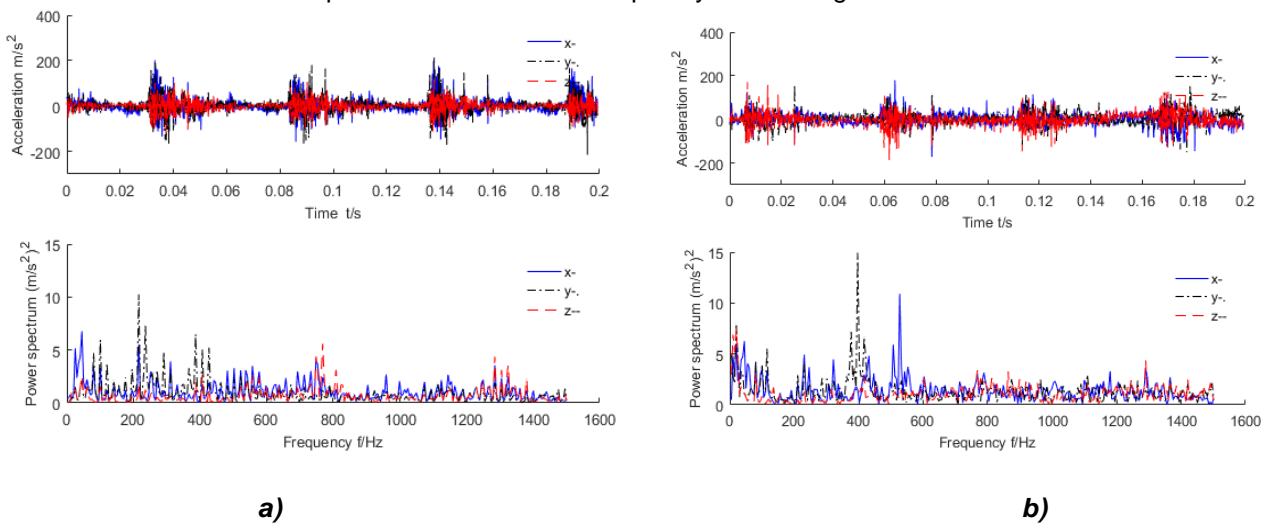


Fig. 3 - Acceleration signal of the mini tiller under different conditions

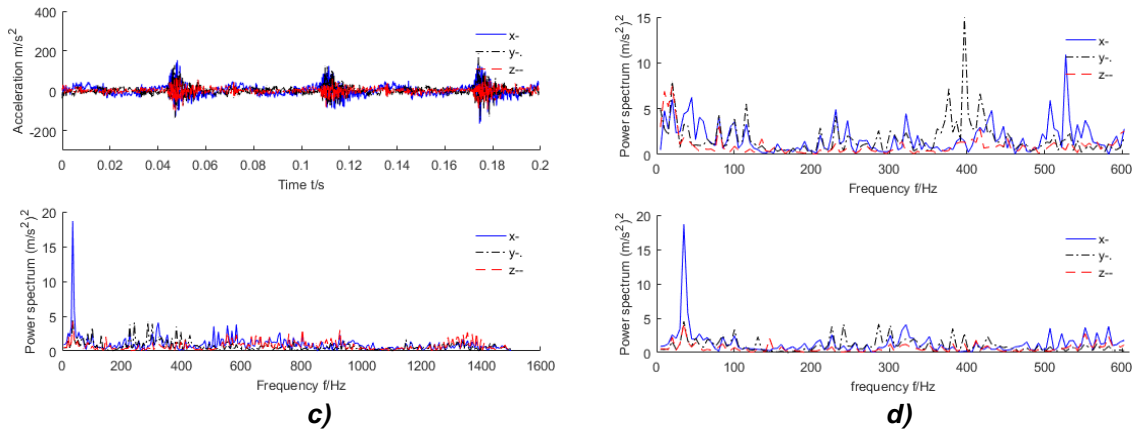


Fig. 3 - Acceleration signal of the mini tiller under different conditions

From Figure 3, it appears that the acceleration signal in the time domain occurs periodically. The primary reason for this could be the configuration of rotary blade which is symmetrical, reflected as the periodicity of curves. The variation in the curves could be attributed to the random firmness and moisture content of the soil. Furthermore, the variable power output of the engine is also reflected in the curves. While in the frequency domain, it is noted that the frequency spectrum is very distinct at the same frequency band. It is hard to find the same peak and trough in Figure 3, and individual signals do not represent characteristic vibrations during tilling. The application of statistics could be useful in describing the vibration process. The root mean square (RMS) value of weighted acceleration is used to analyse the vibration signal in the frequency domain, which can represent the vibrational energy, using the following equation:

$$a_{rms} = \sqrt{\left(\sum_{i=1}^n a_i^2\right) / n} \tag{1}$$

Where: a_i is the measured acceleration amplitude, [ms^{-2}];
 n - the number of acquisitions;
 a_{rms} -the vibration acceleration RMS value, [ms^{-2}].

Accordingly, the results can be seen in Figure 4.

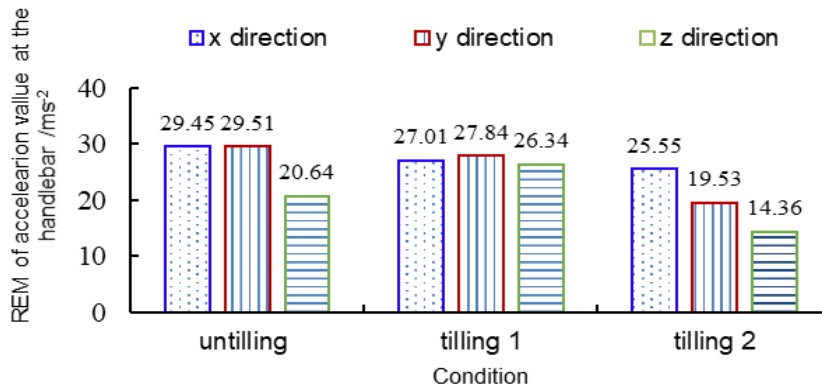


Fig. 4 - Vibration acceleration value in coordinate directions

In Figure 4, the acceleration at the end of the handlebar in the coordinate directions is different, which may be caused by the different stresses in each coordinate direction. The soil surface is uneven which result in the amount of tilling being varied, and the distribution of soil firmness is random. Therefore, the acceleration amplitude in each coordinate direction is unique. In no tilling mode acceleration in the x – coordinate direction it was 43% greater than that in the z – axis direction, while it was similar to the acceleration in the y – axis direction. Compared with tilling 1 and tilling 2 modes, the acceleration in x – coordinate direction was 9% and 15% greater, respectively. Correspondingly, the acceleration in y – coordinate direction was 6% and 51% greater, and acceleration in z – coordinate direction it was -22% and 10% greater, respectively. Overall, the acceleration in each axial direction was irregular, which was generated by the REM values of the different forces exerted.

In the moving mode, the peak of vibration frequencies were 45 Hz, 216 Hz and 768 Hz, and the corresponding amplitudes were 6.8 ms^{-2} , 10 ms^{-2} and 5.6 ms^{-2} , respectively. However, the distribution and amplitude of the frequency in tilling mode 1 were significantly different to the values in the moving mode. The vibration frequency peak in coordinate directions under tilling mode 2 coincided at 35 Hz, which is dissimilar to other modes. In contrast to the moving and tilling mode 1, the acceleration in the x – coordinate direction was 168% and 65% greater, while in the y – coordinate direction, the acceleration was 55% and 70% smaller, and in the z – coordinate direction it was 25% and 44% smaller. The human body is complicated in its reaction to vibration, resulting in different frequencies not being equally disruptive. Namely, different internal organs of the body can have different masses, damping and elasticity, so the resonance frequency within each is unique. For example, 4~8 Hz in the vertical direction and 1~2 Hz in the horizontal direction are more sensitive than other frequencies for most people. Hence, it is necessary to give the distribution of the frequency peaks (Table 2) and the vibration frequency of the mini tiller should be kept greater or smaller than the frequencies humans are sensitive to in order to ensure handling comfort.

Table 2

Human reactions to RMS weighted acceleration levels

Test	x-axis direction		y-axis direction		z-axis direction	
	Vibration frequency	Amplitude	Vibration frequency	Amplitude	Vibration frequency	Amplitude
	[Hz]	[ms^{-2}]	[Hz]	[ms^{-2}]	[Hz]	[ms^{-2}]
Moving	45	6.8	216	10	768	5.6
Tilling 1	527	11	397	15	20	7.5
Tilling 2	35	18.2	35	4.5	35	4.2

From the analysis above, it was noted that vibration frequency is diverse under different tilling conditions. Therefore, enhancing the handling comfort of the mini tiller is difficult. It is convenient to use the total acceleration value a_{rms} in any coordinate axis, because human reaction is a result of the whole vibration input in three coordinate directions. The equation 2 is used for calculating the total weighted acceleration value.

$$a_{sum} = \sqrt{1.4a_x^2 + 1.4a_y^2 + a_z^2} \quad (2)$$

Where:

a_x is the acceleration RMS value in x – coordinate axes, [ms^{-2}];

a_y -the acceleration RMS value in y – coordinate axes, [ms^{-2}];

a_z -the acceleration RMS value in z – coordinate axes, [ms^{-2}];

a_{sum} -the total weighted acceleration value, [ms^{-2}].

Using equation (2), the responding values were calculated as 51.8 ms^{-2} , 52.78 ms^{-2} and 38.41 ms^{-2} , respectively. It is accepted that the acceleration level can be used to evaluate the riding comfort of vehicles (Table 3). Comparing the tilling process results it is shown that the handling comfort of the mini tiller is unacceptable, and possibly the reason why operators of the mini tiller are frequently injured.

Table 3

Human reactions to RMS weighted acceleration levels

Weighted RMS acceleration [ms^{-2}]	Description of human reactions
<0.315	Not uncomfortable
0.315-0.630	A little uncomfortable
0.5-1.0	Fairly uncomfortable
0.8-1.6	Uncomfortable
1.25-2.50	Very uncomfortable
>2	Extremely uncomfortable

Compared with studies reported in the literature (Vaghela, et al., 2013, Bahareh H., et al., 2013, Li, et al., 2016), the RMS of test accelerations in this study were much greater. The distinction between different internal combustion engines was not obvious, so the most probable cause lies in the process of tilling itself, the key to enhance the handling comfort of the mini tiller. The stresses on the rotary blade of the mini tiller are shown in Figure 5.

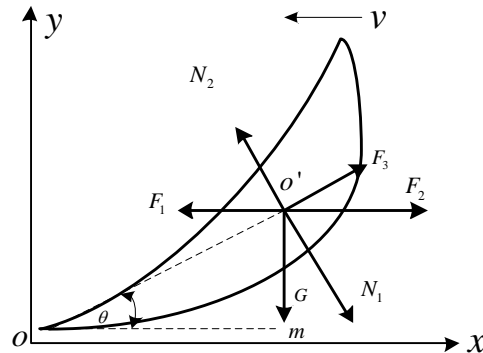


Fig. 5 - The stress analysis of rotary blade during tilling

The mechanism of the equilibrium of the blade can be described by equation 3 as :

$$\begin{cases} G + N_1 \cos \theta - N_2 \cos \theta + F_3 \sin \theta = 0 \\ F_1 - F_3 \cos \theta - F_2 - N_1 \sin \theta + N_2 \sin \theta = 0 \end{cases} \quad (3)$$

Where:

G is the gravity of blade, [ms^{-2}];

θ - the angle between the line Oo' and the line Om , [$^\circ$];

N_1 -the clod pressure above the blade, [N];

N_2 -the clod pressure below the blade, [N];

F_1 -the force of blade roller, [N];

F_2 -the acceleration resistance, [N];

F_3 -the frictional force between the blade and soil, [N].

Furthermore, several forces can be described in more specific forms, which is convenient for calculating results. For example, $F_2 = \delta m \frac{dv}{dt}$, and $F_3 = \mu(N_1 - N_2) + \mu AS$, where δm signifies acceleration mass, μ shows friction coefficient between the blade and soil texture, S expresses the area of adhesive water envelop, and A represents the absorbing load caused by water film. The parameters in equation (3) can be measured and the results recorded under different conditions. Using equation (3), it can be concluded that different tilling depth results in different clod pressures on each coordinate direction, and the mechanical equilibrium also changes. A couple of dynamic parameters, including power output of the engine, firmness of the soil texture, different tilling depths, and different acceleration forces, cause a continuous couple and act on the rack of the mini tiller, creating vibration. If the changes of parameters are large, intense vibration can be produced.

From Figure 5, the rotary blade cuts the soil into a small slice or clod and throws it to the shield in each bite. If the firmness of soil is greater, then a smaller load may be finished in each bite, assuming the power output of the engine is unchanged. Significant variation from the composite force of the blade is generated due to the change of soil firmness and rotating fluctuation of the engine. The situation is aggravated by the single cylinder of the engine which has a lopsided reciprocating and rotary torque. The significant differences in experimental outcomes are due to the firmness of soil, and the relation between the firmness and acceleration is shown in Figure 4.

There is a paradox in Figure 4. The firmness in the first soil texture is smaller than that in the second soil texture, while the acceleration of the handlebar is smaller in the two soils. In addition, the acceleration at the end of the handlebar in the moving mode is greater than that of the acceleration in the tilling mode. These results agree with that reported by Li, et al., 2016. During the process of tilling, more vibrational energy is absorbed by the soil than that transmitted to the handlebar. If the tilling depth is increased, the acceleration is reduced. It is not economical to decrease the acceleration by enlarging the tilling depth, as this will cause higher fuel consumption by the engine and disperse more soil. Whether heightening the tilling depth is feasible should be considered in another study.

CONCLUSIONS

The tilling process is complicated under changing conditions, with further studies, including theoretical analysis and field experiments, needed to understand it.

- The vibration frequency for the mini tiller is wide, and it is hard to keep the frequency within a range to result in satisfactory handling comfort under different terrain and working conditions. It is feasible to design an active system which matches diverse terrains.
- Test results show that the manipulator's body is hurt by the evident vibration during the mini tiller working. In the hilly and mountainous regions, how to transform vibration energy which is produced by the rotary blade and the single cylinder engine into other energy form is more urgent.
- The physical design of the mini tiller should be improved greatly. It is unreasonable to use a rigid structure for the mini tiller. In addition, some elastic components should be included into the assembly of the mini tiller to buffer the vibrational energy.

ACKNOWLEDGEMENTS

This paper was financially supported by the Fundamental Research Funds for the Central Universities (No. XDJK2016B025) and the Doctoral Fund of Southwest University (No.SWU115022).

REFERENCES

- [1] Ahmadian H., Hassan-Beygi R., Ghobadian B., (2012), Determination of a power tiller vibration acceleration envelope curves on transportation mode. *International conference on mechanical Engineering and advanced technology, ICMEAT*, pp.1-5;
- [2] Fabbri A., Cevoli C., Cantalupo G., (2017), A method for handlebars ballast calculation in order to reduce vibration transmissibility in walk behind tractors, *Journal of agricultural engineering*, XLVIII:599, pp. 81-87;
- [3] Fajardo A. L., Suministrado D.C., Peralta E. K., Bato P. M., Paningbatan Jr E. P., (2014), Force and puddling characteristics of the tilling wheel of float-assisted tillers at different lug angle and shaft speed, *Soil & Tillage Research*, 140, pp.118-125;
- [4] Heidary B., Hassan-beygi S. R., Ghobadian B., (2013), Investigating a power tiller vibration transmissibility using diesel-biodiesel fuel blends on stationary conditions, *Journal of mechanical Engineering and technology*, vol. 5, issue 1, pp. 19-31;
- [5] Li G., Chen J., Xie H. J., Wang S. M., (2016), Vibration test and analysis of mini tiller, *Int J Agric. & Biol. Eng.*, vol. 9, issue 3, pp. 97-103;
- [6] Nafchi A. M., Nafchi H. M., Demneh I. A., (2011), Improving steering system for walking tractor-trailer combination to increase operator's comfort and ease of control. *Agricultural Engineering International: CIGR Journal*, vol. 13, issue 3, pp. 1-8;
- [7] Matin M. A., Fielke J. M., Desbiolles J. M. A., (2015), Torque and energy characteristics for strip-tillage cultivation when cutting furrow using three designs of rotary blade. *Biosystems Engineering*, vol. 129, pp. 329-340;
- [8] Mehta C. R., Tiwari P. S., Varshney A.C., (1997), Ride vibration on a 7.5 kW rotary tiller, *J. agric. Engng Res.*, vol. 66, pp.169-176;
- [9] Niu P., Yang M. J., Chen J., Yang L., Xie S. Y., Chen X. B., (2017), Structural optimization of a handheld tiller handrail by vibration modal analysis, *INMATEH Agriculture Engineering*, vol. 52, issue 2, pp. 91-98;

- [10] Ragni L., (1999), Vibration and Noise of Small Implements for Soil Tillage. *Journal of Agriculture Engineer Research*, vol. 74, issue 4, pp. 403-409;
- [11] Vaghela J. G., Jain K. K., (2013), Vibration characteristics of mini-tractor (8.7kW) on tarmacadam, *Agri. Eng. Int: CIGR Journal*, vol. 15, issue 2, pp.1-6;
- [12] Xu F., Zhang L. B., Jiang J. D., Zhang X., (2008), Optimization method of agricultural machinery handle based on FEA and orthogonal experimental design. *Chinese Journal of Mechanical Engineering*, vol. 44, issue 10, pp. 245-249;
- [13] Xu H.B., Chen Y.J., Liu Y., Lu L., (2016), Vibration testing and response analysis of power tiller in non-operational state. *Journal of Chinese Agricultural Mechanization*, vol. 37, issue11, pp. 1-5;
- [14] Yang J, Meng X. W, (2005), Study on vibration mechanism and measures for vibration reducing to the handle of cultivator by virtual prototype technology. *Transactions of the Chinese Society for Agricultural Machinery*, vol. 36, issue 2, pp. 39-42;
- [15] Zhang Y. H., Yang L., Niu P., Li S. T., Xie S. Y., Chen X. B., Yang M. J., (2016), Study on the scoop angle characteristics of a handheld tiller's rotary blade, *INMATEH Agriculture Engineering*, vol. 49, issue 2, pp. 5-12.
- [16] Wang Z., Chen J., Wang S. M., Niu P., Hu C. J., Wang Y. L., Zheng Y. L., (2018), Simulation and experimental study on the vibration response of the pre-stressed mini tiller handle. *Journal of Agricultural Mechanization Research*, vol. 40, issue 4, pp. 195-199;
- [17] *** British Standards Institutions (BS) 6841 Measurement and evaluation of human exposure to whole-body mechanical vibration and repeated shock. London, 1987;
- [18] *** International Standards Organization (ISO) 2631 / 1 Evaluation of human exposure to whole-body vibration – Part 1: General Requirements, Geneva, 1985.

ANALYSIS OF THE WORKS PERFORMED BY PNEUMATIC AND MECHANICAL SEEDING DEVICE WITHOUT USING VACUUM**АНАЛІЗ РОБОТИ ПНЕВМОМЕХАНІЧНОГО ВИСІВНОГО АПАРАТА БЕЗ ВИКОРИСТАННЯ ВАКУУМУ**

Lect. Ph.D. Eng. Vasytkovska K.V., Lect. Ph.D. Eng. Vasytkovskyi O.M.,
Prof. Ph.D. Eng. Sviren M.O., Lect. Ph.D. Agric. Kulik G.A.
Central Ukrainian National Technical University / Ukraine
Tel: +380667103625; E-mail: vasytkovskakv@ukr.net

Keywords: *pneumatic and mechanical seeding device, cell, seed, dosage, angular velocity*

ABSTRACT

The construction of a new pneumatic and mechanical seeding device for precision seeding of tilled crops with peripheral location of cells on a seed disk and a passive device for removing unnecessary seeds in a centrifugal method is suggested. It is assumed that the seeding device works even without the creation of vacuum. The parameters of the seeding device have been determined analytically. It was proved that the proposed design of the pneumatic and mechanical seeding device provides qualitative dosage of seeds without creating vacuum in the system, but with a limited angular velocity of 11.25 rad/s.

To remove extra seeds in the pneumatic and mechanical seeding device we used pockets in the casing of the seeding device above the filling section in which, under the influence of inertia forces, excess seeds get in and are directed back to the filling section. In order not to remove the main seed along with the extra seed when the rotation velocity of the seed disk approaches the velocity of the seeding device, additional force should be applied that would keep the main seed in the cell, that is, the force of suction.

РЕЗЮМЕ

Запропоновано конструкцію нового пневмомеханічного висівного апарата для точного висіву насіння просяних культур з периферійним розташуванням комірок на висівному диску та пасивним пристроєм для видалення зайвого насіння відцентровим способом. Прийнято припущення, що висівний апарат працює навіть без створення вакууму. Аналітичним шляхом визначено параметри висівного апарата. Доведено, що запропонована конструкція пневмомеханічного висівного апарату дозволяє якісно дозувати насіння без створення вакууму в системі, але при обмеженій кутовій швидкості у 11,25 рад/с.

Для видалення зайвого насіння в пневмомеханічному висівному апараті запропоновано використання порожнини в корпусі висівного апарата над зоною заповнення, в яку під дією сил інерції потрапляє зайве насіння та спрямовуються назад до зони заповнення. Для не видалення разом із зайвою насінною основної насінни при наближенні колової швидкості обертання висівного диска до швидкості руху посівного агрегату, необхідно використати додаткову силу, яка утримала б основну насінину в комірці, тобто силу присмоктування.

INTRODUCTION

The formation of a single-seed stream is the main task for seeding devices of tilled crops. The effectiveness of their operation is assessed by the quality of seed flow formation. The quality is higher if the number of misfed seeds and "twin" seeds is lower. Both misfed and "twin" seeds negatively affect the yield of crops. In the first case the number of plants decreases and in the second case the problem is their mass, due to the ineffective distribution of feeding areas of the root system and the competition of the above-ground part for obtaining sunlight.

Many scientists (Boyko A. I., 2003; Sysolin P.V., 2004; Amosov V.V., 2007; Sydorчук O., 2014; Voytyuk, D. G., 2005), studied the problem of the formation of single-seed flow. As a result, the designs of high-performance pneumatic-mechanical seeding devices were created. They exceed technological parameters of the best reliable mechanical devices. However, the quality of the operation of pneumatic and

mechanical seeding devices considerably depends on providing the specified value of rarefaction in the vacuum system for each crop and maintaining its stability.

In real conditions, with the intervention of unmanaged random factors, this is a rather complicated problem which is confirmed by differences in the results of laboratory and field studies.

Therefore, the main task is to create the design of a pneumatic and mechanical seeding device which operates with the least impact of the pressure changes in the system.

Having analyzed the design features of seeding devices for tilled crops precision seeding (Boyko A. I., 2003; Sysolin P.V., 2004; Mursec B., 2007; Amosov V.V., 2007; Sysolin P.V., 2001), a perspective direction of its improvement was determined.

The design of a unique pneumatic and mechanical device (Petrenko M. M., 2011; Petrenko M. M., 2013) (Fig. 1) was developed at the Department of Agricultural Engineering of Central Ukrainian National Technical University. The seed disk 1 has cells 2 which are formed by sectoral cut-outs of the disk and blades 3. Externally, the cells are covered by the device casing 5.

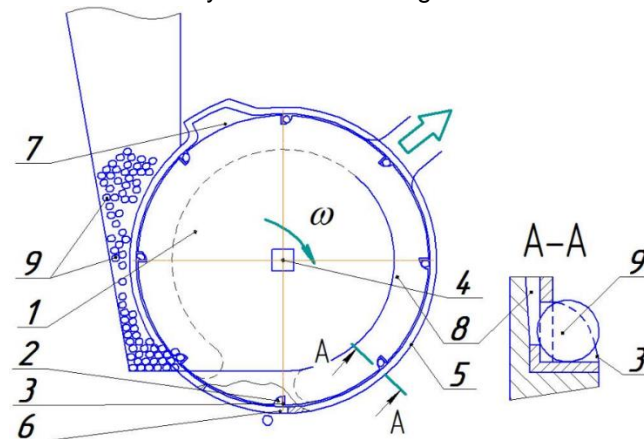


Fig. 1 - The model of the pneumatic and mechanical seeding device

1 – seed disk; 2 – cell; 3 – blade; 4 – driving shaft; 5 – casing; 6 – seeding outlet; 7 – inactive appliance for removing extra seeds; 8 – vacuum chamber; 9 – seeds.

The process of the seeding device operation is as follows. When the disk is rotating, the blades catch a seed and automatically place it in a cell. The vacuum created in the system keeps the seed from transverse tangential and radial displacement. In addition, the blades prevent the trapped particles to fall out in the tangential direction, and the casing prevents falling out in the radial direction. In this way, the particles move to the pocket 7 where the excess "twin" seeds are removed.

The suggested device has a significant advantage over the classical ones, since it ensures the forced seizure of the seeds with blades and the constructive elements to be kept in cells. Let us consider the operation of the device in the worst conditions with the absence of vacuum.

The analysis of the suggested design of the seeding device (Petrenko M. M., 2011; Petrenko M. M., 2013; Vasylykovska K.V., 2016) allows us asserting that seeds can be caught, removed and dropped even without the use of vacuum in the vacuum chamber.

MATERIALS AND METHODS

The objective of the research is to identify the performance of the suggested pneumatic and mechanical seeding device in the conditions of an unstable vacuum in the system, in particular, when it is absent.

Research tasks:

- creation of the physical model of the experimental pneumatic and mechanical seeding device;
- mathematization of the physical model if there is no vacuum;
- obtaining the correspondence which characterizes the performance of the seeding device if there is no vacuum;
- the analysis of the correspondence and development of scientific and methodological recommendations (Vasylykovska K. V., 2014).

Theoretical studies were carried out using the elements of theoretical mechanics, differential and integral calculus and mathematical modelling. The research results were processed by the "MathCAD 14" program.

RESULTS

Let us consider the operation of the suggested pneumatic and mechanical seeding device if there is no vacuum.

At the first stage a seed is caught by a blade (Fig. 2). In this case, it is possible to catch several "twin" seeds in the YOZ plane (Fig. 2b). The tangential movement of the caught seeds with the absence of vacuum is possible due to the corresponding ratio of centrifugal force to the gravity of the grain:

$$K = \frac{I}{G} \geq 1 \tag{1}$$

where K is the property of kinematic mode;

I is the centrifugal force;

G is the gravity force.

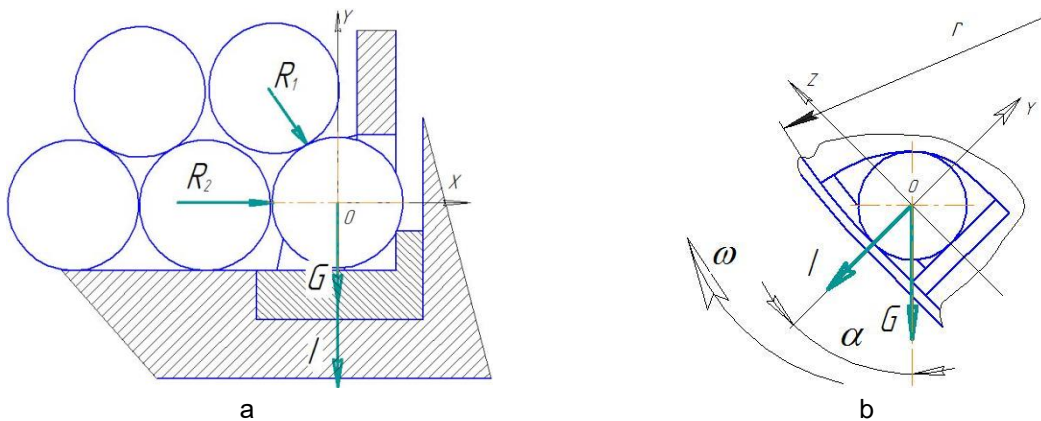


Fig. 2 - Catching a seed by the blade:
a – in the XOY plane; b – in the YOZ plane

Removing the captured "twin" seeds occurs in the pocket of the seeding device casing (Fig. 3).

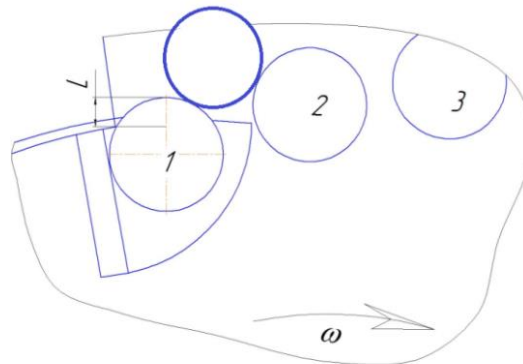


Fig. 3 - Removal of the "twin" seeds in the pocket of the seeding device casing

To prevent the removal of the main seed, the velocity of its radial displacement and the angle of pocket opening ε (Fig. 4) must be such as to follow the assumption:

$$L < \frac{d}{2} \tag{2}$$

where d is the diameter of the seed.

Let us consider the process of moving the main seed on the blade in the moving coordinate system $\tau - n$ in general case with an installed blade at the angle α to the normal (Fig. 4).

The seed is influenced by the gravity force G , the centrifugal force I and the friction force F_{mp} . We shall not take into account other forces as they are not important.

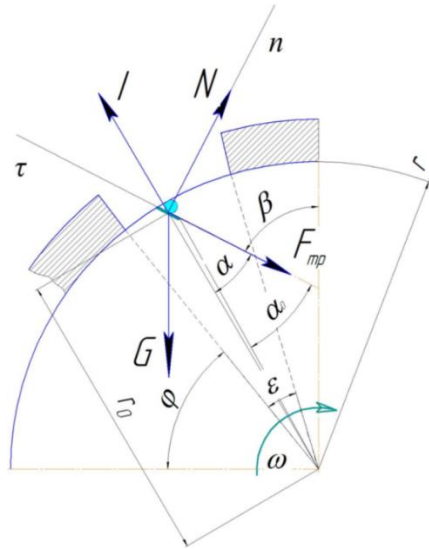


Fig. 4 - Physical model of the seed movement on the blade in the pocket

The differential equation of the seed moving on the blade in the pocket is the following:

$$m \cdot S'' = -f \cdot (-m \cdot \omega^2 \cdot r \cdot \sin \alpha + m \cdot g \cdot \sin \beta) - m \cdot g \cdot \cos \beta + m \cdot \omega^2 \cdot r \cdot \cos \alpha \quad (3)$$

where G is the gravity force, $G = m \cdot g$, [N];

I is the centrifugal force, $I = m \cdot \omega^2 \cdot r$, [N];

F_{mp} is the friction force, $F_{mp} = f \cdot N = f \cdot (-m \cdot \omega^2 \cdot r \cdot \sin \alpha + m \cdot g \cdot \sin \beta)$, [N];

N is the normal response force, [N];

f is the coefficient of the seed friction on the casing material;

m is the mass of the seed, [kg];

β the angle of the blade adjustment vertically, $\beta = \frac{\pi}{2} - \varphi + \alpha_0 + \omega t$;

φ is the angle of the pocket placement;

α_0 is the angle which defines the position of the blade beginning.

To shorten the mass m , we shall have:

$$S'' = (f \cdot \omega^2 \cdot r \cdot \sin \alpha - f \cdot g \cdot \sin \beta) - g \cdot \cos \beta + \omega^2 \cdot r \cdot \cos \alpha \quad (4)$$

From Fig. 4 we have: $r \cdot \sin \alpha = r_0 \cdot \sin \alpha_0 = \text{const}$

Therefore: $r \cdot \cos \alpha = S + r_0 \cdot \cos \alpha_0$

where S is the movement along the axis τ during the period of turning of the disk at the angle ϵ .

We have the equation of second order with the fixed factor relatively to the required function $S = S(t)$:

$$S'' - \omega^2 S = -f \cdot g \cdot \sin\left(\frac{\pi}{2} - \varphi + \alpha_0 + \omega t\right) - g \cdot \cos\left(\frac{\pi}{2} - \varphi + \alpha_0 + \omega t\right) + C \quad (5)$$

$$C = f \cdot \omega^2 \cdot r_0 \cdot \sin \alpha_0 + \omega^2 \cdot r_0 \cdot \cos \alpha_0 .$$

After generation we have:

$$S = \left(\frac{f \cdot r_0 \sin \alpha_0 + r_0 \cos \alpha_0}{2} + \frac{\sqrt{2} \cdot g}{4 \cdot \omega^2} \cos\left(\alpha_0 - \varphi - \frac{\pi}{4}\right) + \frac{\sqrt{2} \cdot f \cdot g}{4 \cdot \omega^2} \sin\left(\alpha_0 - \varphi - \frac{\pi}{4}\right) \right) \cdot e^{\omega t} +$$

$$+ \left(\frac{f \cdot r_0 \sin \alpha_0 + r_0 \cos \alpha_0}{2} + \frac{\sqrt{2} \cdot g}{4 \cdot \omega^2} \sin\left(\alpha_0 - \varphi - \frac{\pi}{4}\right) - \frac{\sqrt{2} \cdot f \cdot g}{4 \cdot \omega^2} \cos\left(\alpha_0 - \varphi - \frac{\pi}{4}\right) \right) \cdot e^{-\omega t} - \quad (6)$$

$$- f \cdot r_0 \cdot \sin \alpha_0 - r_0 \cdot \cos \alpha_0 - \frac{g}{2 \cdot \omega^2} \sin(\alpha_0 - \varphi + \omega t) + \frac{f \cdot g}{2 \cdot \omega^2} \cos(\alpha_0 - \varphi + \omega t)$$

$$S = \frac{r_0}{2} \left(e^{\frac{\omega}{2}t} - e^{-\frac{\omega}{2}t} \right)^2 \cdot (\cos \alpha_0 + f \cdot \sin \alpha_0) + \frac{\sqrt{2} \cdot g}{4 \cdot \omega^2} \cdot \left[(\cos \alpha_1 + f \cdot \sin \alpha_1) \cdot e^{\omega t} + (\sin \alpha_1 - f \cdot \cos \alpha_1) \cdot e^{-\omega t} - \left[-\sqrt{2} \cdot (\sin(\omega t + \alpha - \varphi) - \cos(\omega t + \alpha - \varphi)) \right] \right] \quad (7)$$

or:

$$\alpha_1 = \alpha_0 - \varphi - \frac{\pi}{4}$$

The movement of a seed in the radial direction L is in the range of:

$$0 < L = S \cdot \cos \alpha_0 < \frac{d}{2} \quad (8)$$

To fulfil the assumption (8), the seed should move in radial direction for the period of time needed for the disk to return to angle ε . That determines the size of the pocket of the inactive appliance for removing excess seeds:

$$t = \frac{\varepsilon}{\omega} \quad (9)$$

where ε is the angle which determines the size of the inactive appliance, [rad];

ω is the angular velocity of the seed disk, [rad/s].

Thus, we get:

$$L = \left[\frac{r_0}{2} \left(e^{\frac{\omega}{2}t} - e^{-\frac{\omega}{2}t} \right)^2 \cdot (\cos \alpha_0 + f \cdot \sin \alpha_0) + \frac{\sqrt{2} \cdot g}{4 \cdot \omega^2} \cdot \left[(\cos \alpha_1 + f \cdot \sin \alpha_1) \cdot e^{\omega t} + (\sin \alpha_1 - f \cdot \cos \alpha_1) \cdot e^{-\omega t} - \left[-\sqrt{2} \cdot (\sin(\omega t + \alpha - \varphi) - \cos(\omega t + \alpha - \varphi)) \right] \right] \right] \cdot \cos \alpha \quad (10)$$

We shall form the correspondence of the seed movement on the blade relatively to the disk rotation angle at different angular velocities for the radially installed blade (Fig. 5) (Amosov V.V., 2007; Babak V. P., 2004).

As can we can see on the graph of the dependence of the particle movement on the spade from the disk rotation angle (Fig. 5), to ensure the ascent of the excess seed, the centrifugal force must exceed the seed force of gravity, namely, the angular velocity must exceed the limiting value of 11.25 rad/s. With a smaller value of the angular velocity the particle will move on the shoulder blade backwards which will result in its falling to the pick-up chamber.

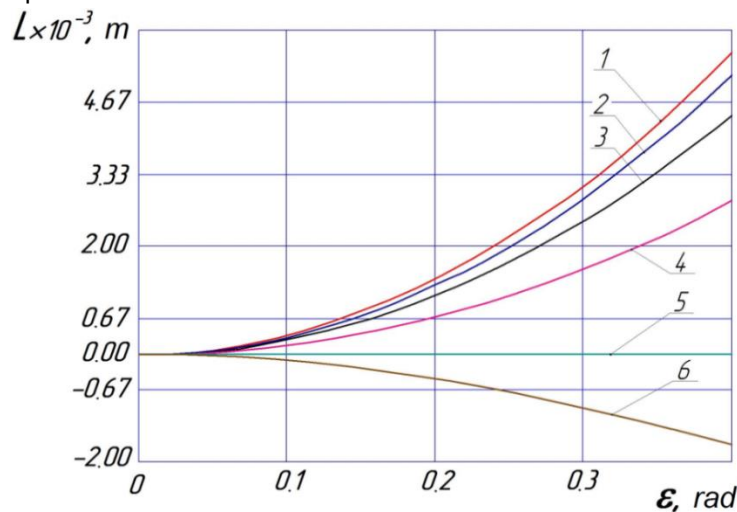


Fig. 5 - Correlation of seed movement on the blade to disk rotation angle at the angular velocity - ω [rad/s]

1 – 30 rad/s, 2 – 25 rad/s, 3 – 20 rad/s, 4 – 15 rad/s; 5 – 11.25 rad/s; 6 – 10 rad/s

However, when the rotation speed of the seed disk is approaching the seed drill speed, the main seed along with the extra seed can be removed from the cell. For the guarantee that the main seed does not fall out, it is necessary to use additional force that would keep it in the cell, which is the force of suction P .

CONCLUSIONS

The design of the new pneumatic and mechanical device increases the angular velocity of cells and reduces their number on the sowing disk and significantly reduces thinning in the vacuum chamber. Therefore, the proposed sowing device increases technological efficiency of seeding tilled crops and reduces energy intensity.

Consequently, the proposed construction of a new pneumo-mechanical seeding machine with peripheral arrangement of cells and inertial removal of excess seed allows the sowing of seeds of different cultivars. Thus, the design of the seeding device can operate without the use of vacuum but with a limited angular velocity of 11.25 rad/s.

The blade, which is behind the cell, allows you to reliably grab the seeds and hold it during movement to the reset zone. In order that the main seed does not fall out together with the extra seed when the rotation speed is approaching the seeding device speed, it is necessary to use additional force to keep the main seed in the cell, that is, the force of suction.

REFERENCES

- [1] Amosov V.V., (2007), Justification of the parameters of a universal seeding machine for cultivating crops: diss., Candidate tech Sciences: special 05.05.11. *Machines and means of mechanization of agricultural production*. 20 p, Kirovohrad /Ukraine;
- [2] Babak V.P., Marchenko, B.G., Frieze, M.S., (2004), Probability Theory, *Random Processes and Mathematical Statistics*. 288 p., Kiev / Ukraine;
- [3] Boyko A. I., Sviren M. O., Shmat S.I., Noshnov M. M., (2003), *New constructions of soil cultivating and sowing machines*. 206 p., Kirovohrad /Ukraine;
- [4] Mursec B., Vindis, P., Janzekovic, M., Cus, F., Brus, M., (2007), Analysis of the quality of sowing by pneumatic sowing machines for sugar beet. *Journal of Achievements in Materials and Manufacturing Engineering*. 22. 1: pp. 85-88, Gliwice / Poland;
- [5] Petrenko M.M., Vasytkovsky M. I., Vasytkovska K. V., (2013), Pat. 77191 U Ukraine, IPC A01S 7/04 (2006.01). *Pneumo-mechanical seeding machine*. №201203339; stated. March 20, 2012; has been published Feb 11, 2013, Bul. No.3;
- [6] Petrenko M.M., Vasytkovsky M. I., Vasytkovska K.V., (2011), Improvement of the pneumo-mechanical seeding machine for precise seeding of cultivating crops seed. *Bulletin of P. Vasilenko Kharkiv National Technical University of Agriculture*. 1. «Mechanization of agricultural production». 107, pp.359-363, Kharkov / Ukraine.;
- [7] Sydorhuk O., Lub P., Malanchuk O., (2014), Impact of meteorological conditions on the need in adaptive performing of technological operations of soil tillage and crop sowing, *ECONTECHMOD: an international quarterly journal on economics in technology, new technologies and modelling processes*. Vol.3, No.4, pp.35-39, Lublin-Rzeszów/Poland;
- [8] Sysolin P.V., Salo V.M, Kropivnyy V.M., (2001), Agricultural machines: theoretical bases, design, engineering, Book 1. *Arable farming machines*, 384 p., Edited by Chernovol M.I., Kyiv / Ukraine.;
- [9] Sysolin P V., Sviren, M.O., (2004), *Seeding machines of seeders*, 160 p., Kirovohrad /Ukraine;
- [10] Vasytkovska K.V., Vasytkovskyy O.M., (2014), Influence of the shape and type of seed cells drive on the quality of dispensing seeds, *Eastern European Journal of latest technology*, Vol.6, No.7 (72),. pp. 33-36, Kharkov / Ukraine, DOI: 10.15587/1729-4061.2014.29272);
- [11] Vasytkovska K.V., Leshchenko S.M., Vasytkovsky O.M., Petrenko D.I., (2016), Improvement of equipment for basic tillage and sowing as initial stage of harvest forecasting, *INMATEH - Agricultural Engineering*. Vol.50, No.3, pp.13-20, Bucharest / Romania;
- [12] Voytyuk D.G., Baranovsky V. M., Bulgakov V.M. and others, (2005), *Agricultural machines. Fundamentals of theory and calculation: textbook*. 464 p., Kiev / Ukraine.

PRODUCTION TESTS OF A SEED DRILL CPH 2000 FOR DIRECT SOWING /

ESSAIS AU CHAMP D'UN SEMOIR CPH 2000 POUR LE SEMIS DIRECT

Warouma Arifa¹⁾, Haidenko Oleh²⁾

¹⁾Dan Dicko Dan Koulodo University of Maradi, Niger Republic

²⁾ Institute of Steppe Agriculture of the National Academy of Agrarian Sciences of Ukraine
Tel: +227 96293475; E-mail: warouma@yahoo.com

Keywords: *direct sowing, energy intensity, quality, drill, efficiency.*

ABSTRACT

Under production conditions it was carried out a test with a drill CPH 2000 for direct seeding. It was evaluated the quality of the drill work and the economical evaluation was done. Obtained results showed that the average value of the practical depth of seeding was of 50.0 ± 2.85 mm and, of practical rate of seed sowing was of 94.0 ± 0.5 seed/m. Economical evaluation of the drill use indicates reduction in fuel and lubricants consumption per hectare of about 20.0 %, in comparison with traditional technology. These results show that this type of drill can be recommended for wide use in agricultural farms.

RESUME

L'essai d'un semoir CPH 2000 pour semis direct a été effectué dans les conditions de production. La qualité du travail du semoir a été évaluée et l'évaluation économique a été faite. Les résultats obtenus ont montré que la valeur moyenne de la profondeur pratique de l'ensemencement était de $50,0 \pm 2,85$ mm et que le rendement pratique de semis était de $94,0 \pm 0,5$ grains/m. L'évaluation économique de l'utilisation du semoir indique une réduction par hectare de la consommation en carburant et en lubrifiant d'environ 20,0% par rapport à la technologie traditionnelle. Ces résultats montrent que ce type de semoir peut être recommandé pour une large utilisation dans les fermes agricoles.

INTRODUCTION

World experience of agriculture proved that deep annual tillage of the soil does not only bring benefits, but also causes irreparable harm, strengthening erosion processes (Sysolin *et al*, 2008; Kosolap *et al*, 2010; Kuksa, 2008). When the human influence on the soil became much more tangible, intensified, agriculture faced the problem of rapid soils degradation and a sharp decrease in their fertility (Lihochvor, 2006; Novatski *et al*, 2007).

Over the past hundred years, black earth soils have lost more than half of their potential fertility (humus, nutrient reserves, structure and other properties) (Panichev, 2007; Skuryatin *et al*, 2008). These phenomena are caused by large plowing of lands, widespread use of plowing, high intensity of tillage and insignificant return of organic matter to soil. This problem can be solved with the help of the latest soil-protective energy, resource- and moisture-saving technologies (Anderson 1997, Carr *et al*, 2007, Endres *et al*, 2007).

The cost of agricultural products depends on the choice of technological operations and technical means for their implementation (Warouma, *et al*, 2010).

According to traditional (classical) technology, a huge amount of resources are spent on tillage: fuel and lubricants, fleet of machinery, working time, fertilizers, as a result, water and wind erosions increased, the content of organic matter in the soil decreased and, on the whole, environmental condition got worse (Markovskaya *et al*, 200; Medvedev 2003; Medvedev *et al*, 2004; Makurina *et al*, 2014).

The traditional technology of growing crops based on the use of plowing and which is a significant consumer of energy resources (which largely affects the cost price of products) has already exhausted itself due to the continuous degradation of soils and huge energy intensity. It has been established that 50% of energy and 25% of labour costs of field mechanized works' total volume account for such a soil treatment system (Marchenko *et al*, 2009; Sysolin P.V., 2001).

Analysis of experimental research results and theoretical developments of the last decade determines two possible ways for the further development of intensive agricultural technologies. The defining feature of both is the desire to reduce spending and cost of production. This can be achieved through the creation of a resource-saving technology, or the introduction of direct seeding technology based on chemicalization and sowing on the minimum prepared field surface.

Recently, in order to save fuel and labour costs, it is recommended to use combined till-plant aggregates more widely (Gaidenko *et al*, 2014; Oleg, 2012; Salo *et al*, 2010).

The creation of combined till-plant machines is caused by high demands on the quality of pre-sowing tillage and the need to reduce the time gap between tillage and seed sowing. Today, the market offers a large number of combined machines with different types of tools (Kravchuk *et al*, 2004, Gaidenko, 2013).

Analyzing the economic indicators of various technologies of soil cultivation and sowing, we can conclude that the transition to energy-saving technologies will provide economy of fuel from 13 to 87% compared to the traditional ones. Significant in this case is also a reduction in labour costs (Ivanishin *et al*, 2006). Direct seeding improves significantly soil lift and saves about 50% of the passage (Chervet *et al*, 2007). Specialized equipment is essential for successful direct seeding. But, for marketing purposes, dealers and manufacturers of agricultural machinery give sometimes fake information on the technical and operational performance of their products (Warouma *et al*, 2010). That's why it's important to test the performance of these machines.

Therefore, in the conditions of each farm, specialists must clearly determine which technology and with which set of agricultural machines the maximum profit will be achieved with minimal financial and energy costs. The aim of this work was to reduce the production cost of plant growing by rational acquisition and efficient use of agricultural park from modern agricultural machines for agrarian formations.

MATERIALS AND METHODS

The test was carried out in 2016 at the State Enterprise "Experimental farm "Elitne" at the Kirovograd state agricultural experimental station of the National Academy of Agrarian Sciences of Ukraine.

The equipment used in traditional plowing is composed of units: tractor T-150 and cultivator 2KPS-4; tractor MTZ-80/82 and seeder CZ-3, 6; tractor MTZ-80/82 and rollers 3KKSH.

The mechanical seed drill CPH 2000 of direct seeding with an operating width of 6.0 m was aggregated with the tractor Case Puma 195 (Fig. 1).



Fig. 1 - Mechanical seed drill CPH 2000 for direct seeding (No-Till) aggregated with a tractor Case Puma195

The mechanical seed drill CP 2000 for direct seeding consists of:

- batteries of disc knives with 34 pieces, staggered at a distance of 17.78 cm from each other, which contributes to self-cleaning from plant residues. The pressure of the knives on the soil is 203 kg, which is sufficient to ensure cutting of plant residues, soil and formation of furrow up to 15.24 cm in depth (Fig.2,a);



Fig. 2 - The components of the mechanical seed drill CPH 2000 for direct seeding with the tractor Case Puma 195: battery of disc knives (a), mechanical seed drill (b)

The investigated coefficients were determined by such formulas (*Listopad et al, 1986*):

- use of driving time:

$$K_d = T_1 / (T_1 + T_2) \quad (4)$$

- technological services:

$$K_1 = T_1 / (T_1 + T_3) \quad (5)$$

- reliability of the technological process:

$$K_2 = T_1 / (T_1 + T_{41}) \quad (6)$$

- reliability of the technical process:

$$K_3 = T_1 / (T_1 + T_{42}) \quad (7)$$

The evaluation of the quality of the drill's work was done in accordance with OST 70.5-1.82 for the following indicators: the correspondence of actual seeding depth to the specified depth; the deviation of the actual rate of seed sowing from the preset one; straightness of longitudinal rows.

The depth of seed sowing was determined by their direct arrangement in a row on the day of sowing. For this purpose, three survey sites with a length of 1 m and a width of two passes of the planter were planned. The distance between the counting sites along the aggregate course was 10 m. The number of measurements was 100.

To determine the practical rate of seed sowing, the sowing machines poured a certain number of seeds with the expectation that it would be enough for several passes of the drill. The rest of the seeds were selected and weighed. By the difference in the weight of the seeds that was covered, and the residues, the amount of seeds actually sown was determined.

The straightness of the longitudinal rows was determined in three rows 25 m long, disposed diagonally. On each of the repetitions of the experiment, the distance from the centre line of the row to the centre of the plants was measured. The centre line was found by placing the cord in the centre of the rows.

To compare the two technologies, the indicators such as costs of time, costs of fuel, labor and lubricants were determined.

RESULTS

• Results

The location of the test had the following characteristics: precursor – annual grasses; number of standing plant residues from 0.3 to 0.5 pcs/m²; average diameter of plant residues from 3 to 5 mm; the average length of standing plant remains is 0.18-0.12 m; weight of plant residues up to 10 g/m²; the relief of the field surface is a plateau levelled, the slope is up to 1°.

The moisture content in the layer from 0 to 5 cm was 8.6%, from 5 to 10 cm – 12.73%. The average moisture content of the sowing soil was 10.66%.

The soil hardness value in the layer from 0 to 5 cm was 2.45 kg/cm², in the layer from 5 to 10 cm – 2.73 kg/cm². The average value of the hardness of the soil seed layer was 2.59 kg/cm².

During the operating movement of the unit, the parameters studied had the following numerical values: engine speed 2043 ± 35 rpm, the slip of driving wheels– 4.86 ± 1%; the operating speed of the unit was 8.64 ± 0.55 km/h (Table 1). Since the tractor, which was part of the seeding unit, passed the running-in period, the value of the engine load index was in the range from 75 to 80%.

Table 1

Values of the studied parameters during the operating movement of the unit

№	Parameter	Repetition							Average value
		1	2	3	4	5	6	7	
1	Engine rotational frequency, rpm	2060	2070	2000	2040	2060	2050	2020	2043±35
2	Slip of driving wheels,%	4	5	5	6	5	4	5	4.86±1
3	Operating speed of the machine, km/h	8.5	8.5	9.5	8.1	8.5	9	8.4	8.64±0.55

When the drill was working on the processed soil, due to the growth of the rolling resistance coefficient, it was self-deepening.

The results of the duration cycles of unit work are shown in Table 2.

Table 2

№	№ of a position	Duration of cycle (min) with:	Repetition			Average value on repetitions (min)
			I	II	III	
1	1-2	Operating stroke	6	6	5	5.40
2	2-3	Turn	2	1	2	1.40
3	3-4	Operating stroke	5	6	6	5.40
4	4-5	Turn	2	2	2	2.0
5	5-6	Operating stroke	6	6	5	5.40
6	6-7	Turn	2	2	2	2.0
7	7-8	Operating stroke	5	6	5	5.20
8	8-9	Turn	1	2	2	1.40
9	9-10	Operating stroke	6	5	5	5.20

Thus, the average operating time of the unit was 5 minutes 32 seconds, of a turn – 1 minute 50 seconds, of the operating cycle – 7 min. 22 seconds. The structure of the operation cycles of the unit during the studied period is shown in Fig. 4.

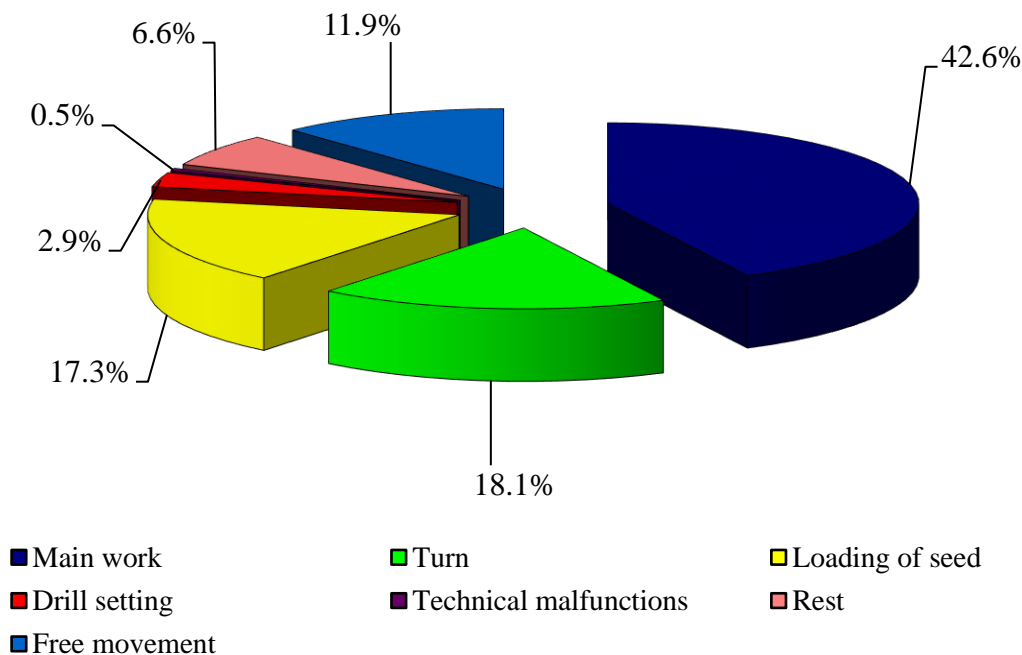


Fig. 4 - Structure of operation cycles of the unit during the period under study

When the indicators of the unit performance were calculated, it was found that within the range of changes in the duration of the operating stroke from 5 min up to 6 min, the value of work productivity varied from 4.6 to 5.5 ha/h. It was established that with an average value of the unit operating stroke duration of 5 min 32 s, the work productivity value per hour of the main time was 4.69 hectares.

The productivity of operative time per hour was 2.56 hectares, variable time – 2.01 hectares, operational – 1.99 hectares.

The investigated coefficients had the following values: use of the movement time 0.7; technological maintenance 0.94; reliability of the technological process 0.99; reliability of the technical process 1; the specific fuel consumption was 7.6 l/ha. According to the results of the researches, the seeding depth value ranged from 47.6 to 53.3 mm. The average seeding depth value was 50 ± 2.85 mm (Table 3).

Table 3

Results of seeding depth measurements

Indicator	Average value on repetitions			Average value of an experiment, mm
	I	II	III	
Depth of seeding, mm	53.3	47.6	49.2	50.0±2.85

According to the results of the researches, the value of actual seed sowing ranged from 93.4 to 94.4 pcs/m. The average value of the actual seed sowing was 94.0 ± 0.5 pcs/m. The deviation of the actual seed sowing from the preset rate ranged from 1.9 to 2.9%. The average value of seed sowing deviation was $2.3 \pm 0.5\%$ (Table 4).

Table 4

Results of determination of seed sowing practical rate

Indicator	Average value on repetitions			Average value of an experiment, pcs/m
	I	II	III	
Seed sowing practical rate, pcs/m	94.2	94.4	93.4	94.0±0,5
Deviation from the preset rate, %	-2.1	-1.9	-2.9	-2.3±0,5

According to the results of the researches, the value of the longitudinal rows straightness fluctuated within ± 5 mm.

The obtained results make it possible to determine the economic efficiency of using this aggregate (Table 5).

Table 5

Economic efficiency of use of a mechanical seed drill CPH 2000 of direct seeding

Indicators	Comparison of technologies	
	Direct Sowing Technology (No-Till)	Traditional
Winter wheat		
Composition of the aggregates that are involved	The Case Puma 195 tractor + seed drill CPH 2000	Tractor T-150 + cultivator 2KPS-4; Tractor MTZ-80/82 + seeder CZ-3,6; Tractor MTZ-80/82 + rollers 3KKSH
Costs of time, man-hour/ha	0.99	0.76
With traditional technology, %	30.3	100
The costs of fuel and lubricants, l/ha	7.6	9.5
With traditional technology, %	-20.0	100
Labour, fuel and lubricants costs UAH*/ha	167.2	209.0
With traditional technology, %	-20.0	100

* UAH- Ukrainian Currency: 1USD = 26 UAH

Economic evaluation of the use of this drill indicates a reduction in the cost of fuel and lubricants and total costs per a hectare by 20.0%, in comparison with the traditional technology.

• Discussions

According to the obtained results, the actual operating speed of the unit (8.64 ± 0.55 km/h) was less than the working speed set by the manufacturer (10 ± 0.5 km/h), this is due to the operation of the unit on the field after preliminary processing of soil, the hardness of which in the upper layers was 2.45 kg/cm².

According to the results of the researches, the seeding depth ranged from 47.6 to 53.3 mm. The average seeding depth was 50.0 ± 2.85 mm, which corresponds to a technologically specified value.

Also, the value of seed sowing practical rate ranged from 93.4 to 94.4 pcs/m. The average value of actual seed sowing was 94.0 ± 0.5 pcs/m, which corresponds to 198.3 kg/ha. The established rate of seed sowing on the seed drill was 203 kg/ha, which corresponds to 96.23 pcs/m. The deviation of the practical seed sowing from a given norm ranged from 1.9 to 2.9%. The average value of the seed sowing deviation was 2.3%, which does not exceed the allowable values of agrotechnical requirements (3.0%).

The value of straightness of longitudinal rows fluctuated within ± 5 mm, which does not exceed the allowable values of agrotechnical requirements ± 10 mm.

When the drill was working on the processed soil, due to the growth of the rolling resistance coefficient, it was self-deepening, which convinces the efficiency of the drill's work on unprocessed soils.

The costs of fuels and lubricants were 9.5 litres per hectare with traditional technology, and 7.6 litres per hectare with direct seeding technology (untreated soils). These figures are not confirmed with the found figures (Salo, 2010) when using the scarifier-drill KRU-4, where the costs of fuel and lubricants were 11.0 l/ha and using the till-plant complex for sowing cereals, where these costs were 9.9 l/ha (Gaidenko, 2014).

Economic evaluation of the use of this drill indicates a reduction in the costs of fuel and lubricants and total costs per hectare by 20.0%, in comparison with the traditional technology. These figures are consistent with the results (Vanishina, 2006), where they were in the range of 13 to 80%, but do not confirm the results (Warouma et al, 2010), where they are between 8.1 and 10.0% in two different fields (Gaidenko, 2013) and where in the implementation of major agrotechnical operations, the reduction of costs were 11.5% compared with the traditional technology.

CONCLUSIONS

The use of direct seeding technology is one of the ways to reduce costs for technological operations. In comparison with conventional tillage, the direct seeding system is characterized by the decrease in fuel consumption, in work time, in labor, in agricultural tools passages number and in tools used number.

The costs of fuels and lubricants for direct sowing and traditional technology have the order of 7.6 l/ha and 9.5 l/ha, respectively; labour costs, fuel and lubricants for direct sowing and traditional technology have the order of 167.2 UAH/ha and 209.0 UAH/ha, respectively.

The use of a mechanical seed drill for direct seeding of the CPH 2000 series, when assembling with the Case Puma 195 tractor, carrying out the technological operation – surface tillage with simultaneous sowing of winter wheat, local application of granular mineral fertilizers in a row and packing of crops, satisfies agrotechnical requirements and according to preliminary conclusions, can be recommended for widespread use in agricultural enterprises.

These results would allow developing a complex of high-productive soil-cultivating and sowing machines, and can be also used in developing typical rates of production and consumption of fuel for this unit.

It would be necessary to continue this research in the future by doing a production performance analysis to make much more complete comparison of the two technologies.

REFERENCES

- [1] Anderson R.L, (1997), A Multi-Tactic Approach to Manage Weed Population Dynamics in Crop Rotation, *Agronomy Journal*, pp.1579-1683;
- [2] Carr P.M., Krall J., Kephart K., Gunderson J., (2007), Impact of Tillage and Crop Rotation in Grain Yield of Spring Wheat I. Tillage Effect, *Dickinson Research Extension Centre Annual Report*, 2007. www.ag.ndsu.nodak.edu/dickinso/research/2006/toweb.htm. Accessed Oct. 29, 2007;
- [3] Chervet A., Gubler L., Hofer P., Maurer-Troxler C., (2007), Semis direct : de l'essai à la pratique, *Revue suisse Agric. Vol.39 (5): I-VI*;
- [4] Endres G., Schatz B., (2007), Carrington Research Extension Centre, *Research Highlights 2006*. www.ag.ndsu.nodak.edu/carringt/06data/06%20Annual%20Report/2006_research_highlights.htm Accessed Oct.29, 2007;
- [5] Gaidenko O., (2012), Simultaneous process and sow, Newspaper of entrepreneurs of agro-industrial complex "Agrobusiness Today", №. 17(240), pp. 62-64;
- [6] Gaidenko O.M., (2013), Results of testing and efficiency of agricultural machines (Результати тестування та ефективність сільськогосподарських машин), *Posibnik ukrainskogoh khlyboroba (Посібник українського хлібороба), Naukovo-praktychniy zbyrnyk (Науково - практичний збірник)*, Vol. 2, pp. 137-142, Kharkyv/Ukraine;
- [7] Gaidenko O., Kernasyuk Y., (2014), Combined complexes on sowing, *The Ukrainian Farmer*, №. 3, 126 p;
- [8] Gritishin M.I., Gorobets R.V, Zaborskiy V.F, Karan N.D, Konyok N.M. Glevakha V., (1992), *Methodical recommendations on production tests of agricultural machinery*, 82 p, Kyiv;

- [9] Ivanishin V., Koval S., Pogorely V., (2006), Ways of energy saving in soil cultivation and sowing of cereals and canola, *Machinery of agro-industrial complex*, №. 9-10, pp. 12-16;
- [10] Kosolap M.P., Krotinov O.P., (2010), Grain production in Ukraine for NO-TILL technology, 2nd edition, corrected, 144 p, Kiev;
- [11] Kravchuk V.I., Gritsishina M.I., Kuznetsova S.M., (2004), Current trends in the development of agricultural machinery designs, *Agrarian Science*, 369 p;
- [12] Kukxa L., (2008), Resource and energy-saving technologies for cultivating the soil for sowing of grain crops // *Propositsiya*, №. 4, pp. 118-125;
- [13] Lihochvor V.V., (2006), Transformation of technologies in plant growing [Text]: bibliography, *Propositsiya*, №8, pp. 38-39;
- [14] Listopad G.E., Demidov G.K., Zonovand B.D., (1986), Agricultural and ameliorative machines, *Agropromizdat*, 688 p;
- [15] Makurina O.N, Milyutkina G.V., (2014), Influence of minimization of soil treatment on its ecological and biochemical characteristics, *Bulletin of the SamSU: Natural Science Series*, - №7(47), pp.128-133;
- [16] Marchenko V.V., Kotko I.G., Opalko V.G., (2009), Technologies and technical means of sowing with minimal and zero processing, *Agrarian engineering and equipment*, №. 1(6), 03, pp. 20-28;
- [17] Markovskaya G.K, Kiryasova N.A., (2007), Influence of minimization of soil cultivation on its biological activity, *Achievements of science and machinery of the agro-industrial complex*, №. 1, pp.16-17;
- [18] Medvedev V., Grabak N.X., (2003), Why is the soil fertility reducing?, *Voice of Ukraine*, №226;
- [19] Medvedev V.V, Grabak N.X., (2004), *Minimization of Soil Treatment in Ukraine*, 86 p, Kharkov;
- [20] Novatski D., Ashley R., Hofman V., (2007), Conservative soil cultivation and equipment for stubble sowing, *NDSU Extension Service, Fargo*, North Dakota 58105;
- [21] Panichev R., (2007), Strategies of soil cultivation, *Agro sector / magazine of modern agriculture*, №. 9 (23), pp. 18-22;
- [22] Salo V.M., Gaidenko O.M., Temchenko A.M., (2010), Substantiation of technical means for conducting direct straw sowing on the example of a scarifier of a drill KRU-4, *KIAPV NAAN*, 28 p, Kirovograd;
- [23] Skuryatin N.F, Bondarev A.V., (2008), The search for an energy-saving way of sowing of grain crops [Electronic resource], *Scientific Journal of KubSAU*, №42 (8), pp. 2-15, Access mode to the Journal: <http://ej.kubagro.ru/2008/08/pdf/06.pdf>;
- [24] Sysolin P.V., (2001), Agriculture without a plow: actual scientific achievements and practical experience, *Journal of Tractors and Agricultural Machines*, №.8, pp.42–46;
- [25] Sysolin P.V., Salo V.M., (2008), Direct sowing of grain crops is a tribute to fashion or a necessity for rural workers, *Technique of the AIP*, №. 8, p.18;
- [26] Warouma A., Gaidenko O., (2010), Field test of a Flexi-coil ST820 pneumatic seed drill in the production conditions of Ukraine (Essai au champ d'un semoir pneumatique Flexi-coil ST820 dans les conditions de production de l'Ukraine), *Annals of Abdou Moumouni University (Annales de l'Université Abdou Moumouni)*, Tome XI-A, pp.216-222.

RESEARCH ON THE RATIONAL REGIMES OF WHEAT SEEDS DRYING

/

ДОСЛІДЖЕННЯ РАЦІОНАЛЬНИХ РЕЖИМІВ СУШІННЯ НАСІННЯ ПШЕНИЦІ

Assoc.Prof. Ph.D.Eng. Paziuk V.M. ¹⁾, Assoc. Prof. Ph.D. Eng. Liubin M.V. ²⁾, Assoc. Prof. Ph.D. Eng. Yaropud V.M. ²⁾,

Assoc. Prof. Ph.D. Eng. Tokarchuk O.A. ²⁾, Assoc. Prof. Ph.D. Eng. Tokarchuk D.M. ²⁾

¹⁾Institute of technical thermal physics NAS of Ukraine

²⁾Vinnitsa National Agrarian University / Ukraine

Tel: +380978399834; E-mail: yaropud77@gmail.com

Keywords: seeds, drying, regimes, germination, wheat, temperature

ABSTRACT

The value of the grain seeds is in the ability to germinate and ensure high yields. The main technological process for preserving the properties of seeds is drying. The proper carrying out and providing of rational modes of drying is a necessary condition to preserve the high ability to germinate. For the object of drying we have taken wheat seeds to determine the rational regimes. The research of the drying process kinetics is carried out on a convective drying stand in the following modes: coolant temperature in the drying chamber $t = 50-80^{\circ}\text{C}$, velocity $V = 0.5-1.5$ m/s. The highest intensity of drying occurs from an increase in the temperature of the coolant from 50 to 80°C in 3 times, but the main indicator is wheat maximum permissible temperature, which, at the coolant temperature of 50°C , is 48.6°C .

The biochemical indicators of wheat seeds were determined in the laboratory of the Institute of Technical Thermophysics according to the method on the 7th day of germination. The results of the researches showed that the best results of wheat germination were at 50°C at the level of 96%. Coolant temperature of 80°C has the most negative influence on wheat germination as the seeds lose their properties.

The analysis of the three-factors of influence, such as temperature and speed of coolant, as well as wheat initial humidity, on seed drying time and germination is done.

The obtained regression equations and obtained response surfaces of seed drying time and germination enable us to evaluate the process in terms of drying parameters' influence.

РЕЗЮМЕ

Цінність насіння зернових культур полягає у здатності пророщування та забезпечення високого врожаю. Основним технологічним процесом для збереження властивостей насіння є сушіння. Правильне проведення і забезпечення раціональних режимів сушіння є необхідною умовою збереження високої здатності до проростання. Для визначення раціональних режимів за об'єкт сушіння нами взято насіння пшениці. Дослідження кінетики процесу сушіння проведені на конвективному сушильному стенді за таких режимів: температура теплоносія в сушильній камері $t = 50-80^{\circ}\text{C}$, швидкість руху $V = 0,5-1,5$ м/с. Найбільша інтенсивність сушіння відбувається від збільшення температури теплоносія від 50 до 80°C в 3 рази, але основним показником є гранично-допустима температура пшениці, що при температурі теплоносія 50°C складає $48,6^{\circ}\text{C}$.

Біохімічні показники насіння пшениці визначались в лабораторії Інституту технічної теплофізики за методикою на 7 день пророщування. Результати досліджень показали, що найкращі результати пророщування пшениці при 50°C на рівні 96%. Найбільш негативно впливає на схожість пшениці температура теплоносія 80°C і насіння втрачає свої насінневі властивості.

Проведений аналіз трифакторного впливу параметрів сушіння – температури та швидкості руху теплоносія, а також початкової вологості пшениці на тривалість сушіння та схожість насіння. Отримані регресійні рівняння та отримані поверхні відгуку тривалості сушіння та схожості насіння, дають можливість оцінити процес від впливу параметрів сушіння.

INTRODUCTION

The problem of drying wheat seeds has been raised by various authors and it requires the choice of the most rational drying regime. Different approaches and different technological equipment may not always accurately reflect the choice of the desired drying regime. The elevated temperatures of the coolant during

wheat seeds drying are given in works (Kovalenko O.A., Kosovska N.V., 2012; Savchenko S.V., 2009) associated with the conditions of passing the grain through the drying chamber of the shaft dryer, where additionally the following drying factors are added: the velocity of the coolant and grain, the height of the grain layer, the hydraulic resistance of the layer, constructive features and other conditions. Under laboratory conditions, when drying in the elementary layer (Matkivska I.Ja., Atamanyuk V. M., Symak D., 2014), drying modes can be characterized more adequately and reliably, but there is a problem with the transfer of research results to industrial installations. The main criterion for evaluating seed grain quality is wheat heating temperature, which is determined by seed germination ability.

To determine wheat seeds germination, the author has proposed to dry the wheat seeds from 80 to 120°C and step modes with an increase in temperature of 80/100 and 80/120°C (Podpryatov G.I., Nasikovskiy V.A., 2005). There is no indication of the effect of these drying conditions on wheat seed properties, only the storage modes are mentioned. In particular, it is indicated that wheat seeds should be stored during the first month with a moisture content of 18.0-18.5%, thus increasing the ability to germinate.

Similar modes of drying are represented in the research work of Kovalenko O.A. for drying wheat at 80 - 120°C and stepwise drying mode at 80/100 and 80/120°C. The presented studies show that at the temperature of 80°C the germination is 89-94,5%, while in stepwise mode it is 63-81%, which cannot be recommended for seed grain at all (Kovalenko O.A., Kosovska N.V., 2012).

In the work of Savchenko S.V. the drying of wheat seeds was carried out in a gravitational-moving layer at the temperature of the heat carrier 70 - 85°C, and at the same time the temperature of heating the grain was 50 - 62°C (Savchenko S.V., 2009). The greatest germination of wheat seeds at the temperature of 70°C is 90%, and at an increase of temperature it is 85 - 83%.

In the research work of Matkivska V., the conditions of wheat seeds drying from 40 to 80 °C were analyzed. The germination at a drying temperature of 40, 50, 60, 80°C, respectively, is 99, 98, 90, 30%. In this case, it is recommended to use the temperature of 60°C, although it would be desirable to choose a temperature of 50°C according to the results of the experiment (Matkivska I.Ja., Atamanyuk V. M., Symak D., 2014).

MATERIALS AND METHODS

The high cost of seed grain and energy has set the task for us: to pick up such drying regimes, that can provide the high quality of seeds, while minimizing the specific heat consumption of the process.

Describing the processes of grain drying, they can be conditionally divided into soft and rigid drying regimes. The first one is characterized by a relatively low temperature and drying agent speed. In a soft mode, the processes of heating and drying the grain pass with a relatively low speed. The rigid mode is characterized by increased temperature and speed of the drying agent. From the economic point of view, it is desirable to dry the grain in rigid mode with a decrease in the drying time. However, in rigid mode due to intense heating and dehydration there is deterioration in its quality: cracking of seeds, change in colour, partial or complete destruction of the embryo, deformation of tissues.

The application of high temperatures at the beginning of wet grain drying process leads to a rapid dehydration of its surface, which makes the shells less permeable to moisture (the phenomenon of thermal "quenching" of the grain). Under these conditions, a water vapour forms in the surface layer, the output of which becomes complicated. It is therefore recommended to dry the seeds at relatively soft temperature regimes. In soft mode, drying does not have a complete guarantee of preservation of seed grain properties, so during prolonged low temperature drying (depending on the environmental parameters) the formation of mould on the surface is possible, and as a result, the damage of the seed material.

The main parameters that determine the choice of the drying mode and the achievement of high quality indicators of dried seeds are the temperature of the drying agent, the grain heating maximum temperature, the seeds initial humidity and the duration of their drying. The initial moisture content of grain ω_0 greatly affects the intensity of the drying process and determines the choice of the maximum allowable temperatures for heating the grain and the maximum temperatures of the drying agent.

The maximum permissible temperature for the grain intended for seed is determined based on the conditions of energy storage of its germination capacity. With the increase in humidity and the duration of grain presence in the heated state, the maximum allowable temperature of it is reduced.

The works of S.D. Ptitsina, M. Hutchison, V.I. Zhidko, O.N. Katkova, V.A. Rezchikov, N.N. Nevsky, V.L. Prokofiev, K.S. Esbolganov are dedicated to the determination of the maximum allowable temperature of heating the grain (table 1).

Finding the maximum-permissible temperature of seed grain in the proposed formulas of S.D. Ptitsina and M. Hutchison depends on the initial humidity and the time of heating the grain t .

V.I. Zhidko determined the maximum allowable temperature of the grain heating by introducing the coefficients and values of the heating time t , n , k and the grain moisture content ω .

O.N. Katkova, V.A. Rezchikov on the basis of processing the experimental data proposed the empirical formula, depending on the mass air velocity $V\rho$, which characterizes the state of the layer (on which the drying time depends), the humidity ω and the initial temperature of the coolant t .

N.N. Nevskaya and V.L. Prokofiev, based on the mass spectrometric radiation of wheat drying features, proposed the dependence of the maximum permissible grain temperature on the humidity ω and the drying time t .

K.S. Esbolganov, under the conditions of recirculation drying, proposed to use grain mass concentration in the heating chamber μ , the temperature of the coolant t and the value of the moisture content ω_c to calculate the maximum permissible temperature of heating wheat seeds.

Table 1

The equation for determining the maximum permissible temperatures for heating the seeds

№	Researcher	Equation	№ Eq.	Source
1	S.D. Ptitsin	$\theta_{TP} = \frac{2350}{0,37(100 - \omega_0) + \omega_0} + 20 - 10 \lg \tau,$ where: ω_0 - initial humidity of grain, %; τ - time of grain heating, min.	(1)	(Melnik B.E., Malin N.I., 1980)
2	M. Hutchinson	$\theta_{TP} = 122,0 - 5,41 \lg \tau - 441 \lg \omega_0,$ where: ω_0 - initial humidity of grain, %; τ - time of grain heating, min.	(2)	(Shchitov S.V., Tikhonchuk P.V., Krivuta Z.F., Kolzov A.V. 2016; Shchitov S.V., Krivueca Z.F., 2012)
3	V.I. Zhidko	$\theta_{TP} = t_0 - n \cdot \omega_0 + k,$ where: t_0 , n are the constant coefficients obtained experimentally for grain with normal gluten $t_0 = 88$, $n = -2,15$; k – coefficient depending on the duration of drying τ and moisture content of the grain: $k = 0,03\omega_c^2 - \frac{\tau - 90}{0,023\omega_c^2}$ where: ω_c - current moisture content of grain, %; τ - time of grain heating, min.	(3) (4)	(Zhidko V.I., Atanazevich V.I., 1982)
4	V.A. Rezchikov, R.P. Dubinicheva	$\theta_{TP} = 1800 \frac{(V\rho)^{0,13}}{\sqrt{\omega t}^{0,4}}$ where: $V\rho$ - mass velocity of air, kg/m ² ; ω - grain moisture content, %; t - coolant temperature, °C	(5)	(Rezchikov V.A., Dubinicheva R.P., 1988)
5	N.N. Nevsky, V.L. Prokofiev	$\theta_{TP} = \frac{900 + 273\omega + \omega^2}{\omega} - 10 \lg \tau,$ where: ω - grain moisture content, %; τ - time of grain heating, min.	(6)	(Tits Z.L., 1967)

It is most appropriate to determine the drying regime according to the biological properties of the grain. Acceptable values of temperatures at different time values of impact on the grains, which does not affect the processes of life in it, depend on the moisture content of the grain – the higher the humidity, the lower the permissible values of temperatures.

An irreversible decrease of wet grain lifetime begins at 55°C (coagulation of protein in the germ and aleuronic layer), and of dry grain at 65°C. During drying it is necessary to reduce the final temperature of heating of seeds by 10-12C, which will allow to preserve the seed properties of the material (fig. 1). (*The results of the investigation of physical processes during the drying of grain, 2018*).

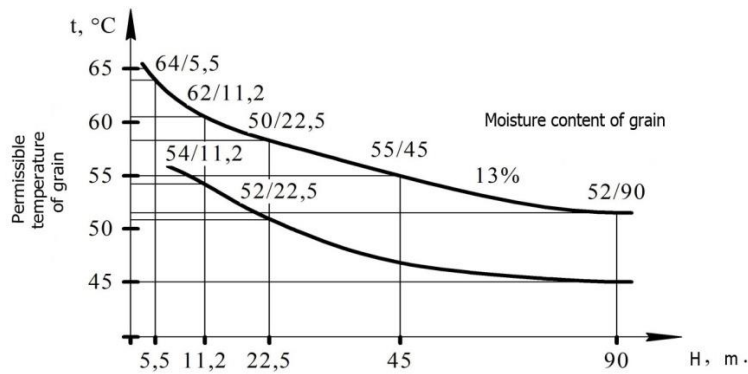


Fig. 1 - Change grain permissible temperature during drying for different humidity of seed grain

It is necessary to apply a milder drying regime for seed grain. According to M.G. Golik, a complete loss of wheat seeds germination occurs when heated to 60°C, at initial moisture content of 20% and higher. The germination of unprocessed seeds at a humidity of 20% was 97%, when heated to 45, 50 and 55°C, the germination was 87, 82 and 47% respectively. The intensity of moisture removal, which should not exceed 5%, was indicated in the work. (Golik M.G., Delidovich V.N., Miller B.E., 1972).

In the work of Savchenko, the studies on the germination of wheat seeds differ significantly from the data presented by M.G. Golik. Experimental studies are carried out at the temperature of 75, 85°C, respectively, heating the grain up to 50.56°C with a germinating capacity of 90 and 85% respectively (Savchenko S.V., 2009).

The temperature change of the grain and the reduction of the material mass were determined using special devices and the developed program in an automatic mode on a convective drying stand. In order to assess the quality of the wheat seeds, the standard methods of research were provided by SS 4138 - 2002 and SS 2240 - 1993 (State Standard 4138 - 2002, 2003; State Standard 2240 - 1993, 1994).

The research program involves removing the wheat drying kinetics by recording the changes in the mass of the material, temperatures of the coolant and in the middle of the material (fig. 2).

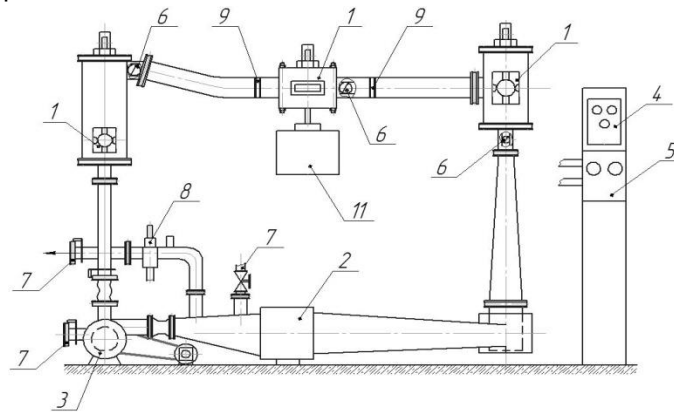


Fig. 2 - Scheme of the experimental stand:

- 1 - drying chamber; 2 - heater; 3 - fan; 4 - temperature controller; 5 - control panel; 6 - thermometers; 7 - pipe fittings;
- 8 - psychrometer; 9 - special gratings; 10 - a bar of scales; 11 – scales

RESULTS

An example of removing the kinetics of the wheat seed drying process at a coolant temperature of 50°C and a flow velocity of a coolant of 0.5 m/s is shown in fig. 3

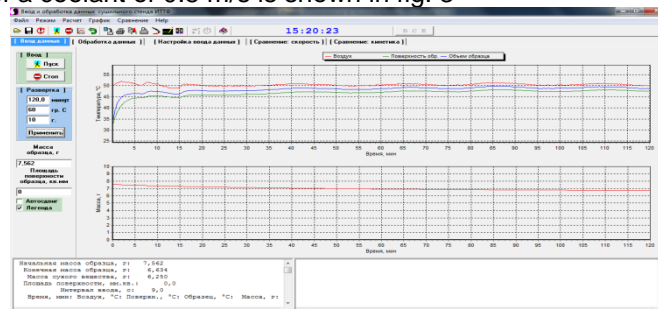


Fig. 3 - Removal of kinetics of wheat drying at the coolant temperature of 50°C and the speed of 0.5 m/s

The main direction of the intensification of wheat seeds drying process is coolant temperature; the higher the temperature, the drying rate increases (fig. 4).

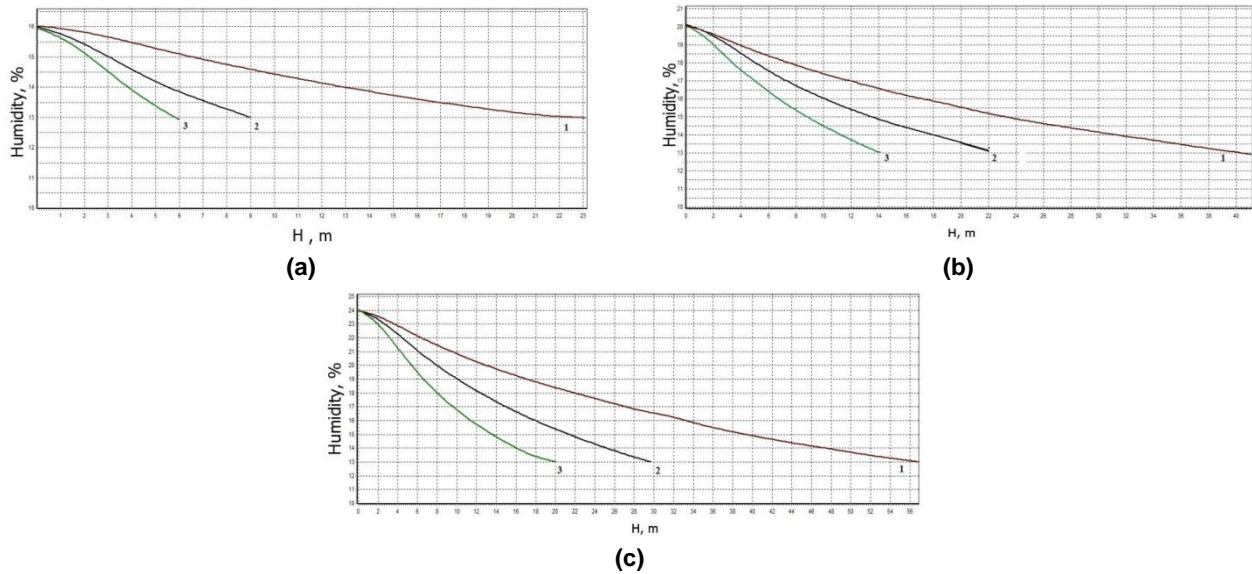


Fig. 4 - Curves of wheat seed drying depending on the coolant temperature, at initial humidity of material 16 (a), 20 (b), 24 (c), 1.5 m/s
 1 - 50°C; 2 - 65°C; 3 - 80°C

The increase of the coolant temperature accelerates the drying process, so at a temperature of 80°C compared with 50°C, the wheat drying is faster by almost 3 times. The initial moisture content of the material increases the drying time, so the duration at a moisture content of 24% to the final moisture of 13% is 57 minutes, and a decrease of moisture up to 20% reduces the duration of the process by 16 minutes.

On the presented temperature curves of wheat seeds heating it can be seen that the material is most rapidly heated for 6 - 8 minutes, and then there is a gradual heating to the final temperature (fig. 5). So the final temperature is: at 50°C - 48,6°C; 65°C - 62,26°C; 80°C - 74,62°C.

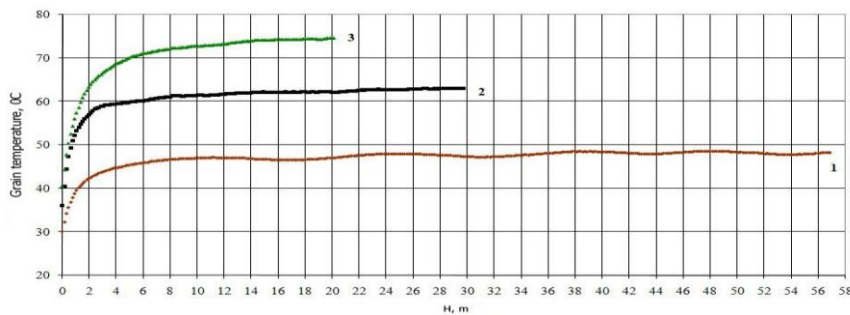


Fig. 5 - Temperature of wheat seeds heating during drying period at initial humidity of material 16 (a), 20 (b), 24 (c), 1.5 m/s
 1 - 50°C; 2 - 65°C; 3 - 80°C

Wheat seeds drying rate, depending on the coolant temperature, is shown in fig. 6. When wheat seeds are dried, there is a period of warming up of the material and a period of falling drying rate. In the period of warming, the material is heated and a partial evaporation of the moisture from the surface layers takes place.

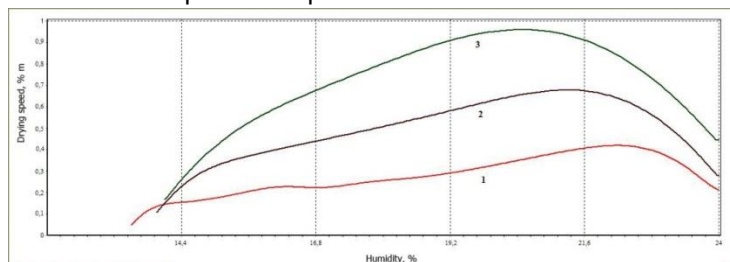


Fig. 6. Curves of wheat drying rate at an initial humidity of 24% and coolant speed 1.5 m/s from temperature
 1 - 50°C; 2 - 65°C; 3 - 80°C

The maximum drying speed at a temperature of 80°C is 0.95%/min., the decrease to 65°C reduces the speed up to 0,67%/min, and when reduced to 50°C, it is 0,41%/min.

The curves of wheat seed drying from the effect of the heat transfer velocity showed that with an increase in the velocity of the coolant from 0.5 to 1.5 m/s, the increase in the drying rate is 7.3%. Drying occurs to the final moisture content of wheat 13%, which corresponds to the equilibrium moisture content of the material (fig. 7).

Fig. 8 shows the curves of the drying speed at different coolant flow velocities, so at coolant velocity of 1.5 m/s the maximum drying speed at 18.6% humidity corresponds to 0.3%/min. At coolant flow velocity of 0.5 m/s, the drying rate is reduced up to 0.25%/min, namely by 20%.

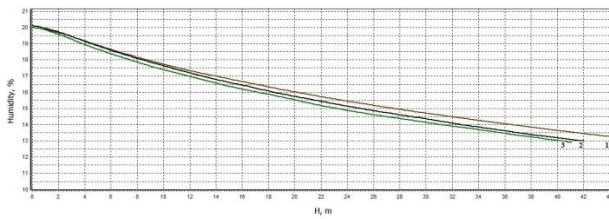


Fig. 7 - Curves of wheat seed drying at coolant flow velocity and a temperature of 50°C
1 – 0,5 m/s; 2 – 1,0 m/s; 3 – 1,5 m/s

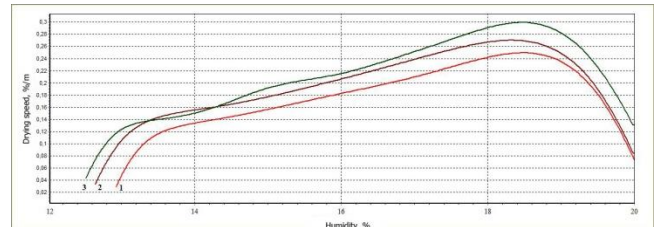


Fig. 8 - Curves of drying rate of wheat seeds from the coolant flow velocity at the temperature of 50°C
1 – 0,5 m/s; 2 – 1,0 m/s; 3 – 1,5 m/s

The rational drying regime was determined by the biochemical properties of wheat seeds, depending on the temperature, the initial humidity and the coolant flow velocity (table 2).

Table 2

The influence of drying parameters on wheat germinating capacity on the 7-th day of germination

Temperature of the drying agent, °C	Initial moisture content of grain,%	Drying agent speed, m/s	Seed germination,%
Output	-	-	99
50	16	1.5	96
50	20	0.5	96
50	24	1.5	96
65	16	1.5	94
65	20	0.5	93
65	24	1.5	90
80	16	1.5	1
80	20	0.5	9
80	24	1.5	0

From the data given in tab. 2, we can draw a conclusion about the significant influence of these parameters in the area of high temperatures. Rational drying mode is the temperature of 50°C, where the influence of the initial moisture and the speed of the drying agent are not significant.

The graphs of the drying parameters' influence on wheat germinating capacity on the seventh day of germination are shown in figure 9.

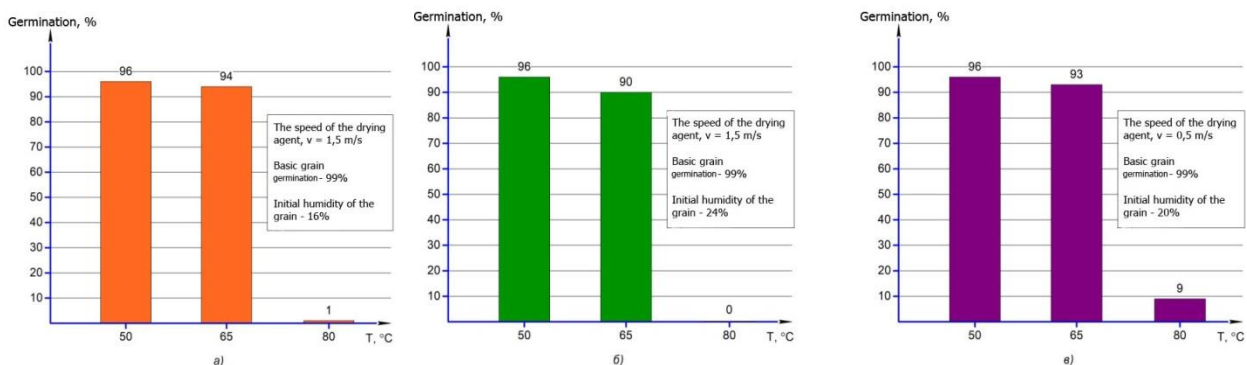


Fig. 9 – The effect of drying parameters on wheat germinating capacity on the 7-th day of germination

We can assess visually the influence of the coolant temperature on the presented fig. 10.



Fig. 10 – The influence of coolant temperature on the germinating capacity of wheat seeds on the 7-th day of germination at the initial moisture content of 20% and the speed of 0.5 m/s

For a mathematical description of the wheat drying process in an elementary layer, we take a three-factor experiment in accordance with an orthogonal compositional plan of the second order.

The total number of points in the plan is determined by:

$$N = 2^n + 2n + N_0; \quad (1)$$

where: $N_1 = 2^n$ - number of points of the factor space, determined by the core of the plan. For a three-factor experiment $n = 3$, that is $N_1 = 2^3 = 8$

$N_2 = 2n = 6$ - the number of stellar points;

$N_0 = 1$ is the number of central (zero) points of the plan.

So, holding a three-factor experiment on three levels requires the conducting of 27 experiments.

That's why it is necessary to establish the optimal amount of experiments required. This task can be solved using modern methods of planning an experiment, in particular mathematical, the basis of which is the creation of a mathematical model in the form of a regression equation.

In orthogonal central planning, the criterion for optimality of the experiment plan is the orthogonality of the planning matrix columns. Because of the planning orthogonality, all the coefficients of the regression equation are determined independently of each other. The core of the composite plan is the plan for a complete factor experiment CFE 2^n .

Experiment planning included the following steps:

- compilation of the coding table of factors and levels of variation;
- drawing up a plan - matrix;
- conducting the experiments according to the plan-matrix
- compilation of the regression equation and definition of the coefficients of the equation;
- analysis of the mathematical model in the form of a regression equation.

In the first stage we will compile a table of factors and levels based on the results of the research on a convective drying stand (table 3):

Table 3

Factors and levels of variation, that influence the wheat seed drying process

Indexes	Factors		
	Heat carrier		Material
	Temperature $t, ^\circ\text{C}$	Speed $V, \text{m/s}$	Initial humidity $W_0, \%$
Top (+1)	80	1.5	24
Average (0)	65	1.0	20
Lower (-1)	50	0.5	16
Variable interval	15	0.45	4
Code mark	x_1	x_2	x_3

According to the plan, the research was conducted using three levels for each factor - upper (+1), zero (0) and lower (-1), the code values of which were determined by the formula:

$$x_1 = \frac{t - t_0}{\varepsilon_1} = \frac{t - 65}{15}; \quad x_2 = \frac{V - V_0}{\varepsilon_2} = \frac{V - 1.0}{0.5}; \quad x_3 = \frac{W - W_0}{\varepsilon_3} = \frac{W - 20}{4}, \quad (2)$$

where: t_0, v_0, w_0 – the value of the factors at the main level, respectively, the temperature and velocity of the coolant, the initial humidity and the height of the canola layer;

$\varepsilon_1, \varepsilon_2, \varepsilon_3$ – the interval of factors variation.

The mathematical models of the process were constructed in the form of regression equations:

$$\hat{y} = a_0 + a_1x_1 + a_2x_2 + a_3x_3 + a_{11}x_1^2 + a_{22}x_2^2 + a_{33}x_3^2 + a_{12}x_1x_2 + a_{13}x_1x_3 + a_{23}x_2x_3. \quad (3)$$

The coefficients of regression can be determined by the following formulas:

$$a_0 = \frac{1}{N} \sum_{k=1}^N y_k - q \sum_{i=1}^N a_{ii}; \quad a_i = b_1 \sum_{k=1}^N x_{ik} y_k; \quad a_{ii} = b_3 \sum_{k=1}^N (x_{ik}^2 - q) y_k; \quad a_{ij} = b_2 \sum_{k=1}^N x_{ik} x_{jk} y, \quad (4)$$

where: q - the value that provides the orthogonality of compositional plans:

$$q = \frac{1}{N} (2^n + 2R^2) = \frac{1}{15} (2^3 + 2 \cdot 1,215^2) = 0,73, \quad (5)$$

b_0, b_1, b_2, b_3 – elements of the plan matrix $b_0 = 0.0667; b_1 = 0.0913; b_2 = 0.125; b_3 = 0.298$.

The estimation of the errors' variance when calculating the estimates of the coefficients of the quadratic regression equation is calculated by the formulas:

$$S_{a_0}^2 = \frac{b_0}{m} S_y^2 + q^2 \sum_{i=1}^n S_{a_{ii}}^2; \quad S_{a_i}^2 = \frac{b_1}{m} S_y^2; \quad S_{a_{ij}}^2 = \frac{b_2}{m} S_y^2; \quad S_{a_{ii}}^2 = \frac{b_3}{m} S_y^2, \quad (6)$$

where:

S_y^2 - estimation of the reproduction dispersion:

$$S_y^2 = \frac{1}{N} \sum_{k=1}^N S_k^2. \quad (7)$$

Recommended form of the plan matrix and the results of experiments on Podolianka variety wheat seeds drying are presented in table 4.

Table 4

The plan matrix and the results of the experiments on Podolianka variety wheat seeds drying

№	Experimental conditions											τ , min	C, %	
	x_1	x_2	x_3	x_1^2	x_2^2	x_3^2	$x_1 x_2$	$x_1 x_3$	$x_2 x_3$	x_1	x_2			x_3
1.	-1	-1	-1	+1	+1	+1	+1	+1	+1	0.27	0.27	0.27	30	95
2.	+1	-1	-1	+1	+1	+1	-1	-1	+1	0.27	0.27	0.27	8	9
3.	-1	+1	-1	+1	+1	+1	-1	+1	-1	0.27	0.27	0.27	23	96
4.	+1	+1	-1	+1	+1	+1	+1	-1	-1	0.27	0.27	0.27	6	1
5.	-1	-1	+1	+1	+1	+1	+1	-1	-1	0.27	0.27	0.27	64	95
6.	+1	-1	+1	+1	+1	+1	-1	+1	-1	0.27	0.27	0.27	24	0
7.	-1	+1	+1	+1	+1	+1	-1	-1	+1	0.27	0.27	0.27	57	96
8.	+1	+1	+1	+1	+1	+1	+1	+1	+1	0.27	0.27	0.27	20	0
9.	-1.215	0	0	+1.472	0	0	0	0	0	0.75	-0.73	-0.73	42	93
10.	+1.215	0	0	+1.472	0	0	0	0	0	0.75	-0.73	-0.73	14	10
11.	0	-1.215	0	0	+1.472	0	0	0	0	-0.73	0.75	-0.73	28	96
12.	0	+1.215	0	0	+1.472	0	0	0	0	-0.73	0.75	-0.73	22.	94
13.	0	0	-1.215	0	0	+1.472	0	0	0	-0.73	-0.73	0.75	17	94
14.	0	0	+1.215	0	0	+1.472	0	0	0	-0.73	-0.73	0.75	31	90
15.	0	0	0	0	0	0	0	0	0	-0.73	-0.73	-0.73	25	93

After carrying out the experiments, the test of experiments' reproduction using the Cochran's criterion is carried out:

$$G_{\max} = \frac{S_{k\max}^2}{\sum_{k=1}^N S_k^2}, \quad (8)$$

where:

S_k^2 is the selective variance of the output quantity y in the k -line of the planning matrix, obtained from "m" of parallel experiments.

$$S_k^2 = \frac{1}{m-1} \sum_{l=1}^m (y_{kl} - y_l), \quad (9)$$

If $G_{\max} < G_{kp}$, with the number of degrees of freedom $\nu_1 = m - 1$, $\nu_2 = N$ and the level of significance $\alpha = 1 - \gamma$, then the hypothesis of dispersion homogeneity is accepted.

The hypothesis about the static significance of the estimates of the coefficients of the regression equation a_i is checked by means of t - the Student's criterion:

$$t_{ip} = \frac{|a_i|}{S_{ai}}, \tag{10}$$

The verification of the mathematical model adequacy by the results of the experiment is carried out according to Fisher's criterion in the form of the ratio:

$$F_p = \frac{S_{inad}^2}{S_y^2}, \tag{11}$$

where: S_{inad}^2 - estimation of inadequacy variance.

$$S_{inad}^2 = \frac{1}{N-r} \sum_{j=1}^N (\bar{y}_j - \hat{y}_j)^2, \tag{12}$$

where: N - number of points of the orthogonal CCP;

r - number of significant parameters of the regression equation;

\hat{y}_j - the value of the response, calculated by the regression equation;

\bar{y} - the average for the series "m" of experiments is the value of a real object reference.

If the condition is fulfilled:

$$F_p < F_{kp}, \tag{13}$$

then the mathematical model is considered adequate, that is, the scattering of the experimental values of the response relative to the values of the regression equation of the same order as the scattering, caused by the experimental errors.

The critical significance of the statistics is according to the corresponding tables for the given level of significance α and the degree of freedom $v_1 = N - r$ and $v_2 = N - (m - 1)$.

The results of a three-factor experiment on an orthogonal compositional plan of the second order are presented in the form of quadratic regression equations:

- for the germinating capacity of wheat seeds:

$$C = 160.4 - 3.618t - 25.06V - 2.53W - 0.16t^2 - 28.72V^2 - 0.57W^2 - 0.21tV - 0.026tW + 0.5VW; \tag{14}$$

- for drying time:

$$\tau = 204.72 - 0.54t - 13.65V + 7.78W + 0.01t^2 + 4.8V^2 + 0.13tV - 0.08tW. \tag{15}$$

Based on the regression equation of wheat seeds' germinating capacity and duration, the response surfaces are constructed (fig. 11).

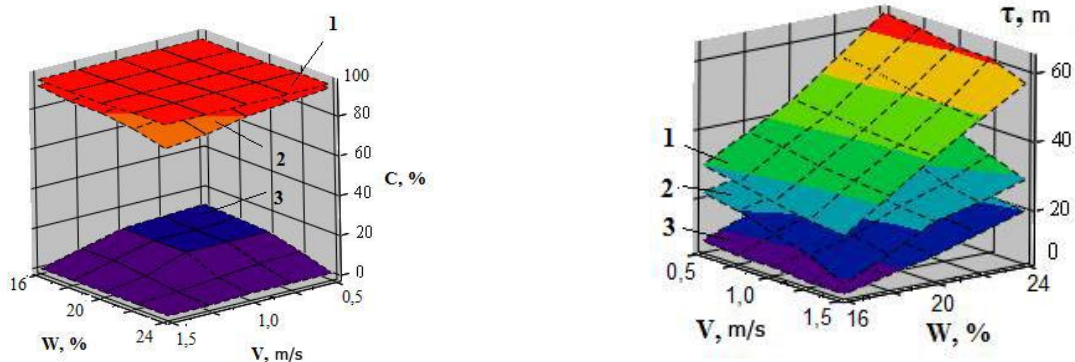


Fig. 11 – Surface response of the germinating capacity and duration of "Podolianka" variety wheat seeds at the action of the coolant temperature, °C
1 - 50; 2 - 65; 3 - 80

CONCLUSIONS

Analyzing the carried out research on the germination of "Podolianka" variety wheat seeds after drying, we can conclude:

- The temperature regime of drying is the most rational at a temperature of 50°C, the germination being 16%.

- At this temperature, the speed of the drying agent in the range $v = 0.5...1.5$ m/s does not significantly affect the germination.
- At this temperature, the initial moisture content of the grain in the range of 16-24% also does not significantly affect the germination.
- At the temperature of the drying agent of 65°C, the germination limits to 93-94% may be at velocity of the drying agent of 1.5 m/s and an initial moisture content of 20%, or at a velocity $v = 0.5$ m/s and an initial moisture content of 16%.
- At the increase in temperature of drying agent to 80°C, the germination is practically small (9%), which goes beyond agrotechnical requirements.

REFERENCES

- [1] Fedorenko V.F., Buklagin D.S., Golyapin V.Ya., (2010), Machines and equipment for post-harvest processing and storage of grain and seeds, *Rosinformagrotekh*, 92 p., Moscow / Russia;
- [2] Gaponyuk O.I. Ostapchuk M.V, Stankevich G.M. (2014), Active ventilation and grain drying, *BMB*, 325 p., Odessa / Ukraine;
- [3] Kovalenko O.A., Kosovska N.V., (2012), Influence of drying modes of winter wheat on the indices of its food and seed qualities. Available at: <http://lib.chdu.edu.ua/pdf/naukpraci/ecology/2012/179-167-16.pdf> (Accessed: 27 August 2018);
- [4] Matkivska I. Ja., Atamanyuk V.M., Symak D., (2014), Basic regularities of filtration drying of wheat grain, *East-European Journal of Advanced Technologies*, No. 5/5 (71). - pp. 14-18, Kharkiv / Ukraine;
- [5] Matkivska I.Ja., Atamanyuk V.M., Symak D., (2014), Basic regularities of the filtration drying of wheat grain, *Eastern-European Journal of Enterprise Technologies*, №5/5(71), pp. 14-18, Kharkov / Ukraine;
- [6] Meledina T.V., Danina M.M., (2015), Planning and processing methods results of scientific research: *Proc. allowance, SPb: NIIT ITMO; IHBT*, 110 p., St. Petersburg / Russia;
- [7] Podpryatov G.I., Nasikovskiy V.A., (2005), Influence of drying modes on the heating temperature and crop properties of wheat grain, *Agrarian Science and Education*, Vol. 6, No. 1-2, pp. 74-77, Mykolayiv / Ukraine;
- [8] Pohozykh M.I., Pak A.O., Pak A.V. (2014), Hydrothermal treatment of cereals using the principles of drying with a mixed heat transfer, *KSUFTT*, 169 p., Kharkiv / Ukraine.
- [9] Poperechnyy A. M., Varvarina N. M., Zhdanov I. V., (2013), Drying of food raw material in a fluidized bed: monograph, *DonNUET*, 303 p., Donetsk / Ukraine;
- [10] Savchenko S.V., (2009), Kinetic model for optimizing the grain drying regime, *Bread products*, №7, p. 38-39, Moscow / Russia;
- [11] Shchitov S.V., Krivueca Z.F., (2012), Optimization of energy inputs in transportation and technological support of agro-industrial complex, Monograph, 151 p., Blagoveshchensk / Russia;
- [12] Shchitov S.V., Tikhonchuk P.V., Krivuta Z.F., Kolzov A.V. (2016), Investigation of the influence of kinematic parameters on the optimization of grain drying process, *Far Eastern agrarian messenger. Scientific and practical journal*, №2(38), pp. 98-102, Blagoveshchensk / Russia;
- [13] Snyezhkin YU.F., Shapar R.O., Chalayev D.M. (2010) The intensification of the drying process of seed grains, *Industrial heat engineering*. P. 42-47, Kiev / Ukraine;
- [14] ***State Standard 2240 – 1993, (1994), Seeds of agricultural crops. Methods for analyzing the moisture content of seeds, *DSSU*, p. 2-10, Kiev / Ukraine;
- [15] ***State Standard 4138 – 2002, (2003), Seeds of agricultural crops. Methods for analyzing the moisture content of seeds, *DSSU*, p. 16-17, Kiev / Ukraine;
- [16] ****Technology of drying and seeding seeds of cereals in the northern regions of the Tomsk region* (2018). Available at: http://sibniit.tomsknet.ru/files/articles/suschka_podrabortka (Accessed: 28 March 2018).
- [17] ****The results of the investigation of physical processes during the drying of grain* (2018). Available at: <http://insightex.com.ua/wp-content/uploads/2014/08/C3MM> (Accessed: 28 March 2018);
- [18] Vasiliev A.N., Severinov O.V., Budnikov D.A., (2012), Mathematical model of optimal control of grain drying with maximum use of drying agent potential, *Collection of reports VIM*, pp. 677-682, Moscow / Russia.

AN ANALYSIS OF EIGHT TILLAGE METHODS IN A SILTY-CLAY SOIL: PROPOSAL FOR FLEXIBLE TILLAGE CYCLES

ANALISI DI OTTO METODI DI LAVORAZIONE DI TERRENI LIMO-ARGILLOSI: PROPOSTA DI CICLI FLESSIBILI DI LAVORAZIONE

Fanigliulo R., Biocca M., Pochi D.

Consiglio per la ricerca in agricoltura e l'analisi dell'economia agraria (CREA), Centro di ricerca Ingegneria e Trasformazioni agroalimentari (Research Centre for Engineering and Agro-Food Processing), Monterotondo (Rome), Italy
Tel: +39 0690675215; E-mail: marcello.biocca@crea.gov.it

Keywords: *conventional tillage, conservation tillage, energy requirements, multivariate statistics, soil quality indexes.*

ABSTRACT

Soil preparation based on ploughing is a conventional method commonly adopted for cereal cultivation in silty-clay soil. Replacing this method with conservation tillage was the subject of this study based on the evaluation of eight implements used in conventional and conservative tillage. By differently combining the implements, we hypothesized eight methods and assessed the overall energy balance and quality of work for each method. Basing on test results, we proposed an approach to the choice of proper tillage methods, aiming at integrating the benefits of conventional and conservative tillage methods.

RIASSUNTO

La preparazione del terreno basata sull'aratura è un metodo convenzionale comunemente adottato per la coltivazione di cereali in terreni limoso-argillosi. La sostituzione di questo metodo con le lavorazioni conservative è stato l'oggetto di questo studio basato sulla valutazione di otto attrezzature usate nelle lavorazioni convenzionali e conservative dei terreni. Combinando tali attrezzi, abbiamo ipotizzato otto metodi e valutato il bilancio energetico e la qualità del lavoro per ciascun metodo. Sulla base dei risultati dei test, abbiamo proposto un approccio alla scelta corretta dei metodi di lavorazione, con l'obiettivo di integrare i vantaggi dei metodi di lavorazione tradizionali con quelli conservativi.

INTRODUCTION

The meanings of the definitions “conventional tillage” and “conservation tillage” imply that such categories cannot be uniquely defined. In other words, each type of intervention on the soil should be assigned to one category or the other depending on the specific type of soil and environmental conditions. On the other hand, the soil tillage methods considered conventional for a given environment are dictated by the experience gained over the centuries and, therefore, can be identified as the most suitable to preserve the characteristics of the soil. From this point of view, there should be a virtual identification between conventional and conservation techniques. Such identification is often interrupted within intensive farming that progressively eliminated practices such as crop rotation and organic fertilization, maintaining traditional (conventional) soil tillage methods and causing, during the years, the occurrence of several problems involving both the aspects of energy requirements and soil fertility.

For instance, the most common conventional method adopted in silty-clay soils of Central Italy to prepare the seedbed for winter cereals, is based on the chopping (rarely the burning) of the residues from previous crop, on a medium depth ploughing (0.20 - 0.30 m aimed at burying the residues, and on the harrowing of the upper layer, by means of a rotary harrow, a disk harrow or a combined seeder (a machine with working tools operated by the tractor's P.T.O. (Power Take-Off) and a pneumatic seed drill).

Unwanted effects of such technique can be: excessive energy requirements (Fanigliulo *et al.*, 2016) and related costs (Fedrizzi *et al.*, 2015), worsening of soil structure due to compaction, loss of nutrients in deeper layers, mineralization of organic matter in upper layers, increasing soil erosion caused by wind and runoff (De Laune and Sij, 2012). Such effects can be limited, in some cases, by adopting conservation methods (Lal *et al.*, 2007; Fanigliulo *et al.*, 2017) that contribute to energy savings and to preserving soil fertility through the reduction of number of passes and of working depth, by using one pass combined machines characterized by wide working width (5-7 m) and working tools with geometry (Godwin, 2007).

Combining these points with the maintenance of a surface coverage of at least 30% and with crop rotation allows reducing soil erosion, surface disturbance and compaction, preserving natural fertility.

Among conservation methods, we can find interventions with different intensity in terms of working depth. The main approaches are (ASABE Standard, 2005): reduced tillage, aimed at soil lifting and shattering, reducing the compaction of both shallow and deep layers, without inversion (e.g. by means of subsoilers or combined cultivators) leaving 15-30% residue cover on soil surface (Townsend *et al.*, 2016); minimum tillage, in which the level of soil manipulation is reduced to the least compatible with crop production (e.g. with use of disk harrows); no tillage, that entails direct sowing into the previous crop stubble with no prior tillage. The comparison among conservation methods was the subject of many studies, especially focused on grain yield, greenhouse gas emissions and economic profitability, as few data were provided on tillage quality parameters. Other studies regarded the measurements of fuel consumption, force of traction and power required by tillage implements (Pochi *et al.*, 2013) under various soil conditions. McLaughlin *et al.* (2008) measured the force of traction and energy inputs of eight tillage implements in a clay loam soil. The results showed that significant energy savings can be realized through the selection of proper tillage methods and tractor-implement coupling.

CREA carried out tests with a series of implements, commonly used for tillage and sowing, collecting, for each of them, the data of energy requirements and tillage quality. Combining the implements and relative data, allowed to hypothesize four conventional (CONT) and four conservation (CT) methods and to assess their relative energy balances and quality of work with the purpose of their comparison, assuming CONT1 as a reference. Lastly, the data of measurements have been used to develop a proposal for an integrated tillage system capable to adapt, time by time, to the actual needs dictated by the conditions of the soil.

MATERIALS AND METHODS

The tests were carried out in the farm of CREA in Monterotondo (Rome, Italy; 42°5'51.26"N; 12°37'3.52"E; 24 m a.s.l.), on flat surface plots (< 1% slope) and on untilled soil classified as silty-clay (clay 543 g kg⁻¹, silt 434 g kg⁻¹, sand 23 g kg⁻¹) according to the USDA soil classification system (USDA, 2014). Before the tests, in ten random points for each plot, the following parameters were measured at a depth of 0.40 m (Table 1): water content, dry bulk density, penetration resistance (cone index) and soil biomass coverage index (SCI). The first two parameters were determined on soil samples of 100 cm³ extracted by means of a manual soil coring tube (Eijkelkamp) and dried in oven at 105°C up to constant mass. Cone index (c.i.) was determined according to the ASAE Standard S313.3 (ASABE Standards, 2004), by means of a hand-operated Penetrologger (Eijkelkamp), measuring the force needed for the penetration in the untilled soil. It provides a detailed vertical profile of soil strength compaction. Then, the SCI was determined by analysing digital pictures of square sections of the ground surface with an area of 1 m². A graphic editor programme (Adobe Photoshop), was used to quantify the percentage of soil areas covered by residues.

Table 1

Average values of the physical-mechanical characteristics of the soil

Implement type	M.U.	Four furrow plough	Rotary harrow	Pneumatic seed drill	Combined seeder	Combined cultivator	Subsoiler	Disk harrow	Seed drill for direct seeding
Water content	%	19.4	18.8	22.7	17.3	16.7	22.5	19.5	15.0
Dry bulk density	kg m ⁻³	1460	1490	1410	1260	1600	1400	1470	1200
Average cone index	MPa	1.90	-	-	-	2.10	1.70	2.25	-

The main technical data of the tested implements are reported in Table 2. The selected implements are commonly used in soil tillage aimed at cereals cultivation. The tests with the seed drills were conducted with filled hoppers (seeding rate: 190 kg ha⁻¹). All implements were operated by a 4WD tractor (Case IH MX 270) with a nominal power of 205 kW and total mass of 11,000 kg. The P.T.O. speed was 104.7 rad s⁻¹ corresponding to an engine speed of 206.7 rad s⁻¹. All tests were performed with diesel fuel in compliance with the EN 590 (EC Standard, 2013). It was always provided by the same supplier. Consequently, its quality was assumed to be constant, with a Low Heating Value of 42.7 MJ kg⁻¹.

The following parameters were measured: width and depth of tillage; speed, time and capacity of work; P.T.O. torque, speed and resulting power; force of traction and resulting power; tractor's slip and corresponding power losses; fuel consumption and energy required per surface unit and per volume unit of tilled soil.

Table 2

Main technical data of the tested implements

Implement type	Four furrow plough	Rotary harrow	Pneumatic seed drill	Combined seeder	Combined cultivator	Subsoiler	Disk harrow	Seed drill for direct seeding
Working tools	skim coulter, knife ploughshare, mouldboard	vertical blades, packer roller	vertical hoe opener	vertical blades, hoe opener	straight shanks, notched disks, roller	straight shanks	notched and plain concave disks	single disk openers, depth band
Tools number	2x4	40	40	24+24	5 + 10 (Ø 610 mm)	7	18+18	33
Lateral tools spacing (mm)	1150	245	125	245/125	950 shanks 480 disks	430	230	180
Total mass (kg)	2560	2910	1930	2680	1730	1670	3465	6380

Before field tests, the tractor's engine performances were verified at the dynamometric brake that provided the updated characteristic curves of the engine. After field tests, the tractor was newly connected to the dynamometric brake used to reproduce the working conditions: the engine speed was set on the same values adopted at the start of each test. Then, the engine load was increased in such a way that the resulting engine speed reductions were equal to the average speeds measured during the field test. This method provided the average values of total torque and power required to the engine and the corresponding fuel consumption (*Pochi and Fanigliulo, 2010*). Multiplying the total power (W_t , kW) by the actual working time (T_o , h ha⁻¹), will provide the energy required per surface unit area:

$$E_{ha} = 3.6 W_t T_o \text{ [MJ ha}^{-1}\text{]} \quad (1)$$

Dividing E_{ha} by the working depth (P , m), will give the energy per unit of volume of tilled soil (E_{vol}), expressed in:

$$E_{vol} = \frac{E_{ha}}{10 \cdot P} \text{ [MJ } 10^{-3} \text{ m}^{-3}\text{]} \quad (2)$$

Knowing the power required by tractor self-dislocation (W_{sd} , kW), it is possible to assess the power losses for slip (W_s , kW), by means of the relation (3):

$$W_s = s (W_{tr} + W_{pto} + W_{sd}) \text{ [kW]} \quad (3)$$

where s is the tractor slip, W_{tr} is the traction power and W_{pto} is the P.T.O. power.

In addition to the aforementioned components or power, the total engine power also includes the power dissipated in the transmission of motion to the wheels (W_{trs} , kW) and to the power take-off. It was assumed the transmission efficiency equal to 0.87.

As to the quality of tillage, the evaluation was based on the determination of: crop residues/biomass burying degree (BBD), soil surface roughness index (SRI), roughness reduction degree (RRD), clod-breaking index (CBI), cloddiness reduction degree (CRD) and seedbed quality index (SQI). They were measured in ten random points in each test.

The BBD is calculated from the values of the SCI determined before and after the implement tillage by means of the equation 4.

$$BBD = 100 \frac{SCI_{us} - SCI_{ts}}{SCI_{us}} \text{ [%]} \quad (4)$$

where SCI_{us} is the soil coverage index of untilled soil and SCI_{ts} is the index of tilled soil.

The SRI and the working depth were determined immediately after the passage of the implement, by means of a profile-meter. The sensor was a laser (Leica Geosystem Disto, Switzerland) moving on a horizontal rail placed perpendicularly to the tilled strip. Running along the rail, every 10 mm the sensor measures its distance from the ground, drawing the surface profile of the ground. A personal computer collects and processes the data. The surface profile is detected in the same point before and after the passage of each implement, obtaining the roughness indexes σ_{r1} and σ_{r2} (standard deviations of the detected heights series). In addition, were also calculated the average levels of surface before and after the tillage, and of the bottom of the tilled layer (after manually removing all the ground).

The RRD resulting from the secondary tillage is calculated as follows:

$$RRD = 100 \frac{\sigma_{r1} - \sigma_{r2}}{\sigma_{r1}} \text{ [%]} \quad (5)$$

The cloddiness was measured digging a 0.5 m side square trench to the working depth. The soil aggregates were removed from the trench avoiding any manipulation and left to dry for at least 20 min. Then they were divided into six size classes by means of hand-operated standard sieves and weighed. An index (I_{ai}), ranging from 0 for the biggest class to 1 for the smallest class, was attributed to each class. The cloddiness results as the percent of each size class mass referred to total mass of the sample. From the cloddiness, the CBI (I_a) is calculated as follows:

$$I_a = \sum_{i=1}^6 \frac{M_i \cdot I_{ai}}{M_t} \quad [\%] \quad (6)$$

where: $M_i \cdot I_{ai}$ is the product of the index assigned to a clod size class and the mass (kg) of ground belonging to the same class; M_t is the total mass of the sample (kg).

Comparing the CBI values observed before (I_{a1}) and after (I_{a2}) the secondary tillage, will provide the CRD by means of the equation 7.

$$CRD = 100 \frac{I_{a2} - I_{a1}}{I_{a2}} \quad [\%] \quad (7)$$

The quality of the seedbed is assessed basing on the cloddiness values observed after the passage of the implements. It is described by the SQI, by means of the Eq. (8):

$$SQI = \frac{M_{\phi \leq 10}}{M_{\phi \geq 10}} \quad (8)$$

where: $M_{\phi \leq 10}$ is the mass of the clods with diameter less or equal to 10 mm and $M_{\phi > 10}$ is the mass of the clods with a diameter over 10 mm (kg).

An instrumental system was used in the tests. A digital encoder, mounted on a rear wheel of the tractor measured wheel revolutions on a given distance, allowing calculation of travel speed under tractor self-displacement, working conditions and slip. Two mono-axial load cells, with full-scale respectively of 98 kN (tests with plough, subsoiler and combined cultivator) and 49 kN (tests with rotary harrow, disk harrow, seed drill and combined seeder), measuring the force of traction as follows. In traction tests, the load cell is lodged in a drawbar properly designed to protect it from transversal stresses and connecting a traction vehicle to the tractor-implement system. This is pulled, with gear in "neutral", at the same working speed set in the actual tillage with the same implement: this test executed with implement working will provide the gross traction force. Repeating the test with implement raised will provide the force required by the self-displacement of the tractor-implement system. The net fraction force will result as the difference between said values. Two torque meters were alternatively applied at the tractor's P.T.O. (full scale 3 kNm and 500 Nm respectively) depending on the characteristics of tested implements. Torque meters measure the P.T.O. torque and speed during the work, required for P.T.O. power calculation. The signals from the sensors were recorded at a scan rate of 10 Hz and collected by an integrated data acquisition system on the tractor (field unit). By means of a radio-modem, the data collected during the tests are transmitted to a support unit (a van equipped as a mobile laboratory) where real time test monitoring and data processing are made.

Working speeds and depths were set considering soil physical-mechanical characteristics and tillage possibility (according to water content). The plough was set in the in-furrow configuration. Three replications were made for each tractor-implement coupling. The experiment was carried out following a randomized distribution of the plots treated with each tillage method. The plots were 100 m long and 20 m wide. Eight tillage methods (Table 3) were considered in this study, including: four conventional tillage (CONT), two reduced tillage (RT), a minimum tillage one (MT) and a no-tillage one (NT). The parameters of field performances were measured for each implement and referred to the surface unit area (hectare). Consequently, the values of actual and operative working time, fuel consumption, energy requirement and energy losses for slip for each tillage method, resulted as the sum of the values measured for each of the implements used in it. As to the slip, for each implement, the average values of each replication were used to calculate power and energy losses. Regarding the tillage quality indexes (SCI, BBD, SRI, CBI and SQI), for each tillage method were considered the values observed after the intervention of the last implement. In the case of no-tillage, the quality indexes were assumed to be identical to those resulting from disk harrowing on untilled soil, given the similarity between the two operations.

The probability of statistically significant differences among tillage methods in terms of field performance parameters and tillage quality indexes was assessed by one-way analysis of the variance (ANOVA) and subsequent multiple pair-wise comparisons, performed by the Tukey's HSD test.

The significance of differences ($\alpha = 0.05$) among treatments was determined after the Bonferroni correction. The statistical procedure was executed by means of the software R (*R Core Team, 2013*). A Principal Component Analysis (PCA) was conducted using the software PAST (*Hammer et al., 2001*), to observe the ordering of treatments and to indirectly analyse which variable best contributes to differentiate treatments. Before the PCA, all variables were standardized (i.e., normalized to mean 0 and variance 1) to avoid problems caused by different units of measurement.

Table 3

Description of the eight tillage methods hypothesized

Type	Method	Operations	Implements
Conventional	CONT1	main tillage + seedbed preparation in a single pass	four-furrow reversible plough + rotary harrow + pneumatic seed drill
	CONT2	main tillage + seedbed preparation in a double pass	four-furrow reversible plough + offset disk harrow + pneumatic seed drill
	CONT3	main tillage + sowing with contemporary seedbed preparation	four-furrow reversible plough + combined seeder
	CONT4	main tillage + sowing with contemporary seedbed preparation	subsoiler + combined seeder
Conservation	RT1	main tillage + seedbed preparation in a single pass	subsoiler + offset disk harrow + pneumatic seed drill
	RT2	combined tillage in a single pass	combined cultivator + pneumatic seed drill
	MT	minimum tillage in two passes	offset disk harrow + pneumatic seed drill
	NT	no-tillage and direct sowing on untilled soil	pneumatic seed drill for direct seeding

RESULTS

Table 4 shows the average values of the parameter measured for each tractor-implement coupling. The highest requirements of energy per surface unit (MJ ha^{-1}) were observed for plough and rotary harrow, implements using considerable power at rather low speed. The energy required per volume unit of moved soil ($\text{MJ } 10^{-3} \text{ m}^{-3}$) was higher for the combined seeder and the rotary harrow (due to the higher power required by the tractor P.T.O.).

Table 4

Average values of the parameters describing the technical performances of the tested machines

Implement	M.U.	A	B	C	D	E	F	G	H	I
		untilled	ploughed	ploughed	ploughed	refined	untilled	untilled	untilled	untilled
Actual working speed	km h^{-1}	4.31	3.36	6.33	5.03	7.94	5.12	5.40	7.46	7.21
Working width	m	2.50	5.03	3.92	3.00	5.00	2.45	3.00	3.92	5.94
Working depth	m	0.41	0.15	0.19	0.10	0.04	0.37	0.35	0.16	0.04
Actual working time	h ha^{-1}	0.94	0.60	0.42	0.67	0.25	0.81	0.65	0.36	0.24
Operative working time	h ha^{-1}	1.44	0.69	0.69	0.89	0.38	1.10	0.81	0.63	0.37
Operative working capacity	ha h^{-1}	0.69	1.44	1.45	1.13	2.63	0.91	1.24	1.60	2.72
Fuel consumption per hour	kg h^{-1}	31.2	33.8	24.4	30.1	13.1	26.7	31.0	26.6	22.3
Fuel consumption per hectare	kg ha^{-1}	29.4	20.2	10.3	20.2	3.3	21.7	20.2	9.6	5.3
Force of traction	kN	60.5	11.9	19.0	19.1	9.7	43.5	52.7	30.0	16.5
Traction power	kW	73.4	11.1	33.4	26.7	21.4	61.8	78.9	62.1	33.1
P.T.O. speed	rad s^{-1}	-	107.2	-	108.2	97.0	-	-	-	104.4
Torque at the P.T.O.	Nm	-	860	-	635	38	-	-	-	70
Power at the P.T.O.	kW	-	92.2	-	68.5	3.7	-	-	-	7.3
Total engine power	kW	119	132.0	85.9	110.6	43.1	91.3	115.0	95.3	91.3
Energy per surface unit	MJ ha^{-1}	403	284	131	267	39	267	270	124	77
Energy per volume unit	$\text{MJ } 10^{-3} \text{ m}^{-3}$	99	191	68	268	-	73	76	77	-
Tractor slip	%	28.9	3.6	7.7	5.9	3.1	14.8	11.0	8.8	1.4
Energy losses	MJ ha^{-1}	125	38	21	39	6	62	55	23	10

Implement: A: reversible plough; B: rotary harrow; C: offset disk harrow; D: combined seeder; E: pneumatic seed drill; F: combined cultivator; G: subsoiler; H: offset disk harrow; I: pneumatic seed drill for direct sowing.

The plough showed the highest fuel consumption for surface unit (kg ha^{-1}), due to high operative working time. The higher values of fuel consumption per hour were obtained for the rotary harrow (33.8 kg h^{-1}), the plough (31.2 kg h^{-1}) and subsoiler (31.0 kg h^{-1}). The average force of traction required for tillage ranged from a minimum of 11.9 kN for the rotary harrow, to a maximum of 60.5 kN for the four-furrow plough, depending on the high variability of working width and depth. Such parameters can vary depending on the conditions of use of each tractor-implement coupling, which, within certain limits, can be managed with the aim of reducing power requirements and losses.

As to the quality of tillage, Table 5 shows the values of the parameters describing the effects of the implements on the soil. The best BBD was provided by the plough (96.6%). Good performance was also provided by the combined cultivator (86.6%), with two ranks of disks with opposite angles, which determine effective reversing of the soil and its mixing with surface biomass residues. The best SRI was produced by the combined seeder, the rotary harrow and the combined cultivator, due to the compacting action of the rear rollers. The best performances on CBI were provided by combined seeder and rotary harrow. Even for this parameter, the result of the combined cultivator is worth mentioning, considering that it operates a deep vertical soil crushing and a good soil breaking in a single pass. As for the SCI, a value higher than 15% was observed only with the offset disk harrow on untilled soil. Thus, the observed surface cover cannot be considered fully adequate for preventing soil erosion. Statistical analysis showed significant variations of soil quality values caused by the implements. Consequently, it was possible to perform, for each parameter, the Tukey's HSD post-hoc test and to separate the averages (i.e. the averages with the same letter are not significantly different) (Table 5).

Table 5

Average values of work quality parameters for each implement and results the Tukey's HSD test (the values followed by the same letter are not significantly different)

Implement type	u.m.	Reversible plough	Rotary harrow	Disk harrow	Combined seeder	Combined cultivator	Subsoiler	Disk harrow
Soil condition		untilled	ploughed	ploughed	ploughed	untilled	untilled	untilled
Coverage index	%	3.31 c	0.28 d	2.07 cd	0.55 d	11.57 b	10.74 b	17.08 a
Biomass burying degree	%	96.59 a	91.67 a	33.03 b	79.14 a	86.56 a	75.93 a	82.92 a
Surface roughness index	-	6.70 a	2.41 e	4.86 b	1.70 f	3.60 d	3.90 c	3.80 c
Roughness reduction degree	%	-	63.7 b	32.8 c	81.1 a	-	-	-
Clod-breaking index	-	0.35 d	0.81 a	0.60 c	0.84 a	0.66 b	0.61 c	0.64 bc
Cloddiness reduction degree	%	-	56.3 a	55.0 a	37.0 b	-	-	-
Seedbed quality index	-	0.20 g	0.87 c	0.43 f	1.08 b	0.82 d	0.75 e	1.47 a

Basing on the values reported in Table 4, we obtained the overall values of the parameter that describe the energy requirements for the eight composed tillage methods. Also in this case the results underwent ANOVA and subsequent Tukey's HSD test to separate the significant differences (Table 6).

Table 6

Technical performances of the eight tillage methods and results of Tukey's HSD test. The averages followed by the same letter do not differ significantly

Parameters	u.m.	CONT1	CONT2	CONT3	CONT4	RT1	RT2	MT	NT
Actual working time	h ha^{-1}	1.79 b	2.05 a	1.61 c	1.32 d	1.33 d	1.07 e	0.97 f	0.24 g
Operative working time	h ha^{-1}	2.51 b	3.20 a	2.33 c	1.69 e	1.88 d	1.49 g	1.63 f	0.37 h
Fuel consumption	kg ha^{-1}	52.9 a	53.4 a	49.6 a	40.4 b	33.9 c	25.0 d	22.5 d	5.3 e
Energy requirement	MJ ha^{-1}	725 a	704 a	670 b	537 c	440 d	307 e	286 e	77 f
Average tractor slip	%	11.9 b	11.8 b	17.4 a	8.5 cd	7.3 cd	9.0 c	6.9 d	1.4 e
Energy losses	MJ ha^{-1}	168 a	172 a	163 a	94 b	82 bc	67 c	52 d	10 e

Figure 1 shows the percent variations in energy requirements obtainable moving towards more CT, compared with CONT1. NT requires about 90% less energy. Moreover, MT and RT2 allow the highest savings of working time.

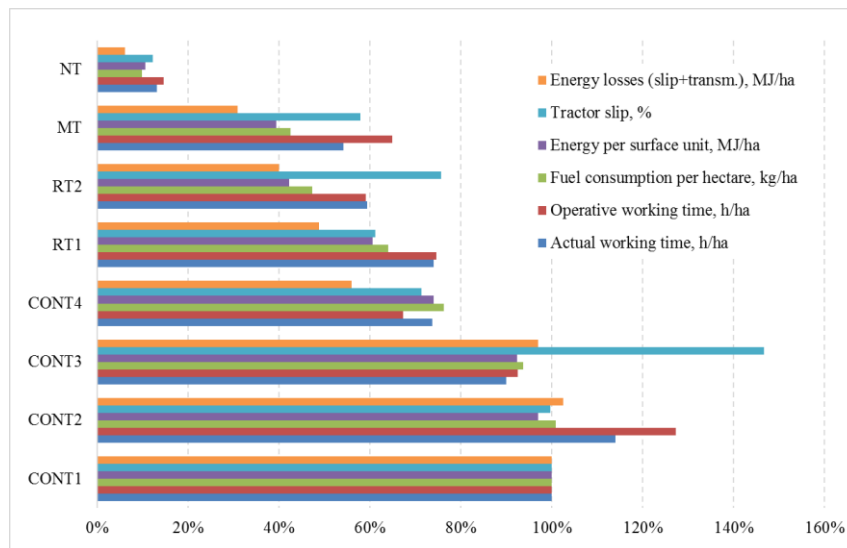


Fig. 1 - Percent reduction of the main technical performance from traditional to more conservation tillage methods compared with CONT1 (CONT2, CONT3, CONT4, RT1, RT2, MT, NT = tillage methods)

The PCA regarded both the energy parameters of Table 6 and the tillage quality indexes of Table 5 assuming, for each tillage method, the same indexes observed for the implements involved. A bi-plot graph (Figure 2) shows the results of the PCA, providing a comprehensive picture of the relationship among parameters and tillage methods.

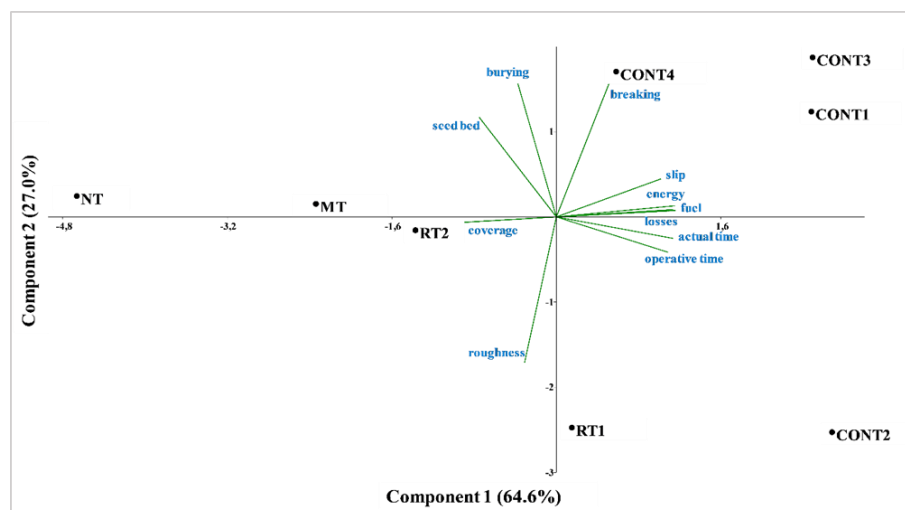


Fig. 2 - Biplot graph with the results provided by PCA

*Energy = energy requirement (MJ ha^{-1}); fuel = fuel consumption (kg ha^{-1}); actual time = actual working time (h ha^{-1}); operative time = operative working time (h ha^{-1}); losses = energy losses for slip and transmission (MJ ha^{-1}); burying = BBD (%); roughness = SRI; seedbed = SQI; coverage = SCI (%); breaking = CBI.
CONT1, CONT2, CONT3, CONT4, RT1, RT2, MT, NT = tillage methods*

The first two principal components (PC) explained 91.6% of the total variance (64.6% for PC 1 and 27.0% for PC 2). PC 1 was responsible for the separation between conventional and RT methods: this was especially evident for CONT1, CONT2 and CONT3 versus MT and NT, while CONT4, RT1 and RT2 were intermediate. NT was the most distant from all other methods. As to PC 2, the visible separation between CONT2 and RT1, compared to CONT1, CONT3 and CONT4 can be related to tillage quality aspects.

The Table 7 shows the PCA loading values, which define the discriminatory power of each variable in the principal component 1 and 2 and its position on the diagram. For instance, the PCA indicates that NT is characterized by low working times, fuel consumption, energy requirement and energy losses. These parameters are highly related to the conventional methods, especially CONT1, CONT2 and CONT3 (i.e. the methods entailing the use of the plough), characterized by the highest energy and fuel requirements and operative and actual working times. RT1, RT2 and CONT4 seem more similar in terms of operative parameters, as they clearly differ for the quality of tillage: CONT4 provides a better seedbed than RT1

(especially in terms of roughness index); the position of RT2 in the diagram is intermediate, (evident with respect to PC2). The methods NT, MT and RT2, different in terms of operative parameters (see position with respect to PC1), are more similar in terms of tillage quality, providing a medium quality of seedbed, with energy saving compared to conventional methods. In this context, the combined cultivator (RT2) seems to be an efficient implement, offering reduced energy requirements and good agronomic performance.

Considering what is conventional or conservation and the environmental conditions of the tests subject of this work, the question is if an indefinite adoption of conservation tillage method is sustainable or not in order to preserve soil fertility. In a medium or long-term perspective, it seems probable that the indiscriminate application of RT, MT or NT methods in a silty-clay soil could negatively affect its fertility. The natural ground settling and the traffic of machines, would determine progressive loosening of structure and increasing soil compaction, accelerated by the lack of organic matter (confined, when present, in the surface layer). Consequently, the soil could gradually lose its nutrients and the capability to store water in depth, becoming asphyxiated and inhospitable to plants' roots. Such a process can have different duration depending on the type of tillage, resulting longer in the case of more energetic techniques (RT1 and RT2) involving deeper interventions that, anyway, beyond relatively limited energy savings, would not allow the organic matter to be incorporated into the soil and to express its beneficial action towards soil structure.

The occurrence of this process could be prevented through a less rigid approach to soil preparation, based on the alternation of different tillage methods. This would lead to the definition of flexible tillage cycles whose duration and constitution (the whole of the interventions on the ground) will depend on the specific environments (e.g.: pedological and climatic characteristics, slope), on the needs of the types of crop to be carried out, on the possibility/willingness to apply crop rotation, on the available types of machines. The criteria that will guide the decision through such factors should be as simple as possible: for example, they could be represented by a few, easily measurable parameters, capable to provide wide and useful information. Soil resistance to penetration and moisture are probably the most comprehensive parameters, requiring simple measurements. The moisture provides the first indications on soil practicability and the risk of damaging its structure. Consequently, the value of field capacity can be assumed as the reference moisture value (30 - 35% for silty-clay soils). In general, with moisture above the field capacity, any soil manipulation should be avoided, but in case of urgency, such as a delayed sowing following a rainy period, MT or NT techniques could represent solutions for seedbed preparation with low impact on the soil. Below the field capacity, the possibility of choosing the tillage method will certainly be wider, but still depend on other soil actual conditions (mostly the structure and the organic matter). The cone index (c.i.) could be a useful parameter to describe the status of the soil. The availability of the trend of the c.i. along the layer explored by the roots, rather than its average value, will increase the quality of information. The diagram of Figure 3 shows the trend of the c.i. at increasing depth (0 cm up to 40 cm), in a silty-clay soil used for the tests described above.

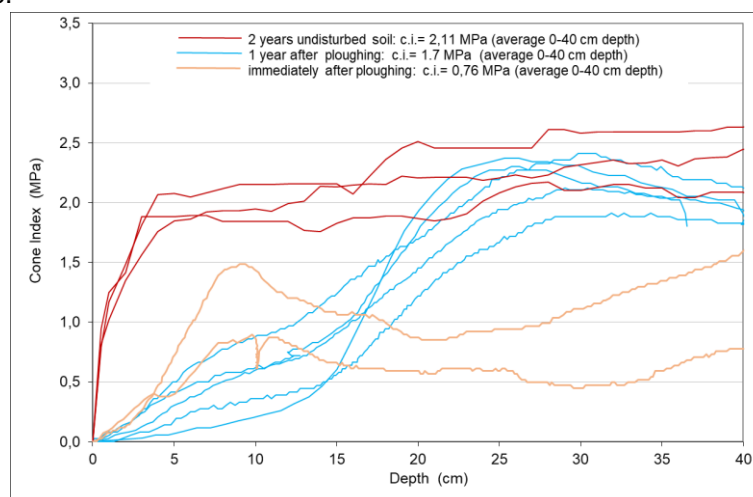


Fig. 3 - Different trend of the c.i. in the same silty-clay soil of the tests, depending on different types of intervention, in the 0 - 40 cm depth layer. All measurements were made with soil moisture between 22 and 24%

The measurements were made during prior CREA's test activities, by means of the described penetrometer. The curves of c.i. are grouped by colour and their shapes clearly differ by each other depending on the three operations to which they refer. After two years of spontaneous soil settling, without

transit of machines, but characterized by rainy weather, the c.i. increases up to over 2 MPa in the first 5 cm of depth. Increasing the depth, the c.i. increases very slowly. The resulting average value is 2.2 MPa. This means a high level of compaction interests the whole layer involved in crop growth. One year after medium depth ploughing, the general shape of the related curves changes showing the maximum (2.0 - 2.3 MPa) at 25 - 30 cm of depth, in correspondence of the bottom of ploughing. In this case the c.i. increases, and in the 0 - 25 cm layer, the soil conditions remain good for the plants. The resulting average c.i. value is 1.7 MPa.

The measurements made immediately after the ploughing, show general lower c.i. values although the presence of big clods affects its trend that increase in the first 10 cm, then decreases and increases again, keeping however distant from the values of the previous cases. The average value is 0.76 MPa. The evolution of moisture and c.i. in the layer explored by the crop roots will suggest the most proper methods to be adopted with the purpose of maintaining the soil characteristics within a range of sustainability for the plants. At the same time, the resulting alternation of methods will allow reducing the overall energy requirements, compared to the continuous use of conventional tillage methods. The test results reported above can be a basis for formulating hypotheses of an integrated tillage system (based on annual cycles) for cereal cultivation and estimating the relative energy demands and the energy savings.

Table 8 shows an example of such an approach, showing the evolution of “cycle 1” followed by the beginning of “cycle 2”. The cycles have not predefined duration and alternation of methods, but evolve, adapting to the actual soil conditions described by c.i. and moisture. In the example, each cycle starts with a conventional technique (CONV1) and ends when the deterioration of soil conditions requires the conventional technique anew. The necessary information is provided by the average values of c.i., by the shape assumed by the curves of the c.i. vs. increasing depth, by the moisture, considering the reference values proposed for these parameters in Figure 3.

Table 8

Example of application of the integrated tillage system with reference to the silty-clay soil of the tests

Cycle	Year	Average cone index* (MPa)	Shape of cone index curves**	Moisture** * (%)	Tillage method adopted	Energy requirements (MJ ha ⁻¹)	Energy losses (MJ ha ⁻¹)
1	1	2.2	1	21	CONT	725	168
1	2	1.8	2	25	RT1	440	82
1	3	2.0	2	35	MT	286	52
1	4	2.2	2	34	MT	286	52
2	1	2.4	1	22	CONT	725	168

* the values reported must be compared with those reported in Figure 3 for that soil. ** The shapes of c.i. curves refer to the diagram of Figure 3, i.e.: “1”: long period of untilled soil, showing high c.i. values already from the first few centimetres, as described by the red curves; “2”: cone index gradually increasing to a maximum in correspondence of the tillage bottom at 25-30 cm, as described by the blue curves. “...n”: c.i. curves with different shapes can be observed depending on actual soil specific manipulations. *** The reference moisture value is the “field capacity”, around 35%

“Cycle 1” starts with CONV1, based on the ploughing, needed because of the high soil compaction level in the surface layer (average cone index: 2.2 MPa; shape of c.i. curve: 1) and lasts 4 years during which the tillage methods vary depending on the evolution of soil moisture and compaction. The moisture does not represent an obstacle to the ploughing. This operation allows the burial of the surface residues, which contribute to restore the organic matter and the structure of the soil. In the 2nd year, the c.i. (average: 1.8; shape: 2) and moisture testify of still good conditions in the first 25 - 30 cm of soil, with probable presence of tillage bottom. RT1 seemed suitable to break it, limiting the risk of water stagnation. In the 3rd and 4th years, the compaction progressively increased, but the high humidity did not allow significant interventions on the soil. Its preparation for the sowing could be done by MT. At the end of the 4th year, the compaction reached the initial level, requiring starting a new cycle, “Cycle 2”, with CONV1, to restore conditions favourable to plants’ growth. The overall energy requirement and losses of the “cycle 1” over 4 years can be estimated by means of the data of Table 6 for each implement. The sum of the annual energy requirements reported in Table 8 is equal to 1,737 MJ ha⁻¹. Adopting CONV1 over 4 years would result in 2,900 MJ ha⁻¹ energy requirements. The about 40% energy saving deriving from the comparison of these values is the consequence of lower overall energy requirements and of lower energy losses. The latter, calculated similarly to the requests, are equal to about 47% compared to CONV1 repeated over 4 years. The lower relative weight of the losses on the global energy balance testifies a progress toward the optimization of the energy use. The results of such calculations probably overestimate the actual achievable benefits,

because indefinitely repeating CONV1 would keep the soil in such conditions that the requirements and losses of energy are lower than those used as reference for the comparison just above.

CONCLUSIONS

This study evaluated the effects of the adoption of eight tillage methods (four conventional, CONT, and four conservative CT methods) on energy requirements and tillage quality in a silty-clay soil. The results showed that CT (specially NT, MT and RT2) allow to achieve significant energy savings (up to 89%), working time reduction (up to 85%) and a satisfactory quality of tillage, compared to CONV1, thus widening the range of possible options for the farmers. Aiming at preserving the soil fertility, the commonly spread distinction between the meanings of CONT and CT gets less rigid, in relation to the characteristics and needs of the soil in question, as in the case of the silty-clay soil of this study. In general, conservation and conventional tillage methods (according to their common definition) should not be considered antithetical and adopting the former or the latter should not be the consequence of ideological, definitive choices, but should derive from the continuous evaluation of actual soil conditions, defining, each time, the more proper type of intervention. This results in the alternation of different tillage methods, according to flexible integrated tillage system, with variable duration, in which the benefits of both conventional and conservation methods are integrated in a compromise solution that should allow achieving an overall reduction of energy requirements compared to conventional methods and maintaining soil fertility at a satisfactory level during time.

REFERENCES

- [1] De Laune P.B., Sij J.W., (2012), Impact of tillage on runoff in long term no-till wheat systems, *Soil & Tillage Research*, vol.124, pp.32-35;
- [2] Fanigliulo R., Biocca M., Pochi, D. (2017), Evaluation of traditional and conservation tillage methods for cereal cultivation in central Italy, *Chemical Engineering Transactions*, vol.58, pp.211-216;
- [3] Fanigliulo R., Biocca M., Pochi, D. (2016), Effects of six primary tillage implements on energy inputs and residue cover in Central Italy, *Journal of Agricultural Engineering*, vol.47 (3), pp.177-180;
- [4] Fedrizzi M., Sperandio G., Guerrieri M., Pagano M., Costa C., Puri D., Fanigliulo R., Bazzoffi P., (2015), Economic competitiveness gap related to the application of the GAEC standards of cross-compliance on farms: Evaluation methodology, *Italian Journal of Agronomy*, vol.10(s1): 696p.;
- [5] Godwin R.J., (2007), A review of the effect of implement geometry on soil failure and implement forces, *Soil & Tillage Research*, vol.97, pp.331-340;
- [6] Hammer O., Harper D.A.T., Ryan P.D., (2001), PAST: Paleontological Statistics Software Package for Education and Data Analysis. *Palaeontologia Electronica*, vol.4 (1), pp.1-9;
- [7] Lal R., Reicosky D.C., Hanson J.D., (2007), Evolution of the plough over 10.000 years and the rationale for no-tillage farming, *Soil & Tillage Research*, vol.93, pp.1-12;
- [8] McLaughlin N.B., Drury C.F., Reynolds W.D., Yang X.M., Li Y.X., Welacky T.W., Stewart G., (2008), Energy inputs for conservation and conventional primary tillage implements in a clay loam soil, *Transactions of the ASABE*, vol.51 (4), pp.1153-1163;
- [9] Pochi D., Fanigliulo R., Pagano M., Grilli R., Fedrizzi M., Fornaciari L., (2013), Dynamic-energetic balance of agricultural tractors: active systems for the measurement of the power requirements in static tests and under field conditions, *Journal of Agricultural Engineering*, vol.44, pp.415-420;
- [10] Pochi D., Fanigliulo R., (2010), Testing of soil tillage machinery, In: *Soil Engineering*, Vol. 20, "Soil Biology" Book Series. Springer, Berlin, Germany, pp.147-168, ISBN: 978-3-642-03680-4;
- [11] R Core Team, (2013), *R: A language and environment for statistical computing*. R Foundation for Statistical Computing, Vienna, Austria. Available at: <http://www.R-project.org/>; accessed 10/6/2016;
- [12] Townsend T.J., Ramsden S.J., Wilson P., (2016), How do we cultivate in England? Tillage practices in crop production system, *Soil Use and Management*, vol.32, pp.106-117;
- [13] ***ASABE Standards, (2004), S313.3: *Soil Cone Penetrometer*, St. Joseph, Michigan, USA;
- [14] ***ASABE Standards, (2005), EP291.3: *Terminology and Definition for Soil Tillage and Soil-Tool Relationships*, St. Joseph, Michigan, USA;
- [15] ***EC Standard, (2013), EN 590: *Automotive Fuels-Diesel-Requirements and Test Methods*, Brussels.

TECHNIQUE FOR CALCULATING THE RESULTANT FORCE AND MOMENT OF SOIL RESISTANCE TO CUTTING BY BLADE OF ROTARY TILLAGE TOOL

/

МЕТОДИКА РАСЧЕТА РЕЗУЛЬТИРУЮЩЕЙ СИЛЫ И МОМЕНТА СОПРОТИВЛЕНИЯ ПОЧВЫ РЕЗАНИЮ ЛЕЗВИЕМ ЛОПАСТНОГО РОТАЦИОННОГО РАБОЧЕГО ОРГАНА

Prof. PhD. Eng. Sc. Akimov A.P.^{*)}, Asst. Prof. PhD. Eng. Sc. Konstantinov Y.V.,
Asst. Prof. PhD. Stepanov A.V.

Chuvash State Agricultural Academy / Russia
E-mail: for.antonstep@gmail.com

Keywords: rotary tools, vane, soil cutting, resultant resistance force, resultant resistance moment.

ABSTRACT

The objective of this study was to develop a technique for calculating the resultant force and moment of soil resistance to cutting by the blade of the earlier proposed rotary tillage tool as functions of the rotation angle on the basis of the developed mathematical model of soil-blade interaction. The dependences taking into account the constructive and functional parameters were obtained and analyzed. It was shown that the blade is subjected to repeated loads during the soil cutting, so the equivalent resultant force of soil reactions acting on the blade changes its magnitude, direction and the point of action periodically with changing the rotation angle. The obtained formulas can be used both for carrying out the long-term strength analysis of the rotary tool and for optimizing its constructive and functional parameters. The proposed technique allows to simplify experiments for determining the rotary tool force characteristics and to reduce their number significantly. Thanks to the commonality of the assumptions it can be transferred mainly to other rotary tillage tools.

РЕЗЮМЕ

Целью данного исследования явилось создание методики расчета результирующего сопротивления почвы и результирующего момента сопротивления почвы резанию лезвием предложенного ранее лопастного ротационного рабочего органа в зависимости от угла его поворота на основе предложенной математической модели взаимодействия лезвия с почвой. Полученные зависимости учитывают влияние конструктивных и режимных параметров. Показано, что при резании почвы лезвие испытывает циклические нагрузки. Результирующая сил реакций почвы на лезвие периодически изменяет свою величину, направление и точку приложения. Полученные формулы можно использовать не только для расчета ротационного рабочего органа на длительную прочность, но также и для оптимизации его конструктивных и режимных параметров. Предложенная методика позволяет существенно упростить эксперименты по определению силовых характеристик рабочего органа и значительно уменьшить их объем. Благодаря общности основных исходных положений предлагаемая методика может быть в основном перенесена на другие ротационные рабочие органы.

INTRODUCTION

The problem of finding the resultant of soil reactions on a rotary tillage tool blade is up-to-date, since its solution allows not only to calculate the strength of the blade, but also to determine the rational values of its constructive and functional parameters.

Professor N. Nerli was one of the first who took into account a distribution of elementary soil reactions, when he determined the resultant of soil reactions on the blade of a flat disk, free rotating in soil (Nerli, 1929). Later, many researchers solved similar problems with different success (Sineokov G.N., 1949; Luchinskij N.D., 1977). The case of the PTO (power take-off) powered flat disk was researched (Medvedev V.I. et al., 1974), and the generalized mathematical theory of soil-disk interaction has been developed (Medvedev V.I. et al., 2001). This model allowed setting and solving the single criterion optimization problem of the disk constructive and functional parameters (Akimov A.P. et al., 2008) and the bicriterion one for the powered disk (Akimov A.P., Konstantinov Y.V., 2016; Akimov A.P., Konstantinov Y.V., 2017).

Directions of elementary soil reactions on the blade of a rotary tillage tool depend not only on the position of its instantaneous rotation axis, but also on the rotation angle. So the resultant of soil reactions on the blade and their resultant moment are functions of that angle.

When researchers determined the resultant soil resistance force to cutting by a rotary tiller blade, they did not take into account the distribution of elementary soil reactions on the blade and it did not allow them to calculate the values of resultant soil resistance and resultant moment of soil resistance at an arbitrary rotation angle value of the blade (Thakur T.C., Godwin R.J., 1989; Thakur T.C., Godwin R.J., 1990; Kalantari D., 2000). Some researchers have plotted the graphs of such dependences on the basis of special experiments (Chertkiattipol S., Niyamapa T., 2010; Niyamapa T., Chertkiattipol S., 2010; Matin M.A. et al., 2015).

As an alternative to existing rotary tillage tools for the purpose of improving the quality of soil treatment and simultaneously reducing its specific tilling energy, the rotary tillage tool (RTT) was proposed, which can be used for various agricultural operations (Medvedev V.I. et al., 1984, Akimov A.P. et al., 2015). The method to determine the resultant force and the resultant moment of soil reaction forces acting only on the surface of this rotary tillage tool depending on the rotation angle was proposed (Akimov A.P., Konstantinov Y.V., 2011; Akimov A.P. et al., 2012; Akimov A.P. et al., 2017). But the soil reactions on the RTT blades have not been taken into account.

The major objective of this study was to develop a technique for determining the resultant force and resultant moment of soil resistance to cutting by a RTT straight rotary blade, which takes into account the distribution of elementary soil reactions and allows determining dependences of these characteristics upon the RTT rotation angle.

MATERIALS AND METHODS

The RTT consists of the flange, to which four identical flat vanes are attached. These vanes are quarters of plate, bounded by an ellipse. The blades of the vane small semi-axes are located in a vertical plane, and the vanes constitute some angle with it. The projection of all the vanes on the plane is a circle of radius r , equal to the small semi-axis of the ellipse. A model sample of the RRT and the RRT row on a shaft of rotary plough are shown in Fig. 1 a, b.

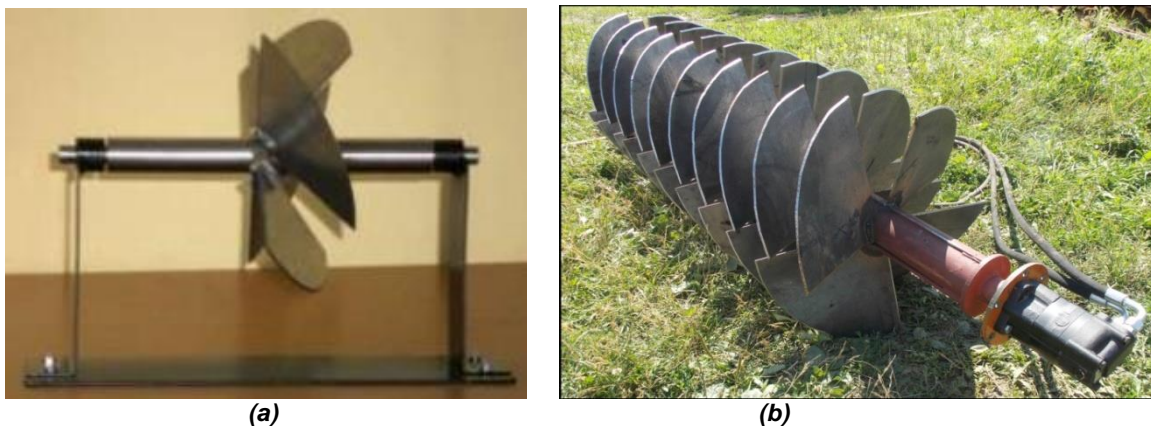


Fig. 1 – A model sample of the RRT (a) and the RRT row on a shaft of rotary plough (b)

This rotary tool can be used also in other rotary machines, which perform various agricultural operations. It can effectively work as a furrow opener in seeders (Medvedev V.I., Kazakov Y.F., 1984), as a ridger in rotary cultivators (Leshhankin A.I., 1991) and as an active coulter (power-take-off driven) in ploughing units (Chatkin M.N., 1990).

For calculating the RTT strength and optimizing the process of its operation it is necessary to develop a mathematical model of the RTT interaction with soil and, in particular, to determine the resultant force of soil resistance to cutting by this rotary tool.

Let us assume that a tillage machine or a unit moves rectilinearly with a constant speed v_0 , the RTT rotates around the rotor axis with a constant angular velocity ω and its blades during work plunge to a maximal depth h into homogeneous soil. The RTT operating regime is characterized by two constant dimensionless parameters: by the ratio of rotor peripheral speed to forward velocity of the tillage machine (kinematic parameter) $\lambda = \omega r / v_0$ and the maximal relative depth $\xi = h / r$.

The minor semi-axis blade of a RTT vane cuts the soil, performing a plane-parallel motion in a vertical plane. In the Oxz coordinate system with the origin O on the RTT axis of rotation and uniformly moving with the RTT, the position of minor semi-axis blade is set by rotation angle α from the vertical (Fig. 2, a). A soil cutting speed, varying along the blade edge, is defined by position of the RTT straight blade instantaneous centre of velocity, located at the point $C(0; a)$, $a = r/\lambda$. Let us also connect with the RTT another coordinate system $Ox'z'$, directing the axis Ox' on the major semi-axis of vane, and the axis Oz' – on its minor semi-axis.

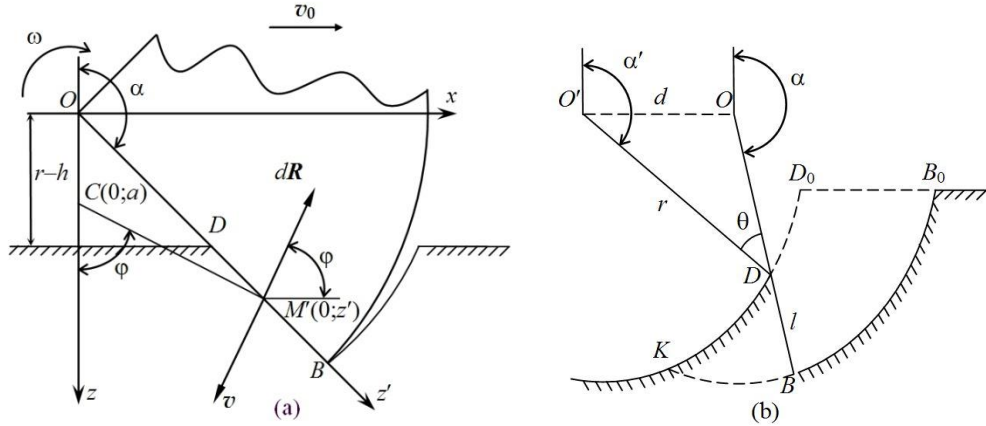


Fig. 2 – Diagram of soil cutting by the first (a) and a non-first (b) blade of the RTT

On an infinitesimal elementary segment of the blade cutting part, adjacent to a point $M(0; z')$, with length dz' , the elementary soil reaction force dR acts, which is directed opposite to the vector of absolute speed v of this point (Fig. 2, a). The magnitude of the force is equal to $dR = Q \cdot dz'$, where Q is the average specific force of cutting per unit length of the blade [N/m].

Let us denote by φ the angle between the force vector dR and the positive direction of Ox axis, then $\cos\varphi = (z-a)/[x^2+(z-a)^2]^{1/2}$, $\sin\varphi = x/[x^2+(z-a)^2]^{1/2}$; and $x=z'\sin\alpha$, $z = -z'\cos\alpha$ (Fig. 2, a). By integrating the equality $dR_x=Qdz'\cos\varphi$ on the segment of the blade cutting part and passing to the dimensionless variable $u = \lambda z'/r$, we obtain the formula for the horizontal component of the resultant of soil resistance to cutting (RSR)

$$R_x = -\frac{Qr}{\lambda} \int_{\lambda \cdot \xi_0}^{\lambda} \frac{(u \cos\alpha + 1) du}{\sqrt{u^2 + 2u \cos\alpha + 1}}, \quad (1)$$

where $\xi_0 = 1-l(\alpha, \xi)/r$, and $l(\alpha, \xi)$ is the length of cutting part of the blade corresponding to the rotation angle value α and the maximal depth of the blade equal to h [m].

Absolutely similarly the formula for the vertical component of this force is obtained:

$$R_z = -\frac{Qr}{\lambda} \int_{\lambda \cdot \xi_0}^{\lambda} \frac{u \sin\alpha du}{\sqrt{u^2 + 2u \cos\alpha + 1}}. \quad (2)$$

Let us choose as the positive direction of the moments of forces the direction coinciding with the RTT rotation direction, then the moment about the point O of an elementary force of soil resistance to cutting will be defined by the equality $dM_O = -z dR_x + x dR_z$ (Fig.2,a). By integrating this equality, we find the resultant moment of soil resistance to cutting (MSR)

$$M_O = -\frac{Qr^2}{\lambda^2} \int_{\lambda \xi_0}^{\lambda} \frac{u(u + \cos\alpha) du}{\sqrt{u^2 + 2u \cos\alpha + 1}}. \quad (3)$$

The integrals in formulas (1) – (3), depending on the variable u and on the parameters λ , ξ_0 , are easily calculated by the method of undetermined coefficients (Gradshteyn I.S., Ryzhik I.M., 2007). The obtained explicit expressions are cumbersome, and we use a way of sequential designations. Let us introduce three functions of two variables:

$$\begin{aligned} F_1(\alpha, u) &= (u^2 + 2u \cos\alpha + 1)^{0.5} \\ F_2(\alpha, u) &= \ln(u + \cos\alpha + F_1(u, \alpha)) \\ F_3(\alpha, u) &= 0,5(u - \cos\alpha) \cdot F_1(u, \alpha) \end{aligned} \quad (4)$$

Then the components of resultant of soil reactions and the resultant moment of soil resistance to cutting by the blade will take the following forms:

$$\begin{aligned} R_x &= -Qr \cdot (G_1(\alpha, \lambda, \zeta_0) \cos \alpha + G_2(\alpha, \lambda, \zeta_0) \sin^2 \alpha) / \lambda, \\ R_z &= -Qr \cdot (G_1(\alpha, \lambda, \zeta_0) - G_2(\alpha, \lambda, \zeta_0) \cos \alpha) \sin \alpha / \lambda, \\ M_O &= -Qr^2 \cdot (G_3(\alpha, \lambda, \zeta_0) - 0,5G_2(\alpha, \lambda, \zeta_0) \sin^2 \alpha) / \lambda^2, \end{aligned} \quad (5)$$

where the functions $G_i(\alpha, \lambda, \zeta_0) = F_i(\alpha, \lambda) - F_i(\alpha, \lambda, \zeta_0)$, $i = 1, 2, 3$.

The sequential expressions (4)–(5) have a simple structure, and are easily programmed. They allow calculating the values of R_x , R_z , and M_O at given values of α , λ and ζ_0 with the help of a computer.

The blade, which is the first to enter into soil (further the first blade), is represented in Fig. 2, a. From the diagram it follows that for the first blade $l(\alpha, \xi) = r + (r - h) / \cos \alpha$, hence for it

$$\zeta_0 = (\xi - 1) / \cos \alpha \quad (6)$$

For any blade entering into soil after the first one (further non-first blade), formula (6) is valid only at the initial stage of cutting. The condition $\zeta_0 = 1$ determines the angle of the beginning of soil cutting process by a blade $\alpha_0 = \arccos(\xi - 1)$. The cutting process by the first blade is completed at $\alpha = 2\pi - \alpha_0$ (Fig.2, a). Thus, formulas (4) – (6) determine the resultant force and the resultant moment of soil resistance to cutting by the first vane blade of RTT at the initial stage ($\alpha_0 \leq \alpha \leq 2\pi - \alpha_0$).

For a non-first vane blade of the RTT formula (6) is valid only until the moment of contact of the blade edge with the upper surface of the cut soil slice in the point D_0 (Fig.2, b). At the final stage of soil cutting the edge of the considered RTT blade crosses the upper surface of the slice in some point D of the trochoid formed by the previous blade. To this point there corresponds the angle α' measured from the vertical through the point O' which is located on the horizontal straight line passing through point O of the considered blade and lying at the distance r from the point D (Fig.2, b). When the RTT rotation axis moves from the position determined by the point O' to the position determined by the point O , the rotary tool rotates through the angle $2\pi/z_b + (\alpha - \alpha')$, and at the same time its rotation axis passes the $O'O$ distance equal to $d = [2\pi/z_b + (\alpha - \alpha')] \cdot r / \lambda$, where $z_b = 4$ is the number of rotary blades. The equality (7) follows from the theorem of sines for the triangle $O'DO$ (Fig.2, b):

$$[2\pi/z_b + (\alpha - \alpha')] \cdot \lambda^{-1} \cos \alpha + \sin(\alpha - \alpha') = 0 \quad (7)$$

As we can see from the Fig. 2, b, $r \sin(\alpha' - \pi/2) = (r - l) \sin(\alpha - \pi/2)$.

Hence:
$$\zeta_0 = \cos \alpha' / \cos \alpha \quad (8)$$

The angle α' is a function of the angle α . This function is defined implicitly by the transcendental equation (7). It is found by means of solving the equation (7) using one of numerical methods. The substitution of this function into the equality (8) allows us to express ζ_0 through the angle α . Thus, equalities (7), (8) and (4), (5) at the final stage of cutting determine the resultant force and the total moment of soil resistance to cutting by a non-first RTT blade as the composite functions of the angle α .

The point D_0 is located on the soil surface and upper surface of slice. Therefore, if we substitute $\alpha' = \arccos(\xi - 1)$ into equation (7), we obtain the transcendental equation for determining the angle $\alpha = \alpha_1$ of the completion of cutting process of the soil surface (initial stage) and the beginning of cutting process of the upper surface of soil slice (final stage). This equation is solved numerically for different values of α .

The value of angle $\alpha = \alpha_2$, corresponding to the completion of soil cutting process by a non-first blade of RTT in the point K of cycloids intersection at the bottom of a furrow (Fig. 2, b), is also determined by using the equation (7). At this point $\zeta_0 = 1$, $\alpha' = 2\pi - \alpha_2$, so we have $\sin \alpha_2 = (\pi - \alpha_2 - \pi/z_b) / \lambda$. This transcendental equation is also solved numerically. If we pass from angle α_2 to angle α'_g by $\alpha'_g = \alpha_2 - \pi$, then equation (7) transforms into the well-known equation, determining the location of crests at the bottom of a furrow during the work of rotary tiller (Sineokov G.N., Panov I.M., 1977).

RESULTS

It follows from formulas (1) and (3) that for the first blade the MSR and the horizontal component of RSR depend only on $\cos \alpha$, therefore their graphs versus α for the relative depth $\xi = 0.5$ and the values $\lambda = 3; 3.5$ and 5 are symmetric relative to the line $\alpha = \pi$ (Fig.3a, c). The component R_x is nonnegative, that is, the resultant of soil resistance to cutting is the driving forward force. The vertical component R_z (Fig. 3, b) is

negative for $\alpha < \pi$, that is, the RSR is the lifting up force and for $\alpha > \pi$ this component is positive, and the soil resistance to cutting is the deepening force. As the MSR is always non-positive, it slows down the RTT rotation, and for overcoming the moment of soil resistance, it is necessary to apply to the rotary tool the positive, equal in modulus, torque. Formulas (1)–(3) show, that for $a < r-h$ the maximal values of the MSR modulus and the RSR horizontal component are reached at the point π and are respectively equal to $P = Q \cdot h$ and to $M = P \cdot (r - h/2)$, and the vertical component of RSR at $\alpha = \pi$ is equal to zero. These expressions must be taken into account to carry out the strength analysis of the RTT and the empirical coefficient Q can be easily determined experimentally. It also follows from these formulas that at the vertical position of the RTT blade reactions of soil resistance to cutting are replaced by the single resultant with the magnitude P , directed horizontally towards the RTT motion and applied to the blade edge at the point lying at distance $h/2$ from its tip. The moduli of the resultant force components and the resultant moment of soil resistance to cutting monotonically increase with increase of the parameter ξ , but with increase of λ only the R_x and MSR moduli slightly increase, while the R_z modulus slightly decreases.

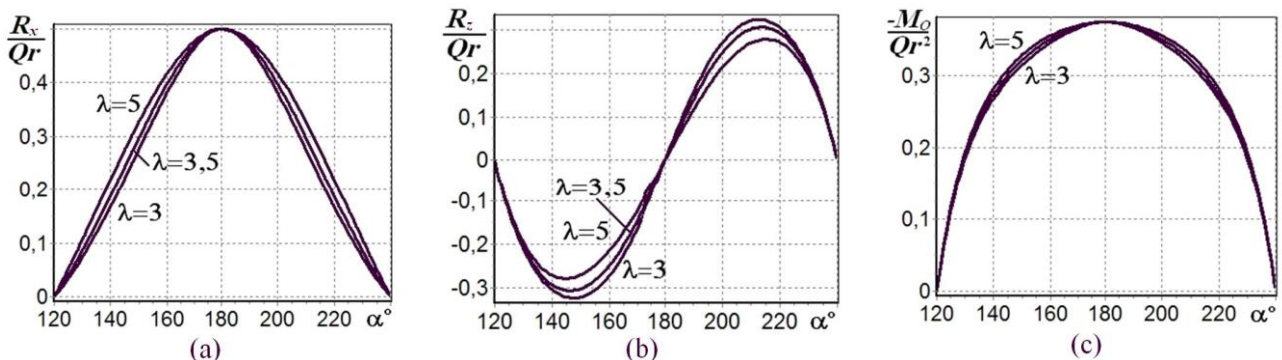


Fig. 3 – Components of the resultant resistance force of soil to cutting on the axis Ox (a), Oz (b) and the resultant resistance moment (c) versus angle α for the first blade

Fig. 4 shows the graphs of the resultant force components and the resultant moment of soil resistance to cutting by the edge of a non-first RTT blade versus the angle α and the parts of the corresponding graphs for the blade which is immediately following the non-first one at $\xi = 0.5$ and $\lambda = 3; 3.5; 5$.

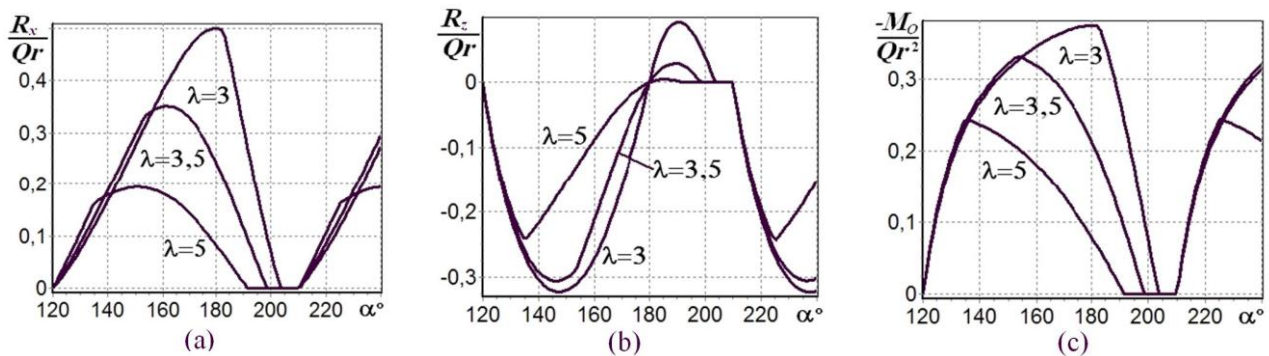


Fig. 4 – Components of the resultant resistance force of soil to cutting on the axis Ox (a), Oz (b) and the resultant resistance moment (c) versus angle α for a non-first blade

With increasing α the horizontal component R_x increases from zero monotonically and almost linearly at the initial stage of cutting, then continues to increase at the beginning of the final stage (for $\lambda = 3.5$ and 5) until it reaches the maximal value and then it decreases to zero again. The graph of R_x versus the angle α has the breaking point in a passage point from the first stage of cutting to the second one. Through the period $360^\circ/z_b = 90^\circ$ the blade of the following vane of the RTT begins to interact with the soil, therefore the specified change of the component R_x repeats again (Fig.4,a). The graph of the vertical component R_z (Fig.4,b) versus α is approximately a join of two halves of sinusoids of different amplitudes (for $\lambda = 3$ and 3.5). The amplitude of lifting action on the RTT at the initial stage of cutting is much more than the amplitude of deepening effect at the final stage. The MSR modulus monotonically increases with increase of the angle α at the initial stage of cutting, and it monotonically decreases at the final stage, reaching the greatest value at the breaking point of the graph of the MSR versus α (Fig. 4, c). With the increase of the ξ parameter, the

maximal values of MRC and the moduli of RSR components significantly increase, and with increase of λ they decrease, that is explained respectively by increase and by decrease of the linear dimensions of a soil slice.

Carrying out the long-term strength analysis of the RTT, it is necessary to take into account that during the interaction of the second and subsequent vanes with soil, the rotary tool is subjected to cyclic loads, the vibration amplitude of which is less than the corresponding greatest values of the forces and the moments, when soil is being cut by the blade of the first vane. At the large values of λ this distinction between the amplitudes is considerable.

The soil-cutting reactions by a blade are generally equivalent to the main vector of forces applied at point O with components, which are given by the expressions (1), (2) and to the couple with the main moment determined by the formula (3). This system of forces can be replaced with the single equivalent resultant force, applied at the point of blade edge, lying from the RTT rotation axis at the distance $r_0 = -|M_0|/[R \cdot \cos(\alpha + \psi)]$, where $R = (R_x^2 + R_z^2)^{0,5}$, and $\psi = -\arcsin(R_z/R)$ is the angle between the resultant and the positive direction of the Ox axis.

The graphs of the ratio r_0/r versus the angle α for the first blade at a relative depth $\xi = 0.5$ practically coincide for the values of $\lambda=3, 3.5$ and 5 (Fig. 5, a). For $\alpha < \pi$ the distance r_0 monotonically decreases from the greatest value $r_0 = r$ at the moment of contact of the blade edge with the soil surface to the least value $r_0 = r - h/2$ at $\alpha = \pi$, and then increases to the value equal to r at the moment, when the edge goes out from soil. On the contrary, the modulus of the resultant R , almost not depending on the parameter λ , at the above mentioned values of ξ and λ , for $\alpha < \pi$ increases monotonically from the least value $R = 0$ to the greatest value P at the point π and then decreases again to zero for $\alpha > \pi$ (Fig. 5, b). The angle ψ , weakly depending on λ , decreases monotonically with increase of α according to an almost linear law (Fig. 5, c).

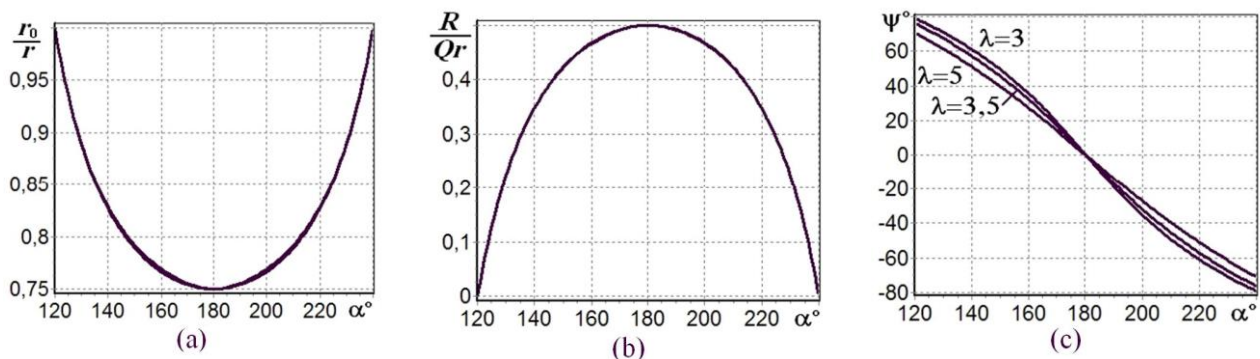


Fig. 5 – The relative distance from rotation axis to point of action of the resultant resistance force of soil to cutting (a), the RSR modulus (b) and the RSR tilt angle (c) versus angle α for the first blade

At $\alpha = \pi$ elementary forces of soil resistance to cutting acting on the blade are equally directed (horizontally) and equal in magnitude, so they are equivalent to the single resultant force with the point of action in the middle of the cutting part of the blade edge. If the instantaneous centre of velocity is located above the soil surface, then for the non-first blade it follows from the formulas (1) – (3), that $R_x = Qr(1 - \zeta_1)$, $R_z = 0$, $M_0 = -Qr^2(1 - \zeta_1^2)/2$, where $\zeta_1 = -\cos(\alpha'(\pi))$. Therefore, the ratio $r_0/r = (1 + \zeta_1)/2$.

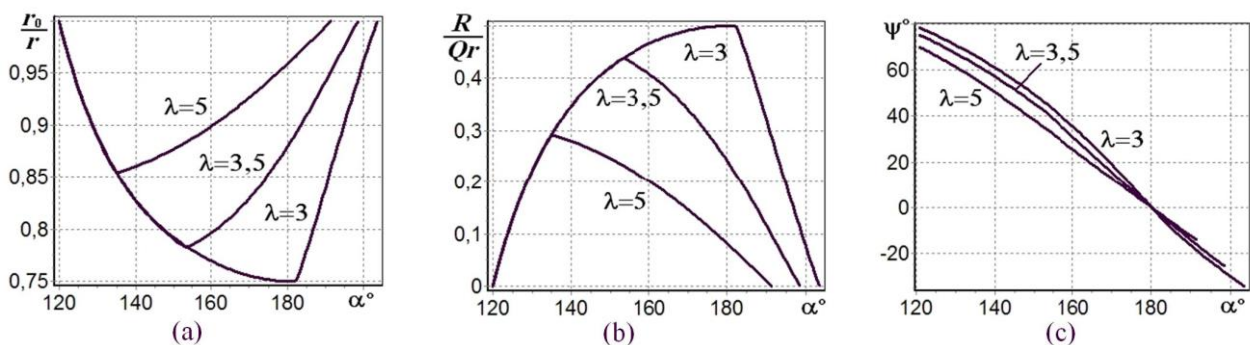


Fig. 6 – The relative distance from rotation axis to point of action of the resultant resistance force of soil to cutting (a), the RSR modulus (b) and the RSR tilt angle (c) versus angle α for a non-first blade

The graphs of the ratio r_0/r versus the angle α for a non-first blade plotted for the values of the ξ and λ parameters mentioned above show, that the ratio r_0/r decreases at the initial stage of cutting and increases on the final one (Fig. 6, a). When soil is being cut, the point of action of the equivalent resultant force changes its position from the most remote one from the RTT rotation axis at the beginning and at the end of the cutting process, to the nearest position at the transition point from the first stage of cutting to the second one at $\alpha=\alpha_1$. With increase of angle α the change character of the modulus of the resultant of soil cutting reactions by non-first blade is similar to the change character of the MSR (Fig. 6, b). The angle ψ monotonically decreases with increase of angle α (Fig. 6, c), and the graphs of ψ versus α practically coincide with the corresponding parts of graphs of the angle ψ for the first blade (Fig. 5, c).

CONCLUSIONS

With the help of the developed mathematical model of soil-blade interaction it is shown that the RTT blade is subjected to repeated loads during the soil cutting. The equivalent resultant force of soil reactions acting on the blade changes its magnitude, direction and the point of action periodically with changing the RTT rotation angle. The proposed technique allows calculating the resultant force and the resultant moment of soil resistance to cutting by the RTT blade as a function of the rotation angle and the RTT parameters.

It was found that the maximal values of the RTT driving force, of the MSR and of the RSR modulus monotonically increase with increasing relative depth ξ for any value of kinematic parameter λ . The angle, which the resultant resistance of soil to cutting constitutes with the positive direction of horizontal Ox axis, decreases almost linearly with increasing rotation angle α .

The obtained formulas can be used both for carrying out the long-term strength analysis of the RTT and for optimizing the RTT constructive and functional parameters.

The developed technique of calculation of the resultant force and the resultant moment of soil resistance to cutting by the RTT blade as functions of the rotation angle and the RTT parameters is valid also for the case of soil cutting by the straight parts (legs) of blades of rotary tillers, and also with some changes it can be transferred to calculating the force characteristics of blades of other rotary tillage tools. This technique allows simplifying the experiments necessary for determining the resultant force and the resultant moment of soil reactions on blades of rotary tillage tools and reducing the number of these experiments considerably.

REFERENCES

- [1] Akimov A.P., Konstantinov Y.V., (2011), A mathematical model of interaction of rotary vane tool and soil (Математическая модель взаимодействия ротационного лопастного рабочего органа с почвой), *Tractors and Farm Machinery (Тракторы и сельхозмашины)*, Issue number 5, pp. 29–35, Moscow/Russia;
- [2] Akimov A.P., Konstantinov Y.V., (2016), Rational choice of parameters of a disk-driver of the tillage unit (Рациональный выбор параметров диска-двигателя почвообрабатывающего агрегата), *Tractors and Farm Machinery (Тракторы и сельхозмашины)*, Issue number 10, pp. 29–33, Moscow/Russia;
- [3] Akimov A.P., Konstantinov Y.V., (2017), *Optimization of parameters and modes of functioning of disks of tillage machines and tools: monograph (Оптимизация параметров и режимов функционирования дисков почвообрабатывающих машин и орудий: монография)*, Cheboksary: FSBEU HE Chuvash State Agricultural Academy, 136 p., ISBN 978-5-906305-24-4, Moscow/Russia;
- [4] Akimov A.P., Konstantinov Y.V., Akvilyanova I.N., (2008), Criteria and optimum parameters of functioning of a cutting disk (Критерии и оптимальные параметры функционирования дискового ножа), *Tractors and Farm Machinery (Тракторы и сельхозмашины)*, Issue number 4, pp. 31–33, Moscow/Russia;
- [5] Akimov A.P., Konstantinov Y.V., Fedorov D.I., (2012) Calculation of driver power of rotary vane tool of tillage machine (Расчет мощности привода ротационного лопастного рабочего органа почвообрабатывающей машины), *Tractors and Farm Machinery (Тракторы и сельхозмашины)*, Issue number 5, pp. 27–32, Moscow/Russia;

- [6] Akimov A.P., Konstantinov Y.V., Fedorov D.I., Akvilyanova I.N. (2015), Influence of a rotational vane tool parameters on the furrow bottom roughness (Влияние параметров ротационного лопастного рабочего органа на неровность дна борозды), *Tractors and Farm Machinery (Тракторы и сельхозмашины)*, Issue number 12, pp. 21–23, Moscow/Russia;
- [7] Akimov A.P., Konstantinov Y.V., Medvedev V.I., (2017), *Kinematics and dynamics of rotational tillage machines and units: monograph (Кинематика и динамика ротационных почвообрабатывающих машин и агрегатов: монография)*, Cheboksary: Chuvash State University, 248 p., ISBN 978-5-7677-2588-5, Moscow/Russia;
- [8] Chatkin M.N., (1990), Recent problems of tillage mechanics. Ploughing unit with active coulters (Современные проблемы земледельческой механики. Пахотный агрегат с активными предплужниками), *Techniques in agriculture (Техника в сельском хозяйстве)*, Issue number 4, p. 33, Moscow/Russia;
- [9] Chertkiattipol S., Niyamapa T., (2010), Variations of torque and specific tilling energy for different rotary blades, *International Agricultural Engineering Journal*, Vol. 19, No. 3, pp. 1-14, Beijing/China;
- [10] Gradshteyn I.S., Ryzhik I.M., (2007), *Table of Integrals, Series and Products*, Elsevier/ Academic Press, Amsterdam, seventh edition, p. 93, sec. 2.252, Amsterdam/Netherlands;
- [11] Kalantari D., (2000), A mathematical model for estimation of rotary tiller power requirement, *World of Sciences Journal*, Vol. 1, Issue 7, pp. 86–93, Vienna/Austria;
- [12] Leshhankin A.I., Kolesnikov N.S., Chatkin M.N., Lyskov A.S., Sedashkin A.N., Ikomasov D.S., (1991), *Rotary cultivator-ridger (Фрезерный культиватор-гребнеобразователь)*, Patent, No. 1679980, Russia;
- [13] Luchinskij N.D., (1977), Some questions of tillage mechanics (Некоторые вопросы земледельческой механики), *Proceedings of VIM*, Vol. 75, pp. 3–77, Moscow/Russia;
- [14] Matin M.A., Fielke J.M., Desbiolles J.M.A., (2015), Torque and energy characteristics for strip-tillage cultivation when cutting furrows using three designs of rotary blade, *Biosystems Engineering*, Vol. 129, pp. 329–340, Amsterdam/Netherlands;
- [15] Medvedev V.I., Kazakov Y.F., (1984), Choice of constructive parameters and operating regimes of furrow openers of sod seeders (Выбор конструктивных параметров и режимов работы бороздовскрывателей дернинных сеялок), *Tractors and Farm Machinery (Тракторы и сельхозмашины)*, Issue number 9, pp. 21–22, Moscow/Russia;
- [16] Medvedev V.I., Kazakov Y.F., Chatkin M.N., Yermolaev N.V., (1984), *Furrow forming tool (Бороздообразующий рабочий орган)*. Patent, No. 1083940, Russia;
- [17] Medvedev V.I., Konstantinov Y.V., Akimov A.P., (2001), The generalized mathematical model of interaction of a cutting disk with soil (Обобщенная математическая модель взаимодействия дискового ножа с почвой), *Tractors and Farm Machinery (Тракторы и сельхозмашины)*, Issue number 2, pp. 34–37, Moscow/Russia;
- [18] Medvedev V.I., Vedeneev A.I., Akimov A.P., (1974), Method of calculation of a driving force of a flat disk-driver (Методика расчета движущей силы на плоском диске-движителе), *Tractors and Farm Machinery (Тракторы и сельхозмашины)*, Issue number 8, pp. 18–20, Moscow/Russia;
- [19] Nerli N., (1929), On the dynamic advantage of the rotating coulter (Sul vantaggio dinamico del coltro rotante), Pisa: Pacini Mariotti, 10 p., Pisa/Italy;
- [20] Niyamapa T., Chertkiattipol S. (2010) Development of blades for rotary tiller for use in Thai soils, *Journal of Food, Agriculture & Environment*, Vol. 8, Issue 3 & 4, pp. 1336-1344, Helsinki/Finland;
- [21] Sineokov G.N., Panov I.M., (1977), Theory and design of tillage machines (Теория и расчет почвообрабатывающих машин), М.: *Mashinostroenie*, 328 p., Moscow/Russia;
- [22] Sineokov G.N., (1949), Disk tools of tillage machines (Дисковые рабочие органы почвообрабатывающих машин), М.: Mashgiz, 86 p., Moscow/Russia;
- [23] Thakur T.C., Godwin R.J., (1990), The mechanics of soil cutting by a rotating wire, *Journal of Terramechanics*, Vol. 27, Issue 4, pp. 291–305, London/Great Britain;
- [24] Thakur T.C., Godwin R.J., (1989), The present state of force prediction models for rotary powered tillage tools, *Journal of Terramechanics*, Vol. 26, Issue 2, pp. 121–138, London/Great Britain.

NUMERIC MODEL OF THE GRAIN MIXTURE FLOW IN A CYLINDRICAL SIEVE WHICH REVOLVES AROUND THE INCLINED AXIS

/

ДОСЛІДЖЕННЯ РУХУ ЗЕРНОВОЇ СУМІШІ В ЦИЛІНДРИЧНОМУ РЕШЕТІ, ЩО ОБЕРТАЄТЬСЯ НАВКОЛО НАХИЛЕНОЇ ОСІ

Lect. Ph.D.Eng. Naumenko M., Lect. Ph.D.Eng. Sokol S., Lect. Ph.D. Eng. Filipenko D.,

Lect. Ph.D. Eng.Guridova V., Prof. Ph.D. Agri.Sci. Kharytonov M.

Dnipro State Agrarian and Economics University, Faculty of Agrarian Engineering / Ukraine;

Tel: 0973456227; E-mail: envteam@ukr.net, S.Yefremovast. 25, Dnipro, Ukraine

Keywords: grain heap, cylindrical sieve, mathematical model

ABSTRACT

A mathematical model of a grain mixture interaction with a cylindrical sieve was proposed. Two options of the model were considered: the axis of the cylindrical sieve rotation is horizontal; the axis is inclined to the horizon at a certain angle.

The calculation scheme of the "a grain heap – a sieve" system assumes that the grain mixtures move integrally affected by the forces of interaction with the sieve, which arise on the contact surface. The forces of weight and the centrifugal forces, which arise during the rotation, also affect the integral motion of the grain mixtures. It is assumed that the consumption of the mixture at the inlet of the sieve is equal to the total grain consumption during the separation and the removed impurities.

The differential equations which describe the motion of the heap along a cylindrical sieve were obtained. These equations can be used both to substantiate the geometric and kinematic characteristics of the sieve, and to choose the rational operating mode.

The graphic illustration of numerical solution of differential equations for a concrete example was given. It allows determining the position of the grain heap in the sieve at any time.

РЕЗЮМЕ

Запропонована математична модель взаємодії зернової суміші з барабаном при очищенні зерна. Розглянуті варіанти для випадків, коли вісь обертання барабана є горизонтальною та для осі нахиленої до горизонту під деяким кутом. Розрахункова схема системи «зерновий ворох – решето» передбачає, що масив зернової суміші рухається як єдине ціле під дією сил взаємодії з решетом, які виникають на контактній поверхні, сил ваги та відцентрових сил, що виникають при обертанні. Приймається, що витрата суміші, що потрапляє в решето дорівнює сумарній витраті зерна при сепаруванні та домішок, які видаляються з масиву під час очистки.

Виведені диференціальні рівняння, що описують рух вороха по циліндричному решету, які можуть бути використаними як при обґрунтуванні геометричних і кінематичних характеристик решета, так і при виборі раціонального режиму його роботи.

Наведена графічна ілюстрація чисельного розв'язку диференціальних рівнянь для конкретного прикладу, яка дозволяє в будь-який момент часу визначати положення зернового вороха в решеті.

INTRODUCTION

Grain production has the biggest impact on the supply of food to the population and the development of forage resources for several agrarian branches (Matveev et al, 2016). The creation of new machines is mostly aimed at improving conventional principles, making basic constructions more complex (Awgichew A., 2017; Werby R., 2010). The grain postharvest cleaning and separation problem is new challenge for implementing advanced technologies and creating next-generation grain cleaners (Linenk et al, 2012). Introducing new grain crops production technologies require high performance of grain cleaning and its compliance with the standards of cleanliness (Nesterenko et al, 2017). It is impossible to improve postharvest cleaning and separation of grain without implementing advanced technologies and creating next-generation grain cleaners (Саров & Shepelev, 2010; Jing Z., 2013). There were several attempts to solve the problem at hand by optimizing the rational set of particular operations and parameters of grain cleaners

that determine the sequential and step-by-step efficient cleaning schemes (Eskhozhin et al, 2016; Tyschenko et al, 2010). Outdated grain cleaners have been replaced by new ones for many years, since no significant progress has been made in the design of new efficient grain cleaners of local manufacture or the development of improved grain cleaning techniques (Li et al. 2009; Mingjie et al, 2012). It is necessary to improve separation of grain and create next-generation grain cleaners (Liang et al 2016). Dynamics of corn cleaning still remains a complex problem. The commonly used approaches on particle dynamics and trajectory tracing and high-speed photography was adopted to quantify the cleaned grain (Li J. et al., 1997; Wenqing et al., 2001; Wenqing et al., 2002). The mainstream efforts of research are mostly of parameterized characteristics, e.g., adjusting physical parameters of processed materials and changing construction and motion to illustrate its cleaning performances (Li H. et al., 2009).

The goal of this work is to develop a mathematical model for the interaction of a grain heap with a drum, which can provide a study of the dependence of the sieve performance on the kinematic and geometric characteristics of the system.

MATERIALS AND METHODS

The research of the grain motion in a cylindrical sieve which rotates around the axis is important for substantiating its geometric and kinematic characteristics. These characteristics are necessary to maintain the predetermined operating modes and the throughput of the drum during the separation. The common approach to the calculation scheme "grain heap - a drum" has not been found yet concerning the interaction of the grain mixture with the surface of the cylindrical sieve. In one case the grain heap is considered as "air-fluidized medium" (Kharchenko S., 2014). In other cases, it can be characterized as a bulk material (Pershin et al, 2009). It was described the movement both homogeneous and heterogeneous, granular media, the vibro viscous factor of which is differently dependent on one of the spatial coordinates. The hydrodynamic theory describes the standard vertical movement of pseudo rarefied mixture on the inner surface of the cylindrical vibratory centrifugal sieve, which rotates at a constant angular velocity around a vertical axis (Tyschenko et al, 2010). The application of the hydrodynamic theory is impossible for cases in which the "air-fluidized medium" does not occur. In addition, there are some doubts regarding the exactness of models of the grain interaction with a sieve, in which the grain is loaded with a centrifugal force of inertia, which is defined by the angular velocity of the drum. For the moment it has not been mentioned how the model can be used to analyse the motion of the grain heap. In this respect, it is interesting to implement a stationary process of grain separation when the axis of the sieve rotation is horizontal. The scheme of forces acting on the grain heap in the sieve in the equilibrium state is shown in Fig. 1.

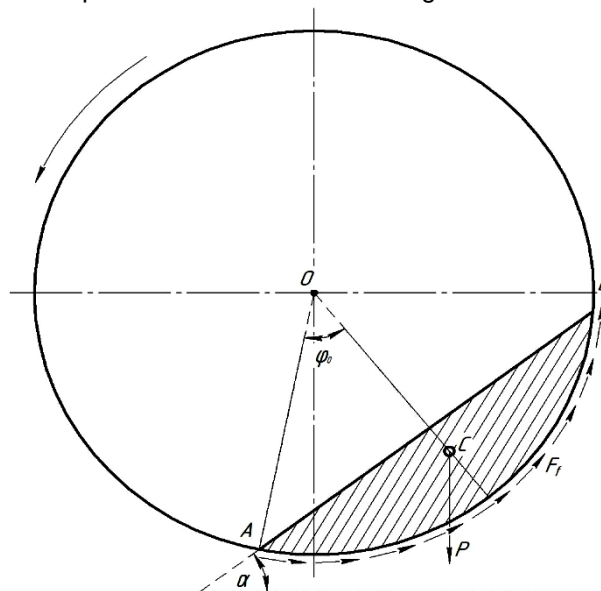


Fig. 1 - The scheme of forces acting on the grain heap in the sieve in the equilibrium state

In this case, the mixture in the sieve is in a state when the free surface of the heap is inclined to the horizon at an angle of natural slope.

For a sieve with horizontal axis of rotation, it is possible to implement a stationary grain separation process in accordance with the scheme shown in Fig. 2.

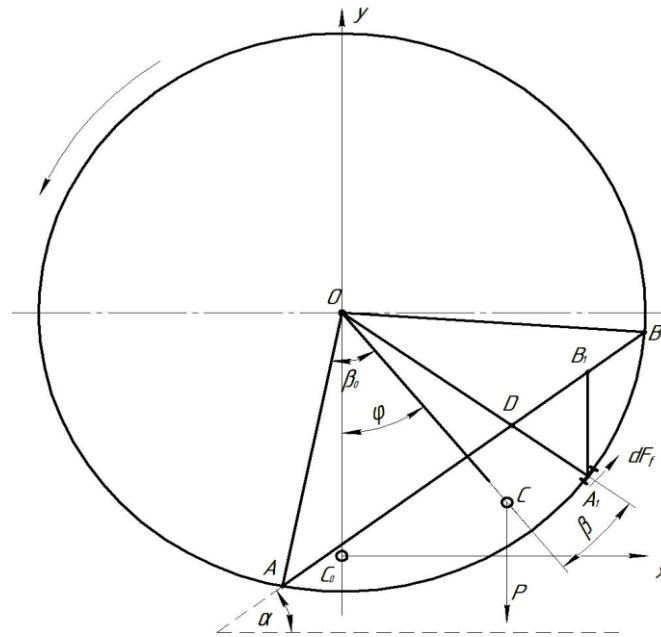


Fig. 2 - Scheme for analyzing the motion of a grain heap in a cylindrical sieve

The friction force Fm and the weight force P are distributed along the interaction area from below, when the material is slid in the sieve. It is assumed that the grain heap, the cross section of which is bounded by a chord AB above and an arc AB below, moves in a sieve with the rotation without deforming from the lower position, in which the axis of symmetry (OC in Fig. 1) occupies the vertical position OC_0 .

The differential equation of the rotational motion of the heap about the sieve axis has the form (Yablonsky and Nykyforova, 1966):

$$I_0 \ddot{\varphi} = M_0(F_f) - P \cdot OC \sin \varphi \quad (1)$$

where

I_0 – is the polar moment of inertia of the heap, the cross section of which is considered to be unchangeable, $kg \cdot m^2$;

$\ddot{\varphi}$ – an angular acceleration of the heap during the rotation, s^{-2} ;

$M_0(F_f)$ – the moment of friction forces that arise between the heap and the sieve about the sieve axis, $N \cdot m$;

P – the weight of the heap, N ;

OC – the distance from the centre of the sieve cross-section to the centre of the weight of the heap cross section, m ;

φ – an angle of rotation, rad .

In determining the frictional forces, we take into account that they will arise from the hydrostatic pressure of the heap on the sieve and from the centrifugal forces which act on the heap during the rotation.

The component of the friction forces, which depends on the hydrostatic pressure of the material at an arbitrary point A (Fig. 1), determined by the angle $(\varphi + \beta)$, is calculated as:

$$dF_{fp} = \gamma \cdot f \cdot H \cdot l \cdot ds \quad (2)$$

where γ – specific weight of the material, N/m^3 ;

H – the distance from point A_1 to the free surface of the heap cross section (A_1B_1 in Fig. 2);

l – the length of the sieve, m ;

ds – elementary section of the arc of the sieve cross section, in the centre of which is the point A_1 , m .

Taking into account that $ds = R d\beta$, for frictional force on the section ds , we obtain:

$$dF_{fp} = f \cdot \gamma \cdot H \cdot l \cdot R \cdot d\beta \quad (3)$$

For the height H of the triangle ADB we obtain:

$$H = R \left(1 - \frac{\cos \beta_0}{\cos \beta} \right) \cdot \frac{\cos \beta}{\cos \varphi} = R \left(\frac{\cos \beta}{\cos \varphi} - \frac{\cos \beta_0}{\cos \varphi} \right) = \frac{R}{\cos \varphi} (\cos \beta - \cos \beta_0) \quad (4)$$

Then

$$dF_{fp} = f \gamma l R^2 \left(1 - \frac{\cos \beta_0}{\sin \beta} \right) \cdot \frac{\cos \beta}{\cos \varphi} d\beta = \gamma f l R^2 \frac{\cos \beta - \cos \beta_0}{\cos \varphi} \quad (5)$$

The centrifugal force that falls on the arc ds is determined by the scheme shown in Fig. 3.

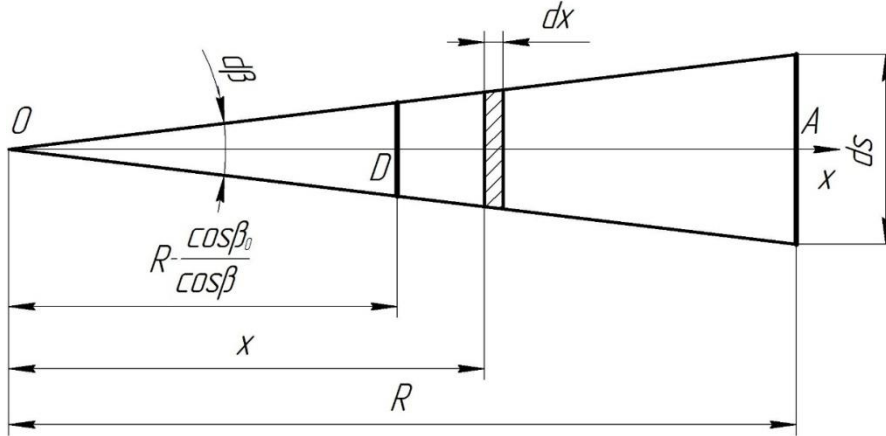


Fig. 3 - Scheme for determining the centrifugal force falling on the elementary arc ds

A centrifugal force acts on an element of mass with dimensions (in Figure 3 its cross-section is shaded):

$$\Delta dF_v = \frac{1}{g} \gamma l x d\beta dx \omega^2 x \quad (6)$$

Integrating this expression from point D to point A we obtain dF_v :

$$dF_v = \frac{1}{g} \int_{R \frac{\cos \beta_0}{\cos \beta}}^R \gamma l \omega^2 d\beta x^2 dx = \frac{1}{3g} \gamma l \omega^2 R^3 \left(1 - \frac{\cos^3 \beta_0}{\cos^3 \beta} \right) d\beta \quad (7)$$

Thus, the total frictional force that falls on a section of width ds is defined as

$$dF_f = f \gamma l R^2 \left[\frac{R \omega^2}{3g} \cdot \left(1 - \frac{\cos^3 \beta_0}{\cos^3 \beta} \right) + \frac{\cos \beta - \cos \beta_0}{\cos \varphi} \right] d\beta \quad (8)$$

For the moment of frictional forces, distributed over the interaction area of the heap with a sieve, it is obtained:

$$M_0(F_f) = f \gamma l R^3 \left\{ \frac{R \omega^2}{3g} \left[2\beta_0 - \sin \beta_0 \cos \beta_0 - \frac{\cos^3 \beta_0}{2} \left(\ln \left| \operatorname{tg} \left(\frac{\pi}{4} + \frac{\beta_0}{2} \right) \right| - \ln \left| \operatorname{tg} \left(\frac{\pi}{4} - \frac{\beta_0}{2} \right) \right| \right) \right] + 2 \frac{\sin \beta_0}{\cos \varphi} - 2 \frac{\cos \beta_0}{\cos \varphi} \beta_0 \right\} \quad (9)$$

According to the known specific weight of the bulk material γ , the square of the heap cross section S and the length of the sieve l , for the moment of the heap weight and for the moment of inertia of the heap about the sieve axis of rotation, respectively:

$$P \cdot OC \cdot \sin \varphi = \gamma R^2 \left(\beta_0 - \frac{1}{2} \sin 2\beta_0 \right) \cdot \frac{4}{3} \frac{R \sin^3 \beta_0}{(2\beta_0 - \sin 2\beta_0)} \cdot \sin \varphi = \gamma \cdot \frac{2}{3} R^3 \sin^3 \beta_0 l \cdot \sin \varphi \quad (10)$$

$$I_0 = \frac{\gamma l R^4}{g} \left(\beta_0 - \frac{1}{3} \sin 2\beta_0 - \frac{1}{12} \sin 4\beta_0 \right) \quad (11)$$

Substituting the expressions for the geometric characteristics of the heap cross section and for the load acting on the heap, after the obvious transformations of the formulas (9), (10) and (11) in equation (1) we obtain:

$$\frac{R}{g} \left(\beta_0 - \frac{1}{3} \sin \beta_0 - \frac{1}{12} \sin 4\beta_0 \right) \cdot \ddot{\varphi} =$$

$$= f \left\{ \frac{R\omega^2}{3g} \left[2\beta_0 - \sin \beta_0 \cos \beta_0 - \frac{\cos^3 \beta_0}{2} \ln \frac{\operatorname{tg} \left(\frac{\pi + \beta_0}{4 + \frac{\beta_0}{2}} \right)}{\operatorname{tg} \left(\frac{\pi - \beta_0}{4 - \frac{\beta_0}{2}} \right)} \right] + 2 \frac{\sin \beta_0}{\cos \varphi} - 2 \frac{\cos \beta_0}{\cos \varphi} \beta_0 \right\} -$$

$$-\frac{2}{3} \sin^3 \beta_0 \sin \varphi. \quad (12)$$

RESULTS

The differential equation (12) makes it possible to analyse the motion of a heap in a sieve, the axis of which is horizontal. The motion of the heap will be considered as composition of a rotational motion around the axis and translational along the x - axis, when the sieve is rotated about the axis, inclined to the horizon at angle ψ (Fig. 4).

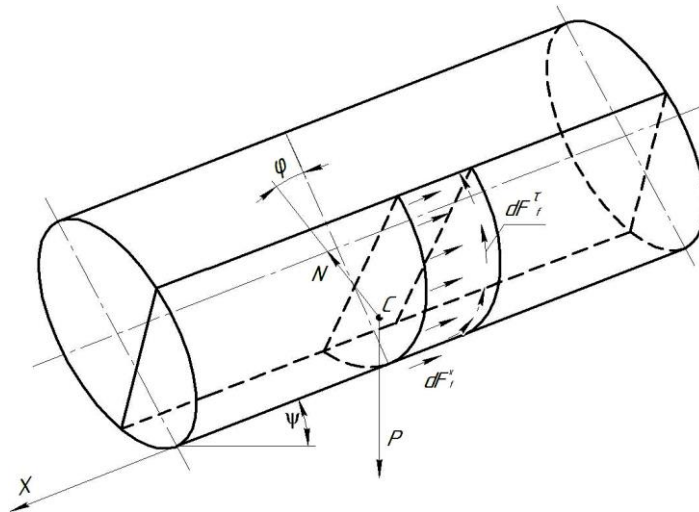


Fig. 4 - The scheme of frictional forces acting on the elemental volume of the heap in the sieve with an inclined axis of rotation to the horizon

The differential equation of rotational motion will have the form:

$$I_0 = M_0 (F_f^\tau) - P \cdot OC \cdot \sin \varphi \cos \psi \quad (13)$$

where ψ – an angle of inclination of the sieve, rad ; $M_0 (F_f^\tau)$ – moment of friction forces, $N \cdot m$.

The differential equation of motion of the heap along the sieve has the form:

$$m\ddot{x} = P \sin \psi - F_f^x \quad (14)$$

where m – mass of the heap, kg ; \ddot{x} – projection of acceleration on the x -axis; F_f^x – resultant frictional forces directed along the axis of the sieve, N .

Taking into account the information mentioned above, for differential equations of the heap motion we obtain:

- for the rotational component movement

$$\begin{aligned} & \frac{R}{g} \left(\beta_0 - \frac{1}{3} \sin \beta_0 - \frac{1}{12} \sin 4\beta_0 \right) \cdot \ddot{\varphi} = \\ & = f \left\{ \frac{R\omega^2}{3g} \left[2\beta_0 - \sin \beta_0 \cos \beta_0 - \frac{\cos^3 \beta_0}{3} \ln \left| \frac{\operatorname{tg} \left(\frac{\pi + \beta_0}{4 + \frac{\beta_0}{2}} \right)}{\operatorname{tg} \left(\frac{\pi - \beta_0}{4 - \frac{\beta_0}{2}} \right)} \right| \right] + 2 \frac{\sin \beta_0 - \beta_0 \cos \beta_0}{\cos \varphi \cos \psi} \right\} \times \\ & \times \frac{R\omega}{\sqrt{\dot{x}^2 + R^2 \omega^2}} - \frac{2}{3} \sin^3 \beta_0 \sin \varphi \cdot \cos \psi; \end{aligned} \tag{15}$$

- for the translational component motion of the heap along the axis of rotation

$$\begin{aligned} & \ddot{x} \frac{l\gamma R^2}{g} \left(\beta_0 - \frac{1}{2} \sin 2\beta_0 \right) = \\ & = f \gamma l R^2 \left\{ \frac{R\omega^2}{3g} \left[2\beta_0 - \sin \beta_0 \cos \beta_0 - \frac{\cos \beta_0}{3} \ln \left| \frac{\operatorname{tg} \left(\frac{\pi + \beta_0}{4 + \frac{\beta_0}{2}} \right)}{\operatorname{tg} \left(\frac{\pi - \beta_0}{4 - \frac{\beta_0}{2}} \right)} \right| \right] + 2 \frac{\sin \beta_0 - \beta_0 \cos \beta_0}{\cos \varphi \cos \psi} \right\} \times \\ & \times \frac{\dot{x}}{\sqrt{\dot{x}^2 + R^2 \omega^2}} + l\gamma R^2 + \left(\beta_0 - \frac{1}{2} \sin 2\beta_0 \right) \sin \psi. \end{aligned} \tag{16}$$

The considered mathematical model allows us to investigate the motion of the grain heap in the sieve during its rotation. The numerical solution of the system of differential equations, (15) and (16) is carried out by the Runge - Kutta method (Porshnev and Belenkova, 2005) according to the initial data given in the table 1.

Table 1

Output data to a numerical solution

R [m]	β_0 [rad]	ψ [rad]	f	g [m/s ²]	l [m]	φ_0 [rad]	ω_0 [rad/s]	V_0 [m/s]	Δt [s]
0.45	0.8	0.1	0.3	9.81	1.2	0	0	0	0.01

In integration it was assumed that the grain heap, the cross section of which is determined by the radius of the sieve R and the loading angle β_0 , moves from the rest state, with $\varphi = 0$; $\omega = 0$; $V = 0$.

The integration process with the step $\Delta t = 0.01$ s was completed at the passage of weight centre of the heap cross section along the entire length of the sieve ($l = 1.2$ m). The graphic illustration of the solution shown in fig.5 makes it possible to determine: the position of the centre of the sieve cross section along the sieve length for any moment of its movement (curve 1); the angle of deviation in the normal section of the sieve (curve 3); the angular velocity at any moment of time (curve 2).

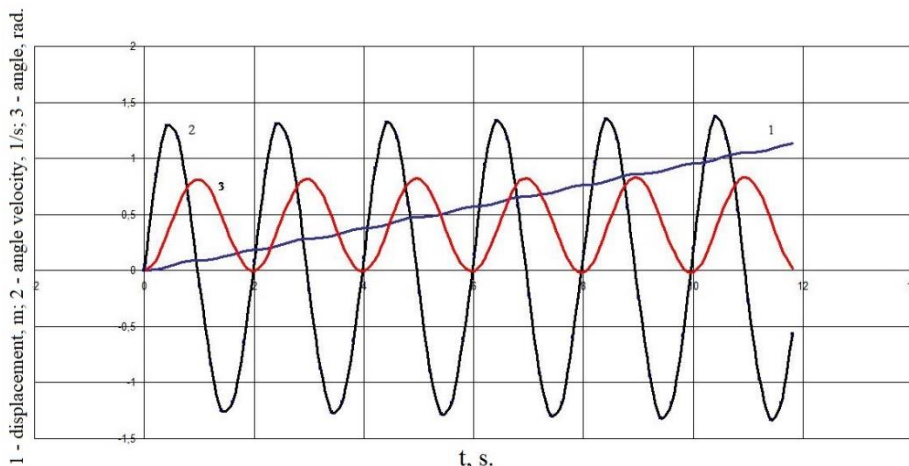


Fig. 5 - Kinematic characteristics of the grain heap during the interaction with the sieve

The numerical solution of the equations above, (15) and (16), allows, based on the analysis of the motion of the grain mixture in the sieve, to assign the most efficient operating mode for grain separation.

CONCLUSIONS

The mathematical model of interaction of the grain heap with a drum, which rotates around an axis inclined to the horizon, has been suggested.

The solution of differential equations of motion allows determining the speed and time of the egress of grain during the separation in a sieve.

The given mathematical model of a grain heap interaction with a drum can be used in substantiating the geometric and kinematic characteristics of the sieve, as well as in choosing a rational mode of its operation.

ACKNOWLEDGEMENT

The work has been funded by the Ukrainian Ministry of Education and Science.

REFERENCES

- [1] Awgichew A., (2017), Performance evaluation of the grain and chaff separation and cleaning machine. *International Journal of Scientific and Research Publications*, Volume 7, Issue 7, pp.2250-3153, ISSN 2250-3153;
- [2] Capov S. N., Shepelev S. D., (2010), Improving the effectiveness of grain harvesting and grain cleaning through coordination. *Achievements of Science and Technology in the Agro-Industrial Complex*, (12), pp.76–78, Moscow/Russia;
- [3] Eskhozhin D.Z., Nukesheva S.O., Capov S.N., Baishugulova S.K., Dikhanova M.B., (2016), A Theoretical Substantiation of a Grain Cleaner with a Compound Motion of the Operating Device, *International journal of environmental & science education*. vol.11, no.18, pp.11385-11392, Budapest/Hungary;
- [4] Jing Z., (2013), Design of New Grain Threshing Cleaning Device. *Journal of London University*, 1, 17, London/UK;
- [5] Kharchenko S.A., (2014), To the construction of a three-dimensional hydrodynamic model of a bubbly fluidized grain mixture along a structural vibrating screen. *Melitopol University Issues (Траци Мелітопольського університету)* 14, Vol.2, pp.80-85, Melitopol/Ukraine;
- [6] Li J., Zhao Y., (1997), Experiment and Computer Simulation of Tossing Motion of Agricultural Materials on Oscillating Sieve [J]. *Transactions of the Chinese Society Agricultural Engineering*. 13 (4), pp.46-65, Madison/Wisconsin;
- [7] Li H., Gong H., Yin W., (2009), Design of simulation strategy for corn cleaning on discrete element method. IFIP International Federation for Information Processing. Volume 293, *Computer and Computing Technologies in Agriculture*, Volume 1, eds. D.Li, Z.Chunjiang, (Boston: Springer), pp. 603–611, Boston / USA;
- [8] Liang Z., Li Y., Xu L., Zhao, Z. (2016), Sensor for monitoring rice grain sieve losses in combine harvesters. *Biosystems Engineering*, 147, pp.51–66;
- [9] Linenk, A. V., Tuktarov, M. F., Akruhin, S. V., (2012), Analysing the performance of the sieve boot driving gear in an experimental grain-cleaning rig with a linear motor. *Ulyanovsk State Agricultural Academy Journal (Вестник Ульяновской сельскохозяйственной академии)*, (2), 18, pp.97-100, Ulyanovsk/Russia;
- [10] Matveev, Y. V., Valieva, E. N., Kislov, O. V., Trubetskaya, A. G. (2016). Globalization and Regionalization: Institution Aspect. *IEJME-Mathematics Education*, 11(8), 3;
- [11] Mingjie L., Wei S., Jianguo C., (2012), Design of grain combine harvester cleaning overflow fan. *Journal of Agricultural Mechanization Research*. 8, pp.90–92, China;
- [12] Nesterenko A.V., Leshchenko S.M., Vasylovskiy O.M., Petrenko D.I., (2017), Analytical assessment of the pneumatic separation quality in the process of grain multilayer feeding. *INMATEH Agricultural Engineering*, Vol. 53, No. 3, pp.65-70, Bucharest/Romania;
- [13] Pershin V.F., Odnol'ko V.G., Pershina S.V., (2009.) Processing of bulk material in the drum-type apparatus (Обработка сыпучих материалов в аппарате барабанного типа), *Mashinostroyeniye (Машиностроение)*, 220 p., Moscow/Russia;

- [14] Porshnev S.V., Belenkova I.V., (2005), *Numerical methods of integration in Mathcad (Численные методы интеграции на основе Маткад)*, 464p., St. Petersburg/Russia;
- [15] Tyschenko L.M., Ol'shanskiy V.P., Ol'shanskiy S.V., (2010) *Hydrodynamics of grain separation (Гидродинамика сепарирования зерна)*, 174p., Kharkyv/Ukraine;
- [16] Yablonsky A.A., Nykyforova V.M. (1966), *Course of theoretical mechanics (Курс теоретической механики)*. Part. 1, 438p., Moscow/USSR;
- [17] Wenqing Y., Kutzbach H. D. (2002), Experimental Research on Cleaning Shoe with Circular Vibrating Sieve [J]. *Transactions of the CSAE*. Vol.18 (6), pp.81-83, Madison/Wisconsin;
- [18] Wenqing Y., Wacker P., Kutzbach H. D., (2001), Combine harvester - cleaning system investigations for excitation by circular oscillator (Mähdrescher - Reinigungsanlage Untersuchungen zur Anregung durch Kreisschwinger) [J], *Landtechnik*, (4), pp.276-277, Germany;
- [19] Werby R.A., (2010), Performance Cleaning Unit for Clover Grains Affecting Some Physical and Mechanical Properties. *Misr Journal of Agricultural Engineering*. 27(1), pp.266- 283, Egypt.

**RESEARCHES ON THE MONITORING OF AIR PRESSURE IN THE TIRES
AT ROAD TRANSPORT MEANS**
/
**CERCETARI PRIVIND MONITORIZAREA PRESIUNII AERULUI DIN PNEURI
LA MIJLOACELE DE TRANSPORT RUTIERE**

Ph.D. Eng. Ciupercă R., Ph.D. Stud. Eng. Persu C., Ph.D. Eng. Nedelcu A.,
Ph.D. Eng. Popa L., Ph.D. Stud. Eng. Zaica A., Ph.D. Stud. Eng. Ștefan V.
National Research-Development Institute for Machines and Installations designed to Agriculture
and Food Industry - INMA Bucharest / Romania
E-mail: ciupercaradu@yahoo.com

Keywords: *transport, tire pressure monitoring, efficient rolling*

ABSTRACT

Traffic parameters of the road transport means are influenced beside the loads to be transported, the travel speeds, the constructive and functional characteristics by the air pressure in the tires which has a direct impact on the tire tread wear, rolling resistance, compaction, soil compaction and rolling track wear, and finally on the transport operation costs.

This paper presents the research on a transport articulated vehicle made up of an agricultural tractor and a semi-trailer, aiming at continuous monitoring of the transported load in order to determine the optimal air pressure in the tires.

In order to monitor the tire pressure, which is directly influenced by the tire load, an installation was created and placed on the articulated vehicle that continuously measures and monitors, in real time, the transported load, consisting mainly of two force transducers, two force amplifiers, a micro PLC (Programmable logic controller), an operating terminal, and the connection elements between them.

The records made during experiments are managed using software specifically created for these researches.

The experiments were performed at different loads of the semi-trailer, the results obtained from the tests allowing us to determine the authenticity of the software created, on the one hand and the value evolution of the measured parameters, on the other hand.

The determined results allow the operator to make optimal decisions on the air pressure in the tire corresponding to the measured load, also taking into account the nature of the transported load, the type and condition of the rolling track.

REZUMAT

Parametrii de rulare ai mijloacelor de transport rutiere sunt influențați, pe lângă sarcinile de transportat, vitezele de deplasare, caracteristicile constructive și funcționale, și de presiunea aerului din pneuri, care are impact direct asupra uzurii benzii de rulare a pneurilor, a rezistenței la rulare, a tasării, compactării solului și uzurii căii de rulare, și, în final, asupra cheltuielilor efectuate cu operația de transport.

În lucrarea de față se prezintă cercetările efectuate asupra unui autotren de transport alcătuit dintr-un tractor și o semiremorcă agricolă, scopul fiind monitorizarea continuă a sarcinii transportate, în vederea stabilirii presiunii optime a aerului din pneuri

Pentru monitorizarea presiunii din pneuri, care este influențată în mod direct de sarcina pe pneu, a fost realizată și amplasată pe autotren o instalație care masoară și monitorizează continuu, în timp real, sarcina transportată, alcătuită în principal din două traductoare de forță, două amplificatoare de forță, un micro PLC (Controler logic programabil), un terminal de operare și elementele de conexiune între acestea.

Înregistrările efectuate în timpul experimentărilor sunt gestionate cu ajutorul unui soft, special creat pentru aceste cercetări.

Experimentările s-au efectuat la diferite sarcini de încărcare a semiremorcii, rezultatele obținute în urma testărilor permițându-ne să stabilim veridicitatea softului creat, pe de o parte, și evoluția valorică a parametrilor măsoarați, pe de altă parte.

Rezultatele determinate permit operatorului să ia decizii optime privind presiunea aerului din pneu, corespunzătoare sarcinii măsurate, ținând seama totodată și de natura sarcinii transportate, de tipul și starea căii de rulare.

The normal reaction of the ground on the semi-trailer wheels (tire load) Z_s , is determined from the momentum equation written in coupling point C, according to the equation (1):

$$Z_s \cdot L_1 - G_s \cdot a_s = 0 \quad (1)$$

By grouping the terms, we determine the expression of the Z_s reaction according to the equation (2):

$$Z_s = \frac{G_s \cdot a_s}{L_1} \quad (2)$$

Component R is determined with the equation (3):

$$R = G_s - Z_s \quad (3)$$

Substituting the expression of the Z_s reaction with its expression in equation (2), results the expression for the component R , according to the equation (4).

$$R = G_s - \frac{G_s \cdot a_s}{L_1} = \frac{G_s(L_1 - a_s)}{L_1} \quad (4)$$

The normal ground reaction on the semi-trailer wheels, Z_s is the size that will be continuously measured and monitored by the monitoring installation, which determines the value of the optimal air pressure in the tires, depending on the tire type, the travel speed, the nature and the condition of the rolling track.

To accomplish this, an operating program was designed, according to the logical schema presented in (Fig. 2).

Input data:

- fixed: tire type; air pressures in the tire recommended by the manufacturer, depending on the load and travel speed; rolling track type.

- variable: load measured by the monitoring installation.

Output data: optimal air pressure in the tire.

Operating mode: Select the travel speed of the means of transport and the rolling track type and, depending on the load measured by the monitoring system, the operating program will show the optimal air pressure in the tire on the display.

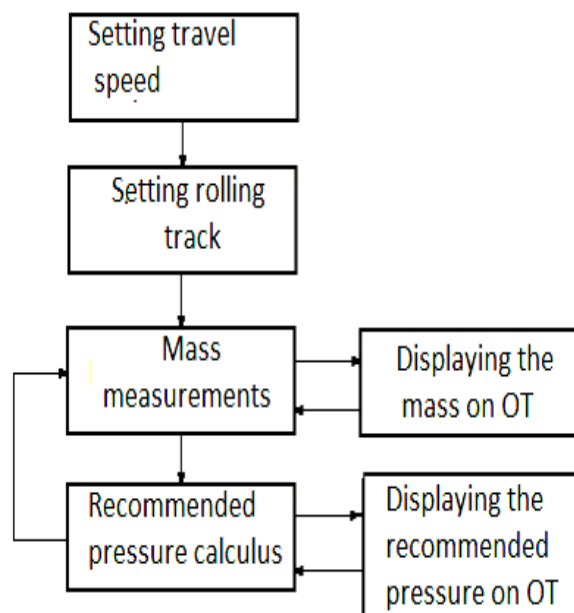


Fig. 2 – Operating program logical schema

OT – Operating terminal

The tests were carried out with a transport articulated vehicle consisting of an autotractor and a means of transport at rest on a horizontal land, in this case a New Holland TD80D agricultural tractor and an agricultural semi-trailer equipped with bogie-type drivetrain (Fig. 3), the semi-trailer being equipped with a load monitoring installation, (Fig. 4).



Fig. 3 – Articulated vehicle: New Holland TD80D agricultural tractor and agricultural semi-trailer

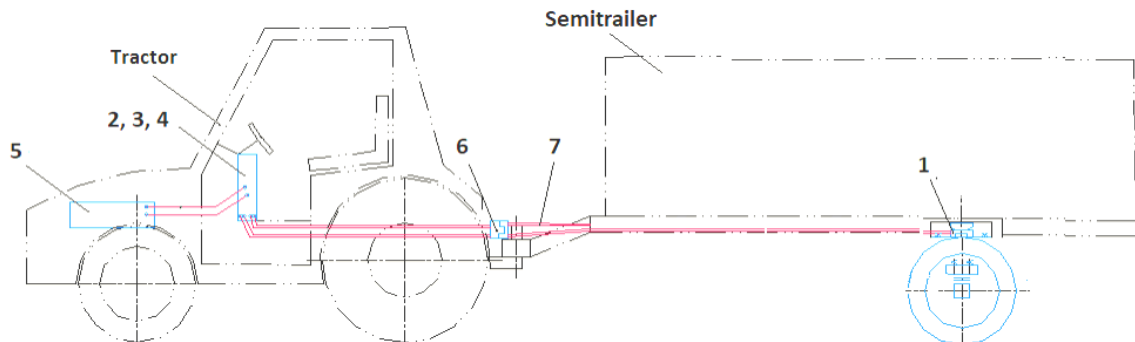


Fig. 4 – Load monitoring installation scheme:

1 – force transducer; 2 – force amplifier; 3 - micro PLC; 4 – operating terminal;
5 - accumulator battery; 6 – double pole fuse; 7 – connecting cables.

In the case of the present paper, we were interested in the forces acting on the semi-trailer, namely Z_s ; R based on which the operating program determines the required air pressure in the tires.

Working methodology

In the first stage of the tests, the semi-trailer's own mass G_p , and its distribution Z_p , R_p , were determined by weighting when stationary using the classic system (the weighting machine), and its constructive dimensions were measured and calculated (fig.3), the results being:

- $G_p = 4310$ daN; $Z_p = 3770$ daN; $R_p = 540$ daN.

where: Z_p - distribution of G_p on the semi-trailer axle; R_p - the component of G_s that is transferred to the tractor.

Also, the constructive dimensions of the semi-trailer were measured and calculated as follows:

$L_1 = 4.8$ m; $a_s = 4.2$ m; $b_s = 0.6$ m; $h_s = 1.6$ m; $h_c = 0.45$ m

Since the monitoring system transducers were located between the trailer chassis and the top of the rolling system, as shown in (Fig. 4), the weight monitored by them is reduced by the weight of the rolling system, the operating program of the system being realized accordingly.

For these reasons, in order to verify the viability of the previous relations, in the second stage the value of the weight measured by the two transducers was set at $3770/2 = 1885$ daN each, the actual load sustained by the tires on the same side of the trailer.

In the third stage, the same parameters were determined by weighing and measurements, with the semi-trailer loaded at $G_s = 7250$ daN (own weighting + load) for three values of G_s , the determined values being:

- $G_s = 7250$ daN; $Z_s = 6080$ daN; $R = 1170$ daN;

$L_1 = 4.85$ m; $a_s = 4.07$ m; $b_s = 0.78$ m; $h_s = 1.65$ m; $h_c = 0.42$ m

where: Z_s - distribution of G_s on the semi-trailer axle; R_s - the component of G_s that is transferred to the tractor.

In the fourth stage tests were carried out to check the functionality of the monitoring system for three values of G_s (own mass + load), the established values being determined by the existing used load (metal tare weights), respectively:

1. $G_{s1} = 7250(4310+2940)$ daN;
2. $G_{s2} = 6830(4310+2520)$ daN;
3. $G_{s3} = 5570(4310+1260)$ daN.

Equipment used for experiments

- The weighting machine: max. capacity 10t; accuracy class 0.1 – it weights the semi-trailer mass.
- The monitoring installation: placed as shown in (Fig. 4):
 - *force transducer*: max. capacity 10 t; protection class IP 68; accuracy class, 0.05; input resistance, $\geq 4350 \Omega$; high output signal of 2.85mV/V – It converts the mechanical force into an electric signal;
 - *force amplifier*: output, $\pm 10V$, 0...10 V and 4...20mA; protection class IP 20. - It amplifies the electrical signal received from the transducer;
 - *micro PLC*: no I/O 14; electrical connecting, 24 VDC; digital input, 8; work blocks max. 200. – It processes the signal received;
 - *operating terminal*, main characteristics: power terminal, 24 VDC; number of touch keys, maximum 50 keys/screen; user memory 512 kB or less - It displays the results obtained and represents the operator interface.

RESULTS

The results determined by the monitoring system are presented in Table 1.

Table 1

Values determined for Z_s and R

Test no.	Parameter determined	Values			
		Determined by the monitoring system [daN]	Determined by weighting machine [daN]	Difference [daN]	Deviation [%]
1	G_s [daN]	5558	5570	-12	- 0.2
	Z_s [daN]	4854	4860	-6	- 0.1
	R [daN]	704	710	-6	- 0.8
2	G_s [daN]	6840	6830	+10	0.1
	Z_s [daN]	5975	5968	+7	0.1
	R [daN]	865,,	862	+7	0.3
3	G_s [daN]	7261	7250	+11	0.2
	Z_s [daN]	6082	6080	+2	0
	R [daN]	1179	1170	+9	0.8

It can be noticed that the differences between the values determined by the classic system and those by the monitoring system were insignificant, so the monitoring installation is functioning correctly, the deviations having values that fall within the constructive error margin of the used measuring equipment.

Using the data specified in Table 1, the operating program determined the optimal tire pressures p_a , in accordance with the rolling track type and the pre-set travel speeds, the results being shown in Table 2, for the tire equipped with the 16.00-20/12PR outer cover.

Table 2

Values determined for the air pressure in the tire

Test no.	Parameter determined	Values determined by the monitoring system		
		Speed = 15 km/h Ground road	Speed = 30 km/h Concrete road	Speed = 40 km/h Highway
1	G_s [daN]	5558	5558	5558
	p_a [bar]	1,25	2	2,25
2	G_s [daN]	6840	6840	6840
	p_a [bar]	1,5	2,25	2,5
3	G_s [daN]	7261	7261	7261
	p_a [bar]	1,75	2,5	2,75

The operating program interface is presented in (Fig. 5).

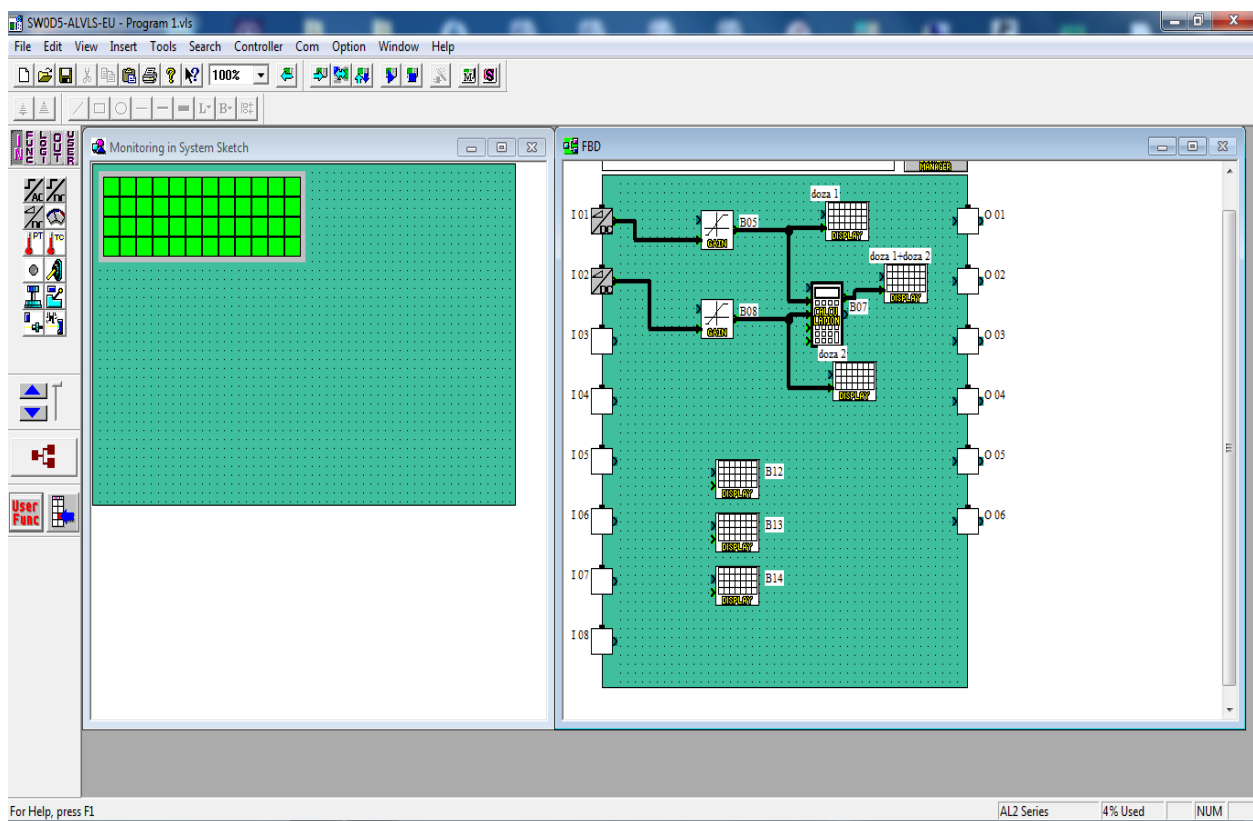


Fig. 5 – The operating program interface

The variation of the values of the components Z_s and R at the same amount of G_s depends on the position of load placement in the trailer to the axis of the driving system. A placement more toward the tractor could lead to a situation in which the value of R exceeds the value of the maximum permissible load on the tractor from the articulated vehicle, as declared by the manufacturer, which can be dangerous.

The information provided by the monitoring system, on the operating terminal, can avoid this situation because the operator has information about the value of R reconnected during loading of the trailer and can coordinate the proper placement of the load in the trailer.

For the experiments carried out in his work, with articulated vehicle, the variation of R according to the position of the load on the trailer, determined by the cart a_s , is presented in (Fig. 6), in which is marked the maximum value of R , allowed by the tractor from the articulated vehicle.

Experiments have been carried out for the $G_s = 7261$ daN.

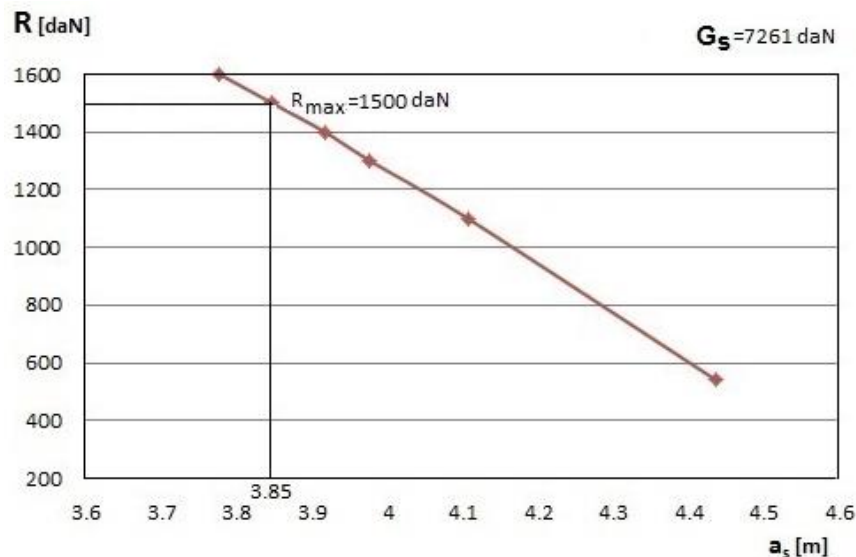


Fig. 6 – The variation of the component R depending on the position of the load on the trailer
Articulated vehicle: New Holland TD80D agricultural tractor and agricultural semi-trailer

CONCLUSIONS

1. The rolling system which was the subject of the present paper is equipped with a load monitoring installation that performs real-time, continuous measurement of the weight sustained by the trailer rolling system and its variation as a result of the weight transferred to the tractor;

2. The values measured in the experiments for the trailer weight G_s , the soil reaction to the trailer rolling system Z_s and the weight transfer from the semi-trailer to the tractor R was very close to those determined theoretically with the mathematical relations, the deviations calculated as the ratio of the theoretically calculated value to the value measured in experiments ranging between 0.1 - 0.8%, values that fall within the constructive error margin of the measuring equipment;

3. The operating program that was realized is working properly, providing the operator with information regarding the load on the rolling system and the optimal air pressure in the tires;

4. Continuous, real-time monitoring of the transported loads provides useful information to the operator so that he can optimally control the articulated vehicle rolling parameters by adapting the air pressure in the tires according to the transported load, the rolling track type and the travel speed, thus reducing the imminent dangers that may occur during the transport operation and ensuring an efficient transport.

ACKNOWLEDGEMENTS

The paper was performed under the project "Increasing the competitiveness of SC ELECTROPUTERE VFU PASCANI SA through assimilation into production of an Intelligent rolling system, designed to general and technological land transport equipment", Contract 5/PTE/2016 funded by the Executive Agency for Higher Education, Research, Development and Innovation Funding - UEFISCDI within the PN-III-CERC-CO-PTE-2016 Program.

REFERENCES

- [1] Badescu M., Iordache S., Ivancu B., Persu C., Bunduchi G., Epure M., Vladut V., (2014), Theoretical Study of the System of Forces and Moments Acting on Tractor-Semitrailer Aggregate, into Rectilinear Motion, *ANNALS of Faculty Engineering Hunedoara – International journal of Engineering*, Tome XII, Fascicule 3 (August);
- [2] Battiato A., Diserens E., (2017), Traction performance simulation on differently textured soils and validation: A basic study to make traction and energy requirement accessible to practice, *Soil and Tillage Research*, Vol. 166, pp. 18-32, Elsevier;
- [3] Biriş S. Şt., Vladut V., Ungureanu N., Matache M., Voicea I., (2012), Researches on the Development of an Equation for the Contact Area Calculus for Agricultural Tires, *40 Symposium "Actual Tasks on Agricultural Engineering"*, Opatija, Croatia;

- [4] Brixius W. W., (1987), Traction prediction equations for bias ply tyres, *ASAE, Paper No. 871622*, St. Joseph, Michigan;
- [5] Cardei P., Muraru V., Sfaru R., (2007), Interaction between vehicle wheel and soil – Estimation of soil compaction *INMATEH Agricultural Engineering*, no. 22, Vol. IV, pp.74-78, Bucharest, Romania;
- [6] Ciuperca R., Zaica A., Nedelcu A., Anghelut A., (2018), Monitoring work parameters for road transport means, *Engineering for Rural Development*, pp. 1962-1968, Jelgava, Latvia;
- [7] Dinu L., (2010), *Researches regarding the manufacturing of systems of pressure adjustment in tractor tires according to field features and movement conditions*, Ph.D. thesis, University TRANSILVANIA Brasov, Romania;
- [8] Diserens E., Défossez P., Duboisset A., Alaoui A., (2011), Prediction of the contact area of agricultural traction tyres on firm soil, *Biosystems engineering*, Vol. 110, pp. 73-82;
- [9] Popescu S., Ene T. A., Constantinescu A. (2006) - Theoretical and experimental researches regarding the influence of tyre parameters on soil settlement and compaction, *INMATEH Agricultural Engineering*, vol. 17, No. 2/2006, pp. 133...140, Bucharest, Romania;
- [10] Robescu V.O., Elekes C., (2008), Soil damaging as result of compaction process, a severe problem in Romanian agriculture, *Scientific Papers –vol. 51(2), series Agronomy*, pp.176 – 182, USAMV Iasi;
- [11] Xia K., (2011), Finite element modeling of tire/terrain interaction: Application to predicting soil compaction and tire mobility, *Journal of Terramechanics*, Vol. 48, pp. 113-123;
- [12] Roșca R., Cârlescu P., Țenu I., (2014), A semi-empirical traction prediction model for an agricultural tyre, based on the super ellipse shape of the contact surface, *Soil and Tillage Research*, Vol. 141, pp.10-18;
- [13] Tiwari V.K., Pandey K.P., Pranav P.K., (2010), A review on traction prediction equations, *Journal of Terramechanics*, Vol. 47, pp. 191-199, Elsevier;
- [14] Roșca R., Cârlescu P., Țenu I., (2017), Comparative analysis of some tire deformation models used for the prediction of traction characteristics, *INMATEH Agricultural Engineering*, Vol. 53, No.3, pp. 151-158, Bucharest, Romania;
- [15] Tecusan N., Ionescu A., (1982), *Tractors and Automobiles (Tractoare și automobile)*, Didactic and Pedagogical Publishing House Bucharest, pp. 65-88, Bucharest, Romania;
- [16] Żebrowski J., (2010), Traction efficiency of a wheeled tractor in construction operations, *Automation in Construction*, vol. 19, Issue 2, pp. 100-108.

**RESEARCHES REGARDING THE OPTIMIZATION OF IMPURITIES REMOVAL
TECHNOLOGY FROM THE CEREAL AND INDUSTRIAL PLANT SEEDS FOR
ESTABLISHING ECOLOGICAL CROPS**

/

**CERCETĂRI PRIVIND OPTIMIZAREA TEHNOLOGIEI DE ELIMINARE A
IMPURITĂȚILOR DIN MASA DE SEMINȚE DE CEREALE ȘI PLANTE TEHNICE
DESTINATE ÎNFIINȚĂRII CULTURILOR ECOLOGICE**

Ph.D. Eng. Păun A. ¹⁾, Eng. Stroescu Gh. ¹⁾, Ph.D. Eng. Vișan A.L. ¹⁾,
Ph.D. Eng. Olan M. ¹⁾, Ph.D. Stud. Eng. Zaica Alexandru ¹⁾, Lect.Ph.D.Eng. Moiceanu G. ²⁾

¹⁾ National Institute of Research-Development for Machines and Installations designed to
Agriculture and Food Industry – INMA / Bucharest, Romania;

²⁾ Politehnica University of Bucharest / Romania
Tel: 02 1/269.32.50; E-mail: ani_paun@yahoo.com

Keywords: seeds, conditioning, cylindrical sieves, seed conditioning installation

ABSTRACT

To ensure maintaining the biological quality of harvested seeds represents a challenge for scientific research in ecological agriculture. The production of seed material, organic certified, depends to a great extent on the functional quality of seed conditioning equipment and installations, but also on the quality of the raw material. Given the importance of knowing the conditioning process of different culture seeds the paper presents a seed conditioning technology and installation that combines two functioning principles: counterflow aspiration and separation on cylindrical sieves. From the results obtained in the experimental research a comparative analysis of the performances of the equipment that could be used by the producers was made.

REZUMAT

Asigurarea menținerii calității biologice a semințelor recoltate, reprezintă o provocare pentru cercetarea științifică în agricultura ecologică. Producția de material semincer certificate ecologic, depinde în mare măsură de calitatea funcțională a echipamentelor și instalațiilor de condiționare a semințelor, dar și de calitatea materiei prime. Având în vedere importanța cunoașterii procesului de condiționare a diferitelor semințe de cultură, lucrarea prezintă o tehnologie și o instalație de condiționare a semințelor, care combină două principii de funcționare: aspirație în contracurent și separarea pe sitele cilindrice. Din rezultatele obținute în cercetarea experimentală s-a realizat analiza comparativă a performanțelor echipamentului ce poate fi utilizat de producătorii.

INTRODUCTION

After the harvesting process, agricultural products (seeds, fruits, vegetables, etc.) cannot be used directly for various purposes such as: preservation, consumption, industrialization, marketing, sowing, etc., as they also contain impurities (plant remains, seeds, weeds, other bodies, etc.) and damaged products. Prior to receiving a specific destination, it is necessary and obligatory for the harvested products to undergo cleaning and sorting operations. In order to reduce and even eliminate the negative influences of the cereal grain impurities, it is necessary to make a pre-cleaning with different equipment or installations. At the same time, for the use of cereal and industrial plant seeds as sowing material, it is necessary to eliminate foreign bodies, which differ from the seeds of agricultural crops in general, by their physical characteristics, as well as the removal of seeds with low germinating capacity, poorly developed ones and cracks. For this reason, the realization of cleaning and sorting technical equipment is a necessity.

MATERIALS AND METHODS

Within the primary processing operations of agricultural products for obtaining high quality final products are also the cleaning and sorting operations, which involve an adequate technological flow (Brăcăcescu C., Găgeanu I., Popescu S., Kemal C.S., 2016).

If currently, in some countries, the focus is on predominantly organic agriculture, it is estimated that in the next few years, the importance of technical equipment for cleaning and sorting cereal and technical plant seeds will obviously increase due to the high degree of crop contamination resulting from the elimination of chemical processes to prevent factors that negatively influence their development (herbicide application, chemicalization, etc.) (Ciobanu V.G., Vişan A.L., Păun A, Nedelcu A., 2015).

The cleaning operation, as the first operation within the technological flow of processing agricultural products requires, first of all, cleaning and sorting equipment having its working process based on the difference between the physical characteristics of seeds and those of foreign bodies.

In order to meet the needs of cereal and technical plant processors and agricultural farmers, INMA Bucharest has developed a technology, (Fig.1) (Păun A., et al., 2016) and a pilot installation for seed conditioning ISC (Fig. 2) (Păun A., et al., 2016), which is composed of high capacity combined-type technical equipment (pre-cleaning module and cylindrical sieve) (Păun A., et al.-2016).

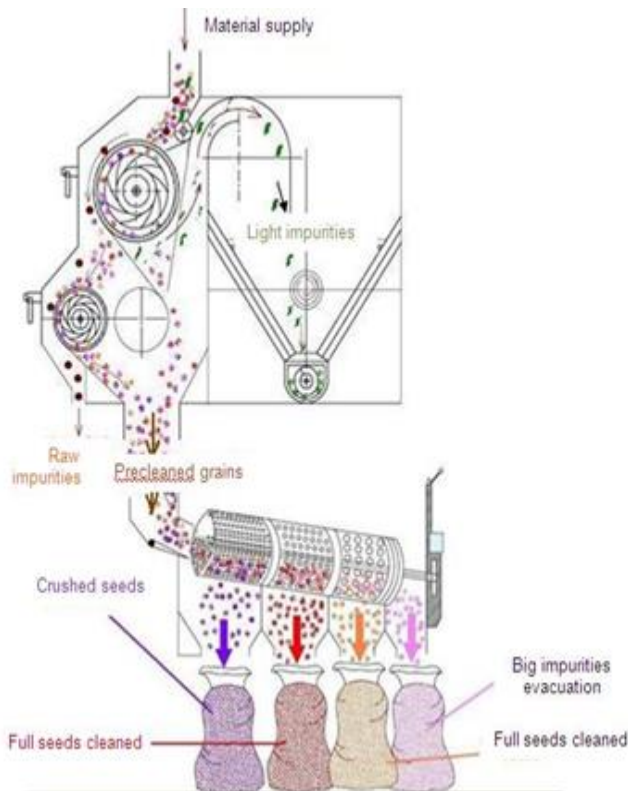


Fig. 1 - Seeds for conditioning technology [9]

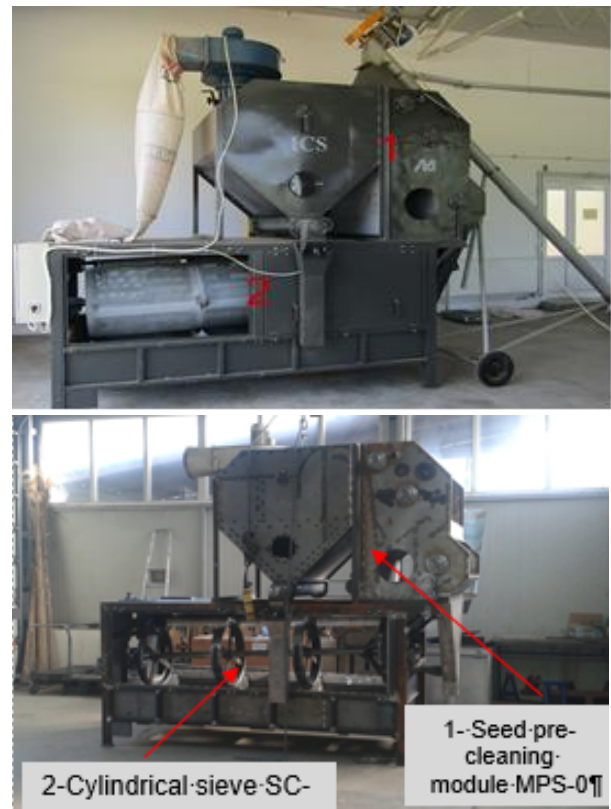


Fig. 2 – ICS seed conditioning installation

The seed conditioning installation is designed to improve harmonised technologies for the production of organic seed in cereals, legumes for grains, oilseeds, industrial and fodder plants, aromatic and medicinal plants, to solve practical problems concerning the production of organic seed for field cultures and planting material, organic certified, at farmers. It has the role of removing from the processed product the impurities that affect its quality.

Aligned to the most modern trends, incorporating the latest design solutions, the ICS installation uses in the seed pre-cleaning process, within the pre-cleaning module, two combined principles: separation on two sieve drums and the counter flow aspiration of the product. The product, pre-cleaned of coarse foreign bodies and light impurities, reaches the cylindrical sieve where separation in several fractions takes place.

The adopted constructive solution allows changing the inclination angle of the cylindrical sieve and also, to increase the productivity and the technological sorting effect, it is provided with inner inclined planes (Păun A. et al., 2016).

Main technical and functioning characteristics of the pilot installation ICS are:

- **Seed pre-cleaning module MPS-0.** This equipment has a productive capacity of 8 [t/h] for a standard product, respectively a working capacity higher than 5 [kg/h] for wheat (humidity of 6 ÷ 8 [%]) and a cleaning degree of 40 ÷ 50 [%];

• **Cylindrical sieve SC-0.** This equipment presents a selection capacity of 3 ÷ 4 [t/h], a sieve rotation frequency of 14 [min⁻¹] and an installed power 75 [kW].

In order to determine cereal seed pre-cleaning degree, experiments were carried out with the seed conditioning installation, at INMA, under operating conditions, using as raw material seeds of: wheat that was not pre-cleaned, camelina and soy, purchased on the market.

Considering the technological role of the seed conditioning installation, samples were taken and laboratory analyses were performed at: seeds entering the pre-cleaning module; seeds going out from the pre-cleaning module; the outlet of the product decanted in the cyclone; the outlets (sieved products) from the three segments of the cylindrical sieve and the plus material on the last element of the cylindrical sieve.

The technological effect of the installation was analysed against product standards and assessed according to the following results obtained at a single pass through the installation of the product to be processed (Tarcolea C. et al, 2008, Paun A. et al, 2012).

During the experimental research activities of the pilot installation, the following determinations were made: large impurities extraction evaluated using the E_{csM} [%] coefficient and defined in eq. (1); small impurities extraction evaluated using the E_{csm} [%] coefficient and defined in eq. (2) and light impurities extraction (weeds, dust particles, bents, vegetal pieces, husks with dimensions smaller than 1.5 [mm]) evaluated using the E_{csu} [%] coefficient and presented in eq. (3).

$$E_{csM} = [(C_{sMi} - C_{sMe}) / C_{sMi}] \times 100 \text{ [%]} \quad (1)$$

$$E_{csm} = [(C_{smi} - C_{sme}) / C_{smi}] \times 100 \text{ [%]} \quad (2)$$

$$E_{csu} = [(C_{sui} - C_{sue}) / C_{sui}] \times 100 \text{ [%]} \quad (3)$$

The terms used in the above equations have the next significations: the C_{sMi} is the content of large impurities at installation inlet, [%]; the C_{sMe} is the large impurities content at the installation outlet, [%]; the C_{smi} is the small impurities content at the installation inlet, [%]; the C_{sme} is the content of small impurities content at the installation outlet, [%]; the C_{sui} is the light impurities content at the installation inlet, [%] and the C_{sue} is the content of light foreign bodies at the installation outlet [%].

RESULTS

The results obtained from experimental research activities carried out under operating conditions of the ICS installation that is equipped with MPS module are presented in Tables 1 and 2.

During the laboratory analyses were obtained the humidity and impurity of the samples extracted from the supply and evacuation seed material and their pictures are presented in Fig. 3, 4 and 5.

Table 1

Experimental results obtained from ICS under operating conditions

Measured parameter	Sample no.	Camelina seeds		Soy seeds		Wheat seeds	
		Product inlet	Product outlet	Product inlet	Product outlet	Product inlet	Product outlet
Humidity [%]	S I	7.6	7.4	7.355	7.35	7.6	7.4
	S II	7.4	7.5	7.358	6.6	7.4	7.3
	S III	7.7	7.5	7.356	6.5	7.7	7.35
	Average value	7.57	7.47	7.36	6.82	7.57	7.35
Seed mass [kg/hl]	S I	61.2	61.2	69.35	69.168	74.3	74.1
	S II	63.3	63.3	69.35	69.05	79.3	79.05
	S III	64.1	64.1	69.35	68.95	79.1	78.95
	Average value	62.87	62.87	69.35	69.06	77.57	77.37
Seed purity [%]	S I	63.01	93.05	90.5	98.54	96.2	98.9
	S II	63.1	93.15	91.3	98.82	94.8	99.1
	S III	63.28	93.1	91.1	97.64	95.1	98.8
	Average value	63.13	93.10	90.97	98.33	95.37	98.93

Table 2

Determinations regarding the quality of processed seeds

Measured parameter	Sample no.	Camelina seeds			Soy seeds			Wheat seeds		
		Product inlet	Product outlet		Product inlet	Product outlet		Product inlet	Product outlet	
Light impurities content collected at fan evacuation [%]		C_{sui}	C_{sue}	E_{csu}	C_{sui}	C_{sue}	E_{csu}	C_{sui}	C_{sue}	E_{csu}
	S I	19.58	3.7	81.10	0.54	0.006	98.89	0.72	0.19	73.61
	S II	19.7	3.68	81.32	0.59	0.005	99.15	0.68	0.2	70.59
	S III	19.68	3.74	81.00	0.47	0.006	98.72	0.65	0.17	73.85
	Average value	19.68	3.71	81.15	0.533	0.006	98.87	0.68	0.19	72.06
Small impurities evacuated by the helical horizontal conveyor [%]		C_{smi}	C_{sme}	E_{csm}	C_{smi}	C_{sme}	E_{csm}	C_{smi}	C_{sme}	E_{csm}
	S I	13.63	2.61	80.85	0.24	0.008	96.67	0.22	0.04	81.82
	S II	13.6	2.64	80.59	0.22	0.007	96.82	0.25	0.04	84.00
	S III	13.65	2.66	80.51	0.25	0.009	96.40	0.23	0.06	73.91
	Average value	13.63	2.63	80.70	0.237	0.008	96.62	0.23	0.047	79.57
Large impurities evacuated by the tram [%]		C_{sMi}	C_{sMe}	E_{csM}	C_{sMi}	C_{sMe}	E_{csM}	C_{sMi}	C_{sMe}	E_{csM}
	S I	3.51	0.54	84.62	1.5	0.3	80.00	1.7	0.2	88.24
	S II	3.59	0.58	83.84	1.55	0.4	74.19	1.9	0.28	85.26
	S III	3.58	0.6	83.24	1.42	0.3	78.87	1.65	0.3	81.82
	Average value	3.56	0.56	84.27	1.49	0.33	77.85	1.75	0.26	85.14
Cracks [%]	S I	-	-		2.10	0.4		1.5	0.2	
	S II	-	-		2.01	0.6		1.7	0.25	
	S III	-	-		1.74	0.9		1.4	0.21	
	Average value	-	-		1.95	0.63		1.53	0.22	



Quality of unprocessed camelina seeds



By product collected after MPS



Camelina seeds sieved by sieve no.1



Camelina seeds sieved by sieve no.2



Camelina seeds sieved by sieve no.3



Material evacuated by sieve no.3

Fig. 3 - Samples collected during the technological flow of ICS when it processed the camelina seeds

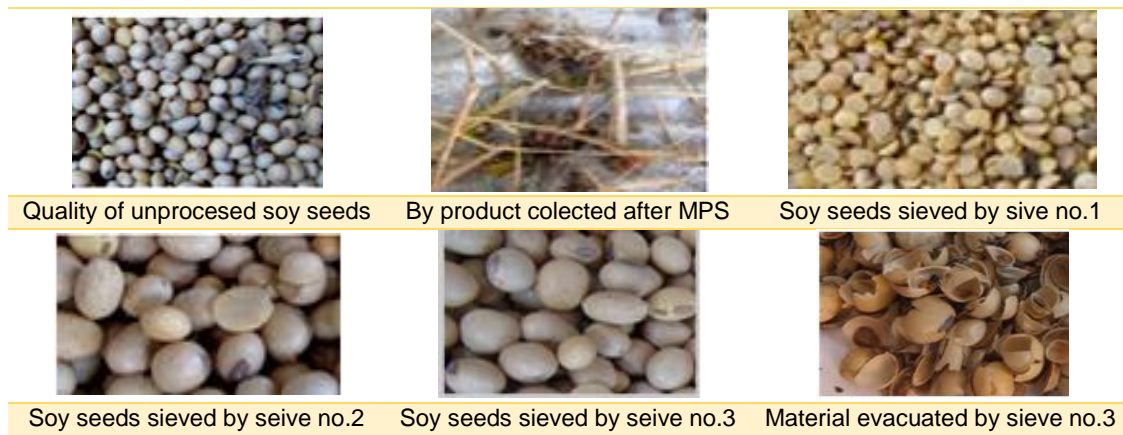


Fig. 4 - Samples collected during the technological flow of ICS when it processed the soy seeds

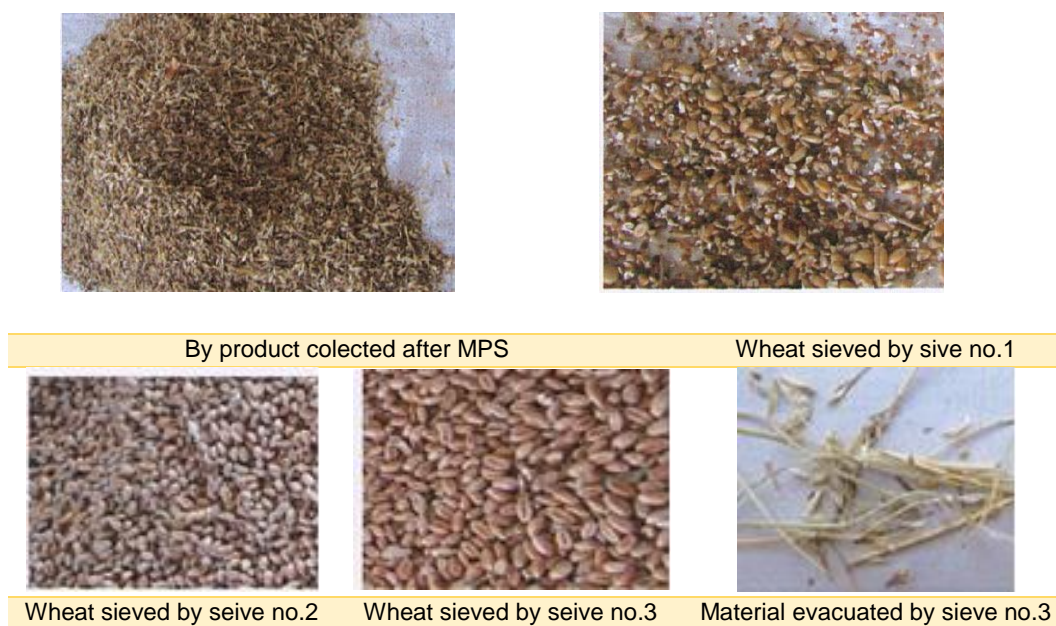


Fig. 5 - Samples collected during the tehcnological flow of ICS when it procesed the wheat

In fig. 6 is presented the graphical distribution of impurities extraction from seed mass during the ICS technological process for different types of seeds, beginning form the small ones – camelina seeds and ending with soy seeds.

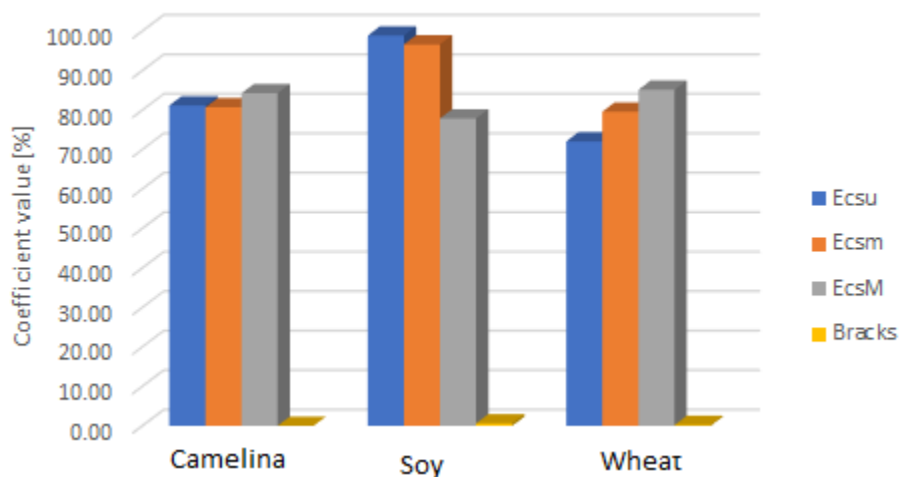


Fig. 6 - The distribution of the impurities extraction from seeds that are processed by ICS installation

Analysing this data can be concluded that the separation process by fractions can be easily made if the seed dimensions are considerably higher, but at the same time the amount of breakage is much higher (see also Table 2) while the cracks evacuation percentage is maintained at the same value.

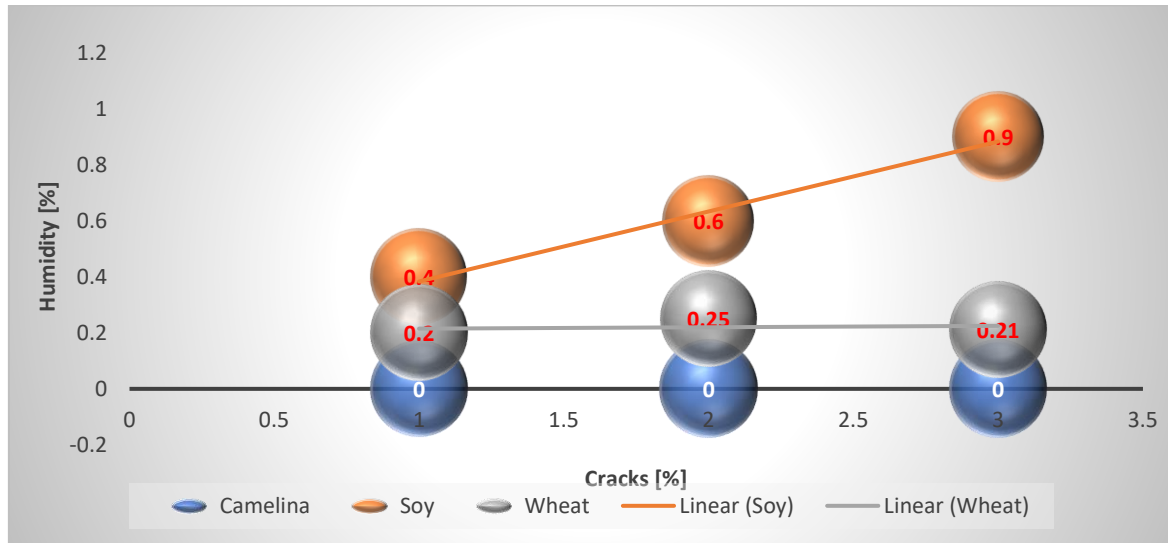


Fig. 7 - The distribution of the cracks from procesed seed mass in acordance with material humidity

If we take a close look at the crack percentage of cracks in the processed seed material it can be seen that it has increased. The most concerning case is that of the soy beans because its tendency increased rapidly by almost 50% from sample to sample, even if the feeding material is maintained constant and the humidity has decreased only by 0.855 [%].

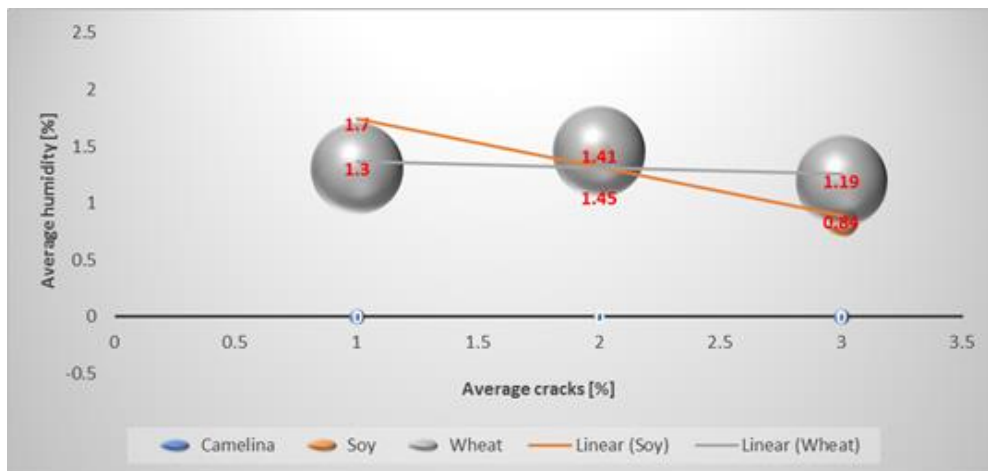


Fig. 8 - The distribution of the cracks from procesed seed mass in acordance with material humidity

In fig. 8 is presented an important aspect of the seed mass processing: if the separation process takes place into the air tunnel, the seeds can modify their humidity and sometimes can increase their fragility; this way, the processed seed mass can increase the cracks percentage, as it can be seen in Table 2.

In fact, the camelina seed mass has no cracks and their humidity can be compared easily with the wheat material, but the dimensions are smaller and also their external surface, fact that has no influence during the seed dynamics and assures its integrity during the technological process.

Comparing wheat humidity with soy seeds, it can be noticed that there is a slight difference, and if it is correlated with dimensional and mass aspects it can be clearly concluded that, from a certain point, the technologic parameter must be controlled in order to decrease the cracks percentage in the processed material. If this aspect is not considered, the technological process cannot be adequately controlled and that leads to the fact that the separation process can be compromised.

CONCLUSIONS

This installation has the ability to remove impurities of unthreshed wheat seeds and due to the pre-cleaning process performed by ICS they are successfully eliminated. This process must be well controlled so that the speed of the air flow above the seed flow limit can aspirate beside the impurities also the good seeds that are then directed to the cyclone and from there to the residues, applying the principle of impurities separation based on the difference in aerodynamic properties between seeds and impurities. The separation module has the ability to adjust the flow rate of the air flow in the suction channels by altering the geometry of the transverse section thereof by actuating some control valves.

To eliminate large impurities like straws, cobs, ears, etc. which can cause installation clogging, which obstruct or stop the grains flowing from the installation, the module with cylindrical sieves is mounted. The pre-cleaning module MPS-0 ensures an optimum drive mode of the seeds and impurities mass using two sieve drums which can be replaced depending on the seeds undergoing pre-cleaning.

The ICS has been designed to ensure high-purity cereal and industrial plant seeds used in organic crops establishment, a need that is increasingly present to farmers who want to set up crops with high nutritional and economic value.

In this paper are underlined some technological aspects that must be considered during the seed separation process in order to lead to a product in line with market product standard. In the next papers will be presented further research results on different seeds with different humidity, and will be presented a dedicated controlling system that will allow adapting the process parameters to seed humidity and dimensions.

ACKNOWLEDGEMENTS

This paper was financed with the support of ADER Project-ADER 1.2.2. Development of an integrated system for producing seed and planting material, organic certified, at field cultures: cereals, legumes for grains, oilseeds, industrial plants and fodder, aromatic and medicinal plants.

REFERENCES

- [1] Brăcăcescu C., Găgeanu I., Popescu S., Kemal C.S., (2016), Researches concerning impurities separation process from mass of cereal seeds using vibrating sieves in air flow currents, *Proceedings of 5th International Scientific Conference "Engineering for rural development 2016"*, ISSN1691-5976, pp.364-370, Jelgava, Latvia;
- [2] Căsăndroiu T., (1993), *Primary processing and agricultural products storing*, Lithographed course, Politehnica University of Bucharest, Romania, p.176;
- [3] Căsăndroiu T., David L., (1994), Equipment for primary processing and preservation of agricultural products. (Echipamente pentru procesarea primară și conservarea produselor). Guidelines for laboratory work, chap. 4, *Ed. Politehnica University of Bucharest*, Bucharest/Romania;
- [4] Ciobanu V.G., Vișan A.L., Păun A., Nedelcu A., (2015), Comparative study regarding seed sorting equipment and the importance of implementing smart systems within the working process, *JoKULL Journal*, vol. 64, no. 9, ISSN 0449-0576, pp. 91-100;
- [5] Coskuner Y., Karababa E., (2007), Physical properties of coriander seeds (*Coriandrum Sativum L.*), *Journal of Food Engineering*, Vol. 80, Issue 2, pp. 408-416, Los Angeles/California;
- [6] Costin I., (1988), *Miller book (Cartea morarului)*, Technical Publishing House, Bucharest/Romania;
- [7] Dziki D., Laskowsky J., (2005), Wheat kernel physical properties and milling process (Właściwości fizyczne ziarna pszenicy a proces przemiału), *Acta Agrophysica*, Vol. 6(1), pp. 59-71, Institute of Agrophysics, Polish Academy of Sciences, Lublin/Poland;
- [8] Găgeanu P., (2001), *Study on corn seeds sorting*, Doctoral Thesis, Politehnica University of Bucharest, Faculty of Biotechnical Systems Engineering, 185 p;
- [9] Karimi M., Kheiralipour K., Tabatabaeefar A. et al., (2009), The effect of moisture content on physical properties of wheat, *Pakistan Journal of Nutrition*, Vol. 8, Issue 1, pp. 90-95, Faisalabad/Pakistan;
- [10] Păun A., Pirnă I., Găgeanu P., Vlăduț V., (2012), Increasing the added value of processed products in the milling industry by implementing a combined calibrator in wheat preparation technological scheme, *INMATEH - Agricultural Engineering*, vol. 36, no. 1, ISSN: 2068 – 2239; ISSN: 2068-4215, pp. 63-68, Bucharest, Romania;

- [11] Păun A., Ionita Gh., Milea D., Ganea–Christu I., (2016), *Seed conditioning technology*, Patent application no. A/00887;
- [12] Păun A., Ionita Gh., Milea D., Ganea–Christu I., (2016), *Seed conditioning installation*, Patent application A/00688;
- [13] Paun A., Bracacescu C., Dumitru M., Bunduchi G., (2016) Researches on producing organic certified seeds and planting material, *Proceedings of International Symposium ISB-INMA' TEH 2016*, pp. 731, Bucharest, Romania;
- [14] Târcolea C., Căsandroiou T., Voicu Gh., (2008), Stochastic models for simulating seed separation process on sieves, *Proceedings of the 36th International Symposium "Actual Tasks on Agricultural Engineering"*, pp. 293-306, Croatia;
- [15] Voicu Gh., Orășanu N., (2009), Considerations regarding the study on particle motion on the sieve plan with circular motion, *International Conference "Research People and Actual Tasks on Multidisciplinary Sciences"*, vol. 2, Lozenec, Bulgaria;
- [16] Yan J., Liu C., Zhao L., (2010), Dynamic characteristics of vibrating screen with determinate structure and statistically indeterminate structure, *Applied Mechanics and Materials*, no. 34-35, pp.1850-1854;
- [17] *** (2012), General testing procedure PGI-01.20, Pre-cleaning and cleaning installations for cereals and technical plants, Testing Department - INMA Bucharest/Romania.

RESEARCH OF YELLOW-FEATHER CHICKEN BREEDING MODEL BASED ON SMALL CHICKEN CHAMBER

基于小型鸡舍的黄羽鸡精细化养殖模式研究

MAE. Stud. Heyang Yao ¹⁾, Ms. Qiyue Sun ¹⁾, Assoc. Prof. Ph.D. Xiuguo Zou ^{*1)}, MEE. Stud. Siyu Wang ²⁾,
Senior Exper. Shixiu Zhang ¹⁾, MAE. Stud. Shikai Zhang ¹⁾, Ms. Shuyue Zhang ¹⁾

¹⁾ College of Engineering, Nanjing Agricultural University / China;

²⁾ School of environmental science and Engineering, Nanjing University of Information Science and Technology / China

Tel: +862558606585; E-mail: xiuguo zou@gmail.com

Keywords: *small chicken chamber, yellow-feather chicken, heat stress, ammonia, fine particulate matter*

ABSTRACT

Yellow-feather chicken is a common breeding chicken in China. In view of the uncontrollable factors of pasture-raised chickens, the team proposes a precise breeding method of small chicken chamber. In this way, two problems are solved, including heat stress and the effects of environmental factors, such as bedding, fodder, water, wind speed, ammonia and fine particulate matter (PM_{2.5}) on chickens. This experiment studies heat stress and air quality during the 20-day experiment period using the method of a negative pressure fan controlled by an inverter. The experimental results show that under design conditions, all the environments are up to standard, and the weight gain efficiency of chickens is higher than that of free-range chickens and no death is witnessed. This experiment proposes a new breeding model which has been approved by some breeding companies and thus has a broad application prospect.

摘要

黄羽鸡是中国常见的一种养殖鸡，针对散养鸡各方面因素不可控，团队提出小型鸡舍精细化养殖方式，在这种养殖方式下，重点解决两个问题，一是热应激，二是垫料、饲料、水、风速、氨气和 PM_{2.5} 等环境因素对鸡的影响。本次实验采用变频器控制负压风机的方案，在为期 20 天实验时间内研究热应激和空气质量情况。最终实验结果表明，在设计条件下各方面环境均达标，鸡增重效率高于散养，没有鸡死亡。本实验提出一种新型的养殖模式，已经得到部分养殖基地认可，有很好的推广前景。

INTRODUCTION

With the popularization of the scientific concept of “animal welfare”, environmental quality is an important factor that restricts the health welfare and production performance of chickens (Liu Y., 2015). In Jianghuai Region of China, it often appears high temperature and high humidity in summer. Due to the lack of sweat glands and the difficulty in heat dissipation of chickens, different heat stress response occur at this time (Farooqi H., 2005). The heat stress response of chicken refers to a series of abnormal reactions caused by temperature regulation and physiological dysfunction under high temperature conditions, which have different effects on feed intake, production function and feed conversion rate of chickens, and even causes shock and death of chickens (Yuan J., 2007). Saffar and Rose (2002) studied that the physiological function of poultry was greatly influenced by environmental factors, among which ambient temperature was one of the most important factors (Al-Saffar A., 2002).

At the same time, air quality in the chicken house also affects the health of chickens. For traditional chicken houses in China, a scraper-type defecating system is used for dung removal, which has problems such as long cleaning cycle, incomplete cleaning and water leakage of drinking water equipment. As a result, the fecal fermentation in the chicken house is easy to occur, resulting in high temperature, humidity and ammonia concentration in the chicken house (Kocaman B., 2006). In chicken house, ammonia is produced by microorganisms degrading substances such as feces. Higher concentrations of ammonia may damage the respiratory lining of chickens, decrease their immune function, increase their risks of infectious and respiratory diseases, and adversely affect their weight gain, feed conversion rates, carcass quality, thereby reducing their breeding benefits (Beker A., 2004; Lin T., 2016; Xing H., 2015). Studies show that the dust in chicken house mainly comes from feed, feces, chicken skin, feathers, the foam produced during cackling, airborne microorganisms and fungus (Chen F., 2014). Ammonia is also an important source of PM_{2.5} (Li Q., 2014).

Only a small amount of pathogenic microorganism inhaled by chickens can lead to airborne infection, affecting normal life and health of chickens, and leading to the decline of production performance (Yang W., 2016). In order not to affect the health and normal production performance of chickens, China's livestock and poultry farm environmental standard (NY/T 388-1999) stipulates that the concentration of ammonia in chicken houses shall not exceed $10\text{mg}/\text{m}^3$.

To solve the above mentioned problems, this paper studies the precise breeding mode of yellow-feather chickens based on small chicken chamber and analyzes the effects of heat stress, $\text{PM}_{2.5}$ and ammonia on the growth performance of yellow-feather chickens in terms of colour of excreta, feed and water, wind speed in the chamber, concentration of ammonia and $\text{PM}_{2.5}$ particles.

MATERIALS AND METHODS

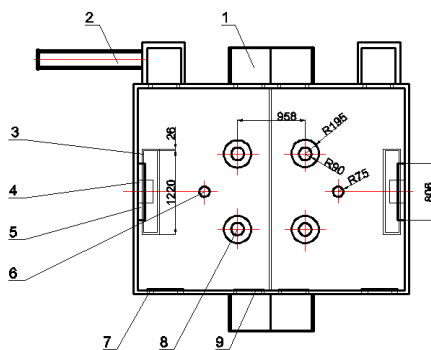
The experiment was conducted at Jinniuhu Street, Luhe District, Nanjing City, Jiangsu Province, China. The geographical coordinates of the chicken house are $32^{\circ}26'77''\text{N}$ in latitude and $118^{\circ}52'64''\text{E}$ in longitude. The chicken house has two symmetrical structure chambers and the walls of chambers are designed by two layers of steel plate with heat insulation cotton in the middle. Each chamber is 1.9m in width, 2.9m in length and covers a total area of 5.51m^2 . The roof is a slope, and its west side is 1.88m in height and east side is 1.77m in height, which makes rain drain easy. In the chamber, temperature and humidity monitoring system, ammonia monitoring system, inner and external circulated ventilation system, and video monitoring system were equipped.

The experiment began on July 20, 2018, and the yellow-feather chickens were 24-day old. The experimental period is 20 days. On the first day of the experiment, each chicken was numbered. The yellow-feather chickens after registration were put into two chambers for feeding according to their identifications. The 35 chickens in Chamber 1 are numbered consecutively from the number of 101 and a plastic ring is put on their feet for identification, while the 35 chickens in Chamber 2 are numbered consecutively from the number of 201.

Figure 1 (a) shows the location and surrounding environment of the chicken house. The red frame the red arrow points at is the chicken house used in the experiment. The internal structure of the two chambers and their internal landscape are shown in Figure 1 (b) and Figure 1 (c).



(a) The Location of the chicken house



(b) The internal structure of the chambers



(c) The internal landscape of one chamber

Fig. 1 - Overview of the experimental chicken house

1. internal circulated air outlet, 2. external circulated air outlet, 3. Drinking water pipe, 4. water tank, 5. air conditioner, 6. camera, 7. internal circulated air inlet, 8. feeder, 9. external circulated air inlet

During the 20-day experiment, the water trough in the chicken chamber is cleaned every morning to avoid water contamination problems caused by clogged water outlets or the accumulation of the bedding in the water trough as a result of movement of yellow-feathered chickens.

At the same time, temperature changes in the chicken chamber also need to be recorded in the control room many times per day. If the temperature exceeds 30°C, the inlet air brake of the chicken chamber needs to be adjusted to the largest degree to speed up heat dissipation and slow down temperature rise speed in the chamber, and when the temperature in the chamber exceeds 34°C, the air conditioner will be open (set to 30°C) for cooling until the external temperature of chicken chamber drops to lower than 34°C to avoid mortality of chickens because of heat stress.

The daily work is arranged as follows:

(1) Daytime (6:00 AM - 11:00 PM): check the status of the chicken every hour, record the temperature of the chicken chamber and check every half hour when the temperature is high at noon. The recording time shall be precise to minute.

(2) Adjust the frequency of variable frequency fan according to the temperature reference table.

(3) At high temperature: C1, C2 > 34°C, use inner cycle fan, close damper, open air conditioning, air conditioning set at 30°C, set frequency converter of internal cycle fan to 30Hz, frequency converter of external cycle fan to 0HZ, constantly monitor temperature. When the temperature outside the chicken chamber drops to 34°C, open frequency converter of the external cycle, frequency converter of the internal cycle and the external cycle are set to 50Hz, close air conditioning.

(4) Other arrangements are as follows:

11:00 PM ~ 5:00 AM (the next day): Detect particulate matter mass and ammonia concentration at night.

6:00 AM ~ 8:00 AM: Check and clean the chicken chambers, and check feed and water to ensure water level is no less than 70cm.

8:00 AM ~ 2:00 PM: Detect particulate matter mass and ammonia concentration etc.

2:00 PM ~ 4:00 PM Check feed, water and chickens status.

4:00 PM ~ 10:00 PM Detect particulate matter mass and ammonia concentration etc.

The whole experiment mainly consists of the following aspects.

The experimental plan of bedding

Good quality bedding encourages yellow-feather chickens to engage in some natural behaviours and physiological activities, such as foraging for water, combing their feathers and walking back and forth. In this experiment, wood chip is used as bedding. Wood chip bedding is flat and loose, not prone to agglomeration, and can effectively absorb the excreta of yellow-feather chickens (*Robins A., 2011*).

On the day when the experiment ends (Day 20 of the experiment), a small amount of the bedding samples will be collected at 2 points at external and internal circulated air outlets of the chicken chamber (10 cm from the air outlet), 2 points at external and internal circulated air inlet (10 cm from air inlet), 2 points at water area centre and feed area centre, and 1 point at the centre of chicken chamber. These samples will be analyzed and tested.

The experimental plan of feed and water

This experiment adopts Zhengda 511 chicken feed (suitable for 22-day chickens to chickens 7 days before yielding). Ingredients: corn flour, soybean meal, protein powder, rice bran, fish meal, calcium phosphate, copper sulfate, ferrous sulfate, compound vitamin, amino acid, etc., and it contains all the nutrients required for the growth of chicken. This product is puffed and thus easier to intake.

Studies show that the addition of vitamin C can maintain a normal body temperature and normal concentrations of calcium, protein and cortisol in the blood, thus relieving heat stress response of the chickens. Addition of vitamin C to daily ration is good for chickens at high or low temperatures to maintain body temperature (*Al-Masad M., 2012*). Therefore, vitamin C is added to feed in 1‰ or drinking water in 0.5‰.

The experimental plan of real-time environmental monitoring

Temperature and humidity monitoring system, ammonia monitoring system and video monitoring system are installed in chicken chambers.

Temperature and humidity monitoring system: temperature and humidity sensor of Swiss Sensirion SHT11 is adopted, and the maximum temperature error: $\pm 0.4^{\circ}\text{C}$, and the maximum humidity error: $\pm 3\% \text{RH}$. Four temperature and humidity sensors monitor the temperature and humidity in Chamber 1 and Chamber 2, in front of the chambers and in back of the chambers.

Ammonia monitoring system: Daan Instruments gas monitoring host and electrochemical ammonia gas sensor are adopted. The sensor range is 0-200ppm and the resolution is 1ppm. The sensor is mounted (equipped) on a wall 30cm above the top of the chambers.

Video monitoring system: HIKVISION N1W monitoring host and hemispheric network camera are adopted, and the camera focus is 2.8mm and pixel is 2 million.

The control room with the control system is shown in Figure 2.



Fig. 2 - Control room and control system

The experimental plan of ventilation system

A small chicken chamber for precise breeding mode must have a perfect ventilation system. A reasonable ventilation system can promote indoor gas flow and exchange indoor and outdoor air to a certain extent, and has the effect of eliminating harmful gases, lowering temperature, and improving the environment inside the chamber (Cheng L., 2015; Wu P., 2013; Zhao F., 2014). The ventilation system adopted in the experiment is mainly composed of frequency converter and negative pressure fan. Each chamber has two sets of frequency converter and fan, including internal and external circulated ventilation systems, and cycle power is driven by negative pressure fan controlled by frequency converter. The negative pressure fan of external circulation exhausts directly to outside and the air inlet directly intakes fresh air from outside. For external circulation, the negative pressure fan returns the air through the air passage under the floor is used to complete the internal air circulation. The return air passage has a length to width ratio of 2900mm*550mm*270mm.

The plan of negative pressure fan controlled by the inverter is shown in Table 1 (Du Y., 2016). It is proved by literature and pre-experiment.

Table 1

The plan of negative pressure fan controlled by the inverter

Temperature	The frequency of external circulated inverter	The internal circulated air inlet	The frequency of internal circulation inverter	The air conditioner
Less than 24°C	10 Hz	Open to 30%	0	OFF
24°C~26°C	20 Hz	Open to 30%	0	OFF
26°C ~28°C	30 Hz	Open to 60%	10Hz	OFF
28°C ~30°C	40 Hz	Open to 60%	20 Hz	OFF
30°C ~32°C	50 Hz	Open to 100%	30 Hz	OFF
32°C ~34°C	50 Hz	Open to 100%	50 Hz	OFF
Greater than 34°C	0	Close	30 Hz	Turned on to 30°C

The experimental plan of wind speed detection

15 detecting points are set in Chamber 1 and Chamber2, respectively. The first detecting point starts from the air inlet and the points set in the two chicken chambers are symmetrical. The positions of the specific detection points are shown in Figure 3. The high precision hand-held anemometer of Testo 405i with the precision of $\pm 0.1\text{m/s}$ is used for wind detection and the results are transmitted to the smartphone via Bluetooth.

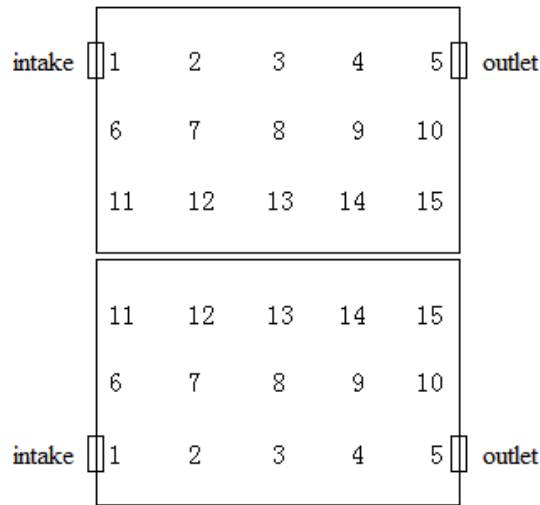


Fig. 3 – The distribution of the wind speed detecting points in Chamber 1 & Chamber 2

The experimental plan of ammonia concentration detection

ZG-1 gas sampling pump and ammonia detection tube made in the Research Institute of Beijing Labour Protection Science are used for ammonia detection. During the experiment, ZG-1 sampling pump is stopped after extracting 100ml air and kept still until the indicator in the tube stops changing colour. The data can be read from the scale corresponding to the yellow column. 9 detecting points are set in Chamber 1 & Chamber 2, respectively. The first detecting point starts from the air inlet and the points set in the two chicken chambers are symmetrical. The positions of specific detection points are shown in Figure 4.

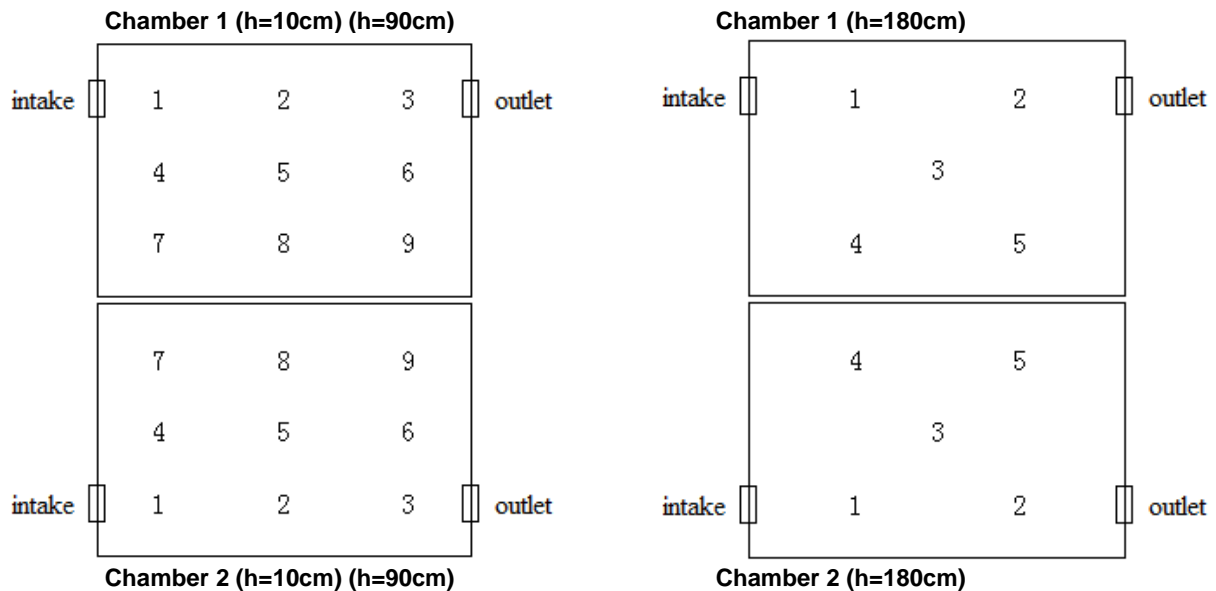


Fig. 4 - The distribution of the ammonia detecting points in Chamber 1 & Chamber 2

The experimental plan of PM_{2.5} mass detection

The lighting time of chicken chamber is from 5:00 AM to 11:00 PM and the lights-out time is from 11:00 PM to 5:00 AM. LB-120F PM_{2.5} sampler in an intermediate flow produced by Qingdao Lubo Weiye Environmental Protection Technology co., LTD is used during the lighting and lights-out time, and the collection of PM_{2.5} is implemented by $\Phi 90\text{mm}$ super fine glass fibre filter membrane working for 6 hours at the sampling rate of 100 litres per minute.

The filter membrane is weighed by ESJ182-4A automatic electronic analytical balance with the accuracy of 0.01mg and maximum range of 30g before and after sampling. For each weighing, the analytical balance is first internally calibrated. The filter membrane is weighed three times after zero clearing and the mean value of the weighting values is taken as the mass. The mass of PM_{2.5} can be calculated by calculating the mass difference of each filter membrane before and after sampling.

Figure 5 (a) shows the working condition of PM_{2.5} sampler in the chamber and Figure 5 (b) shows the experimenter weighing the filter membrane at a certain temperature (26~30°C) and humidity (45~55%).

(a) PM_{2.5} sampler in the chamber

(b) The experimenter weighing the filter membrane

Fig. 5 - The experiment of PM_{2.5} mass detection

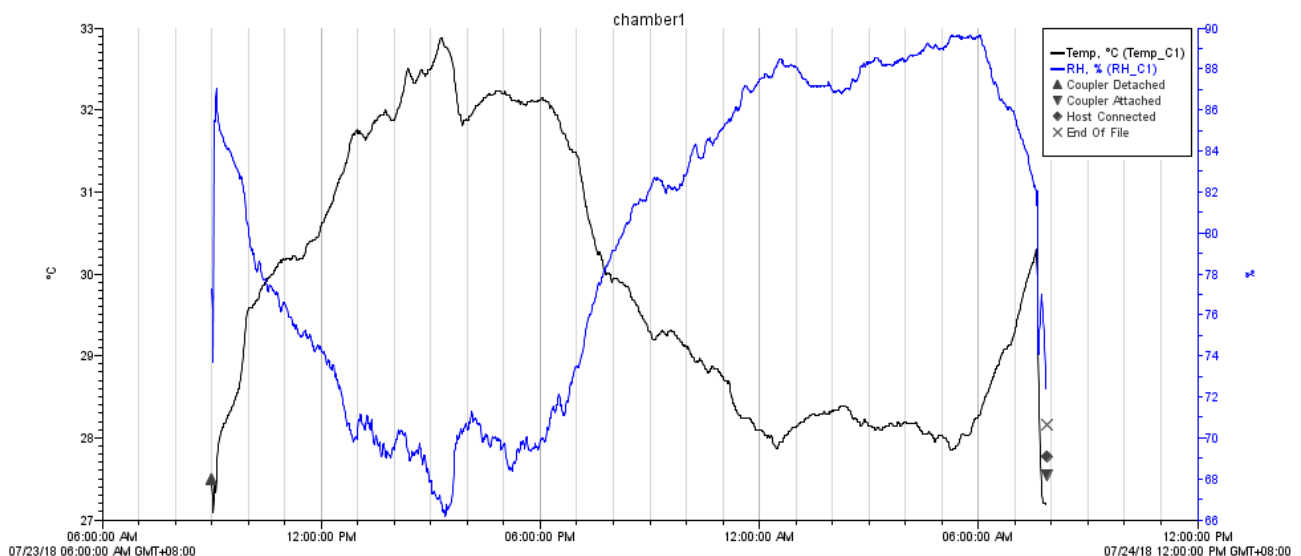
RESULTS

During the 20 days of the experiment, a large number of yellow-feather chickens gathered at the air outlet of chicken chamber each day at the high temperature of 32~34°C and their body got close to the bedding, with their mouth open for breathing and reluctant to move. It suggests that when the temperature reaches 32°C, yellow-feather chickens have already had heat stress symptoms. Once the temperature drops below 32°C, life condition of chickens will restore to a relatively normal state. They will move actively in the chicken chamber, increase water drinking and food intake.

In this experiment, HOBO temperature and humidity instrument, Testo 405i high-precision hand-held anemometer, ZG-1 gas sampling pump and sampling tube and LB-120F PM_{2.5} sampler are used. The collected data are analyzed by software to provide the following results.

Temperature and humidity recording results

In the experiment, the HOBO thermo-hygrometer is set to collect temperature and humidity per minute. After the data collected, the HOBOWare Software is used to read data that can be visualized to view the data or stored as CSV format for further analysis. Graphical results in HOBOWare are shown in Figure 6.

**Fig. 6 – The result of HOBO thermo-hygrometer**

After statistics in HOBOWare, the number of minutes in Chamber 1 where the temperature is greater than 32°C is 3,844 minutes while that in Chamber 2 is 2,854 minutes during the 20-day experiment. The time of high temperature experienced by the chickens of Chamber 1 is 1.35 times as large as that of Chamber 2.

Wind speed measurement results

The wind speed data are measured at 30 points in Chamber 1 and Chamber 2 with Testo 450i and the specific results are shown in Table 2 and Table 3.

Table 2

The results of the wind speed measurement in Chamber 1 related to the inverters

Point	FOECI:10HZ FOICI: 0HZ	FOECI:20HZ FOICI: 0HZ	FOECI:30HZ FOICI: 10HZ	FOECI:40HZ FOICI: 20HZ	FOECI:50HZ FOICI: 30HZ	FOECI:50HZ FOICI: 50HZ
1	0.17	0.24	0.48	0.74	1.13	1.44
2	0.12	0.17	0.29	0.34	0.36	0.48
3	0.04	0.04	0.08	0.11	0.23	0.32
4	0.05	0.15	0.06	0.16	0.25	0.36
5	0.25	0.45	0.86	1.13	1.50	1.77
6	0.01	0.01	0.01	0.04	0.04	0.07
7	0.09	0.13	0.18	0.28	0.39	0.46
8	0.08	0.06	0.10	0.22	0.46	0.60
9	0.05	0.03	0.12	0.16	0.35	0.38
10	0.00	0.01	0.02	0.02	0.03	0.03
11	0.02	0.07	0.41	0.71	1.25	1.74
12	0.01	0.01	0.07	0.20	0.60	0.71
13	0.04	0.01	0.09	0.13	0.44	0.58
14	0.01	0.01	0.06	0.17	0.41	0.49
15	0.02	0.04	0.22	0.60	0.97	1.81

FOECI: frequency of external circulation inverter

FOICI: frequency of internal circulation inverter

Table 3

The results of the wind speed measurement in Chamber 2 related to the inverters

Detecting point	FOECI:10HZ FOICI: 0HZ	FOECI:20HZ FOICI: 0HZ	FOECI:30HZ FOICI: 10HZ	FOECI:40HZ FOICI: 20HZ	FOECI:50HZ FOICI: 30HZ	FOECI:50HZ FOICI: 50HZ
1	0.21	0.44	0.51	1.02	1.73	1.79
2	0.13	0.35	0.52	0.84	0.90	1.55
3	0.08	0.23	0.24	0.25	0.34	0.59
4	0.02	0.16	0.24	0.39	0.26	0.19
5	0.22	0.48	0.81	1.26	1.81	1.97
6	0.01	0.01	0.01	0.02	0.04	0.12
7	0.03	0.01	0.07	0.14	0.18	0.46
8	0.01	0.06	0.04	0.29	0.33	0.40
9	0.04	0.04	0.05	0.11	0.25	0.34
10	0.00	0.01	0.01	0.04	0.05	0.06
11	0.03	0.04	0.36	0.59	1.24	2.32
12	0.01	0.02	0.18	0.44	0.41	0.95
13	0.01	0.02	0.15	0.24	0.08	0.67
14	0.02	0.03	0.07	0.05	0.13	0.59
15	0.01	0.06	0.13	0.43	0.96	1.59

FOECI: frequency of external circulation inverter

FOICI: frequency of internal circulation inverter

Wind speed at air inlet and outlet during heat stress response at 32~34°C meets ventilation requirements of 1.78 ~ 2.03 m/s; this is also the reason why the chickens gather at air inlet and outlet during heat stress response.

Ammonia detection results

Ammonia is not detected since insufficient chicken excrement accumulates on the bedding at the early stage of the experiment. Table 4 shows the concentration of ammonia measured at each test point in Chamber 1 at a height of 10 cm from the ground on August 2, 2018. Table 5 shows the concentration of ammonia measured in chambers at a height of 10cm, 90cm and 180cm from the ground on August 6, 2018.

From Table 4 and Table 5, the ammonia concentration distribution also indicates that the chickens prefer to gather at the air inlet and outlet. According to the environmental quality standard of livestock and poultry farm of the Ministry of Agriculture, the ammonia gas concentration in the chicken chamber for chickens within 50 days should be less than 10ppm. After multi-point detection, the ammonia concentration value is less than 10ppm, meeting the breeding requirements.

Table 4**The ammonia concentration in Chamber 1 on Aug. 2, 2018**

Height	Detecting point	Detecting value (unit: ppm)
10cm	1	2.5
10cm	2	1.5
10cm	3	2.0
10cm	4	1.5
10cm	5	0.5
10cm	6	1.5
10cm	7	1.5
10cm	8	1.0
10cm	9	1.5

Table 5**The ammonia concentration in Chamber 1 & 2 on Aug. 6, 2018**

Height (cm)	Detecting point	Detecting value (unit: ppm)	
		Chamber1	Chamber2
10	1	6.0	4.5
10	2	3.5	3.8
10	3	4.5	4.5
10	4	4.5	5.0
10	5	5.5	4.0
10	6	5.0	4.0
10	7	4.0	6.0
10	8	4.0	4.5
10	9	4.5	4.0
90	1	4.0	4.2
90	2	3.8	3.8
90	3	3.0	4.0
90	4	3.8	4.0
90	5	3.5	3.8
90	6	3.0	4.0
90	7	3.8	4.5
90	8	3.5	4.0
90	9	3.0	4.0
180	1	4.0	4.0
180	2	3.8	4.0
180	3	4.0	4.5
180	4	4.0	3.8
180	5	4.0	4.0

PM_{2.5} detection results

Statistical results after measuring PM_{2.5} mass are shown in Table 6. Table 6 shows that in the daytime when chickens are active, the mass of PM_{2.5} in the chicken chamber is much higher than that outside the chicken chamber, which is about three times higher. In the lights-out time for 6 hours when the chickens are sleeping, the PM_{2.5} mass is measured to be much less than that of the chickens when they are active during the day, which is less than 10% of that during the daytime. Moreover, in the lights-out time at night, the PM_{2.5} mass inside and outside of the chicken chamber is similar under the effect of air exchange.

Table 6**PM_{2.5} mass per hour both inside and outside of the chambers during the daytime and lights-out time**

Chamber Number	Daytime		Lights-out time	
	PM _{2.5} mass per hour inside the chamber (unit: g)	PM _{2.5} mass per hour outside the chamber (unit: g)	PM _{2.5} mass per hour inside the chamber (unit: g)	PM _{2.5} mass per hour outside the chamber (unit: g)
1	0.00180	0.00066	0.00015	0.00021
2	0.00249	0.00074	0.00020	0.00021

Weight of chicken

At the end of 20 breeding days, the yellow-feather chickens in Chamber 1 and Chamber 2 are weighed and the weight of yellow-feather chickens measured on the 1st and 20th day in each chamber is averaged, thus the weight gain rate is obtained using formula (1) as follows.

$$Growthrate = \frac{W_{after} - W_{before}}{W_{before}} \times 100\% \quad (1)$$

where:

Growth rate denotes the growth rate of chickens, W_{before} denotes the average weight of chickens before being put in Chamber 1 or Chamber 2, W_{after} denotes the average weight of chickens after being bred in Chamber 1 or in Chamber 2 for 20 days.

After calculation, the final result is obtained as shown in Table 7.

Table 7**Statistical result of chickens weight gain in Chamber 1 & Chamber 2**

Chamber number	The average weight of chickens on the 1st day (unit: g)	The average weight of chickens on the 20th day (unit: g)	Growth rate
Chamber 1	217.0	399.7	84.22%
Chamber 2	215.9	420.2	94.64%

CONCLUSIONS

At the end of the 20-day experiment, there is no mortality of yellow-feather chickens due to heat stress or air quality problems and the following conclusions are obtained via the experiment.

(1) The heat stress response will slow down the growth of broilers and change the colour of excreta. Under the effect of the ventilation system, yellow-feather chickens will have slight heat stress response at 32 ~ 34°C, but not life-threatening. If the ambient temperature of the chicken chamber keeps 32°C above for a long time, the chickens grow slowly. If the ambient temperature is controlled within 32°C, the chickens grow faster.

(2) When proper bedding and feed are selected and reasonable ventilation management system is set, the concentration of ammonia gas and PM_{2.5} can be effectively reduced, the air quality in the chicken chamber can be improved, so that the normal growth of yellow-feather chickens can be guaranteed. It also suggests that this kind of small chicken chamber is easy to carry out precision control and the health of chickens can be further guaranteed.

ACKNOWLEDGEMENTS

This work was supported by China Postdoctoral Science Foundation (2015M571782), the Fundamental Research Funds for the Central Universities of China (KYTZ201661), and Jiangsu Agricultural Machinery Foundation (GXZ14002).

REFERENCES

- [1] Al-Masad M., (2012), Effects of Vitamin C and Zinc on Broilers Performance of Immunocompetence Under Heat Stress, *Asian Journal of Animal Sciences*, Vol. 6, Issue 2, pp. 76-84, Dubai/UAE;
- [2] Al-Saffar A., and Rose S., (2002), Ambient temperature and the egg laying characteristics of laying fowl, *World's Poultry Science Journal*, Vol. 58, pp. 317-331, Cambridge/England;
- [3] Beker A., Vanhooser S., Swartzlander J. et al., (2004), Atmospheric ammonia concentration effects on broiler growth and performance, *Journal of Applied Poultry Research*, Vol. 13, Issue 1, pp. 5-9, Savoy/USA;
- [4] Chen F., (2014), Research on particulate matter and harmful gas concentration in cage layer house, *Kunming University of Science and Technology*, Kunming/China;
- [5] Cheng L., Wu Y., Wang Y., et al., (2015), Effect of manure cleaning method on air quality in layer house and the physicochemical properties of manure, *China Poultry*, Vol. 37, Issue 18, pp. 22-27, Jiangsu/China;
- [6] Du Y., Pang L. and Wang Y., (2016), Research and application of "precise" ventilation technology for laying hens, *Poultry Science*, Vol. pp. 25-27, Shandong/China;
- [7] Farooqi H., Khan M., Khan M. et al., (2005), Evaluation of betaine and vitamin C in alleviation of heat stress in broilers, *International Journal of Agriculture & Biology*, Vol. 7, pp. 744-746, Faisalabad/Pakistan;
- [8] Kocaman B., Esenbuga N., Yildiz A. et al., (2006), Effect of environmental conditions in poultry houses on the performance of laying hens, *International Journal of Poultry Science*, Vol. 5, Issue 1, pp. 26-30, Dubai/UAE;
- [9] Li Q., Wang-Li L., Shah S. et al., (2014), Ammonia concentrations and modeling of inorganic particulate matter in the vicinity of an egg production facility in southeastern USA, *Environ Sci Pollut Res Int*, Vol. 21, Issue 6, pp. 4675-4685, Berlin/ Germany;
- [10] Lin T., Shah S., Wang-Li L., et al., (2016), Development of MOS sensor-based NH₃ monitor for use in poultry houses, *Computers and Electronics in Agriculture*, Vol. 127, pp. 708-715, Oxford/England;
- [11] Liu Y. and Li B., (2015), Research progress of welfare-oriented breeding mode and technical equipment for laying hens, *Transactions of the Chinese Society of Agricultural Engineering*, Vol. 31, Issue 23, pp. 214-221, Beijing/China;
- [12] NY/T388-1999, *Ministry of Agriculture*, Beijing/China;
- [13] Robins A. and Phillips C., (2011), International approaches to the welfare of meat chickens, *World's Poultry Science Journal*, Vol. 67, Issue 02, pp. 351-369, Cambridge/England;
- [14] Wu P., (2013), Research about variation of semi-open sheds in different seasons on environmental parameters and its effect on the performance of laying hens *Hebei Agricultural University*, Hebei/China;
- [15] Xing H., (2015), Effect of ammonia in house on lipid metabolism of broilers, *Chinese Academy of Agricultural Sciences*, Beijing/China;
- [16] Yang W., (2016), Detection and analysis of components of airborne microbes and PM_{2.5} in poultry house, *Shandong Agricultural University*, Shandong/China;
- [17] Yuan J., Zhang K. and Hu X., (2007), Study on the effect of environment factors on the growth of broiler chickens, *Journal of Domestic Animal Ecology*, Vol. 28, Issue 16, pp. 135-138, Shaanxi/China;
- [18] Zhao F., Luo Y., Zhang L., et al., (2014), Effect of roof with ceiling on air quality in laying house, *China Poultry*, Vol. 36, Issue 10, pp. 25-28, Jiangsu/China.

RESEARCH ON TEMPERATURE PREPARATION OF DIESEL BIOFUEL IN AN ENERGY VEHICLE FUEL TANK

/

ДОСЛІДЖЕННЯ ТЕМПЕРАТУРНОЇ ПІДГОТОВКИ ДИЗЕЛЬНОГО БІОПАЛИВА В ПАЛИВНОМУ БАКУ ЕНЕРГОЗАСОБУ

Prof.D.Sc. Golub G.A.¹⁾, Ph.D. Eng. Chuba V.V.¹⁾, Ph.D. Eng. Керко О.І.²⁾

¹⁾National University of Life and Environmental Sciences of Ukraine, Kyiv / Ukraine;

²⁾Uman National University of Horticulture, Uman / Ukraine

Tel: +380630499929, E-mail керко@meta.ua

Keywords: diesel biofuel, fuel tank, diesel engine of internal combustion, heating of biofuel

ABSTRACT

The expediency of using diesel biofuel heating in a fuel tank at low ambient temperatures has been substantiated. The article represents a mathematical model of dynamics of diesel biofuel heating in a fuel tank, with the help of a cooling liquid, of the internal combustion engine. Comparative experimental and theoretical studies of diesel biofuel heating in a fuel tank have been made. On the basis of the obtained data, a mathematical dependence has been generated to determine the additional operating costs of diesel fuel associated with the use of diesel biofuel on the basis of fatty acids as the main fuel. The work presents the results of the carried out tests.

РЕЗЮМЕ

Обґрунтовано доцільність використання підігріву дизельного біопалива в паливному баку при низьких температурах навколишнього середовища. В статті представлено математичну модель динаміки нагріву дизельного біопалива в паливному баку за допомогою охолоджуючої рідини двигуна внутрішнього згорання. Виконано порівняльні експериментальні та теоретичні дослідження процесу нагріву дизельного біопалива в паливному баку. На основі отриманих даних сформовано математичну залежність для визначення додаткових експлуатаційних витрат дизельного палива пов'язаних з використанням в якості основного палива дизельного біопалива на основі жирних кислот. Робота представляє результати проведених випробувань.

INTRODUCTION

Lack of energy resources, high prices and environmental problems associated with the use of fossil fuels encourage the production and use of alternative energy sources derived from renewable raw materials. Diesel biofuel based on fatty acids of vegetable or animal fats manufactured using the reaction of transesterification, has the most similar properties in comparison with standard fuel of diesel engines. Physical and chemical properties allow using diesel biofuel with minimal changes of constructions and settings of existing diesel engines.

Mentioning the advantages of using diesel biofuel, a number of shortcomings should be noted, which should include high indicators of kinematic viscosity, temperature of turbidity and hardening in the first place (Agarwal A.K., Gupta J.G., Dhar A., 2017; Alptekin E., Canakci M., 2009; Dunn R.O., 2009). The analysis of physical and mechanical properties of diesel biofuel obtained from various vegetable and animal fats indicates problems associated with the use at temperatures below plus 10 degrees (Pérez Á., Casas A., Fernández C., Ramos M., Rodríguez L., 2010; Sandhya K. Vijayan, Mary Naveena Victor, Abinandan Sudharsanam, Velappan Kandukalpatti Chinnaraj, Vedaraman Nagarajan, Sandhya K. Vijayan, 2018). The use of diesel biofuel at low ambient temperatures leads to blockages of filters and fuel lines (Kerschbaum S., Rinke G., Schubert K., 2008; Ramos M.J., Fernandez C.M., Casas A., Rodriguez L., Perez A., 2009; Park J. Y., Kim D.K., Lee J.P., Park, S.C., Kim Y.J., Lee, J.S. 2008), the appearance of uncharacteristic vibrations (Lapuerta M., Herreros J. M., Garcia-Contreras R., Briceno Y., 2008) in structural elements of fuel equipment, the formation of soluble and insoluble precipitates in fuel tanks and storage tanks (Kerschbaum S., Rinke G., Schubert K., 2008; Dwivedi G., Verma P., Sharma M.P., 2016).

Peculiarities of low temperature of biofuel are associated with the length and branching of the fatty acids structural chain, the location of double bonds along the length of the chain and the degree of

unsaturation of the molecules (Dunn R.O., 2009; Sierra-Cantor J.F., Guerrero-Fajardo C.A., 2017; Ramos M.J., Fernandez C.M., Casas A., Rodriguez L., Perez A., 2009; Yuan M.H., Chen Y.H., Chen J.H., Luo Y.M. 2017). Nowadays quite a lot of studies have been carried out allowing to improve the low-temperature properties of diesel biofuel to some extent, but the proposed methods will require the implementation of additional technological operations (Knothe G., Krahl J. & Gerpen J Van., 2015; Pérez Á., Casas A., Fernández C., Ramos M., Rodríguez L., 2010), additional components (Maximo G.J., Magalhães A.M.S., Gonçalves M.M., 2018; Udomsap P., Sahapatsombat U., Puttasawat B., Krasae P., 2008; Ali O.M., Mamat R., Abdullah N.R., Abdullah A.A., 2016; Lapuerta M., Herreros J. M., Garcia-Contreras R., Briceno Y., 2008) and leads to a decrease in the output of the finished product (Pérez Á., Casas A., Fernández C., Ramos M., Rodríguez L., 2010), which negatively affects the profitability of production and the economic attractiveness of this fuel for the end user.

The work (Trehub M.I., Chuba V.V., 2008; Golub G.A., Chuba V.V., Pavlenko M. U., 2012) considers the temperature aspects of using pure diesel biofuels and their mixtures with petroleum fuels. The authors propose the use of pre-heating diesel fuel in a fuel tank during the cold season in order to optimize viscosity to ensure fluidity and filtration. In terms of quality of the filtration process - the best filtering of diesel fuel with coarse filters and fine purification occurs when the kinematic viscosity of fuel in the range 2.5-4.0 mm²/s. For diesel biofuels, this kinematic viscosity can be reached in the temperature range from 30 to 45°C, and heating of fuel to this temperature range can be achieved without significant changes to existing fuelling systems of the internal combustion engine.

The goal of this work is to increase the efficiency and assess the use of diesel biofuel by substantiating the performance indicators of the heating system.

MATERIALS AND METHODS

To determine the cloud point and pour point the fuel samples were previously dehydrated. After dehydration, the fuel was poured into two transparent glass tubes. The test tube, which had double walls, was placed into a cooling thermostat, the other one served as a standard. When the temperature dropped by 0.1°C the tubes were lit, with signs of cloudiness it was recorded the appropriate temperature. With further cooling, the tube was periodically pricked, when the fuel lost mobility at an angle of 45 degrees, the pour point was fixed.

Viscosity of diesel biofuel and its mixtures with diesel fuel of oil origin was determined using liquid viscometers, which were placed into a thermostat maintaining a constant set temperature.

To study the effectiveness of diesel biofuel heating, the fuel system of the tractor type “MT3-100” was modernized according to the scheme (Golub G.A., Trehub M.I., Chuba V.V., Pavlenko M. U., 2018). A diesel fuel tank is equipped with a liquid heat exchanger, which is included in the small circle of the cooling system of the diesel engine for internal combustion (fig. 1).

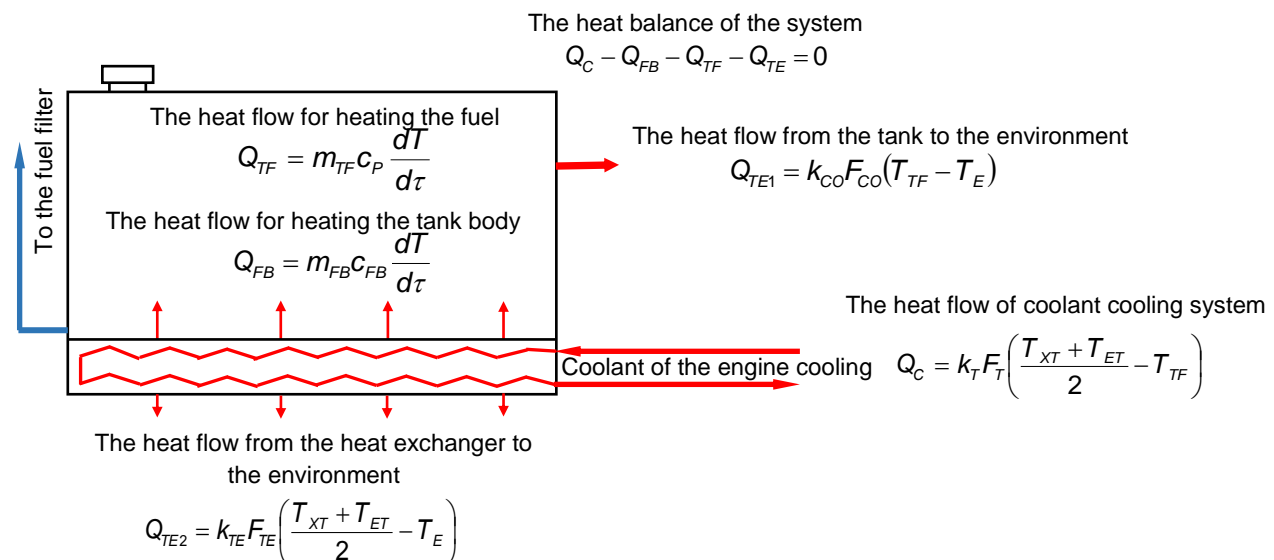


Fig. 1 - Scheme for calculating diesel biofuels heating

The notations in the figure are:

Q_C – the heat flow that gives the heat-carrier during the passage of the heat exchanger, W; Q_{FB} – a heat flow transmitted to the fuel tank body, W; Q_{TF} – a heat flow transmitted to fuel, W; Q_{TE} – a heat flow lost to the environment, W; m_{TF} – is the fuel mass in a tank, kg; c_P – specific heat of fuel, J/kg°C; m_{FB} – tank mass, kg; c_{FB} – specific heat of a tank material, J/kg°C; k_T – a coefficient of heat transfer through a flat wall between the heating medium and fuel, W/m²°C; F_T – the area of heat exchange between the heating medium and the fuel in the tank, m²; T_{XT} – the temperature of the coolant at the inlet to the heat exchanger, °C; T_{ET} – temperature of the cooling fluid at the outlet of the heat exchanger, °C; T_{TF} – the fuel temperature in the tank, °C; k_{CO} – the coefficient of heat transfer through the outer walls of the tank to the environment W/m²°C; F_{CO} – the area of the external surface of the tank in contact with the environment, m²; T_E – ambient temperature, °C; k_{TE} – a coefficient of heat transfer through the external wall of the heat exchanger to the environment, W/m²°C, F_{TE} – the area of the external surface of the heat exchanger in contact with the environment, m².

To measure the temperature of the fuel in the fuel tank, the temperature of the coolant at the inlet to the heat exchanger and at the exit from it, a thermocouple is installed. The temperature change recording was carried out continuously with the help of program- hardware complex on the basis of the personal computer “ASUS” and a temperature meter “Regmik”. The coolant flow through the heat exchanger was fixed using a liquid flow meter. The velocity of air motion in the basin area of the tank was measured using an anemometer. General view of experimental equipment during research is shown in fig. 2.



Fig. 2 - General view of experimental equipment during research

a - general view of a tractor with a biofuel tank with heating; b - diesel biofuel tank with heating

Before the measurement, the engine was heated to the working temperature, and the ambient and fuel temperatures in the fuel tank were recorded. After reaching the working temperature, the engine opened the supply of the heated coolant to the heat exchanger of the fuel tank and the changes in fuel temperature in the fuel tank were measured, as well as the temperature of the coolant at the inlet and outlet of the heat exchanger. The research was carried out at engine idling mode at constant turnovers, and during the study period the coolant flow rate and air flow velocity were determined.

Using the experimental data obtained, a theoretical modelling of the diesel fuel heating time in a fuel tank was performed. A comparison of the obtained theoretical and experimental dependence has been performed. On the basis of the obtained data, a mathematical dependence has been generated to determine the additional operating costs of diesel fuel when using biofuels.

RESULTS

The obtained indicators of the cloud point and pour point of diesel biofuels produced from the main oilseeds of Ukraine for determining the maximum temperature range of the use of diesel biofuels are shown in table 1. The cloud point of diesel biofuel characterizes the appearance of particles that can clog the fuel line and the filter elements of the engine.

Table 1

Cloud point and pour point of diesel biofuel

Indicator	Diesel biofuel based on		
	soybean oil	sunflower oil	rapeseed oil
Cloud point, °C	10.0	9.6	7.9
Pour point, °C	2.7	0.9	-0.8

The analysis of the obtained results allows asserting the inexpediency of the use of diesel biofuel at a temperature of less than 10°C.

An important parameter that provides fuel filtration is the kinematic viscosity. We have performed comparative studies to determine the effect of temperature on the viscosity of diesel biofuel produced from rapeseed and soybean oil depending on temperature (table 2). It should be noted that in order to improve the low-temperature properties, diesel biofuel based on soybean oil is additionally frozen.

Table 2

Fuel type	Temperature, C					
	0	3	8.5	14	17.5	20
Diesel fuel	10.22	8.43	6.13	5.27	4.85	4.5
Diesel biofuel from rapeseed oil	17.42	13.31	10.97	8.92	8.2	7.64
Diesel biofuel from soybean oil	14.23	11.06	8.5*	7.21	6.68	6.15

* – data is recorded at a temperature of 8.2 °C.

It was found that in the studied temperature range from 14 to 20°C the kinematic viscosity of diesel biofuel from rapeseed and soybean oils when compared to diesel fuel is higher by 70% and 37%, respectively. When comparing diesel fuel with biofuel from soybean oil, the viscosity of diesel biofuel from rapeseed oil is higher by 24%.

One of the directions of diesel biofuel use is the use of mixtures with diesel fuel of oil origin. We have researched the effect of temperature on the viscosity of mixtures of diesel biofuels based on soybean and rapeseed oils with the addition of 30 and 50 percent of diesel fuel of oil origin (table. 3).

Table 3

Fuel	Temperature, °C				
	0	3	8	14	19
70 % biofuel from rapeseed oil +30 % diesel fuel	15.23	11.34	8.96	7.36	7.22
70 % biofuel from soybean oil +30 % diesel fuel	11.92	9.97	7.74	6.42	6.27
50 % biofuel from rapeseed oil +50 % diesel fuel	14.83	10.83	8.29	6.94	6.02
50 % biofuel from soybean oil +50 % diesel fuel	11.42	9.31	7.18	6.09	5.91

The analysis shows that the kinematic viscosity of fuel mixtures also decreases with increasing fuel temperature. Fuel mixtures with 30% of diesel fuel content have a kinematic viscosity higher by 2-8% when compared to a mixture containing 50% of diesel fuel depending on the temperature. This proportion is typical for both rapeseed and soybean oil biofuels.

Studies have shown that at a temperature of 19°C, the addition of biofuel from rapeseed oil and 30% of diesel fuel leads to a decrease in the viscosity of the mixture by 5.5%, and the addition of 50% of diesel fuel reduces the viscosity of the mixture by 13 %. When the temperature drops down to 14°C the difference in kinematic viscosity increases up to 17% and 27%, respectively. The addition of diesel fuel to biofuels from soybean oil reduces the kinematic viscosity by 2 % and 4 % at 19°C, respectively, for mixtures containing 30% and 50% of diesel fuel and 11% and 17% at 14°C. Consequently, the addition of diesel fuel leads to a certain decrease in the kinematic viscosity of diesel biofuel, but does not allow increasing its kinematic viscosity at low temperatures.

In Ukraine, a significant number of technological operations of agricultural production are carried out at an ambient temperature below 10°C. In this case, the most appropriate way to improve the efficiency of diesel biofuels use is its heating in the fuel tank.

Taking into account the expressions for determining the heat flow, the equation of heat flows balance of a fuel tank with a liquid heat exchanger takes the form:

$$\left(m_{TF}c_p + m_{FB}c_{FB}\right) \frac{dT}{d\tau} = (k_T F_T - k_{TE} F_{TE}) \left(\frac{T_{XT} + T_{ET}}{2}\right) - (k_T F_T + k_{CO} F_{CO}) T_{TF} + (k_{TE} F_{TE} + k_{CO} F_{CO}) T_E \quad (1)$$

Having solved the differential equation (1), we obtain the equation for changing the final temperature of fuel in the tank from the values of the parameters of the heat transfer equation:

$$T_{FTT} = \frac{(k_T F_T - k_{TE} F_{TE}) \left(\frac{T_{XT} + T_{ET}}{2} \right) + (k_{TE} F_{TE} + k_{CO} F_{CO}) T_E}{(k_T F_T + k_{CO} F_{CO})} \times$$

$$\times \left(1 - \exp \left(- \frac{(k_T F_T + k_{CO} F_{CO})}{(m_{TF} c_p + m_{FB} c_{FB})} \tau \right) \right) + T_{ITT} \exp \left(- \frac{(k_T F_T + k_{CO} F_{CO})}{(m_{TF} c_p + m_{FB} c_{FB})} \tau \right) \quad (2)$$

where:

T_{ITT} – the initial temperature of fuel in the tank, °C;

T_{FTT} – the final temperature of fuel in the tank, °C;

τ – time of fuel heating in the fuel tank, s.

The given equation (2) determines the relationship between the technological and structural parameters of a fuel tank and a liquid heat exchanger for heating fuel in a fuel tank.

In order to verify the obtained theoretical dependence (2), experimental research of the process of diesel fuel heating in a fuel tank was carried out at engine running at idle speed, the parameters of the heat exchange process (Table 4) were determined, and an experimental dependence of the temperature change of fuel in a fuel tank (Fig. 3) was obtained. Heat transfer coefficients (Table 4) are calculated in accordance with the well-known formulas and empirical dependencies.

Using the dependence (2), on the basis of the parameters of the heat exchange process and the structural parameters of the fuel tank (Table 4), the theoretical modelling of the fuel heating process in the fuel tank was made, and the theoretical dependence of the heating fuel dynamics (Fig. 3) was constructed.

The value of the deviation of the experimental and theoretical values of the fuel temperature is estimated by the determination index, which is $\eta^2 = 0.953$, which gives an opportunity to draw a conclusion on the correctness of the chosen method of theoretical calculations. The discrepancy between experimental and theoretical data is due to the fact that during theoretical research, due to the complexity of the determination, the heat loss wasn't taken into account during the heat transfer between the tank and the tractor body parts at the points of the tank fixing.

Table 4

Constructive and technological parameters of the heat exchange process of diesel biofuel heating during theoretical calculation

No	Parameter name	Parameter marking and measure unit	Parameter value
1	The area of the tank outer surface	F_{CO} , m ²	0.388
2	The thickness of the tank wall	δ_{TW} , m	0.004
3	The thermal conductivity coefficient of the tank wall material	λ_{TC} , W/m °C	51.5
4	Air movement speed	V_{AM} , m/s	2
5	The coefficient of heat transfer through the tank outer wall to the environment	k_{TV} , W/m ² °C	13.275
6	The area of heat exchange between the heating medium and fuel in the tank	F_T , m ²	0.08
7	Coolant flow rate	V_T , m/s	0.01683
8	Heat transfer coefficient from the heating medium to the fuel	k_T , W/m ² °C	220.196
9	The area of the heat exchanger external surface in contact with the environment	F_{TE} , m ²	0.268
10	The coefficient of heat transfer through the heat exchanger exterior wall to the environment	k_{TE} , W/m ² °C	13.295
11	The temperature of the engine coolant at the inlet to the heat exchanger	T_{XT} , °C	81
12	The temperature of the engine coolant at the output of the heat exchanger	T_{ET} , °C	77
13	Ambient temperature	T_E , °C	13
14	Initial fuel temperature in the fuel tank	T_{ITT} , °C	13
15	Mass of fuel in the tank	m_{FB} , kg	25
16	Specific heat of diesel biofuel	c_p , J/kg °C	2100
17	Tank mass	M_{BK} , kg	30
18	Specific heat capacity of the tank material	c_{FB} , J/kg °C	462

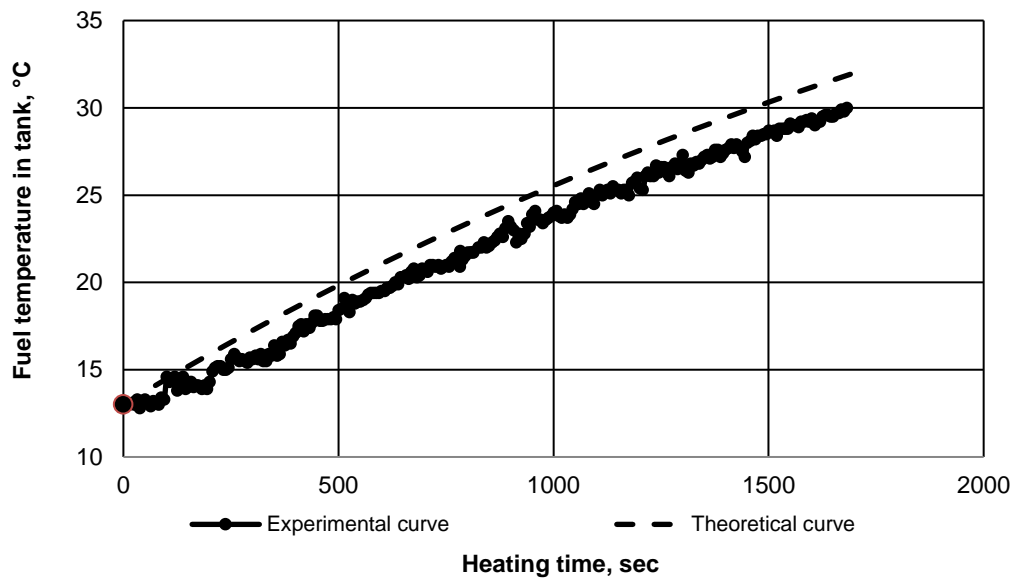


Fig. 3 - Dynamics of the process of heating diesel fuel in a fuel tank

In order to prevent the introduction of diesel biofuel into motor oil, the start of diesel engine while working on diesel biofuel should be carried out only on diesel fuel. The variable consumption of diesel fuel associated with starting of the engine can be determined based on the design features, in the formula:

$$Q_{DF}^V = k_{RR} (V_{CFF} + V_{FFF} + V_F + V_{IVHP}) \quad (3)$$

where:

Q_{DF}^V – variable diesel fuel consumption for engine start, l ;

k_{RR} – reserve coefficient, relative unit;

V_{CFF} – volume of a coarse fuel filter, l ;

V_{FFF} – volume of fine fuel filter, l ;

V_F – internal volume of fuel lines, l ;

V_{IVHP} – internal volume of the head of the high-pressure fuel pump, l .

The variable fuel consumption of diesel fuel when the diesel fuel tank is heated at an ambient temperature below 10°C can be determined as follows:

$$Q_{DF}^H = t_H G_{HF} \quad (4)$$

where:

Q_{DF}^H – variable diesel fuel consumption for engine start and fuel heating in the fuel tank, l ;

t_H – an operating time of the engine on diesel fuel, required for heating diesel biofuels in a fuel tank, h ;

G_{HF} – hourly fuel consumption, at the operation mode of the engine in the heating of diesel biofuel, l .

The total additional consumption of diesel fuel when diesel oil is replaced by biofuel, can be determined based on the consumption of diesel fuel as follows:

$$Q_{DF}^D = \frac{Q_{DF}}{Q_{VF}} [k_{DF} k_{RR} (V_{CFF} + V_{FFF} + V_F + V_{IVHP}) + (1 - k_{DF}) t_H G_{HF}] \quad (5)$$

where:

k_{DF} – is a coefficient of diesel fuel consumption distribution, in accordance with the maximum temperature of diesel fuel without heating, relative unit;

Q_{DF} – amount of diesel fuel spent on the execution of the unit or volume of work, l ;

Q_{VF} – average fuel consumption variable, l .

The obtained dependence (5) allows calculating the consumption of diesel fuel due to the operational features of the use of diesel biofuel and the need for its heating at low temperatures.

CONCLUSIONS

The results of studies on the cloud point and pour point, as well as the kinematic viscosity of diesel biofuels and its mixtures with diesel fuel at temperatures ranging from 0 to 20°C , indicate that the effective range of use of diesel biofuels, in which the properties of biofuels will not significantly affect the operation of

the diesel engine, is at a temperature higher than 10°C. At ambient temperatures below 10°C, to ensure fuel filtration, it is advisable to use preheating of fuel in the fuel tank.

The differential equation of diesel biofuel heating in a fuel tank has been defined, which connects the design parameters of the fuel tank, the temperature conditions of the environment and the parameters of the heat exchange process.

The comparative theoretical and experimental studies allow stating the adequacy of the solution of the differential fuel heating equation in the fuel tank. The obtained mathematical dependence can be used in further research on operation modes of the internal combustion engine and the heating of a fuel tank, from an optimization method of diesel biofuel heating time in a fuel tank.

As a result of the analysis of the diesel engine performance when using diesel biofuel, an expression has been obtained to determine the additional operating costs of diesel fuel associated with starting the engine and heating diesel fuel in a fuel tank.

The obtained results allow to design the operating modes of the engine during diesel fuel heating in a fuel tank at low ambient temperatures and to evaluate the additional operating costs of diesel fuel of oil origin.

REFERENCES

- [1] Agarwal A.K., Gupta J.G., Dhar A., (2017), Potential and challenges for large-scale application of biodiesel in automotive sector, *Progress in Energy and Combustion Science*, 61, pp. 113-149;
- [2] Ali O.M., Mamat R., Abdullah N.R., Abdullah A.A., (2016), Analysis of blended fuel properties and engine performance with palm biodiesel-diesel blended fuel. *Renewable Energy*, 86, pp. 59-67;
- [3] Alptekin E., Canakci M., (2009), Characterization of the key fuel properties of methyl ester-diesel fuel blends. *Fuel*, 88 (1), pp. 75-80;
- [4] Dunn R.O., (2009), Effects of minor constituents on cold flow properties and performance of biodiesel. *Progress in Energy and Combustion Science*, 35, pp. 481–489;
- [5] Dwivedi G., Verma P., Sharma M.P., (2016), Impact of oil and biodiesel on engine operation in cold climatic condition. *Journal of Materials and Environmental Science*, 7 (12), pp. 4540-4555;
- [6] Golub G.A., Chuba V.V., Pavlenko M. U., (2012), Areas of improvement of production and use of diesel biofuels (Напрямки удосконалення виробництва і використання дизельного біопалива). *Collection of scientific works Vinnytsia National Agrarian University (Збірник наукових праць Вінницького державного аграрного університету)*, 10 (1), pp. 20-23;
- [7] Golub G.A., Trehub M.I., Chuba V.V., Pavlenko M. U., (2018), *Fuel heating system for diesel internal combustion engine (Система нагріву палива для дизельного двигуна внутрішнього згорання)*. Patent No. 116375. Ukraine;
- [8] Kerschbaum S., Rinke G., Schubert K., (2008), Winterization of biodiesel by micro process engineering. *Fuel*, 87(12), pp. 2590–2597;
- [9] Knothe G., Krahl J., Gerpen J Van., (2015), *The Biodiesel Handbook* (2nd. ed.). Urbana, Illinois: AOCS Press;
- [10] Lapuerta M., Herreros J. M., Garcia-Contreras R., Briceno Y., (2008), Effect of the alcohol type used in the production of waste cooking oil biodiesel on diesel performance and emissions. *Fuel*, 87(15-16), pp. 3161-3169;
- [11] Maximo G.J., Magalhães A.M.S., Gonçalves M.M., (2018), Improving the cold flow behaviour of methyl biodiesel by blending it with ethyl esters. *Fuel*, 226, pp. 87-92;
- [12] Park J. Y., Kim D.K., Lee J.P., Park, S.C., Kim Y.J., Lee, J.S., (2008), Blending effects of biodiesels on oxidation stability and low temperature flow properties. *Bioresource Technology*, 99 (5), pp. 1196-1203
- [13] Pérez Á., Casas A., Fernández C., Ramos M., Rodríguez L., (2010), Winterization of peanut biodiesel to improve the cold flow properties. *Bioresource Technology*, 101(19), pp. 7375-7381;
- [14] Ramos M.J., Fernandez C.M., Casas A., Rodriguez L., Perez A., (2009), Influence of fatty acid composition of raw materials on biodiesel properties. *Bioresource Technology*, 100(1), pp. 261–268;
- [15] Sandhya K. Vijayan, Mary Naveena Victor, Abinandan Sudharsanam, Velappan Kandukalpatti Chinnaraj, Vedaraman Nagarajan, (2018), Winterization studies of different vegetable oil biodiesel, *Bioresource Technology Reports*, 1, pp. 50-55.
- [16] Sierra-Cantor J.F., Guerrero-Fajardo C.A., (2017), Methods for improving the cold flow properties of biodiesel with high saturated fatty acids content: A review. *Renewable and Sustainable Energy Reviews*, 72, pp. 774-790;

- [17] Trehub M.I., Chuba V.V., (2008), Method of using biodiesel fuel, made on basis of vegetable oil (Спосіб використання біодизельного пального, виготовленого на основі рослинної олії). NSC «IAEE» *"Mechanization and electrification of agriculture: collected papers"*, (92), pp. 312 - 318;
- [18] Udomsap P., Sahapatsombat U., Puttasawat B., Krasae P., (2008), Preliminary research on cold flow improvers for palm-derived biodiesel blends. *Journal of Metals, Materials and Minerals*, 18(2), pp. 99-102;
- [19] Yuan M.H., Chen Y.H., Chen J.H., Luo Y.M., (2017), Dependence of cold filter plugging point on saturated fatty acid profile of biodiesel blends derived from different feedstocks. *Fuel*, 195, pp. 59-68.

NUMERICAL ANALYSES OF AIR VELOCITY AND TEMPERATURE DISTRIBUTION IN POULTRY HOUSE USING COMPUTATIONAL FLUID DYNAMICS

آنالیز عددی توزیع سرعت و دما در مرغداری با استفاده از دینامیک سیالات محاسباتی

Ph.D. Stud. Eng. Pourvosoghi N¹⁾, Assoc.Prof. Ph.D. Eng. Nikbakht A.M.¹⁾,
Assoc.Prof. Ph.D. Eng. Sharifian F.¹⁾, Assist.Prof. Ph.D. Eng. Najafi R²⁾

¹⁾Department of Mechanical Engineering of Biosystems, Urmia University / Iran

²⁾Department of Animal Science, Urmia University / Iran

Tel: +98 44 2770555, E-mail: a.nikbakht@urmia.ac.ir

Keywords: Poultry house, differential pressure, air velocity, temperature distribution, CFD

ABSTRACT

Experimental analysis of air velocity and temperature distribution in poultry houses is laborious, especially for large scale houses. Enhanced broiler yield can be obtained when the house is suitably ventilated. Therefore, efficient prediction tools would be vital. Computational fluid dynamics (CFD) provides detailed data on indoor flow patterns, air velocity and temperature distribution in poultry houses giving promising outlooks as an efficient and cost-effective tool to establish optimum ventilation systems. This work focused on evaluation and numerical analysis of the influence of differential pressure (20, 30 and 40 Pa) and fan activation scenarios on indoor air velocity and temperature distribution in a poultry house. Results showed that air velocity tends to be maximum toward the centre of the cross-section of the house and minimum near the floor next to the side walls. Furthermore, it is elucidated that considerable thermal discomfort for chickens is likely due to temperature variation at the proximity to the exhaust fans. Based on the evaluations of pressure variation on the air velocity distribution, quick estimation of the air velocity can be obtained in the zones occupied by chickens. Generally speaking, numerical computation of the equations dominating the poultry house leads to desirable control model of the ventilation and aeration. This would be vital in decision making and economical management of the house.

خلاصه

تجزیه و تحلیل تجربی توزیع سرعت هوا و دما در مرغداری‌ها، بخصوص در مرغداری‌های بزرگ، بسیار دشوار است. بیشترین و بهترین عملکرد مرغداری‌ها موقعی حاصل می‌شود که سالن به‌خوبی تهویه شود. بنابراین نیاز به ابزار پیش‌بینی‌موتری، حیاتی است. دینامیک سیال محاسباتی (CFD) اطلاعات دقیق‌تر الگوی جریان‌ها، نحوه توزیع سرعت هوا و دما در مرغداری‌ها فراهم می‌کند که به عنوان یک ابزار کارآمد و مقرون به صرفه، برای ایجاد سیستم‌های تهویه مطلوب چشم‌اندازهای امیدوارکننده‌ای ارائه می‌دهد. این مطالعه به ارزیابی و تجزیه و تحلیل عددی، تاثیر اختلاف فشار (20، 30 و 40 پاسکال) و کارکرد هواکش‌ها بر توزیع سرعت هوا و دمای سالن در مرغداری، متمرکز شده است. نتایج نشان داد که سرعت هوا به حداکثر مقدار خود در خط مرکزی مرغداری و حداقل مقدار خود در نزدیکی کف و کنار دیوارهای جانبی می‌رسد. به علاوه، مشخص است که شرایط نامساعد قابل توجهی برای جوجه‌ها در مجاورت هواکش‌ها، به علت تغییرات دما، وجود دارد. بر اساس ارزیابی‌ها تاثیر تغییرات فشار در توزیع سرعت هوا، می‌توان برآورد سریعی سرعت هوا در مناطق اشغال شده توسط جوجه‌ها را به دست آورد. به طور کلی، محاسبه عددمعادلات غالب در مرغداری، منجر به یافتن مدل کنترلی مطلوب برای تهویه و هوادهی می‌شود. این موضوع در تصمیم‌گیری و مدیریت اقتصادی مرغداری بسیار حیاتی است.

Nomenclature			
P	Pressure, Pa	AH	total chicken heat, W
ρ	Density, kg m ⁻³	AHS	sensible heat from chicken, W
S_h	Total entropy, J K ⁻¹	AHL	latent heat from chicken, W
τ	Stress tensor, Pa	m	mass of chicken, kg
E	Total energy, J	Ti	indoor temperature, °C
k_{eff}	Heat transmission coefficient	Sm	Mass source, kg m ⁻³
h	Specific enthalpy, J kg ⁻¹	J	Component of diffusion flux, kg m ⁻² s ⁻¹

INTRODUCTION

Meat production in poultry is a crucial and economical industry in the world (Mostafa et al., 2012). Controlling poultry conditions is an increasingly important issue in rearing processes. Environmental control systems in poultry houses include heating, ventilation and cooling which in turn are featured by temperature, air velocity, relative humidity, concentration of oxygen, ammonia, carbon dioxide, dust and microbial contamination (Blanes-Vidal et al., 2007). Ventilation in poultry houses is an action that prepares required air and oxygen, thermal comfort and reduces polluted gas concentration of chickens. The most common system

in poultry houses is forced ventilation based on negative-pressure. Velocity range at the animal level, rate of air exchange and air distribution are three basic principles for ventilation design (MWPS., 1990; ASAE EP270.5., 2009; Pedersen., 1999). Operational factors such as fan operation, adjustment of air inlet openings and pressure drop are essential to define an optimal ventilation system (Bustamante et al., 2012). Among ventilation systems, tunnel ventilation is extensively used in most poultry houses in order to remove extra heat and to simultaneously prepare the required amount of fresh air during hot seasons (Kwon et al., 2015). A significant distinction between tunnel ventilation and conventional poultry housing is the uniformity of air movement. The uniform air movement results in increased cooling for the birds throughout the house. In ventilation systems, poultry breeders usually control the internal environment by changing the amount of slot opening inlets and the activity of fans. These changes are performed by automatisms that cause changes in the differential pressure and air velocity values (Bustamante et al., 2013). Air flow rate in the zone occupied by the birds is one of the main parameters affecting the creation of an appropriate indoor environment (Zajíček and Kic, 2013). When the ambient climate is hot and humid, temperature inside the poultry house rises above the recommended levels. As a result, air flow rate strongly affects convective animal heat losses and plays a vital role in animal welfare. However, experimental measurement of air velocities in poultry houses has obstacles such as lack of comprehensive details of interior air velocity in various parts of the building, high cost of measuring devices and finally sensitivity of some electronic devices to environmental parameters which distort the output data (Blanes-Vidal et al., 2008).

In the last few years there has been a growing interest in using computational fluid dynamics (CFD) in order to remove experimental measurement limitations and get careful results (Lee et al., 2007; Seo et al., 2009). This method has several benefits for setting the experimental conditions within poultry houses, enabling airflow predictions. Hence, CFD has been widely used for ventilation of concentrated agricultural systems, such as greenhouse (Bartzanas et al., 2002; Campen and Bot, 2003; Campen, 2005; Fatnassi et al., 2006; OuldKhaoua et al., 2006; Baeza et al., 2008; Bournet et al., 2007), poultry houses (Norton et al., 2010; Li, 2012; Zajicek and Kic, 2012; El Mogharbel et al., 2013; Rojano et al., 2015; Bustamante et al., 2015), livestock houses (Bjerg et al., 2013; Wu et al., 2012) and storage (Ghoreishi-Madiseh et al., 2015; Tseng et al., 2016). CFD has been considered as a strong and versatile tool for analyzing complex phenomena, such as turbulent flow or heat transfer, according to various environmental conditions (Kwon et al., 2015). CFD could also save the cost, time and effort associated with field experiments to establish the optimum system (Lee et al., 2009). Another effective parameter inside the poultry house is static pressure. Indeed, when the exhaust fan is active, it pulls air out of the house. Air from outside the house moves into the house to replace the air removed by the exhaust fan. Theoretically, when the fans are active, they could pull all the air out of the house and creating a vacuum (Czarick et al., 2002). The higher static pressure the harder the fans have to work. As the level of static pressure increases, the amount of air moved by a fan decreases and power usage increases (Czarick et al., 2010).

In this work, we study a poultry house equipped with tunnel ventilation, using a powerful numerical method, CFD, to characterize the accurate internal environment. Thermohydraulic parameters governing the house ventilation and hence optimum management are quantified. The impact of static pressure and number of active fans on the air velocity and temperature distribution in the zone occupied by the birds (0.2 m above of floor) are argued.

MATERIALS AND METHODS

Simulated broiler house

The poultry house simulated in this study was typical of that popularly used in Iran. It was located in the city of Nooshin Shahr (latitude: 37°, 43', longitude: 45°, 3' and 1320 m above sea level). Fundamental geometric dimensions of the hall are as follows: length, 80 m; width, 15.80 m; side-wall height, 2.7 m, and the maximum distance from floor to ceiling, 3.6 m. This broiler house uses a mechanically ventilated tunnel system by negative pressure with multiple tunnel fans during the summer and a mechanically cross-ventilated system using a number of inlets in the winter. The house was provided with 10 side-wall inlets, each 120 cm wide and 100 cm high, whose central horizontal axis was located 1.1 m above the floor, and seven fans located at the end wall with a diameter of 0.65 m. Brick was the main material used in all the walls and polystyrene as insulation between bricks and sandwich panels with a thickness of 4 cm used for roof (Fig. 1).

The actual arrangement of the house is given in Fig 2. Characteristic of poultry house used in simulation are indicated in Table 1.

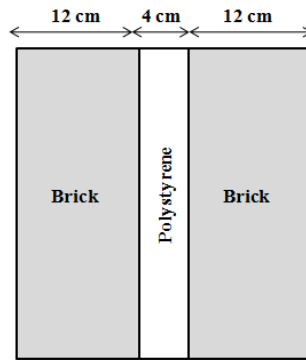


Fig. 1 -Structure of poultry houses walls

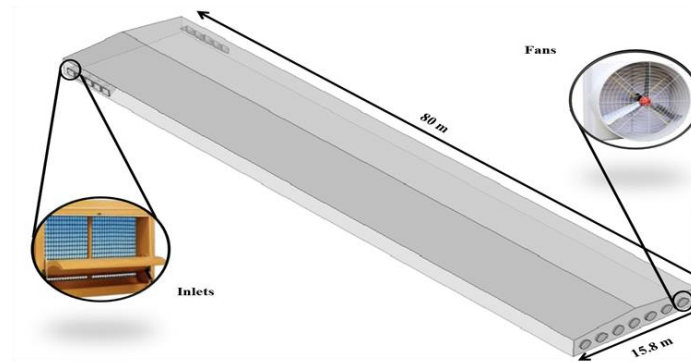


Fig. 2 -Schematic and dimensions of poultry house

Table 1

Characteristic of poultry house used in simulation	
Poultry house dimensions	
Length	80 m
Width	15.8 m
Height	2.7 m
Ceiling height	3.6 m
Chicken number	19000
Chicken density	15 chickens per m ²
Chicken age	3 weeks
Number of exhaust fans	7 (diameter 1.3 m)
Number of air inlets	10 (1.20 * 1.00 m)

Numerical model

Numerical methods for calculating air velocity and temperature distribution of poultry house are attractive in terms of time and costs given the difficulty to experimentally determining the flow and temperature field. In this study, three-dimensional CFD models were generated by COMSOL Multiphysics (ver. 5.1) software. Fine and dense meshes were used to improve the accuracy of the CFD model. The standard k- ω model was used to simulate the air velocity and temperature in the summer (high ventilation rate) conditions and simulations were carried out under steady-state conditions. This model performs excellent near the wall, as a result of its simple low Reynolds number formulation and its ability to accurately compute flows with weak adverse pressure gradients (Yang, 2004).

Governing equations

CFD indeed acts as a powerful alternative for implementation of sensors and massive experimentation. The fundamental theory behind all CFD methods is the resolution of a set of nonlinear partial differential equations where the equations correspond to conservation of mass (Eq. (1)) or continuity, momentum (Eq. (2)) or Navier-Stoke's law and energy (Eq. (3)) (Shivkumar, 2014; Mostafa et al., 2012 ; Seo et al., 2009; El Mogharbel et al., 2013).

$$\frac{\partial P}{\partial t} + \nabla \cdot (\rho \vec{v}) = S_m \tag{1}$$

$$\frac{\partial}{\partial t}(\rho \bar{v}) + \nabla \cdot (\rho \bar{v} \bar{v}) = -\nabla P + \nabla \cdot (\bar{\tau}) + \rho \bar{g} + \bar{F} \quad (2)$$

$$\frac{\partial}{\partial t}(\rho E) + \nabla \cdot (\bar{v}(\rho E + P)) = \nabla \cdot \left(k_{eff} \nabla T - \sum_j h_j \bar{J}_j + (\bar{\tau} \bar{v}) \right) + S_h \quad (3)$$

Boundary condition

Boundary conditions for air inlets and outlet fans, differential pressure was chosen. The differential pressure variable was set at 20, 30 and 40 Pa. At each pressure level, two groups of fans worked: first stage 5 fans active and second stage 7 fans active. Average ambient temperature for summer conditions in western Azerbaijan was chosen 25°C and heat flux boundary condition for the floor, instead of the heat generated by the hens, determined with Eq. (4), was applied. Also for heat exchange with the exterior, heat flux boundary condition were considered. Eq. (5) and Eq. (6) compute the produced sensible and latent heat, respectively (CIGR, 2002).

$$AH = 10.62 m^{0.75} \times \left(1 + \frac{20(20 - T_i)}{1000} \right) \quad (4)$$

$$AH_s = 0.61 \times AH - \left(\frac{0.228}{1000} \right) \times T_i^2 \quad (5)$$

$$AH_L = AH - AH_s \quad (6)$$

RESULTS

The main objective of this article is to show effect of differential pressure between inlet and outlet on air velocity and temperature distribution in the zone occupied by the birds by CFD methods. A comparison of velocity profiles and temperature profiles at various differential pressure and fans activation was done.

Air velocity variation

Fig. 3 illustrates the air velocity distribution of the poultry house at 20 Pa differential pressure and 5 fans active conditions. The results, as seen in fig. 3, indicate that maximum value for air velocity obtained in centerline of the house and the region near the inlets. In half end of house distribution of air velocity is approximately uniform. It can be seen in fig. 3 that air velocity tends to be highest toward the center of the house cross-section and lowest near the floor next to the side walls. There are similarities in the distribution of velocities between the present study and (Blanes-Vidal et al., 2007; Czarick et al., 2015) study. Variation of air velocity at 30 and 40 Pa differential pressure and 5 fans active condition are shown in figures 4 and 5, respectively.

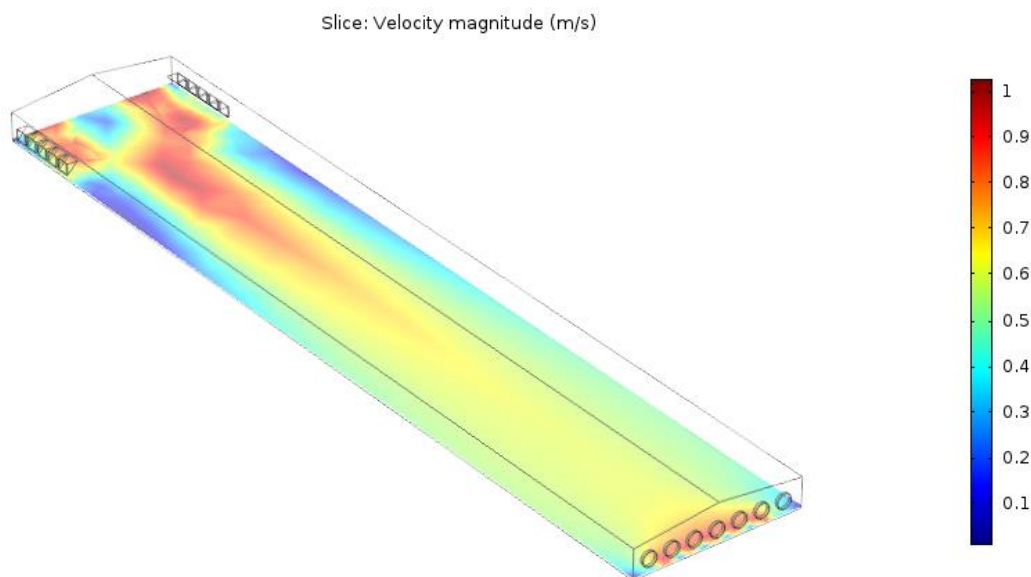


Fig. 3 - Variation of air velocity at 20 Pa differential pressure and 5 fans active condition

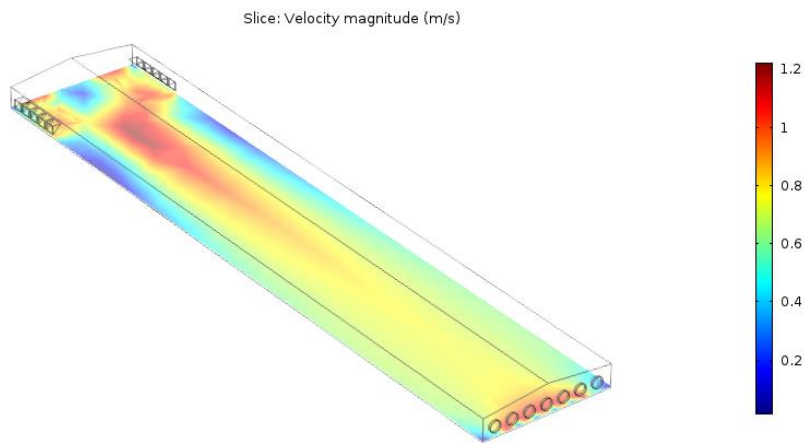


Fig. 4 - Variation of air velocity at 30 Pa differential pressure and 5 fans active condition

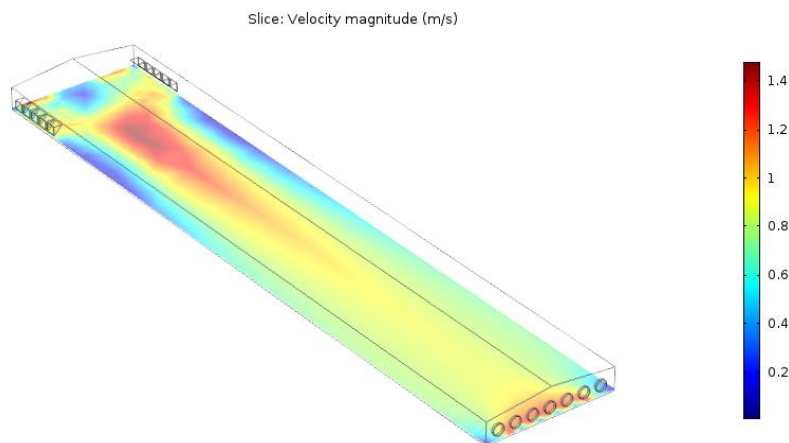


Fig. 5 - Variation of air velocity at 40 Pa differential pressure and 5 fans active condition

Fig. 6, 7 and 8 present the distribution of air velocity within the poultry house at various differential pressures (20, 30 and 40 Pa) and 7 fans active condition, respectively. The maximum value for air velocity in the centerline of the house at 20, 30 and 40 Pa differential pressures is 1.2, 1.8 and 2 m/s, respectively. Proper air velocity in the poultry house is essential for ensuring thermal homogeneity in the zone occupied by the chickens. Also sufficient air velocity is required to keep the litter inside the house dry. When ambient temperatures are above that in the chicken zone, air velocity must be kept relatively high to reduce bird body heat (Mostafa *et al.*, 2012). According to (Bustamante *et al.*, 2015) high air velocity values (~2 m/s) in the poultry house can help for chicken thermoregulation by increasing the convective flux heat of them and therefore decrease their thermal stress and reduce mortality. Also this finding corresponded to (Czarick *et al.*, 2010) who indicate that with increasing static pressure, speed increases. This result is shown in figure 9.

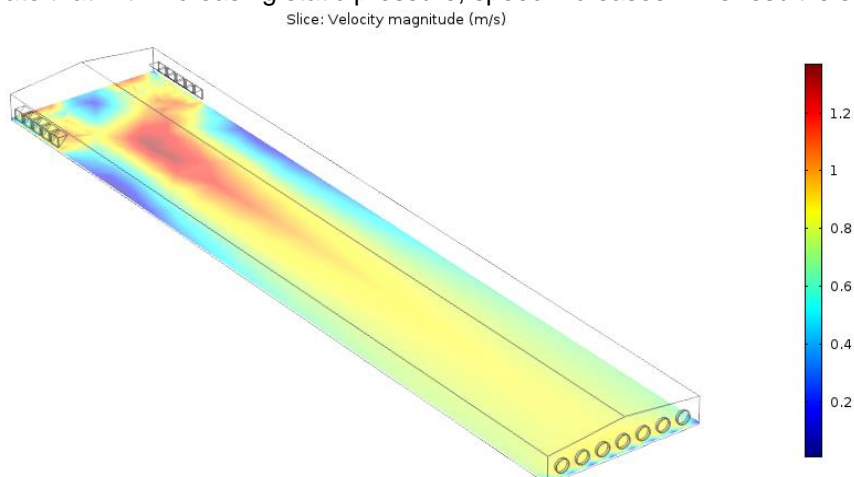


Fig. 6 - Variation of air velocity at 20 Pa differential pressure and 7 fans active condition

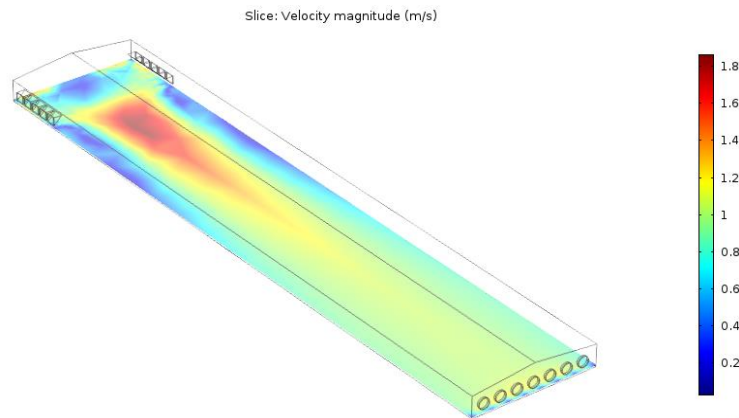


Fig. 7 - Variation of air velocity at 30 Pa differential pressure and 7 fans active condition

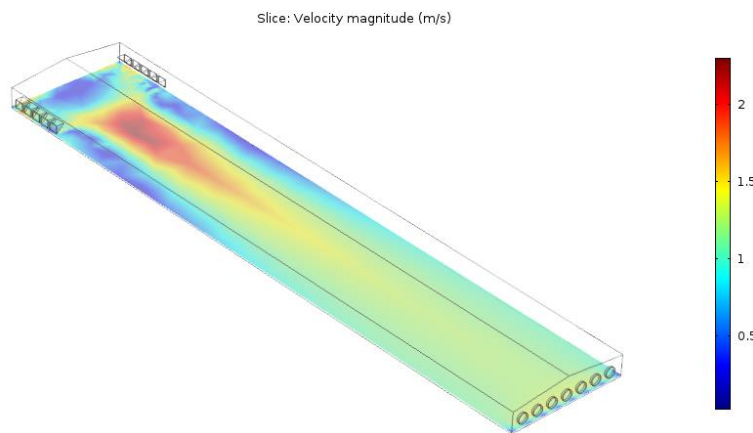


Fig. 8 - Variation of air velocity at 40 Pa differential pressure and 7 fans active condition

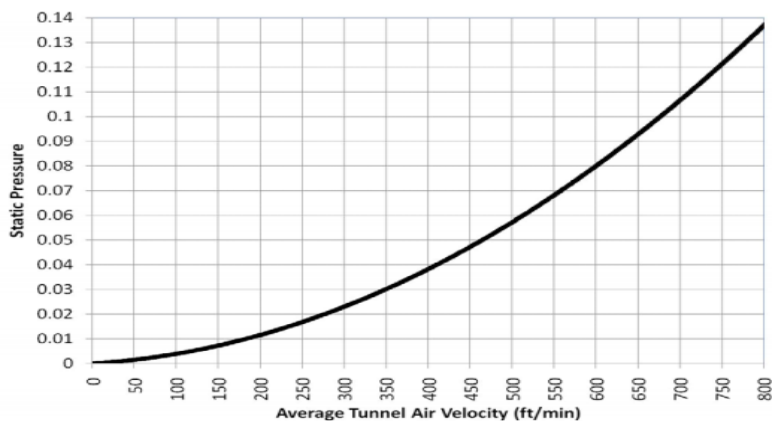


Fig. 9 - Relationship between air velocity and the static pressure in tunnel-ventilated houses (Czarick et al., 2010)

Temperature variation

Figures 10-12 describe the monitored thermal distribution along the zone occupied by the chickens (0.2 m above the floor) according to the variables of differential pressure (20, 30 and 40 Pa) and 5 fans active, respectively. It is shown in figure 10 that air temperature increases when it moves through the poultry house length. When entering air temperature was 25°C, the CFD model predicted an increase in air temperature in the order of 4 or 5°C at the outlets; This increase is due to heat production by animal. Therefore, additional heat is transported from the inlet towards the outlet. This result has best agreement with (Lee et al., 2007; Osorio et al., 2011; Rocha et al., 2014) searches. Also this temperature increasing for figures 11 and 12 observable, but value of output temperature reduces due to increasing air velocity.

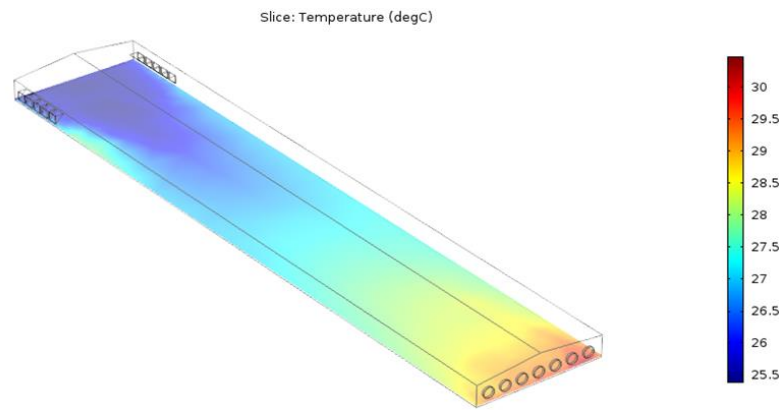


Fig. 10 - Distribution of temperature at 20 Pa differential pressure and 5 fans active condition

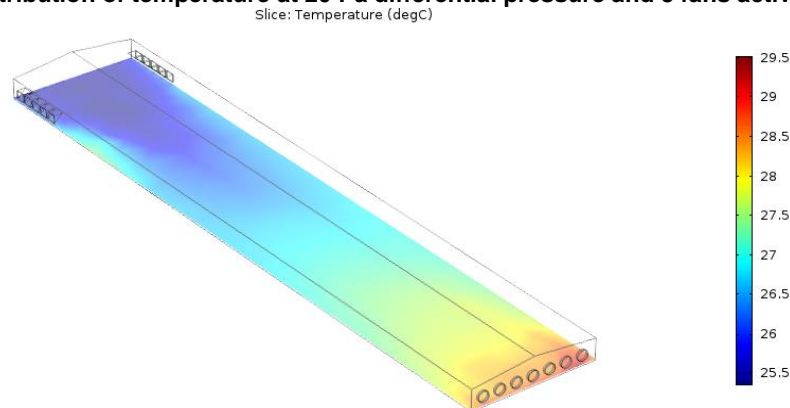


Fig. 11 - Distribution of temperature at 30 Pa differential pressure and 5 fans active condition

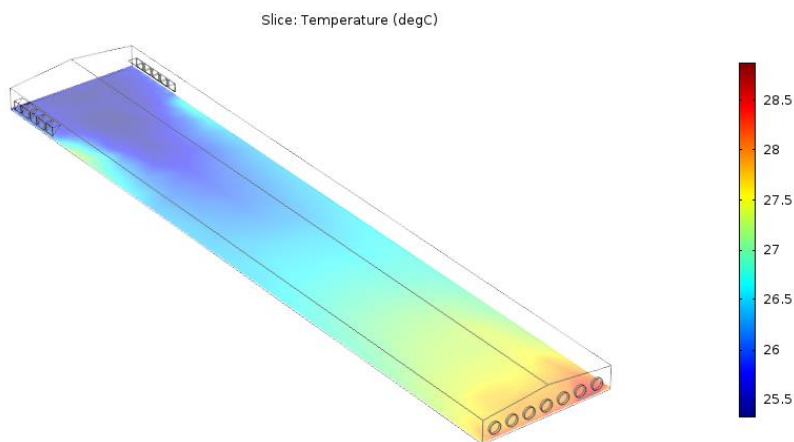


Fig. 12 - Distribution of temperature at 40 Pa differential pressure and 5 fans active condition

The maximum temperature in the zone occupied by the chickens by CFD in the poultry house is 33, 28 and 27.5°C which is shown in fig. 13, 14 and 15 respectively. These figures show that temperature gradient variation proximity to the exhaust fans causes thermal discomfort for chickens. For ventilation with 20 Pa differential pressure (fig.13), temperature at the bird's height varied between 26 and 33°C. The lower efficiency of this system may be explained by the fact that this system generates a low velocity which prevents the convective transport of heat produced by the chickens (*Osorio et al., 2013*). Increasing air velocity makes the animals increase the heat loss and causes thermal comfort. According to (*Simmons et al., 1994*) for chickens in fifth week of age with outside temperature of 29°C and air velocity increasing from 1.01 to 3.05 m.s⁻¹, the loss of heat increases from 1.19 to 2.09 W kg⁻¹ and in the sixth week of age from 1.30 to 2.33 W kg⁻¹. The result obtained from figures 14 and 15 indicated that increasing differential pressure from 30 Pa to 40 Pa has no significant effect on outlet air temperature. Considering the previous results, it was concluded that the suggested CFD simulation can be used to sufficiently characterize the air velocity and temperature distribution inside poultry houses.

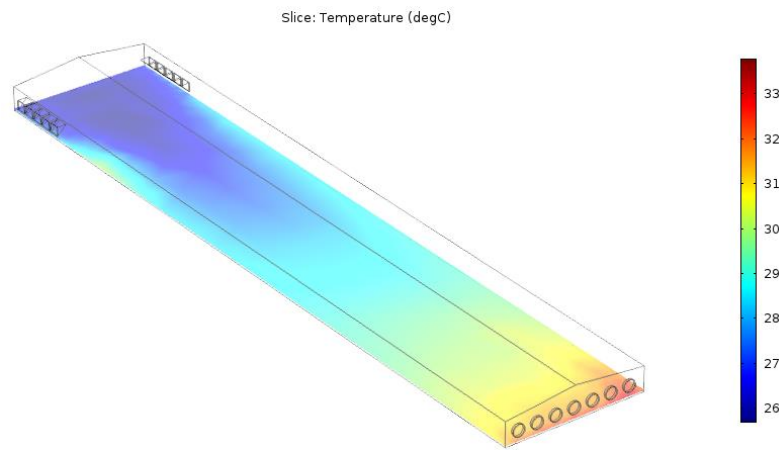


Fig. 13 - Distribution of temperature at 20 Pa differential pressure and 7 fans active condition

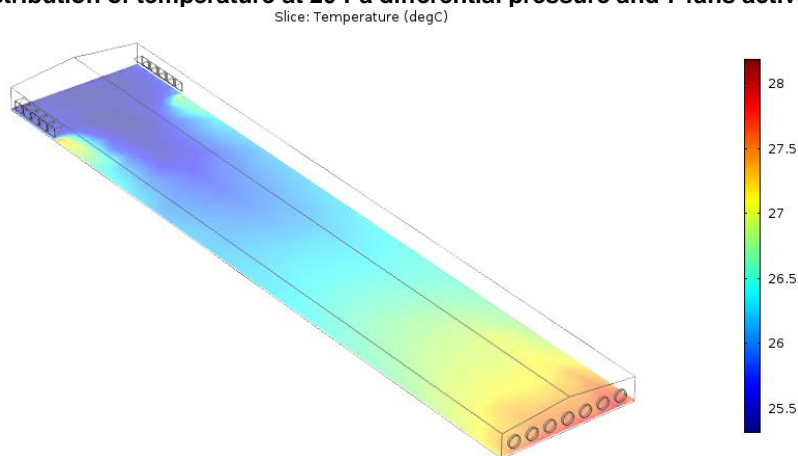


Fig. 14 - Distribution of temperature at 30 Pa differential pressure and 7 fans active condition

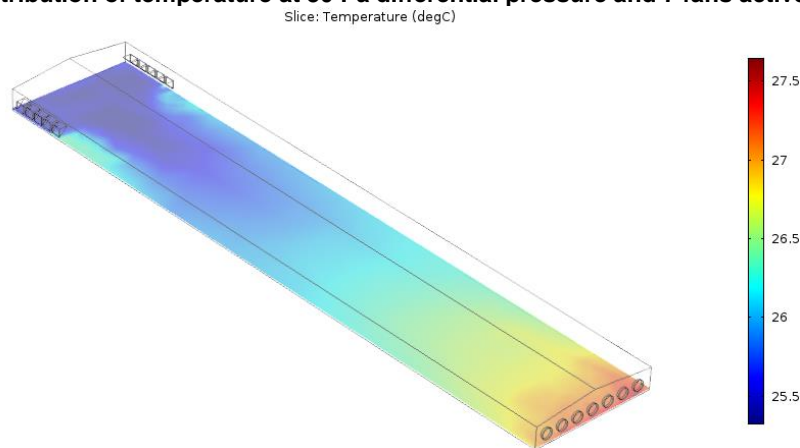


Fig. 15 - Distribution of temperature at 40 Pa differential pressure and 7 fans active condition

CONCLUSIONS

The present work demonstrates the advantages of using the numerical method (CFD) modeling in the environmental control process of a poultry house. Commercial CFD software (COMSOL Multiphysics) was used to conduct the numerical simulations. Differential pressure (20, 30 and 40 Pa) and fans activation (5 fans active and 7 fans active) are main variable parameters in poultry simulation. This simulation is useful for investigating the effect of differential pressure and fan activation on the parameters of comfort (air velocity and temperature distribution). The result showed that in differential pressure variation (20, 30 and 40 Pa) and 7 fans active condition the maximum value for air velocity in the poultry house centreline is 1.2, 1.8 and 2 m/s, respectively. Also it results for all conditions that air temperature increases when it moves through the poultry house length and additional heat is transported from the inlet towards the outlets. The generated model can be used to help enhancing poultry design, in terms of enhancing the efficiency of the ventilation system.

REFERENCES

- [1] ASAE EP270.5. (2009), Design of Ventilation Systems for Poultry and Livestock Shelters. In ASABE Standards. *American Society of Agricultural and Biological Engineers (ASABE)*, pp. 1–19;
- [2] Baeza E.J., Perez-Parra J.J. Lopez J.C., (2008), CFD Simulation of Natural Ventilation of a Parral Greenhouse with a Baffle Device below the Greenhouse Vents. *Acta Horti*, Vol. 801 ,pp. 885-892;
- [3] Bartzanas T., Boulard T., Kittas C., (2002), Numerical simulation of the airflow and temperature distribution in a tunnel greenhouse equipped with insect-proof screen in the openings. *Comput. Electron. Agric.* Vol. 34, No. 1–3, pp. 207–221;
- [4] Bjerg B., Cascone G., Lee I.B. et al., (2013), Modelling of ammonia emissions from naturally ventilated livestock buildings. Part 3: CFD modeling, *Biosystems Engineering*, Vol. 116, pp. 259-275;
- [5] Blanes-Vidal V., Fitas V., Torres A., (2007), Differential pressure as a control parameter for ventilation in poultry houses: effect on air velocity in the zone occupied by animals. *Spanish Journal of Agricultural Research*, Vol. 5, No.1, pp.31-37;
- [6] Blanes-Vidal V., Balasch S., Torres A.G., (2008), Application of computational fluid dynamics to the prediction of air flow into mechanically ventilated commercial poultry building, *Biosystems Engineering*, Vol. 100, No.1, pp. 105-116;
- [7] Bournet P.E., Ould Khaoua S.A. Boulard T.,(2007), Numerical prediction of the effect of vent arrangements on the ventilation and energy transfer in a multi-span glasshouse using a bi-band radiation model. *Biosystems Engineering*, Vol. 98, pp. 224–234;
- [8] Bustamante E., Guijarro E., García-Diego F.J. et al., (2012), Multisensor system for isotemporal measurements to assess indoor climatic conditions in poultry farms. *Sensors*, Vol.12, pp. 5752–5774;
- [9] Bustamante E., García-Diego F.J., Calvet S. et al., (2013), Exploring Ventilation Efficiency in Poultry Buildings: The Validation of Computational Fluid Dynamics (CFD) in a Cross-Mechanically Ventilated Broiler Farm. *Energies*, Vol. 6, No. 5, pp. 2605–2623;
- [10] Bustamante E., García-Diego F.G., Calvet S. et al., (2015), Measurement and Numerical Simulation of Air Velocity in a Tunnel-Ventilated Broiler House. *Sustainability*, Vol. 7, pp.2066-2085;
- [11] Campen J.B., (2005), Greenhouse design applying CFD for Indonesian conditions. *Acta Horticulturae*, Vol. 691, pp. 419–424;
- [12] Campen J.B., Bot G.P.A., (2003), Determination of greenhouse-specific aspects of ventilation using three-dimensional computational fluid dynamics. *Biosystems Engineering*, Vol. 84, pp. 69–77;
- [13] CIGR., (2002), Heat and moisture production at animal and house level. In S. Pedersen, & K. Sallvik (Eds.), 4th Report of working group on climatization of animal houses. Horsens, Denmark: CIGR. *Published by Danish Institute of Agricultural Sciences*;
- [14] Czarick M., Fairchild B. Dartnell, D., (2002), Answers to basic questions about negative pressure ventilation. *Poultry Housing Tips, The University of Georgia*, Vol. 14, No. 9, pp. 1 - 6. <https://www.poultryventilation.com/tips/vol14/n9>;
- [15] Czarick M., Fairchild B. Dartnell D., (2010), Measuring Static Pressure in Tunnel-Ventilated Houses. *Poultry Housing Tips, The University of Georgia*, Vol. 22, No. 9, pp. 1 - 4. <https://www.poultryventilation.com/tips/vol22/n9>;
- [16] Czarick M., Fairchild B. Dartnell D., (2010), High Tunnel Air Velocities = High Static Pressures. *The University of Georgia*, Vol. 22, No. 8, pp.1-3. <https://www.poultryventilation.com/tips/vol22/n8>;
- [17] Czarick M., Fairchild B., Dartnell D., (2015), Average Tunnel Air Velocity. *Poultry Housing Tips, The University of Georgia*, Vol. 26, No. 4, pp.1-4. <https://www.poultryventilation.com/tips/vol27/n4>;
- [18] El Mogharbel O., Ghali K., Ghaddar N. et al., (2013), Simulation of a localized heating system for broiler brooding to improve energy performance. *Int.J.Energy Res*, pp.125-138;
- [19] Fatnassi H., Boulard T., Poncet C. et al., (2006), Optimisation of greenhouse insect screening with computational fluid dynamics. *Biosystems Engineering*, Vol. 93, pp. 301–312;
- [20] Ghoreishi-Madiseh S.A., Sasmito A.P., Hassani F.P. et al., (2015), Heat transfer analysis of large scale seasonal thermal energy storage for underground mine ventilation. *Energy Procedia*, Vol. 75, pp. 2093–2098;
- [21] Kwon K.S., Lee I.B., Zhang G.Q., et al., (2015), Computational fluid dynamics analysis of the thermal distribution of animal occupied zones using the jet-drop-distance concept in a mechanically ventilated broiler house. *Biosystems Engineering*, Vol. 136, pp. 51-68;
- [22] Lee I.B., Sase S., Han H., et al., (2009), Ventilation design for a chick incubator using computational fluid dynamics. *Japan Agricultural Research Quarterly*, Vol. 43, No. 3, pp. 227-237;

- [23] Lee I.B., Sase S. Sung S.H., (2007), Evaluation of CFD accuracy for the ventilation study of a naturally ventilated broiler house", Japan Agricultural Research Quarterly, Vol. 41, No. 1, pp.53-64;
- [24] Li Y., (2012), Numerical simulation and analysis for indoor air quality in different ventilation. *Health*, Vol.4, No.12, pp.1352-1361;
- [25] Mostafa E., Lee I.B., Song S.H., Kwon K.S. et al., (2012), Computational fluid dynamics simulation of air temperature distribution inside broiler building fitted with duct ventilation system. *Biosystems Engineering*, Vol. 112, No. 4, pp. 293-303;
- [26] MWPS, (1990), Mechanical Ventilating Systems for Livestock Housing. 1st ed.; Midwest Plan Service, Iowa State University: Ames, IA, USA;
- [27] Norton T., Grant J., Fallon R. et al., (2010), Improving the representation of thermal boundary conditions of livestock during CFD modeling of the indoor environment. *Computers and Electronics*, Vol. 73, pp. 17-36;
- [28] Norton T., Grant J., Fallon R., et al., (2010), Optimising the ventilation configuration of naturally ventilated livestock buildings for improved indoor environmental homogeneity. *Building and Environment*, Vol. 45, pp. 983–995;
- [29] Osorio J.A., Aredes Martins M., Oliveira Rocha,K.S., et al., (2013), Use of Computational Fluid Dynamics to Simulate Temperature Distribution in Broiler Houses with Negative and Positive Tunnel Type Ventilation Systems. *Rev. U.D.C.A Act. &Div. Cient.*, Vol. 16, No. 1, pp.159–166;
- [30] Osorio J.A., Oliveira K.S., Ferreira I.F. et al., (2011), Use of CFD modeling for determination of ammonia emission in non-insulated poultry houses with natural ventilation. *ASABE Annual International Meeting Sponsored by ASABE Gault House Louisville, Kentucky*, pp.1-10;
- [31] Ould Khaoua S.A., Bournet P.E., Migeon C. et al., (2006), Analysis of greenhouse ventilation efficiency based on computational fluid dynamics. *Biosystems Engineering*, Vol. 95, No.1, pp. 83–98;
- [32] Pedersen S., (1999), Forced Ventilation. In CIGR Handbook of Agricultural Engineering: Animal Production & Aquacultural Engineering. *American Society of Agricultural Engineers (ASAE)*, St. Joseph, MI, USA, pp. 68–87;
- [33] Rocha K.S.O., Ferreira T., Martins J.H. et al.,(2014), Modeling and simulation of internal environment conditions in high-density poultry houses with ventilation using computational fluid dynamics. *International Conference of Agricultural Engineering, Zurich*;
- [34] Rojano F., Bournet P.E., Hassouna M. et al., (2015), Modelling heat and mass transfer of a broiler house using computational fluid dynamics. *Biosystems Engineering*, Vol.136, pp. 25–38;
- [35] Seo I.H., Lee I.B., Moon O.K., et al., (2009), Improvement of the ventilation system of the naturally ventilated broiler house in the cold season using computational simulations. *Biosystems Engineering*, Vol. 104, No.1, pp.106-117;
- [36] Shivkumar A.P., (2014), *Flow Testing and CFD Modeling of Poultry Engineering Chamber*. M.S. Thesis, North Carolina State University;
- [37] Simmons J.D., Lott B.D., May J.D., (1994), Heat loss from broiler chickens subjected to various air velocities and ambient temperatures. *Applied Engineering in Agriculture*, Vol. 13, No. 5, pp. 665-669;
- [38] Tseng Y.S., Lin C.H., Shih C. et al., (2016), Evaluating the feasibility of new surveillance concept for Dry Storage System through CFD methodology. *Nuclear Engineering and Design*, Vol. 304, pp.1–10;
- [39] Wu W., Zhai J., Zhang G. et al., (2012), Evaluation of methods for determining air exchange rate in a naturally ventilated dairy cattle building with large openings using computational fluid dynamics (CFD). *Atmospheric Environment*, Vol. 63, pp.179-188;
- [40] Yang T., (2004), *CFD and Field Testing of a Naturally Ventilated Full-scale Building*, PhD thesis, University of Nottingham;
- [41] Zajicek M. Kic P., (2012), Improvement of the broiler house ventilation using the CFD simulation. *Agronomy Research Biosystem Engineering Special*, Vol. 1, pp.235-242;
- [42] Zajíček M., Kic P., (2013), Simulation of the broiler house ventilation. *Scientia agriculturae bohemia*, Vol. 44, pp. 32–37.

RESEARCH ON SUNFLOWER SEEDS SEPARATION BY AIRFLOW / ДОСЛІДЖЕННЯ ПРОЦЕСУ СЕПАРАЦІЇ НАСІННЯ СОНЯШНИКУ ПІД ДІЄЮ ПОВІТРЯНОГО ПОТОКУ

Ph.D. Aliev E.B.¹⁾, Ph.D. Yaropud V.M.²⁾, Ph.D. Dudin V.Yr.³⁾,
Ph.D. Pryshliak V.M.²⁾, Ph.D. Pryshliak N.V.²⁾, Ph.D. Ivlev V. V.³⁾

¹⁾Institute of Oilseed Crops NAAS, Zaporizhzhia / Ukraine,

²⁾Vinnitsa National Agrarian University / Ukraine, ³⁾ Dnipro State Agrarian and Economic University / Ukraine

Tel: +380688614437; E-mail: aliev@meta.ua

Keywords: seeds, sunflower, separation, air, flow, modeling

ABSTRACT

Investigation of the process of sunflower seeds separation during its movement under the influence of air flow has been carried out in two stages. The first (theoretical) stage is implemented in the software package STAR-CCM+ using the corresponding physical models. The second stage has been made to carry out the experimental research on the installation with the base of the aerodynamic separator of the "Almaz" series. The results of numerical simulation and experimental researches of the sunflower seed separation process during its movement in the airflow are presented. As a result of numerical simulation and experimental studies of the mechanical and technological process of sunflower seeds separation during movement under the influence of air flow, there has been developed the dependences of the distribution of each seed fraction on the length of the area (average value, average square deviation, filling factor, distribution coefficient) and the consumed power from the seed effective diameter, air flow velocity and the seed supply. Statistical analysis has showed that the correlation coefficient between the theoretical and experimental dependencies in the variation of the factors' values in the given range is 0.96. During the research, a compromising problem was solved, namely, there had been reached minimization of consumed power at the maximum value of the distribution coefficient and the seed supply.

РЕЗЮМЕ

Дослідження процесу сепарації насіння соняшнику при його переміщенні під дією повітряного потоку проводились в два етапи. Перший (теоретичний) етап реалізовано в програмному пакеті STAR-CCM+ з використанням відповідних фізичних моделей. Другим етапом було проведення експериментальних досліджень на установці із базою аеродинамічного сепаратора серії «Алмаз». Представлені результати чисельного моделювання і експериментальних досліджень процесу сепарації насіння соняшнику при його переміщенні під дією повітряного потоку. В результаті чисельного моделювання і експериментальних досліджень механіко-технологічного процесу сепарації насіння соняшнику при його переміщенні під дією повітряного потоку отримані залежності розподілу кожної фракції насіння по довжині області (середнє значення, середньоквадратичне відхилення, коефіцієнт заповнення, коефіцієнт розподілу) і споживану потужність від ефективного діаметра насінини, швидкості подачі повітря та подачі насіння. Статистичний аналіз показав, що коефіцієнт кореляції між теоретичною і експериментальною залежностями при варіюванні значеннями факторів в заданому діапазоні складає 0,96. В процесі досліджень була вирішена компромісна задача, а саме мінімізація споживаємої потужності при максимальному значенні коефіцієнта розподілу і подачі насіння.

INTRODUCTION

The unsatisfactory quality of sunflower seeds results in a significant reduction in agricultural productivity and a high over expending of seed material (Zaika P., 2006). According to the current standards, oilseed crop varieties and crop yields are determined mainly by their varietal purity, which should equal 99.6-99.9% for the elite seed (elite, superelite) - depending on the crop (Aliev E., 2016).

The task of separating sunflower seeds by density (specific weight, texture) is reduced to its previous calibration by geometric dimensions (Tishchenko L., Olshansky V., Olshansky S., 2010). In other words, there are two variables: sailing and density. It is obvious that at the seed with same density and smaller mass flies further under the air flow influence, than seeds of greater mass that fly shorter distances.

In addition, depending on the orientation of the seed to the vector of the air flow velocity, the sailing range appears, which leads to a random trajectory of the movement of seeds (Nurullin E., Salakhov I., Dmitriev A., 2014). Of course, within the long-term airflow impact, the seed will take the best aerodynamic position in which the lowest resistance is observed (Aliiev E., Shevchenko I., 2017).

In addition to the above, the air flow must have a uniform structure, in terms of the turbulence parameters (scale and intensity), and on the speed diagram (Aliiev E., Yaropud V., 2017).

Considering all the difficulties of the task, the process of sunflower seeds separation during their movement under the air flow influence must be theoretically and experimentally explored.

MATERIALS AND METHODS

Investigation of the process of sunflower seeds separation during their movement under the influence of air flow has been carried out in two stages.

The first (theoretical) stage is implemented in the software package STAR-CCM+ using the corresponding physical models. The initial positions and velocities of sunflower seeds and the air flow have been determined using the finite element method. Then, based on this initial data, given physical laws of contact interaction, the forces acting on each seed at each interval of time have been calculated. For each seed, the resulting force has been calculated and the Cauchy problem has also been solved on the selected time interval, the result of which is the initial data for the next step. The following physical models have been selected for numerical modeling: k-ε disturbed flow turbulence model, gravity field, Van der Waals real gas model, discrete element model, multiphase interaction model (Aliiev E., Bandura V., Pryshliak V., Yaropud V., Trukhanska O., 2018). The method of discrete elements is based on the laws of conservation of impulse and impulse momentum for Lagrangian models of a multiphase environment. However, to construct a physico-mathematical model, one must assume that the seeds are represented in the form of identical ellipsoids with a defined density and effective diameter.

According to previous researches of physical and mechanical properties of Prometheus variety sunflower seeds, selected by the Institute of Oilseeds of NAAS, (Burenko K., Vedmedeva E., Pershin A., 2012; Aliiev E., Shevchenko I., 2017; Aliiev E., Yaropud V., 2017) the following averaged values were adopted for numerical modeling: Poisson's coefficient – 0.5; Young's modulus – 0.2 MPa; density – 200-1000 kg/m³; coefficient of friction of rest – 0.8; normal recovery factor – 0.5; tangential recovery factor – 0.5; coefficient of rolling resistance – 0.3. Properties of the environment have been fixed as follows: environment – air; dynamic viscosity – 1.85508·10⁻⁵ Pa·s; Prandtl's turbulent number – 0.9; free fall acceleration – 9.8 m/s²; temperature – 293 K; pressure – 101325 Pa. The size of the grid cell modeling is 0.001 m. The exposure is from 3 to 7 s.

For the implementation of numerical simulation, a computational scheme of sunflower seed separation process has been made when it was moved under the air flow influence (Fig. 1).

For the factors of numerical modeling, the following most important technological parameters have been adopted: seed effective diameter D_p , air supply rate V , seeding Q .

The effective diameter of sunflower seed D_p was determined by the formula

$$D_p = \sqrt[3]{l_x \cdot l_y \cdot l_z} \quad (1)$$

where: l_x , l_y , l_z – length, width and thickness of sunflower seed, respectively, mm.

According to researches (Vedmedeva K., Makhova T., Kirpichova N., 2017), the geometric dimensions of sunflower seed are $l_x = 8-15$ mm, $l_y = 3-8$ mm, $l_z = 2-4$ mm, so it can be stated, that the effective diameter of sunflower seeds D_p varies in the range of 3-7 mm. Due to the fact that the seeds can be integral, partial and empty, then, according to researches (Vedmedeva K., Makhova T., Karpychova N., 2017), their density can vary in the range of 200-1000 kg/m³. Therefore, the seed flow has been represented by 5 fractions, the weight of 1000 seeds of each being presented in Table 1.

Table 1

Weight of 1000 seeds for a determined effective diameter m_{1000} , g					
Effective diameter of seed D_p , mm	Seeds density ρ , kg/m ³				
	200	400	600	800	1000
3	3	6	9	12	15
5	13	26	39	52	65
7	36	72	108	144	180

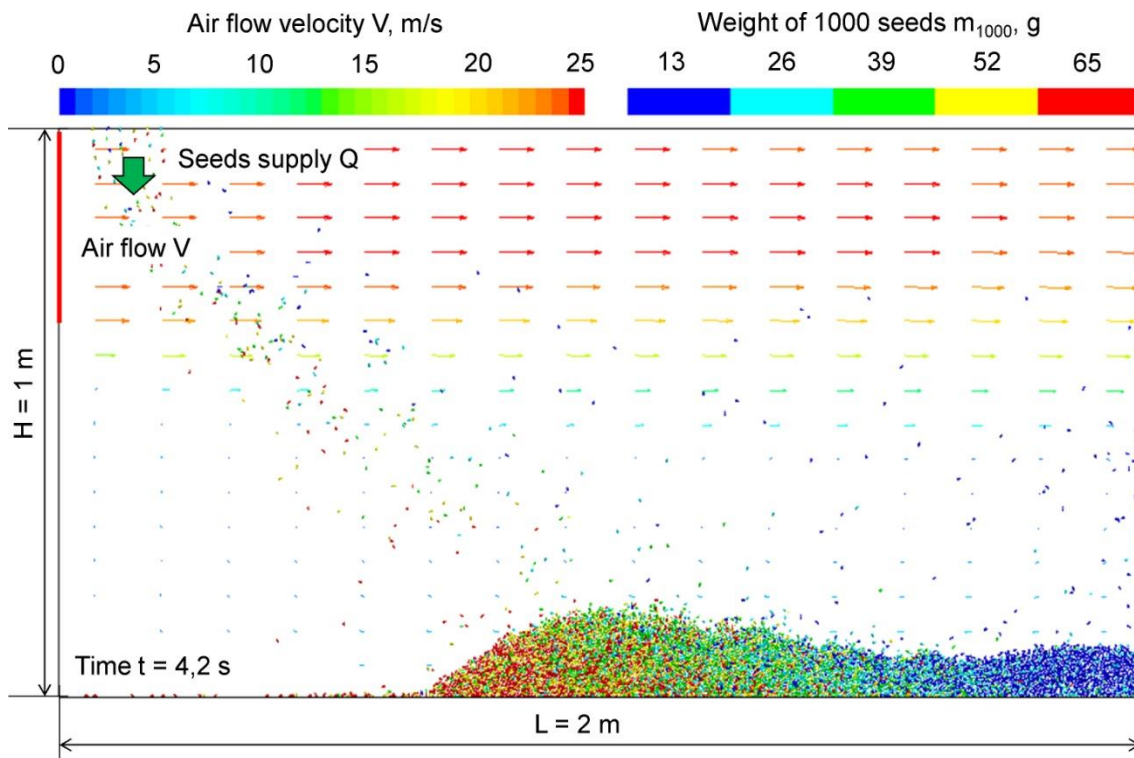


Fig. 1 – Scheme of numerical simulation of the sunflower seed separation process during its movement under the air flow influence

Numerical simulation has been conducted on a complete factorial study with a total number of experiments – $3^3 = 27$. The numerical modeling factors variation boundaries are presented in Table 2 based on the previous studies (Aliiev E., 2017).

Table 2

Factors variations levels in numerical simulation of the seeds movement in the air flow

Factors variations level	Factors		
	Seeds' effective diameter D_p , mm	Seeds supply Q , kg/s	Air flow velocity V , m/s
Top level (+)	7	0.09	25
Base level (0)	5	0.06	20
Low level (-)	3	0.03	15
Factors variations interval	2	0.03	5

As a result of the seeds separation under the air flow influence, the distribution of each fraction along the length of the area can be represented by a normal distribution with a defined value and a value deviation σ (fig. 2). For a normal distribution in the area, a probability of 95.45 % is observed.

According to fig. 2, the best separation (95.45 %) is achieved with the condition:

$$2\sigma_1 + 2(2\sigma_2 + 2\sigma_3 + 2\sigma_4) + 2\sigma_5 \leq \bar{x}_5 - \bar{x}_1 \tag{2}$$

or

$$\theta = \frac{\bar{x}_5 - \bar{x}_1}{2\sigma_1 + 2(2\sigma_2 + 2\sigma_3 + 2\sigma_4) + 2\sigma_5} \rightarrow \max \tag{3}$$

where: θ – filling factor.

It should be noted that the entire area has been divided into 20 identical vertical zones, each of which determines the amount of seeds in each fraction.

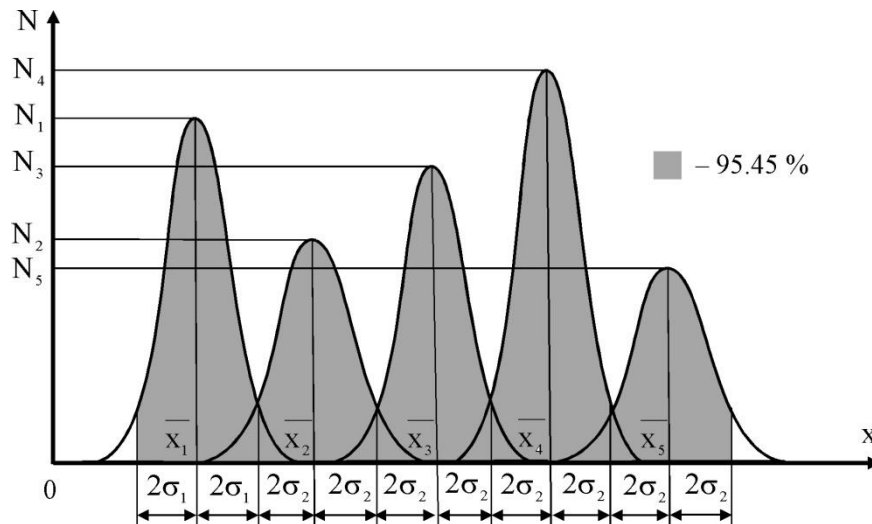


Fig. 2 – Functions of normal distribution of each fraction by area length

The fill factor θ , mentioned before, means values of the fractions distributions in length and their square deviations σ characterize the size and location of the gathering areas (samplings). However, in existing aerodynamic separators, preservatives of the same size are used, which complicates the assessment of the separation process quality. Therefore, another criterion for the quality of fractions distribution in the receptacles is introduced – the distribution coefficient δ , which is defined as follows. Let the input material be divided into N fractions, then the number of gatherable areas should be N . For each fringe area, the fractional composition of the seed mixture is determined, which can be mathematically represented in the form of a square matrix $N \times N$:

$$\begin{pmatrix} w_{11} & w_{12} & \dots & w_{1N} \\ w_{21} & w_{22} & \dots & w_{2N} \\ \dots & \dots & \dots & \dots \\ w_{N1} & w_{N2} & \dots & w_{NN} \end{pmatrix} \tag{4}$$

where: w_{ij} – mass fraction of fraction i in the collection j :

$$w_{ij} = \frac{m_{ij}}{\sum_{i=1}^N \sum_{j=1}^N m_{ij}} \cdot 100\% \tag{5}$$

m_{ij} is the mass of fraction i in the collection j .

The distribution coefficient δ is defined as the largest sum of the diagonal elements of the matrix (4):

$$\delta = \max \left(\sum_{k=1}^N w_{kk}, \sum_{k=1}^N w_{k(k+1)}, \dots, \sum_{k=1}^N w_{k(k+N-1)}, \sum_{k=1}^N w_{(k+1)k}, \dots, \sum_{k=1}^N w_{(k+N-1)k} \right) \tag{6}$$

where: k is a natural number.

The second stage has been made to carry out the experimental research on the installation with the base of the aerodynamic separator of the "Almaz" series (produced by the PE PF "Agrotech"), consisting of a bunker 1 for loading seed material to be separated from a vibroplate 2, generator of air jet cascades 3, which is installed below it and connected to the pressures air flow source 4 into generator 3 and separation chamber 5. Under the separation chamber 5 are the collections of fractions 6 (I-IV). A collection of dust and light fraction 7 (V) was mounted at the end of the separation chamber 5. The design and technological scheme and the general view of the experimental installation are presented in Fig. 3. To ensure a certain supply of seeds, a calibrated valve 8 is used to limit input performance. The specified air supply is set using the 9 (Danfoss VLT Micro Drive) frequency converter, and controlled using the anemometer 10 (Benetech GM-816).

The source material during the experimental researches was represented by sunflower seeds of the Prometheus variety, selection of the Institute of Oilseed Crops NAAS, which were calibrated to a fraction of 3.2-3.4 mm. One experiment was conducted by passing through a pilot sample of a supply unit of 100 kg of seeds.

Factors for experimental studies are the air supply rate V and the supply of seed Q . The intervals and levels of variation by these factors coincide with the theoretical ones (Table 1).

As optimization criteria were adopted: power consumption – P , kW and distribution coefficient – δ . The power consumed by the fan drive is measured using one of the additional functions of the Danfoss VLT Micro Drive frequency converter. Since the task of separating sunflower seeds during its movement under the influence of air flow is the division into 5 fractions (integral, partial, naked core, empty and dust), then at the experimental installation exposed 5 fence regions. For each experiment, for each fringe area, fraction composition is determined according to the generally accepted methodology (GOST 10854-88, 2010) and the corresponding distribution coefficient δ is calculated according to the formula (6).

Experimental studies have been conducted on the D -optimal second-order Boxing-Benkin plan for 2 factors (9 trials) in a three-time repetition. The processing of the research results has been carried out by the mathematical factor planning of experiments method, using the Mathematica software package. The mathematical model is determined by one optimization criterion.

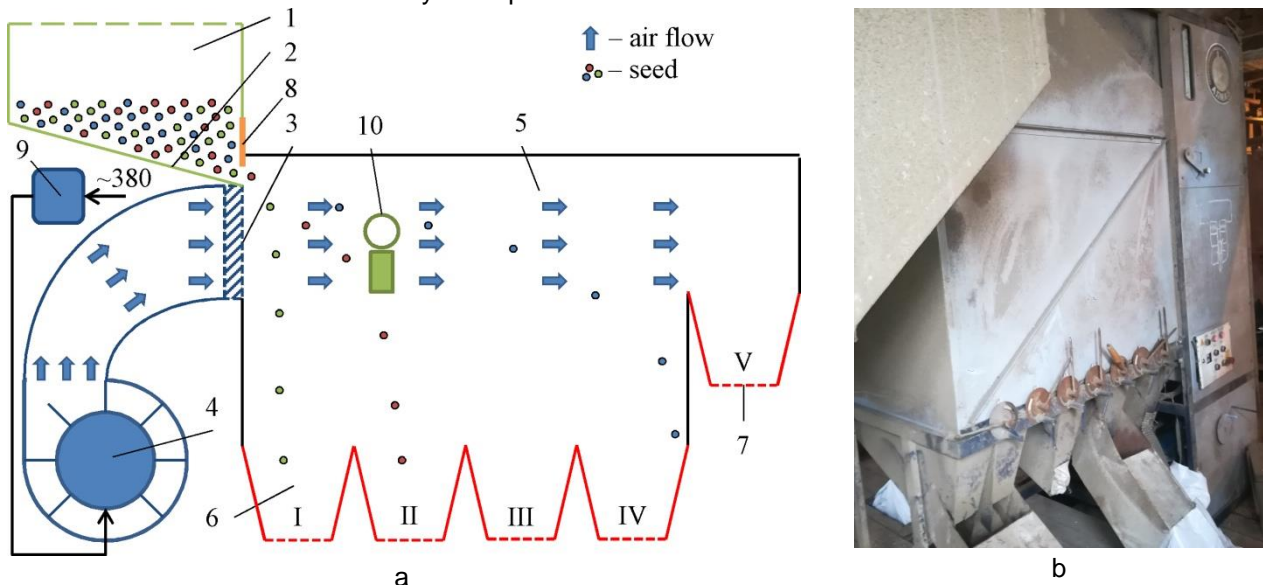


Fig. 3 – Structural-technological scheme (a) and general view (b) of an experimental plant for studying the process of sunflower seeds separation when they are displaced by airflow

1 – bunker; 2 – vibroplate; 3 – air jets oscillator; 4 – fan; 5 – separation chamber; 6 – collections of fractions; 7 – dust collector and light fraction; 8 – valve; 9 – frequency converter 10 – anemometer

RESULTS

According to the first stage, as a result of numerical simulation, a visualization of the technological process of sunflower seeds separation was obtained when they were displaced under the influence of air flow (fig. 4).

The average value and the average square deviation σ have been calculated for each experiment, for each fraction of seeds accordingly. According to the data obtained by formula (3), the filling factor θ is calculated. Using Mathematica software package, a mathematical expression is compiled in a skilled form after the reduction of non-significant parts of the equation according to Student's criterion, which links the coefficient of filling θ with the research factors:

$$\theta = 0.658343 - 0.065448 D_p - 0.00711689 D_p^2 - 4.31791 Q + 0.00181584 V + 0.00683085 D_p V + 0.159939 QV - 0.00138784 V^2 \quad (7)$$

The graphical interpretation of the dependence (7) is shown in Fig. 5. The optimum parameters of equation (7) under the condition of the maximum filling factor θ are $D_p = 3$ mm, $Q = 0.03$ kg/s, $V = 15$ m/s. As it can be seen from Fig. 5: with the increase of the seed diameter D_p , the fill factor θ decreases by parabola; with an increase in the seeds supply Q , the fill factor θ decreases linearly; and for the air flow velocity $V = 15$ m/s, the optimal value of the fill factor θ is present.

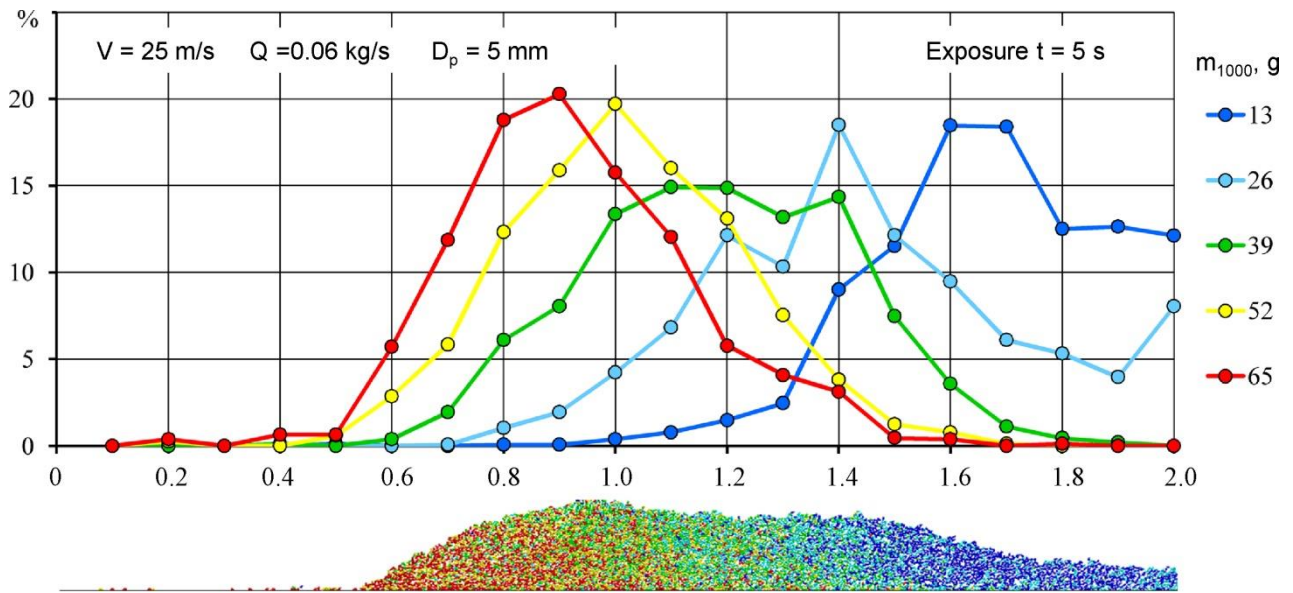


Fig. 4 – Distribution of seed fractions with effective diameter $D_p = 5$ mm along the length of the area formed by the air flow influence

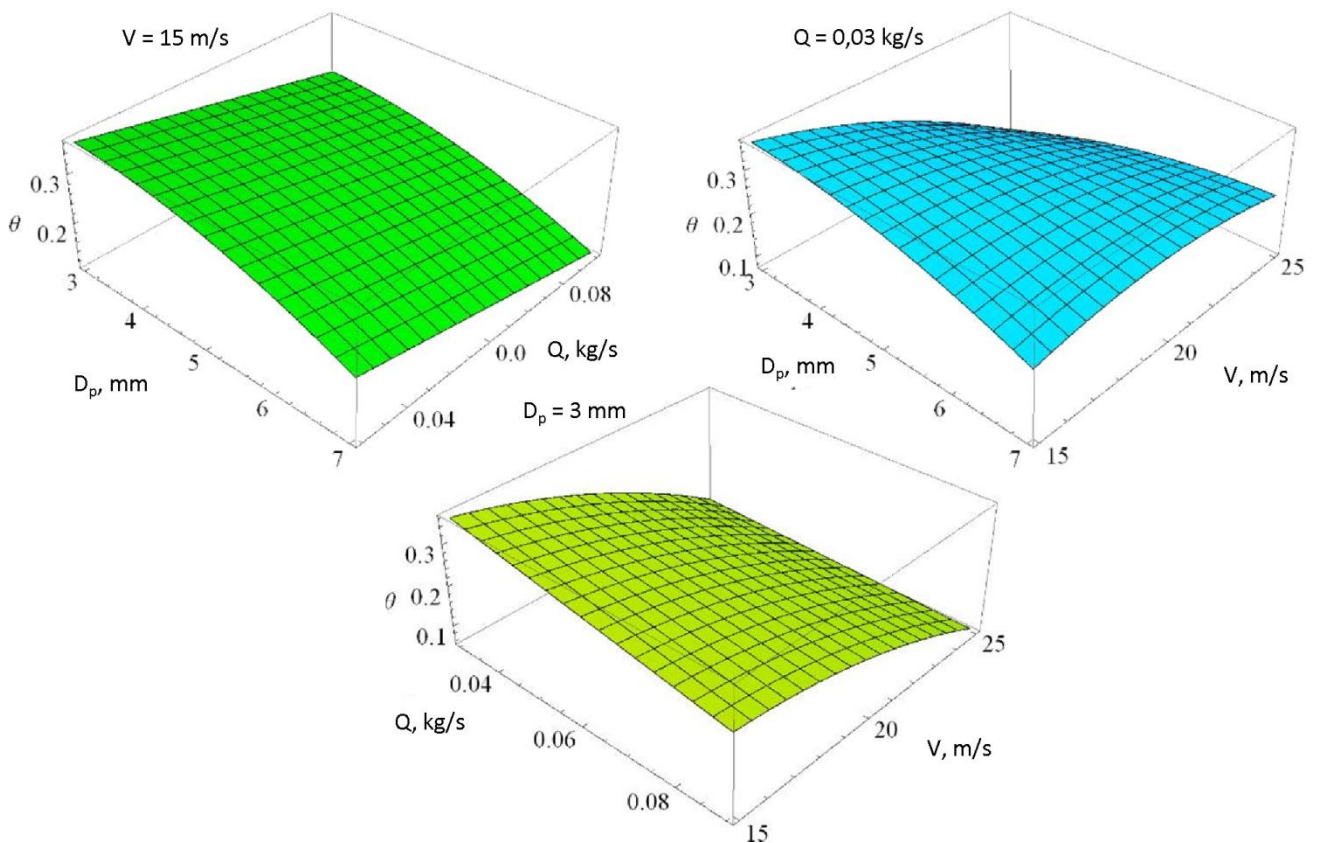


Fig. 5 – The dependence of the filling factor θ on the effective diameter of the seed D_p , the supply of seed Q and the air velocity V

According to the obtained data, the coefficient of distribution δ is calculated by the formula (6). Using Mathematica software package, a mathematical expression is compiled in a skilled form after the reduction of non-significant parts of the equation according to Student's criterion, which links the coefficient of distribution δ to the factors of research:

$$\delta = 67.568 - 4.87605 D - 0.537449 D^2 - 152.139 Q - 1.22609 V + 0.542871 D V + 6.11275 Q V - 0.0510141 V^2 \quad (8)$$

The graphical interpretation of the dependence (8) is shown in Fig. 6. The optimum parameters of equation (8) under the condition of the maximum distribution coefficient δ are $D_p = 3$ mm, $Q = 0.03$ kg/s, $V = 15$ m/s. As it can be seen in Fig. 6, with increasing the seeds supply, the distribution factor θ decreases by parabola; the diameter of the seed D_p and the air velocity V affects the distribution coefficient δ by the function of the hyperbolic paraboloid.

The second stage, namely experimental research, has been carried out using the method of mathematical planning of the multifactorial experiment, which allows determining the mathematical processes' models in the form of regression equations. The obtained mathematical model of the influence of the investigated factors on the coefficient of distribution δ is the following:

$$\delta = 36.8588 - 0.87431 x_1 + 0.0222222 x_1^2 + 3.12163 x_2 + 0.883579 x_1 x_2 - 1.25313 x_2^2 \quad (9)$$

For this equation, the 95 % probability level of the dispersion is homogeneous, the value of the Cochran criterion $G = 0.2594 < G_{0.05} (2; 9) = 0.4755$. Dispersion of the adequacy of the mathematical model $S_{aad}^2 = 1.879$; variance of experimental error $S_y^2 = 1.4870$; Fisher's value $F = 1.26 < F_{0.05} (5; 18) = 2.77$. The model is adequate at any level of confidence probability. According to the calculated values of the correlation coefficients and Student's criterion $t_{0.05} (18) = 2.1$, all coefficients are significant at the confidence level of over 95 %. In a sketched form, the model (9) has the following form:

$$\delta = 6.07089 - 29.1437 Q + 2.62933 V - 0.0501251 V^2 \quad (10)$$

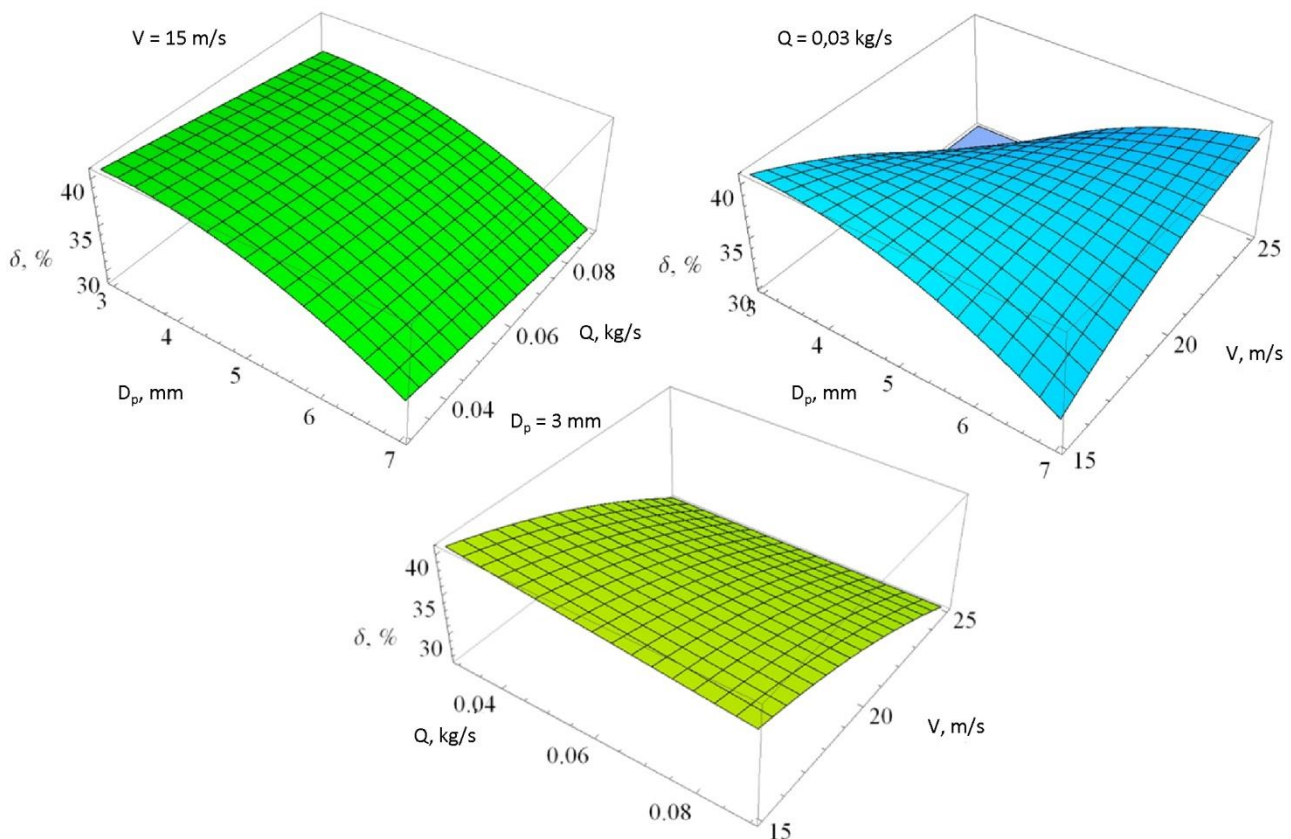


Fig. 6 – The dependence of the distribution coefficient δ on the effective diameter of the seed D_p , the seeding Q and the air flow velocity V

Analyzing equation (10), it can be argued that the factor of distribution δ is affected by all of the above-mentioned factors. At the same time, with increasing air flow velocity V , the distribution coefficient δ increases. And with increasing seed Q supply, the distribution coefficient δ decreases. The graphical interpretation of the experimental (10) and theoretical dependences (8) obtained at $D_{p1} = 6$ mm and $D_{p2} = 7$ mm is shown in Fig. 7. Statistical analysis showed that the correlation coefficient between the theoretical (8) and experimental (10) dependencies in the variation of the factors' values in the given range is 0.96.

The mathematical model of the influence of the investigated factors on the power consumed by the experimental installation, has the form:

$$P = 1.62667 + 0.0116667 x_1 - 0.0183333 x_1^2 + 0.995556 x_2 - 0.000833333 x_1 x_2 - 0.01 x_2^2 \quad (11)$$

For this equation, the 95 % probability level of the dispersion is homogeneous, the value of the Cochran criterion $G = 0.1675 < G_{0.05} (2; 9) = 0.4755$. Dispersion of the adequacy of the mathematical model $S_{aad}^2 = 0.00215$; variance of experimental error $S_y^2 = 0.00135$; value of Fisher's criterion $F = 1.59 < F_{0.05} (7; 18) = 2.58$; the model is adequate at any level of confidence probability. According to the calculated values of the correlation coefficients and Student's criterion $t_{0.05} (18) = 2.1$, all coefficients are significant at the confidence level of over 95 %. In a sketched form, the model (11) has the form:

$$P = -2.35556 + 0.199111 V \tag{12}$$

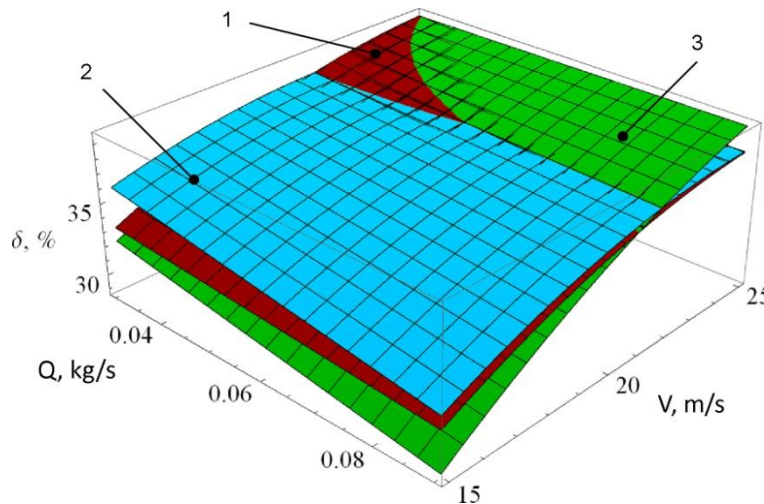


Fig. 7 – The dependence of the distribution coefficient δ on the seeds supply Q and air flow velocity V
 1 – experimental dependence (10); 2 – theoretical dependence (8) with $D_{p1} = 6 \text{ mm}$;
 3 – theoretical dependence (8) with $D_{p2} = 7 \text{ mm}$

The graphic interpretation of the obtained dependence (12) is presented in Fig. 8. Analyzing Equation (12), it can be argued that the power consumed by the experimental installation linearly affects only the air flow velocity V .

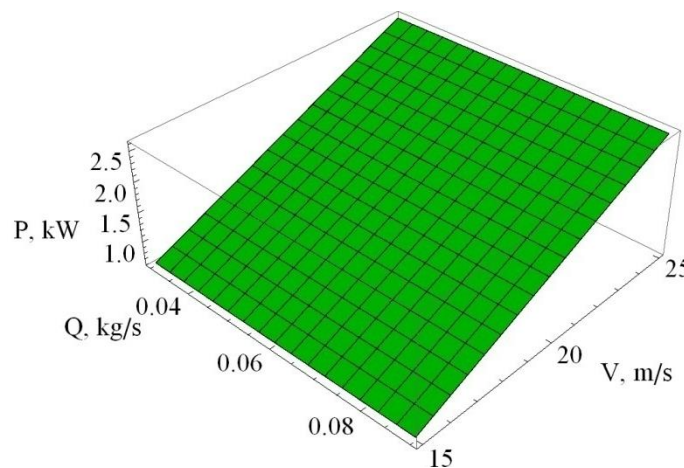


Fig. 8 – The dependence of the power P , consumed by the experimental installation, on the seeds supply Q and air velocity V

The task of solving a compromise problem was to minimize the power P consumed by the experimental installation, with the maximum value of the distribution coefficient δ and the seeds supply Q , that is:

$$\begin{cases} \delta(Q, V) \rightarrow \max, \\ P(Q, V) \rightarrow \min, \\ Q \rightarrow \max. \end{cases} \tag{13}$$

Convert the system of equations (13) to the form:

$$\frac{P(Q,V)}{Q \times \delta(Q,V)} \rightarrow \min . \quad (14)$$

The solution of the problem (14) with the aid of Mathematica software package leads to optimal technological regimes of the sunflower seeds separation during movement under the influence of air flow: $Q = 0.09$ kg/s, $V = 15$ m/s, $\delta = 31.6$ %, $P = 0.63$ kW.

CONCLUSIONS

As a result of numerical simulation of the mechanical and technological process of sunflower seeds separation during movement under the influence of air flow, there has been developed the dependences of the distribution of each fraction of the seeds on the length of the area (average value, average square deviation σ , filling factor θ , distribution coefficient δ) from the seed effective diameter D_p , air flow velocity V and the seed supply Q . Under the condition of a maximum filling factor θ and a distribution coefficient δ , rational regime parameters of the specified process are defined: for effective diameter of the seed $D_p = 5$ mm supply is $Q = 0.03$ kg/s, and air velocity $V = 15$ m/s.

As a result of experimental studies of the mechanical and technological process of sunflower seed separation during its movement under the action of air flow, a physical-mathematical model was developed that linked the distribution coefficient δ and the consumed power P to the supply of seed Q and air velocity V . Statistical analysis has showed that the correlation coefficient between the theoretical and experimental dependencies in the variation of the factors' values in the given range is 0.96.

During the research, the compromise problem has been solved, in particular, the minimization of the power P consumed by the experimental installation with the maximum value of the distribution coefficient δ and the seeds supply Q : $Q = 0.09$ kg/s, $V = 15$ m/s, $\delta = 31.6$ %, $P = 0.63$ kW.

REFERENCES

- [1] Aliev E.B., (2017), Numerical modeling results of the mechano-technological process of the oilseed seeding material transfer under the air flow influence, *Bulletin of Zhytomyr National Agroecological University (Вісник Житомирського національного агроекологічного університету)*, №1 (58), Т.1, pp. 173–180, Zhytomyr / Ukraine;
- [2] Aliev E.B., (2016), Technical and technological support of oil crop seeds purification and separation processes, *Records of the Ukrainian Scientific and Practical Conference of Young Scientists and Specialists from May 25-26, 2016 The role of scientific research in providing the processes of the Ukrainian agrarian production innovative development./ NAAS, GA ISC NAAS, Ministry of Agrarian Policy and Food of Ukraine, Ukrainian Institute of Plant Variety Expertise (Матеріали Всеукраїнської науково-практичної конференції молодих вчених і спеціалістів 25–26 травня 2016 р. Роль наукових досліджень в забезпеченні процесів інноваційного розвитку аграрного виробництва України. / НААН, ДУ ІЗК НААН, М-во аграр. політики та прод. України, Укр. ін-т експертизи сортів рослин.)*. pp. 4-5, Vinnytsya/Ukraine;
- [3] Aliev E.B., Bandura V.M., Pryshliak V.M., Yaropud V.M., Trukhanska O.O., (2018), Modeling of mechanical and technological processes of the agricultural industry, *INMATEH Agricultural Engineering*, Vol. 54, Nr. 1, pp. 95–104, Bucharest/Romania;
- [4] Aliev E.B., Shevchenko I.A., (2017), Investigation of aerodynamic properties of oilseeds, *Bulletin of Agrarian Science (Вісник аграрної науки)*, №3 (769), pp. 63–65, Kiev/Ukraine;
- [5] Aliev E., Yaropud V., (2017), Research of physical and mechanical properties of oilseed crops, *MOTROL. Commission of Motorization and Energetics in Agriculture*, Vol. 19, No 3, pp. 103–108, Lublin/Poland;
- [6] Aliev E.B., Yaropud V.M., (2017), Physical and mathematical apparatus of seeds movement in the air flow, *Ukrainian scientific journal "Technology, energy, transport, agribusiness" (Всеукраїнський науково-технічний журнал «Техніка, енергетика, транспорт АПК»)*, №2 (97), pp. 19–23, Vinnytsia/Ukraine;
- [7] Burenko K.S., Vedmedeva E.V., Pershin A.F., (2012), Studying of sunflower collection for the trait of large fruit (Изучение коллекции подсолнечника по составляющим признакам крупноплодности), *Scientific and technical bulletin Institute oilseeds NAAS (Науково-технічний бюлетень Інституту олійних культур НААН)*, № 17, С. 42–47, Zaporizhia/Ukraine;

- [8] GOST 10854-88 (2010), Oilseeds. Methods for determining the weed, oil and specially accounted impurity, Enter: 23.12.88. *Standartinform*, 10 p, Moscow/Russia.
- [9] Nurullin E.G., Salakhov I.M., Dmitriev A.V., (2014), Mathematical model of the seeds movement in the main chamber of the pneumatic and mechanical treating machine, *Bulletin of the Kazan State University of Agriculture (Вестник Казанского ГАУ)*, № 1 (31), pp. 69–72, Kazan/Russia;
- [10] Tishchenko L.N., Olshansky V.P., Olshansky S.V., (2010), *Hydrodynamics of grain separation: monograph (Гидродинамика сепарирования зерна: монография)*, 174 p, Kharkiv/Ukraine;
- [11] Vedmedeva K.V. Makhova T.V., Kirpichova N.M., (2017), The result of selection for a large-fatty line and a sunflower variety, *Collection of scientific works of the Selection-Genetic Institute of the National Centre for Seed and Selection Studies (Збірник наукових праць селекційно-генетичного інституту Національного центру насіннезнавства та сортовивчення)*, issue 29 (69), pp. 26–34, Odessa/Ukraine;
- [12] Zaika P.M., (2006), The theory of agricultural machines. Volume 3, Section 7. *Cleaning and sorting seeds (Теорія сільськогосподарських машин. Том.3, розділ 7. Очистка і сортування насіння)*, 407 p, Kharkiv/Ukraine.

DESIGN OF SHAPED-HOLE VOLUME-VARIABLE PRECISION SEEDER

/ 变容量型孔轮式排种器设计

Lect. Ph.D. Jiaxin Zheng¹, M.S. Yanyu Gao¹, Lect. Ph.D. Hongfang Yuan², Lect. Ph.D. Rong Chen^{*1}¹ School of Mechanical and Electrical Engineering, Yunnan Agricultural University, Kunming 650201, China;² Key Laboratory of Bionics Engineering, Ministry of Education, Jilin University, Changchun 130025, China

Tel: 15808841895; E-mail: 15808841895@163.com

Keywords: seeder, volume-variable hole, compulsory seed metering, seed spacing**ABSTRACT**

To improve the seed spacing consistency of vertical-disc seeders and starting from the mechanical compulsory seed metering, we designed a variable-volume hole precision seeder that adopts a cam push-rod structure to realize the compulsory seed metering. We studied the overall design of this new seeder. The optimal hole parameters were determined. Response surface method (RSM) was used in trial design, and this scheme was implemented on the discrete element software EDEM. RSM regression and prediction optimization show the optimal hole parameters are hole diameter 10 mm, depth 6.5 mm, and chamfer 2 mm. Comparative tests on the bench show that the new seeder is over the vertical-disc device showing 14%-21% higher longitudinal consistency and 18%-26% higher transversal consistency. The hole-typed volume-variable precision seeder with a cam push-rod structure would significantly improve the seed spacing consistency.

摘要

本文提出提高排种器的粒距一致性需具备的“两个条件”，并由机械式强制排种入手，设计出采用凸轮推杆机构实现定点强制排种的型孔容积可变式精密排种器，对该排种器进行了整体设计。为求出型孔参数的最优解，利用响应曲面方法进行试验设计，并在离散元软件 EDEM 中实施试验方案；经响应曲面回归分析和预测寻优，得出型孔参数最优解为，直径 10mm、深度 6.5mm、倒角 2mm。为验证仿真试验的准确性，又进行了离散元和 JPS-12 排种器试验台对比试验，试验结果相近，表明离散元仿真试验得出的结果是准确的，型孔参数的最优解可信。经与普通垂直圆盘排种器精播大豆粒距分布台架对比试验，得出型孔容积可变式精密排种器的合格粒距一致性可提高 14%~26%。

INTRODUCTION

During precision seeding, the number (single-seed or multi-seed), space and depth of seeds are precisely controlled as per the agronomic requirements and plowed into soils. As a result, the seed spacing consistency is improved, which facilitate the growth, development of seeds and finally improve the crop yield (Zheng, 2017).

The premise of precision seeding is precise seed metering of the seeder. Precision seeders can be divided by the working principle into mechanical and pneumatic ones. Precision seeders are limited in maintaining the consistency of seed spacing. 1) As for mechanical devices, due to the difference in seed sizes (Arzu and Adnan, 2014) and the impacts of metering structures, three seed dropping methods (prompt dropping, delayed dropping and compulsory dropping) coexist. As a result, the seeds are not dropped from the same position of the seeder and at the same start speed at a constant time interval. 2) As for pneumatic devices, the consistency of seed spacing is impacted by the air pressure, rotating speed of seeder and the number and size of suction holes. Due to the difference in seed sizes, the pneumatic device is not as stable or reliable as the mechanical one. Even though the suction holes on the suction cup can precisely fill seeds, the departing speeds of seeds from the metering device would differ, which leads to the differences in seed spacing (Zdzislaw et al., 2015; Fang et al., 2018; Rasool and Qayoum, 2018).

Two commonly-used precision machinery seeders are vertical-disc and horizontal-disc devices. The seed spacing consistency can be improved if the seed dropping methods of these two devices are restricted to one method such as compulsory seed dropping, so that the seeds would be ejected from the same position of the metering device.

There is rare research on the seed spacing consistency from the perspective of compulsory seed metering. For instance, the addition of a vertical disc or a ball-roll pusher seed planter significantly improves the seed spacing consistency of horizontal-disc seeders.

Compared with the pneumatic one, the precision mechanical metering device is superior with simple structure, low machining cost, working stability and reliability, and ability in improving the seed spacing consistency (Ike, 2018). Among the mechanical seeders, the vertical-disc device is more able to maintain the seed spacing consistency due to the height and direction of seed dropping. Thus, we selected the vertical-disc seeder and made the research from the perspective of mechanical compulsory seed metering. We aim to establish a shaped-hole volume-variable soybean precision seeder with point-fixed compulsory seed metering (Yao, 2018).

MATERIALS AND METHODS

Experiment part

Design of a Novel Seeder

This seeder was built by adding a cam push rod structure into the traditional vertical-disc seeder. This cam push rod structure had a fixed cam and was driven by the hole disc to rotate around the cam. The push rod was controlled by the cam outline curve to regularly shrink in the hole, which thereby changes the hole volume, so that the compulsory seed metering is adopted when the hole shrinks.

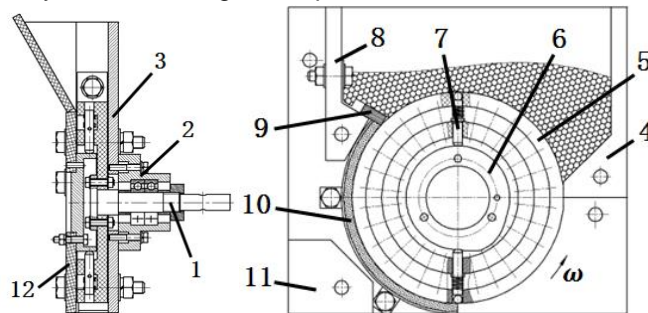


Fig. 1 - The structure of volume-variable hole precision seeder

1. Transmission shaft; 2. Bearing seat; 3. Front lid of seed box; 4. Upper right support; 5. Hole disc; 6. Cam; 7. Push rod; 8. Upper left support; 9. Seed brush; 10. Protection board; 11. Lower left support; 12. Rear lid of seed box;

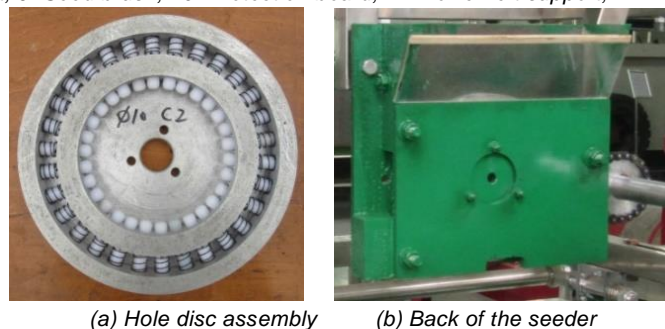


Fig. 2 - The shaped-hole volume-variable soybean precision seeder

Soybean used in the Experiment

The properties of the soybean (Hefeng 50) used here are listed in Table 1. The equivalent diameter of soybean approximately obeys the normal distribution with a mean of 6.52 mm and standard deviation (SD) of 0.31 mm. The beans with equivalent diameter within 6.00-7.20 mm account for 88.7%.

Table 1

Properties of soybean			
Water content	Density	Poisson's ratio	Shear modulus
9.4 %	1.27 g/cm ³	0.413 ³⁴	45.56 MPa ³⁴

Table 2

Properties of materials that get in contact with soybeans				
	Al	Rubber	Q235	PMMA
Poisson's ratio	0.334	0.49	0.26	0.33
Shear modulus (GPa)	25.5	0.006	81.34	0.08
Density(g/cm ³)	2.7	1.52	7.85	1.19

Table 3

Mechanical parameters between soybeans and contact materials					
	Seed&Seed	Seed&Q235	Seed&PMMA	Seed&Rubber	Seed&Al
Recovery coefficient	0.47 ²⁹	0.6 ³⁴	0.58 ²⁹	0.60 ^{34,38}	0.6 ³⁴
Static friction coefficient	0.27 ³⁵	0.23 ³⁶	0.32 ³⁷	0.34 ²⁶	0.25 ³⁹
Rolling friction coefficient	0.05 ³⁴	0.20 ²⁹	0.1 ²⁹	0.26 ²⁷	0.19

Parameter setting on EDEM software

The use of EDEM software into design of seeders helps to improve the research and design levels, shorten the development period and increase the performance.

The use of DEM (Discrete Element Modeling) into simulation of seeders necessitates the provision of multiple physico-mechanical parameters such as water content, density, three-axis dimensions, and static rolling friction coefficient.

The fault Hertz-Mindlin (No Slip) model was selected as the between-seed and seed-boundary contact physical model. The physical properties of the seeds and boundary were set as per Tables 1 and 2. The contact parameters between the seeds and the components of the seeder were set as per Table 3. The simplified seeder model was introduced. The material properties of all components were added as per Table 3. The seed spacing was set as 50 mm, when the seeder worked at the limit speed 2.57 km/h. After simulation tests with different speeds, we determined the final rotating speed to be 25.56 rpm (at the real working speed of 2.3 km/h). A spherical model was used to simulate beans. Their diameters within 6.00-7.20 mm obeyed the normal distribution with mean of 6.52 mm and SD of 0.31. During the simulations, totally 1500 seeds were generated, and their sizes and positions were randomly formed (Bilonoga Y., Maksysko O., 2018). The time step length was 9.79×10^{-6} s, about 20% of Rayleigh time step. The simulation duration was 22 s, data collection interval was 0.01 s and mesh size was 2R.

Description of test Equipment

We conducted verification tests with this seeder on a JPS-12 seeder bench. The trial scheme was that trials were conducted on EDEM and the test bench separately. The working speeds (seed spacing =5cm) and the rotating speeds of the seeder are listed in Table 4.

Table 4

The working speeds and the rotating speeds of the seeder						
Working speed (km/h)	1	1.5	2	2.5	3	3.5
Rotating speed (rpm)	11.1	16.7	22.2	27.8	33.3	38.9

The bench trials were conducted on a JPS-12 seeder performance test bench (Jointly developed by Heilongjiang Institute of Agricultural Machinery Engineering Science and Harbin Bona Technology Co. Ltd).

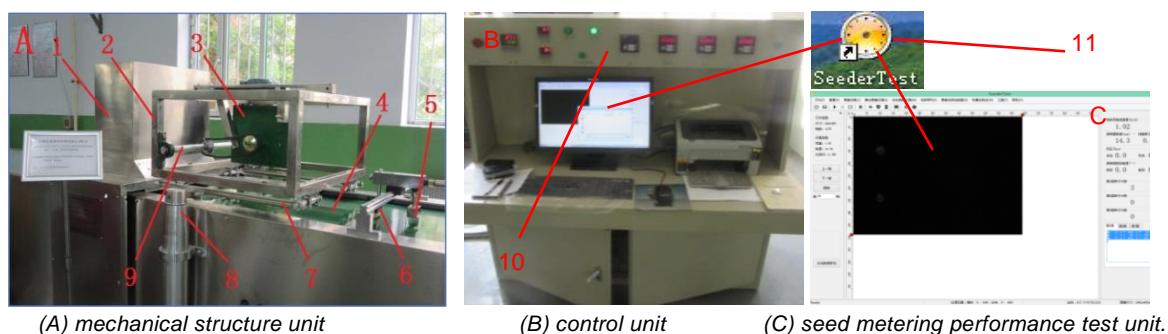


Fig. 3 - Overall composition of the seeder test bench

1. Industrial camera 2. Metering device universal mounting bracket 3. Variable-volume hole precision seeder. 4. Oil zone 5. Nozzle 6. Oil brush 7. Mounting bracket front and rear inclining angle adjusting device 8. Mounting bracket height and left/right inclining angle adjusting device 9. seed metering shaft 10. bench operation control plane 11. metering performance test software

Research Method

The parameters of hole structure are all continuous, so the significant ones should be selected as per regression fitting, factor analysis and interactions. Finally, the parameters are optimized (Liu, 2018). The response surface method (RSM) is more suitable for optimization of hole structure parameters of seeders. Here the Box-Behnken RSM trial design from Design-Expert was used to optimize hole structure parameters.

Simulation experiment: There were totally 17 trials including 12 trials of factor analysis, 5 trials of zero tests. Each trial was conducted in triplicate.

The factor levels and trial design are showed in Table 5.

Table 5

Level	Factor/mm		
	diameter(A)	depth(B)	chamfer(C)
1	10	7	3
0	9	6.7	2
-1	8	6.4	1

Contrast experiment: Like the simulations, with reference to the results of simulation processing and manufacturing material, the new seeder and a vertical-disc seeder (a bristle brush wheel seeder) were sent into seed spacing consistency comparative test on the JPS-12 test bench, so as to validate whether the new device can improve the seed spacing consistency.

To more precisely study the consistency of qualified seed spacings, we used longitudinal consistency (longitudinal seed spacing consistency) and transversal consistency (transversal seed spacing consistency) to measure qualified grain interval consistency. Specifically, the longitudinal seed spacing consistency was reflected by the seed spacing SD (σ_z), while the transversal seed spacing consistency was measured by the SD away from the centreline (σ_H).

RESULTS

Hole parameter optimization with the seeder.

Regression analysis

Table 6

Final analysis of variance (ANOVA) of single-seed rate					
Source	Sum of squares	df	Mean Square	F Value	p-value
Model	6892.60	5	1378.52	161.18	<0.0001
A	2733.19	1	2733.19	319.57	<0.0001
C	2831.66	1	2831.66	331.09	<0.0001
AC	991.62	1	991.62	115.94	<0.0001
A²	89.17	1	89.17	10.43	0.0080
C²	230.00	1	230.00	26.89	0.0003
Residual	94.08	11	8.55		
Lack of fit	64.46	7	9.21	1.24	0.4403
Pure Error	29.62	4	7.40		
Total	6986.67	16			
Std.Dev	2.92		R²	0.9865	
Mean	80.63		Adj R²	0.9804	
C.V.%	3.63		Pred R²	0.9676	
PRESS	226.66		Adeq Precision	45.416	

1) At the significance level $p < 0.05$, the significant items are A, C, AC, A², C², at the insignificance level $p > 0.1$, there is no insignificant item.

2) The F-value of the regression equation is 161.18, indicating significant ($p < 0.01$).

3) The regression equation shows no lack-of-fit ($p < 0.05$). The coefficient of determination ($R^2 = 0.9865$) and adjusted R square ($Adj R^2 = 0.9804$) are both close to 1, indicating this regression equation is precise and effective significantly.

The predicted R^2 ($Pred R^2 = 0.9676$) and precision value ($Adeq Precision = 45.416 > 4$) suggest this regression equation predicts well within the preset range.

Moreover, the significance levels of all factors rank as follows: chamfer > diameter > depth.

After substitution into the coding equation, we get the regression equation of single-seed rate against the real factors:

$$\text{Single-seed Rate} = -802.90 + 132.70d + 190.04\delta - 15.75d\delta - 4.60d^2 - 7.38\delta^2 \quad (1)$$

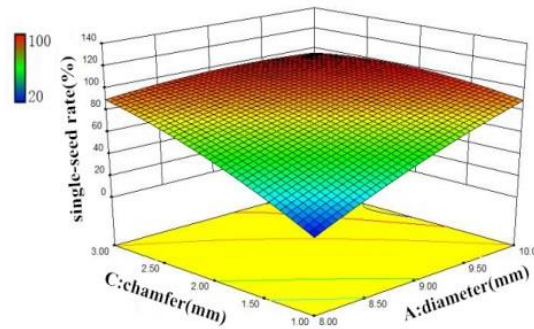


Fig. 4 - Contours of diameter (A) and chamfer (C) against single-seed rate (R1)

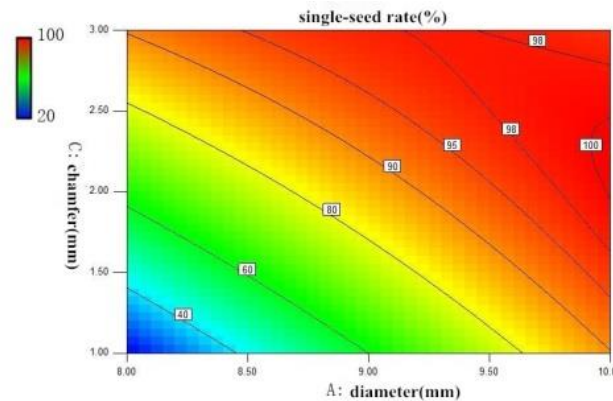


Fig. 5 - Response surfaces of diameter (A) and chamfer (C) against single-seed rate (R1)

The contours and response surfaces can be used to determine whether the impact of a factor on the effect is significant, the changing trend of effect against the factor and the area of the optimal value. The contours (Fig. 4) and response surface (Fig. 5) of hole diameter (A) and chamfer (C) against single-seed ratio (R_1) were plotted on Design-Expert. The contours show that the single-seed rate (R_1) is significantly affected by the hole diameter (A) and chamfer (C). The single-seed rate increases from 20% at $A=8$ mm to 100% at $A=10$ mm. The single-seed rate rises from 20% at $C=1$ mm to 100% at $C=3$ mm and then declines. The interactive effect between A and C on single-seed rate is very significant. The maximum of single-seed rate is obtained at $A=10$ mm and within $C=2-3$ mm. This phenomenon is also revealed on the response surface. Similarly, the final ANOVA of cavity rate is showed in Table 7.

Table 7

Final ANOVA of cavity rate						
Source	Sum of squares	df	Mean Square	F Value	p-value	
Model	6676.60	5	1335.32	146.03	<0.0001	
A	2665.23	1	2665.23	291.47	<0.0001	
C	2601.73	1	2601.73	284.52	<0.0001	
AC	1036.84	1	1036.84	113.39	<0.0001	
A ²	76.35	1	76.35	8.35	0.0147	
C ²	279.08	1	279.08	30.52	0.0002	
Residual	100.59	11	9.14			
Lack of fit	70.97	7	10.14	1.37	0.4009	
Pure Error	29.62	4	7.40			
Total	6777.18	16				
Std.Dev	3.02			R ²	0.9852	
Mean	19.77			Adj R ²	0.9784	
C.V.%	15.30			Pred R ²	0.9629	
PRESS	251.17			Adeq Precision	43.846	

1) The significant items are A, C, AC, A², C²; there is no insignificant item.

2) The F-value of the regression equation is 146.03, indicating significant ($p < 0.01$).

3) The regression equation shows no lack-of-fit ($p = 0.4009 < 0.05$).

The coefficient of determination ($R^2 = 0.9852$) and adjusted R square ($Adj R^2 = 0.9784$) are both close to 1, indicating this regression equation is precise and effective significantly.

The predicted R^2 ($Pred R^2 = 0.9629$) and precision value ($Adeq Precision = 43.846 > 4$) suggest this regression equation predicts well within the preset range. Moreover, the significance levels of all factors rank as follows: diameter > chamfer > depth.

After substitution into the coding equation, we get the regression equation of cavity rate against the real factors:

$$Cavity\ Rate = 881.05 - 127d - 195.45\delta + 16.1d\delta + 4.25d^2 + 8.13\delta^2 \quad (2)$$

The contours and response surface of hole diameter (A) and chamfer (C) against cavity rate (R^2) were plotted on Design-Expert. The contours show that the cavity ratio (R^2) is significantly affected by the hole diameter (A) and chamfer (C). The cavity rate increases from 80% at $A = 8$ mm to 0 at $A = 10$ mm. The cavity rate first declines and then rises with the increase of C from 1 to 3 mm. The interactive effect between A and C on cavity rate is very significant. The minimum of cavity rate is obtained at $A = 10$ mm and within $C = 2$ -3 mm. This phenomenon is also revealed on the response surface.

The working performance of the seeder is jointly reflected by the single-seed rate, cavity rate, and double-seed rate. During the simulations, nearly no double-seed in one hole was found. The data obtained during the trials were insufficient to build a regression equation of diameter (A), depth (B) or chamfer (C) against double-seed rate. According to experiences, when the hole chamfer and diameter are very large, the seeds are more likely to fall into holes, but if the depth only accommodates one seed, other seeds will be cleaned outside anyway.

Prediction optimization

The RSM is feasible for prediction optimization. In the design domain, we provided the maximum of single-seed rate, the minimum of cavity rate, and obtained the contours and response surface of fitness.

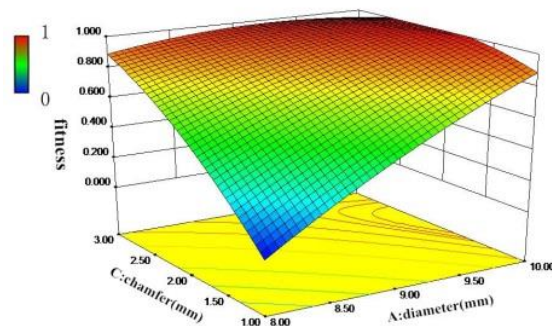


Fig. 6 - Contour of fitness

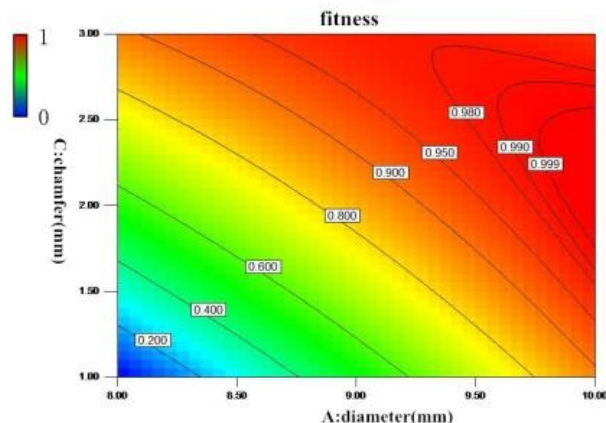


Fig. 7 - Response surface of fitness

As showed in Fig. 7, in the area with the fitness close to 1, we obtain the optimal solution. The optimal solution is found at hole diameter of 10 mm and chamfer of 2 mm. When the diameter and chamfer were assigned with integers, it facilitated the hole machining. Thus, we set hole diameter = 10 mm and chamfer = 2 mm. The hole depth has no significant effect on single-seed rate or cavity rate, but at large depth, the hole accommodates two seeds. The equivalent diameters of the seeds are 5.45-7.46 mm (mean 6.52), so the hole depth was set at 6.5 mm. Finally, the optimal combination of hole parameters is listed in Table 8.

Table 8

Optimal combination of hole parameters (mm)

Diameter d	Depth h	Chamfer δ
10	6.5	2

Contrast experiment

In this section, the new seeder and a vertical-disc seeder (a bristle brush wheel seeder) were sent into seed spacing consistency comparative test, so as to validate whether the new device can improve the seed spacing consistency.



(a) volume-variable hole precision seeder; (b) bristle brush wheel seeder.

Fig. 8 - Comparative test of seeders

To more precisely study the consistency of qualified seed spacings, we used longitudinal consistency (longitudinal seed spacing consistency) and transversal consistency (transversal seed spacing consistency) to measure qualified grain interval consistency. Specifically, the longitudinal seed spacing consistency was reflected by the seed spacing SD (σ_z), while the transversal seed spacing consistency was measured by the SD away from the centreline (σ_H).

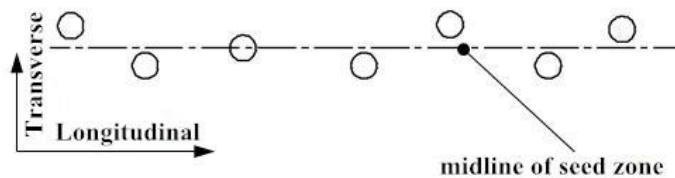


Fig. 9 - Seed zone transversal and longitudinal schematic diagrams

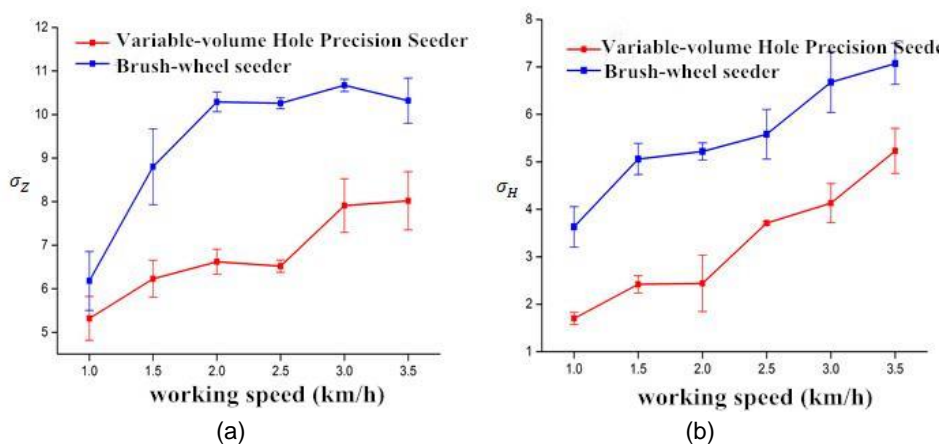


Fig. 10 - σ_z σ_H of two seeders

Note: A- σ_z changes with velocity; B- σ_H changes with velocity

Comparative tests on the JPS-12 test bench show that the new seeder is superior over the vertical-disc seeder in terms of 14%-21% higher longitudinal consistency and 18%-26% higher transversal consistency. The variable-volume hole precision seeder with a cam push-rod structure would significantly improve the seed spacing consistency.

CONCLUSIONS

1) To improve the seed spacing consistency of vertical-disc seeders, we, starting from the mechanical compulsory seed metering, designed a variable-volume hole precision seeder that adopts a cam push rod structure to realize the compulsory seed metering. We studied the overall design of this new seeder.

2) The hole parameters of the new seeder were optimized via Box-Behnken trials. The trial scheme was implemented on the discrete software EDEM. Response surface regression and prediction optimization were conducted on Design-Expert. The single-seed rate and cavity rate were significantly affected by both hole diameter and chamfer. The regression equations of hole diameter, depth and chamfer against the single-seed rate or cavity rate were determined separately. The optimal solution of hole parameters is: diameter 10 mm, depth 6.5 mm and chamfer 2 mm.

3) Comparative tests on the bench show that the new seeder is superior to the vertical-disc device in terms of 14%-21% higher longitudinal consistency and 18%-26% higher transversal consistency. The shaped-hole volume-variable precision seeder with a cam push-rod structure would significantly improve the seed spacing consistency.

ACKNOWLEDGMENTS

This work is supported by Polygonatum kingianum Coll. et Hems! Adaptive Seedbed Establishment Technology for High-Altitude Hilly Areas, 2018, Yunnan Education Department Scientific Research Fund (2018JS272), Yunnan Younth Fund (2017FD080), the 12th Five-Year Plan for National Science and Technology (No.2014BAD06B03) and Jilin Province Science and Technology Development Plan Projects (20140204050NY).

REFERENCES

- [1] Arzu Y., Adnan D., (2014), Measurement of seed spacing uniformity performance of a precision metering unit as function of the number of holes on vacuum plate. *Measurement*, vol.56, pp. 128-135;
- [2] Bilonoga Y., Maksysko O., (2018), Specific features of heat exchangers calculation considering the laminar boundary layer, the transitional and turbulent thermal conductivity of heat carriers, *International Journal of Heat and Technology*, vol. 36, issue 1, pp. 11-20;
- [3] Fang K., Zhou H., Lu Z., (2018), Research on optimization of drill hole gas pre-drainage process in low permeability outburst coal seam, *Chemical Engineering Transactions*, vol.66, pp. 667-672;
- [4] Gauthier T., Weidner S., Martinez B. (2017), Pressure measurements using pressure sensitive paint in supersonic flow, *Instrumentation Mesure Metrologie*, vol.16, issue 1-4, pp. 115-141;
- [5] Ike C.C., (2018), Exponential Fourier integral transform method for stress analysis of boundary load on soil, *Mathematical Modelling of Engineering Problems*, vol.5, issue 1, pp. 33-39;
- [6] Ike C.C., (2018), Flexural analysis of rectangular Kirchhoff plate on Winkler foundation using Galerkin-Vlasov variational method, *Mathematical Modelling of Engineering Problems*, vol. 5, issue 2, pp. 83-92;
- [7] Liu F., (2018), Numerical analysis of droplet atomization in wet electrostatic precipitator based on computational particle-fluid dynamics, *International Journal of Heat and Technology*, vol.36, issue. 1, pp. 215-221;
- [8] Yao Y., (2018), Application of mechanical arm sliding mode variable structure control in thermal cutting of metal materials, *Chemical Engineering Transactions*, vol.66, pp.685-690;
- [9] Zdzislaw K., Piotr M., Andrzej A., (2015), Frictional properties of selected seeds. *Technical Sciences*, vol.18, issue 2, pp.85-101;
- [10] Zheng J.X., (2017), *Furrow Construction Technology and Furrowing Machine for Soybean Precision Planters*, Jilin University, Changchun/China.

RESEARCH AND DEVELOPMENT OF AIR-SUCTION CORN PRECISION SEED METERING DEVICE

气吸式精量玉米播种器的研究与开发

Prof. Ph.D. Eng. Lv Xiaorong*¹⁾, Prof. Ph.D. Eng. Zhang Lihua¹⁾, Ph.D. Eng. Lv Xiaolian²⁾,
M.A. Stud. Eng. Tian Zhiwei¹⁾

¹⁾ Sichuan Agricultural University, College of Machinery & Electronics/China;

²⁾ Chuzhou University, College of Machinery & Automotive Engineering/China

Tel: 08352882182; E-mail: lrxj2008@163.com

Keywords: corn, seed metering device, detection and control system, reseeding device, performance test

ABSTRACT

The air-suction seed metering device with automatic detection and reseeding function was designed. The device is mainly composed of metering disc, reseeding device, detection system, signal processing and control system, alarm device and power supply. Based on the photoelectric sensors, the seed metering device is detected. The timed reseeding function was realized through the detection and control system. The correlation performance tests were done by comprehensive weight score value method. The test results had shown that: under the operating conditions of 4kPa and 15r/min, the seed metering device has the best seeding effect; the qualification rate of the seed metering device with the reseeding device is 93.68%, the over-seeding rate is 3.91%, the miss-seeding rate is 2.38%; compare the installed reseeding device with the uninstalled reseeding device, the qualification rate of the seed metering device is increased by 2.34% and the miss-seeding rate is dropped by 3.09%, and the seeding quality of the seed metering device has been greatly improved.

摘要

设计了一种带有自动检测与补种功能的气吸式播种器。该装置主要由排种盘、补种装置、检测系统、信号处理与控制系统、报警装置及电源等部分组成。基于光电传感器检测播种器漏播情况，通过检测控制系统实现播种器实时补种功能。采用综合加权评分法进行了试验，结果表明：当真空度为 4kPa，转速为 15r/min 时，播种器作业效果最优，装有补种装置的播种器的播种合格率为 93.68%，重播率为 3.91%，漏播率为 2.38%，相对未安装补种装置的播种器播种合格率上升 2.34%、漏播率下降 3.09%，播种质量有了较大的提升。

INTRODUCTION

Air-suction precision seeding is the main direction of corn precision seed metering device development, but currently there is a large miss-seeding problem in the seeding work (Lv X.L. *et al*, 2012; Shi Song *et al*, 2014). In recent years, many researchers have been made in the field of timed detection method and detection system for miss-seeding of the seed metering device. SINGH and others (Singh T.P. *et al*, 2011) used electronic control measurement system to timed monitor and feedback the seeding process of metering seed device. Jae Wan Lee and others (Jae Wan Lee *et al*, 2013) have studied the relationship between the vibration frequency of the metering seed disks and the PTO vibration frequency of the tractor in FlexPDE and ANSYS software. Zhou Liming and others (Zhou Liming *et al*, 2012; Zhu Ruixiang *et al*, 2014) have studied the monitoring system of the seeding performance of the corn precision seed metering device. Tian Liquan and others (Tian Liquan *et al*, 2016) have developed the seed metering device with the function of missing seed compensation and the device satisfied the accurate and effective reseeding requirements. Wu Jianmin and others (Zhang Xiaodong *et al*, 2013; Cao Dong, 2013) have researched and designed the missing seed detection and compensation system for the potato seed metering device. Ding Youchun and others (Ding Youchun, 2014; Li Ming *et al*, 2010) have studied the timed detection system for the missing seed of rape planting. At present, the method of delay time reseeding is adopted in the missing seed detection and reseeding systems for the precision seed metering device. It has the problems of complex structure and inaccurate reseeding. The foreign research is relatively mature, but its cost is high and unsuited for the planting mode of our country. In the paper, the air-suction corn precision seed metering device with automatic detection and reseeding device was designed, and the test was done on the influence of the working factors and the effect of the reseeding.

OVERALL SCHEME DESIGN

Structure and composition

The seed metering device mainly consists of main seed metering disc, reseeding device, detection and control system, transmission shaft, seed chamber, gas chamber and seeding pipe, as shown in Fig.1. The seed chamber and the gas chamber are installed on the transmission shaft. The gas chamber is connected with the seed chamber by the bolts. The gas chamber is connected to the fan through the gas pipe. The negative pressure of sucking seed is provided by the fan. The reseeding disc is installed on the drive shaft, and is fitted with the outside of the seed chamber. On both sides of the main seeding disc and reseeding disc a pair of photoelectric sensors is separately installed. The signal transmitter is fixed in the corresponding position of seed chamber. The signal receptor is fixed on the outside shell of the gas chamber, and corresponds to the transmitter. The sensors are used to detect the sucking seed situation on the seed metering discs. The seeding tube is installed on the frame and is located under the seed metering discs. A pair of sensors is installed in the pipe to detect the seeds flowing. The sensors are connected with the Microcontroller Unit (MCU) to transfer and deal with the signals. The MCU is connected with the stepper motor driver and control the reseeding disk sucked seed and timed reseeding.

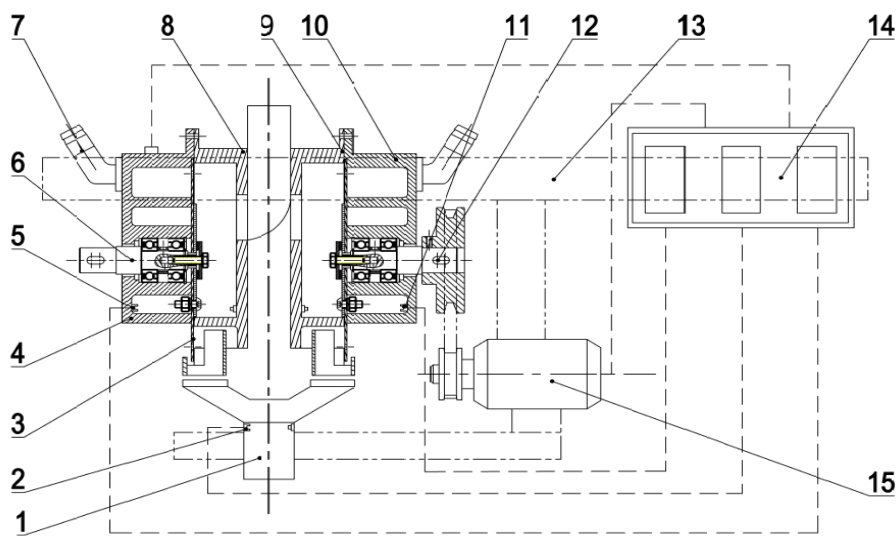


Fig. 1 - Structure diagram of the air-suction corn seed metering device

- 1- Seeding pipe; 2- Detection sensor I ; 3- Main seed metering disc; 4- Gas chamber; 5- Detection sensor II; 6- Main drive shaft; 7- Gas pipe; 8- Seed chamber; 9- Reseeding chamber; 10- Reseeding gas chamber; 11- Detection sensor III ; 12- Reseeding drive shaft; 13- Rack; 14- Single chip microcomputer; 15- Stepper motor

As shown in Fig. 2, the detection and control system is mainly composed of the detection module, the MCU, the reseeding device, the stepper motor, the alarm module and the power supply module.

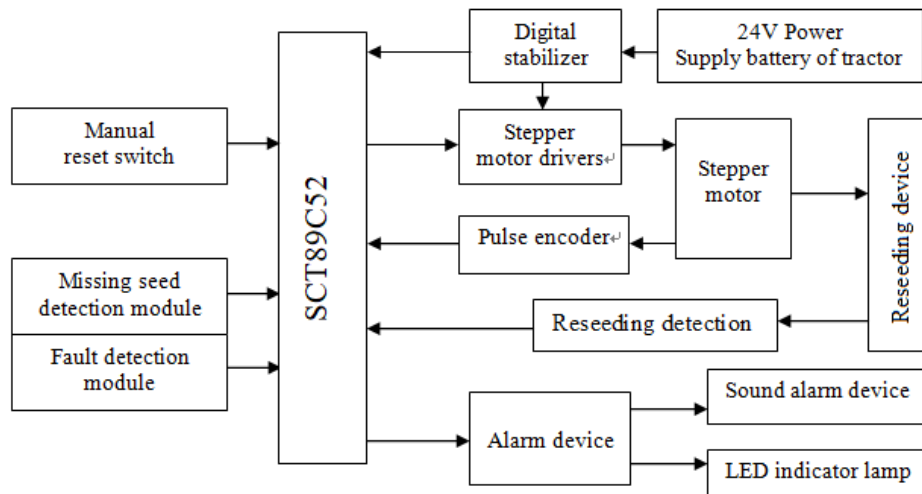


Fig. 2 - Structure block diagram of hardware system of reseeding detection

The detection module consists of three pairs of photoelectric sensors. The MCU is the core of the detection and control system. It deals with the transfer signal of the detection module and controls the operation of the reseeding device and alarm system. In order to ensure the safety and reliability of the system, the aeronautical plugs were used for the connection between each module. The working power is generated by the 24VDC power of the tractor.

MATERIALS AND METHODS

Working principle

With main seed metering disc rotated, the seeds were adsorbed on the suction holes by gas chamber negative pressure. The photoelectric sensor detected the sucking seeds situation. If the seeds were sucked on the suction hole, the signal receptor didn't receive the emission light of signal transmitter and the detection circuit was not changed so the reseeding device is in the static state. The seeds were carried out of the seed chamber. The negative pressure disappeared and the seeds fell into the seeding pipe. When there weren't seeds on the suction hole, the signal receptor received the light of the signal transmitter and the detection circuit was changed. The MCU sent out work instructions to the reseeding device according to the program setting, and started the stepper motor to drive the reseeding disc. At the same time, the photoelectric sensor installed on both sides of the reseeding disks was used to detect the next suction seed hole of the reseeding disc. When the seeds were adsorbed on the suction hole, the MCU sent out the stop instruction to the stepper motor. The sensor on the seeding pipe timely sent the pulse signal to the MCU. The seed dropping speed was reflected through the frequency of the transmitted signal. When the seed metering device has a problem, the MCU doesn't receive the pulse signal in the set time range and the alarm device starts.

DESIGN OF AUTOMATIC RESEEDING SYSTEM

Reseeding device

As shown in Fig.3, the reseeding device is mainly composed of the reseeding gas chamber, reseeding drive shaft, reseeding disc, reseeding chamber and gas pipe. The gas chamber is connected with the fan through the gas pipe and generates negative pressure. The gas chamber is installed on the drive shaft through a bearing and fixedly connected with the bracket. The reseeding chamber is installed on the gas chamber. The reseeding disc is installed on the driver shaft and is attached to the outside of the gas chamber and of the reseeding chamber. The reseeding disc rotates to the gas chamber and the reseeding chamber by the reseeding drive shaft. The MCU controls the rotation of the reseeding disc to real-time reseeding. When the seed metering device missed a seed, the control system controlled the metering seed disc to perform timed reseeding. The motor received the pulse signal from the control system, and then converted the pulse signal into the angular value (*Li Leixia, 2012*). The stepper motor 86BYGH250C is adopted. The 32 bit DSP digital type stepper motor driver HB-860H is selected, adopts PWM current control and the working voltage is 24VDC.

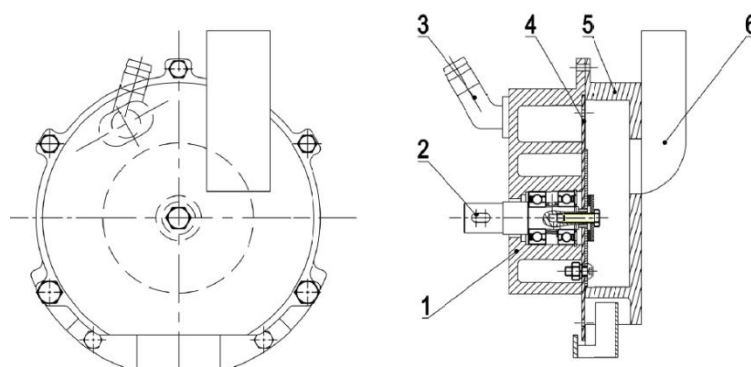


Fig. 3 - Structure diagram of the reseeding device of air suction corn precision seed metering device

1- Reseeding gas chamber; 2-Reseeding drive shaft; 3- Gas pipe; 4-Reseeding disc; 5-Reseeding chamber; 6- Adding seed pipe

Detection and control system

The detection device is provided the reseeding signal according to the output level of the sensor. When the suction seed hole had seed, the light of the laser transmitter was shielded, the laser receptor was unable to receive the light signal and output the high level. When the suction seed hole had no seed, the

laser receptor received the optical signal and outputted a low level. When the seed was normally falling, the sensor outputted a continuous high level signal. When the device had a problem, the sensor outputted a continuous low level signal. The starting of the alarm device is determined by the test result of the discriminating circuit. The M12 laser sensor is used to detect seed on the suction seed hole, and the HD-DS25CM-3MM photoelectric sensor is used to detect the seed flowing in the seeding pipe. The signal conversion circuit of the photoelectric sensor is shown in fig. 4.

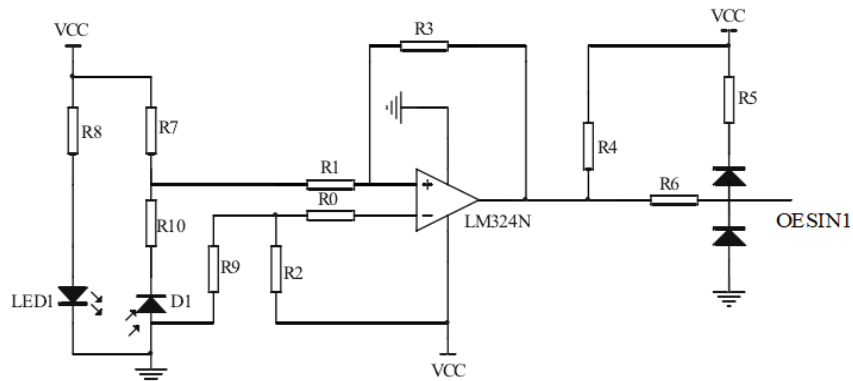


Fig. 4 - Circuit diagram of the signal conversion

The signal processing and control module is the core of the detection and control system (Sun Wei et al, 2016; WANG Lifen, 2015). As shown in Fig. 5, the system needs to deal with more comprehensive information, so that the digital analog hybrid circuit is used. The STC89C52 MCU is adopted in the reseeding system. The clock circuit in this module connects with the controlled reverse phase amplifier through the XTAL1 and XTAL2 pins of the MCU. The MCU was controlled by external oscillator. The value of the capacitor of the oscillator is 30pF and X1 crystal oscillator is 12MHz. After pressing the reset button, the high level was transmitted to the RST terminal, and the components' reset was realized to avoid unnecessary operations. The alarm module detects seed flowing by photoelectric sensors inside the seeding pipe. The work of metering seed device and the seeding pipe are judged by the sending high and low level signals of the sensor. If the sensor continuously sends the low level signal in the set time range, the MCU starts the alarm device. The alarm device adopted the buzzer and LED.

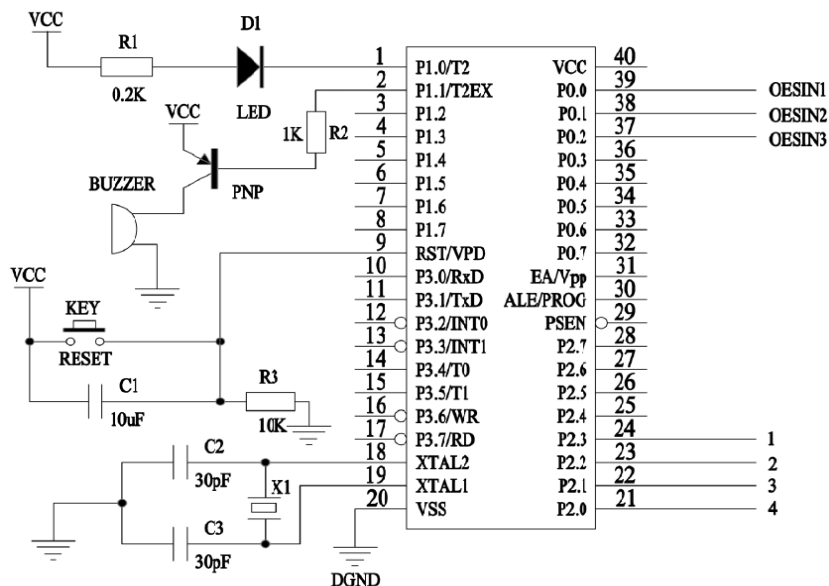


Fig. 5 - Circuit diagram of the control system

The software of automatic reseeding device

The main program flow chart of the detection and control system is shown in Fig. 6. The program executes the initial value setting of the global variable and the start of the photoelectric sensor, and presses the reset key to realize the reset of the system. First, the program is to monitor whether the components are in normal state, initializes the parameter, then receives the detection signal of the photoelectric sensor and

determines whether the seed metering device missed seeding, then it controls the corresponding action of the stepper motor. The action of the stepper motor is controlled by sensors on the main seed metering disc and reseed disc. The detection device provides the reseed signal through level of the sensor. In the process of the detection, when there were seeds on the suction hole of the main metering seed disc with the metering seed disc rotating, the laser receptor didn't receive the light signal, the high level was outputted and the stepper motor did not start. When there were no seeds on the suction hole of the main metering seed disc, the low level was outputted, the stepper motor was rationed the set angle for reseed. At the same time, the next suction hole was detected. If there was no seed on the next suction hole, the stepper motor was controlled to continue turn 18° (the angle between the two holes), and the next suction hole was detected. Until the seed was detected on the suction hole, the stepper motor stopped. The seed flowing situation in the seeding pipe is detected by the output signal in the set time. When the seeds normally fell, the sensor outputted a continuous high level signal. When no seeds fell, the sensor outputted a continuous low level signal. If there were no seeds falling in a set time, the LED was lighted and the buzzer started for real-time alarm.

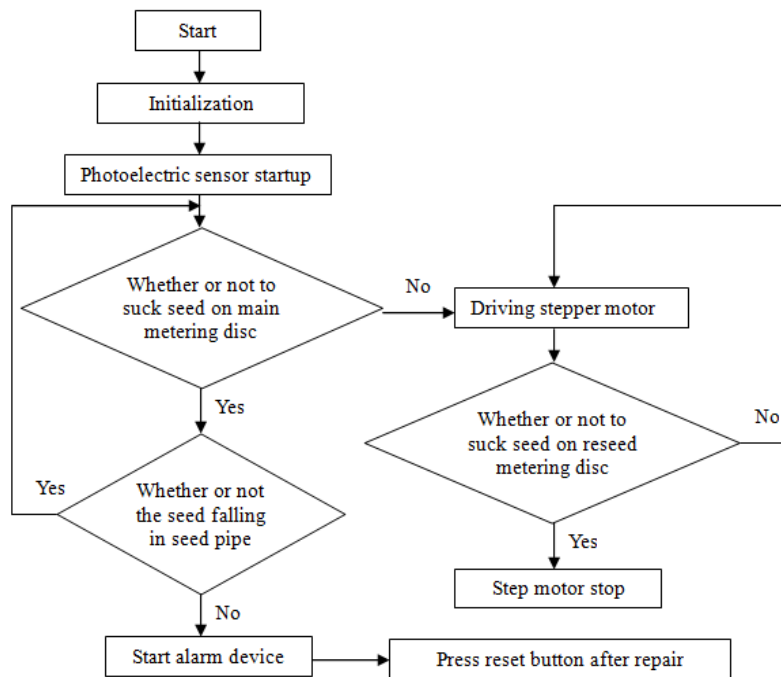


Fig. 6 - The flow chart of main program of the automatic reseed system

MATERIALS AND METHODS

As shown in Fig.7, the designed air-suction precision corn seed metering device was installed on the JPS-12 automatic test bench to test the performance of the seed metering device. In order to simulate the actual seeds falling into the seedbed, the oil was coated on the seeding area of the seedbed to accept and carry the seeds. The Guiyu No. 1 corn seed was selected in the test. The seeds of the reseed were coated with red, which is different from the planting seeds.



Fig. 7 - Test bench of the seed metering device performance

The seeding performance of the seed metering device were tested, mainly including: The orthogonal experiment of the influence effect of working factors, and the comparison experiment of the working effect of the seed metering device without the reseeding device and the seed metering device with the reseeding device. The planted seeds were selected as samples during the seedbed belt and metering device stable working. The test results were processed according to the “GB/T6973-2005 single grain (precision) seed metering device test method” (Wu Nan et al, 2016; Yi Shujuan et al, 2014). For the orthogonal experiment, the seed metering device had uninstalled reseeding device. The seeding spaces of the 150 seeds were measured in the each test, and the test was repeated 3 times to get the average value. The comparison test done at the vacuum degree was 4KPa and the speed of the reseeding disc was 15r/min. The seeding spaces of the 150 seeds were measured in each test. Whether the seeding was qualified, it was judged according to the seed spacing. The theory seed spacing was $X_r = 250\text{mm}$ in the test. When X_i was greater than $1.5 X_r$, it was the miss-seeding; When X_i was greater than or equal to $0.5 X_r$ and less than or equal to $1.5 X_r$, it was the qualified one; When X_i was less than $0.5 X_r$, it was over-seeding.

RESULTS

Orthogonal test of the seeding performance

In the orthogonal test, the influencing factors were the vacuum degree A and the rotation speed B of the seeding disks, and the indexes were the qualification rate Q, the over-seeding rate O and the miss-seeding rate M. The factor and level are as shown in table 1.

Table 1

Factor and level table for orthogonal test		
Factor	Vacuum degree	Rotating speed of the seed metering disc
	A [kPa]	B[r/min]
1	3.5	15
2	4	20
3	4.5	25

When the seed metering device is operated, the influencing effect of each factor to different operation indexes is different. In order to determine the optimal combination of the factors, the comprehensive weighted score method was adopted to evaluate the orthogonal test results. According to the importance degree of each test index in the test, the weight proportion is determined. The evaluation matrix of the test index is as follows:

$$X = \begin{pmatrix} x_{11} & \cdots & x_{1j} \\ \vdots & \ddots & \vdots \\ x_{i1} & \cdots & x_{ij} \end{pmatrix} \quad (1)$$

Where, i —test number, j —the three index in test, the qualified rate, over-seeding rate and miss-seeding rate. In the test, the expected change direction of the qualified rate, over-seeding rate and miss-seeding rate is different. In order to make the direction of each index change consistent, the rule of the chosen the score is that if the value is the smaller the better. The test index is converted by formula (2).

$$y_{ij} = \begin{cases} x_{ij}, & j \in U_1 \\ x_{j_{\max}} - x_{ij}, & j \in U_2 \end{cases} \quad (2)$$

where, U_1 -miss-seeding rate and over-seeding rate, U_2 -qualified rate.

According to the formula (2), the magnitude of the index is unified and the dimension is eliminated. The standardized evaluation matrix for the test index is $Z=(y_{ij})$.

$$Z_{ij} = 100 \times \frac{(y_{ij} - y_{j_{\min}})}{(y_{j_{\max}} - y_{j_{\min}})} \quad (3)$$

where

$$y_{j\min} = \min \{y_{ij} | i = 1, 2, \dots, n\}, y_{j\max} = \max \{y_{ij} | j = 1, 2, \dots, m\}$$

Referring to the relevant agricultural technology requirements and experience (HU Zhichao et al, 2013; Wang Xiaoyan et al, 2013), and considering the importance degree of each index, the weights of each index are: the weights of qualified rate is $w_1=0.6$, the weights of over-seeding rate is $w_2=0.1$, the weights of miss-seeding rate is $w_3=0.3$. The weights are substituted into the formula (3), and the score of each index is as follows:

$$f_i = \sum_{j=1}^m w_j z_{ij} \quad i=1, 2, \dots, n \quad (4)$$

Where, w_j - the weight of each index.

The result of the test, comprehensive weighted score value and the result of the range analysis, is shown in Table 2.

Table 2

Test and analysis results							
No.	Factor			Index value			Comprehensive weighting score value f_i
	A	B	AxB	Qualified rate [%]	Over-seeding rate [%]	Miss-seeding rate [%]	
1	1	1	1	83.11	3.38	13.51	64.4
2	1	2	2	76.58	4.43	18.99	98.0
3	1	3	3	84.71	1.91	13.38	55.3
4	2	1	2	94.96	2.16	2.88	3.9
5	2	2	3	92.11	3.29	4.61	19.1
6	2	3	1	85.19	1.23	13.58	52.4
7	3	1	3	92.81	5.23	1.96	17.0
8	3	2	1	87.12	1.84	11.04	43.1
9	3	3	2	91.52	1.82	6.67	21.0
K1	72.6	28.4	53.3	Sequence of factors: A>B>AxB Optimal combination: A ₂ B ₁			
K2	25.1	53.4	41.0				
K3	27.0	42.9	30.5				
R	47.5	25.0	22.8				

In table 2, it can be obtained: the influence order of the factors is A > B > AxB. When Comprehensive weighting score value was the smallest, the factors combination was the optimal combination. The optimal combination was A₂B₁, it was that the vacuum degree of the gas chamber was 4kPa and the rotating speed of metering seed disc was 15r/min. Under the optimal combination condition, the qualified rate of the seed metering device was 94.96%, the over-seeding rate was 2.16%, and the missing seed rate was 2.88%, and all indexes can meet the technical requirements of seeding performance.

Comparison test of the automatic reseeding performance of the seed metering device

When the vacuum degree of the gas chamber was 4kPa and the rotating speed of metering seed disc was 15r/min, the comparative test of the seeding effect was done on the seed metering device of not install the reseeding device to the seed metering device of the install the reseeding device. The results of the test had shown in Table 3, and the comparison results of the indexes had shown in Figure 8.

Table 3

Comparative test results of air suction seed metering device

No.	Qualification rate [%]		Over-seeding rate [%]		Miss-seeding rate [%]		Comprehensive weighted score value	
	No reseeded	reseeded	No reseeded	reseeded	No reseeded	reseeded	No reseeded	reseeded
1	92.26	93.24	2.58	4.73	5.16	2.03	35.93	45.25
2	93.88	96.60	2.04	2.72	4.08	0.68	12.45	3.50
3	91.84	96.00	2.72	1.33	5.44	2.67	42.02	16.72
4	90.54	95.92	2.03	3.40	7.43	0.68	63.59	11.05
5	91.95	93.66	2.68	3.52	5.37	2.82	40.43	43.19
6	88.82	90.58	1.97	5.23	9.21	3.92	90.06	80.33
7	91.45	89.61	0.66	4.55	7.89	5.84	52.98	98.11
8	92.11	95.07	5.26	4.23	2.63	0.70	31.73	20.55
9	91.67	93.79	1.92	4.14	6.41	2.07	46.56	39.28
10	88.67	91.56	3.33	4.55	8.00	3.90	89.05	70.09
11	89.33	92.72	8.00	5.30	2.67	1.99	67.63	50.92
12	93.55	95.42	5.16	3.27	1.29	1.31	9.93	18.68
average value	91.34	93.68	3.20	3.91	5.47	2.38	48.53	41.47

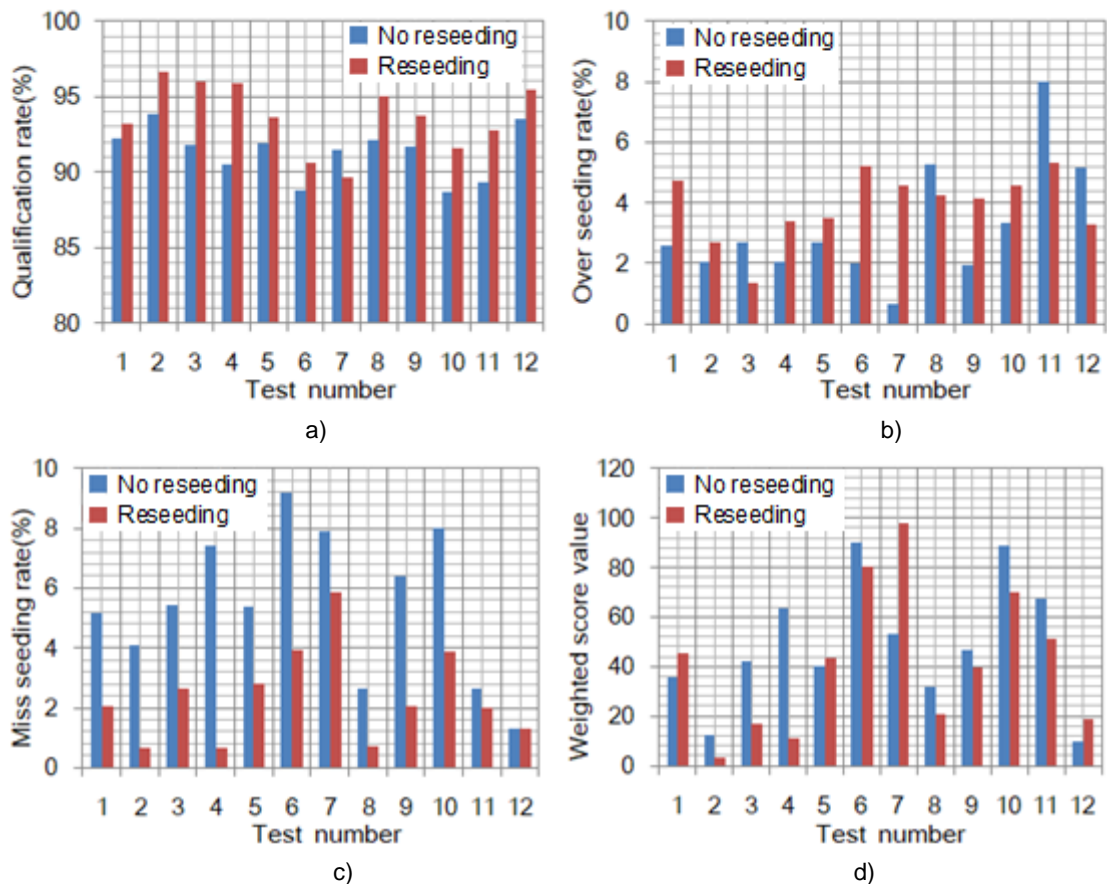


Fig. 8 - Distribution contrast diagram of test results

Table 3 shows that: when the vacuum degree was 4kPa and the rotating speed was 15r/min, when the seed metering device had a reseeding device installed, it was that the highest qualified rate was 96.60%, the maximum over-seeding rate was 5.84%, the minimum comprehensive weighted value was 3.50, the average qualified rate was 93.68%, the average over-seeding rate was 3.91%, the average miss-seeding rate was 2.38%, the comprehensive weighted average value was 41.47; when the seed metering device had no reseeding device installed, the highest qualified rate was 93.88%, the maximum over-seeding rate was 9.21%, the minimum comprehensive weighted score value was 12.45, the average qualified rate was 91.34%, the average over-seeding rate was 3.20%, the average miss-seeding rate was 5.47%, the comprehensive weighted average value was 48.53. When the seed metering device had a reseeding device installed, the qualified rate was increased by 34% and the miss-seeding rate was decreased by 3.09%. As shown in Figure 8, the effect of automatic reseeding device was very significant to improve the seeding performance of the seed metering device. When the automatic replanting device had been installed, the qualified rate was greatly increased, the miss-seeding rate was reduced, and the comprehensive weighted average value was reduced. The influence of the over-seeding rate was not obvious and the analysis shows that the environment conditions of the work were very complicated and the detection system sometimes had some misjudgements, which led to the increase of the over-seeding rate.

CONCLUSIONS

The air-suction corn precision seed metering device with automatic reseeding device was designed. The scheme of automatic reseeding detection and control system was designed. The STC89C52 MCU was chosen as the core of signal processing and control system of the reseeding device. The photoelectric sensors were adopted as reseeding detection element. The design and selection of hardware parts of the detection and control system were finished, and the software program of the system were written.

(1) The orthogonal test of the seed metering device working performance was carried out. The comprehensive weighted score method was adopted to comprehensively evaluate the test indexes, and the comprehensive weighted score value was used to evaluate the seeding effect of the seed metering device. The analysis of the test results showed that: when the vacuum degree was 4kPa and the rotation speed was 15r/min, the seeding performance was the best and the qualified rate was 94.96%, the over-seeding rate was 2.16%, the miss-seeding rate was 2.88%.

(2) When the vacuum degree was 4kPa and the rotation speed was 15r/min, the comparison test was done about the seeding effect of the seed metering device without the reseeding device and the seed metering device with the automatic reseeding device. The result showed that: when the seed metering device had a reseeding device installed, the qualified rate was increased by 2.34% and the miss-seeding rate was decreased by 3.09%, the comprehensive seeding performance was greatly improved. The automatic reseeding device had obvious effect on improving the seeding quality of the air suction corn precision seed metering device.

ACKNOWLEDGEMENTS

The study was supported by the National corn industry system project (CARS-02-29), and the Planning project of Chuzhou University (KJZ06).

REFERENCES

- [1] Cao Dong, (2013), Study on Loss Sowing Monitoring and Early Warning System of Potato Precision Seed metering device [D], *Yangling: North West Agriculture and Forestry University*, Yangling/China;
- [2] Ding Youchun, Wang Xueling, Liao Qingxi, (2014), Method of real-time loss sowing detection for rapeseed precision seed metering device based on time changed window, *Transactions of the Chinese Society of Agricultural engineering (Transactions of the CSAE)*, Vol.30, Issue 24, pp.11-21, Beijing/ China;
- [3] Hu Zhichao, Lü Xiaolian, Peng Baoliang, et al, (2018), Optimization of the Working Performance of Half-Feeding Peanut Picking Device Based on Response Surface Methodology, *INMATEH – Agricultural Engineering*, Vol.54, Issue 1, pp.121-128, Bucharest/ Romania;
- [4] Jae Wan Lee, Young Joo Kim, Seong Il Kang, Joon Yong Kim, Dong Pyo Hong, (2013), The Analysis of the Dynamic Characteristics on Seed Plate of The Vacuum Planters for Precision Sowing, *Applied Mechanics and Materials*, Vol.284-287, pp.968-972, Zurich/Switzerland;

- [5] Li Leixia, Hao Zhiming, Yang Wei et al, (2012), Design of seeding performance detection system for precision seed metering device, *Agricultural Engineering*, Vol. 2, Issue 8, pp.16-19, Beijing/ China;
- [6] Li Ming, Ding Youchun, Liao Qingxi, (2010), Loss sowing detection in field of pneumatic precision seed metering device for rapeseed, *Transactions of the Chinese Society of Agricultural Engineering (Transactions of the CSAE)*, Vol.26, Issue Supp.1, pp.27-31, Beijing/ China;
- [7] Lv X.L, Liu M J, Wang H.O., Hu Z.C, (2012), Research development of peanut seeding technology and equipment on the film, *Chinese Agricultural Mechanization*, Issue1, pp.89-92, Nanjing/ China;
- [8] Shi Song, Zhang Dongxing, Yang Li, Cui Tao, Zhang Rui, Xiaowei, (2014), Design and experiment of pneumatic corn precision seed-metering device with combined holes, *Transactions of the Chinese Society of Agricultural Engineering (Transactions of the CSAE)*, Vol.30, Issue 5, pp.10-18, Beijing/ China;
- [9] Singh T.P., Mane D.M., (2011), Development and laboratory performance of an electronically controlled metering mechanism for okra seed, *AMA-Agricultural Mechanization in Asia Africa & Latin America*, Vol.42, Issue 2, pp.63-69, Tokyo/Japan
- [10] Sun Wei, Wang Guanping, Wu Jianmin, (2016), Design and experiment on loss sowing testing and compensation system of spoon-chain potato seed metering device, *Transactions of the Chinese Society of Agricultural Engineering (Transactions of the CSAE)*, Vol.32, Issue 11, pp.8-15, Beijing/ China;
- [11] Tian Liquan, Wang Jinwu, Tang Han et al, (2016), Design and performance experiment of helix grooved rice seeding device, *Transactions of the Chinese Society for Agricultural Machinery*, Vol.47, Issue 5, pp.46-52, Beijing/ China;
- [12] Wang Lifan, (2015), Single-chip Microcomputer Control Applied on the Corn Seed metering device [D]. *Hebei: Hebei University of Science and Technology*, Hebei/ China;
- [13] Wang Xiaoyan, Liang Jie, Shang Shuqi et al, (2008), Design and experiment of half feeding type peanut picker, *Transactions of the CSAE*, Vol.24, Issue 9, pp.94-98, Beijing/ China;
- [14] Wu Nan, Lin Jing, LI Baofa et al, (2016), Design and test on performance monitoring system of no-tillage planter seed-metering device [J/OL], *Transactions of the Chinese Society for Agricultural Machinery*, Vol.47, Issue Supp., pp.69-75, Beijing/ China
- [15] Yi Shujuan, Liu Yongfen, Wang Chun et al, (2014), Experimental study on the performance of bowl-tray rice precision seed metering device, *International Journal of Agricultural and Biological Engineering*, Vol.7, Issue 1, pp.17-25, Beijing/ China;
- [16] Zhang Xiaodong, Wu Jianmin, Sun Wei, et al, (2013), Design of automatic compensation system for potato planter, *Journal of Gansu agricultural university*, Vol.48, Issue 1, pp.145-149, Lanzhou/ China;
- [17] Zhou Liming, Wang Shumao, Zhang Xiaochao et al, (2012), Seed monitoring system for corn planter based on capacitance signal, *Transactions of the Chinese Society of Agricultural Engineering*, Vol.28, Issue 13, pp.16-21, Beijing/ China;
- [18] Zhu Ruixiang, Ge Shiqiang, Zhai Changyuan et al, (2014), Design and experiment of automatic reseeded device for miss-seeding of crops with large grain, *Transactions of the Chinese Society of Agricultural Engineering*, Vol.30, Issue 21, pp.1-8, Beijing/ China

DESIGN AND EXPERIMENTAL STUDY OF THE FINGER-TYPE LIFTER TEST BENCH FOR *Cerasus humilis* BRANCHES

拨指式钙果扶禾试验台的设计与试验

As. M.S. Stud. Eng. Yongqiang He, Prof. Ph.D. Eng. Junlin He^{*}), Ph.D. Stud. Eng. Xiaobin Du, M.S. Stud. Eng. Dawei Fang

College of Engineering, Shanxi Agriculture University, Taigu/China;
Tel: +86-0354-6288400; E-mail: hejunlin26@126.com

Keywords: agricultural machinery, lifter, experiment, design, *Cerasus humilis*

ABSTRACT

We developed finger-type lifter test bench to address low fruit removal rate and high breakage rate during the lodging of *Cerasus humilis* branches. The bench is mainly composed of a frame, branches lifter, gripping delivery device, fruit removal device and control system. A single factor experiment was carried out, and fruit removal rate and breakage rate were used as the evaluation indexes. The elevation angle, declination angle, poking finger speed and conveying speed were selected as the experimental factors. Results showed that the influence of the declination angle was small. To determine the optimum parameter combination, we performed the three factors and three levels central composite orthogonal experiment, using the fruit removal rate and breakage rate as the evaluation indexes, while elevation angle, speed of poking fingers and conveying speed as the experimental factors. The results showed that elevation rate had the largest effect on removal rate, followed by poking fingers speed and conveying speed. Meanwhile, conveying speed had the largest effect on breakage rate, followed by poking fingers speed and elevation angle. The optimal parameter combination includes elevation angle of 56°, poking fingers speed of 1.02 m/s and conveying speed of 0.27 m/s and corresponding fruit removal rate of 96.07% and breakage rate of 4.58%. The bench verification experiment was performed according to the combination of the parameters, and the results showed that the removal rate was 97.28% and the breakage rate was 5.01%. The relative errors of the experimental value and the theoretical optimisation value were 1.24% and 8.58%, respectively.

摘要

针对钙果枝条倒伏造成收获时脱果率低、破损率高等问题, 本文设计了拨指式钙果扶禾试验台, 主要由机架、扶禾装置、夹持输送装置、脱果装置、控制系统组成。以脱果率和破损率为评价指标, 选择仰角、偏角、拨指线速度、输送速度为试验因素分别进行单因素试验, 试验表明偏角影响不显著。为确定最优扶禾参数组合, 以脱果率和破损率为评价指标, 以仰角、拨指线速度、输送速度为试验因, 进行三因素三水平中心组合正交试验, 试验表明: 影响脱果率的主次顺序为仰角>拨指线速度>输送速度; 影响破损率的主次顺序为输送速度>拨指线速度>仰角; 最优参数组合为: 仰角 56°、拨指线速度 1.02 m/s、输送速度 0.27 m/s, 对应的脱果率为 96.07%、破损率为 4.58%。根据该参数组合进行台架验证试验, 得到脱果率为 97.28%、破损率为 5.01%, 与理论优化值的相对误差分别为 1.24%、8.58%。

INTRODUCTION

Cerasus humilis is a new and unique fruit plant resource in China (Sun et al., 2016; Liang et al., 2006), and its yield reaches 15,000 kg/hm² (Liu, 2003). The fruit is rich in minerals, vitamins and amino acids, has high edible and medicinal value and a broad development prospect (Li, 2015; Liang et al., 2008). However, a single fruiting branch has high mass, so lodging remains a serious problem in the mature period (Zhang et al., 2018). Thus, mechanical harvesting is very difficult, and thus the fruits are mainly picked by hand. Consequently, harvesting incurs substantial economic loss (Liu et al., 2013; Kang et al., 2017) because it has low efficiency despite the high labour intensity and the best picking time is delayed. The lodging of branches restricts the development of the *Cerasus humilis* industry, so lifting becomes a problem that needs to be solved in the process of harvesting *C. humilis*.

Crop lifting has been extensively investigated. The tilted maize stalks can be quickly straightened and fed into a picking area orderly by a new type of maize harvester with reel star wheel, which improves picking performance (Hao et al., 2014). The parameters of a soybean lifter can be optimised by a virtual prototype, and lifter angle and conveying speed greatly influence the performance of a soybean lifter (Chen et al., 2012).

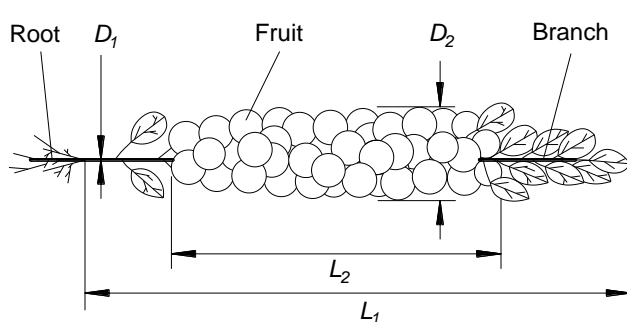
To solve the problem of rice lodging, an electric drive system was developed. Rice harvesting efficiency can be improved by automatically adjusting the speed of poking fingers in the range of 0.7–1.0 m/s with a PWM governor (Pan *et al.*, 2016). The lifting device of a safflower harvester retains its relative position with the safflower plants, thereby improving harvesting efficiency (Gu *et al.*, 2018). A study found that using a guide rod ensures that a corn stalk has a good upright posture when it enters a picking mechanism, so this device ensures orderly feeding and reduces the loss of cutting (He *et al.*, 2007). Another study found that the forward speed of the lifting device, poking fingers speed, elevation angle, declination of a lifter considerably affect the angle of lodging of sugarcane (Mou *et al.*, 2009). However, no research has been reported on lifting of *C. humilis*.

In this paper, we designed a finger-type lifter test bench to address the problem in lodging mature *C. humilis* branches. The design considers the growth characteristics of the branches. Fruit removal rate and breakage rate were used as evaluation indexes, while elevation angle, declination angle, poking fingers speed and conveying speed were used as experimental factors. Our aim is to obtain an optimal structure and working parameter combination for the design of *C. humilis* picking machine.

MATERIALS AND METHODS

Cerasus humilis variety and sample preparation

C. humilis branches were obtained from Juxin Modern Agriculture Base in Taigu County, Shanxi Province, China (E 112°29', N 37°23'), and the variety was 'Nongda 6'. The harvest date was August 15, 2018. The diameter D_1 of the branches was 4–6 mm, the length L_1 was 600–800 mm, the diameter D_2 of the fruiting zone was 50–60 mm and the length L_2 of the fruiting zone was 400–500 mm (Fig.1a). The mass of a single-branched fruit branch was 0.8–1.2 kg, which easily caused lodging (Fig.1b).



a. The physical parameters of the *Cerasus humilis* branch



The *Cerasus humilis* branch

b. The lodging phenomenon of *Cerasus humilis* branch

Fig. 1 - The characteristics of *Cerasus humilis* branches

Design of lifter test bench

As shown in Fig. 2, the bench was mainly composed of a frame, branches lifter, gripping delivery device, fruit removal device and control system. The branches lifter was used to guide the fruiting branches towards the fruit removal device and straighten them. The dividing plate gathered the fruiting branches towards the branches lifter. The gripping delivery device mainly transports the initially lodging fruiting branches to the branches lifter and fruit removal device. During transportation, the branches lifter first straightened the branches, and then the fruit removal device detached the fruit. The elevation angle α of the branches lifter was adjustable from 20° to 90°, the declination angle β was -15° to +15°, the speed v_t of poking fingers was 0–4.7 m/s and the conveying speed v_m was 0–1.0 m/s.

Before the experiments, the branch root was fixed to the gripping delivery device. At this time, the branch was in a lodging state because of gravity. Then we adjusted the elevation angle α and the declination angle β of the branches lifter to change the direction angle of the poking fingers movement. During the experiments, the gripping delivery device conveyed the branch to the branches lifter in a linear motion at a speed v_m . The poking fingers turned the branches up continuously at the speed of v_t and lifted the branch up to provide good posture conditions for the follow-up fruit removal device.

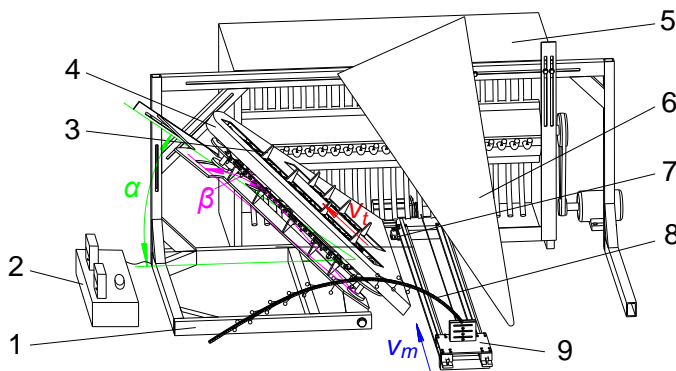


Fig. 2 - The branches lifter test bench of *Cerasus humilis*

1 – Rack; 2 – Control system; 3 – Poking finger; 4 – Stalk lifter; 5 – Fruit removal device; 6 – Dividing plate; 7 – Limit switch; 8 – *Cerasus humilis* branch; 9 – Gripping delivery device

Experiment design

Design of single factor experiment

To clarify the effects of elevation angle α , declination angle β , poking fingers speed v_t and conveying speed v_m on the fruit removal rate and breakage rate, we design the single factor experiment. The experimental factors and levels are shown in Table 1.

Table 1

Scheme of single factor experiment

Item	1	2	3	4	5	6	7	8	9	10	11	12	13	14	15	16	17	18	19	20
α [°]	30	40	50	60	70	50					50					50				
β [°]	0					-	-	0	+7.5	+15	0					0				
v_t [m/s]	1.2					1.2					0.8	1.0	1.2	1.4	1.6	1.2				
v_m [m/s]	0.4					0.4					0.4					0.2	0.3	0.4	0.5	0.6

Design of orthogonal experiment

The results of the single factor experiment showed that the declination angle in the experiment range had no significant influence on the fruit removal and breakage rates, whereas elevation angle, poking fingers speed and conveying speed had considerable influences.

To study the influences of interactive factors on the performance of lifting, the three factors at three levels central composite orthogonal experiment was carried out. Fruit removal rate and breakage rate was used as the evaluation indexes and the elevation angle, the poking fingers speed and the conveying speed as the experimental factors. The experimental factors and levels are shown in Table 2.

Table 2

Coding schedule of experimental factors

Coded value	Elevation angle, α	Poking fingers speed, v_t	Conveying speed, v_m
	[°]	[m/s]	[m/s]
	A	B	C
Lower level (-1)	30	0.8	0.2
Middle level (0)	50	1.2	0.4
Upper level (1)	70	1.6	0.6

Note: factors encoding: A= α , B= v_t , C= v_m .

To reduce the number of experiments and obtain the regression equation, the mathematical method of the experiment planning based on Box-Behnken Centre combination method (Golub *et al.*, 2018) was used.

Performance evaluation of lifting

The key factors affecting lifting performance were selected for the test. The factors included elevation angle, declination angle, poking fingers speed and conveying speed. Lifting performance was evaluated by using the important indicators of fruit removal rate and breakage rate during the harvesting process. The calculation method of fruit removal rate and breakage rate is shown in Formulas (1) and (2). To reduce the experiment error, each group of the tests was conducted three times, and the results were averaged.

$$\mu = \frac{N_1}{N} \quad (1)$$

$$\eta = \frac{N_2}{N_1} \tag{2}$$

Where: μ is the fruit removal rate, [%];
 η is the breakage rate, [%];
 N_1 is the number of *Cerasus humilis* fruit removed;
 N_2 is the number of fruit damaged in the removed *Cerasus humilis* fruit;
 N is the total number of *Cerasus humilis* fruit on the branch before the experiment.

RESULTS

Results and analysis of single factor experiment

Data analysis was conducted using SAS 9.1. The results of the single factor experiment are shown in Fig.3. Fig.3a shows the polynomial relationship between elevation angle and fruit removal rate and breakage rate, with r^2 values greater than 0.93 and 0.88, respectively. With the increase of the elevation angle, the fruit removal rate increased from 91.3% to 97.7%, then decreased to 90.9%, and the breakage rate decreased from 9.7% to 2.5%.

Fig.3b shows the polynomial relationship between declination angle and fruit removal rate and breakage rate, with r^2 values greater than 0.64 and 0.80, respectively. With the increase of deviation angle, the variation trend of fruit removal rate and breakage rate was not obvious, and the difference between the maximum and minimum values of fruit removal rate and breakage rate were only 1.2% and 0.84% respectively.

Fig.3c shows the polynomial relationship between the poking fingers speed and the fruit removal rate and breakage rate, with r^2 values greater than 0.96 and 0.90, respectively. With the increase of the poking fingers speed, the fruit removal initially increased from 92.8% to 95%, then decreased to 91.8%, and the breakage rate gradually increased from 2.64% to 8.79%.

Fig.3d shows the polynomial relationship between the conveying speed and the fruit removal rate and breakage rate, with r^2 values greater than 0.83 and 0.97, respectively. With the increase of conveying speed, the fruit removal rate decreased gradually from 98.2% to 93.0%, whereas the breakage decreased initially from 8.12% to 2.82%, then increased to 10.5%.

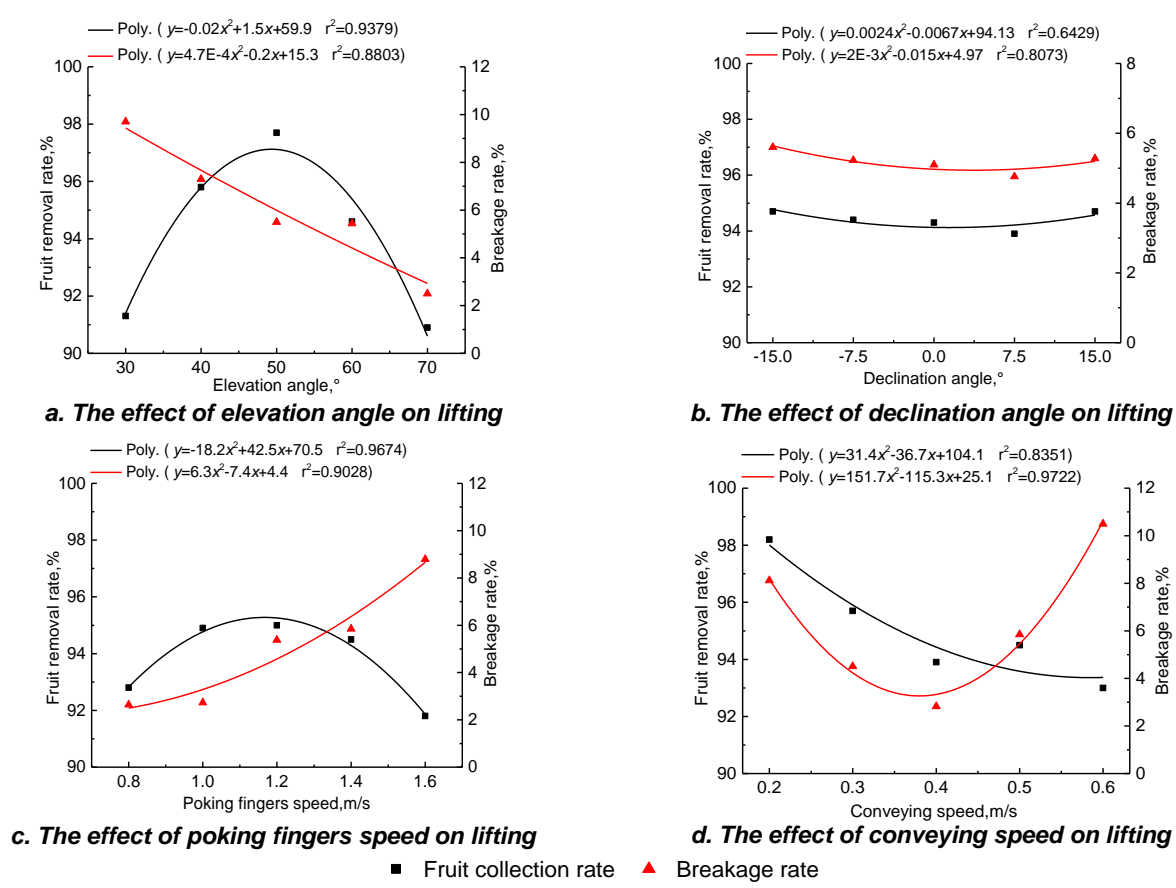


Fig. 3 - Results of single factor experiment

Results and analysis of orthogonal experiment

The Box-Behnken Centre combination plan was used for the three-factor and three-level experimental design. The plan included 17 test points, of which the points 1–12 were factorial design points and the points 13–17 were central design points for the estimation of experimental error. The results are shown in Table 3.

Table 3

The orthogonal test results

No.	Elevation angle A	Poking fingers speed B	Conveying speed C	Fruit removal rate Y ₁	Breakage rate Y ₂
	[°]	[m/s]	[m/s]	[%]	[%]
1	-1	-1	0	88.4	6.08
2	1	-1	0	90.1	3.66
3	-1	1	0	89.2	6.24
4	1	1	0	90.3	5.85
5	-1	0	-1	92.4	6.45
6	1	0	-1	94.2	5.27
7	-1	0	1	91.5	8.35
8	1	0	1	90.7	6.15
9	0	-1	-1	96.8	5.44
10	0	1	-1	96.7	7.52
11	0	-1	1	94.7	6.35
12	0	1	1	93.7	8.10
13	0	0	0	95.1	4.31
14	0	0	0	94.7	4.59
15	0	0	0	96.2	4.65
16	0	0	0	94.4	4.39
17	0	0	0	93.5	5.24

Analysis of variance and regression model

Variance analysis was performed on the experiment results (Table 4). The regression equations are shown in Equations (3) and (4). The quadratic regression models of fruit removal rate Y_1 and breakage rate Y_2 were extremely significant, and the r^2 values of the regression equation were 0.956 and 0.963, respectively. These results indicated that the predicted value of the regression model was well fitted to the actual value and thus can be used in the prediction and analysis of the influences of elevation angle, poking fingers speed and conveying speed on the fruit removal rate and breakage rate in the lifting process.

Table 4

The results of variance analysis

Item	Degree of freedom	Mean square	F Value	P Value	Item	Degree of freedom	Mean square	F Value	P Value
Model 1	9	11.87	16.87	0.0006**	Model 2	9	3.01	19.96	0.0003**
A	1	59.87	85.09	<0.0001**	A	1	1.03	6.82	0.0348*
B	1	4.15	5.90	0.0456*	B	1	1.21	8.02	0.0253*
C	1	4.17	5.92	0.0452*	C	1	3.51	23.24	0.0019**
AB	1	0.09	0.13	0.7312	AB	1	1.03	6.83	0.0348*
AC	1	1.69	2.40	0.1651	AC	1	0.26	1.72	0.2306
BC	1	0.20	0.29	0.6083	BC	1	0.027	0.18	0.6838
A ²	1	77.04	109.49	<0.0001**	A ²	1	0.29	1.92	0.2089
B ²	1	4.23	6.01	0.0440*	B ²	1	1.32	8.73	0.0212*
C ²	1	12.13	17.24	0.0043**	C ²	1	11.56	76.61	<0.0001**

Note: $P < 0.01$ (extremely significant, **), $P < 0.05$ (very significant, *); Model 1 is variance analysis of fruit removal rate; Model 2 is variance analysis of breakage rate.

$$Y_1 = 61.31 + 1.18 \cdot A + 17.07 \cdot B - 28.39 \cdot C - 0.16 \cdot AC - 2.81 \cdot BC - 0.01 \cdot A^2 - 6.27 \cdot B^2 + 42.44 \cdot C^2 \quad (3)$$

$$Y_2 = 18.52 - 0.15 \cdot A - 9.22 \cdot B - 26.05 \cdot C + 0.06 \cdot AB - 0.06 \cdot AC - 1.03 \cdot BC + 3.50 \cdot B^2 + 41.43 \cdot C^2 \quad (4)$$

Where:

- A is elevation angle, [°]; B is poking fingers speed, [m/s]; C is conveying speed, [m/s];
- Y_1 is the fruit removal rate, [%]; Y_2 is the breaking rate, [%].

Analysis of the influence of interaction factors on lifting performance

The 3D response surface was generated according to the Box-Behnken Centre combination method, and the comprehensive influence of the three factors: elevation angle A , poking fingers speed B and conveying speed C on the evaluation indexes was analysed according to the response surface.

1) Analysis of the test factors on the fruit removal rate

The response surface of elevation angle A , poking fingers speed B and conveying speed C to the fruit removal rate Y_1 is shown in Fig.4a–4c. When the conveying speed was 0.4 m/s, the fruit removal rate increased initially before decreasing with the increase of the elevation angle and poking fingers speed. However, the variation range of the response surface along the elevation angle was large, indicating that the elevation angle had more influence than poking fingers speed (Fig.4a). When the poking fingers speed was 1.2 m/s and the conveying speed was low, the influence of elevation angle on the fruit removal rate increased. With the increase of elevation angle, the fruit removal rate obviously increased first before decreasing. However, with the increase of the conveying speed, the fruit removal rate decreased significantly, indicating that the elevation angle had larger effect on the fruit removal rate than the conveying speed (Fig.4b). When the elevation angle was 50°, the interaction between poking fingers speed and conveying speed had no considerable effect on the fruit removal rate (Fig.4c).

As indicated by the change range of the response value of the experimental factors to the fruit removal rate, the order of influence of the experimental factors on the fruit removal rate was elevation angle $A >$ poking fingers speed $B >$ conveying speed C . The overall influence trend was that the poking fingers speed B is moderate when the elevation angle A is moderate and that the fruit removal rate increases when conveying speed C is low. The main reasons were as follows: when the elevation angle was moderate, the branches were lifted to an appropriate elevation angle. This process is conducive to the carding operation by the fruit removal device. When poking fingers speed was moderate, the branches were in the appropriate angle range under the action of the fingers. When conveying speed was low, the effect frequency of fruit removal device on branches increased, thus improving the fruit removal rate.

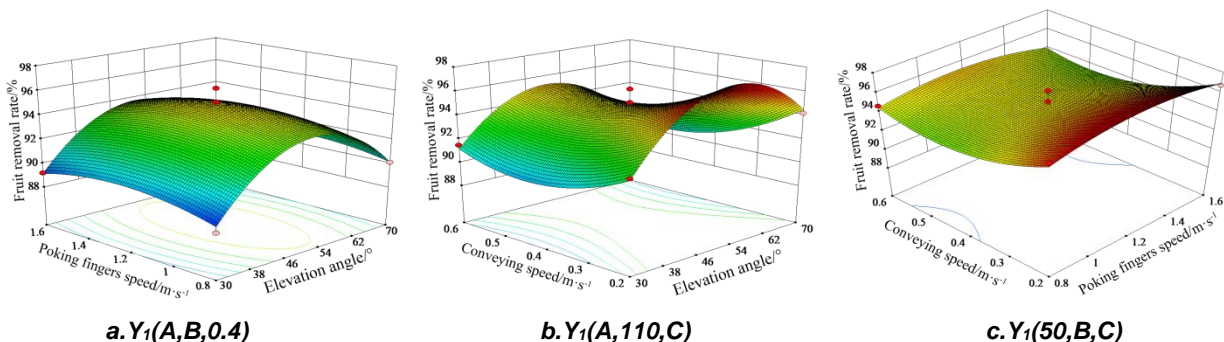


Fig. 4 - Response surface of various factors on fruit removal rate

2) Analysis of the test factors on the breakage rate

The response surface of elevation angle A , poking fingers speed B and conveying speed C to the breakage rate Y_2 is shown in Fig.5a–5c. When the conveying speed was 0.4 m/s, the breakage rate increased considerably with the increase of elevation angle and poking fingers speed (Fig.5a). When the poking fingers speed was 1.2 m/s, the breakage rate decreased significantly with the increase of elevation angle (Fig.5b). When the elevation angle was 50°, the breakage rate decreased first and then increased with the increase of conveying speed, and the breakage rate increased with the increase of the poking fingers speed (Fig.5c).

The change range of response value of the experimental factors to the breakage rate indicated that the significant order of influence of the experimental factors on the breakage rate was conveying speed $C >$ poking fingers speed $B >$ elevation angle A . The overall influence trend was that the poking fingers speed B is moderate when elevation angle A is large and that breakage rate decreases when conveying speed C is low. The main reasons were as follows: the elevation angle was extremely large, and the branches were relatively erect when they entered the fruit removal device. This condition prevented damage to the *C. humilis* fruit. When the poking fingers speed was extremely low, the impact force of the finger on the fruit was small, and the *C. humilis* fruit was not easily damaged. At an extremely low conveying speed, the number of

collisions of the fruit removal device on the *Cerasus humilis* fruit increased. At an extremely fast conveying speed, the collision speed of the *C. humilis* fruit and the fruit removal device increased the damage rate.

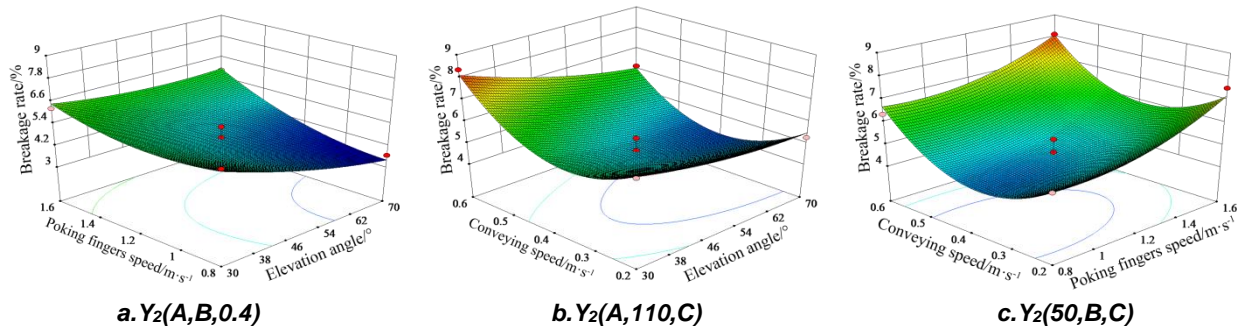


Fig. 5 - Response surface of various factors on breakage rate

Parameter optimization and validation

The best lifting performance yields high fruit removal rate and low breakage rate. By analysing the effects of interaction factors on fruit removal rate and breakage rate, we found that moderate elevation angle and poking fingers speed and low conveying speed are required for increasing the fruit removal rate. Moreover, breakage rate can be decreased by increasing the elevation angle, decreasing the poking fingers speed and using a moderate conveying speed. Given that the impact of each evaluation index on each factor varies, multi-objective optimisation is needed. In the range of the test factors, where the elevation angle A was 30–70°, poking fingers speed B was 0.8–1.6 m/s and conveying speed C was 0.2–0.6 m/s, the fruit removal rate was set to its maximum value, whereas the breakage rate was set to its smallest value. The weight coefficient was 0.5, looking for the optimal combination of parameters under the condition of the above two objective functions. Combined with the actual test conditions, the optimal results of this paper were as follows: elevation angle of 56°, poking fingers speed of 1.02 m/s, conveying speed of 0.26 m/s. The comprehensive response value of the model surface was optimal, and the fruit removal rate and breakage rate were 96.07% and 4.58%, respectively.

To verify the accuracy of the prediction model, we tested the optimised parameter combination three times, and the results were averaged. The elevation angle was set to 56°; the poking fingers speed, to 1.02 m/s and conveying speed, to 0.27 m/s. The test was carried out under this scheme and the fruit removal rate and breakage rate were 97.28% and 5.01%, respectively. The relative errors with the predicted values were 1.24% and 8.58%. The test results are consistent with the predicted values and the test error is small, so the parameter prediction model is reliable.

CONCLUSIONS

1) The finger-type lifter test bench designed in this paper is mainly composed of frame, branches lifter, gripping delivery device, fruit removal device and control system, which can adjust several key parameters, such as elevation angle, declination, poking fingers speed and conveying speed. By combining these parameters, the effect of lifting effect on the rate of fruit removal and the rate of breakage was studied.

2) The single factor experiment results found that declination had no significant effect on the effect of lifting. A quadratic multiple response model was established. The research analysed the influence of elevation angle, finger speed and conveying speed on the rate of fruit removal and breakage rate. The results showed that elevation angle had the largest effect on the removal rate, followed by poking fingers speed and conveying speed. Meanwhile, conveying speed had the largest effect on breakage rate, followed by poking fingers speed and elevation angle.

3) The Box-Behnken Centre combination test method was used for the optimisation of the analysis, the optimal parameters of the operation of lifting were as follows: elevation angle, 56°; poking fingers speed, 1.02 m/s and conveying speed, 0.27 m/s. The analysis predicted that the fruit removal rate reached 96.07%, and the breakage rate reached 4.58%. The bench verification test had an elevation angle of 56°, poking fingers speed of 1.02 m/s and conveying speed of 0.27 m/s. The fruit removal rate and breakage rate were 97.28% and 5.01%, respectively, and the corresponding relative errors with the predicted values were 1.24% and 8.58%.

ACKNOWLEDGEMENTS

This research titled ‘Design and experimental study of the finger-type lifter test bench for *Cerasus humilis* branches’ was funded by the Key Research and Development Plan of Shanxi Province, China (201703D221029-1). The authors are grateful and honoured to have obtained support from the Laboratory of Key Technology and Equipment for Dry Farming Machinery.

REFERENCES

- [1] Chen H.T., (2012), Optimization of parameters for soybean lifter based on dynamic simulation of virtual prototype. *Transactions of the Chinese Society of Agricultural Engineering*, Vol.28, Issue 18, pp.23-29, Beijing/P.R.C;
- [2] Gu L.L., (2018), Design and parameter analysis of the precision spoon-wheel seed meter for corn. *Journal of Agricultural Mechanization Research*, Vol.40, Issue 3, pp.17-21, Harbin/P.R.C;
- [3] Golub G.A., (2018), Research on a boiler furnace module effectiveness working on small fracture wastes. *INMATEH-Agricultural Engineering*, Vol. 55, No.2, pp.9-18, Bucharest/Romania;
- [4] He J.L., (2007), Kinematic simulation of no-row feed-in mechanism with guide-rod for corn harvester. *Transactions of the Chinese Society of Agricultural Engineering*, Vol.23, Issue 6, pp.125-129, Beijing/P.R.C;
- [5] Hao F.P., (2014), Design and experiment of corn harvester head with reel star wheel. *Transactions of the Chinese Society for Agricultural Machinery*, Vol.45, Issue 6, pp.112-117, Beijing/P.R.C;
- [6] Kang S.L., (2017), Design and finite element analysis of harvesting device for the *Cerasus humilis*. *Journal of Shanxi Agricultural University (Natural Science Edition)*, Vol.36, Issue 6, pp.439-443, Jinzhong/P.R.C;
- [7] Liang Y.H., (2006). Development of fermented milk drinks containing calcium fruits. *Modern Food Science and Technology*, Vol.22, Issue 2, pp.183-184, Guangdong/P.R.C;
- [8] Liu S.T., (2003). Cultivation technology and application prospect of red *Cerasus humilis*. *Chinese Journal of Eco-Agriculture*, Vol.11, Issue 1, pp.106-106, Hebei/P.R.C;
- [9] Li X.L., (2015). Determination and analysis of nutritional content in prunus humilis. *Journal of Agriculture*, Vol.5, Issue 8, pp.97-100, Beijing/P.R.C;
- [10] Liang W.Z., (2008). Study on brewing technology of Chinese dwarf cherry fermented wine. *Chinese Brewing*, Issue 22, pp.72-74, Beijing/P.R.C;
- [11] Liu H.F., (2013). Experimental study on technical parameters of *Cerasus humilis* picking device. *Journal of Shanxi Agricultural University (Natural Science Edition)*, Vol.33, Issue 4, pp.342-345, Jinzhong/P.R.C;
- [12] Mou X.W., (2009), Experiment of the finger-chain type sugarcane-lifter. *Transactions of the Chinese Society for Agricultural Machinery*, Vol.40, Issue 8, pp.49-53. Beijing/P.R.C;
- [13] Pan Y.X., (2016), The design research of the electric drive type rotary taking grain system of the semi-fed rice combine harvester. *Machinery Design & Manufacture*, Issue 5, pp.79-82, Shenyang/P.R.C;
- [14] Sun Z.B., (2016), Experimental on physical parameter and biomechanical properties of *Cerasus humilis* 5. *Agricultural Engineering*, Vol.6, Issue 2, pp.1-4, Beijing/P.R.C;
- [15] Zhang W., (2018). Simulation analysis and experiment of combing pluck of *Cerasus humilis*. *Agricultural Engineering*, Vol.8, Issue 5, pp.89-94, Beijing/P.R.C.

DESIGN AND TEST ON CONTROL SYSTEM OF AUTOMATIC SEEDLING FEEDING MECHANISM FOR TRANSPLANTING MACHINE

移栽机自动送苗机构控制系统设计和试验

As. Ph.D. Stud. Eng. Yong Zhang^{1,2)}, A/Prof. Ph.D. Eng. KaiXing Zhang^{*1)}, M.S. Stud. Eng. Chao Song¹⁾,
Prof. Ph.D. Eng. XianXi Liu.¹⁾, Prof. Ph.D. Eng. ZhengHe Song³⁾

¹⁾ College of Mechanical and Electrical Engineering, Shandong Agricultural University, Taian 271000, China;

²⁾ School of Information and Electronic Engineering, Shandong Technology and Business University, Yantai 264005, China;

³⁾ College of Engineering, China Agricultural University, Beijing 100083, China

Tel: +86 13563800102; E-mail: kaixingzhang@139.com

Keywords: *transplanting machine, seedling-feeding (SF) mechanism, positioning control, Kalman filter (KF), incremental Proportional-Integral-Derivative (PID)*

ABSTRACT

The purpose of this study is to improve the operation reliability and running positioning accuracy of full automatic vegetable transplanting machine. To this end, in this paper, a horizontal automatic seedling-feeding (SF) mechanism for transplanting machine was designed, and the initial-position positioning control and the incremental Proportional-Integral-Derivative (PID) control algorithm based on Kalman filter (KF) were adopted to improve its operational reliability and positioning accuracy. Then, the mathematical model of the transfer function in this mechanism was analysed and MATLAB simulation was performed; the simulation results show that the KF-based incremental PID control can well suppress the influence of external disturbance to avoid system overshoot and improve the robustness and reliability of the system. Finally, the actual operation test was carried out, the test results show that at the seedling tray speed below 350mm/s, the error of moving a new seedling tray (570mm) is $\leq 4.19\text{mm}$, and the positioning accuracy is $\geq 99.27\%$; the error of moving a column distance (42mm) is $\leq 1.05\text{mm}$ and the positioning accuracy is $\geq 96.79\%$. The automatic SF mechanism of the transplanting machine designed in this paper has a wide range of running speed and high positioning accuracy, which can meet the requirements of the positioning accuracy for the full-automatic transplanting machine feeding mechanism. This provides a reference for the design of the transplanting machine.

摘要

为了提高全自动蔬菜移栽机运行可靠性和运行定位精度, 首先, 设计了一种水平式移栽机自动送苗机构, 并采用初始位置定位控制和融合卡尔曼滤波的增量式 PID 定位控制算法, 以提高其运行可靠性和定位精度; 然后, 分析了该机构传递函数的数学模型, 并进行 MATLAB 仿真, 仿真结果表明融合了卡尔曼滤波的增量式 PID 控制能很好的抑制外界干扰的影响, 可以避免系统出现超调现象, 提高了系统的鲁棒性和可靠性。试验结果表明苗盘速度在 350mm/s 以下时, 移动一个新苗盘(570mm)的误差 $\leq 4.19\text{mm}$, 定位精度 $\geq 99.27\%$, 移动一列距离(42mm)时误差 $\leq 1.05\text{mm}$, 定位精度 $\geq 96.79\%$ 。本文所设计的移栽机自动送苗机构运行速度范围大、定位精度高, 可以满足全自动移栽机送苗机构定位精度的要求, 为移栽机送苗机构的设计提供了参考。

INTRODUCTION

Seedling transplanting is the main planting method in the production of protected vegetable in China. With the increase of planting quantity and labour cost, mechanical transplanting has been more applied. However, the currently used transplanting machinery is mostly the semi-automatic transplanting machine with artificial seedling feeding, which cannot fundamentally solve the problems of high labour intensity, low efficiency of transplanting and low accuracy of transplanting etc.

The field transplanting technology of plug seedlings in the developed countries is relatively mature and advanced. The Japanese full automatic transplanting machine (Tsuga, 2000; Nambu and Tanimura, 1992) relies on pure mechanical structures such as cam grooves etc. to realize full-automatic transplanting, but it has very complicated structure and poor adaptability to different types of plug seedlings. The Ferrari's automatic transplanting machine (Zhou, 2009) in Italy operates pneumatically or hydraulically, with high efficiency in the seedling picking and feeding process. In addition, the price of transplanting machines in

developed countries is very high and they're developed according to the transplanting process of foreign plug seedlings, which is not applicable to domestic conditions (Ni *et al.*, 2015).

At present, only a few scientific research units in China have been developing full automatic transplanting machines. The typical one is developed by Wei *et al.* (2016). It can realize high-speed transplanting of plug seedlings. However, the seedling-pick up mechanism remains in a high-speed operation state with excessive workload and has low reliability during long-term operation. The automatic seedling pick-up and feeding device of the plug seedling transplanting machine developed by Han *et al.* (2013) uses high pressure gas as the power source. It has a simple mechanical transmission system, but the vibration of the pneumatic system is large, the positioning accuracy is low and the pot seedling matrix loss is also higher. Wu *et al.* (2013) developed a full automatic transplanting machine with a gas-liquid damping cylinder as the driving component, but it has the disadvantages of high cost, large mechanical vibration and unstable performance. On the whole, domestic transplanter technology is relatively backward. Domestic field transplanting machines are all semi-automatic machines. Now, the development of automatic transplanting machines for field transplanting stays at the experimental research stage and there still exist the problems such as low precision and poor reliability.

In this paper, the SF mechanism of automatic transplanting machine needs to cooperate with the seedling picking mechanism for continuous start and stop, and then accurately send the seedling tray to the designated position. Too much dynamic positioning error can cause failure in the seedling picking. During operation, this SF mechanism will be affected and disturbed by such factors as seedling mass, running speed, high-frequency signal of power supply, etc., and its mechanical characteristics of the mechanism will also change after long-term operation, resulting in low long-term operational reliability and operational positioning and directly affecting the performance of the entire transplanter. In view of that above, combined with the structure of the seedling picking mechanism and feeding mechanism etc. for the full automatic transplanting machine mentioned, a horizontal automatic seedling feeding mechanism (Han *et al.*, 2013) for transplanting machine was designed in this paper. Besides, the incremental PID positioning control algorithm based on Kalman filter was proposed, and the simulation analysis and prototype operation test were carried out, in order to improve the positioning accuracy and long-term reliability of the mechanism.

MATERIALS AND METHODS

Working principle and running speed of transplanting machine automatic seedling feeding mechanism

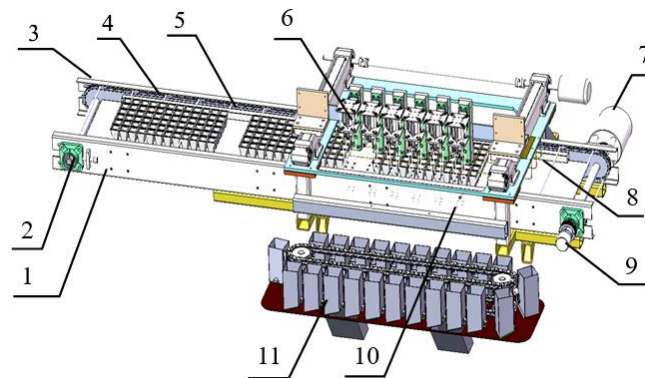


Fig. 1 - Structural diagram of automatic seedling feeding mechanism

1. Side plate 2. Tensioning wheel 3. Sprocket 4. Seedling support rod 5. Support rail 6. Seedling picking mechanism 7. Stepper motor 8. Seedling tray clamp 9. Rotary encoder 10. Position switch 11. Horizontal seedling feeding mechanism

Fig.1 shows the seedling feeding mechanism in the automatic transplanting machine. For the SF mechanism, the total length is 2,100 mm and the width is 450 mm. By the chain drive mode, the chain tension is changed by the tensioning wheel; the power source is a stepper motor which is mounted on the side plate and connected together by the coupler and the sprocket to drive the chain conveyor. The seedling support rod is installed on the chain, and three support rods support a 540 mm-wide seedling tray; the support rod is fixed with a support wheel with an outer diameter of 15mm, and the support wheel rolls on the support rail to support the chain and the load of the seedlings on the chain, thus reducing the operating resistance of the mechanism. The position of the seedling tray is settled by its position switch, i.e., Hall

sensor, which is composed of a sensor probe and a circular permanent magnet. The circular permanent magnet is mounted on the support rod of the seedling conveyor belt and the sensor probe is fixed on the frame. The position is adjusted to ensure that the new seedling tray moves and stops at the set position.

During operation, three seedling trays can be placed on the SF mechanism at the same time, with the tray spacing of L_1 (30 mm). The seedling picking mechanism is used to grab the seedlings in the rightmost seedling tray, and the new seedling tray is placed on the left or the middle for the next-time picking. The design of the transplanting machine in this paper is applicable to 6 rows, 12 columns and 72 holes of seedling trays, with the spacing between the two seedlings of M (42 mm). The seedling picking mechanism has 6 seedling hands which pick seedlings per row and simultaneously work so as to improve the picking efficiency. Due to the limited spacing between adjacent seedlings, the method of picking seedlings at intervals was adopted. In operation, the seedling picking mechanism first takes the odd-numbered seedlings, and grabs the seedlings of the first to sixth rows successively. Then the seedling feeding mechanism moves a distance M (one column) from left to right shown in Fig. 2 and grabs the even-numbered seedlings. After grabbing, the conveyor belt moves the distance $L_2=W+L_1=570$ mm to bring a new seedling tray and the empty seedling tray automatically falls into the seedling tray collection box on the right. The seedling feeding mechanism automatically repeats the above working process until a stop command is issued. Each time one seedling tray is completed, the seedling tray is repositioned by its position switch to avoid the cumulative error.

The automatic SF mechanism needs to start and stop frequently during the running process. Its running speed determines whether it can deliver the seedling tray to the designated position in time at the seedling picking interval, and also directly affects the design of the positioning control algorithm. The running speed of the automatic SF mechanism is determined by the design index of the full automatic transplanting machine for the plug seedlings. The design indicators include: (1) operating speed, ranging from 0.8 to 1.5 km/h; (2) plant spacing, i.e., the distance between the two adjacent seedlings in the same row of 300-500 mm; (3) the number of rows in operations, with two rows working simultaneously.

The transplanting interval between two adjacent seedlings is calculated as:

$$t = \frac{3.6 l}{v} \times 10^{-3} \quad (1)$$

where: l - plant spacing, mm;

v - operation speed of transplanting machine, km/h.

According to the design index of transplanting machine, at the fastest speed of 1.5 km/h and the shortest plant spacing of 300 mm, the shortest interval of transplanting between two adjacent seedlings is calculated as $t_{\min}=0.72$ s; at the longest plant spacing and the slowest speed, the longest time interval $t_{\max}=1.5$ s. The transplanting machine adopts two-row working system with six seedling hands running at the same time; each time three seedlings are transplanted in the same row, the seedling tray moves once; the move time interval is $t \times 3$ three times of the transplanting time interval between the adjacent seedlings.

The highest speed of the seedling conveyor belt appears when the new seedling tray is moved to the designated position. At this time, the longest moving distance of the seedling tray is up to $L_2=570$ mm. For the running speed of the seedling tray, according to formula (2), by taking the shortest running time interval $t_{\min} \times 3$, removing the seedling picking time of the mechanism, and plus certain time margin $t_y=0.5$ s, it's calculated as $v_{\max}=343.5$ mm/s.

The sprocket bearing diameter D of belt is 96.5 mm and the maximum working speed of the stepper motor can be calculated according to formula (3) as $v_{s,\max}=68$ rpm. Substituting t_{\max} , it's derived as $v_{\min}=142.5$ mm/s, $v_{s,\min}=28.3$ rpm. Then, the running speed of the stepper motor is calculated to be 28.3-68rpm, which can meet the design requirements of the transplanter.

$$v = \frac{L}{3t - t_y} \quad (2)$$

where:

v - operation speed of seedling tray, mm/s;

L - moving distance, mm;

t - transplanting time interval, s.

t_y - time margin, s

$$v_s = \frac{v}{\pi D} \cdot 60 \quad (3)$$

where: v_s - stepper motor speed, rpm;
 D -sprocket bearing diameter, mm.

Positioning control algorithm

The automatic SF mechanism of the transplanting machine is a closed-loop control system composed of a stepper motor, a position switch and a rotary encoder under the control of the PLC. In order to achieve accurate positioning, an appropriate positioning control algorithm needs to be designed.

Positioning control precision analysis

The SF mechanism of the transplanting machine is driven by the stepper motor and the relationship between the running distance of the feeding mechanism and the pulse number of the stepping motor issued by the PLC is:

$$n = \frac{L}{\pi D} \cdot \frac{360 \cdot H}{\theta_0} \quad (4)$$

where:

L - running distance, mm

θ_0 - standard step angle of stepping motor, 1.8°;

H - the number of subdivisions for the stepper motor driver, 16;

The maximum angle error of the stepper motor occurs when the picking is changed from the odd-numbered seedlings to even-numbered ones. The distance travelled by the stepper motor to drive the SF mechanism is L_1 ; according to formula (4), the number of pulses in the stepper motor is $n_1=443.32$ and the rounding error is $\Delta n_1=0.32$. Based on the stepper motor parameters of Table 3, the accuracy is $\pm 5\%$, and the relative error of the maximum angle for the stepping motor can be calculated as $\alpha_1=0.089\%$ by the formula (5).

$$\alpha = \frac{\Delta n_1 + 1.8 \times 5\%}{n_1} \times 100\% \quad (5)$$

The relative error of the maximum position for positioning the seedling tray is calculated by the formula (6) to be $\beta_1=8.33\%$ and the positioning accuracy is $1-\beta_1=91.67\%$.

$$\beta = \frac{s}{L_1} \times 100\% \quad (6)$$

where, s is the maximum position error allowed by the seedling tray positioning, which is $\pm 3.5\text{mm}$ by experiment. If it exceeds this value, it will cause the failure of seedling picking, seedling damage or excessive damage of seedling substrate.

Similarly, the maximum angle relative error of the stepping motor when the seedling mechanism moves a new seedling tray to the designated position can be calculated as $\alpha_2=0.011\%$, the relative error of the maximum position is $\beta_2=0.61\%$ and the positioning accuracy is $1-\beta_2=99.39\%$.

According to $\alpha_1 < \beta_1$ and $\alpha_2 < \beta_2$, it can be concluded that the running accuracy of the stepper motor can fully meet the seedling tray positioning requirements of the SF mechanism. However, in the actual operation process, the positioning accuracy of the seedling tray is interfered by various factors, e.g., the chain conveyor belt has nonlinear errors caused by the tooth gap, the insufficient rigidity of the drive disk component causes the stepping motor to lose the step, and the randomness of the seedling tray quality and the complexity/variability of the field operation environment disturbs the control signal. The simple positioning control is not enough to meet the system requirements and then an effective control algorithm should be taken to achieve accurate positioning control.

Kalman filter-based incremental PID Control

In order to improve the positioning accuracy, this paper designs an incremental PID position control based on Kalman filter. The block diagram of the control system is shown in Fig.2.

The trapezoidal curve, exponential curve, S-curve and PID control algorithm are often used to make position control of stepper motor. The first three algorithms can play a certain role in preventing sudden changes in speed, but with the fixed motor speed in the algorithm. After the step loss and overshoot phenomenon occurs, it must be processed by another program, which is inflexible. PID control is widely used

in the field of motion control and process control, which can greatly improve the control effect. Since the stepper motor is a control object with an integral mechanism, the increments should be also controlled. Thus, in this paper the incremental PID control (Zhao et al., 2015) was adopted, and the incremental PID control algorithm is given as Eq. 7-10.

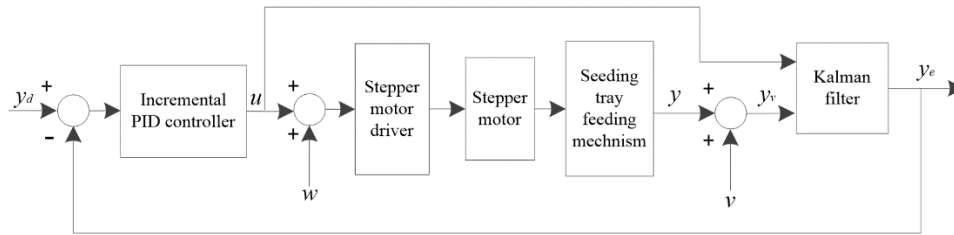


Fig. 2 - Kalman filter-based PID control system

$$u_t = u_{t-1} + \Delta u_t \tag{7}$$

$$u_{t-1} = K_p(e_{t-1} + K_i \sum_{j=0}^{t-1} e_j + K_d(e_{t-1} - e_{t-2})) \tag{8}$$

$$\Delta u_t = u_t - u_{t-1} \tag{9}$$

$$\Delta u_t = K_p(e_t - e_{t-1}) + K_i e_t + K_d(e_t - 2e_{t-1} + e_{t-2}) \tag{10}$$

where:

- u_t, u_{t-1} -control amount at the time t and $t-1$;
- e_t, e_{t-1}, e_{t-2} -position error at the time $t, t-1$ and $t-2$;
- K_p -proportional coefficient;
- K_i -integral coefficient.

From formula (7), it can be seen that the incremental PID control algorithm does not need to be accumulated and the control increment Δu_t is only related to the last two samplings, so it is influenced slightly when the malfunction occurs, so as to achieve a better control effect.

The stepper motor adopts the PTO (Pulse Train Output) pulse control mode and the PID controller output quantity u_t is the pulse frequency, at the low speed of stepper motor. In order to avoid overshoot phenomena etc., the upper limit of the u_t pulse frequency is set. According to formula (11), the pulse frequency of the stepper motor control signal corresponding to different running speeds of the seedling tray is calculated and the calculated value is rounded to obtain the upper limit of the pulse frequency (Table 1).

$$h = \frac{v}{\pi D} \frac{360 \times 16}{\theta_0} \tag{11}$$

where, θ_0 is the standard step angle of the stepper motor, 1.8°; 16 is the subdivision number of the stepper motor driver.

Table 1

Upper limit of control signal pulse frequency						
Speed (mm/s)	150	200	250	300	350	400
Upper limit of the frequency (Hz)	1585	2115	2640	3170	3700	4230

Incremental PID has little calculation and also small impact range when the controller fails. However, since the transplanting machine SF mechanism is subject to a lot of interference from the outside during the operation, KF has a good effect in suppressing interference and weakening noise. For this, this paper incorporates Kalman Filtering algorithm on the basis of incremental PID control (Kalman, 1960; Halber and Chakravarty, 2018; Washha et al., 2017).

The KF uses the recursive algorithm in the time domain to perform filtering processing and estimate the state value of the current moment by using the estimated value of the previous moment and the observed value of the current moment. This algorithm can effectively suppress the control interference signals and measurement noise signals that may occur during the working process through the estimation of the system state (Chen and Du, 2012).

The mathematical model of control system is discretized as:

$$x_t = A x_{t-1} + B (u_t + w_t) \quad (12)$$

$$y_{v,t} = C x_t + v_t \quad (13)$$

where:

x_t - system state vector

$y_{v,t}$ - system measurement vector

u_t - stepper motor control

w_t - control interference signal

v - measuring interference signals

A - system state matrix

B - system control matrix

C - output observation matrix

According to the system model, the current state can be predicted based on the previous state of the system.

$$\hat{x}_{(t|t-1)} = A \hat{x}_{(t-1|t-1)} + B u_t \quad (14)$$

Where:

$\hat{x}_{(t|t-1)}$ - state prediction result at the time ($t-1$)

$\hat{x}_{(t-1|t-1)}$ - state optimal value at the time ($t-1$)

The covariance matrix $P_{(t|t-1)}$ corresponding to $\hat{x}_{(t|t-1)}$ is:

$$P_{(t|t-1)} = A P_{(t-1|t-1)} A^T + Q \quad (15)$$

Where:

$P_{(t-1|t-1)}$ - the covariance matrix corresponding to $\hat{x}_{(t-1|t-1)}$

A^T - transpose matrix of A .

Q - system process noise covariance

Combining the measured values of the system in formula (13) with the prediction results of the current state in formula (14), the optimal estimate of the current state is derived as:

$$\hat{x}_{(t|t)} = \hat{x}_{(t|t-1)} + K_t (y_{v,t} - C \hat{x}_{(t|t-1)}) \quad (16)$$

where, K_t is the Kalman gain

$$K_{(t)} = \frac{P_{(t|t-1)} C^T}{C P_{(t|t-1)} C^T + R} \quad (17)$$

where: C^T - transpose matrix of C

R - measurement noise covariance matrix.

To ensure the continuous operation of KF, it is also necessary to update the covariance of the current moment:

$$P_{(t|t)} = (I - K_t C) P_{(t|t-1)} \quad (18)$$

Since the system is a single-model single measurement, then $l=1$ in the formula above.

The KF output is given as:

$$y_{e,t} = C \hat{x}_{(t|t)} \quad (19)$$

Automatic seedling feeding system simulation and seedling feeding operation test

Simulation analysis of automatic seedling feeding system

The automatic SF system is mainly composed of a stepper motor, a stepping motor driver, a driving belt and a rotary encoder. Its transfer functions are $G_d(s)$, $G_s(s)$, $G_m(s)$ and $G_r(s)$, respectively. The total

transfer function of the system is:

$$G(s) = \frac{G_d(s)G_s(s)G_m(s)G_r(s)}{1 + G_d(s)G_s(s)G_m(s)G_r(s)} \tag{20}$$

According to the literature (Wang et al., 2013), the transfer function of stepper motor is given as:

$$G_d(s) = \frac{L_0 i^2 Z_r^2 / 2J}{s^2 + Ds / J + L_0 i^2 Z_r^2 / 2J} \tag{21}$$

where: L_0 -inductance, [mH]; i -rated current, [A]; Z_r - number of rotor teeth; J -moment of inertia, [kg.cm²]; D -viscous damping coefficient.

Table 2

Parameters of stepper motor

Type	Number of rotor teeth	Step angle (°)	Rated voltage (V)	Rated current (A)	Resistance (Ω)	Inductance (mH)	Static torque (N.m)	Moment of inertia (g.cm ²)	Vicious damping coefficient	Mass (kg)
HBS860H	50	1.8±5%	3.36	5.6	0.6±10%	5.5±20%	8.5	2500	0.06	4.1

According to Table 2, substituting the relevant parameters into formula (21), the stepper motor driver adopts a bridge circuit, which can be regarded as a proportional element; then, taking the subdivision selection into consideration, its transfer function is $G_d(s)=10$. The SF mechanism converts the angular displacement into the linear displacement of the seedling conveyor belt through bearing rotation, which can be regarded as a proportional element, and its transfer function is $G_m(s)=(\pi d^2)/360=0.84$. The rotary encoder can also be seen as a proportional element with a transfer function of $G_r(s)=0.1$.

$$G(s) = \frac{263.4}{s^2 + 0.04s + 577} \tag{22}$$

The system simulation program was written in M language under MATLAB. The lsqnonlin () nonlinear least squares function in MATLAB was used to optimize the PID parameters and then obtain the initial K_p , K_i and K_d . Based on this, the NCD (nonlinear control design) optimization was performed to complete the PID parameter tuning. The final setting is $K_p=14.5$, $K_i = 1.8$, $K_d = 0.2$.

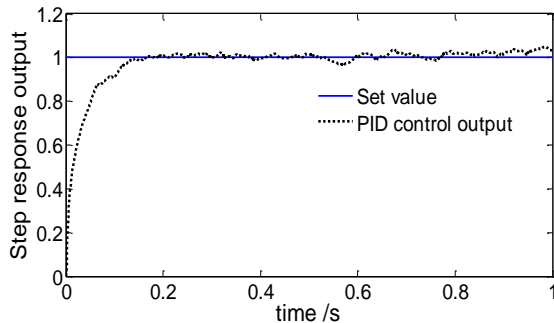


Fig. 4 - Incremental PID control response output curve

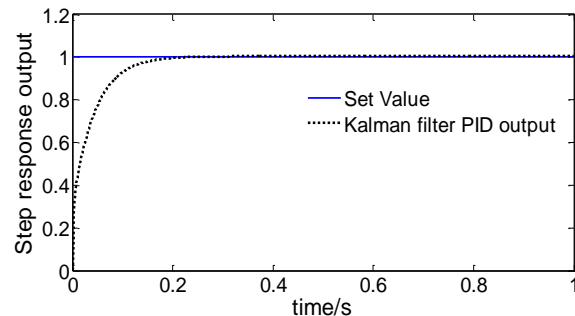


Fig. 5 - Kalman filter incremental PID control response output curve

Fig.4 and 5 show the system simulation results. The given signal by the test is a unit step signal. The blue line in the figure shows that the control interference signal and the measurement interference signal are both white noise signals with amplitude of 0.002. Fig.4 indicates that the incremental PID control is obviously affected by the external interference signal; Fig.5 indicates that the KF-based PID control effect is significantly improved, which has a good suppression of external interference, so as to avoid the overshoot phenomenon and promote the robustness and stability of the system.

Operation test of automatic seedling feeding mechanism

Test location and materials

The operation test was carried out in the Agricultural Machinery Equipment Laboratory, College of Mechanical and Electrical Engineering of Shandong Agricultural University. The 6x12 seedling tray was adopted. The transplanting machine in this paper was designed for the seedling transplanting of the eggplant, tomato, pepper, and lettuce etc. In the test, about 24-day eggplant seedlings were selected having an average seedling mass of 40 g and certain quality of the seedling substrate.

Test plan

The main purpose of this operation test is to verify the accuracy of the automatic SF mechanism under the control of the positioning algorithm (Fan et al., 2017; Yu et al., 2018). By adding the seedling substrate for different seedling tray tests, the running speed and moving distance of the SF mechanism were set through the touch screen, as shown in Fig. 6.



Fig. 6 - Test control system interface of touch screen



Fig. 7 - Operation test of seedling feeding

Main test indicators:

$$\alpha = \left| 1 - \frac{L_m}{L_n} \right| \times 100\% \tag{23}$$

where:

- α -positioning accuracy
- L_m -actual displacement, mm
- L_n -theoretical displacement, mm

Test results and analysis

Fig.7 shows the feeding operation test. During the test, the SF mechanism ran smoothly under the driving of the stepping motor and the initial positioning was performed when the new seedling tray moved to the seedling position, to avoid the cumulative error and ensure accurate system positioning. Six operating speeds of 150, 200, 250, 300, 350 and 400 mm/s, and the seedling mass of 40, 50 and 60g were selected. The running speed and the average mass were combined in pairs. Each group ran 10 times and then took the average. The test results are shown in Table 3.

Table 3

Test results

Speed (mm/s)	Seedling quality (g)	Mobile new seedling tray			Moving one column (42mm)		
		Distance (mm)	Time (s)	Accuracy (%)	Distance (mm)	Time (s)	Accuracy (%)
150	40	567.83	3.961	99.62	41.83	0.478	99.59
	50	568.74	3.968	99.78	41.83	0.475	99.59
	60	569.04	3.971	99.83	42.74	0.485	98.23
200	40	568.74	3.044	99.78	41.83	0.409	99.59
	50	570.25	3.052	99.96	42.44	0.412	98.95
	60	570.86	3.054	99.74	43.05	0.415	97.5
250	40	569.95	2.480	99.98	42.14	0.369	99.67
	50	568.52	2.474	99.74	43.05	0.372	97.5
	60	571.16	2.485	99.79	42.74	0.391	98.23
300	40	568.13	2.094	99.67	42.44	0.341	98.95
	50	572.07	2.107	99.64	42.74	0.342	98.23
	60	572.98	2.110	99.48	43.35	0.345	96.79
350	40	571.46	1.832	99.74	42.44	0.321	98.95
	50	573.28	1.838	99.43	42.14	0.32	99.67
	60	574.19	1.841	99.27	42.75	0.322	98.21
400	40	572.68	1.672	99.53	42.44	0.306	98.95
	50	574.8	1.677	99.16	42.44	0.311	98.95
	60	575.71	1.689	99.01	43.66	0.322	96.05
Average value		571.13		99.62	52.56		98.53

It can be seen from Table 3 that the average positioning accuracy is 99.62% when moving a new seedling tray to the seedling position. The positioning accuracy decreases with the increase of speed and the mass of tomato seedlings. At the speed of 400mm/s, the maximum error is up to 5.7mm and the positioning accuracy is low. At the moving speed of the seedling tray of 350mm/s or less, the SF mechanism can meet the system positioning accuracy requirements.

When the seedling tray moves a distance of one column, the average value of the total positioning accuracy is 98.53%, but the maximum error is 1.6mm, meeting the positioning accuracy requirements. The main reason for the error is that with the short moving distance, the encoder can only count the integer value.

In the test process, there are also phenomena such as stepper motor overload alarm, blocking, and pulse loss etc. The running time of the stepper motor is slower than the theoretical calculation time by 0.1-0.2s, especially when the speed is greater than 350mm/s. The reason is that the torque of the stepping motor decreases as the rotation speed increases and the resistance of the feeding mechanism is greater than the torque of the stepper motor.

CONCLUSIONS

(1) In view of the high precision requirements, great load change and multiple external interference factors during the automatic seedling tray operation, the initial positioning control and the incremental PID positioning control algorithm based on Kalman filter were adopted. Based on the Siemens S7-1200 programmable controller, the electric control system of the automatic SF mechanism for the transplanting machine was designed, so as to achieve the stable operation of the seedling tray transportation.

(2) The control system model of the SF mechanism was established. The simulation experiment was carried out with MATLAB. The results show that the Kalman filter-based PID controller can effectively suppress external interference, avoid overshoot and improve the robustness and stability of the system, meeting the positioning accuracy requirements of the seedling mechanism.

(3) The eggplant seedlings in the 20-day nursery period were used for actual experiment. When the seedling speed is below 350mm/s, the error of moving a new seedling tray is ≤ 4.19 mm and the positioning accuracy is $\geq 99.27\%$; the error for moving a column distance is ≤ 1.05 and the positioning accuracy is $\geq 96.79\%$, which can meet the requirements of the positioning accuracy for the feeding mechanism.

(4) In order to ensure the resistance of the SF mechanism within the torque range of the stepper motor, the maximum running speed of the mechanism is set to be 350mm/s, keeping the sprocket, etc. in good lubrication state and reducing the system resistance.

ACKNOWLEDGEMENTS

The work is supported by The National Key R&D Program (2017YFD0700100), Shandong Key R&D Program (2016GNC112008) and Shandong Province "Double First Class" Award Fund Project (SYL2017XTTD14)

REFERENCES

- [1] Chen X.H., Du M., (2012), Multipoint temperature information fusion using sequential dual Kalman filter for temperature control system of portable RT-PCR instrument, *Journal of instrument*, vol.33, issue 2, pp.263-270;
- [2] Fan G.J., Wang Y.Z., Zhang X.H., Zhao J.Y., Song Y.P., (2017), Design and experiment of automatic leveling control system for orchards lifting platform, *Transactions of the Chinese Society of Agricultural Engineering (Transactions of the CSAE)*, vol.33, issue 11, pp.38-46;
- [3] Guo J.B., Niu H.L., Han Y.H., Dong R.J., Liu X.X., Pang C.L., (2017), Design and Experiment of Farm Ammonia Bio-oxidation Device Based on PLC, *Transactions of the Chinese Society for Agricultural Machinery*, vol.48, issue 3, pp.310-316;
- [4] Halber A., Chakravarty D. (2018), Investigation of wireless tracking performance in the tunnel-like environment with particle filter, *Mathematical Modelling of Engineering Problems*, vol.5, issue 2, pp. 93-101.
- [5] Han L.H., Mao H.P., Mou X.H., Hu J.P., Yang X.J., (2013), Design of Automatic Picking Up Seedling End-effector Based on Mechanical Properties of Plug Seedlings, *Transactions of the Chinese Society for Agricultural Machinery*, vol.44, issue 11, pp.260-265;

- [6] Han Z.J., Yang W.Z., Zhang X.J., Guo H., Yin W.Q., (2013), Design and test of automatic feed system for tray seedlings transplanter, *Transactions of the Chinese Society of Agricultural Engineering (Transactions of the CSAE)*, vol.29, issue 8, pp.51-61;
- [7] Kalman R.E., (1960), A new approach to linear filtering and prediction problems, *Transaction of the ASME Journal of Basic Engineering*, vol.82, issue 3, pp.35-45;
- [8] Liu J.D., Cao W.B., Xu H.Z., Tian D.Y., Jiao H.B., Ouyang Y.N. (2017), Adaptive fuzzy-PID control of accurate orientation for auto-detect seedling supply device, *Transactions of the Chinese Society of Agricultural Engineering (Transactions of the CSAE)*, vol.33, issue 9, pp.37-44;
- [9] Nambu T., Tanimura M., (1992), Development of automatic transplanter using chain pot for vegetable crops, *International Symposium on Transplant Production Systems*, issue 319, pp.541-546;
- [10] Ni Y.L., Jin C.Q., Liu J., (2015), Design and experiment of system for picking up and delivering seedlings in automatic transplanter, *Transactions of the Chinese Society of Agricultural Engineering (Transactions of the CSAE)*, vol.31, issue 23, pp.10-19;
- [11] Ryu K.H., Kim G., Ting K.C., (2001), Development of a robotic transplanter for bedding plants, *Journal of Agricultural Engineering Research*, vol.78, issue 2, pp.141-146;
- [12] Tsuga K., (2000), Development of fully automatic vegetable transplanter, *Japan Agricultural Research Quarterly*, vol.34, issue 1, pp.21-28;
- [13] Wang Q., Cao W.B., Zhang Z.G., Zhang P., Wang P., (2013), Location control of automatic pick-up plug seedlings mechanism based on adaptive fuzzy-PID, *Transactions of the Chinese Society of Agricultural Engineering (Transactions of the CSAE)*, vol.29, issue 12, pp.32-39;
- [14] Washha M., Mezghani M., Sèdes F. (2017), Behavioural account-based features for filtering out social spammers in large-scale twitter data collections, *Ingenierie des Systemes d'Information*, vol.22, issue 3, pp. 65-88;
- [15] Wei X.H., Bao S., Liu X.K., Liu C.L., Mao H.P., (2016), Design and Experiment on Potted-seedling Automatic Transplanter Control System for Motion Coordination, *Transactions of the Chinese Society for Agricultural Machinery*, vol.47, issue 12, pp.1-7;
- [16] Wu J.M., Yan H., Jin X., Guo Y., Chen K., Dong Z., (2013), Research on Disk Conveying Device and Positioning Control System for Transplanter, *Transactions of the Chinese Society for Agricultural Machinery*, vol.44, issue S1, pp.14-18;
- [17] Youssef A.M., (2018), Operations of electric vehicle traction system, *Mathematical Modelling of Engineering Problems*, vol.5, issue 2, pp.51-57;
- [18] Yu X.X., Zhao Y., Chen B.C., Zhou M.L., Zhang H., Zhang Z.C., (2014), Current Situation and Prospect of Transplanter, *Transactions of the Chinese Society for Agricultural Machinery*, vol.45, issue 8, pp.44-53;
- [19] Zhang H., Liu F., (2018), Spatial and temporal disparities in agricultural carbon emissions in Xinjiang and decomposition of impact factors, *Chemical Engineering Transactions*, vol.66, pp.553-558;
- [20] Zhao D.A., Jia W.K., Zhang Y., Zhao Y.Y., Ji W., (2015), Design of Agricultural Robot Autonomous Navigation Control Based on Improved Self-adaptive Filter, *Transactions of the Chinese Society for Agricultural Machinery*, vol.46, issue 5, pp.1-6;
- [21] Zhou T., (2009), Greenhouse hole tray seedlings transplanting machine design and experimental research, *Nanjing agricultural university*.

THE EFFECT OF POTATOES' COMPRESSIVE MECHANICAL PROPERTIES UNDER DIFFERENT MOISTURE CONTENTS: AN EXPERIMENTAL STUDY

不同含水率下马铃薯压缩力学特性影响的试验研究

Ph.D. Yu Fan^{1,2)}, A. Prof. Ph.D. Ping Zhao^{*1)}, Prof. Ph.D. Lichun Qiu¹⁾, M.S. Jizhe Zhao¹⁾

¹⁾ Agricultural University of Shenyang, Shenyang 110886, China

²⁾ Heilongjiang Agricultural Economy Vocational College, Mudanjiang 157041, China

Tel: +8615945306697; E-mail: 117636078@qq.com

Keywords: early-maturing variety, moisture content, mechanical property, potato

ABSTRACT

Based on the viewpoint and theory of the integration between agricultural machinery and agronomy, by taking five early-maturing varieties of potato widely planted in western Liaoning Province as the research object, this paper applies the universal material testing machines and electric drum drying ovens etc. in the experiment and obtains the change law of moisture content of potatoes after harvest within 0-5 months, the compressive mechanical properties of potato with different moisture content were tested. The variation of breaking force, maximum deformation and elastic modulus of potato with different moisture content were obtained. Therefore, the experimental results can provide necessary mechanical parameters and theoretical references for the harvesting, storage, the design research on processing/transportation equipment, and the placement method of early-maturing potato in western Liaoning.

摘要

基于农机与农艺结合的观点与理论, 本文以辽西地区广泛种植五个早熟品种马铃薯为试验对象, 应用万能材料试验机和电热鼓风干燥箱等仪器设备, 测试得到马铃薯收获后 0-5 个月之内含水率的变化规律, 并进行了以含水率为单因素的压缩力学特性试验, 得到了不同含水率下马铃薯的破裂力、最大变形量和弹性模量的变化规律。试验结果可为辽西地区早熟马铃薯的收获、贮藏及加工运输设备的设计研究和摆放方式提供必要的力学参数和理论参考。

INTRODUCTION

Potato is the world's fourth largest food crop after rice, wheat and corn. With its production advancement as staple food, the potato will surely achieve regionalization of cultivation, mechanization of production, industrialization of operations, refinement of processing and diversification of staple food varieties, further leading to its great growth of grading, transportation and storage capacity, and wide distribution in the market (Chen, 2014; People's Daily, 2015; Tian et al., 2015). During the process of harvesting, transporting, grading and storage, potatoes are subjected to external loads, which are likely to cause mechanical damage. This will not only damage the epidermis tissue of the potato, affect its appearance, but also easily cause internal decay and deformation, reduce its quality and economic value; it can even affect their germination rate if these potatoes are used as seeding material next year (Lu, 2016; Wang et al., 2014). In the potato tuber, the moisture occupies a large proportion and the degree of moisture content greatly affects the compression mechanics of the potato; only with enough hardness and strength will it not be damaged. Currently, the research on the moisture content is mostly concentrated on items such as soybeans, corn, walnuts and fruits, and it has been demonstrated that the degree of moisture content has a significant influence on the mechanical properties of fruits (Shen et al., 2016; Gao et al., 2012; Li et al., 2018). Therefore, it is very necessary to understand the compressive mechanical properties of potato with different moisture content and to further study the compressive mechanical indexes such as rupture force, elastic modulus and maximum deformation of the potato under pressure, aiming to provide the basis and reference for reducing the damage in storage and transportation, guiding the relevant agricultural machinery design, making assessment and detection of potato quality.

At present, scholars in China and abroad have conducted relevant researches on the mechanical properties of potatoes. M.G. Scanlon et al. performed the compression and stretching tests on potatoes, and demonstrated that the moisture content of potato has an effect on the mechanical properties (Scanlon et al.,

1996); *Bentini et al. (2009)* carried on the quasi-static compression tests on two potato varieties harvested for two years and identified that Young's Modulus and Poisson's ratio are related to storage time. The domestic scholars, *Wu Yali and Guo Yuming (2011)* conducted experiments on general mechanics of potatoes and then obtained mechanical property indexes such as compressive strength and shear strength of potatoes; *Shi Linyi and Zhang Fengwei et al.* determined the significant effects of loading direction and loading rate on the potato rupture force through the compression mechanical test of the whole potato tubers (*Shi and Wu, 2014; Zhang et al., 2014*); *Wang Yumei et al. (2015)* achieved the main factors affecting the mechanical properties of potato by compressive mechanical properties test of potato. However, among the existing research results, there have been no relevant reports on the different early-maturing potato varieties planted in western Liaoning and there are also relatively few researches on the moisture content test and its effect on compressive mechanical properties under different storage time after harvest.

The western part of Liaoning Province is the well-known home of potato in China, where the potato planting area is about 13% of the total planting area, and the potato planting area in Jianping County is up to 150,000 ha (*Xiao, 2013; Zhang and Lu, 2015*). Mainly by taking the five early-maturing varieties planted in Jianping County of western Liaoning Province as the research objects, this paper carries out the moisture content test at various time periods within five months after harvest and finally conducts the single factor compression mechanics test for different moisture contents. It aims to study the variation rule of moisture content in different potato varieties under natural conditions and the effect of different moisture contents on the compression mechanical properties of potato, in order to provide the theoretical basis for potato harvest, storage and design of processing equipment in western Liaoning, as well as for the selection of reasonable placement methods, transport time and related parameters of deep processing machinery for these potato varieties in transportation and storage etc.

MATERIALS AND METHODS

Test materials

In our experiment, the research objects were selected from the potato experimental field jointly built by Shenyang Agricultural University and Jianping Agricultural Technology Promotion Centre, and the experimentally related early-maturing potato varieties were planted, mainly including the Netherland 15#, Fujin, Youjin, Favorita and Zaodabai. They were artificially harvested on July 20, 2017, where 50 were selected from each variety, and 4-6 pest-free, non-porous and non-injurious fresh potatoes were selected for each plant. After harvest, they were stored at room temperature for about two weeks. The Vernier caliper was used to measure the three-dimensional size of fresh potatoes of each variety so as to select the potatoes with similar size and shape for about 100 g, label and store them; then the whole tuber compression test was performed, as shown in Fig.1. To determine the moisture content of potatoes in different storage time periods, the potatoes for the experiment were stored in the agricultural product processing and storage laboratories and cellars at Shenyang Agricultural University at the temperature of 2-8°C and humidity of 80%-85%. The storage lasted from August 1, 2017 to January 1, 2018, for 5 months in total.



Fig. 1 - Potato samples used for the test

Test equipment and instruments

The test equipment includes Instron 3344-series universal material physical testing machine (American Instron Corporation) and Model 101 electric drum drying oven (Beijing Yongguangming Medical Instrument Co., Ltd.), electronic balance (accuracy 0.01g), Vernier caliper (measurement Range 0-300mm,

resolution 0.01mm), fresh-keeping bags and paper labels. The universal material physical testing machine was used to test the mechanical properties of potato static loading. It mainly consists of the data acquisition system and test bench (Fig. 2) which can display the compression load, displacement, velocity and test curve in real time; electronic balance and 101 electric drum drying oven were adopted to measure the moisture content of the potato; the Vernier caliper measured the three-dimensional size of the potato sample.



Fig. 2 - Universal material physical testing machine
1-Rack and Rail; 2-Indenter; 3-Base; 4-Computer

Test design and method

(1) Determination of potato moisture content

In order to study the effects of different moisture contents on the compression mechanical property of potato, the test method of moisture content based on the storage time was adopted in this experiment. After one day from harvesting (fresh potatoes 6), the first moisture content determination and compressive mechanical test were conducted; after 15 days, the second test was conducted; after 30 days, the third trial; after 45 days, the fourth trial; after 60 days, the fifth trial; in this way the moisture content was tested once every 15 days, and only the last test was conducted every 30 days, 150 days in total. So, it's expected to obtain the variation of moisture content with the change of storage time and find out its impact on compression mechanics.

There are lots of methods for moisture determination, where the internationally accepted methods are vacuum drying and air blast drying currently (Ma and Gu, 2003; Sun et al., 2018). Based on the existing conditions in the laboratory, the moisture content of potatoes was measured using the blast drying method and the mass weighing method according to GB/T12078-2008. Firstly, the selected potato was subjected to the compression mechanics test. Immediately after the test, the moisture content was tested: ten samples for each potato variety were firstly prepared, which were cut into the thin slices with similar thickness (weight: over 2g), and numbered separately; afterwards, the weight of samples was measured and the initial weight was recorded; then, they were uniformly placed on the tray and in the blast drying box at the temperature of 85°C, and dried for 0h, 1h, 2h, 3h, 3.5h and 4h respectively; in the drying process, at the specified time, the related varieties were taken out of the box for weighing and data recording. Those that didn't reach the specified drying data shall be put back into the blast box for continuous drying; but if the weight no longer changed, it meant the end of drying. The moisture content of potato samples was calculated as:

$$X = \frac{m_1 - m_2}{m_1} \% \quad (1)$$

where X is the moisture content of the potato, %; m_1 is the mass of the sample, g; m_2 is the mass of the sample after drying to constant weight, g.

(2) Compressive mechanical properties test

In the harvesting, storage and transportation process, potatoes are generally subjected to external loads under natural placement conditions. Therefore, it is very valuable to test the mechanical properties of whole potato tubers in natural states (Guo et al, 2014). The test steps of potato compression characteristics are: the fixed loading speed is 15 mm/min and the loading directions are Z directions. (X is placed upright, Y is placed lateral, Z is flatwise) as shown in Fig.3a and 3b. The single-factor determination test of moisture content was conducted. The potato tubers of five varieties were selected respectively. They were subjected

to Z-direction compression under the moisture content of the natural storage at different time periods, so as to obtain the epidermis rupture force, elastic modulus and maximum deformation of the potato. Then the study was conducted for the effect of moisture content on the compressive mechanics property through the static loading mechanical properties. For each variety, five repeated tests were carried out at the same moisture content. The data were statistically analysed to take the average and variance. During the test, the rigid plate was used as the loading device. The whole tuber of the potato was placed in the centre of the indenter, and the upper indenter was adjusted to just not touch the potato. Then, the test program control interface was entered and the control setting parameters were selected in the method interface, including loading rate 15 mm/min, upper limit load 2000 N, upper limit displacement 50 mm, the upper limit load-descending percentage 20%, and the upper limit load-descending 10N. In the test interface, the steps were followed by clicking Load Zero, Reset Gage, Start and Finish. In order to reduce the experimental/test error, each test was repeated 5 times under the same conditions and finally averaged.

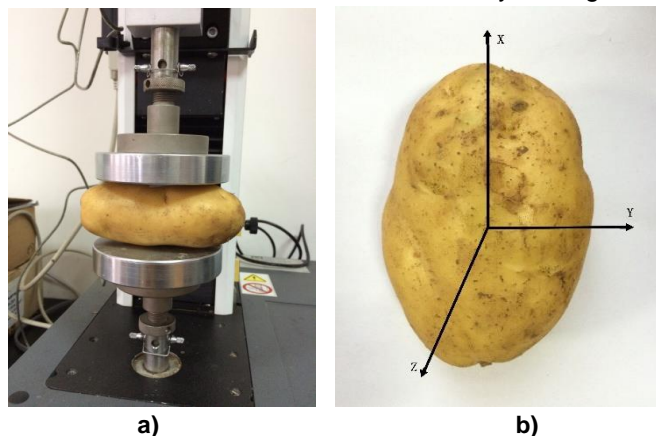


Fig. 3 - Diagram of potato compression loading device
 a) Z-direction loading device b) Diagram of potato directions

(3) Experimental factors and indexes

In this paper, potato moisture contents are selected as the experimental factors. The maximum load received when the potato tuber breaks, deformation and elastic modulus under compression were used as test indexes.

RESULTS

Variation rule of moisture content for different varieties

The measurement results of moisture content for the five varieties within 0 to 5 months after harvest were collected and analysed (Fig.4). It can be seen that the fresh potato's moisture content of the five varieties reached 80%-84% at harvest, but with storage time increasing, the moisture content of the five varieties showed a downward trend: in the first 0-30 days of storage the moisture content decreased more rapidly; at about 45 days, the decline of moisture content tends to decrease more slowly, reaching about 75%-80%. At the 60 days of storage, the moisture content of Zaodabai was the lowest and also tended to be stabilized. From the 75th day onwards, the moisture content of potatoes in the four varieties of Fujin, Youjin, Favorita, and the Netherlands 15# also increased slightly. Taking Favorita as example, the moisture content of its fresh potatoes reached 83.8% at the beginning; after 30 days, it dropped to 80.5%, which was a drop of 3% or so. The moisture content at the 60th day was 78.2% and the data became stable. After about 120 days, the data was further increased. For different potato varieties, their moisture contents also vary, esp., Favorita had a significant drop in moisture content at the beginning of storage (0-60d). But the other four varieties did not change so dramatically. In general, despite the different varieties, the variation rules of the potato tubers' moisture content are similar.

Through the reason analysis, it's found that: after harvesting, although the photosynthesis stops immediately, the potato is still a living organism. Its life metabolism is still being carried out in an orderly manner. The potato epidermis has not been completely corked and the respiration inside the potato block is strong, so the moisture evaporates actively and the water is easily lost, causing it to lose weight and lose freshness. With the increase of storage time, the potato will go into dormancy, followed by the reduced metabolism, the decreased water transpiration, and the weakened respiration. Therefore, the relevant moisture content will decline slowly and tends to be stable. Considering that the potato contains starch,

sugar and other carbohydrates in addition to water, it is certain that potato tubers are not fully mature with the tender epidermis within 0-20 days from the beginning of potato harvest, and the cork layer isn't formed with high moisture content and easy peeling. But it can be used for processing food such as mashed potatoes. However, fresh potatoes with high moisture content are not suitable for long-distance transportation. Thus, it can be concluded that after two months from potato harvest, the water loss rate of the above five varieties of potatoes is between 4% and 6%, and the relevant energy is converted into other dry matter.

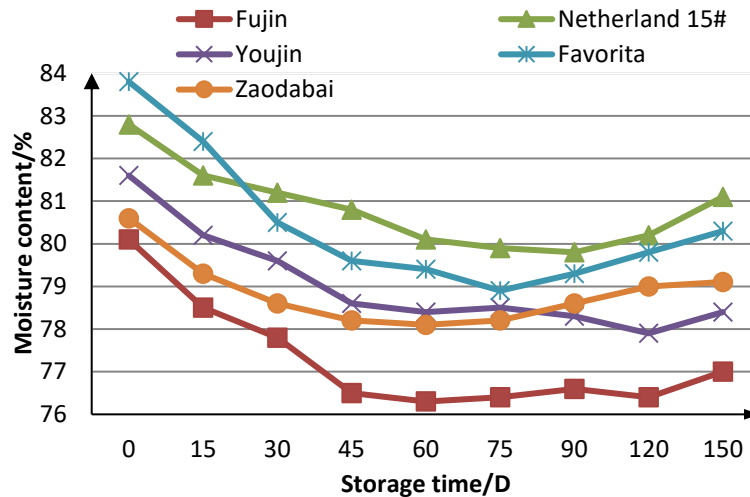


Fig. 4 - Variation of potatoes with storage time

Compressive mechanical properties of potato under different moisture contents

Due to the fact that most tubers are placed in piles during the transport and storage of potatoes, the most common interaction between tubers is mutual extrusion. So, this paper focuses on the mechanical experiment of uniaxial compression of potato under natural flat state. Through the stress test, the mechanical properties of different varieties of potato under different moisture contents were obtained (Table 1).

(1) Relationship between moisture content and rupture force. The rupture force of potato mainly refers to the maximum value of the external load when the potato breaks. In Table 3, it can be seen that as the moisture content decreased, the compressive load that the potato can withstand increased and the moisture content of the potatoes of each variety at the early harvesting stage was more than 80%; after the natural storage for 30 days, moisture content declined rapidly, e.g., for the Zaodabai, the relevant compressive force rose from 1,196.19N to 1,424.53N; then, after 45-day storage, the change of compressive force tended to be stable; with the increase of storage time, at about 120 days of storage, when the moisture content decreased, the rupture force further decreased.

The main reason of analysing the effect of moisture content on potato rupture strength is that potato is the viscoelastic solid agricultural material, and the different moisture contents lead to the difference in its internal structure and mechanical strength. The higher the moisture content, the softer the internal tissue of the potato, the lower the resistance to rupture; when subjected to external loads, the fluid inside the cell can cause the internal pressure to act on the cell wall. This allows the cells to be in a state of elastic pressure, showing elastic properties, thus, the potato is easily deformed and its pressure capacity decreases. As the moisture content decreases, the cellular pressure in the inner tissue of the potato decreases, showing an increase in the rigidity and elasticity of the inner cell wall, besides, the inner tissue is tightly bound, the hardness of the potato fruit increases, and the loading capacity is improved accordingly. Based on the MATLAB software, the relational graph of storage time, moisture content and rupture force of each variety was fitted in the diagram. Due to the limited space, in this paper, only the relational graph of Fujin potato variety is given in Fig.5.

According to the test data and the MATLAB fitting graph of various varieties, it can be seen that the compressive loads of Fujin, Youjin, and Zaodabai potatoes did not change much at the beginning of storage; after 45 days or so, the maximum compressive force increased sharply, which was 1.5 times the initial value, indicating that these three varieties have become more solid at this time, besides, from the perspective of storage and transportation, the external load pressure does less damage to the potato, so it's the best time for transport. For the other two varieties Netherlands 15# and Favorita, their changes were relatively small,

and the overall upward trend was relatively slow; at the 60th day of storage, these two varieties bear a greater load. This is related to the change of their internal moisture content: the effect of different moisture contents on the potato is still relatively large, and the compressive force of the potato among different varieties also varies, which mainly depends on their different internal structure.

The single-factor relational expression between potato rupture force and moisture content of five different varieties was fitted by MATLAB software, which was approximated by the cubic function relation, with the determination coefficient above 0.98. The related formula is expressed in Table 2.

Table 1

Compressive mechanical property values under different moisture contents

Variety	Moisture content %	Max. rupture force/N	Max. compression deformation/mm	Elastic modulus/MPa
Favorita	83.8	997.63	12.27	16.01
	82.4	1073.81	13.21	17.86
	80.5	1125.39	14.54	21.68
	79.1	1203.48	15.05	24.93
	78.2	1341.03	16.45	26.88
	78.3	1318.97	16.49	26.95
	78.6	1287.91	15.96	25.82
	79.3	1165.32	14.61	25.26
	79.8	1163.02	14.06	24.22
Netherland 15#	82.8	986.7	13.43	24.34
	81.2	1097.1	14.89	26.93
	80.6	1047.34	15.31	28.21
	80.3	1057.8	15.78	28.70
	79.6	1254.97	16.59	30.66
	79.5	1265.27	16.61	30.99
	79.8	1171.82	15.99	30.24
	80.2	1063.44	15.61	28.52
	81.1	1048.82	14.69	26.91
Zaodabai	81.6	1196.19	17.30	22.84
	79.3	1339.57	16.06	26.39
	78.6	1424.53	15.65	28.67
	77.8	1418.84	14.56	30.49
	78.1	1592.44	15.18	28.68
	78.2	1390.78	15.11	28.54
	78.8	1342.9	15.36	28.17
	79.2	1322.43	15.59	26.44
	79.5	1311.73	15.84	26.17
Youjin	81.8	958.4	16.03	21.25
	80.2	974.48	15.41	23.65
	79.6	1059.1	14.53	25.13
	78.3	1180.85	12.63	27.72
	78.4	1178.27	12.96	27.97
	78.5	1170.34	13.01	27.95
	78.8	1129.2	12.83	25.95
	79.4	1049.24	13.34	24.36
	79.9	1062.44	13.06	21.11
Fujin	80.1	846.91	15.79	16.03
	78.5	1054.77	13.59	18.54
	77.8	1148.61	12.66	19.56
	76.5	1267.51	11.42	21.23
	76.3	1286.23	11.88	21.75
	76.4	1269.78	11.89	21.31
	76.6	1243.37	11.56	21.38
	76.4	12633.2	11.53	21.67
	77	1120.93	12.19	19.12

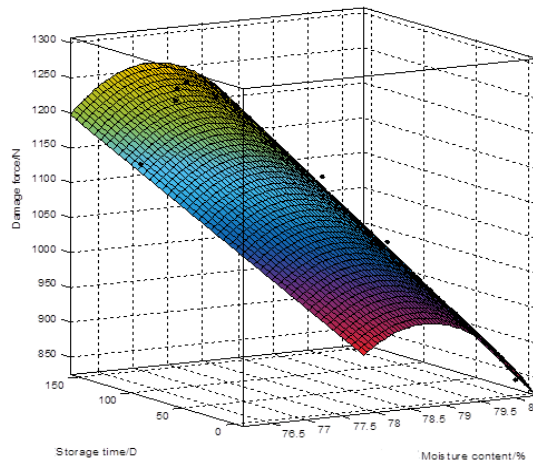


Fig. 5 - Relational graph between rupture force and moisture content

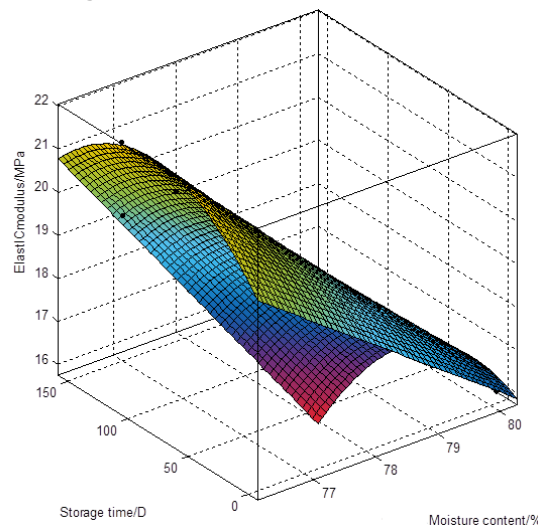


Fig. 6 - Relationship between elastic modulus and moisture content

Table 2

Fitting function of potato rupture force and moisture content		
Varieties	Fitting function	R ² determination coefficient
Zaodabai	$F(x) = 4.14x^3 - 992.7x^2 + 79240 - 2105000$	0.979
Favorita	$F(x) = -5.317x^3 + 1300x^2 - 106000x + 2881000$	0.993
Netherland 15#	$F(x) = -62.3x^3 + 15190x^2 - 123500x + 3344000$	0.985
Youjin	$F(x) = 5.578x^3 - 1320x^2 + 10400x - 2729000$	0.987
Fujin	$F(x) = -20.35x^3 + 4769x^2 - 37250x + 9703000$	0.980

where F(x) is the maximum loading force when the potato is placed flat, N; X is the moisture content of the potato.

(2) Relationship between moisture content and elastic modulus. The elastic modulus of potato is a measure of the difficulty degree of deformation. The greater the elastic modulus is, the greater the pressure of the external load is, and the smaller the elastic deformation is. The INSTRON universal material testing machine used in this test has the function of automatically measuring and recording the elastic modulus, and it can measure the elastic modulus of potato under any pressure and deformation.

From the test data in Table 1, it can be seen that the modulus of the five varieties increased with the decrease of moisture content, and the elastic modulus values of Zaodabai and Netherlands 15# were the largest, but after four months, the changes of the elastic modulus for the five varieties were similar, where the modulus value of Favorita potatoes was the maximum, followed by the Zaodabai, Netherlands 15# and Fujin, and Youjin's elastic modulus was the minimum. The higher the elastic modulus value, the better its tuber firmness. The reason analysis shows that after the moisture content is reduced, the elastoviscosity of the potato is reduced and the density of the material is increased. So, the potato is close to the rigid body

and is not easily deformed under pressure with a certain load carrying capacity. According to MATLAB software, the relational graph of storage time, moisture content and elastic modulus of each variety was fitted. Due to the limited space, only the relational graph of Fujin potato variety was given in this paper as shown in Fig.6.

The single-factor relational expression between the elastic modulus and moisture content of five different varieties of potato was fitted by Matlab software, which was approximated by the cubic function relation, with the determination coefficient above 0.96. The related formula is expressed in Table 3.

Table 3

Fitting function of potato elastic modulus and moisture content		
Varieties	Fitting function	R^2 determination coefficient
Zaodabai	$E(x) = 0.02537x^3 - 5.871x^2 + 450.5x - 11420$	0.975
Favorita	$E(x) = 0.06203x^3 - 15x^2 + 1206x - 32260$	0.986
Netherland 15#	$E(x) = -0.1365x^3 + 33.49x^2 - 2741x + 74580$	0.981
Youjin	$E(x) = -0.2594x^3 + 62.55x^2 - 5029x + 13480$	0.965
Fujin	$E(x) = -0.3418x^3 + 80.2x^2 - 6274x + 16360$	0.992

Note: $E(x)$ in the formula is the elastic modulus of the potato when it is laid flat; X is the moisture content of the potato

(3) Relationship between moisture content and compressive deformation. The compressive deformation of potato refers to the deformation of potato under the action of external compressive load, which is the maximum displacement of potato at the rupture point. From the test data in table 3, it can be seen that as the moisture content decreased, the amount of deformation tended to decrease, and the trend of change among different varieties was the same. E.g., for the variety Fujin, the variation of potato deformation with moisture content is shown in Fig. 8; when the moisture content decreased from 80.1% to 76.5%, the deformation showed a downward trend, but on the whole, the downward trend was relatively slow; after 45-day storage, when the moisture content dropped to approximately 76%, the changes of deformation were small and potato variation in other varieties had their own characteristics; the Netherlands 15#, Favorita and Fujin had less variation, while the Zaodabai and Youjin changed significantly, but the overall trend was the same. According to MATLAB software, the relational graph of storage time, moisture content and deformation amount of each variety was fitted. Due to the limited space, only the relational graph of Fujin potato variety was given in this paper, as shown in Fig.7.

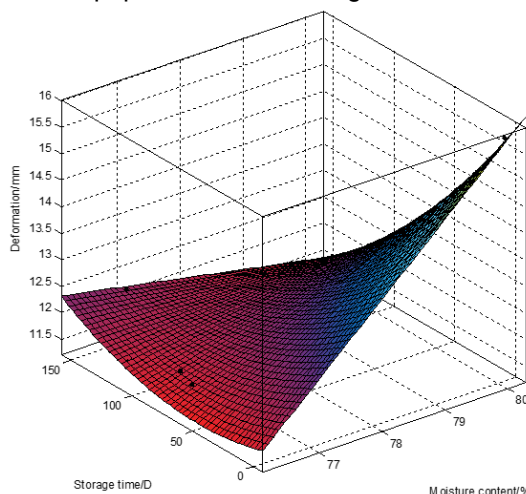


Fig. 7 - Relationship between deformation amount and moisture content

The reason analysis shows that the moisture content of potato is the main factor affecting its tissue cell turgor pressure. The freshly harvested potato with more moisture content shall have a higher internal cell turgor pressure. As the storage time increases, the moisture content gradually decreases, and the potato internal tissue gradually becomes more compact; besides, the degree of maturity increases, the hardness increases, and the ability to resist external loads becomes stronger, so the amount of deformation decreases. In comparison, in order to reduce the potato's compression damage during transportation, it is most reasonable to transport the potato in the minimal-deformation period.

The single-factor relational expression between the deformation and moisture content of five different varieties of potato was fitted by MATLAB software, which approximated by the cubic function relation, with the determination coefficient above 0.97. The related formula is expressed in Table 4.

Table 4

Fitting function of potato deformation and moisture content		
Varieties	Fitting function	R^2 determination coefficient
Zaodabai	$S(x) = 0.1261x^3 - 30.14x^2 + 2401x - 63750$	0.976
Favorita	$S(x) = -0.06224x^3 + 15.19x^2 - 1237x + 33580$	0.993
Netherland 15#	$S(x) = -0.06283x^3 + 15.37x^2 - 1254x + 34150$	0.987
Youjin	$S(x) = -0.2852x^3 + 68.23x^2 - 5440x + 14450$	0.991
Fujin	$S(x) = -0.06469x^3 + 15.32x^2 - 1209x + 31750$	0.982

Note: $S(x)$ is the maximum deformation displacement when the potato is placed flat, mm; x is the moisture content of the potato.

CONCLUSIONS

Through experiments on the static mechanical properties of different potato varieties in western Liaoning Province, the mechanical properties of the whole potato tubers and their variations were explored with different moisture contents, and the relations between moisture content and rupture force, elastic modulus, and maximum deformation of all five potato varieties were analysed. The main conclusions are made as follows:

(1) The moisture content of five varieties of potatoes in the period after harvest of 5 months has been studied. The moisture content of different varieties has similar change law. The moisture content of potatoes in the early harvest period is high. At about 60 days, the moisture content decreases to the lowest level, and then increases. Among them, the moisture content of Fujin is lowest.

(2) The moisture content greatly affects the mechanical properties of the potato such as rupture force, elastic modulus and deformation: the elastic modulus and rupture force increase with the decrease of the moisture content, and the deformation decreases with the decrease of the moisture content. The correlation coefficients of polynomial regression fitting are all above 0.95, indicating that the regression equation is well-fitted, and the numerical value changes regularly, which can be used for routine judgment.

(3) Potatoes with low moisture content show better static pressure mechanical property, therefore, from the perspective of reducing potato damage, storage and transportation should be made about 45-60 days after harvesting, when the moisture content drops below 80%, the hardness of potatoes increases, and the ability to resist deformation is improved to avoid damage.

ACKNOWLEDGEMENT

The authors gratefully acknowledge the national natural science foundation of China for its funding (51505305).

REFERENCES

- [1] Bentini M., Caprara C., Martelli R., (2009), Physico-mechanical properties of potato tuber during cold storage, *Biosystems Engineering*, vol.104, issue 1, pp.25-32;
- [2] Chen H.L., (2014), Research status and existing problems of potato harvesting machinery, *Scientific and technological information*, issue 20, pp.91;
- [3] Gao L.X., Jiao W.P., Yang D.X., Zhao Z.G., Zhao X.G., Liu D.J., (2012), Effect of moisture content on mechanical properties of soybean seed under static pressure, *Transactions of the Chinese Society for Agricultural Machinery*, vol.28, issue 15, pp.40-44;
- [4] Guo W.B., Wang C.G., Gao J., (2014), Study on Correlation between Starch Content and Parameters in Viscoelastic Model of Potato Tuber, *Transactions of the Chinese Society of Agricultural Engineering (Transactions of the CSAE)*, vol.1, issue 1, pp.191-193;
- [5] Li X.P., Xiong S., Geng L.X., Ji J.T., (2018), Effect of moisture content on the compressive properties of maize ear, *Journal of agricultural engineering*, vol.34, issue 2, pp.25-31;
- [6] Lu Q., (2016), Experimental study of potato injury mechanism and design of combine harvester, *Xi'an: northwest agriculture and forestry university*;
- [7] Ma Y., Gu R.X., (2003), Potato deep processing technology, *Beijing: China light industry press*, Issue 1, pp.35-36;

- [8] Scanlon M.G., Pang C.H., Biliaderis C.G., (1996), The effect of osmotic adjustment on the mechanical properties of potato parenchyma, *Food Research International*, vol.29, issue 5, pp.481-488;
- [9] Shen L.Y., Zhang H., Li Y., Tang Y., (2016), Experimental Study on Mechanical Properties of Wen 185 Walnut Kernel under Different Moisture Content, *Journal of Henan Agricultural Sciences*, vol.45, issue 7, pp.143-147;
- [10] Shi L.R., Wu J.M., (2014), Mechanical compression of whole tuber potato, *Journal of Northwest Ag-F University*, vol.42, issue 5, pp.190-196;
- [11] Sun G.Z., Zhang R.L., Tian K.Y. (2018), The dynamic evolution model and experimental study of gas permeability under multiple factors, *International Journal of Heat and Technology*, vol.36, issue 1, pp.49-55;
- [12] Tian S.L., Tian J.C., Ge X., (2015), Current situation and development prospect of Chinese potato storage technology, *Potato industry and modern sustainable agriculture*, China crop association potato professional committee, Issue 6;
- [13] Wang Y.M., Sun W., Wang G., (2015), Experimental Research on Compression Mechanical Properties of Potato, *Journal of agricultural mechanization research*, vol.626, issue 1, pp.191-193;
- [14] Wang Y.M., Sun W., Wang G.P., (2014), Study on mechanical damage in potato harvest, *Anhui agricultural science*, vol.42, issue 9, pp.2837-2840;
- [15] Wu Y.L., Guo Y.M., (2011), Research on the conventional mechanical properties of potatoes, *Proceedings of the Chinese academy of agricultural engineering 2011*, Chongqing: China agricultural engineering society;
- [16] Xiao J.M., (2013), A brief discussion on potato mechanization harvesting technology in western Liaoning province, *Modern agriculture*, vol.3, issue 33, pp.96;
- [17] Zhang F.W., Shi L.R., Wang L.J., Dai F., Han Z.S., (2014), Experimental Study on Mechanical Compression of Potato, *Advanced Materials Research*, vol.926-930, pp.993-996;
- [18] Zhang G.Z., Lu Y., (2015), The reasons and solutions for the decay of potato during storage, *Modern Agriculture*, issue 11, pp.76;
- [19] ***People's Daily, (2015), February 7, China.

THE INFLUENCE OF BULK MATERIAL FLOW ON TECHNICAL AND ECONOMICAL PERFORMANCE OF A SCREW CONVEYOR

ВПЛИВ ПОТОКУ СИПКОГО МАТЕРІАЛУ НА ТЕХНІКО-ЕКОНОМІЧНІ ПОКАЗНИКИ РОБОТИ ГВИНТОВОГО КОНВЕЄРА

Prof. Ph.D. Eng. Hevko R.B.¹⁾, Prof. Ph.D. Eng. Baranovsky V.M.²⁾, Prof. Ph.D. Eng. Lyashuk O.L.,²⁾
 Prof. Ph.D. Eng. Pohrishchuk B.V.¹⁾ Assoc. Prof. Ph.D. Eng. Gumeniuk Y.P.¹⁾ Assoc. Ph.D. Eng. Klendii O.M.,³⁾
 Assoc. Ph.D. Eng. Dobizha N.V.¹⁾

¹⁾Ternopil National Economical University / Ukraine; ²⁾Ternopil Ivan Puluj National Technical University,

³⁾Separated Subdivision of National University of Life and Environmental Sciences
 of Ukraine Berezahany Agrotechnical Institute / Ukraine;

E-mail: klendii_o@ukr.net

Keywords: flow movement, bulk material, impact of material particles, rational parameters, changes in energy consumption

ABSTRACT

The paper covers theoretical investigations of the movement of bulk material flow when it is fed by a pneumatic screw conveyor. Process calculation of the impact of bulk material particles during their transportation in guiding covers has been conducted. A mathematical model, which characterizes the overall energy spent on the impact of two particles, depending on impact velocity, physical and mechanical properties of bodies and impact conditions, has been developed. The limits of design and kinematic parameters that provide the effective application of pneumatic screw conveyors for transporting bulk materials have been defined.

РЕЗЮМЕ

В статті наведено теоретичні дослідження руху потоку сипких матеріалів при їх подачі пневмо-шнековими транспортерами. Проведено розрахунок процесу співудару частинок сипкого матеріалу під час його транспортування в направляючих кожухах. Побудовано математичну модель, яка характеризує загальну енергію, втрачену під час співудару двох частинок, залежно від швидкостей співудару, фізичко-механічних властивостей тіл та умов середовища удару. Встановлено межі конструктивно-кінематичних параметрів, які забезпечують ефективне застосування пневмо-шнекових транспортерів для переміщення сипких матеріалів

INTRODUCTION

There is a number of scientific works, which deal with the problems of material transportation in airflow (Ackerman N.I. and Shen H.H., 1982; Haydl H.M., 1986; Hewko B.M. et al., 2015; Hevko R. Et al., 2018; Hevko R.B. et al., 2017; Hevko R.B. et al., 2018; Li Y. and Li Y.Z. , 2008; Loveikin V. and Rogatynska L., 2011; Owen Philip J. and Cleary Paul W., 2010; Tian Y. Et. Al., 2018; Lyashuk O.L. et al., 2015; Lyashuk O.L. et al., 2018; Rogatynska O. et al., 2015; Rohatynskiy R.M. et al, 2016; Lech M., 2001; Roberts Alan W. and Bulk Solids, 2015; Yao Y.P. et al., 2014; Yoshihama S. et al., 2016). These works are aimed at solving the problems that are connected with the improvement of technical production performance of screw conveyors. The improvement of the process of bulk material transportation can be achieved by means of using the combination or the integration of their pneumatic and mechanical movement, taking into consideration material flow properties, which is covered in the papers (Humatylin R.I., 1987; Hychin B.M., 2000; Manjula E.V.P.J. and Hiromi W.K., 2017; Naveen Tripathi, 2015). In the process of conducting theoretical investigations, basic developments that are presented in the papers (Baranovsky V.M. et al., 2018; Hychin B.M., 2000; Loveikin V. and Rogatynska L., 2011; Rogatynska O. et al., 2015) were used. However, these problematic issues are not solved to the full extent. That is why, this paper is the continuation of our investigations, which are partially presented in the papers (Baranovsky V.M. et al., 2018; Hevko R.B. et al., 2018).

MATERIALS AND METHODS

In order to provide bulk material transportation in airflow in case it is fed by a screw feeder, pneumatic screw conveyors have been developed and their detailed design description is presented in the papers (Baranovsky V.M. et al., 2018; Hevko R.B. et al., 2018).

The movement of single particles or their separate groups in a pneumatic pipeline takes place under the action of the forces of a carrying air flow in the form of an air-fuel mixture. A distinction is made between two main kinds of pneumatic transport: general pneumatic transport (material parts are conveyed by an air flow along a pneumatic pipeline by means of “jumps”) and pneumatic transport with a continuous flow.

Let us consider the investigation of the process of bulk material transportation in case of its transportation in the form of a continuous flow.

The energy spent during the process of transportation in case of a pneumatic way of bulk material conveyance generally depends on the motion modes of the flow of bulk material parts. Motion modes of a particle flow are connected with physical and mechanical properties of the transported bulk materials, the design of a pneumatic transport unit, the geometry of a pipeline and its routing, the operation pressure and the travelling speed of a carrying flow motion, the consistency of bulk material feeding to a pipeline etc.

The main factors of physical and mechanical properties, which influence the motion modes of the flow of bulk material particles, are the following: density, particle size, coefficients of internal and external friction etc. The speed of flow motion is the dominant factor of the energy spent in the process of transportation. Energy spending during such a process is the minimum at wave and batch material movement in an aerated condition that is achieved due to the creation of an airflow, which is fed to a pipeline through inlet nozzles. It is typical of the process that is presented in Fig.1.

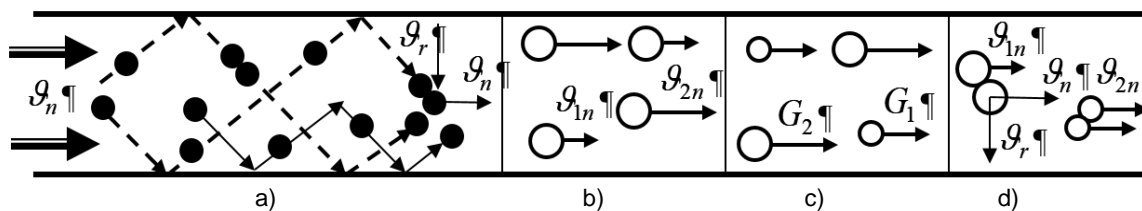


Fig. 1 - Motion patterns of the particles, which move in a pipeline
a) – particle movement types; b), c), d) – cases of the impact of particles

The main envelopes of the available motion modes of bulk material particle motion for the horizontal segments of a pipeline are presented in the form of the operation field of the three ways of conveying bulk materials in a pneumatic transport: continuous mass displacement, pneumatic conveyance while in flight of separate particles or groups of material particles in suspension, intermediate motion modes.

Formal characterization of the transportation process lies in the following – let us assume that, while in flight along a pipeline, particles of bulk material move only alongside forward and their form and mass remain.

In this case, there are three main characteristic movement types of particles or particle groups in the horizontal direction in the air flow of a pipeline relative to the contact with its internal surface (Fig. 1 a): along a lower wall, having impacts with a lower wall, having impacts with both walls.

The analysis of the motion modes of the flows of bulk material particles shows that they are followed by the relative motion of particles that have a very complex nature. On one side, due to various velocities of the translational motion of particles in a pipeline, they have relative displacement velocity and, on the other side, due to relative contacts (impacts) of particles, they acquire additional components of the travelling velocity of their random motion.

Material particles, which fly in a transport medium, collide only if their travelling velocities are different in value $g_{1n} \neq g_{2n}$ (Fig. 1 b) or in direction. The difference between the velocities of particles is particularly important, if particles differ significantly in their weight $G_1 \neq G_2$ (Fig. 1 c) or in air flow resistance force. However, particles of equal size can collide as well, if there are radial (normal) and tangential speeds (Fig. 1 a, d), besides axial (instantaneous) speeds that are equal for all the material parts.

Let us consider the impact process of the two spherical particles of bulk material, which move in the air flow of a pipeline following the pattern of contacting with the external surface of a pipeline (Fig. 1 a), here, let us consider the material of particles to be elastic.

The analytic model of the impact process of two spherical parts 1, 2 of bulk material is presented in Fig. 1, here, the impact process is considered in case of the movement of the two spherical particles after their contact with the pipeline wall 3.

According to the theory of granulated medium motion, it is known that at flow displacement, the velocity of particles is the sum of three related velocity components: the velocity of fluctuation, travelling (average) and rotational velocities, and, in case of solving the problems of displaced material flows, a kinetic theory of continuous gases is applied.

The analysis of the known state equation of bulk material during its movement $p(y)\bar{\varepsilon}(y) = \chi \left(\frac{d\vartheta}{dy} \right)^2$ shows that, on the right side, the product of the squared velocity of bulk material movement $d\vartheta/dy$ by the coefficient of the physical constant χ is identical to the specific value of the work, which is required for moving the layer of particles, calculated for 1 m², and, on the left side, the product of the hydrostatic pressure analog $p(y)$ by the dilatancy (porosity) of grain medium $\bar{\varepsilon}(y)$ in the physical meaning is identical to the kinetic energy of relative random particle motion due to the complex movement of bulk grain medium.

The interaction of two particles 1 and 2 takes place mostly due to the exchange of impact pulses on an oblique impact, here, the vectors \bar{g}_1 and \bar{g}_2 , which characterize impact velocities, are directed at the angle α_c to the horizon.

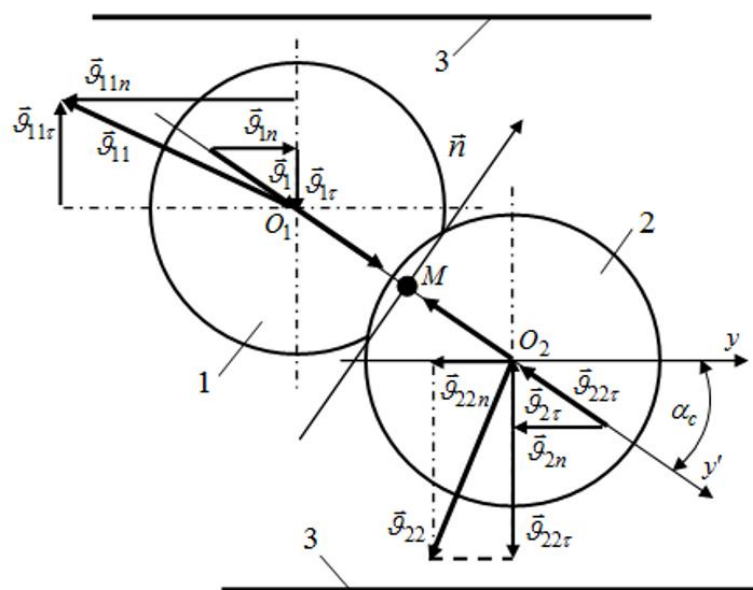


Fig. 2 - Calculation scheme of the impact process of bulk material particles

According to the law of energy conservation, the total sum energy E (J), which is spent during the impact of two particles 1 and 2 of a bulk material is the following:

$$E = \frac{1}{2} m_{1c} g_1^2 + \frac{1}{2} m_{2c} g_2^2 - \frac{1}{2} m_{1c} g_{11}^2 - \frac{1}{2} m_{2c} g_{22}^2 \quad (1)$$

where m_{1c} , m_{2c} – the reduced mass of the particles 1 and 2, kg, respectively; g_1 , g_2 – the movement velocity of the particles 1 and 2 before the impact, m/s, respectively; g_{11} , g_{22} – the movement velocity of the particles 1 and 2 after the impact, m/s, respectively.

After the reduction of (1), we obtain:

$$E = \frac{1}{2} m_{1c} (g_1^2 - g_{11}^2) + \frac{1}{2} m_{2c} (g_2^2 - g_{22}^2) \quad (2)$$

Having denoted the difference in velocities $(g_1^2 - g_{11}^2)$ and $(g_2^2 - g_{22}^2)$ by Δg_1 and Δg_2 , respectively, and having taken into consideration that $m_{ic} = V_{ic} \rho = \rho \pi d_{ic}^3 / 6$, where $V_{ic} = \pi d_{ic}^3 / 6$ – the volume of the particle i (m³), d_{ic} – the diameter of the particle i (m), we can write down the following:

$$E = \frac{1}{12} \pi d_{1c}^3 \rho (\Delta \mathcal{G}_1)^2 + \frac{1}{12} \pi d_{2c}^3 \rho (\Delta \mathcal{G}_2)^2 = \frac{1}{12} \pi \rho \left[d_{1c}^3 (\Delta \mathcal{G}_1)^2 + d_{2c}^3 (\Delta \mathcal{G}_2)^2 \right] \quad (3)$$

Let us determine the components of the difference in before-impact and after-impact velocities $\Delta \mathcal{G}_1$ and $\Delta \mathcal{G}_2$ from the following considerations.

Random particle movement results in the transverse mass transfer (of particles), which is followed by the transfer of the impulse, the carriers of which are the particles that move with various velocities depending on the coordinates, which results in the intensity of the relative movement of bulk material particles.

According to Gauss hypothesis, it is known that the connection between the values of contacting and normal impulses on impact is formed similar to Coulomb's law for friction

$$\Delta \mathcal{G} = -f(1+k)\mathcal{G}' \quad (4)$$

where $\Delta \mathcal{G}$ – the change of relative tangential velocity, as a result of an impact, m/s; \mathcal{G}' – the velocity of particle fluctuation, m/s; k – the coefficient of recovery on impact.

The velocity of fluctuation \mathcal{G}' characterizes the coefficient of transverse quasi-diffusion $D_{kd} = 0.5 \mathcal{G}'s$, where s – the average distance between the particles relative to their reduced mass (m), which, in its turn, regulates the intensity of the relative motion of bulk material particles. Here, the intensity of particle motion increases proportionally to D_{kd} and to the velocity gradient $d\mathcal{G}/dy$ of relative particle motion in the direction of their displacement velocity.

However, the dependence (4) does not take into account the physical properties of the surfaces of the particles, which collide at the contact point M .

In addition, it is known that the closest relationship between the values of contacting and normal impulses on impact is described by "λ-hypothesis", according to which, the change in the relative tangential velocity $\Delta \mathcal{G}$ as a result of the impact of colliding points is proportional to the before-impact value of this velocity \mathcal{G}

$$\Delta \mathcal{G} = -\bar{\lambda} \mathcal{G} \quad (5)$$

where $\bar{\lambda}$ – the average value of the coefficient that characterizes the properties of the surfaces of the particles, which collide; \mathcal{G} – the before-impact velocity of a particle, m/s.

Having taken into account the peculiarities of the problem of the impact of two spherical bodies, let us apply these two hypotheses (4), (5) by means of their combination or considering them when determining the change in the relative tangential velocity $\Delta \mathcal{G}$, which is the result of the collision of two bodies.

Having taken into account the scheme of the impact process (Fig. 2) and the fact that

$$k = \mathcal{G}_{ii} / \mathcal{G}_i = \frac{dS_{ii}}{dt} / \frac{dS_i}{dt} = \frac{dS_{ii}}{dS_i}, \text{ where } \mathcal{G}_{ii}, \mathcal{G}_i \text{ – the velocity of the } i \text{ particle before and after the impact, respectively, m/s; } dS_{ii}, dS_i \text{ – the distance covered by the } i \text{ particle before and after the impact, respectively, (m); } t \text{ – particle movement time, (s), let us combine these two borderline cases (4), (5) by a continuous function in the form of:}$$

respectively, m/s; dS_{ii}, dS_i – the distance covered by the i particle before and after the impact, respectively, (m); t – particle movement time, (s), let us combine these two borderline cases (4), (5) by a continuous function in the form of:

$$\left. \begin{aligned} \Delta \mathcal{G}_1 &= -f \left(1 + \frac{dS_{11}}{dS_1} \right) \mathcal{G}'_1 \sin^2 \alpha_1 - \bar{\lambda} \frac{dS_1}{dt} \cos^2 \alpha_1; \\ \Delta \mathcal{G}_2 &= -f \left(1 + \frac{dS_{22}}{dS_2} \right) \mathcal{G}'_2 \sin^2 \alpha_2 - \bar{\lambda} \frac{dS_2}{dt} \cos^2 \alpha_2 \end{aligned} \right\} \quad (6)$$

where

α_1, α_2 – the angle between the velocity vector of the impact of the particles 1 and 2 and the impact line y' , respectively (deg.).

Having substituted the values of the corresponding velocity components from (6) into the dependence (3), we obtain:

$$E = \frac{1}{2} \pi \rho f^2 \left\{ \begin{aligned} & d_{1c}^3 \left[\left(1 + \frac{dS_{11}}{dS_1} \right) \mathcal{G}'_1 \sin^2 \alpha_1 - \bar{\lambda} \frac{dS_1}{dt} \cos^2 \alpha_1 \right]^2 + \\ & d_{2c}^3 \left[\left(1 + \frac{dS_{22}}{dS_2} \right) \mathcal{G}'_2 \sin^2 \alpha_2 - \bar{\lambda} \frac{dS_2}{dt} \cos^2 \alpha_2 \right]^2 \end{aligned} \right\} \quad (7)$$

In order to simplify the solution of the problem, let us assume that the particles 1 and 2 of bulk material are of the same mass, that is to say $m_{1c} = m_{2c} = m_c$, here, the correct identities are the following: $d_{1c} = d_{2c} = d_c$, $\mathcal{G}'_1 = \mathcal{G}'_2 = \bar{\mathcal{G}}'$, $\alpha_1 = \alpha_2 = \alpha$, respectively, where d_{1c} , d_{2c} , d_c – the diameter of the particles 1 and 2 and the average particle diameter, respectively, (m).

Thus, having taken into account this assumption, let us write the dependences (3) and (6) in a simplified form:

$$E = \frac{1}{12} \pi d_c^3 \rho \left[(\Delta \mathcal{G}_1)^2 + (\Delta \mathcal{G}_2)^2 \right] \quad (8)$$

$$\left. \begin{aligned} \Delta \mathcal{G}_1 &= -f \left(1 + \frac{dS_{11}}{dS_1} \right) \bar{\mathcal{G}}' \sin^2 \alpha_c - \bar{\lambda} \frac{dS_1}{dt} \cos^2 \alpha_c; \\ \Delta \mathcal{G}_2 &= -f \left(1 + \frac{dS_{22}}{dS_2} \right) \bar{\mathcal{G}}' \sin^2 \alpha_c - \bar{\lambda} \frac{dS_2}{dt} \cos^2 \alpha_c \end{aligned} \right\} \quad (9)$$

where $\bar{\mathcal{G}}'$ – the average value of the velocity of particle fluctuation, m/s.

Having substituted the values of the corresponding velocity components from (9) into the dependence (8) and after the transformation and the simplification of the expression, we obtain:

$$E = \frac{1}{2} \pi d_c^3 \rho \left\{ \begin{aligned} & f^2 (\mathcal{G}')^2 \cos^4 \alpha_c \left[\left(1 + \frac{dS_{11}}{dS_1} \right)^2 + \left(1 + \frac{dS_{22}}{dS_2} \right)^2 \right] - \\ & 2f \bar{\lambda} \mathcal{G}' \sin^2 \alpha_c \cos^2 \alpha_c \left[\left(1 + \frac{dS_{11}}{dS_1} \right) \frac{dS_1}{dt} + \left(1 + \frac{dS_{22}}{dS_2} \right) \frac{dS_2}{dt} \right] + \\ & + \bar{\lambda}^2 \cos^4 \alpha_c \left[\left(\frac{dS_1}{dt} \right)^2 + \left(\frac{dS_2}{dt} \right)^2 \right] \end{aligned} \right\} \quad (10)$$

The dependence (10) is a mathematical model, which characterizes the general energy that is spent during one impact of two spherical particles of bulk grain material, depending on the velocity components of the impact process, physical and mechanical properties of colliding bodies and the conditions of impact medium. This model can be used in order to analyse the accepted expression of the “temperature of grain medium” and, further, bulk material state during particle movement in a pipeline.

If the assumption is made that the coefficients of the recovery of the particles 1 and 2 on their impact are maximally adequate or even equal in their value, then the dependence (10) can be written in the following form:

$$E = \pi d_c^3 \rho \left\{ \begin{aligned} & f^2 (\mathcal{G}')^2 (1+k)^2 \cos^4 \alpha_c - \\ & -(1+k) f \bar{\lambda} \mathcal{G}' \sin^2 \alpha_c \cos^2 \alpha_c \left(\frac{dS_1}{dt} + \frac{dS_2}{dt} \right) + \\ & + 0,5 \bar{\lambda}^2 \cos^4 \alpha_c \left[\left(\frac{dS_1}{dt} \right)^2 + \left(\frac{dS_2}{dt} \right)^2 \right] \end{aligned} \right\}. \quad (11)$$

RESULTS

Fig. 3 presents the characteristic curve of the change in the general energy E spent during one impact of two spherical particles of bulk material depending on: a – the coefficient of recovery k and the coefficient of the internal friction f ; b – the diameter of the particles d_c and the angle between the vector of impact velocity and the line of collision α_c ; c – the diameter of particles d_c and the bulk weight of material ρ .

The analysis of the graphical plotting shows that if the coefficient of recovery k increases within the limits of $0 \leq k \leq 1$ and the coefficient of internal friction f increases within the limits of $0 \leq f \leq 1$, the general energy E spent on the impact of two spherical particles of bulk material increases on average from 0.1 to 0.3 J (Fig. 3, a), here, the dominant factor of the change in E is the coefficient of recovery k .

The increase of the energy E (Fig. 3, b, c) spent on the impact of two particles with the diameter of $d \leq 0.002$ (s) is not significant and its average value is 0.01 J, if there is a change in the angle between the vector of impact velocity and the line of collision α_c within the limits of $0 \leq \alpha_c \leq 0.5$ (rad) and the change in bulk weight within the limits of $900 \leq \rho \leq 1500$ (kg/m³), and with further increase of α_c the increase in energy spending E is practically near zero (Fig. 3, b). Significant energy E spending takes place during the transportation of particles with the diameter of more than 2 mm, here, there is a sharp increase of E from 0.02 to 0.14 J for $\rho = 1300$ kg/m³ (Fig. 3, b) or from 0.05 to 0.3 J (Fig. 3 c).

In order to provide a contact (impact) of the particles 1 and 2, the angle α_c (Fig. 2) must be within the limits of the interval $(0, \pi/2)$.

Having taken into account that particle movement in a flow of a pipeline has a complex nature, let us write the kinetic energy of relative bulk medium movement in the form of the sum of particle kinetic energies in their relative translational motion during their displacement and during their random motion in the process of transverse mass transfer, that is to say:

$$E_c = E_g + E_{g'} + E_n \quad (12)$$

where:

E_c – the kinetic energy of particle relative motion;

(J); E_g , $E_{g'}$, E_n – the kinetic energy of translational motion, random motion (fluctuation) and transverse mass transfer of bulk medium particles, respectively, (J).

Correspondingly, the kinetic energy of the particles in their relative translational motion in the direction of their displacement E_g , in their random motion (fluctuation) $E_{g'}$ and in the process of transverse mass transfer E_n of the particles of a bulk medium, is determined from the following expressions

$$\left. \begin{aligned} E_g &= \frac{1}{12} \pi d_c^3 \rho (\Delta y)^2 \left(\frac{d\mathcal{G}}{dy} \right)^2; \\ E_{g'} &= \frac{1}{2} \frac{\pi d_c^3}{6} \rho (\mathcal{G}')^2 = \frac{2\pi d_c^3}{3} \rho v_c^2 s^2; \\ E_n &= \frac{1}{4} \frac{\pi d_c^3}{6} \rho s \mathcal{G}' \frac{d\mathcal{G}}{dy} = \frac{1}{12} \pi d_c^3 \rho v_c s^2 \frac{d\mathcal{G}}{dy} \end{aligned} \right\} \quad (13)$$

where:

Δy – the difference in the coordinates of the particles' centres of the adjacent layers of a bulk medium, (m);

v_c – the average frequency of the impact of bulk medium particles, (1/s).

Here,

$$\Delta y = c_1 - c_2; \quad \mathcal{G}' = 2s v_c \quad (14)$$

where: c_1 , c_2 – the centre coordinates of the adjacent layers, respectively, and the average frequency of an impact v_c is determined by means of Ackerman-Shen method:

$$v_c = \frac{\tau}{K_d N} \frac{d\mathcal{G}}{dy}, \quad (15)$$

Where:

τ – displacement potential, (Pa); K_d – the dissipation of the kinetic energy of particle impact on one contact, (J); N_c – the number of particles per unit layer volume, (1/m³).

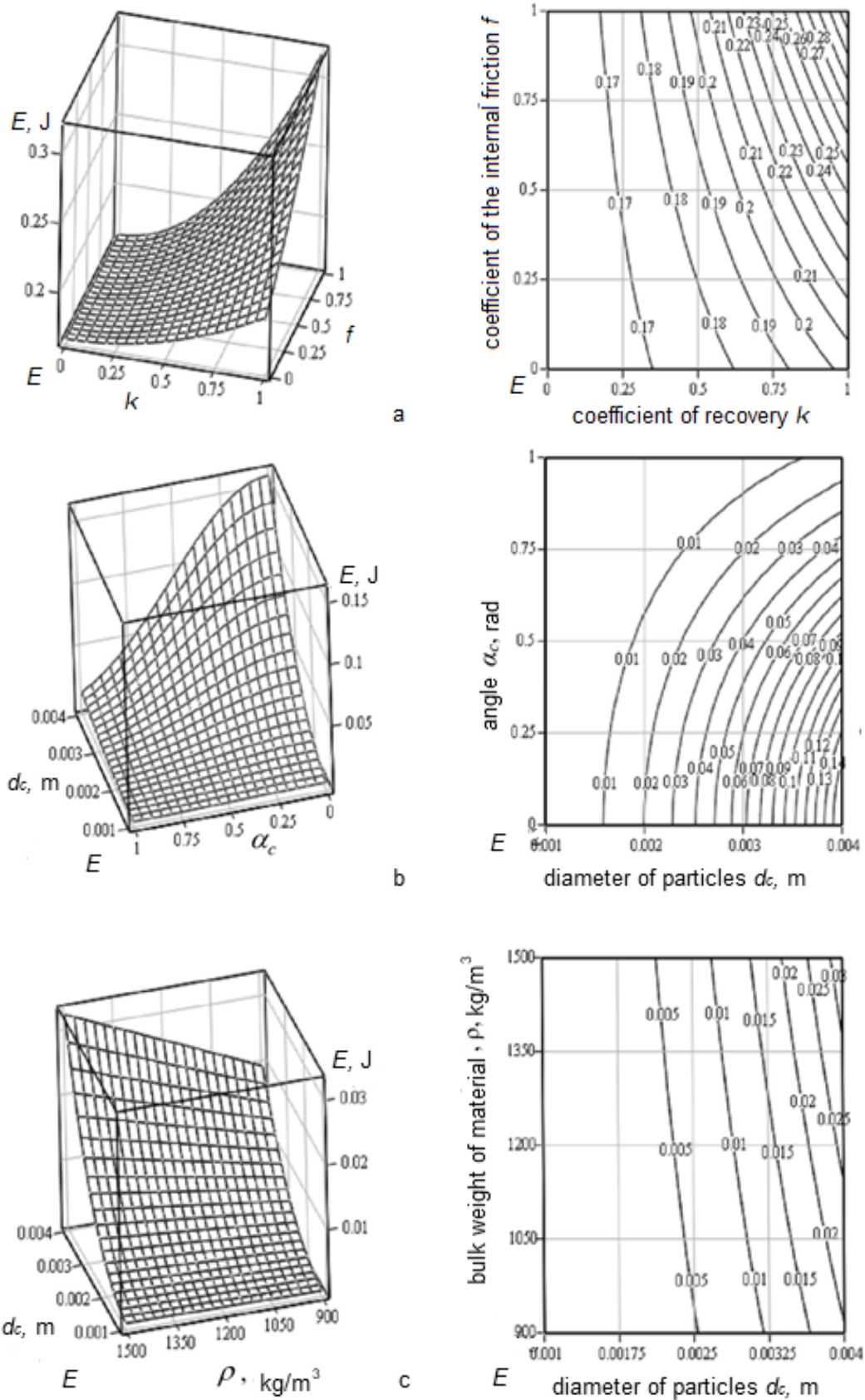


Fig. 3 - Energy change dependence as a function:
 a - $E = f(f, k)$, b - $E = f(d_c, \alpha_c)$, c - $E = f(d_c, \rho)$

The dissipation of the kinetic energy K_d of the impact of particles on one contact is determined from Ackerman-Shen formula:

$$K_d = \frac{1}{12} \pi d_c^3 \rho \left(\frac{1-k^2}{4} + \frac{f(1+k)}{\pi} - \frac{f^2(1+k)^2}{4} \right) (\mathcal{G}')^2 \quad (16)$$

Then, according to (14), (15) and (16), the average frequency of the impact ν_c of bulk medium particles is determined as follows:

$$\nu_c = \frac{24\tau}{d_c^3 \rho \left[\pi(1-k^2) + 4f(1+k) - \pi f^2(1+k)^2 \right] (\mathcal{G}')^2 N} \frac{d\mathcal{G}}{dy}. \quad (17)$$

Having substituted the values of Δy from (14) and the values of ν_c from (17) into the equation (13), we obtain:

$$\left. \begin{aligned} E_g &= \frac{1}{12} \pi d_c^3 \rho (c_1 - c_2)^2 \left(\frac{d\mathcal{G}}{dy} \right)^2; \\ E_{g'} &= \frac{2\pi s^2}{3d_c^3 \rho} \left(\frac{24\tau}{\left[\pi(1-k^2) + 4f(1+k) - \pi f^2(1+k)^2 \right] (\mathcal{G}')^2 N} \right)^2 \left(\frac{d\mathcal{G}}{dy} \right)^2 \\ E_n &= \frac{2\pi s^2 \tau}{\left[\pi(1-k^2) + 4f(1+k) - \pi f^2(1+k)^2 \right] (\mathcal{G}')^2 N} \left(\frac{d\mathcal{G}}{dy} \right)^2. \end{aligned} \right\} \quad (18)$$

Thus, having substituted (18) into (13) and after the transformation and the simplification of the expression, the kinetic energy E_c of the relative motion of bulk material particles is determined by the following dependence

$$E_c = \frac{\pi}{12} \left[d_c^3 \rho (c_1 - c_2)^2 + s^2 \left(\frac{8\Omega^2}{d_c^3 \rho} + \Omega \right) \right] \left(\frac{d\mathcal{G}}{dy} \right)^2 \quad (19)$$

where $\Omega = \frac{24\tau}{\left[\pi(1-k^2) + 4f(1+k) - \pi f^2(1+k)^2 \right] (\mathcal{G}')^2 N}$.

The equation (19) characterizes the so called “temperature of grain medium” during the relative motion of bulk medium particles.

Having taken into consideration (19), the known equation $p(y)\bar{\varepsilon}(y) = \chi(d\mathcal{G}/dy)^2$ of a bulk material state during its motion can be written in the following form

$$p\bar{\varepsilon} = \chi' \frac{\pi}{12} \left[d_c^3 \rho (c_1 - c_2)^2 + s^2 \left(\frac{8\Omega^2}{d_c^3 \rho} + \Omega \right) \right] \left(\frac{d\mathcal{G}}{dy} \right)^2 \quad (20)$$

where χ' – the coefficient of the physical constant, which is identical to the specific value of work that is required for moving the layer of particles, calculated for 1 m²; $\bar{\varepsilon}$ – the average porosity of a grain medium.

The obtained dependence (20) can be used for further analysis and substantiation of the process flow parameters of pneumatic screw conveyors.

CONCLUSIONS

The article presents the design of a pneumatic screw conveyor, which provides bulk material transportation with less dust concentration due to impulse air feeding.

The calculation of the impact process of bulk material particles during their transportation in a pipeline has been conducted. In addition, a mathematical model, which characterizes the general energy spent on the impact of two particles, depending on impact velocities, physical and mechanical body properties and impact medium conditions, has been developed.

It has been determined that the increase of the energy E spent on the impact of two particles with the diameter of $d \leq 0.002$ (m) is insignificant and on average it equals 0.01 (J) on the change of the angle between the vector of impact velocity and the collision line α_c within the limits of $0 \leq \alpha_c \leq 0.5$ (rad) and of the bulk weight within the limits of $900 \leq \rho \leq 1500$ (kg/m³), and with further increase of α_c , the energy E spending is practically near zero. Significant energy spending E takes place during the transportation of the particles, the diameter of which is more than 2 mm, here, there is a sharp increase of E from 0.02 to 0,14 (J) for $\rho = 1300$ (kg/m³) or from 0.05 to 0.3 (J).

REFERENCES

- [1] Ackerman N.I., Shen H.H., (1982), Stresses in rapidly Fluid–Solid Mixtures, *Journal of the Engineering Mechanics Division- ASCE*, vol.108, pp. 95-113;
- [2] Baranovsky V.M., Hevko R.B., Dzyura V.O., Klendii O.M., Klendii M.B., Romanovsky R.M., (2018), Justification of rational parameters of a pneumoconveyor screw feeder, *INMATEH: Agricultural Engineering*, vol.54, no.1., pp. 15-24, Bucharest/Romania;
- [3] Haydl H.M., (1986), Design aspects of large-diameter tubular conveyor galleries, *Proceedings of the institution of civil engineers, Part 1 – Design and construction*, Vol. 80, pp. 633-639, London/England;
- [4] Humatylin R.I., (1987), *Dynamics of multiphase mediums (Динамика многофазовых сред)*, by publishing “Nauka” (Издательство Наука), 1987, 464 p., Moscow/Russia;
- [5] Hevko B.M., Hevko R.B., Klendii O.M., Buriak M.V., Dzyadykevych Y.V., Rozum R.I., (2018), Improvement of machine safety devices. *Acta Polytechnica, Journal of Advanced Engineering*, Vol.58, no.1, pp.17-25, Prague/Czech Republic;
- [6] Hevko B.M., Popovich P.V., Diachun A.Y., Lyashuk O.L., RO Liubachivskiyi, (2015), The study of bulk material kinematics in a screw conveyor-mixer, *INMATEH Agricultural Engineering*, vol.47, no.3., pp. 156-163, Bucharest/Romania;
- [7] Hevko R., Brukhanskyi R., Flonts I., Synii, S. Klendii O. (2018), Advances in Methods of Cleaning Root Crops, *Bulletin of the Transilvania University of Braşov, Series II*, vol.11(60), pp.127-138, Braşov/Romania;
- [8] Hevko R.B., Yazlyuk B.O., Liubin M.V., Tokarchuk O.A., Klendii O.M., Pankiv V.R. (2017) - Feasibility study of mixture transportation and stirring process in continuous-flow conveyors, *INMATEH Agricultural Engineering*, vol.51, no.1, pp.49-59, Bucharest/Romania;
- [9] Hevko R.B., Liubin M.V., Tokarchuk O.A., Lyashuk O.L., Pohrishchuk B.V., Klendii O.M. (2018) - Determination of the parameters of transporting and mixing feed mixtures along the curvilinear paths of tubular conveyors, *INMATEH Agricultural Engineering*, vol.55, no.2, pg.97-104, Bucharest/Romania;
- [10] Hevko R.B., Strishenets O.M., Lyashuk O.L., Tkachenko I.G., Klendii O.M., Dzyura V.O., (2018), Development of a pneumatic screw conveyor design and substantiation of its parameters, *INMATEH: Agricultural Engineering*, vol.54, no.1, pg.153-160, Bucharest/Romania;
- [11] Hychin B.M., (2000), Recovery of the movement structure of air-fuel mixtures in a pneumatic transporting pipeline (Восстановление структуры движения аэросмесей в пневмотранспортном трубопроводе), *Bulletin of National Technical University of Ukraine KPI. Mechanical Engineering (Вестн. Нац. Техн. Ун-та України КПІ. Машиностроєння)*, vol. 38, no. 2, pp. 158-162, Kyiv/Ukraine;
- [12] Lech M., (2001), Mass flow rate measurement in vertical pneumatic conveying of solid, *Powder Technology*, Vol.114, Issues 1–3, pp. 55-58;
- [13] Li Y., Li Y.Z., (2008), New equipment for bulk cargo conveying screw-gas bulk sucking and taking equipment, *6th International Conference on Material Handling (ICMH 2008)*, pp. 243-247, Shanghai/China;
- [14] Loveikin V., Rogatynska L., (2011), A Model of Loose Material Transportation by Means of High-Speed Conveyors with Elastic Operating Devices (Модель транспортування сипкого вантажу швидкохідними гвинтовими конвеєрами з еластичними робочими органами). *Bulletin of I.Pyliui Ternopil National Technical University (Вісник ТНТУ ім. І.Пуллюя)*, Vol.16, pp.66-70, Ternopil/Ukraine;

- [15] Lyashuk O.L., Rogatynska O.R., Serilko D.L., (2015), Modelling of the vertical screw conveyor loading, *INMATEH Agricultural Engineering*, vol.45, no.1, pp.87-94, Bucharest/Romania;
- [16] Lyashuk O.L., Sokil M.B., Klendiy V.M., Skyba O.P., Tretiakov O.L., Slobodian L.M., Slobodian N.O. (2018) - Mathematical model of bending vibrations of a horizontal feeder-mixer along the flow of grain mixture, *INMATEH Agricultural Engineering*, vol.55, no.2, pp.35-44, Bucharest/Romania;
- [17] Manjula E.V.P.J., Hiromi W.K. Ariyaratne, Ratnayake Chandana, Morten C. Melaaen, (2017), A review of CFD modelling studies on pneumatic conveying and challenges in modelling offshore drill cuttings transport, *Powder Technology*, Vol.305, pp.782-793;
- [18] Owen, Philip J., Cleary, Paul W. (2010) - Screw conveyor performance: comparison of discrete element modelling with laboratory experiments. *Progress in computational fluid dynamics*, Vol. 10, Issue 5-6, pp.327-333, Geneva/ Switzerland;
- [19] Tian Y., Yuan P., Yang F., Gu J., Chen M., Tang J., Su Y., Ding T., Zhang K., Cheng Q. (2018) - Research on the Principle of a New Flexible Screw Conveyor and Its Power Consumption, *Applied Sciences*, vol.8, no.7;
- [20] Tripathi Naveen, Sharma Atul, Mallick S.S., Wypych P.W., (2015), Energy loss at bends in the pneumatic conveying of fly ash, *Particuology*, vol.21, pp. 65-73;
- [21] Rogatynska O., Liashuk O., Peleshok T., Liubachivskyi R., (2015), Investigation of the Process of Loose Material Transportation by Means of Inclined Screw Conveyors (Дослідження процесу транспортування сипкого вантажу похилими гвинтовими конвеєрами), *Bulletin of I.Pyliui Ternopil National Technical University (Вісник ТНТУ ім. І.Пулюя)*, Vol.79, pp.137-143, Ternopil/Ukraine;
- [22] Roberts Alan W., Bulk Solids, (2015), Optimizing Screw Conveyors. *Chemical engineering*. Vol.122 (2), pp.62-67, New York/USA;
- [23] Yao Y.P., Kou Z.M., Meng W.J., Han G., (2014), Overall Performance Evaluation of Tubular Scraper Conveyors Using a TOPSIS-Based Multiattribute Decision-Making Method, *Scientific World Journal*, New York/USA;
- [24] Yoshihama S., Takano S., Yamada Y., Nakamura T., Kato K., (2016), Powder Conveyance Experiments with Peristaltic Conveyor using a Pneumatic Artificial Muscle, *IEEE ASME International Conference on Advanced Intelligent Mechatronics*, pp. 1539-1544, Banff/Canada.

THE NUMERICAL SIMULATION OF HYDRODYNAMICS AND MASS TRANSFER PROCESSES FOR VENTILATING SYSTEM EFFECTIVE LOCATION

/

ЧИСЕЛЬНЕ ДОСЛІДЖЕННЯ ГІДРОДИНАМІКИ І ТЕПЛОПЕРЕНОСУ У ПТАШНИКУ ДЛЯ ЕФЕКТИВНОГО РОЗМІЩЕННЯ ВЕНТИЛЯЦІЙНОГО ОБЛАДНАННЯ

Prof. Ph.D. Eng. Gorobets V.G.¹⁾, Senior lecturer Ph.D. Eng. Trokhaniak V.I.¹⁾,
Assoc. Prof. Ph.D. Eng. Rogovskii I.L.¹⁾, Senior lecturer Ph.D. Eng. Titova L.L.¹⁾,
Senior lecturer Ph.D. Eng. Lendiel T.I.¹⁾, Assoc. Prof. Ph.D. Eng. Dudnyk A.O.¹⁾, PhD student Masiuk M.Yu.¹⁾.

¹⁾ National University of Life and Environmental Sciences of Ukraine;
E-mail: Trohaniak.v@gmail.com

Keywords: *computational fluid dynamics, heat and mass transfer processes, poultry house, ventilation equipment*

ABSTRACT

In this paper the numerical evaluation for heat and mass transfer during the air ventilation in poultry houses' premises was provided. The analysis of the proposed conditions for heat and mass transfer in poultry houses depends on the ventilators location in the poultry house's altitude. The efficiency of this equipment's location was determined. The observed climate-control supporting system for poultry-houses is based on the external air cooling by water from underground wells. The simulation was made for 2D computational fluid dynamics (CFD) analyses by ANSYS Fluent software. The CFD analysis for the air flow analysis scheme CFD and heat condition inside the poultry house was proposed. The geometrical ventilation equipment and the best ways of its location in the poultry house were found by the results of numerical simulation.

РЕЗЮМЕ

У роботі проведено чисельне моделювання процесів тепло- і масопереносу при вентиляції повітря в птахівничих приміщеннях. Проведений аналіз умов тепло- і масопереносу у пташнику в залежності від розміщення вентиляторів по висоті пташника та визначена ефективність розташування такого обладнання. Система підтримання мікроклімату в пташниках розглядалась при наявності системи охолодження зовнішнього повітря водою з підземних сверловин. Моделювання проведено для 2D CFD моделей за допомогою програмного забезпечення ANSYS Fluent. Представлені результати CFD аналізу схеми потоку повітря і теплового стану всередині пташника. В результаті чисельних досліджень знайдено геометрію розташування вентиляційного обладнання, при якій умови вентиляції птахівничих приміщень будуть найкращими.

INTRODUCTION

There are some ventilating equipment systems that depend on the air vent and exhaust ventilator location (Campbell J. et al., 2007). The present analysis showed that the most energy efficient ventilation system is the tunnel ventilation. This system would be chosen as the base during the modulation and numerical simulation of heat and mass transfer in poultry houses premises (Curi T. et al. 2017).

A paper (Zajicek M., Kic P., 2013) researched the influence of maximum air exchange and intensive cooling of poultry by the high air velocities during the poultry houses ventilation in the summer period of the year. The air exchange numerical simulation in different configurations of ventilating systems inlet and outlet holes were executed by ANSYS Fluent software. The dimensions and forms of inlet holes and their locations on the poultry houses' walls were changed during the stimulation of heat and mass transfer in poultry houses premises.

The CFD simulation of airflow and heat and mass transfer in poultry houses premises are provided in the paper. The side ventilation system is used in this process. The authors (Blanes-Vidal V. et al., 2008; Bustamante E. et al., 2017) considered that the method of side mechanical ventilation system is the most effective in comparison with other methods. It allows decreasing the heat stress and poultry productivity increase during the summer period of the year. The results of numerical simulation were compared with the data of experimental researches. The deviation was of 12%. The authors (Blanes-Vidal V. et al., 2008;

Bustamante E. et al., 2017) have concluded that the non-enough air velocity and the absence of the cooling system resulted in productivity decrease during the poultry growing. This absence favours the non-homogeneity of air flow and the existence of stagnation zone decreases the conditions for poultry's thermal regulation.

Another paper (*Zajicek M. and Kic P., 2012*) presents the CFD solution of miscellaneous improved cases for the various flow and shape configurations of the poultry house. Effects of the transversal and longitudinal ventilation are combined with the changes of inlet air streams directions and also with the different cross-section shaping obtained using curtains.

This paper is the next stage of researches for supporting the climate-control systems in poultry houses (*Gorobets V.G. et al. 2018*). The cooling system for external air by special construction heat exchanger is observed. The underground wells' water is used as cooling medium in these heat exchangers.

MATERIALS AND METHODS

In this paper is observed the effective location of exhausting ventilation equipment in poultry-house's altitude. The measures are directed for the ventilating system improving and microclimate enhancement. The observed air cooling system is based on the water usage from underground well and heat exchanger recuperators. (*Gorobets V.G. et al., 2018*). The specified technique allows decreasing the external air temperature without increasing their relative humidity comparing with the cooling system of water spraying. The paper's aim is to propose theoretical researches connecting with the heat and mass transfer in poultry houses. These processes run inside the house and run through its walls, by the geometry ventilators location change.

The poultry house of standard type has the following main characteristics:

- Building's data – 90x20x5m
- External barriers are made of claydite – concrete with thickness of 0.2 m.
- External air temperature in the summer period +40°C.
- Building's volume 7200 m³.
- Internal air temperature as per norm +17°C

The research of heat exchange and mass transfer in poultry houses is the basic aim of the present paper. The height of the ventilating equipment has important value for decreasing the stagnation zones dimension. These zones are characterized by the high temperature of heated air in poultry houses and by the decrease of growing poultry productivity. These researches allow to evaluate the hydrodynamic and heat conditions for supporting a normalized microclimate and to determine the efficiency of present ventilation system operating. The air velocity in the poultry house is within: 2.58 through 1.64 m/s with average temperature +27°C (*Gorobets V.G. et al., 2018*) according to the standards. The evaluated average value is 1.97 m/s and it is at the border «Inlet_2D» (see fig.2a). The views of rear and lateral surfaces in 2-D mode are showed schematically in Figure 1. This line runs through the centreline of separate ventilators.

The poultry is kept in the floor storage mode. Poultry is the source of heat generation. The general quantity of poultry is 1000 heads. The distance between the poultry and the ventilating equipment should not be less than 3 m. The barrier is installed on the border with the poultry. It is designed for avoiding the poultry entrance into the ventilators. These barriers protect the equipment against poultry break. The barrier influence was not considered on the hydrodynamics and heat transfer for the simplifying model. The safe distance was chosen for the poultry and ventilators in spite of it. The poultry's average temperature was accepted +41°C. The poultry's high concentration was considered and accepted 7 heads per 1m². The present source of heat generation around the floor was accepted at +41°C (fig.2b). The exhausting ventilating equipment of the present system was supplied with an accepted diameter of the wheel of 1.25 m. The ventilators were located at the height of 1.125, 1.5 and 1.875 m to the centre line of ventilators (see fig.1).

The proposed poultry houses' hydrodynamic flow and thermal fields' analysis (*Gorobets V.G., et al., 2018*) showed the best conditions for vertical areas. These flows run through the ventilator's centre. These flows slightly changed independently from the ventilator's location toward to lateral walls. Some differences were only observed for extreme ventilators. They didn't influence on the general view of flow and temperature separation in the whole poultry. The 2D model may be used during the modeling. This way

facilitates the numerical simulation without influence on the physical data of heat exchange and mass transfer in poultry houses premises. The calculations were done from the centreline through the poultry house length. (Gorobets V.G. et al. 2018). The air velocity alignment was observed through all cross sections of premises and it became the same on the first approximation through the whole section.

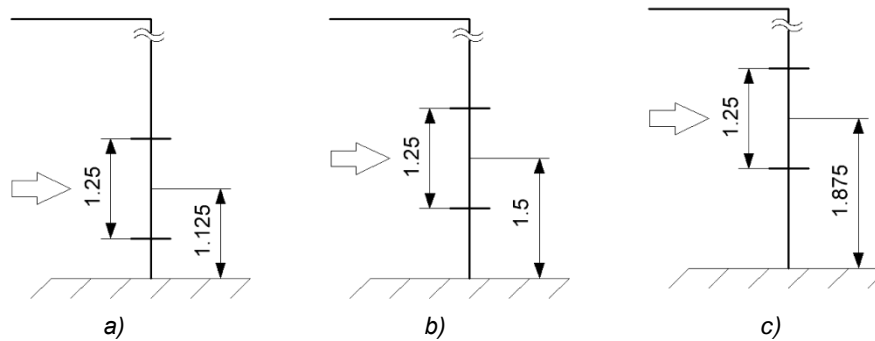


Fig. 1 - The ventilator location configuration from centreline to the floor in terms of height:
a – 1,125 m; b – 1,5 m; c – 1,875 m

Numerical mathematical simulation of hydrodynamic and heat and mass transfer processes in an industrial greenhouse was conducted. For this purpose, computer-generated simulation method based on ANSYS Fluent software was used. Navier-Stokes equations (Khmelnik S.I., 2018) and energy-transfer equations for convective currents are the basis for this mathematical model.

Navier-Stokes equation:

$$\left. \begin{aligned} \rho \left(\frac{\partial u}{\partial t} + u \frac{\partial u}{\partial x} + w \frac{\partial u}{\partial z} \right) &= - \frac{\partial p}{\partial x} + \mu \left(\frac{\partial^2 u}{\partial x^2} + \frac{\partial^2 u}{\partial z^2} \right), \\ \rho \left(\frac{\partial w}{\partial t} + u \frac{\partial w}{\partial x} + w \frac{\partial w}{\partial z} \right) &= - \frac{\partial p}{\partial z} + \mu \left(\frac{\partial^2 w}{\partial x^2} + \frac{\partial^2 w}{\partial z^2} \right), \end{aligned} \right\} \quad (1)$$

where ρ – medium density, [kg/m³]; μ – medium dynamic viscosity, [Pa·s]; p - pressure, [Pa]; u, w – velocity field of vectors; t – time, [s].

A continuity equation:

$$\frac{\partial u}{\partial x} + \frac{\partial w}{\partial z} = 0 \quad (2)$$

An energy-conservation equation:

$$\rho \cdot C_p \left(V_x \frac{\partial T}{\partial x} + V_z \frac{\partial T}{\partial z} \right) = \frac{\partial}{\partial x} \left(\lambda \frac{\partial T}{\partial x} \right) + \frac{\partial}{\partial z} \left(\lambda \frac{\partial T}{\partial z} \right) \quad (3)$$

where T – point temperature, [°K]; λ – coefficient of medium heat transfer capacity, [W/m °K]; C_p – specific heat capacity of a medium, [J/kg °K].

Boundary Conditions

- by inlet on poultry houses centreline (fig.2a):

$$x = 0; 0 \leq z \leq z_{1ch}; z_{2ch} \leq z \leq H_i; W = W_{inlet_2D}; T = T_{inlet_2D}; i = 1, 2, \dots, 7; \quad (4)$$

where z_{1ch}, z_{2ch} are vertical coordinates of the heat generation source.

It was produced by poultry arrangement during the floor storage;

H -is the distance from the floor to the roof in terms of poultry house altitude for i -ventilator.

So the number of installed ventilators equals 7, $W_{inlet_2D}, T_{inlet_2D}$ is the velocity and temperature of air flow on inlet to poultry house centreline:

- on outlet vent doors, which locate ventilation on the rear and wall (fig. 2a):

$$x = L; z_{1v} \leq z \leq z_{2v}; W = W_{outlet_2D}; T = T_{outlet_2D}; \quad (5)$$

- conditions for the absorption of heat and air temperature at the back of the poultry house (fig.2b):

$$x = L; 0 \leq z \leq z_{1v}; z_{2v} \leq z \leq H; W = 0; T = T_{wall_2D} \quad (7)$$

- pollution terms and roof temperature (fig.2b):

$$z = H_i; 0 \leq x \leq L; W = 0; T = T_{wall_roof_2D} \quad (8)$$

- pollution terms and floor temperature (fig.2b):

$$z = 0; 0 \leq x \leq L; W = 0; T = T_{wall_floor_2D} \tag{9}$$

- pollution terms of heat generation on surface source, which is formed by poultry (fig.2b):

$$z_{1ch} \leq z \leq z_{2ch}; 0 \leq x \leq L_{ch}; W = 0; T = T_{wall_chicken_2D} \tag{10}$$

where: L – poultry house length from centreline to rear wall, [m];

L_{ch} – the length of the area of the poultry house on which the birds are located [m];

T_{wall_2D} , $T_{wall_roof_2D}$, $T_{wall_floor_2D}$, $T_{wall_chicken_2D}$ ceiling wall temperature poultry house, on the floor, roof, surface source of heat generation, respectively [°C]

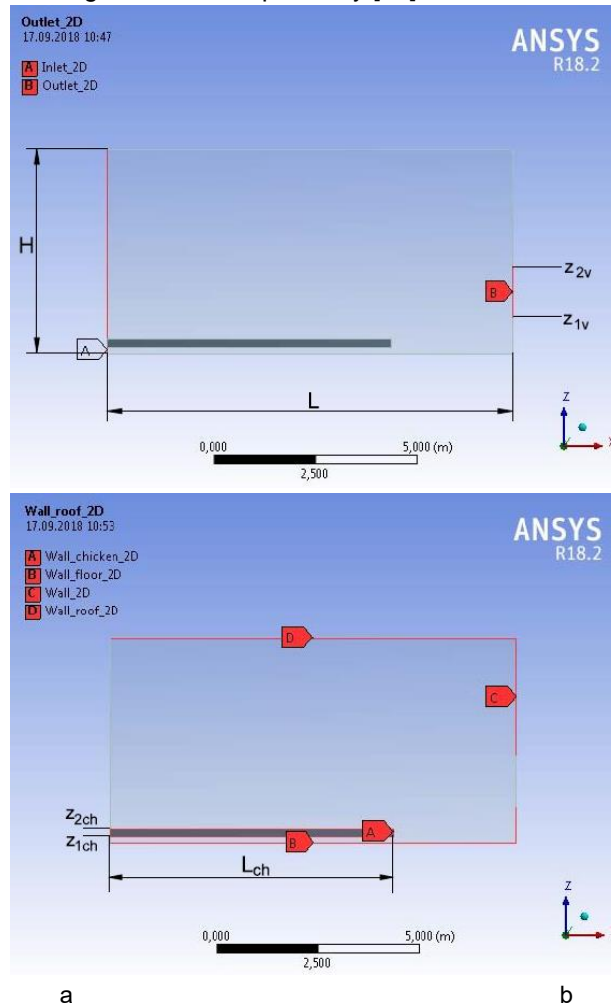


Fig. 2 - The poultry house projection view in 2 D cross-section which runs by the ventilator’s centre line by the poultry house’s length

a-boundary conditions at the inlet and outlet of air exchange system in the poultry house; *b*- boundary conditions on the surface of the interaction of the heat source with the plane of the poultry house on which the birds are located; H -poultry house’s terms of height, m ; L - poultry house’s length, m ; L_{ch} – the length of the location on which the birds are located in the poultry house, m .

The turbulence model by Spalarta-Allmarasa (*Spalart P.R. and Rumsey C.L., 2007; Allmaras S.R. et.al., 2012; Bailly C. and Comte-Bello G., 2015*) and Discrete Ordinates (DO) radiation model (*ANSYS, 2017*) were used in design. The cooling system of enforced air by water from underground wells in heat exchanger – recuperators (*Gorobets V.G., et.al., 2018*) designs were provided.

RESULTS

The finite element method was used for the numerical simulation of hydrodynamics and heat and mass transfer. The mesh building was made in the ANSYS Meshing mesh generator. The method of local mesh control was used for mesh building. The index of Orthogonal Quality is 1. The mesh building of poultry houses premises runs through the centreline of separate ventilator through the premises. This mesh is in fig.3.

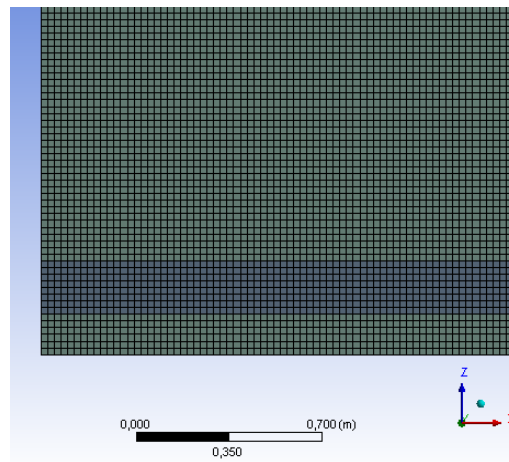


Fig. 3 - The building of mathematical mesh of centreline through ventilator centreline by the premises length

The calculation results of computer mathematical simulation for poultry house were provided in figures 4-7.

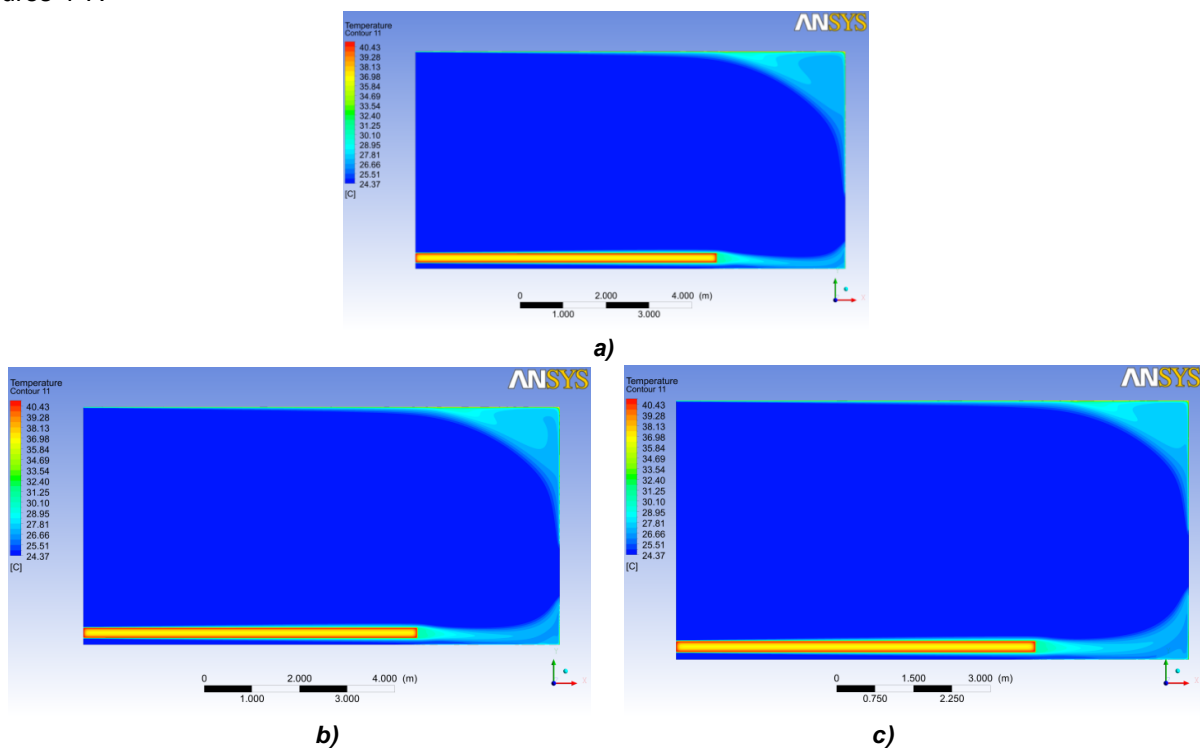


Fig. 4 - Thermal fields (°C) in longitudinal section of premises by the ventilator centreline on coordinates Ox from ventilators location from centreline to floor on height:
a – 1.125 m; *b* – 1.5 m; *c* – 1.875 m

The thermal fields by the premises height in longitudinal section by the ventilator centreline on coordinate Ox for all ventilators' location on the poultry house rear wall are shown in fig. 4. The air inlet temperature +27°C cools the poultry. It locates in the lowest part of the poultry house. The air's external temperature and radiation background were considered. The increased air temperature is observed around the ceiling. The heated air has a temperature +30°C. It is caused by the heat release from poultry heads. The heated air runs to the exhausting ventilating units after the poultry cooling.

The poultry house air velocity data, especially around the poultry is located. Is one of the important data for poultry keeping. The velocity field by the poultry house premises' height and length is shown in fig 5-7. Maximum velocity on the poultry house inlet and outlet areas doesn't surpass 2 m/s. The air velocity equals zero, especially in stagnant areas of some premises places. But the average velocity around the poultry, for the height of 0.5 m from the floor, was considered 1.97 m/s in spite of high turbulence and flow non-homogeneity. The air velocity on ventilator's outlet is considered nearly 8.4 m/s (fig. 5-7) independently from ventilators' location.

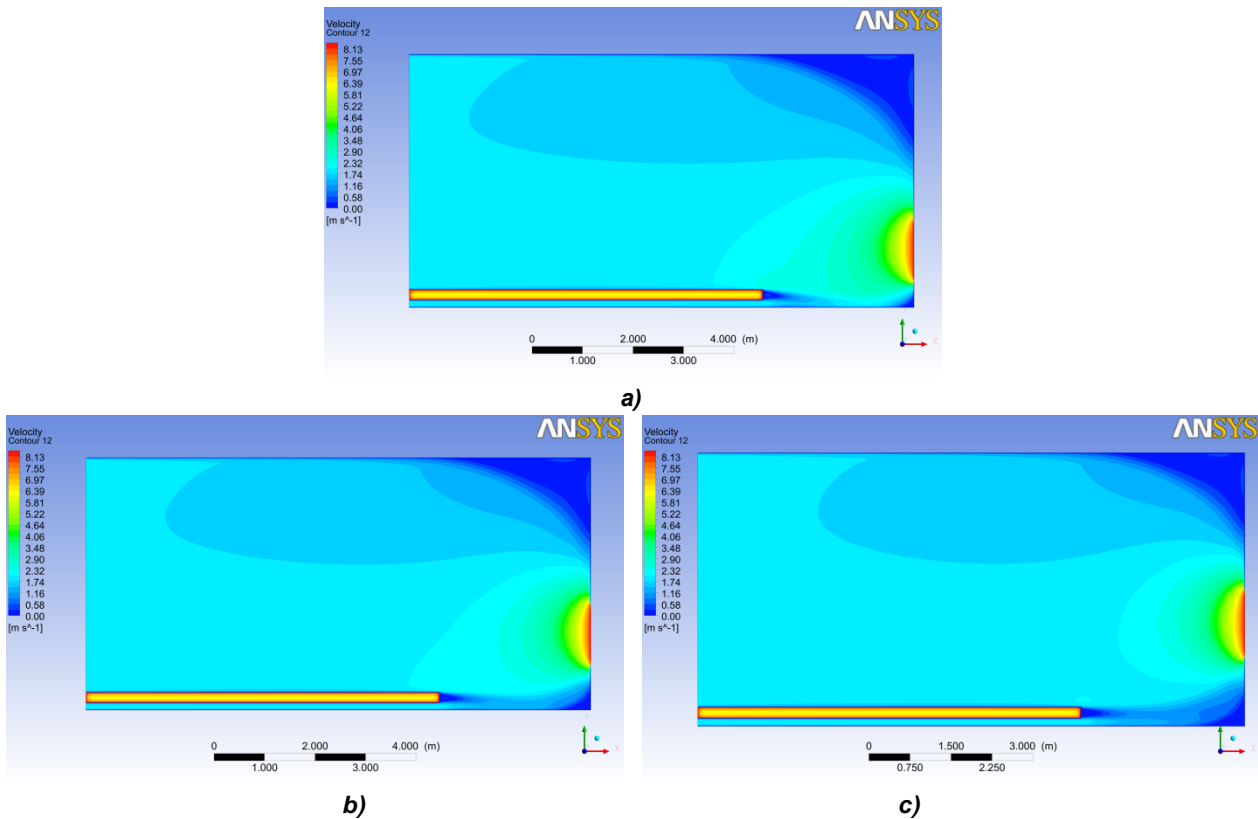


Fig. 5 b,c – Field of velocities (m/s) in premises’ cross-section by coordinate Ox with ventilator’s location from centre line to floor in terms of height: a – 1.125 m; b – 1.5 m; c – 1.875 m

The vortex zones are observed in the form of elliptical region in the upper part of the poultry house. The air velocity decreases to 1.65 m/s (fig. 5-7). The excessive stagnation area is observed in the upper angle area in fig. 5a-7a. The vortex appears in the lower part of the premises in fig. 5b-7b. The ventilator’s location at the height of 1.5 m makes the vortex minimizing the stagnation areas in the angle parts of the poultry house (fig. 5b- 7b).

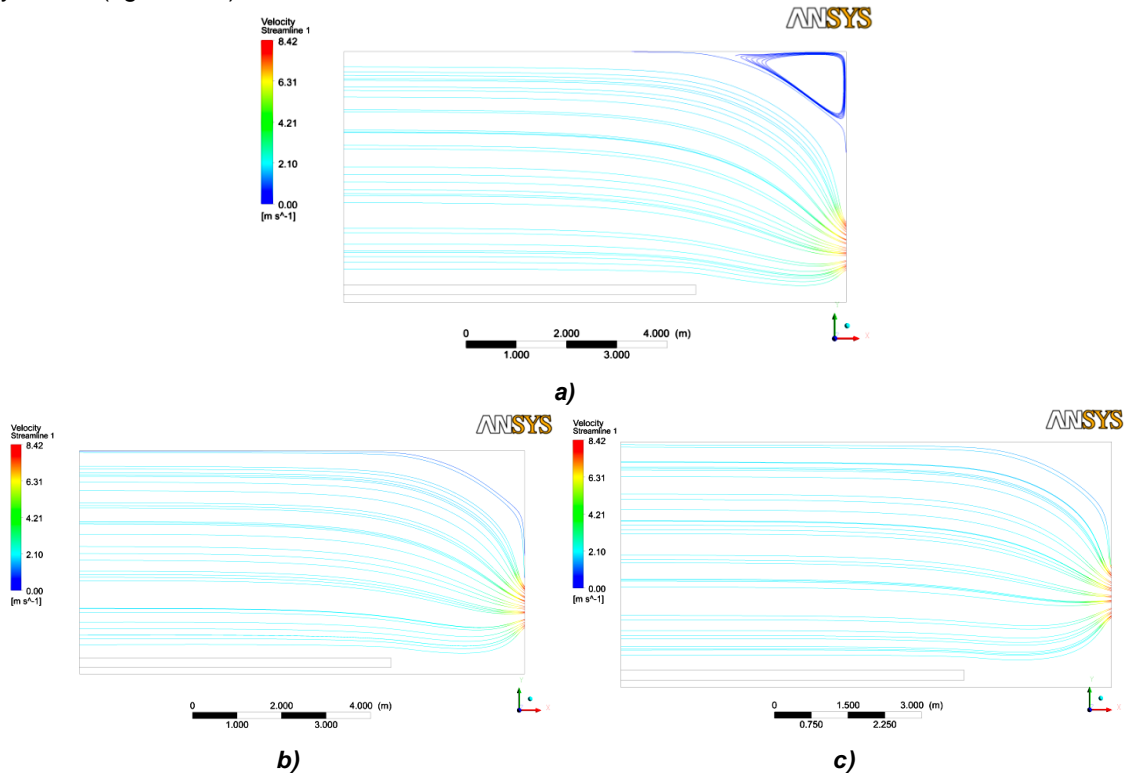
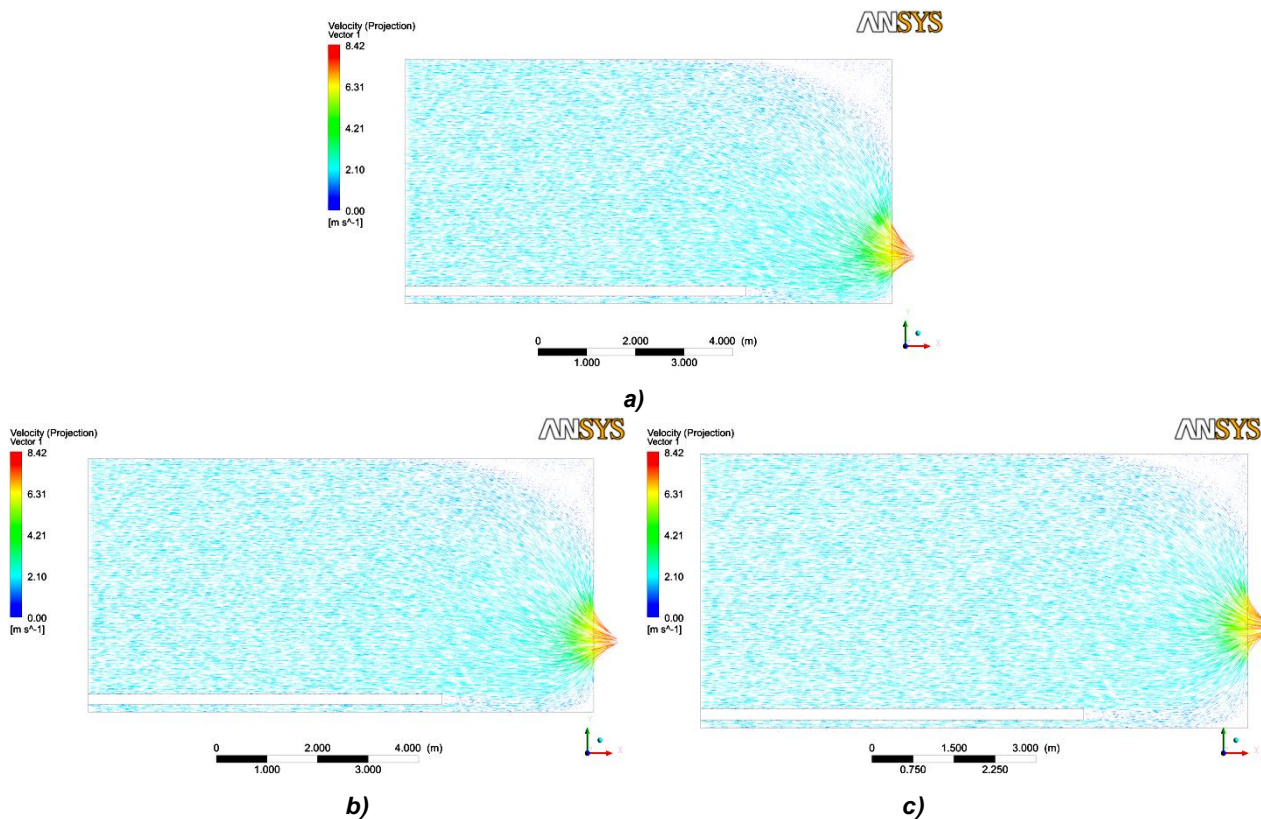


Fig. 6 - Streamlines (m/s) in premises’ longitudinal section by the ventilator centreline by coordinate Ox with ventilators location from centreline to floor in terms of height: a – 1.125 m; b – 1.5 m; c – 1.875 m

The stagnation area may be observed in the premises' upper part in fig. 6a. The ventilators streamlines and air rate velocity (fig. 6a and 7a) direct downside. That is why the air velocity around the poultry increases. It may cause the excessive poultry cooling. The decrease in poultry's temperature may cause poultry disease. It will have a negative impact on the poultry farms operation indexes.



**Fig. 7 - The velocity vector (m/s) in premises longitudinal section by the ventilator by coordinate Ox with ventilators location from centreline to floor in terms of height:
a – 1.125 m; b – 1.5 m; c – 1.875 m**

CONCLUSIONS

The numerical simulation of poultry's heat exchange and mass transfer were provided. The velocity and temperature distribution were received by the centreline of separate ventilator by the longitudinal section. The velocity field analysis showed the presence of stagnation areas in poultry houses' angle regions. The multiple calculations of mass transfer and heat exchange during the different geometry of ventilating equipment location on the rear wall were provided with the aim to minimize the stagnation areas, air flow aligning and temperature indexes increasing. It is necessary to install the ventilating equipment at the height of 1.5 m. It allows decreasing the dimension of stagnation areas and non-equality distribution of air velocity around the poultry. Such ventilators location allows equalizing flow considering the poultry house's terms of height. It will not cause the excessive poultry cooling. The average air temperature for such conditions is 1.97 m/s. The poultry house's outlet air temperature is +27°C. Such mode favours the productivity increase during the poultry farming.

REFERENCES

- [1] Allmaras S.R., Johnson F.T., Spalart P.R., (2012), Modifications and Clarifications for the Implementation of the Spalart-Allmaras Turbulence Model, *7th International Conference on Computational Fluid Dynamics*, pp. 9-13, Big Island/Hawaii;
- [2] ANSYS, (2017), *ANSYS Fluent Theory Guide. Release 18.2*, Published in the USA, 832 p.;
- [3] Bailly C., Comte-Bello G., (2015), Turbulence. Series: Experimental Fluid Mechanics, *Springer International Publishing*, 360 p., Heidelberg/Germany;
- [4] Blanes-Vidal V., Guijarro E., Balasch S., Torres A.G., (2008), Application of computational fluid dynamics to the prediction of airflow in a mechanically ventilated commercial poultry building. *Biosystems Engineering*, vol.100, no.1, pp. 105-116, San Diego/USA;

- [5] Bustamante E., Calvet S., Estelles F., Torres A.G., Hospitaler A., (2017), Measurement and numerical simulation of single-sided mechanical ventilation in broiler houses, *Biosystems Engineering*, vol.160, pp. 55-68, San Diego/USA;
- [6] Campbell J., Donald J., Simpson G. and other (2007), Keeping birds cool costs down in summertime heat, *Auburn University in association with the US poultry and egg association*, no.48, pp. 12-15;
- [7] Curi T., de Moura D.J., Massari J.M., Mesquita M., Pereira D.F., (2017), Computational fluid dynamics (CFD) application for ventilation studies in broiler houses, *Engenharia Agrícola*, vol. 37, no.1, pp. 1-12, Jaboticabal/Spain;
- [8] Gorobets V.G., Bohdan Yu.O., Trokhaniak V.I., Antypov I.O., (2018), Experimental studies and numerical modelling of heat and mass transfer process in shell-and-tube heat exchangers with compact arrangements of tube bundles, Paper presented at the *MATEC Web of Conferences*, vol. 240, <https://doi.org/10.1051/mateconf/201824002006>, Cracow/Poland;
- [9] Gorobets V.G., Trokhaniak V.I., Antypov I.O., Bohdan Yu.O., (2018), The numerical simulation of heat and mass transfer processes in tunneling air ventilation system in poultry houses, *INMATEH: Agricultural Engineering*, vol.55, no.2, pp.87-96, Bucharest/Romania;
- [10] Khmelnik S.I., (2018), Navier-Stokes equations. On the existence and the search method for global solutions, *Mathematics in Computers – MiC*, 134 p., Bene-Ayish/Israel;
- [11] Spalart P.R., Rumsey C.L., (2007), Effective inflow conditions for turbulence models in aerodynamic calculations, *Aiaa Journal*, vol. 45, no. 10, pp. 2544-2553, doi:10.2514/1.29373, Reston/USA;
- [12] Zajicek M., Kic P., (2012), Improvement of the broiler house ventilation using the CFD simulation, *Agronomy Research*, vol. 10, Special Issue 1, pp. 235–242, Tartu/Estonia;
- [13] Zajicek M., Kic P., (2013), Longitudinal ventilation of broiler house – simulation of variants, *12th International Scientific Conference Engineering for Rural Development*, pp. 198-202, Jelgava/Latvia.

STUDY ON NDVI OPTIMIZATION OF CORN VARIABLE FERTILIZER APPLICATOR

变量施肥机 NDVI 的优化研究

Ph.D. Hongli Liu¹⁾, Prof. Xi Wang^{*2)}, M.S. Jin Bing-kun³⁾¹⁾ College of Engineering, Heilongjiang Bayi Agricultural University, Daqing/China;²⁾ College of Engineering, Heilongjiang Bayi Agricultural University, Daqing/China;³⁾ Western University, 1151 Richmond Street, London, Ontario / Canada

Tel: +13836961962 E-mail: ndwangxi@163.com

Keywords: NDVI; soil reflectance; variable fertilizer applicator**ABSTRACT**

The large error exists in Normalized Difference Vegetation Index (NDVI) data because of soil reflectance. An optimal corn canopy NDVI data processing method was proposed in this study. The method was employed to reduce the effect of soil reflectance error under different leaf areas on corn canopy NDVI. First, an experiment was established using different plant spacings to obtain different canopy leaf area treatments. Then, the average NDVI of the largest leaf area (dense plant spacing) was used as the evaluation standard value. The NDVI mean values after error elimination by Box-plot, Dixon rule and Pauta criterion were obtained under other leaf area treatments. The difference between the NDVI mean and the standard value, the R^2 of the regression model between the NDVI mean value of each algorithm with corn parameter were used to evaluate the performance of the algorithm. Results demonstrate that the difference between the NDVI mean of the Box-plot and the standard control value is the smallest at 9% and 16% under normal plant spacing and sparse plant spacing, respectively. The R^2 between the NDVI mean of the Box-plot and corn plant height has the best effect, increasing to 0.7676 and 0.5966 under normal plant spacing and sparse plant spacing, respectively. The R^2 between the NDVI mean of the Box-plot and the nitrogen content of corn has a similar result, increasing to 0.7154 and 0.5739, respectively. These findings indicate that the Box-plot reduces the interference of soil background on corn canopy NDVI and improves the estimation ability of corn parameters.

摘要

土壤反射对冠层 NDVI 造成较大的干扰。本研究提出了一种最佳的玉米冠层 NDVI 数据处理方法。该方法用于降低不同叶面积下土壤反射率误差对玉米冠层 NDVI 的影响。首先，使用建立差异性的玉米株距处理得到不同的叶面积。随后，NDVI 平均值和标准值之间的差异及 NDVI 平均值与玉米参数（株高，氮含量）之间的回归模型的 R^2 来评估各算法的性能。结果表明，在正常植物间距和稀疏植物间距下，箱图的 NDVI 平均值与标准对照值之间的差异最小，分别为 9% 和 16%。箱形图的 NDVI 平均值与玉米株高之间的 R^2 达到最大值，在正常植物间距和稀疏植物间距下分别增加至 0.7676 和 0.7154。箱形图的 NDVI 平均值与玉米氮含量之间的 R^2 具有相似的结果，分别增加至 0.5966 和 0.5739。这些结果表明，箱形图减少了土壤背景对玉米冠层 NDVI 的干扰，提高了玉米参数的估算能力。

INTRODUCTION

Top-dressing, which is among the available measures of increasing corn production, is popular in agricultural practices. The amount of fertilizers received in several regions is uneven because of crop growth or spatial differences in soil nutrient (Chen P. et al, 2010). Fertilizer cycle exhibits dynamic changes, and predicting the supply of various nutrients to plants is difficult. Therefore, the unified quantitative fertilization method results in low fertilizer use efficiency (Fangfang Zhang et al, 2017). China's comprehensive fertilizer utilization rate was 34% in 2017 (Sun S.K. et al, 2018).

Previous studies have shown that a variable fertilizer applicator for corn top-dressing can effectively improve fertilizer utilization (Torsten I., 1982). The variable decision of the fertilizer applicator in previous studies was based on the normalized difference vegetation index (NDVI) (Geipel J., Link J., 2014). Commercialized products have been introduced for variable fertilizer applicators based on this approach, and examples include the Case 3230, which is equipped with Greensseeker to detect crop canopy NDVI and thus reflect differences in growth. Greensseeker has been employed to control the motor and adjust the flow of liquid fertilizer in real time for variable fertilization (Cicek H. et al, 2010). However, corn top-dressing in China

uses solid fertilizer, the variable fertilizing device is mechanical and the speed of variable fertilization regulation is limited. A variable fertilizer application machine adopts a uniform fertilizer amount on a fixed area. The average method is employed to express the overall situation of the fixed area's NDVI (Ali A.M. et al, 2015). This process has become a great challenge in the accurate assessment of NDVI because of numerous influencing factors, such as leaf shape difference, corn canopy difference, and soil reflection. On the basis of the analysis above, this study examines a core problem in the improvement of NDVI's detection accuracy.

Greenseeker is the most widely utilized near-surface plant canopy spectral detection sensor. The direction of Greenseeker measurement for corn canopy spectral reflectance detection has been tested, and results showed that the variation in the crop nutritional parameters of the output value of longitudinal measurement is higher than that of transverse measurement (Ali A.M. et al, 2014). The optimal height for Greenseeker measurements is 70–110 cm and sunlight exerts a minimal effect on Greenseeker's performance (Enciso J. et al, 2017). A previous study added an adjustment factor based on NDVI to establish a soil-adjusted vegetation index (SAVI) and showed that corn nitrogen content prediction improves when the corn canopy coverage is 50% of the leaf area (Chua T. et al, 2003). Another study used mathematical iteration methods to perform an infinite number of iterations for removing the adjustment factors and established a modified SAVI (MSAVI); However, the feasibility of the index was not further verified (Gianquinto G. et al, 2011). Currently, NDVI is still the most widely used parameter in the estimation of plant nitrogen content. Using statistical methods to optimize NDVI can also effectively reduce the interference of background factors. For example, the maximum method has been applied to perform noise reduction processing on cotton canopy NDVI data and obtain the average NDVI of the detection area, thus reflecting the overall NDVI trend in the detection area (Ramirez M.B., Schjoerring J K, 2015). The following problems are encountered under actual production conditions. First, the corn leaf area cannot be obtained in real time. Second, a difference exists between cotton and corn canopy, and the application of the maximum method in the NDVI quantification of the corn canopy has not been verified.

A method of evaluating four types of algorithms for error culling to reduce the error data of NDVI by Greenseeker under different leaf areas was proposed. The NDVI of the optimal algorithm has the highest correlation with the plant height and nitrogen content of corn. The applicability of the maximum method to the NDVI of corn was also verified.

MATERIALS AND METHODS

The study area is located at the Heilongjiang Bayi Agricultural University research base in Daqing City, with latitude 46°63'–46°64'N and longitude 125°20'–125°21'E. The area of the research base is 50 hm^2 . The soil type is chernozem, in which the thickness of the black soil layer is 25–40 cm and the organic matter mass fraction is high at 3.0%–4.0%. The basic conditions of the soil are shown in Table 1 (tested using the soil nutrient status system research method).

Table 1

The basic characteristics of the soil

Definition of the parameter	Parameter values
A. PH	6–7
B. Electrical Conductivity	232 $\mu s/cm$
C. Available Nitrogen	50 ppm
D. Total Nitrogen	32 ppm
E. Organic content	22 g/kg
F. Soil type	Chernozem

The research data were acquired using a ground-based remote sensing platform. The Greenseeker plant canopy spectral detector mainly obtains NDVI data of the corn canopy and its own narrow-band light emitting diode with red light at 660 nm and near-infrared light at 770 nm is used as the active light source. The second-generation optical sensor (N Tech) is used as a detection sensor to acquire plant spectral information under two bands. It has a measurement area of 61 cm \pm 10 cm (width) \times 1.5 cm \pm 0.5 cm (length). The RT100 GPS (Trimble Company) obtains position information with an error of 1 cm.

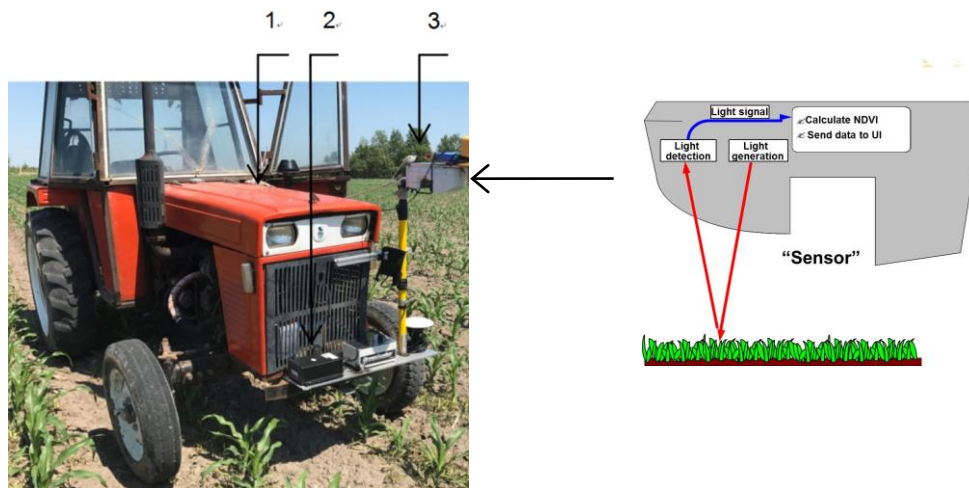


Fig.1 - Test data acquisition platform

1 – Tractor of 405; 2 – GPS; 3 – Greenseeker sensor

Test Design

Three different plant spacings of corn were set (Fig. 2): dense plant spacing (N1: 12 cm), normal plant spacing (N2: 18 cm) and sparse plant spacing (N3: 22 cm). Each plot area was 1.3 m x 100 m. Fertilizer was applied as urea, P₂O₅ and K₂O, in the ratio of 3:1:1 to give a total fertilizer application rate of 250 kg/hm².

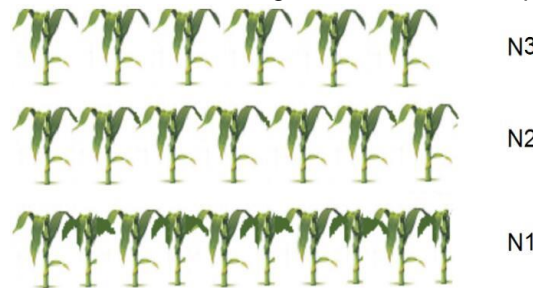


Fig. 2 - Experimental setup for different plant spacing

Data Detection Methods

The data processing interval was 3 s, according to the operating speed (1.4 m/s) and separation of Greenseeker from the tailstock spreader (4.1 m). The Greenseeker vertical distance was 70 cm from the canopy and the detection direction was consistent with the ridge. The NDVI and GPS output frequencies were 26 times/s and 5 times/s, respectively.

Data Processing Methods

The error based on experience was an abnormally low value. First, the maximum method was used for data pre-processing. The 24 maximum values were selected based on the data processing interval (3 s), operating speed (1.4m/s) and standard plant spacing (18cm). Further error elimination of pre-processed data used the following methods:

Pauta criterion: If the difference between the measured value (x_n) and the average value (\bar{x}) is greater than N times the standard deviation (σ), then (x_n) will be eliminated. In this study n was 1 based on experience (Cheng Shen et al, 2017).

$$\alpha = |x_n - \bar{x}| > n\sigma \tag{1}$$

Dixon criterion: Calculates the r values in different orders according to formula (2) after arranging the data by size. This method compares the difference between the r value and the Dixon criterion test critical value; the data are eliminated when r_{max} and r_{min} are greater than the corresponding critical value $F(0.05, m)$, or less than the corresponding critical value $F(0.05, m)$ (Grubbs F., 2012; Serth R.W. et al, 1986; Özyurt D., Pike P., 2004).

$$\begin{cases} r_{max} = \frac{x_n - x_{n-1}}{x_n - x_1}, r_{min} = \frac{x_2 - x_1}{x_n - x_1} (3 \leq n \leq 7) \\ r_{max} = \frac{x_n - x_{n-1}}{x_n - x_2}, r_{min} = \frac{x_2 - x_1}{x_{n-1} - x_1} (8 \leq n \leq 12) \\ r_{max} = \frac{x_n - x_{n-1}}{x_n - x_3}, r_{min} = \frac{x_3 - x_1}{x_{n-2} - x_1} (13 \leq n) \end{cases} \quad (2)$$

The Box-plot method: The 25% quantiles, 75% quantiles, top borders and bottom borders were obtained after sorting the data by size to create a Box plot, which describes the overall distribution of the data. The box contains most of the normal data, with outliers outside the upper and lower boundaries of the box (Zhengjiang Zhang et al, 2014).

Evaluation Methods

The NDVI of 42 meters (10 intervals) in the middle area was selected under each plant spacing. The dense plant spacing was basically free of soil exposure, so the NDVI mean value was employed as the evaluation standard value. Using different algorithms to eliminate the outliers of NDVI in each interval and obtain the overall mean at different plant spacings. The performance of different algorithms was evaluated by comparing the differences between the mean and the standard values. Five corn plants with uniform growth were selected in each interval to measure the mean value of nitrogen content and plant height under each plant spacing. The regression equations of NDVI, nitrogen content and plant height were established, and the fitness (R^2) was employed as the evaluation standard for each algorithm performance.

RESULTS

In Fig. 3, a, b, and c are the NDVI time series data obtained by the plant spacing of 12 cm, 18 cm and 22 cm, respectively. The change in NDVI data was gradual with the change in plant spacing because the area of corn canopy leaf increased and the soil background had less influence on the detection of crop canopy reflectance with the increase in plant spacing. When the plant spacing increased from 12 to 18 cm, the mutual shielding effects of the leaves became smaller, and the exposed area of the soil background increased. This led Greenseeker to integrate the measured values of the soil into the measured values of the crop canopy NDVI, resulting in a smaller NDVI detection value. Significant surface exposure was observed between plants, and the lowest value of canopy NDVI was detected when the maximum distance between rows was the largest. The NDVI continuous data obtained from the mean value of the largest plant spacing could not accurately describe the overall NDVI trend.

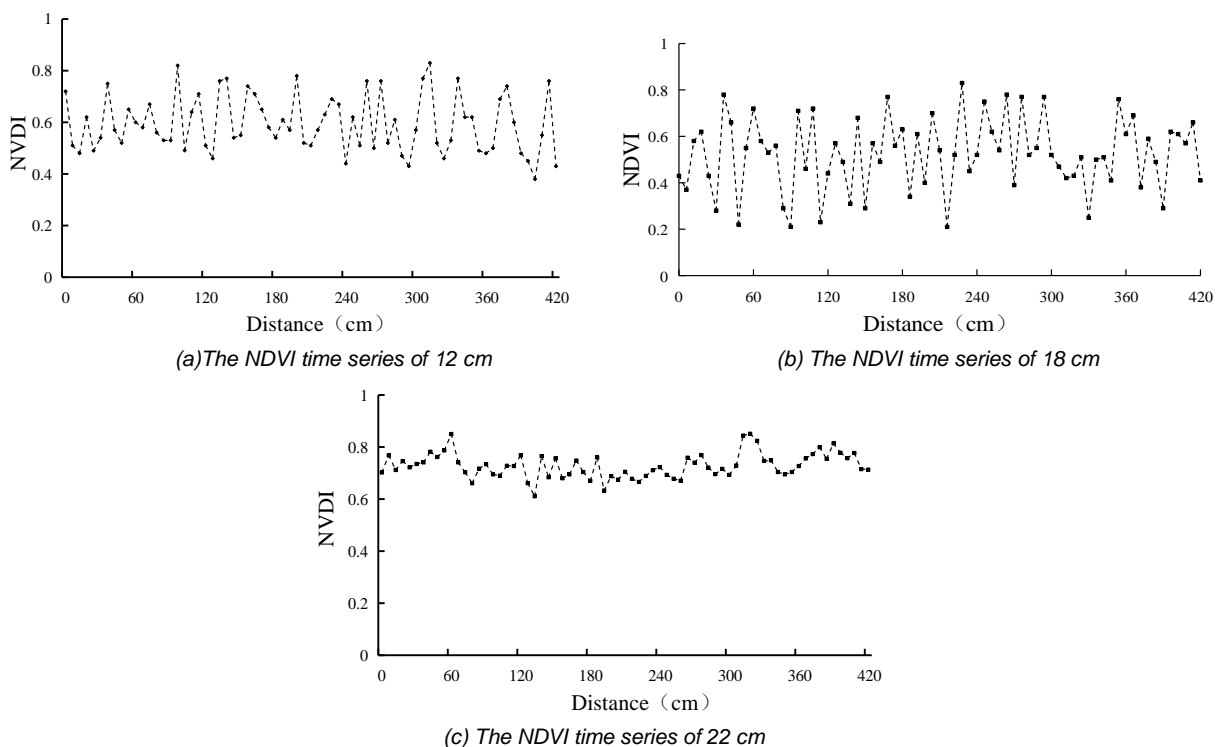


Fig. 3 - Change of NDVI data with different plant distance within a certain distance

The mean after pre-processing the NDVI data of each plant spacing using the maximum value method increased significantly, but there was still a large difference between the mean and the standard control value (Table 2). Therefore, the NDVI maximum value needs to be further processed to reduce the error rate.

Table 2

Maximum value processing mean			
Treatment	Plant spacing (cm)	The mean of NDVI	Mean value of NDVI processed by the maximum value
N1	12	0.781	0.786
N2	18	0.51	0.66
N3	22	0.42	0.53

Data Processing Algorithm Performance

Pauta criterion: After the elimination of data by comparison of the standard deviation of pre-processed data using formula (1). As shown in Fig. 4, the mean of Pauta criterion for N2 and N3 were 0.709 and 0.657, respectively. The average N2 data processed by Pauta criterion was not significantly different from the mean of Maximum method and the difference from the standard value was 11%. The average N3 data processed by Pauta criterion was no significantly different ($F > 0.05$) from the mean of Maximum method and the difference from the standard value was 18%.

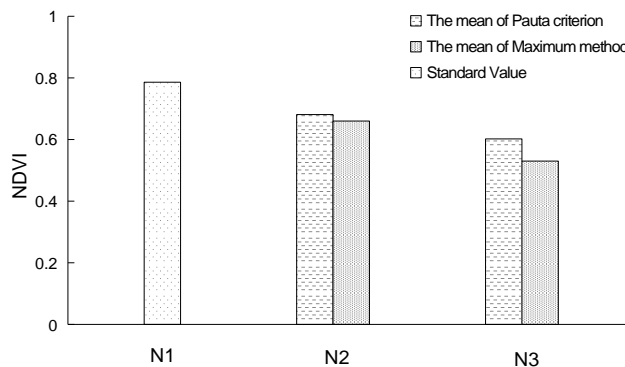
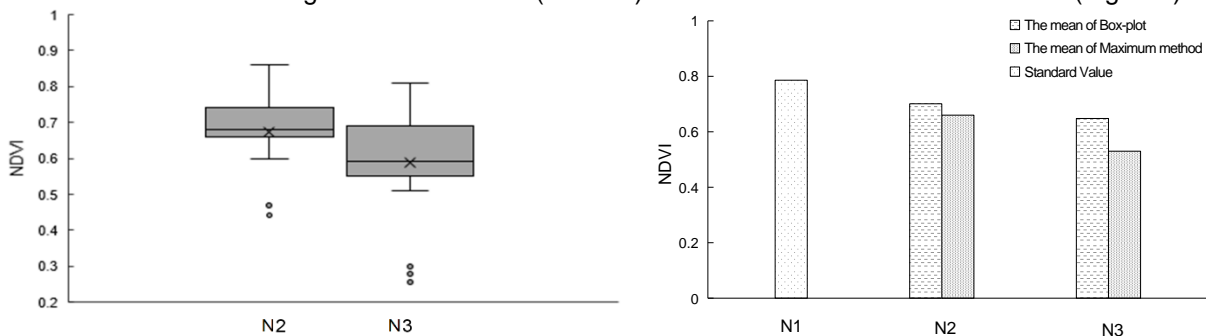


Fig. 4 - The treatment of NDVI mean by Pauta criterion

The Box-plot method: As shown in Fig. 5-a, there were two error points and three error points for N2 and N3 which were eliminated by Box-plot, respectively (Fig. 5-a). The mean of Box-plot for N2 was 0.722; its difference with the standard values was 9% and it had no significant difference ($F > 0.05$) with the mean of Maximum method (Fig. 5-b). The mean of Box-plot for N3 was 0.689, its difference with the standard values was 16% and it had no significant difference ($F > 0.05$) with the mean of Maximum method (Fig. 5-b).



(a) The error values of Box-plot

(b) The average value of Box-plot

Fig.5 - Line map box of different plant distance processing

Dixon criterion: The r_{max} and r_{min} for all data were calculated according to the Dixon criterion confidence factor (as shown in Fig. 6-a) and formula (2). The mean of Dixon criterion for N2 was 0.693, its difference with the standard values was 12%. The mean of Dixon criterion for N3 was 0.649, its difference with the standard values was 19%. At same time, the mean of Dixon criterion for N2 and N3 had no significant difference with the mean of Maximum method (Fig. 6-b).

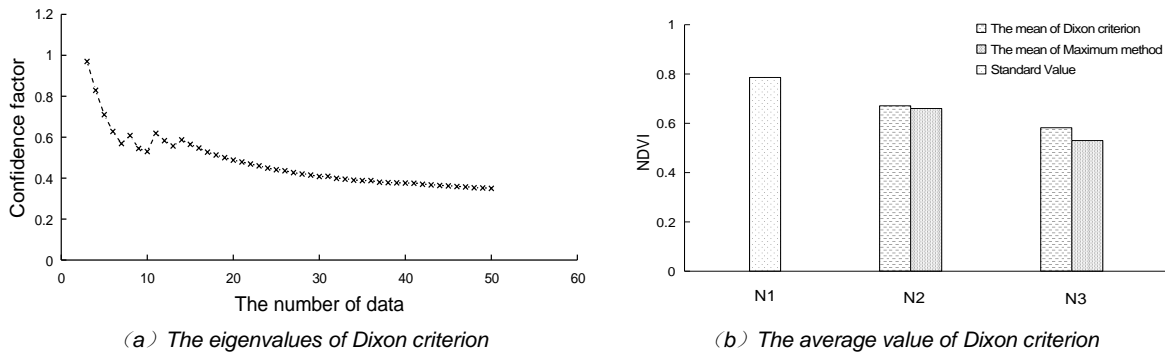


Fig 6 - Different plant distance processing of Dixon criterion

Estimation of corn nitrogen content and plant height at different plant spacings

As shown in Fig.7a, at the close planting distance, the R^2 between NDVI and plant height was of plant height and nitrogen content 0.877, and the R^2 between NDVI and nitrogen content was 0.8134. At this time, it accurately inverted the growth state of corn. With the increase of plant spacing, the soil background interference existed under normal plant spacing, but the fitting degree R^2 of plant height and nitrogen content were greater than 0.6 (Fig.7-b), the NDVI could predict the growth parameters. At sparse plant spacing, the R^2 of plant height and nitrogen content were significantly lower than other plant spacing, indicating that NDVI could not be used for corn parameter estimation (Fig.7-c).

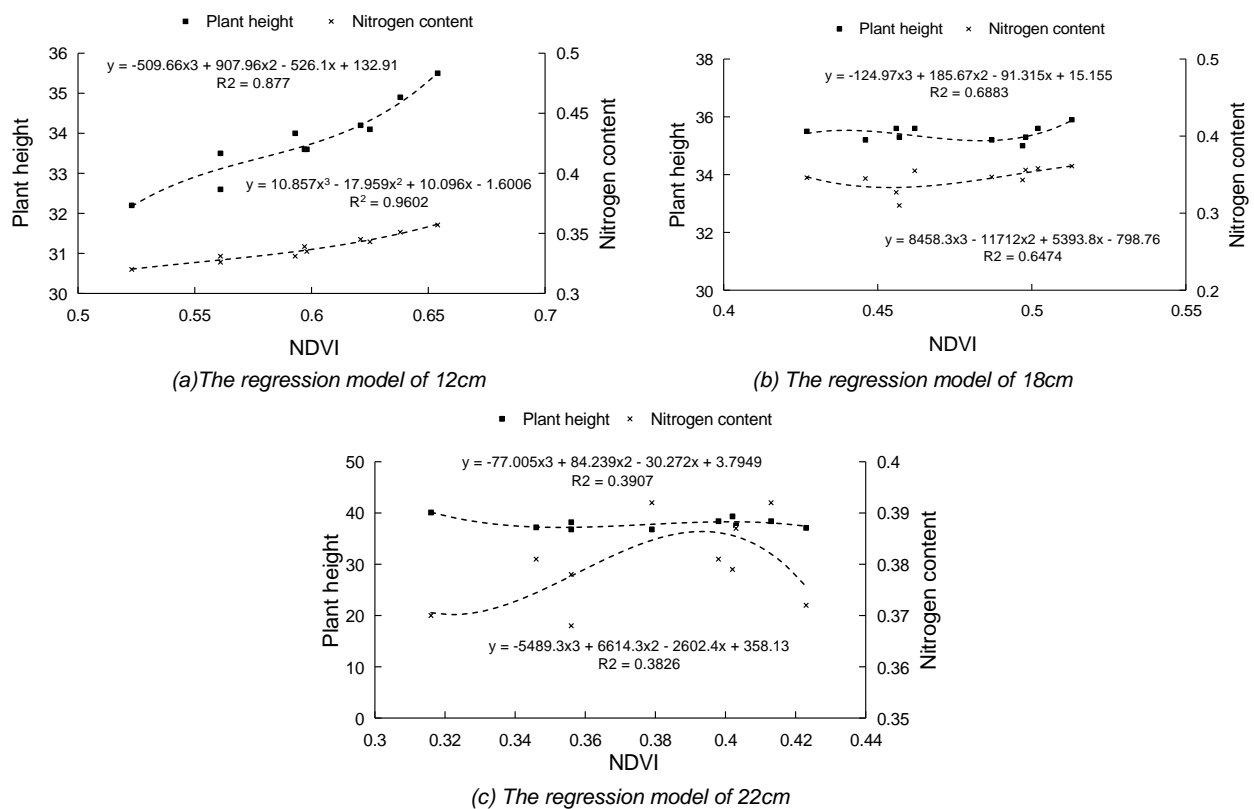


Fig 7 - Estimation of plant height and nitrogen content of original NDVI data with different row spacing

In Fig. 8, a, b, and c represent the regression model of the plant height and nitrogen content of the Pauta criterion, the Box-plot and the Dixon law under the normal plant spacing (N2), respectively. The R^2 of the plant height and nitrogen content were improved to different degrees by different algorithms. The R^2 of the Box-plot were processed having the maximum value. Compare with the dense plant spacing, the difference rates of R^2 were 10.6% and 13.7%, respectively. However, the R^2 change was not obvious compared to the original data, indicating that the abnormal value had no significant effect on the accuracy of corn canopy NDVI under normal plant spacing.

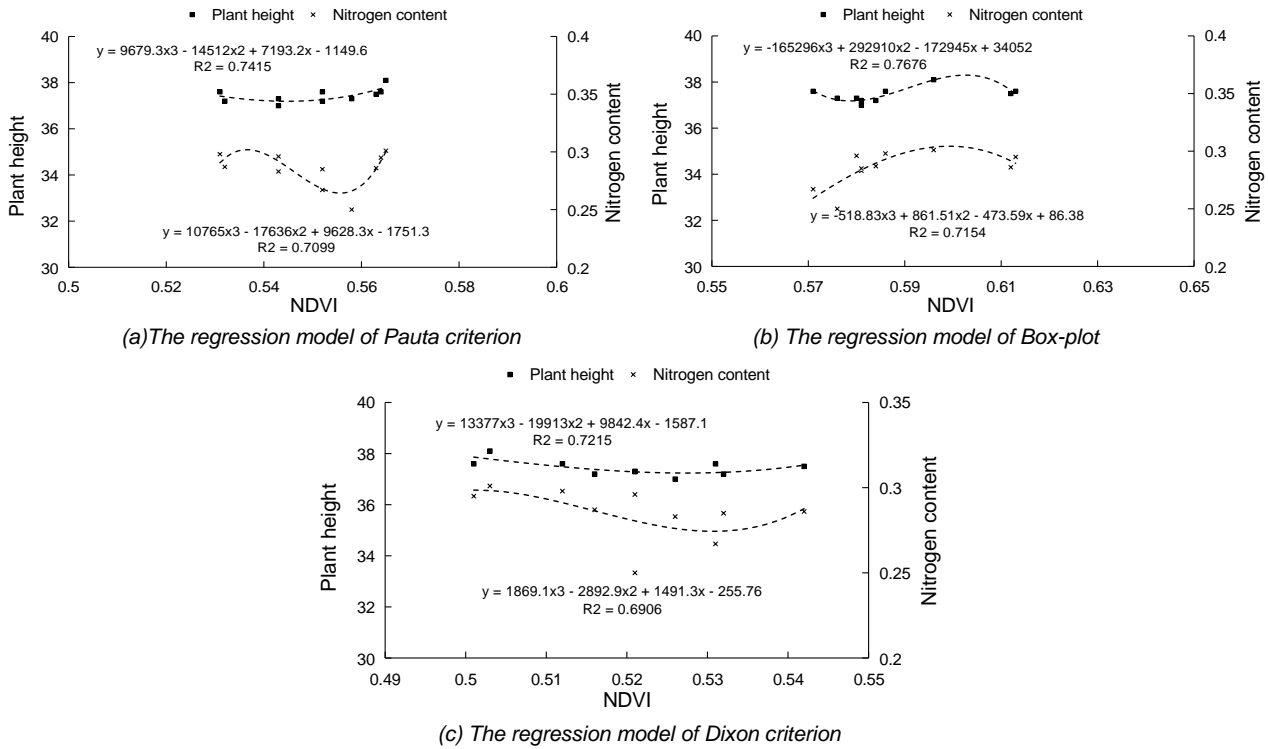


Fig 8 - Estimation of plant height and nitrogen content of NDVI at normal plant spacing

Compared with the original data, the R^2 has been significantly improved by the data processed by different algorithms under the sparse plant spacing (N3). The Box-plot has the best results and the R^2 of the plant height and nitrogen content have maximum value, which are 36% and 30% higher than the original data, respectively. There was no significant difference between R^2 after treatment under normal plant spacing, indicating that the NDVI data processed by the Box-plot under sparse plant spacing significantly reduced the disturbance of soil background.

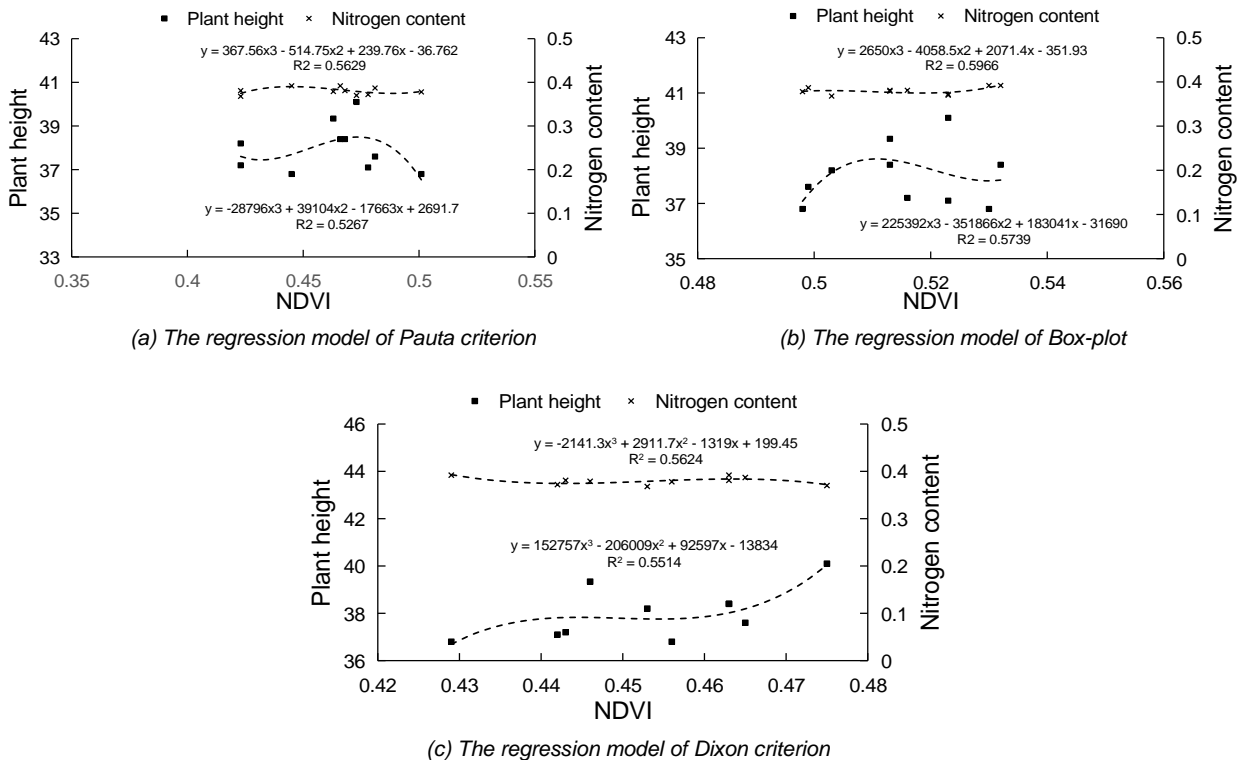


Fig 9 - Estimation of plant height and nitrogen content of NDVI at sparse plant spacing

Discussion

In this study, the NDVI of corn canopy obtained from Greenseeker was used to study the effects of different NDVI data error elimination algorithms to reduce the interference of soil background under different leaf area. The NDVI mean after error elimination was used to accurately describe the overall trend of NDVI in the detection area.

The corn canopy spectral reflectance is the key to real-time monitoring of corn nitrogen status. The canopy reflectance of plants is measured by satellite, aircraft and ground equipment equipped with spectral image sensors or plant spectral detectors. Satellite and aircraft remote sensing platforms have limited application in crop management because of their own operational cycles and cloud, weather and low resolution (Cicek H. et al, 2010; Geipel J., Link J., 2014). Ground remote sensing is a good way to overcome the above problems, as it is conducted close to the plants (50–150 cm) and can be used in conjunction with variable-rate fertilizer applicators for real-time variable fertilization (Nakajima Teruyuki T. et al, 1996; Michael T et al, 2016).

The bare soil light reflectance is the main problem that affects the accuracy of NDVI of corn canopy. It is difficult to strip soil reflectance from NDVI data. Statistical methods are employed to reduce the interference of soil background on NDVI. For example, the Curve fitting (Bradley et al, 2007; Chen J., Per J., 2004), asymmetric Gaussian function fitting (Nan Cong, 2012; Zhuokun Pan et al, 2015) and Fourier transform (Quiroz R. et al, 2011; Yang Shao et al, 2016; Du Ming Tsai and Wan-Ling Chen, 2017) methods were employed to reconstruct NDVI data and reduce outliers. The appeal methods are based on the least-squares method and the time-frequency conversion principle, which are limited in real-time applications because of computational complexity. The experimental design was based on the work of (Ramirez M., Schjoerring J.K, 2015) and verified the efficiency of the algorithm in corn applications. The results showed that the optimal algorithm reduced the influence of soil light reflectance on corn canopy NDVI to a certain extent, but the large errors in the NDVI data after processing because the canopy is different between cotton and corn (Atanassov R. et al, 2009). Alternative data processing methods, such as Pauta criterion and Dixon criterion are tested because they are simple to calculate and can be applied under actual production conditions. All of the data processing methods remove outliers based on their particular threshold values. The Dixon criterion automatically set the threshold according to the amount of data. In this study, The Box-plot determines the threshold according to the characteristics of the data. It does not require prior knowledge and accurately removes outliers of NDVI data when compared with other algorithms. Simultaneously, the correlation between the mean value of NDVI by the Box-plot and the nitrogen content is 0.94. Accuracy of nitrogen content estimation is improved compared to other studies (Scharf P.C et al, 2002; Kyle W et al, 2007). Application of the Box-plot effectively improved the accuracy of the NDVI-based variable fertilization model.

The test plant spacing, evaluation criteria and area of the test space are set according to the characteristics of the fertilizer application or for a certain purpose. With the development of the electronically controlled fertilization device, the NDVI method for a smaller area can be studied to further improve the refinement of corn canopy growth and further reduce the amount of fertilizer applied. At the same time, the applicability of this method can be studied in other crops such as rice, wheat, soybean, and cotton. The method can be applied to forestry surveys, land use monitoring (Michael T et al, 2016) and other applications, to improve the popularization of the method and to be able to use remote sensing error analysis, remote sensing applications in statistical techniques and for other applications.

CONCLUSIONS

To reduce the interference of soil reflection on corn canopy NDVI under different leaf areas, a case study was made to compare the performance of three types of error culling algorithms. A novel method based on the Box-plot method was developed to reduce the effect of soil background on corn effective NDVI and improve the accuracy of NDVI estimation of corn plant height and nitrogen content. The following conclusions were obtained.

- (1) The NDVI error depends on the leaf area. When the leaf area is small, NDVI has a large error.
- (2) Under a different leaf area, the Box-plot method exhibits the best performance. When NDVI has a large error, the Box-plot method considerably improves the estimation of NDVI, corn plant height and nitrogen content.

(3) Although the maximum method improves the effectiveness of NDVI compared with the averaging method, a large error is observed when the leaf area is small. The method is suitable for small leaf crops, such as cotton.

The resulting method considers the variation in leaf area to achieve a highly accurate simulation of the actual application. However, leaf area is affected by many factors and the proposed method is limited to considering the influence of plant spacing. Future research should consider other influencing factors.

ACKNOWLEDGMENTS

The authors would like to thank Edanz Editing and anonymous reviewers for their constructive comments and suggestions to improve the quality of the study. This work was partially supported by National Key R & D project (2016YFD020060802).

REFERENCES

- [1] Ali A.M., Thind H.S., Sharma., Varinderpal-Singh, (2014), Prediction of dry direct-seeded rice yields using chlorophyll meter, leaf colour chart and GreenSeeker optical sensor in north-western India. *Field Crops Research*, Vol.161, Issue.5, pp.11-15, Elsevier, Amsterdam/Netherlands;
- [2] Ali A.M., Thind H.S., Varinderpal-Singh., Bijay-Singh, (2015), A framework for refining nitrogen management in dry direct-seeded rice using GreenSeeker™ optical sensor. *Computers and Electronics in Agriculture*, Vol.110, Issue.1, pp.114-120, Elsevier, Oxford/England;
- [3] Atanassov R., Bose P., Couture M., Maherwari A., Morin P., Paquette M., Smid M., Wuher S., (2009), Algorithms for optimal outlier removal. *Journal of Discrete Algorithms*, Vol. 7, Issue.2, pp.239-248, Elsevier, New York/U.S.A.;
- [4] Bradley B., Jacob R., Hermance J., Mustard J., (2007), A curve fitting procedure to derive inter-annual phenologies from time series of noisy satellite NDVI data. *Remote Sensing of Environment*, Vol.106, Issue.2, pp.137-145, Elsevier, New York/U.S.A.;
- [5] Chen P., Haboudane D., Tremblay N., Wang Jihua, Vigneault P., Li Baoguo, (2010), New spectral indicator assessing the efficiency of crop nitrogen treatment in corn and wheat. *Remote Sensing of Environment*, Vol.114, Issue.9, pp.1987-1997, Elsevier, New York/U.S.A.;
- [6] Cheng Shen, Xuejing Bao, Jiubin Tan, Shutian Liu, Zhengjun Liu, (2017), Two noise-robust axial scanning multi-image phase retrieval algorithms based on Pauta criterion and smoothness constraint. *Optics Express*, Vol.25, Issue.14, pp.16235-16249, OSA Publishing, Washington/U.S.A.;
- [7] Chua T., Bronson K., Booker J.D., Keeling W., Mosier A., Bordovsky J., Lascano R., Green C., Segarra E., (2003), In-Season nitrogen status sensing in irrigated cotton: Leaf nitrogen and biomass. *Soil Science Society of America Journal*, Vol.67, Issue.5, pp.1428-1438, Amer Statistical Assoc, Alexandria/ U.S.A.;
- [8] Cicek H., Sunohara M., Wilkes G., (2010), Using vegetation indices from satellite remote sensing to assess corn and soybean response to controlled tile drainage. *Agricultural Water Management*, Vol.98, Issue.2, pp.261-270, Elsevier, Amsterdam/Netherlands;
- [9] Du Ming Tsai, Wan-Ling Chen, (2017), Coffee plantation area recognition in satellite images using Fourier transform. *Computers and Electronics in Agriculture*, Vol.135, Issue.4, pp.115-127, Elsevier, Oxford/England;
- [10] Enciso J., Maeda M., Landivar J., Jung J., Chang A., (2017), A ground based platform for high throughput phenotyping. *Computers and Electronics in Agriculture*, Vol.141, Issue.9, pp.286-291, Elsevier, Oxford/England;
- [11] Fangfang Zhang., Qingsong Wang., Jinglan Hong., Wei Chen., (2017), Life cycle assessment of diammonium- and monoammonium-phosphate fertilizer production in China, *Journal of Cleaner Production*, Vol.141, Issue.10, pp.1087-1094, Elsevier, Oxford/England;
- [12] Freemana K., Girmab K., Arnall D., Mullen R., Martin K., Teal R., Raun W., (2007), By-Plant Prediction of Corn Forage Biomass and Nitrogen Uptake at Various Growth Stages Using Remote Sensing and Plant Height, *Remote Sensing*, Vol.99, Issue.2, pp.530-536, Molecular Diversity Preservation International, Basel/Switzerland;
- [13] Geipel J., Link J., Claupein W., (2014), Combined Spectral and Spatial Modeling of Corn Yield Based on Aerial Images and Crop Surface Models Acquired with an Unmanned Aircraft. *Remote Sensing*, Vol.11, Issue.6, pp.10335-10355, Molecular Diversity Preservation International, Basel/Switzerland;

- [14] Gianquinto G., Orsini F., Fecondini M., Mezzetti M., Sambo P., Bona S., (2011), A methodological approach for defining spectral indices for assessing tomato nitrogen status and yield. *European Journal of Agronomy*, Vol. 35, Issue.3, pp.135-143, Elsevier, Amsterdam/Netherlands;
- [15] Grubbs F., (2012), Procedures for Detecting Outlying Observations in Samples. *Technometrics*, Vol.11, Issue.1, pp.1-21, Amer Statistical Assoc, Alexandria/U.S.A.;
- [16] Jin Chen, Per. Jönsson., Masayuki Tamura., Zihui Gu., Bunkei Matsushita., Lars Eklundh, (2004), A simple method for reconstructing a high-quality NDVI time-series data set based on the Savitzky–Golay filter. *Remote Sensing of Environment*, Vol.91, Issue.3-4, pp.332-344, Elsevier, New York/U.S.A.;
- [17] Nakajima Teruyuki., Tonna Glauco., Rao Ruizhong., Boi Paolo., Kaufman Yoram., Holben Brent., (1996), Use of sky brightness measurements from ground for remote sensing of particulate polydispersions. *Applied Optics*, Vol. 35, Issue.15, pp.2672-2686, OSA Publishing, Washington/U.S.A.;
- [18] Nan Cong., Shilong Piao., Anping Chen., Xuhui Wang., Xin Lin., Shiping Chen., Shijie Han., Guangsheng Zhou., Xiping Zhang., (2012), Spring vegetation green-up date in China inferred from SPOT NDVI data: A multiple model analysis. *Agricultural and Forest Meteorology*, Vol.65, Issue.15, pp.104-113, Elsevier, Amsterdam/Netherlands;
- [19] Özyurt D., Pike P., (2004), Theory and practice of simultaneous data reconciliation and gross error detection for chemical processes. *Computers & Chemical Engineering*, Vol.28, Issue.3, pp.381-402, Elsevier, Oxford/ England;
- [20] Quiroz R., Yarlequé C., Posadas A., Mares V., Immerzzel W., (2011), Improving daily rainfall estimation from NDVI using a wavelet transform. *Environmental Modelling & Software*, Vol.26, Issue 2, pp.201-209, Elsevier, Oxford/England;
- [21] Ramirez M., Allen P., Freeland R., Wilkerson J., (2015), Ground-Based NDVI Sensing: Separating the Ground Surface from the Cotton Canopy. *ASABE*, Vol.58, Issue.3, pp.597-605, U.S.A.;
- [22] Schaefer M., Lamb D., (2016), A Combination of Plant NDVI and LiDAR Measurements Improve the Estimation of Pasture Biomass in Tall Fescue (*Festuca arundinacea* var. Fletcher). *Remote Sensing*, Vol.8, Issue.2, pp.109-119, Molecular Diversity Preservation International, Basel/Switzerland;
- [23] Serth R.W., Heenan W.A., (1986), Gross error detection and data reconciliation in steam metering systems. *AIChE*, Vol. 32, Issue.5, pp.733-742, John Wiley & Sons, Hoboken/U.S.A.;
- [24] Shao Yang, Lunetta R., Wheeler B., Iames J., Campbell J., (2016), An evaluation of time-series smoothing algorithms for land-cover classifications using MODIS-NDVI multi-temporal data. *Remote Sensing of Environment*, Vol.174, Issue.1, pp.258-265, Elsevier, New York/U.S.A.;
- [25] Scharf P., Lory J., (2002), Calibrating Corn Colour from Aerial Photographs to Predict Side-dress Nitrogen Need. *Agronomy Journal*, Vol.94, Issue.3, pp. 397-404, Amer Soc Agronomy, Madison/U.S.A.;
- [26] Sun S.K., Lu Y.J., Gao H., Jiang T.T., Du X.Y., Shen T.X., Wu P.T., Wang Y.B., (2018), Impacts of food wastage on water resources and environment in China. *Journal of Cleaner Production*, Vol. 185, Issue.1, pp.732–739, Elsevier, Oxford/England;
- [27] Torsten I., (1982), Relative addition rate and external concentration; Driving variables used in plant nutrition research. *Plant, Cell & Environment*, Vol.5, Issue.6, pp.443–453, Wiley-Blackwell Publishing, Malden/U.S.A.;
- [28] Zhengjiang Zhang, Junhui Chen., (2014), Simultaneous data reconciliation and gross error detection for dynamic systems using particle filter and measurement test. *Computers & Chemical Engineering*, Vol.69, Issue.3, pp.66-74, Elsevier, Oxford/England;
- [29] Zhuokun Pan., Jingfeng Huang., Qingbo Zhou., Qingbo Zhou., Limin Wang., Yongxiang Cheng., Hankui Zhang., George Alan Blackburn., Jing Yan., Jianhong Liu., (2015), Mapping crop phenology using NDVI time-series derived from HJ-1 A/B data. *International Journal of Applied Earth Observation and Geoinformation*, Vol.34, Issue.2, pp.188-197, Elsevier, Amsterdam/Netherlands;

EFFECT OF PRE-SOAKING AND GRAIN SHAPE ON COOKING ENERGY OF PARBOILED AND RAW RICE

තම්බන ලද සහ කැකුළු සහල් ඇටවල හැඩය හා පිසීමට කලින් පොඟවීම සහල් පිසීමේ ශක්ති පරිභෝජනය මත බලපෑම

K. G. Gunasekara ¹⁾, D. A. N. Dharmasena ²⁾ and F. H. C. A. Silva ^{*2)}

¹⁾ Postgraduate Institute of Agriculture, University of Peradeniya, Peradeniya, Sri Lanka

²⁾ Department of Agricultural Engineering, Faculty of Agriculture, University of Peradeniya, Sri Lanka.

Tel: +94 715 451 630 E-mail: fhcasilva@gmail.com

Keywords: rice cooking energy, cooking time, sorption, Peleg’s model, pre-cook condition

ABSTRACT

Rice is the staple food of Sri Lankans and both parboiled and raw rice forms of medium and slender grain types are popular in Sri Lanka. These two shaped grain varieties were selected and the optimum pre-soaking duration was calculated using the Peleg’s model. The optimum rice to water ratios were determined for different rice types. A three factor factorial experiment was used to analyse the cooking energy and cooking time, considering the grain shape, rice grain process condition and pre-cooking condition. Soaking durations for 86% rice grain saturation was 10 minutes for both shapes in raw form and the optimum rice: water ratio was 1:2.

Parboiled forms, slender grains and un-soaked rice consumed considerably higher amounts of cooking energy and time than raw rice forms, medium type grains and pre-soaked rice. When considering pre-cooking condition and process condition, highest cooking energy and time is consumed by un-soaked parboiled form of rice. Pre-soaked raw rice requires the least and saved about 40% of energy and time compared to the un-soaked parboiled rice. With respect to process condition and grain type, Parboiled slender grains consume the highest cooking energy and cooking time while cooking Raw medium type grains saves about 40% of those requirements.

සාරාංශය

ශ්‍රී ලාංකිකයන්ගේ ප්‍රධාන ආහාරය වන සහල්, කැකුළු සහ තම්බන ලද යන දෙවර්ගයන්ම ජනතාව අතර ප්‍රචලිතය. මධ්‍ය සහ සිහින් හැඩති සහල් වර්ග දෙකක් මෙම පර්යේෂණයේදී අධ්‍යයනයට තෝරා ගන්නා ලද අතර විවිධ ප්‍රශස්ථ පොඟවීමේ කාල පරාසය ජලයේ දුර්භය මගින් ගණනය කරන ලදී. තවද සහල් පොඟවීම සඳහා අවශ්‍ය ප්‍රශස්ථ සහල් : ජල අනුපාතයන්ද විවිධ සහල් වර්ග සඳහා නිර්ණය කරන ලදී.

සහල් පිසීමේ ශක්ති පරිභෝජනය සහ ගතවන කාලය තුන් සාධක ක්‍රමාරෝපිත සංවිභවන අධ්‍යයනයක් මගින් ඇගයීමට ලක් කරන ලදී. මෙහිදී ප්‍රධාන සාධක ලෙස ධාන්‍ය හැඩය, සැකසුම් තත්වය සහ පෙර පිසීමේ තත්වය යන සාධක තුන භාවිත කරන ලදී. කැකුළු සහල් වල අධ්‍යයනය කරන ලද හැඩයන් දෙක සඳහා 86%ක සංතෘප්ත ප්‍රතිශතයක් ලබා ගැනීමට මිනිත්තු 10ක කාලයක් ගත විය. ප්‍රශස්ථ සහල් ජල අනුපාතය 1:2 ලෙස විය.

පිසීමේ ශක්ති පරිභෝජනය සැලකීමේදී තම්බන ලද, සිහින් සහ පෙර නොපොඟවූ සහල් වල ශක්ති පරිභෝජනය මධ්‍ය හැඩති පෙර පොඟවූ කැකුළු සහල් වල ශක්ති පරිභෝජනයට වඩා වැඩි විය. පෙර පිසුම් තත්වයන් සහ සැකසුම් තත්වයන් සැලකීමේදී තම්බන ලද පෙර නොපොඟවූ සහල් වැඩි පිසීමේ ශක්ති ප්‍රමාණයක් සහ කාලයක් පරිභෝජනය කරන ලදී. කලින් පොඟවන ලද කැකුළු සහල් සඳහා අවම ශක්ති පරිභෝජනයක් වාර්තා වූ අතර 40% ක ශක්ති හා කාල ඉතුරුවක් තම්බන ලද නොපොඟවූ සහල් වලට සාපේක්ෂව ලබා දෙන ලදී. සැකසුම් තත්ව සහ ධාන්‍ය වල හැඩය සැලකීමට ගැනීමේදී තම්බන ලද සිහින් හැඩති සහල් වැඩිම පිසීමේ ශක්තියක් හා කාලයක් පරිභෝජනය කරන ලද අතර මධ්‍ය හැඩති කැකුළු සහල් වීම පරිභෝජනයෙන් 40%ක ඉතිරියක් ලබා දීමට සමත් විය.

INTRODUCTION

Energy cost is one of the most important issues in Sri Lanka similar to most of the countries in the world. At present, the highest amount of primary energy in Sri Lanka is provided by the biomass (43%), followed by the petroleum (37%), hydropower (13%) and coal (4%). Electricity remains as the main secondary energy source (Energy, 2015). According to the available statistics in 2014, households, commercial and other sectors accounted for the largest share of energy being 44.7% while the transport and industry sector accounted for 29.4% and 25.9%, respectively (SLSEA, 2014). Another study reveals that 50% of domestic energy use is for cooking purposes (Wijayatunga, Attalage, 2002). In the cooking context,

rice is the staple food which is consumed two or three meals a day in almost all households and the per-capita rice consumption is about 105 kg/year (*WorldBank, 2010*). Therefore, rice cooking accounts for a significant fraction of the cooking energy at each household; a population of 20.8 million cooks approximately 2.18 million tons of rice annually. Energy conservation in rice cooking has a national importance in reducing cost of living and minimizes the national energy crisis while reducing greenhouse gas emissions to the environment.

The basic dimension used for the rice grain classification is size (length of the grain) and the shape (length/width ratio). Both USDA (United States Department of Agriculture) and FAO (Food and Agriculture Organization of the United Nations) classification systems are being used by the scientists. Out of different rice grain types, classified according to shape classification under both systems, slender and medium types are of the prime importance as they are the most popular two grain types consumed by Sri Lankans (*Gunasekara, Dharmasena, 2011*).

A study has been carried out to investigate the effect of soaking on cooking energy conservation of a rice variety (Belleputana) (*Roy, Shimuzu, Kimura, 2004*). However, in this study only three selected soaking durations were considered instead of moisture saturation percentage and physical characteristics of grains. Two other studies have reported a comparison of energies to cook un-soaked and pre-soaked rice of the variety "Bangara Thigadu" with different cooking appliances (*Das et al, 2006*) and a kinetic analysis has been carried out for cooking at both pre-soaked and un-soaked conditions with different levels of water with the same paddy variety (*Chakkaravarthi et al, 2008*). The temperature on soaking had a significant effect on chemical composition, glycemic index and starch characteristics of rice (*Kale et al, 2015*). Effect of thermodynamic properties on pre-soaking was studied in another research and they have used five different temperatures as 35°C, 45°C, 55°C, 65°C and 75°C for soaking. Peleg model was used for curve fitting of the experimental data and the results revealed that the constants of the Peleg model (k_1 and k_2) decreased with increasing temperature, indicating a higher initial absorption rate and higher product water absorption capacity, respectively (*Paulo et al, 2016*). (*Gunasekara, Dharmasena, 2011*), the same research group of this study has studied the effect of grain shape and pre-soaking conditions and established a model for soaking pattern for two common polished rice grain types but limited only for parboiled rice.

Therefore, the objective of this study was to extend the model for polished rice grain soaking patterns and to compare the effect of pre-soaking on cooking time and cooking energy of Raw and Parboiled rice as it has a paramount importance at national and global perspective.

MATERIALS AND METHODS

As the consumer preference is mostly governed by the size and the shape of the rice grains, two popular varieties were selected to represent both long grain varieties and medium grain varieties as shown in Table 1 (*Gunasekara, Dharmasena, 2011*). Like most of the Sri Lankan rice varieties, the selected two varieties are falling into intermediate category (70 -74°C) according to their gelatinization temperature (*Gunasekara, Dharmasena, 2011*).

Table 1

Classification of BG 360 and BG 94-1 rice varieties according to USDA and FAO classification system

Rice variety	Length (mm)	Width (mm)	Length/Width ratio	Classification according to size (Length)		Classification according to Shape (Length/Width)	
				USDA	FAO	USDA	FAO
BG 94-1	6.58	1.87	3.66	Medium	Long	Slender	Slender
BG 360	4.5	1.72	2.67	Short	Short	Medium	Medium

A two-parameter empirical formula that was proposed by Peleg (*Peleg, 1988*) for milk powder was reported as satisfactory in modeling hydration kinetics in vacuum soaking of paddy (rough rice) (*Bello, Tolaba, Suarez, 2008*). The same model was used to derive sorption curves for each of the factorial combinations after testing its fitness for sorption of polished rice grains. The Peleg model relates the instantaneous moisture content with the initial moisture content and the soaking time as given in equation (1).

$$m(t) = m_o + \frac{t}{k_1 + k_2 t} \quad (1)$$

The variation of moisture content is denoted as $m(t)$, in decimal dry basis, with the time t and m_o is the initial moisture content (decimal dry basis) while k_1 , k_2 being constants. The Mean Relative Deviation

Modulus (P), one of the statistical tools used in assessing the goodness of fit of the Peleg model with data was calculated using the equation (2).

$$P = \left(\frac{100}{n}\right) \sum \left(\frac{|M_a - M_p|}{M_p}\right) \quad (2)$$

where P is the Mean Relative Deviation Modulus, M_a is the actual Experimental Moisture content; M_p is the predicted moisture content; and n is the number of observations. P value less than 5, between 5-10 and greater than 10 indicates that the model has an extremely good fit, reasonably good fit and poor fit respectively, with the experimental data.

Since the Parboiled and Raw rice forms are popular among the consumers from different parts of the country, four 100 g samples of both BG 94-1 and BG 360 in both Parboiled and Raw rice forms were soaked in 300 mL of distilled water under room temperature ($27 \pm 2^\circ\text{C}$) and at atmospheric pressure. Subsequently the samples were drawn at 15 minutes intervals for 2.5 hours. After the surface moisture was removed from rice kernels, the samples were kept in oven at 120°C for 24 hours (AOAC, 2000) and dry weights were obtained and the moisture contents were calculated at each time period.

The model fitting procedure of the previous study (Gunasekara, Dharmasena, 2011) was followed for the raw rice as well. According to the Peleg model, the highest moisture content (Equilibrium Moisture Content (EMC)) is achieved when $t \rightarrow \infty$. Even though the Peleg model, gives the highest moisture content or EMC when $t \rightarrow \infty$, prolonged soaking enhances the microbial fermentation resulting in bad odour development. Further, the longer soaking durations are not practical with the present lifestyles. Therefore, the maximum allowable soaking time was limited to 2.5 hours as previously reported by the same research team (Gunasekara, Dharmasena, 2011). In order to provide the equal conditions for both samples of raw and parboiled, the factor combination in which the sorption process is the slowest (parboiled types), was only allowed to hydrate 150 minutes and the moisture content at that particular time and wetted percentage with respect to the EMC was back calculated using the Peleg model. Then the required soaking duration was calculated for the other factor combinations taking the above wetted percentage as a constant.

Four parboiled and raw samples of 250 g each from slender (BG 94-1) and medium grain types (BG 360) were cooked in an electric rice cooker using four different rice to water volume ratios; 1:2, 1:2.5, 1:3 and 1:3.5. After the rice was cooked, few kernels were taken out and pressed between two glass plates. Minimum rice to water ratio which produced cooked rice without having an opaque core when pressed was considered as the optimum rice to water ratio. It was found the 1:2 as the optimum volume ratio for raw rice of both grain types. (Gunasekara, Dharmasena, 2011) have already found that 1:2.5 is the optimum ratio for parboiled rice of both grain types (BG 94-1 and BG 360 varieties).

A three factor factorial experiment was conducted considering the pre-cooking condition (un-soaked and soaked conditions as two levels), rice grain process condition (parboiled and raw rice forms as two levels) and the rice grain type/variety (with two levels as BG 94-1 and BG 360) as the considered factors. Four replicates were tested for each of the factor combination. A rice sample of 300 mL was cooked using 750 mL of distilled water for samples containing parboiled rice while the same amount of rice was cooked in 600 mL of distilled water for raw rice. A Mitsubishi electric rice cooker (Model NJ-Z18T) was used to conduct the cooking trials, while an 110V digital watt meter (Model P4400 KILL A WATT™) (Fig. 1) was employed to obtain the data on cooking energy and cooking time. The data were analyzed by General Linear Model (GLM) using Minitab 15® (2006) statistical software.

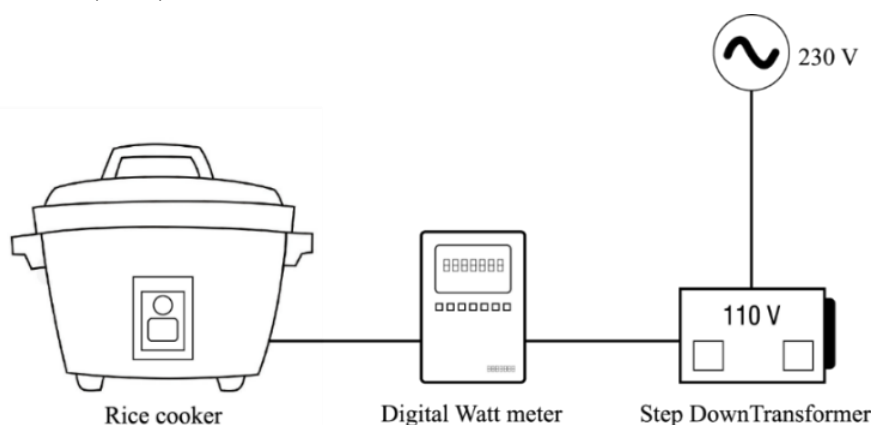


Fig. 1 - Instrumentation setup for the measurement of rice cooking energy

RESULTS

• **Mathematical model fitting for moisture sorption of polished rice grains**

The characteristic hydration curves obtained for raw rice samples of both varieties are shown in Fig. 2. Hydration curves for parboiled rice is extracted from a previous study by the same research team for the comparison purpose of two different forms. The rapid hydration rates shown in the initial phase were diminished to reach a plateau towards the Equilibrium Moisture Contents (saturation) in each of the four cases (Gunasekara, Dharmasena, 2011). According to the hydration curves, the parboiled forms of both rice varieties took much more time to reach the plateau when compared to the raw rice form. The parboiled form of the slender type took the longest time in comparison with all other types. Hydration curves of the raw rice forms of both varieties were more or less similar and almost overlapping with each other. In the parboiled context, there was a huge variation of sorption pattern between two rice types or varieties. Medium grain variety showed higher initial hydration rate compared to the slender grain variety. However, the parboiled medium rice achieved its predetermined moisture content (86% saturation) quickly, in 44 minutes, compared to that of parboiled slender grain variety that took 150 minutes (Gunasekara, Dharmasena, 2011).

In the mathematical model fitting procedure, the corresponding Peleg's coefficients, Residual Sums of Squares (RSS), correlation coefficients (R²), Mean Relative Deviation Modulus values (P) are given in Table 2.

Table 2

Peleg's model fitting for curves of rice hydration as a function of time

Variety	k ₁	k ₂	RSS	R ²	P
Slender Grains (BG 94-1)	45.28 ± 7.58	1.485 ± 0.074	0.00514	0.987	2.38
Medium Grains (BG 360)	19.32 ± 3.34	1.973 ± 0.047	0.00166	0.993	1.53
Slender Grains (BG 94-1)	11.69 ± 5.53	4.065 ± 0.107	0.00059	0.988	1.59
Medium Grains (BG 360)	12.15 ± 8.97	4.112 ± 0.173	0.00147	0.972	2.28

Source: (Gunasekara, Dharmasena, 2011)

According to Table 3, BG 94-1 parboiled slender rice saturated 86% with respect to its EMC in water or water saturation within 150 minutes of soaking, while BG 94-1 slender raw rice, BG 360 medium parboiled and BG 360 medium raw rice forms took 10, 44 and 10 minutes, respectively to reach the pre-determined 86% saturation.

Table 3

Comparison of soaking times of different rice types to reach predetermined saturation level and the Peleg's sorption model parameters

Variety	Mo	t	MC(t)	Me	Soaking%
BG94-1 Parboiled	0.138	150	0.698	0.811	86
BG94-1 Raw	0.166	10	0.353	0.409	86
BG360 Parboiled	0.156	44	0.570	0.663	86
BG360 Raw	0.157	10	0.348	0.403	86

Source: (Gunasekara, Dharmasena, 2011)

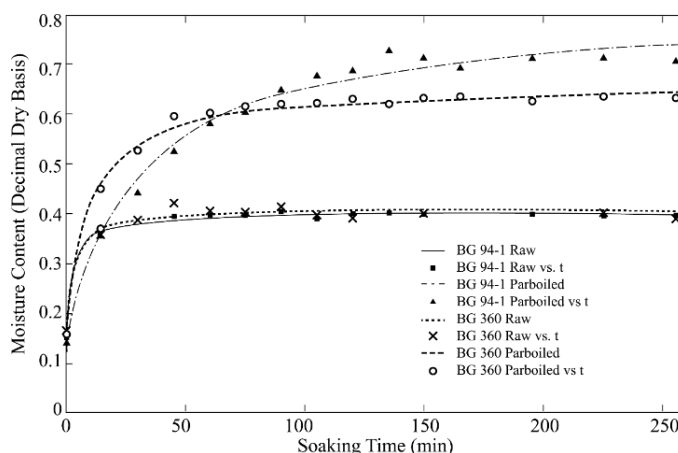


Fig. 2 - Comparison of sorption curves of parboiled and raw rice forms of both slender and medium grain varieties at the room temperature (27 ± 2°C) and at atmospheric pressure

• **Comparison of optimum rice to water volume ratios for cooking**

Main effects of all the factors: pre-cook condition (pre-soaked or not), process condition (Raw or Parboiled) and the rice grain type (slender or medium) were significant for both cooking energy and cooking time. Even though pre-cook x process condition and process condition x grain shape were significant for cooking energy, the pre-cook condition x grain shape interactions were not significant for the cooking energy ($p > 0.05$). The three way interaction: pre-cook condition x process condition x grain shape was also not significant for the cooking energy ($p > 0.05$) (Table 4). Similarly for cooking times, all the main effects were significant and the two way interaction of pre-cook x process condition and process condition x grain shape were significant ($p \leq 0.05$). However, the two way interaction of pre-cook condition x grain shape and the three way interaction; pre-cook condition x process condition x grain shape were not significant ($p > 0.05$) (Table 5).

Table 4

Analysis of variance for cooking energy, using adjusted sums of squares for tests

Source	DF	Seq SS	Adj SS	Adj MS	F	P
Pre-cook	1	0.0200	0.0200	0.0200	369.2300	0.000
Process	1	0.0946	0.0946	0.0946	1746.6900	0.000
Grain	1	0.0200	0.0200	0.0200	369.2300	0.000
Pre-cook x Process	1	0.0025	0.0025	0.0025	45.2300	0.000
Pre-cook x Grain	1	0.0000	0.0000	0.0000	0.2300	0.635
Process x Grain	1	0.0032	0.0032	0.0032	59.0800	0.000
Pre-cook x Process x Grain	1	0.0000	0.0000	0.0000	0.2300	0.635
Error	24	0.0013	0.0013	0.0001		
Total	31	0.1416				

Table 5

Analysis of variance for cooking time, using adjusted sums of squares for tests

Source	DF	Seq SS	Adj SS	Adj MS	F	P
Pre-cook	1	157.530	157.530	157.530	225.720	0.000
Process	1	693.780	693.780	693.780	994.070	0.000
Grain	1	166.530	166.530	166.530	238.610	0.000
Pre-cook x Process	1	19.530	19.530	19.530	27.990	0.000
Pre-cook x Grain	1	2.530	2.530	2.530	3.630	0.069
Process x Grain	1	22.780	22.780	22.780	32.640	0.000
Pre-cook x Process x Grain	1	1.530	1.530	1.530	2.190	0.152
Error	24	16.750	16.750	0.700		
Total	31	1080.970				

• **Effect of pre-soaking on cooking time and cooking energy**

Fig.3 illustrates the cooking time and cooking energy requirements of four main factor combinations: soaked raw and parboiled and un-soaked raw and parboiled types. According to the graph, pre-soaking requires less cooking energy and cooking time for both parboiled and raw rice types. The amount of cooking energy and cooking time conservation with respect to highest energy consuming factor combination considering pre-cook condition and the process condition are illustrated in Table 6. According to Turkey mean comparison test, pair wise comparisons among all the levels of pre-cook condition x process condition interactions were significantly different ($p \leq 0.05$).

Table 6

Mean percentage energy and time saving in cooking Parboiled and Raw rice

	Un-soaked-Parboiled	Un-soaked-Raw	Soaked-Parboiled	Soaked-Raw
% Energy Reduction	0	-32	-17	-40
% Time Reduction	0	-33	-18	-41

Fig. 4 illustrates the cooking time and cooking energy comparisons of slender and medium grain types processed as parboiled or raw. According to the graph, slender grain of both parboiled and raw consume more energy and time than medium grain type. According to data, parboiled slender consumes the highest cooking energy and cooking time and Table 7 provides the percentage energy and time saving for above four rice types with respect to parboiled slender rice type. The pair wise comparisons among all the levels of process condition x grain type interactions were significantly different ($p \leq 0.05$) for cooking energy and cooking time.

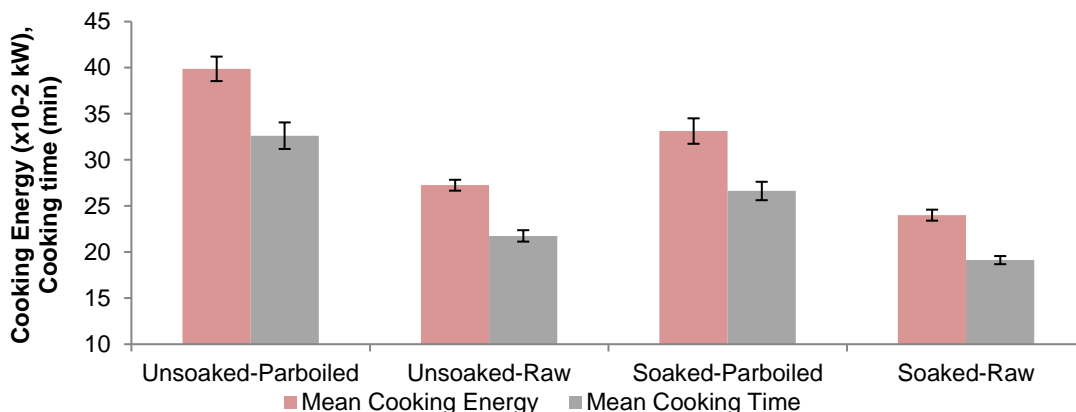


Fig. 3 - Mean cooking energy and cooking times for Parboiled and Raw rice types in both un-soaked and pre-soaked conditions

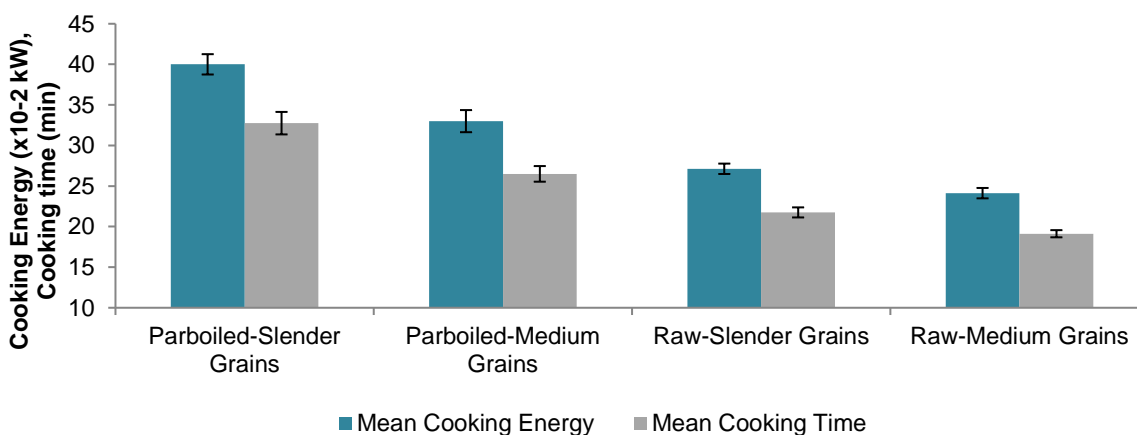


Fig. 4 - Mean cooking energy and cooking times for Parboiled and Raw rice of both slender and medium types

Table 7

Mean percentage energy and time saving in cooking different types of rice				
	Parboiled-Slender	Parboiled-Medium	Raw-Slender	Raw-Medium
% Energy Reduction	0	-18	-32	-40
% Time Reduction	0	-19	-34	-42

• Discussion

Establishment of a mathematical model for moisture sorption for polished rice soaking in water is very important for predicting sorption related unknown parameters. The same research team has reported that the Peleg’s model fits well for the sorption of parboiled rice. In the evaluation of the acceptability of Peleg’s mathematical model, very low RSS values, very high R² values (0.97 to 0.98) and Mean Relative Deviation Modulus (P) value less than five (5) confirms that the Peleg model fits extremely well with the all four types of polished rice grain sorption data. Therefore, the Peleg model can be used to accurately estimate instantaneous moisture content of polished raw rice as well as the parboiled rice when soaking in water at room temperature and atmospheric pressure.

It has been previously reported that prior soaking reduces the energy consumption and cooking time during normal cooking, while the pre-soaking does not contribute to the energy conservation in the case of controlled cooking in electric rice cooker (Das *et al*, 2006). Soaking rice prior to cooking, an established energy saving practice, resulted in energy savings to the extent of 5–11% in normal cooking and 3–18% in controlled cooking and also pre-soaking shows only a marginal reduction (Lakshmi *et al*, 2007).

However, according to another study (Roy, Shimuzu, Kimura, 2004) cooking of milled raw and parboiled rice by adopting the pre-soaking method for 60 minutes with an electric rice cooker reduces the cooking energy of cooked rice (66% moist) by 4% and 6 to 11% respectively. However, information on grain type, gelatinization temperature and the grain saturation level are not considered in all above studies.

According to the results of this experiment, 40% of cooking energy and 41% of cooking time reduction is evident by cooking raw rice after being soaked for 10 minutes (86% saturation), 32% energy and 33% cooking time for un-soaked-Raw rice, and 17% energy and 18% cooking time for soaked Parboiled rice compared to cooking of un-soaked parboiled rice. Therefore, it is clearly evident that significant amount of energy and cooking time could be conserved by switching to soaked raw rice instead of un-soaked parboiled rice. Further, pre-soaking has reduced about 17% energy for parboiled type and about 8% for raw rice type. The percentage energy saving for raw rice is observed as twice as the value reported in a previous study (Roy, Shimuzu, Kimura, 2004) and the percentage cooking energy saving for Parboiled rice is also considerably higher than their reported range. This may be due to the differences in physicochemical properties of the grain varieties used in Sri Lanka, optimization of water requirement and the degree of pre-soaking of the rice grains.

In addition, cooking of Raw-Medium shape grain type has shown a 40% reduction in energy and 42% reduction in cooking time compared to Parboiled-Slender shape grain type. The cooking energy and cooking time reduction of Parboiled-Medium shape grain type was 18 and 19%, and Raw-Slender shape grain type was 32 and 34% respectively, compared to that of the Parboiled-Slender grains. Therefore, it is evident that the process condition; raw or parboiled as well as pre-cook condition; pre-soaked or un-soaked have influenced on the reduction of cooking energy and cooking time requirement. The cooking energy reduction in pre-soaked rice may be due to the uniformity of heat and mass transfer during cooking in the pre-soaked rice grains. Rice cooking is a process governed by two mechanisms; [1] moisture diffusion from surface to core and [2] physicochemical reactions of grain components. According to kinetics, rice cooking is similar to a first order chemical reaction. In the case of un-soaked rice cooking, there are two falling rate periods similar to drying of hygroscopic foods with two corresponding rate constants. This is due to the initial formation of an outer cooked impervious layer which acts as a barrier for moisture diffusion to the reaction site at the core of the rice grain. Therefore, the initial reaction rate is dropped down after about 80% of gelatinization and enters into a second reaction phase. However, in cooking pre-soaked rice, there is only one reaction rate as the grain is adequately hydrated for gelatinization. This is the main reason for cooking energy and cooking time conservation in pre-soaked rice (Chakkaravarthi *et al*, 2008).

According to results of the experiment, both slender and medium types of parboiled rice consumed significantly higher cooking energy and time than raw types. A previous study carried out using μ -CT and MRI technologies to identify the grain microstructure's effect on cooking behaviour and reported that the increasing porosity within the grain reduces the cooking time (Mohoric *et al*, 2009). During parboiling the starch crystals are being gelatinized and become amorphous molecules resulting less porous within the rice grains. Therefore, the hydration time during the cooking process is prolonged for parboiled rice resulting higher cooking time, leading to higher cooking energy than raw milled rice (Otegbayo, Osamuel and Fashakin, 2001).

CONCLUSIONS

The Peleg's mathematical model fits well with the moisture sorption data of polished raw rice. The optimum rice to water ratios for cooking raw rice is 1:2. Parboiled forms, slender grain types and un-soaked rice require considerably higher amounts of cooking energy and time than raw rice forms, medium type grains and at least 86% pre-soaked rice. When considering pre-cook condition and process condition, highest cooking energy and cooking time is consumed by un-soaked Parboiled form of rice. Pre-soaked raw rice requires the least and could be saved about 40% of energy and time required for un-soaked parboiled rice. With respect to process condition and grain type, parboiled slender grains consumes the highest cooking energy and time while cooking raw medium type grains save about 40% of those requirements.

REFERENCES

- [1] Ameresekere, R.V.W.E., (1984), Interaction between agriculture, nutrition, and food science in Sri Lanka, *Interaction between agriculture, nutrition, and food science*, 418 p, *Proceedings of a workshop held at Hyderabad, India, 10-12 November 1981*, ISBN 92-808-0478-2, Hyderabad: United Nations University, Tokyo/Japan;
- [2] Bello M.O., Tolaba M.P., Suarez C, (2008), Hydration kinetics of rice kernels under vacuum and pressure, *International Journal of Food Engineering*, Vol: 4 (4), pp. 181-186;
- [3] Chakkaravarthi A., Lakshmi S., Subramanian R., Hegde V.M., (2008), Kinetics of cooking un-soaked and presoaked rice, *Journal of Food Engineering*, Vol. 84, pp. 181-184;
- [4] Das T., Subramanian R., Chakkaravarthi A., Singh V., Ali S. Z., Bordoloi P. K, (2006), Energy conservation in domestic rice cooking, *Journal of Food Engineering*, Vol. 75, pp. 156-166;
- [5] Gunasekara K.G., Dharmasena D.A.N, (2011), Effect of grain shape and pre-soaking on cooking time and cooking energy, *Tropical Agricultural Research*, Vol 22 (2), pp. 194-203;
- [6] Kale S. J., Jha J. K., Jha G. K., Sinha J. P., Lal S. B., (2015), Soaking Induced Changes in Chemical Composition, Glycemic Index and Starch Characteristics of Basmati Rice, *Rice Science*, pp. 227-236;
- [7] Lakshmi S., Chakkaravarthi A., Subramanian R., Singh V., (2007), Energy consumption in microwave cooking of rice and its comparison with other domestic appliances, *Journal of Food Engineering*, Vol 78, pp. 715-722;
- [8] Mohoric, A., Vergeldt F., Gerkema E., Van Dalen G., Van denDoel L.J., Van Vliet L.J., Van As H., Van Duynhoven J., (2009), The effect of rice kernel microstructure on cooking behaviour, *Food Chemistry* Vol. 115, pp 1491-1499;
- [9] Otegbayo B.O., Osamuel F., Fashakin J.B., (2001) Effect of parboiling on physicochemical quality of two local rice varieties in Nigeria, *The Journal of Food Technology in Africa*, Vol. 6 (4), pp. 130-132;
- [10] Paulo C.C., Gabriel H.H.D.O., Ana Paula L.R.D.O., Fernando M.B., André L.D.G., (2016), Thermodynamic properties of drying process and water absorption of rice grains, *CyTA-Journal Of Food*, pp. 1-7;
- [11] Peleg M., (1988), An empirical model for the description of moisture sorption curves, *Journal of Food Science*, Vol. 53, pp. 1216-1219;
- [12] Roy P., Shimuzu N., Kimura T., (2004), Energy Conservation in cooking of Milled Raw and Parboiled Rice, *Food Science and Technology*, Vol. 10 (2), pp. 121-126;
- [13] Wijayatunga P.D.C., Attalage R. A., (2002), Analysis of household cooking energy demand and its environmental impact in Sri Lanka, *Energy Conversion and Management*, Vol. 43 (16), pp 2213–2223;
- [14] *** AOAC, (2000), *Official methods of analysis 17th Edition*, USA: Association of analytical communities, Ed Gaithersburg, MD, USA;
- [15] *** Ministry of Power and Energy, (2015) *Sri Lanka energy sector development plan for a knowledge-based economy 2015-2025*;
- [16] *** SLSEA, (2014), Total Energy Demand in Household, Commercial and Other Sectors, *Sri Lanka Energy Balance 2014 - An Analysis of Energy Sector Performance*, Vol. 85, Colombo: Sri Lanka Sustainable Energy Authority;
- [17] WorldBank, (2010), *Food Prices Increases in South Asia*. Sustainable Development Department, Washington, DC: The International Bank for Reconstruction and Development.

DETECTION AND CLASSIFICATION OF BRUISES IN “RED DELICIOUS” APPLE FRUITS BY APPLYING PIEZOELECTRIC TRANSDUCERS

/

تشخیص و طبقه‌بندی کوفتگی سیب "رد دلیشز" با استفاده از ترانسدیوسرهای پیزوالکتریک

Ph.D. Stud. Mehrdad Foj Laley¹⁾, Assoc. Prof. Parviz Ahmadi Moghadam¹⁾, As Prof. Ali Hasanpour¹⁾,
As prof. Vahid Rostampour¹⁾

¹⁾ Department of Mechanical Engineering of Biosystems, Urmia University, Urmia, Iran
Tel: 0984432779558; E-mail: P.ahmadi@urmia.ac.ir

Keywords: apple, bruises, piezoelectric transducers, vibration, wavelet

ABSTRACT

Bruising is one of the most important factors of apple wastes. In this study, the performance of both stimulator and receptor piezoelectric transducers in the diagnosis of Red Delicious apple bruising was evaluated. The evaluations were conducted on damaged apples at level 1 (depth of 0.3 cm and 1.58 cm in diameter), level 2 (depth of 0.4 cm and 2.22 cm in diameter) and level 3 (depth of 0.6 cm and 3.4 cm in diameter). The signal processing was carried out in both time and time-frequency domains and two properties of Root Mean Square (RMS) and Kurtosis were calculated. To transmit signals in time-frequency domain, wavelet transform with 4 levels of decomposition including approximate a1 to a4 and details d1 to d4 were used. Results showed that in the time domain, the value of RMS of level 1 damaged apples was 22% less than safe apples ($P < 0.05$), but there was neither significant difference between damage levels, nor in the value of kurtosis. In the time-frequency domain, the RMS values of safe apples in a1, a2 approximates and d2 and d3 details were significantly higher than level 1 damage ($P < 0.01$), but no significant difference was found between damage levels. In this domain, the value of kurtosis of damaged apples in level 1 in details d4 was 86% higher than safe apples and in the a4 approximate, the difference between the levels of kurtosis was significant in levels of damage 1, 2 and 3 ($P < 0.01$). Therefore, piezoelectric transducers are able to detect apple bruising.

چکیده

کوفتگی از مهمترین عوامل ضایعات سیب می باشد. در این تحقیق کارایی دو مبدل پیزوالکتریک تحریک کننده و دریافت کننده ارتعاش در تشخیص کوفتگی سیب رد دلیشز مورد ارزیابی قرار گرفت. ارزیابی ها روی سیب های آسیب دیده سطح یک (عمق 0/3 سانتی متر و قطر 1/58 سانتی متر)، سطح دو (عمق 0/4 سانتی متر و قطر 2/22 سانتی متر) و سطح سه (عمق 0/6 سانتی متر و قطر 3/4 سانتی متر) انجام شد. پردازش سیگنالها در دو حوزه زمان و زمان-فرکانس انجام شد و دو ویژگی ریشه میانگین مربعات و کورتوسیس محاسبه شد. برای انتقال سیگنالها به حوزه زمان-فرکانس از تبدیل موجک با 4 سطح تجزیه شامل اپروکسیمیت های a1 تا a4 و دیتیلزهای d1 تا d4 استفاده شد. نتایج نشان داد که در حوزه زمان مقدار ریشه میانگین مربعات سیب های آسیب دیده سطح 1، 22% کمتر از سیب های سالم بود ($P < 0.05$) ولی بین سطوح آسیب 1، 2 و 3 اختلاف معنی داری وجود نداشت. در این حوزه اختلاف مقدار کورتوسیس ها معنی دار نبود. در حوزه زمان-فرکانس مقدار ریشه میانگین مربعات سیب های سالم در اپروکسیمیت های a1 و a2 و دیتیلزهای d2 و d3 بیشتر از آسیب سطح 1 بود ($P < 0.01$) ولی بین سطوح آسیب 1، 2 و 3 اختلاف معنی دار نبود. در این حوزه مقدار کورتوسیس سیب های آسیب دیده سطح 1، در دیتیلز d4، 86% بیشتر از سیب های سالم بود و در اپروکسیمیت a4 اختلاف بین مقدار کورتوسیس سطوح آسیب 1، 2 و 3 معنی دار بود ($P < 0.01$). بنابراین ترانسدیوسر های پیزو الکتریک با استفاده از ویژگی کورتوسیس قادر به تشخیص غیر مخرب سطوح لهدگی سیب می باشند.

INTRODUCTION

The apple fruit (*Malus domestica brokh*) is rich in vitamin C and pectin. It has high calorie content (Nunes, 2008). Iran has the eighth ranking between the apple producers of the world in 2015 with the production of 1.7 million tons (FAO, 2015). The fruit quality can be determined by external (i.e. weight and colour) and internal (i.e. firmness, sugar content and acidity) characteristics (Rostampour et al., 2013). The apple quality contains different factors such as external features, texture, acidity, and soluble solid contents (SSC). There are different methods for measuring these criteria including destructive and non-destructive techniques. It can be said that non-destructive methods have no invasive effect on thermal, chemical, mechanical, photo physical, and photo chemical properties of agricultural products. The principle of using sound properties of materials (acoustic method) is one of the non-destructive evaluations (Arana et al., 2004).

In recent decades, various non-destructive methods are presented to evaluate bruises in fruits. Most of these methods are sensitive to the physical characteristics of the fruit. These characteristics are mechanical (force-deformation curve, sound and impact responses, and ultrasonic methods), optical (visible and NIR spectroscopy), electromagnetic (nuclear magnetic resonance), and chemical (the olfactory machine) (ElMasry *et al.*, 2009). The non-destructive methods are providing higher velocities in quality measurements. The bruises are one of the external damages of fruits that occur during harvest and post-harvest operations. The bruises are the second important factor of quality after flourished in apple (Stajniko *et al.*, 2004). It happens due to applying a mechanical force to the texture of fruits. Bruise detection in "Red Delicious" apples by using image analysis and similar techniques has a low accuracy (Kleynen *et al.*, 2005). Bennedsen *et al.* (2005) used digital imaging technique for bruise detection in apples. The results showed that it was able to distinguish bruised fruits from intact ones with the accuracy of 85%. The sound and vibration response method is one of the non-destructive methods to evaluate the textural quality of agricultural products.

The amount of bruises depends on elastic parameters of the environment called Young's modulus E(Pa) or shear stress modulus G(Pa) (García *et al.*, 2005). Vibrational sensors, used for identifying and measuring the propagated signals by fruits, are classified into contact and non-contact sensors. The contact sensors (usually piezoelectric device or accelerometer) are connected directly to the surface of fruit, but non-contact sensors (usually microphone) do not have any contact with the samples.

According to the high importance of quality control in post-harvest period and separation of damaged textures in fruits, the objective of the current study is checking out the ability of piezoelectric transducer as a non-destructive method aimed at detecting bruised textures. Herein, two piezoelectric transducers have been used to detect the bruises in "Red Delicious" apples. The performance of the developed system is evaluated in bruise detection at three levels. The signals are processed in time and time-frequency domain by wavelet transformation. Then, two features, RMS and Kurtosis, are extracted from signals.

MATERIALS AND METHODS

SAMPLE PREPARATION

"Red Delicious" apples have been harvested from a garden in West-Azerbaijan province of Iran in 2017. Then, samples were washed and allowed to dry under the free flow of air. The samples were transferred to post-harvest laboratory in the Biosystems department of Urmia University in order to perform the related tests. Different levels of bruises have been shown in table 1.

Table1

Different levels of bruises			
Level3	Level2	Level1	Bruises levels
0.6	0.40	0.30	Depth (cm)
3.4	2.22	1.58	Diameter (cm)

PIEZOELECTRIC SET-UP

The experimental set-up based on sonic vibration response was designed and made. Piezoelectric transducers contain two PZT layers with the thickness of 0.19mm. In this system, a linear voltage amplifier (Model EPA-104) has been used. The non-destructive device has been shown in Fig1.



Fig.1- Non-destructive set-up to evaluate bruises

This set-up contains a soft bed with two piezoelectric transducers: one for sample excitation and another as a sensor. The vibration passes the fruit and is received by the receiver sensor. For this reason, the received signal goes into a microprocessor. Then, noise and disturbing vibrations were removed by low-pass filters. Finally, filtered signal appears in voltage through the amplifier. The received signal has been sent to a PC by USB port with a 1000 Hz sampling speed. It is notable that the receiver sensor was on bruise areas during the experiments.

SIGNAL PROCESSING

The vibrational signals were processed in time and time-frequency domains by wavelet transformation. In this study, two features, Root Mean Square (RMS) and Kurtosis, were used to compare the output signals from fruits.

ROOT MEAN SQUARE (RMS)

Root Mean Square (RMS) is one of the popular quantities in vibration science. RMS is calculated from Equation (1) for digital and random signals (Mohammad et al, 2013):

$$a_{RMS} = \left[\sum_{k=1}^N a^2(t_k) \right]^{\frac{1}{2}} \quad (1)$$

Where a is the amplitude at the moment of t_k and N is the number of samples.

KURTOSIS

Kurtosis expresses the magnitude and sharpness of signal extreme. Kurtosis (K) is calculated from Equation (2) for digital and random signals ($x(t)$) with N samples (Hong & Dhupia, 2014):

$$k = \frac{\frac{1}{N} \sum_{i=1}^N x(i)^4}{\left(\frac{1}{N} \sum_{i=1}^N x(i)^2 \right)^2} \quad (2)$$

WAVELET TRANSFORMATION

In Wavelet transformation, the signal is passed through a series of upstream and downstream filters. Signal is divided in two parts; the section, which passes from a high-pass filter, contains high frequency data i.e. noise. It is called details. The second section, which passes from a low-pass filter, contains low frequency data and identity features of signals. In general, if $x(t)$ is the main signal and is decomposed into x levels, the first signal can be achieved from the sum of approximation signal at the last level and detail functions at different levels (Equation (3)) (Zanardelli et al., 2005; Soman et al., 2010):

$$x(t) = a_n(t) + \sum_{j=1}^n d_j(t) \quad (3)$$

Decomposition operations can be continued until there is no significant data in approximations. So, the first signal can be rebuilt using details signals without losing any necessary data. Function type selection is different for various problems in wavelet transformation. The Daubechi function (DB) has been used in most of the studies. The efficiency of Daubechi function is acknowledged. Hence, the mentioned function is used in this research to decompose the signals. Herein, Daubechi function with four decomposition levels was selected after try and error. Therefore, the signal can be written as Equation (4), (d_1 - d_4 are details and a_4 is approximation):

$$x[n] = a_4 + d_4 + d_3 + d_2 + d_1 \quad (4)$$

Where $x[n]$ is the main signal and indexes are related to the decomposition level of signal.

STATISTICAL ANALYSIS

The received signals from intact and damaged apples were compared with each other. In total, there were 48 samples and data acquisition was repeated 12 times per treatment. MATLAB R 2014a software was used for signal processing. Duncan method compared the means with each other and SAS 9.1 software was used for statistical analysis.

RESULTS

SIGNAL PROCESSING IN TIME DOMAIN

Fig. 2 shows the received signals from intact and damaged apples at levels 1, 2, & 3 in time domain. As seen, the received signals were same for both intact and damaged samples. Consequently, there was no obvious difference between them. Therefore, RMS and kurtosis was extracted from the signal for an accurate processing.

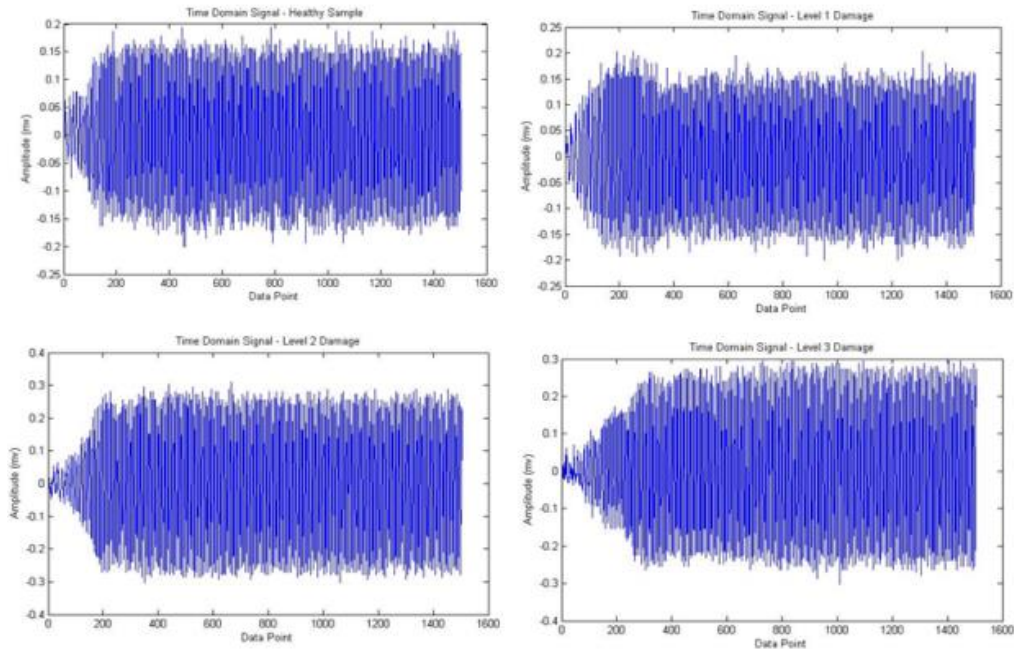


Fig. 2 - Time domain signals for intact and damaged samples at levels 1, 2, & 3

RMS and kurtosis amounts are shown in Fig. 3 for time domain signals of intact and damaged samples at levels 1, 2, & 3. The RMS amount for damaged apples of level 1 was 22% less than for intact ones ($p < 0.5$). However, there is no significant variation in RMS amount according to the increase in the damage region from level 1 to level 2 and from level 2 to level 3. So, the RMS can detect presence or absence of injuries in apples at the confidence level of 95%, but it cannot be considered as a suitable criterion in detecting different levels of injuries.

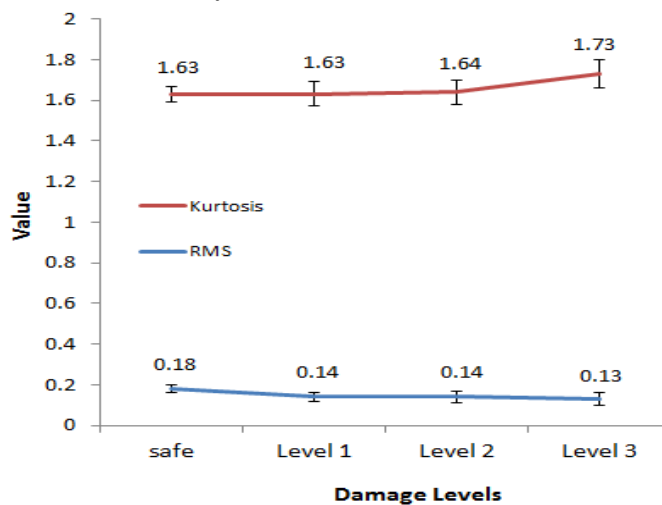


Fig. 3 - RMS and kurtosis amounts for intact and damaged samples at levels 1, 2 & 3 in time domain

Additionally, the kurtosis amount was approximately same for intact and damaged samples in time domain signals and means differences were not statistically significant. Hence, kurtosis in time domain signals was not able to detect damages.

SIGNAL PROCESSING IN TIME-FREQUENCY DOMAIN

Due to accurate processing of signals, wavelet transformation was used. It transferred signals to time frequency domain and converted the main signal to some sub-signals. An example of a main signal and sub-signals is shown for intact and damaged samples at level 3 in Fig. 4 and Fig. 5 respectively.

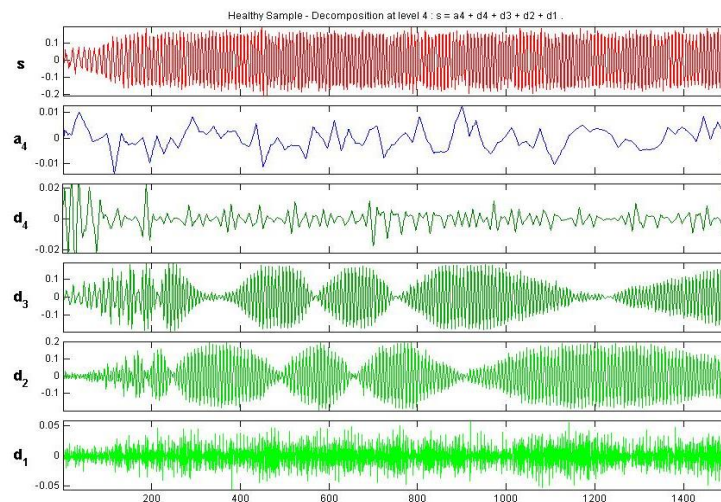


Fig. 4 - The main signal and sub-signals for an intact apple

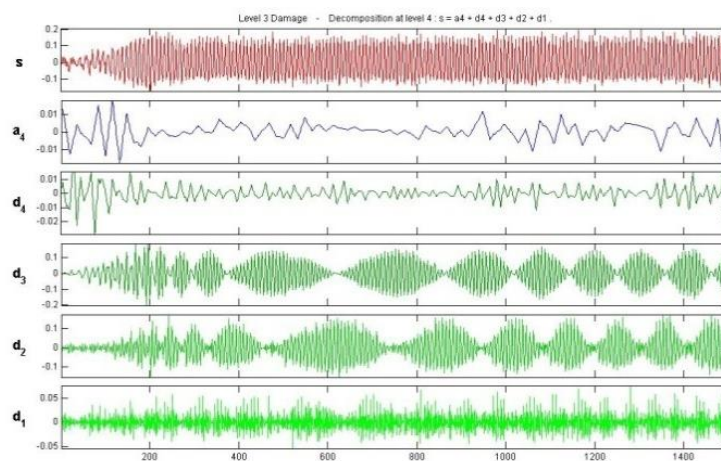


Fig. 5 - The main signal and sub-signals for a damaged apple at level 3

The main signals (s) in Fig. 4 and Fig. 5 do not show any difference among the studied treatments, but some differences can be seen with the naked eye after decomposing signals and studying sub-signals. For example, the amplitude of d_4 sub-signal for damaged samples of level 3 is less than that for intact ones at first moments of applying vibration. It can be also seen that d_2 and d_3 sub-signals in damaged apples of level 3 have more beating situation than intact ones. This difference can be related to the presence of weakness in system structure and consequently manipulate the output signal. However, there was no definite conclusion, and for better comparison, RMS and kurtosis values of decomposed signals were calculated.

In Fig. 6 the RMS values of sub-signals and in Fig.7 the kurtosis values of sub-signals, in two sections of approximates and details for healthy and damaged apples, in levels 1, 2 and 3 are shown. Given that the signals were decomposed in 4 levels, the results are presented in 4 levels of approximation (a_1 to a_4) and 4 levels of details (d_1 to d_4).

As seen in Fig. 6 RMS amount in damaged samples is less than that in intact ones according to all sub-signals of approximations ($a_1 - a_4$) and details ($d_1 - d_4$). Decreasing the RMS can be due to softening the texture of damaged fruits and attenuating the passing signal from fruit. RMS amounts of intact and damaged fruits were not significantly different at third and fourth approximations (a_3 & a_4) (Fig.6).

However, the RMS amounts of intact and damaged fruits were significantly different at first and second approximations (a_1 & a_2) ($p < 0.01$). It shows that RMS amounts among damaged samples of levels 1, 2, & 3 are not statistically significant. Also, this amount is not significantly different in first and fourth details (d_1 & d_4), but it is statistically significant in second and third details (d_2 & d_3) at the confidence level of 1%.

It demonstrates that RMS is not significantly different among damaged samples of levels 1, 2, & 3. Consequently, RMS feature is not suitable for detecting damaged samples of levels 1, 2, & 3 from each other even using wavelet transformation and decomposing the main signal to sub-signals. Hence, the RMS can only detect intact apples from damaged samples of level 1 in some sub-signals.

In Fig.7, the comparison of kurtosis amounts between details sub-signals shows that kurtosis in damaged samples of level 3 is 221% more than that in damaged apples of level 2 in fourth approximation sub-signal (a_4). Additionally, this amount for damaged apples of level 2 is 325% more than that for damaged ones of level 1. As shown in Fig. 7, the kurtosis in damaged samples of level 1 is 86% more than that in intact ones according to the fourth details sub-signal (d_4). It can be concluded that the kurtosis in the fourth details sub-signal (d_4) is used for detecting damaged samples of level 1 from intact ones.

However, the kurtosis in fourth approximation sub-signal (a_4) can be used for separating different levels of injuries. The sensitivity of a_4 and d_4 toward the changes in fruit conditions can be due to the destruction of homogenous structure in intact apples and disorders in passing signals from the texture of damaged samples. These disorders in damaged samples of level 1 make little changes in general process of signal and can be only shown in the main sub-signal of details (d_4). However, the mess in the vibrational signal increases with the increase of injuries to levels 2 and 3. So, it influences the general structure of signal or fourth approximation (a_4).

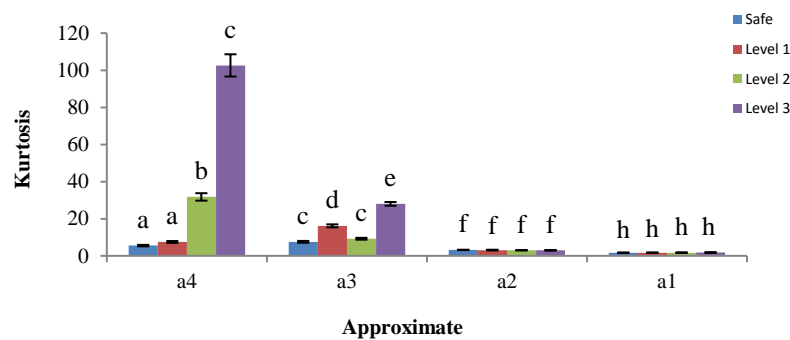


Fig. 6- The kurtosis of intact and damaged samples in approximations signals

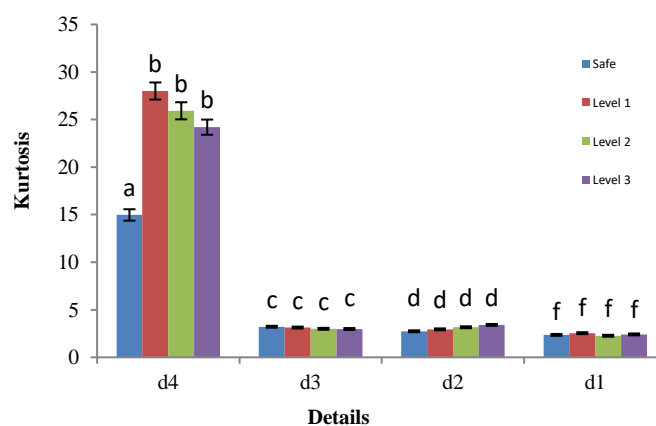


Fig. 7- The kurtosis of intact and damaged samples in details signals

CONCLUSIONS

In this article, two piezoelectric transducers were used to detect bruises in “Red Delicious” apples, non-destructively. In this technique, vibrational signals were passed through the texture of fruits. These signals were processed in time and time frequency (decomposition with wavelet transformation) domains. The results demonstrated that piezoelectric transducers could correctly detect the bruises in “Red Delicious”

apples. The detection of different levels of damages was impossible in time domain, but it was possible by using wavelet transformation and sub-signals processing. Signal analysis in time domain showed that only RMS could distinguish intact apples from damaged ones, but it was not helpful in the detection of different levels of injuries using wavelet transformation in time-frequency domain and comparing the kurtosis of sub-signals could be useful in detection of intact samples from damaged apples and in separating the different levels of damages from each other.

REFERENCES

- [1] ElMasry G., Wang N., Qiao C. V., ElSayed A, (2008), Early detection of apple bruises on different background colours using hyperspectral imaging, *LWT- Food Science and Technology*, Vol. 41, Issue 2, pp. 337-345;
- [2] ElMasry G., Wang N., Vigneault C, (2009), Detecting chilling injury in Red Delicious apple using hyperspectral imaging and neural networks, *Postharvest Biology and Technology*, Vol. 52, pp. 1-8;
- [3] Enes A. M., Fracarolli J. A., Fabbro I. M. D., Rpdrigues S, (2012), Biospeckle supported fruit bruise detection, *International Journal of Biological, Biomolecular, Agricultural, Food and Biotechnological Engineering*, Vol. 6, Issue 10, pp. 889-891;
- [4] García-Ramos F.J., Valero C., Homer I., Ortiz-Cañavate J. & Ruiz-Altisent M, (2005), Non-destructive fruit firmness sensors - a review, *Spanish Journal of Agricultural Research*, Vol. 3 , Issue 1, pp. 61-73;
- [5] Kleynen O., Leemans V., Destain M-F, (2005), Development of a multi-spectral vision system for the detection of defects on apples, *Journal of Food Engineering*, Vol. 69, pp. 41-49;
- [6] Konopacka D., Pocharski W.J, (2004), Effect of storage conditions on the relationship between apple firmness and texture acceptability, *Postharvest Biology and Technology*, Vol. 32, pp. 205-211;
- [7] Ma Y., Haung M., Zhu Q., Li Y., Bu P, (2014), Recognition of bruise and pest infestation apple based on hyperspectral imaging technique, *Transactions of the ASABE*, No. 141908135;
- [8] Macrelli E., Romani A., Paganelli R. P., Sangiorgi E., Tartagni M, (2013a), Piezoelectric transducers for real-time evaluation of fruit firmness, Part I: Theory and development of acoustic techniques, *Sensors and Actuators A: Physical*, Vol. 201, pp. 487-496;
- [9] Macrelli E., Romani A., Paganelli R. P., Sangiorgi E., Tartagni M, (2013b), Piezoelectric transducers for real-time evaluation of fruit firmness, Part II: Statistical and sorting analysis, *Sensors and Actuators A: Physical*, Vol. 201, pp. 497-503;
- [10] Martinsen P., Oliver R., Seelye R., McGlone, V. A., Holmes T., Davy M., Johnston J., Hallett I., Moynihan K, (2014), Quantifying the diffuse reflectance change caused by fresh bruises on apples, *Transactions of the ASABE*, Vol. 57, Issue 2, pp. 565-572;
- [11] Hong L., Dhupia J. S, (2014), A time domain approach to diagnose gearbox fault based on measured vibration signals, *Journal of Sound and Vibration*, Vol. 333, Issue 7, pp. 2164–2180.
- [12] Soman K. P., Resmi N. G., Ramachandran K. I, (2010), Insight into Wavelets: From Theory to Practice, p. 447;
- [13] Zanardelli W. G., Strangas E. G., Khalil H. K., Miller J. M, (2005), Wavelet-based methods for the prognosis of mechanical and electrical failures in electric motor, *Mechanical Systems and Signal Processing*, Vol. 19, Issue 2, pp. 411–426;
- [14] Rostampour V., Motlagh A. M., Komarizadeh M. H., Sadeghi H.M., Ghanbari T, (2013), Using artificial neural network (ann) technique for prediction of apple bruise damage, *Australian Journal of Crop Science*, Vol. 7, Issue 10, pp. 1442-1448.

WRITING NORMS

Article Types

Three types of manuscripts may be submitted:

1. **Regular articles:** These should describe new and carefully confirmed findings, and experimental procedures should be given in sufficient detail for others to verify the work. The length of a full paper should be the minimum required to describe and interpret the work clearly (max.10 pages, even number);
2. **Short Communications:** A Short Communication is suitable for recording the results of complete small investigations or giving details of new models or hypotheses, innovative methods, techniques or apparatus. The style of main sections has not necessarily to be in accordance with that of full-length papers (max. 6 pages, even number);
3. **Reviews:** Submissions of reviews and perspectives covering topics of current interest are welcome and encouraged (max.10 pages, even number).

Manuscripts should be written in English (American or British usage is accepted, but not a mixture of these) and submitted **electronically** at the following e-mail addresses: ***inmatehjournal@gmail.com***

Please be sure to include your full affiliation and e-mail address (see Sample manuscript)

The authors are responsible for the accuracy of the whole paper and references.

There are allowed 2 papers by each first author.

The text layout should be in single-column format. To avoid unnecessary errors it is strongly advised to use the "spell-check" and "grammar check" functions of your word processor.

Review Process

All manuscripts are reviewed by 2 members of the Scientifically Review Office. Decisions will be made as rapidly as possible and the journal strives to return reviewers' comments to authors in approx.3 weeks.

The editorial board will re-review manuscripts that are accepted pending revision.

NOTE:

Submission of a manuscript implies: that the work described has not been published before (excepting as an abstract or as part of a published lecture or thesis) that it is not under consideration for publication elsewhere.

1. REGULAR ARTICLES

- Manuscripts should be concise, in **1.15 line spacing**, and should have 2 cm all over margins. The font should be **Arial 10 pt.** Ensure that each new paragraph is clearly indicated, using **TAB at 1 cm.**
- Title will be **Arial 12 pt.** and explicit figures will be **Arial 9 pt.**
- Text will be written in English.
- Chapters' titles are written by **Arial 10 pt, Bold, Uppercase** (e.g. **INTRODUCTION, MATERIALS AND METHODS**), between chapters is left a space for 10 pt. At the beginning of each paragraph, TAB of 1 cm.
- The paper body will be written in **Arial 10 pt., Justify alignment.**

TITLE **Arial 12 pt., Uppercase, Bold, Center** (in English language) and **Bold Italic** (in native language).

Should be a brief phrase describing the contents of the paper. Avoid long titles; a running title of no more than 100 characters is encouraged (without spaces).

AUTHORS **ARIAL 9, Bold, Centre alignment**

Under the paper's title, after a space (enter) 9 pt., write **authors' names** and **affiliations (Arial 8 pt.-Regular)**

When the paper has more than one author, their name will be followed by a mark (Arabic numeral) as superscript if their affiliation is different. **Less than 6 authors.**

Corresponding author's name (next row), **(Arial 8 pt.)**. Should be added also: phone, fax and e-mail information, for the paper corresponding author (**font: 8 pt., Italic**).

KEYWORDS **(In English)** about 4 to 7 words that will provide indexing references should be listed (**title: Arial 10pt, bold italic, text Arial 10 pt., italic**).

A list of non-standard **Abbreviations** should be added. In general, non-standard abbreviations should be used only when the full term is very long and used often. Each abbreviation should be spelled out and introduced in parentheses the first time it is used in the text. Standard abbreviations (such as ATP and DNA) need not to be defined.

ABSTRACT **(in English and Native language, Arial 10 pt.)**, the title **bold**; the text of abstract: **italic** should be informative and completely self-explanatory, briefly present the topic, state the scope of the experiments, indicate significant data, and point out major findings and conclusions. The Abstract should be max.250 words. Complete sentences, active verbs, and the third person should be used, and the abstract should be written in the past tense. Standard nomenclature should be used and abbreviations should be avoided. No literature should be cited.

INTRODUCTION (*Arial 10 pt.*) should provide a clear statement of the problem, the relevant literature on the subject, and the proposed approach or solution. It should be understandable to colleagues from a broad range of scientific subjects. We should refer to the current stage of researches performed in the field of the paper to be published, by quoting up-to-date specialty studies, preferably published after 2006, excepting certain referential specialty books/studies, especially papers issued in magazines/journals/conferences/ISI quoted symposia or in other international data bases, which are well known and available.

MATERIALS AND METHODS (*Arial 10 pt.*) should be complete enough to allow experiments to be reproduced. However, only truly new procedures should be described in detail; previously published procedures should be cited, and important modifications of published procedures should be mentioned briefly. Methods in general use need not be described in detail.

RESULTS (*Arial 10 pt.*) should be clearly presented. The results should be written in the past tense when describing findings in the authors' experiments. Results should be explained, but largely, without referring to the literature. Discussion, speculation and detailed interpretation of data should not be included in the Results, but should be put into the Conclusions section.

CONCLUSIONS (*Arial 10 pt.*) The main conclusions drawn from results should be presented in a short Conclusions section. Do not include citations in this section.

Formulae, symbols and abbreviations: Formulae will be typeset in Italics (preferable with the Equation Editor of Microsoft Office 2003) and should be written or marked as such in the manuscript, unless they require a different styling. They should be referred to in the text as Equation (4) or e.g. (4). The formulae should be numbered on the right side, between brackets (*Arial 10 pt.*):

$$P = F \cdot v \quad (1)$$

Terms of the equation and the unit measure should be explained, e.g.

P is the power, [W];

F – force, [N];

v – speed, [m/s]

SI units must be used throughout.

Tables should be self-explanatory without reference to the text. The details of the methods used in the experiments should preferably be described in the legend instead of in the text. [The same data should not be presented both in table and graph form or repeated in the text.](#)

Table's title will be typed *Arial 9 pt, Bold, Centered*

In the table, each row will be written Arial 9 pt, single-spaced throughout, including headings and footnotes.

The table should be numbered on the right side, between brackets (*Arial 10 pt.*):

Figure (*Arial 9 pt., Bold, Center*) should be typed in numerical order (Arabic numerals). Graphics should be high resolution (e.g. JPEG). Figure number is followed by what represent the figure or graph e.g.:

Fig.1 – Test stand

Legend: *Arial 8 pt, Italic, Center, e.g.*

1 - plansifter compartments; 2- break rolls; 3 – semolina machines; 4 – reduction rolls; 5 – flour

ACKNOWLEDGMENTS (*Arial 10 pt.*) of people, grants, funds etc should be brief (*if necessarily*).

REFERENCES (*Arial 10 pt.*)

(In alphabetical order, in English and in the original publication language).

Minimum 10 references, last 10 years, minimum 3 references from the last 2 years

It can be used "References" tool from the *Word Editor*.

References should be cited in the text in brackets as in the following examples:

(Babiciu P., Scripciu V., 2000)

All references must be provided in English with a specification of original language in round brackets.

Authors are fully responsible for the accuracy of the references.

References should be alphabetically, with complete details, as follows:

Examples:

Books: Names and initials of authors, year (between brackets), title of the book (Italic), volume number, publisher, place, pages number or chapter, ISSN/ISBN:

[1] Vlăduț V., (2009), *Study of threshing process in axial flow apparatus (Studiul procesului de treier la aparatele cu flux axial)*, vol.1, ISSN/ISBN, "Terra Nostra" Publishing House, Iași/Romania;

Journal Article: Names and initials of authors, year (between brackets), full title of the paper, full name of the journal (Italic), volume number, publisher, place, ISSN, page numbers:

[1] Lizhi Wu, Yan Di., (2005), *Demonstrational study on the land consolidation and rehabilitation (LCR) project of saline-alkali soil in arid areas: a case study of Lubotan LCR project in Pucheng County, Shaanxi Province (干旱区盐碱化土地整理工程实证研究-以陕西蒲城县卤泊滩土地整理项目为例)*, *Transactions of the Chinese Society of Agricultural Engineering*, vol.21, no.1, pp.179-182, Madison/Wisconsin;

[2] Leonov I.P., (1973), *Basic machine theory for tobacco stringing. Post-harvest care of tobacco and rustic tobacco (Основы теории машин для закрепления табака на шнуры. Послеуборочная обработка табака и махорки)*, *Collection of scientific articles (сборник научно-исследовательских работ)*, pp.37-45;

Conference or Symposium: Names and initials of authors, year (between brackets), full title of the paper (Regular), full name of the conference/symposium (Italic), volume number, publisher, place, ISSN, page numbers

[1] Bungescu S., Stahl W., Biriș S., Vlăduț V., Imbrea F., Petroman C., (2009), *Cosmos program used for the strength calculus of the nozzles from the sprayers (Program Cosmos folosit pentru calculul de rezistență la zgomot al aparatelor de distribuție)*, *Proceedings of the 35 International Symposium on Agricultural Engineering "Actual Tasks on Agricultural Engineering"*, pp.177-184, Opatija / Croatia;

Dissertation / Thesis: Names and initials of authors, year (between brackets), full name of the thesis (Italic), specification (PhD Thesis, MSc Thesis), institution, place;

[1] Popa L., (2004), *Research on the influence of structural and functional parameters of the braking system on the braking performance of agricultural trailers (Cercetări privind influența caracteristicilor constructive și funcționale ale sistemelor de frânare asupra performanțelor de frânare ale remorcilor agricole)*, PhD dissertation, Transylvania University of Brașov, Brașov / Romania.

Patents: Names and initials of authors, year (between brackets), patent title (Italic), patent number, country:

[1] Grant P., (1989), *Device for Elementary Analyses*. Patent, No.123456, USA.

Legal regulations and laws, organizations: Abbreviated name, year (between brackets), full name of the referred text, document title/type (Italic), author, place:

[1] *** EC Directive, (2000), *Directive 2000/76/EC of the European Parliament and of the Council of 4 December 2000, on the incineration of waste, Annex V*, *Official Journal of the European Communities*, L332/91, 28.12.2000, Brussels.

Web references: The full URL should be given in text as a citation, if no other data are known. If the authors, year, and title of the documents are known and the reference is taken from a website, the URL address has to be mentioned after these data:

The title of the book, journal and conference must be written in Italic, the title of the article, chapter of the book, must be written Regular.

Citation in text

Please ensure that every reference cited in the text is also present in the reference list (and vice versa). Do not cite references in the abstract and conclusions. Unpublished results, personal communications as well as URL addresses are not recommended in the references list.

Making personal quotations (one, at most) should not be allowed, unless the paper proposed to be published is a sequel of the cited paper. Articles in preparation or articles submitted for publication, unpublished, personal communications etc. should not be included in the references list.

Citations style

Text: All citations in the text may be made directly (or parenthetically) and should refer to:

- **single author:** the author's name (without initials, unless there is ambiguity) and the year of publication: "as previously demonstrated (*Brown, 2010*)".

- **two authors:** both authors' names and the year of publication: (*Adam and Brown, 2008; Smith and Hansel, 2006; Stern and Lars, 2009*)

- **three or more authors:** first author's name followed by "et al." and the year of publication: "As has recently been shown (*Werner et al., 2005; Kramer et al., 2000*) have recently shown"

Citations of groups of references should be listed first alphabetically, then chronologically.

Units, Abbreviations, Acronyms

- Units should be metric, generally SI, and expressed in standard abbreviated form.
- Acronyms may be acceptable, but must be defined at first usage.



Edited by: INMA Bucharest

6 Ion Ionescu de la Brad Blvd., sect. 1, Bucharest, ROMANIA

Tel: +4021.269.32.60; Fax: +4021.269.32.73

<http://www.inmateh.eu>

e-mail: inmatehjournal@gmail.com